RESERVOIR CHARACTERISATION OF A LAMINATED SEDIMENT

THE RANNOCH FORMATION, MIDDLE JURASSIC, NORTH SEA

Patrick W. M. Corbett, BSc., MSc., Dip.Stat.

Submitted for the
Degree of Doctor of Philosophy
Heriot-Watt University
Department of Petroleum Engineering

July 1993

LIST OF CONTENTS

APPENDICES

LIST OF FIGURES (in text)

LIST OF TABLES (in text)

DEDICATION

This thesis is dedicated to all those who
have played a part in the development of
the probe permeameter.
Their faith has been rewarded,
the little things *are* important.

ACKNOWLEDGEMENTS

The author would like to take this opportunity to acknowledge the many contributions that have helped at all stages of this study. The most important figure has been my supervisor Jerry Jensen whose foresight initiated the project and whose guidance sustained me in those confusing early days. His persistence and dedication to the cause, which started with long-distance telephone calls to Kalimantan, has been rewarded. In addition, the practical assistance and moral support of colleagues in the Edinburgh Reservoir Description Group; Philip Ringrose, Gillian Pickup, Farag Feghi, Ken Sorbie and John Underhill was invaluable. Other members of the department have also provided many useful insights and shared their extensive knowledge of probe permeametry, particularly Jon Lewis and Kjell Rosvoll. The geopseudo ideas grew out of Philip Ringrose's theoretical studies and their application in this real-life case study.

Thanks also go to Adrian Pearce, Greg Geehan and Andy Hurst for promoting and setting up the project. Christian Halvorsen and Statoil are thanked for the painstaking probe measurements that were taken during this project. Statoil's probe permeameter, the care taken in the data acquisition and the resulting high quality of the data contributed much to the weight of my conclusions. Greg Geehan and BP are also thanked for their support of the Bencliff outcrop study. Philip Ringrose, Gerald Corbett and Jon Lewis are thanked for their help during the associated field work. Greg Geehan and Caroline Bajsarowicz assisted in the collection of the Rannoch truncation angle data. Simon Stromberg, Pat Brenchley and BP are also thanked for making the Kennilworth data available for the comparative analysis.

BP, Shell, Statoil and their partners are thanked for providing field data on the Thistle, Statfjord and Cormorant Fields. BP, Chevron, Elf, Exxon, Statoil, Shell, Mobil, Deminex, Enterprise, and the UK Department of Industry are also thanked for funding the various stages of this work. Intera Information Technologies are thanked for the provision of ECLIPSE on which all the numerical simulations were carried out. Cliff Ogle is thanked for his help in the preparation of the photographs for this thesis and the many slides he has been asked to prepare for me during the course of the project.

Finally, and most deeply, I thank Kate for her encouragement, understanding and support that has enabled to achieve an ambition. A doctoral study is, by nature, a lonely journey. Now the destination has been reached, we can resume normal family life again. William, Jessica and Hugo will doubtless appreciate a more relaxed father.

ABSTRACT

The probe permeameter is a recently developed device providing a small scale measurement of permeability. About 15,000 probe permeameter measurements were acquired for analysis during this study. These data were acquired by Statoil from cores in two North Sea wells. These cores are from the Middle Jurassic Rannoch Formation of the Brent Group. This reservoir unit was selected for this study because of its laminated nature and challenge to conventional description and simulation practice.

All aspects of probe permeametry are investigated in this study; the volume of investigation, the compatibility with measurements at larger scales, the measurement statistics, the optimum sample spacing, the relationship of the measurements to the geological description and the scale-up of data for two-phase numerical reservoir simulation.

Careful analysis of probe and traditional plug data shows that the measurements are compatible. Systematic differences could be accounted for by different treatment effects of the material. The probe measurements show that the permeability distribution in the Rannoch Formation is closely related to the primary depositional structure of the sediment, at a hierarchy of scales. This observation is used in combination with conventional simulation techniques to build a more geologically-realistic numerical model of the Rannoch Formation. The scale-up of the small scale measurements is achieved by generation of effective properties for geologically representative elements at various scales and is called the "geopseudo" method. The scale of the natural building blocks within the sediment were determined with the aid of an appropriate outcrop analogue. The model results compare favourably with field production data.

This work demonstrates, for the first time, a systematic method for the scale-up of small scale petrophysical properties associated with lamination in sedimentary rocks, as measured by the probe permeameter. Laminated reservoirs are widely encountered and this work, therefore, makes a significant contribution to reservoir engineering practice.

INTRODUCTION

Reservoir simulation is widely used in the oil industry for planning and monitoring the development of oil and gas fields. Engineers routinely use computer models to plan wells or workovers and to determine the injection and production targets which define the operational priorities and recovery factors for a field under development. With the ever-increasing power of computing, accessability to workstations and sophistication of modelling techniques, reservoir simulation is likely to gain more practitioners and an even higher level of predictive reliance. The development of reservoir simulation is further encouraged by an increasingly detailed level of petrophysical characterisation to match the geological description of reservoir rocks. This study looks at one aspect of characterisation for reservoir simulation, that of a common geological phenomena - a laminated sediment.

A major problem in reservoir simulation has been the scale-up of petrophysical measurements required by the numerical models. Traditionally, reservoir model grid blocks have been relatively large and have been assigned properties from incompatibly small sample volumes by means of various averaging techniques. For this study, measurements at even smaller scales, smaller than were typically available previously, have been made available. Smaller scale measurements should potentially increase the demands of averaging techniques. The smaller scale measurements, however, provide an improved description of the geology (*i.e.*, the lamination) and present a new opportunity for scale-up procedures. Despite the availability of increasingly powerful computers, the averaging or determination of effective properties at larger scales is expected to be needed for some time to come.

Computer models work by solving a well-defined flow equation (*i.e.*, Darcy's Law), under the constraint of mass conservation. The finite difference flow equations are solved between adjacent grid blocks in response to applied pressure gradients representing production or injection wells. The petrophysical properties which govern the location and flow of hydrocarbons (*e.g.*, porosity, permeability, capillary pressure and relative permeability) are assigned to the centre of each grid block. These parameters apply to the volume of the grid block. The size of individual grid blocks is determined by the scale of the modelled reservoir. With 10,000-40,000 grid blocks available from today's computers, these blocks are by necessity large (10's of metres by 100's of metres) relative to the scale of the typical measurement (usually a cylindrical core plug of a few centimetres diameter and length).

As several, or indeed many, core plugs may be available within each grid block at the cored wells, some data reduction or averaging is always required. Away from the wells, statistical and geological techniques are used to extrapolate the limited data set over the remaining reservoir volume. The effectiveness of the averaging and extrapolation techniques will determine the degree to which the models are able to predict real-life. The sampling programme (both volume and spacing) will determine how well real-life is described at the control locations. Appropriate sampling is, therefore, critical to the success of any reservoir simulation excercise.

The oil industry has relied largely on core plugs to provide the petrophysical measurements which form the feedstock of the reservoir models. The core plugs are a non-zero volume of the reservoir rock and therefore give average petrophysical properties for the respective volume. In many reservoir rocks, these core plug volumes are not homogeneous. Layering within the core plug volume (*i.e.*, lamination) can strongly influence the measurement of certain properties, particularly permeability and relative permeability, which become affected by the orientation of the laminae. The measurement of permeability, for example, along laminae and across laminae may show anisotropy. Since permeability is an intensive variable, the desired value is dependent on the imposed boundary conditions. Such variables require careful assessment before scale-up procedures are applied.

Many techniques have been developed for averaging permeability measurements. These vary in complexity from simple algebraic methods for single phase permeability to more complicated procedures, involving numerical simulation or tensor mathematics, for two-phase (oil and water) properties. Each of these methods assumes some arrangement of the sample values (random or ordered) relative to the imposed boundary conditions. The correlation length, or the distance over which knowledge of permeability at one location can help predict the value at a second location, is a statistical measurement of order (or randomness). Averaging or homogenisation should ideally occur over volumes at least as large as the correlation lengths within the data in order to be representative.

Recently, a new device for the measurement of permeability, the probe permeameter, has been developed which, along with some other advantages, allows measurement of permeability at a smaller scale. These measurements, which may be more abundant and potentially more demanding to average, help by clarifying the correlation between permeability and geological features. This improved linkage is illustrated in this work and the geology exploited to determine the spatial structure of the petrophysical properties. Knowing the relationship between permeability and depositional structure, the data collection, averaging and extrapolation can be optimised for a given formation.

Geologists have appreciated for many years that sedimentary rocks consist of a hierarchy of stratal elements. The hierarchy implies a nested structure of correlation lengths. In this work, we show how homogenisation, at scales above the correlation lengths associated with laminae and beds, provides a scale-up procedure that incorporates the geology and mimics the natural architecture of reservoirs.

The Rannoch Formation (Middle Jurassic, North Sea) is a well described and strongly laminated reservoir unit. Flow performance at the larger scale implies an anisotropy (vertical permeability less than horizontal permeability) that is significantly different from that indicated by measurements at the core plug scale. The core plugs are an inappropriate sample volume for the characterisation of laminated reservoirs. Indeed the measured anisotropy is a function of the scale measured. This is illustrated with the help of fine scale probe permeameter measurements and, from these, appropriate anisotropy estimates are derived to provide a different understanding of the production mechanism for this formation.

Laminated sediments are almost universal, resulting from the inherent periodicity in many depositional processes. Measurement of permeability contrasts between laminae is, therefore, the first step in the building of a reservoir model. It is at these small length scales that capillary forces are most apparent. If pervasive high contrast lamination is present within a reservoir unit it is likely to affect the flow performance of the unit.

In this study, an efficient method for the characterisation and scale-up of flow in laminated sediments has been developed. The geopseudo philosophy (*i.e.*, that there exists at some, perhaps several, scales representative elements for which the effective two-phase flow parameters can be determined) provides a focus for the description of reservoir rocks. Application of the geopseudo method in reservoir simulation can improve the prediction of initial oil-in-place, flow performance and remaining oil saturation in petroleum reservoirs.

CHAPTER 1

LAMINATION IN RESERVOIRS

In this chapter, the origin of lamination in sediments is reviewed. A sedimentological perspective suggests that laminated sediments are the norm. The effects of lamination, however, despite being recognised in laboratory experiments in the 1970's has largely been ignored in everyday reservoir simulation practice.

1.1 The Origin of Lamination in Sedimentary Rocks

Lamination or small scale systematic variations in rock texture within clastic reservoirs is ubiquitous as a result of natural depositional processes. Truely massive sands (*i.e.*, those without any internal structure) are very rare, whilst laminated sediments occur in virtually every major environment (Pettijohn *et al.*, 1972, p.100).

The accumulation of detrital sediments dependant on sediment transport (Allen, 1970, p.56). In uniform, steady-state conditions deposition cannot take place. Only when the transport rate changes can either net erosion or deposition occur. In nature, the transport rates in air and water are continuously changing in some periodic or episodic form during storm or flood conditions. Periods of quiescent conditions tend to leave no mark (erosional or depositional) in the geological record. Most sedimentary sequences record the alternation of deposition and erosion and, for all *preserved* sequences, deposition prevailed in the long term.

Sediment particles travelling in a transporting medium (air or water) are subject to several forces of nature: inertial, viscous and gravity. Sediment particles are either transported as bedload in a thin, densely packed layer above the base of the liquid column, by sliding, rolling or saltating or by suspension (carried by turbulence within liquid column). As gravitational forces exceed inertial forces (*i.e.*, as the fluid velocity drops), the grains will either settle out from suspension or their bedload transport cease (Fig. 1.1). As transport velocities vary continuously, the depositional process can be a very effective sorting mechanism.

Bedload transport results in bedforms or spatially periodic mounds and hollows at the sediment liquid interface (Allen 1970, p. 67). Sediment transport by migrating bedforms results in internal lamination or stratification as a result of the periodic movement of that bedform (Allen, 1985, p. 70). Preserved bedforms within sediments deposited subaqueously are the fossilised form of the river or sea bed. In sediments, plane horizontal lamination, undulating lamination and cross-lamination all result from the preservation of the passage of migrating bedforms.

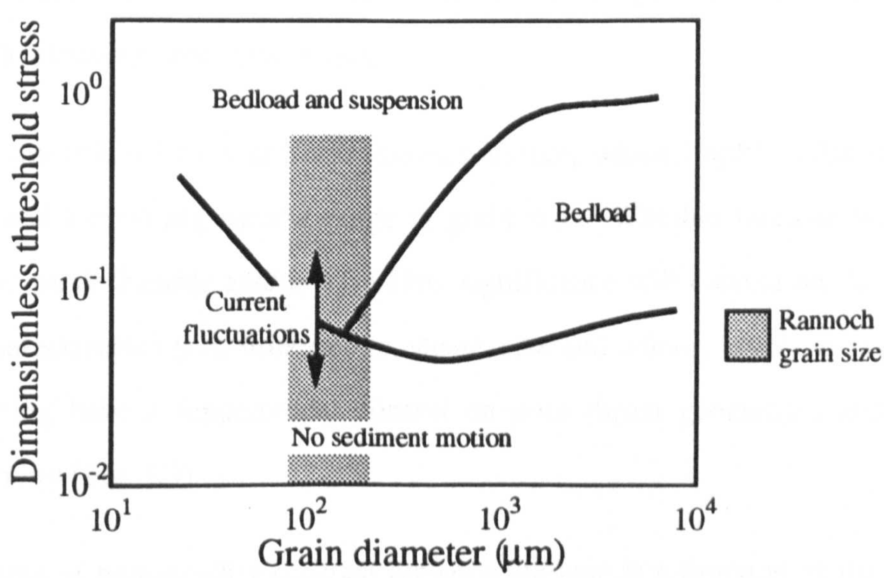

Dimensionless threshold stress =
f(fluid velocity, 1/diameter, fluid density,
1/density contrast)

Figure 1.1: Shield's diagram showing how fluctuations in current strength lead to alternating suspension and deposition of sediment. Range of Rannoch Formation grain size shown (after Allen, 1985).

All detrital sediments will exhibit lamination. A lamina is a mm- to cm-scale stratal element with near uniform properties that is deposited over a relatively short period of time (Campbell, 1967; Van Wagoner *et al.*, 1990). Laminae are the smallest megascopic elements in a hierarchy of stratal elements (Fig. 1.2). Laminae are bounded by laminar surfaces with no internal layering. There is no genetic distinction between a lamina and a uniform bed. Laminae, however, are often arbitrarily defined by a maximum thickness of 1cm (Pettijohn *et al.*, 1972). Other authors are less concerned by such a strict definition (Campbell, 1967; Van Wagoner *et al.*, 1990) and allow a degree of overlap in the scale of elements. Laminae generally have a smaller areal extent and form in a shorter period of time than beds.

In this work, we are primarily interested in the effects due to capillary forces of contrasting laminae or thin beds at length scales up to 5cm (Ringrose *et al.*, 1992). Therefore, it is convenient to consider lamination (*i.e.*, *capillary-sensitive* lamination) to refer to elements 5cm thick or less.

Lamina are defined by a uniform internal texture, which implies relatively good sorting and a resulting narrow range in grain size. Whether laminae within any reservoir are defineable and/or have flow significance will depend on the range of grain characteristics (*i.e.*, minerology, shape, size and colour) involved. Grain size and sorting have a fundamental control on pore throat geometries and, hence, permeability (Fig. 1.3).

The degree of permeability contrast between laminae is a function of the extreme range of current strength and the diversity of sediment available. A sediment that is contains a narrow range of grain sizes is not likely to produce strong permeability contrast laminae. On the other hand, a wider range of grain sizes in a sediment in a strongly fluctuating current can result in high heterogeneity.

Post-depositional process (*e.g.*, dewatering, bioturbation or diagenesis) can modify, either destroying or enhancing, the depositionally-derived permeability fabric.

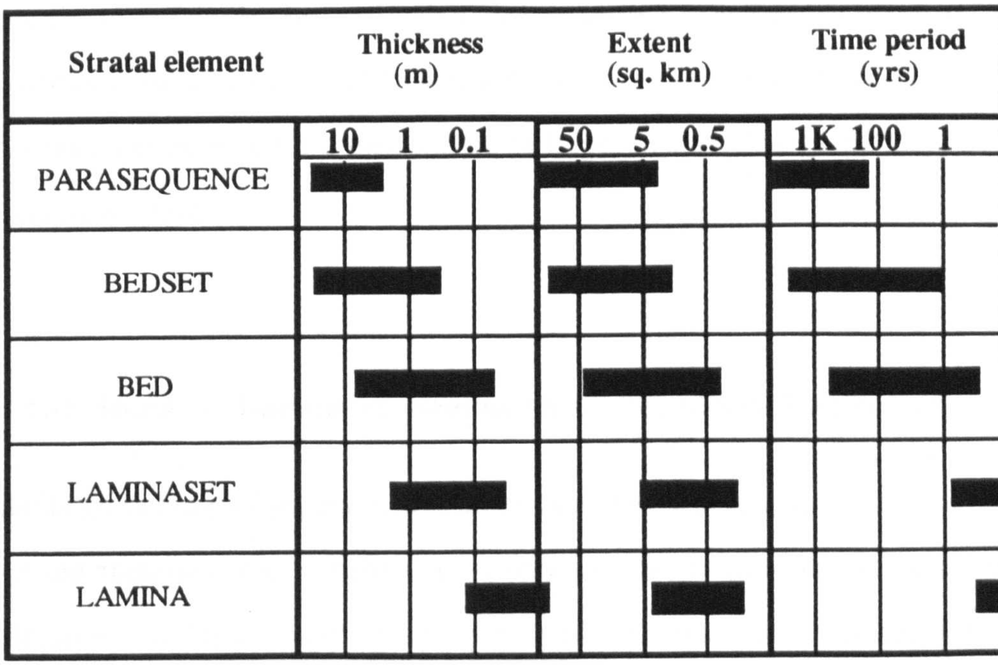

Figure 1.2: The hierarchy of stratal elements. (After Van Wagoner *et al.*, 1990)

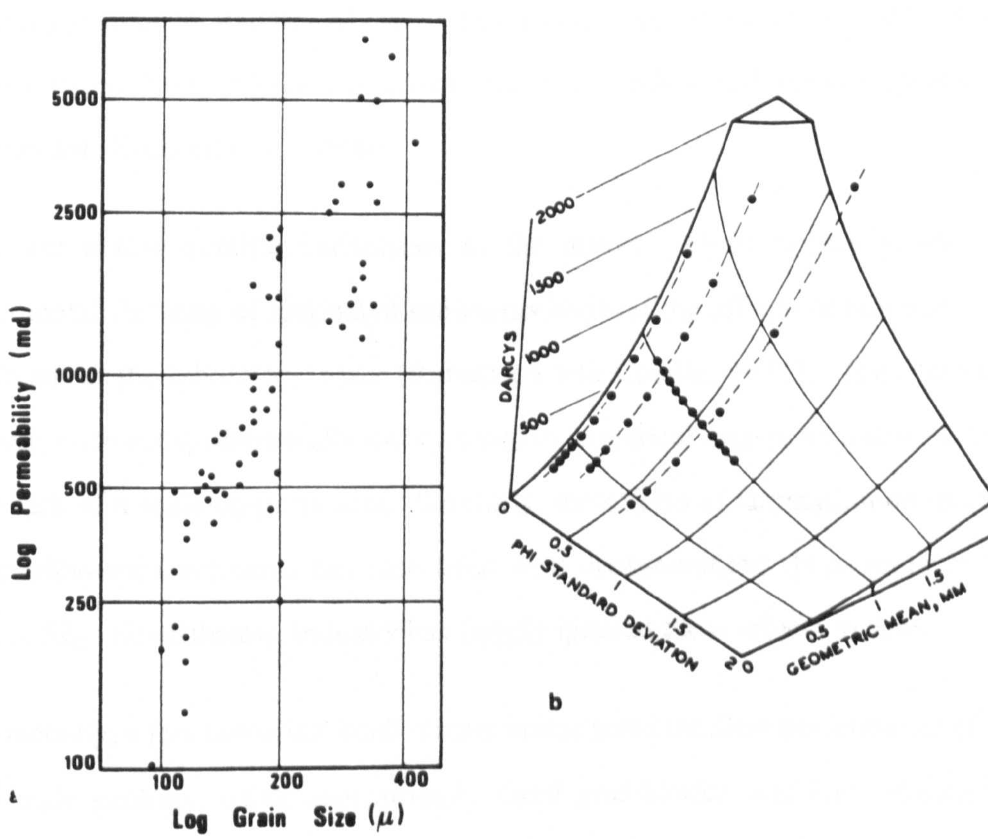

Figure 1.3: Relationships between permeability and grain size; (**a**) from Pettijohn *et al.*, 1972; (**b**) from Krumbein and Monk, 1942.

However, in this study, we confine our investigations to sediments that (excluding compaction) have suffered little apparent post-depositional alteration. In such sediments, the permeability distribution is largely controlled by the depositional sedimentary fabric.

1.2 The Study of Laminated Sediments in Petroleum Engineering

In the large volume of papers published to date, concerning experimental floods of rocks and numerical reservoir simulation, very few specifically consider the effects of lamination. Indeed, many of the petrophysical measurements are made on homogeneous samples (*i.e.*, specifically avoiding laminated rocks) and numerical simulations utilise grid blocks too coarse to require quantification of such small-scale heterogeneity. As a result, the effects of lamination have gone largely unquantified, if not totally unnoticed, to date. Many studies, using inappropriately large grid blocks or flow rates, have mistakenly concluded that such small scale features are insignificant (Kossack *et al.*, 1990).

There are a few notable exceptions to the above. Over twenty years ago, experimental flooding of laminated sediments showed the effects of laminae to be significant at the laboratory scale (Robertson and Caudle, 1971). These effects, however, were not systematically incorporated in numerical reservoir models because of the lack of a scale-up procedure. Similarly, the effects of lamination on relative permeability measurements has also been well docummented (Hornapour et al., 1986, p. 52). Nevertheless, industry has largely ignored these effects to date.

More recently, a few numerical studies have investigated the flow performance of the small-scale geology, using appropriately sized grid blocks, and have shown the effects of systematic lamination (Kortekaas, 1985; Hartkamp-Bakker, 1991) or less ordered permeability fields (Lasseter *et al.*, 1986) to be significant. That the small-scale structure in reservoirs (particularly lamination) can determine the distribution of remaining oil is, however, more widely appreciated (Weber, 1986; van de Graff and Ealey, 1989) if not routinely quantified. For carbonates, the control of small scale structure on residual oil saturation has been well described (Wardlaw and Cassan, 1978).

The effects of small scale geology have largely been ignored in large scale reservoir simulations. A recent study, with more appropriately sized grid blocks (0.25 x 1m), has shown significance of capillary pressure on recovery efficiency (Hoimyr *et al.*, 1993). In this latter study, the grid blocks are still relatively large compared with the primary depositional structure.

CHAPTER 2

THE RANNOCH FORMATION

2.1 The Geological Description of the Rannoch Formation

This study concentrates on a well documented reservoir from a shallow marine setting. The Middle Jurassic Rannoch Formation is a significant oil-bearing and oil-producing reservoir in the northern North Sea offshore area (Fig. 2.1).

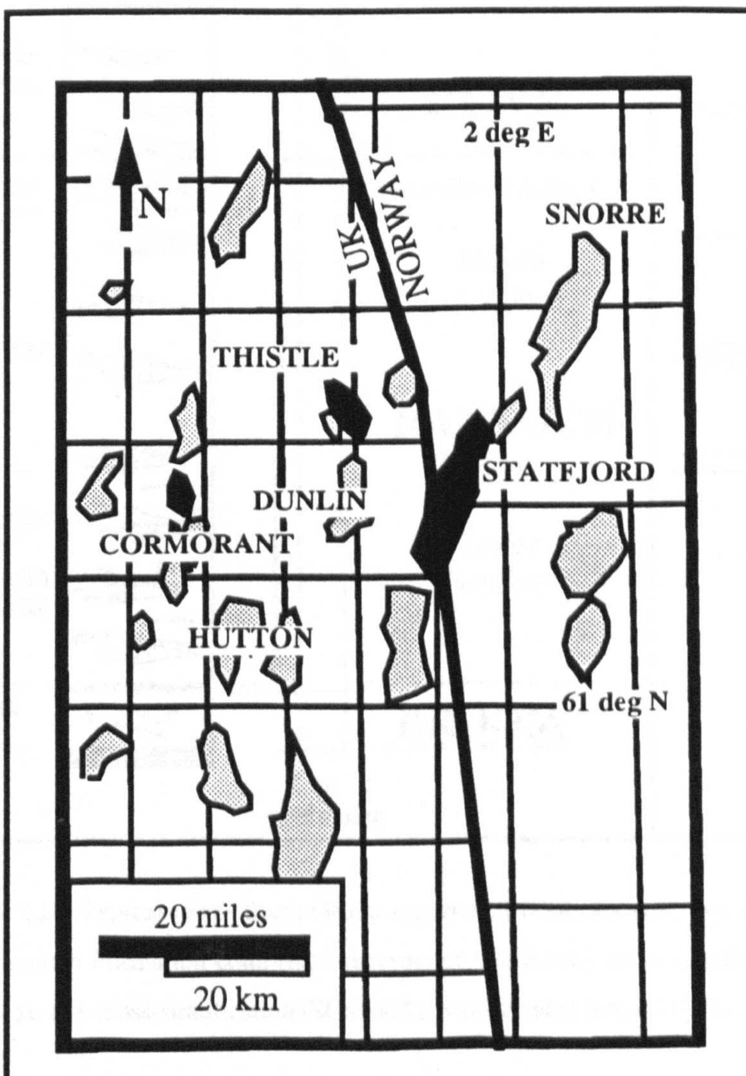

Figure 2.1: Location map for some Rannoch Formation producing fields in the northern North Sea. Light shading shows location of Rannoch-producing fields, dark shading shows fields considered in this study.

The laminated sediments of the Rannoch Formation were deposited along a dissipative shoreline in advance of a northward prograding deltaic system (Budding and Inglin, 1981; Richards and Brown, 1986; Brown *et al.*, 1987; Richards *et al.*, 1988; Brown and Richards, 1987; Graue *et al.*, 1989; Mitchener *et al.*, 1992; Scott, 1992). The Rannoch Formation is characterised by low angle cross-laminated, micaceous, fine to very fine grained sandstone (Fig. 2.2). The Rannoch is directly overlain by the medium to coarse grained, upper shoreface/beach barrier sandstones of the Etive Formation.

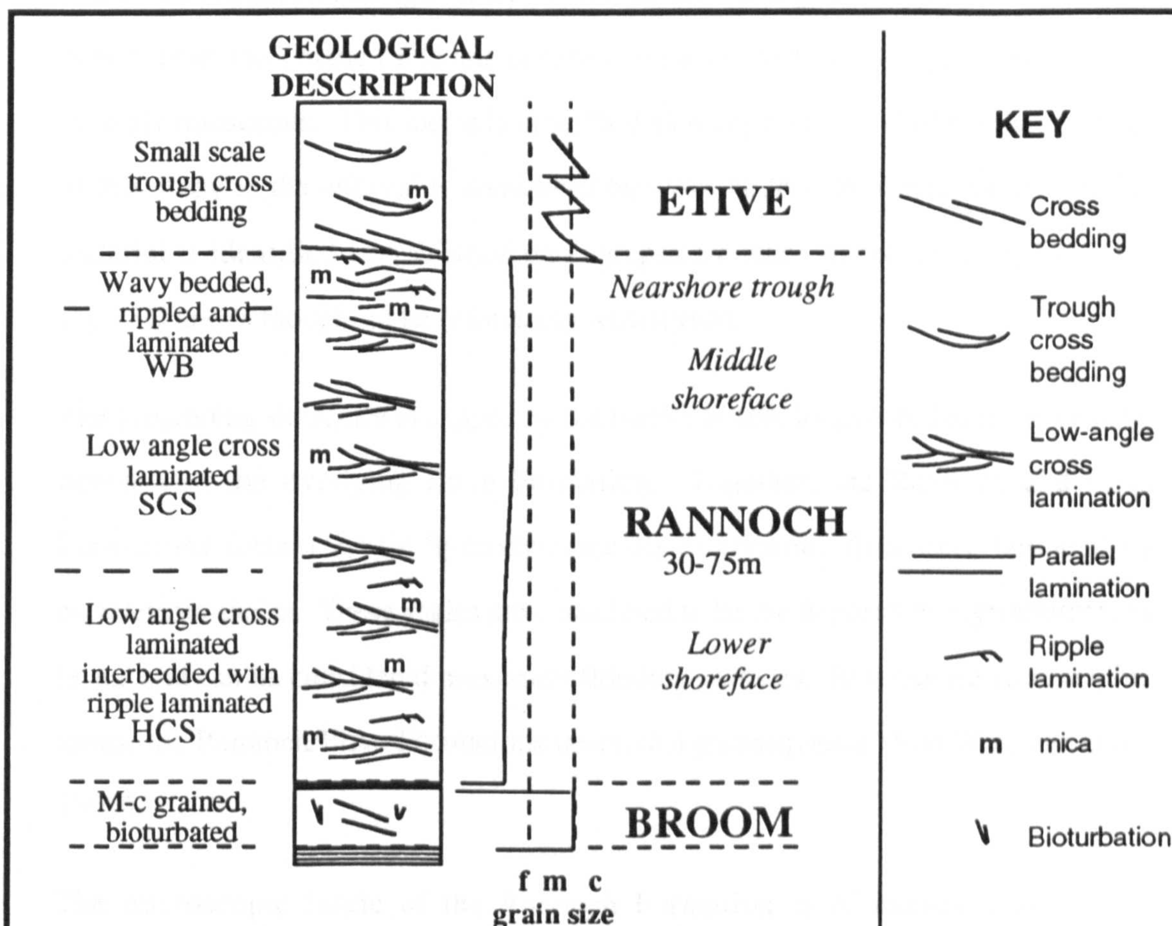

Figure 2.2: Typical lower Brent Group sequence, Middle Jurassic, North Sea. The Rannoch Formation comprises intervals of hummocky cross-stratification (HCS), swaley cross-stratification (SCS) and a wavy bedded interval (WB).

The Broom Formation that underlies the Rannoch Formation is a variably developed, generally coarse grained, transgressive shoreline sandstone of an earlier depositional sequence (Mitchener *et al.*, 1992). The Broom Formation is usually separated from the Rannoch Formation by a thin shale. Together, the Broom, Rannoch and Etive Formations form the lower Brent Group.

More specifically, within the Rannoch Formation, hummocky cross stratification (HCS, Harms *et al.*, 1975; Dott and Bourgeois, 1982; Walker *et al.*, 1983; Duke, 1985; Walker, 1985) of the lower shoreface is overlain by swaley cross-stratification (SCS, Allen and Underhill, 1989) of the middle shoreface and nearshore bar (Fig. 2.2). The low angle cross-laminated sequence (30-60m) is commonly overlain by a thin (3-5m) nearshore trough facies. This nearshore trough facies has been described in core from the Thistle Field and is seen to be wavy bedded to ripple laminated and strongly micaceous. This facies is described as wavy bedded (WB) for the purposes of this study as the interval is dominated by wavy bedded thin sandstones. Similar material is identified in published photographs by other workers (Scott, 1992, her Fig.15a) and is thought to be reasonably widespread.

The prograding shoreface is capped by the barrier beach, longshore bar or rip channel deposits of the overlying Etive Formation. Together, the Rannoch and Etive Formations form a single hydrodynamically-continuous flow unit, bounded by correlatable shales. These shales are considered to be the deposits of high relative sea levels and can be considered maximum flooding surfaces. In sequence stratigraphic terms, the Rannoch/Etive Formations describe a parasequence (Van Wagoner *et al.*, 1990).

The microscopic fabric of the Rannoch Formation is of interest here, as the permeability will be controlled by the grain size and sorting of the sediment at the finest scale. Rannoch Formation sediments are characteristically feldspathic and micaceous. For example, Scotchman *et al.* (1989) describe the Rannoch mineralogy in Northwest Hutton: quartz (67%), felspar (4.8%), calcite (7.4%), mica (2.8%) and clay (16%). The distribution of the mica gives rise to the distinctive banded appearance of the Rannoch (Fig. 2.3) although at the pore-scale the mica is generally dispersed (Fig. 2.4). The quartz is uniform, very fine to fine sand.

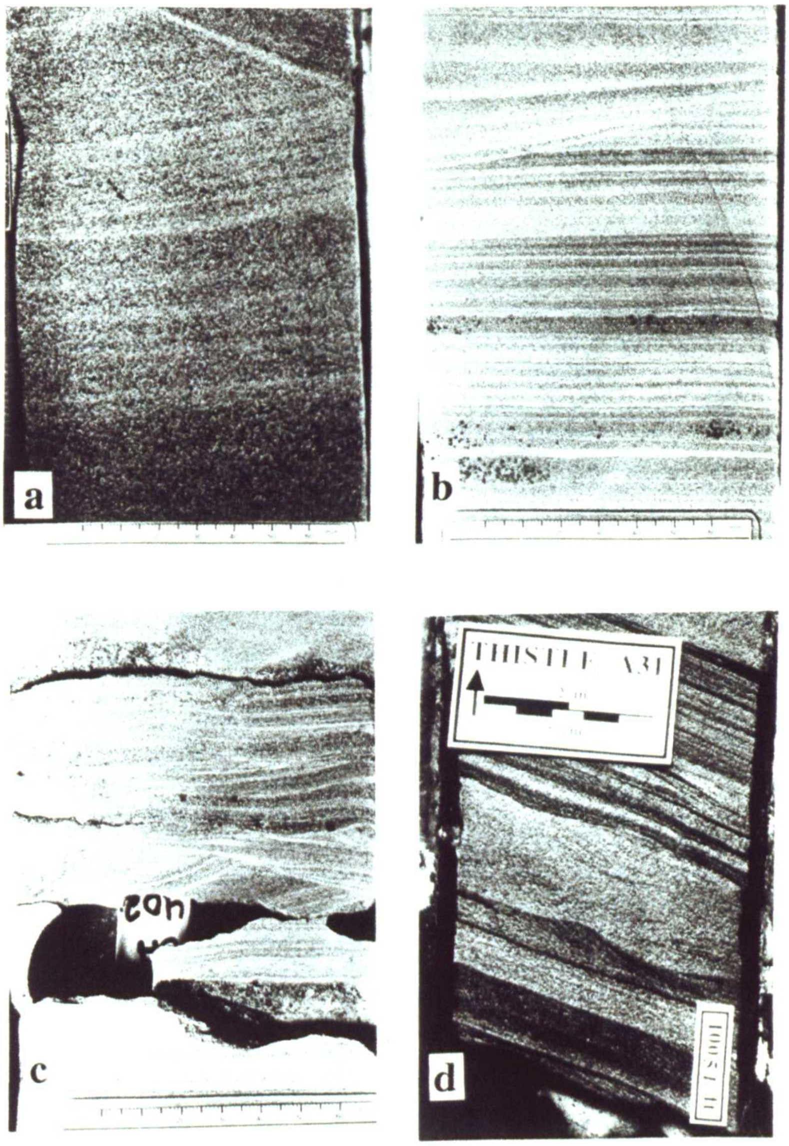

Figure 2.3: Photographs of typical Rannoch lamination types from the various facies: **a)** low mica lamination (HCS/SCS); **b)** high mica lamination (HCS) with the distinctive banded appearance due to the contrast between dark mica-rich and light mica-poor laminae; **c)** ripple lamination (HCS) **d)** wavy bedded lamination (WB)

The hydrodynamic equivalence of medium mica platelets are sand grains approximately 1/12th the grain diameter (Berthois, 1962). The hydrodynamic properties of the mica in the Rannoch is, therefore, very similar to the accompanying sand. Subtle contrasts in the settling velocity of sand grains and mica platelets are therefore enough to generate the sorting into mica-poor and mica-rich couplets (Fig. 2.4).

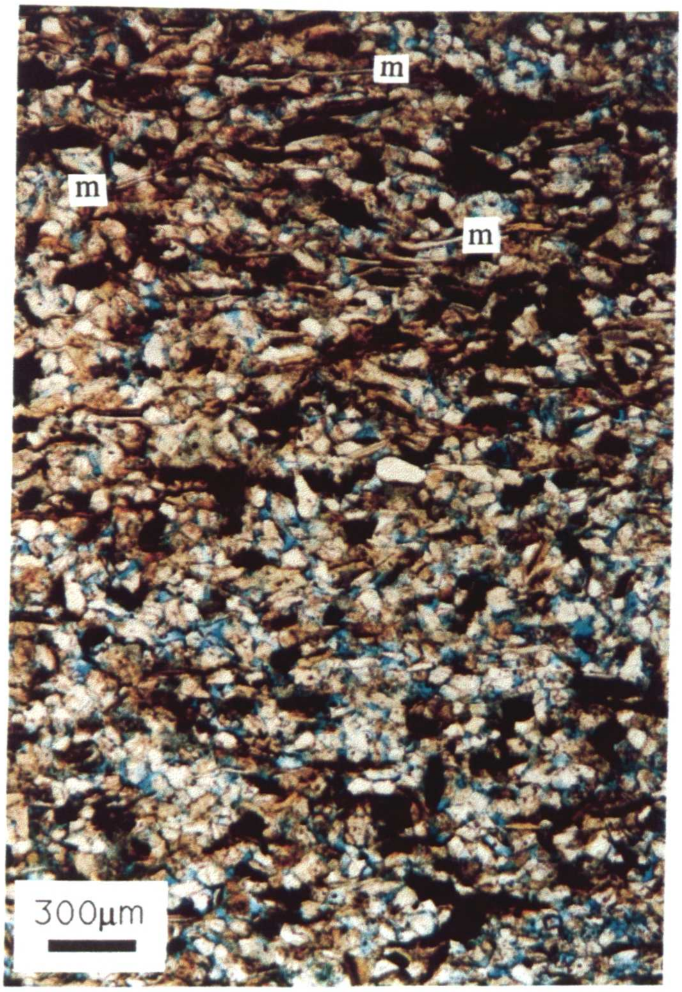

Figure 2.4: Photomicrograph showing typical pore-characteristics of a mica-poor (lower) and mica-rich laminae (upper) in the Rannoch Formation. Note that the mica platelets are disseminated in both elements and in neither do mica platelets form closely packed impermeable layers. (N.B.: m - mica platelets)

There has been much discussion on the depositional processes responsible for HCS/SCS beds (Kreisa, 1981; Duke, 1987; Klein and Marsaglia, 1987; Swift and Nummendal, 1987; Allen, 1989; Brenchley, 1989; Duke *et al.*, 1991) and whether they are produced from pure oscillatory (Southard *et al.*, 1990) or combined oscillatory/translatory flow (Nottvedt and Kriesa, 1987; Allen and Underhill, 1989). HCS bedforms are generally found in fine grained sediments, are characteristically circular in plan view with a lack of any slip face (Fig. 2.5). SCS bedforms are similar in geometry but lack the rippled hummock crests.

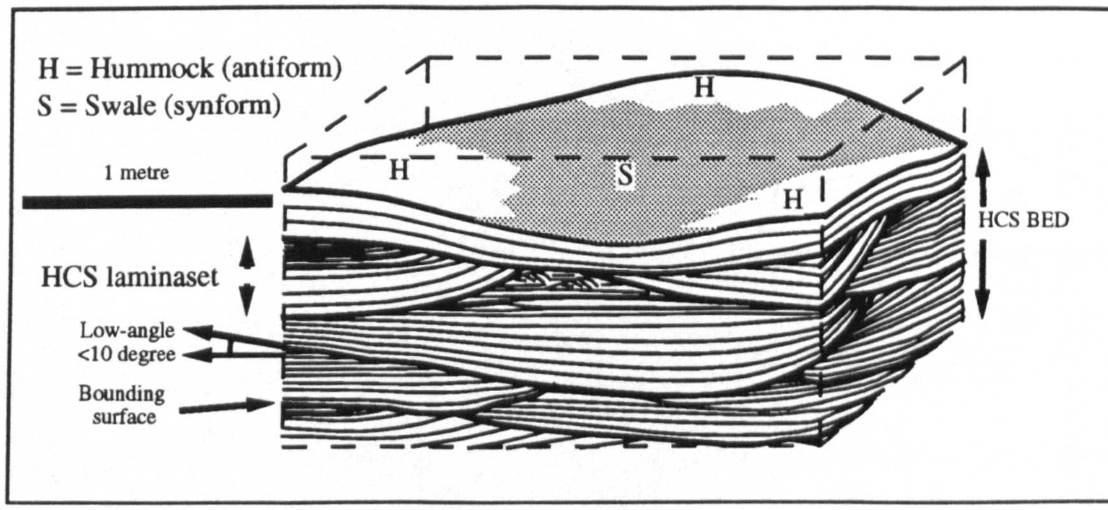

Figure 2.5: Interpreted sketch of the HCS laminasets of the Rannoch Formation. Note the circular plan view of the bedform and the similarity of the orthogonal sections. HCS laminasets are bounded by low angle, erosional bounding surfaces.

In fine grained sediments, however, migrating slipface dune bedforms will not be expected (Fig. 2.6).

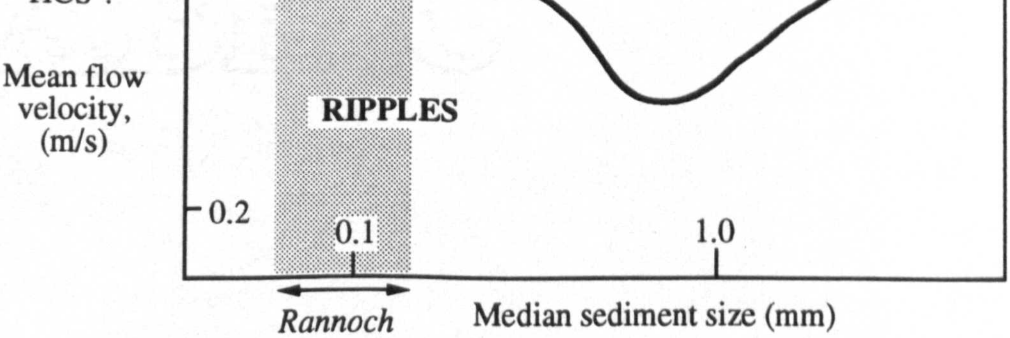

Figure 2.6: Plot of mean flow velocity against median sediment size showing stability field of bed phases. (After Ashley, 1990). Grain size of typical Rannoch sediments indicated.

The fabric of typical HCS sandstones lack consistent particle alignment and imbrication (Cheel, 1991; Yokokawa and Masuda, 1991) suggesting deposition from a predominantly oscillatory flow. Unidirectional sole marks (such as those recognised in Wapiabi Formation HCS, Upper Cretaceous, Canada by Cheel, 1991), on the other hand, would support an initial unidirectional component. Sole marks have not been described to date from the Rannoch Formation HCS. Nevertheless, an early unidirectional component is considered to be the scouring mechanism within the Rannoch (Scott, 1992). In reading the literature, it is clear that the origin of beds described as HCS or SCS cannot be ascribed to a single environment of deposition and that the bedforms probably have a polygenetic origin (Southard *et al.*, 1990).

Thin section analysis of Rannoch Formation sediments shows recurring coarsening-up, mica-poor and fining-up, mica-rich laminae (Scott, 1992). For each lamina, Scott suggests a depositional mechanism. In her model, an initial high-density shear layer near the bed concentrates the coarsest grains at the surface. As the flow velocity falls below the threshold, the bedload freezes as a coarsening-up layer (the mica-poor lamina) and finer sediment falls from suspension forming a fining-up unit (the mica-rich lamina). The platey fabric of the mica also resists subsequent erosion as the flow velocity subsequently increases. The exact process which combines these processes remains speculative but is thought to be wave-oscillatory (*i.e.*, driven by storm waves). Mica-poor and mica-rich laminae are, therefore, considered to form a wave-deposited couplet.

A storm origin in a shoreface setting for the Rannoch Formation (Fig. 2.7) is supported by evidence at all scales - the dominant grain fabric of wave-deposited couplets, the wave rippled and low angle lamination, the HCS/SCS bed associations, and the overlying coarse beach of the Etive. Shoreface sandstones are often extensive along the palaeo-shoreline but can be quite narrow in a seaward direction (Walker, 1985). The Rannoch shoreface unit, however, has been mapped over a large area

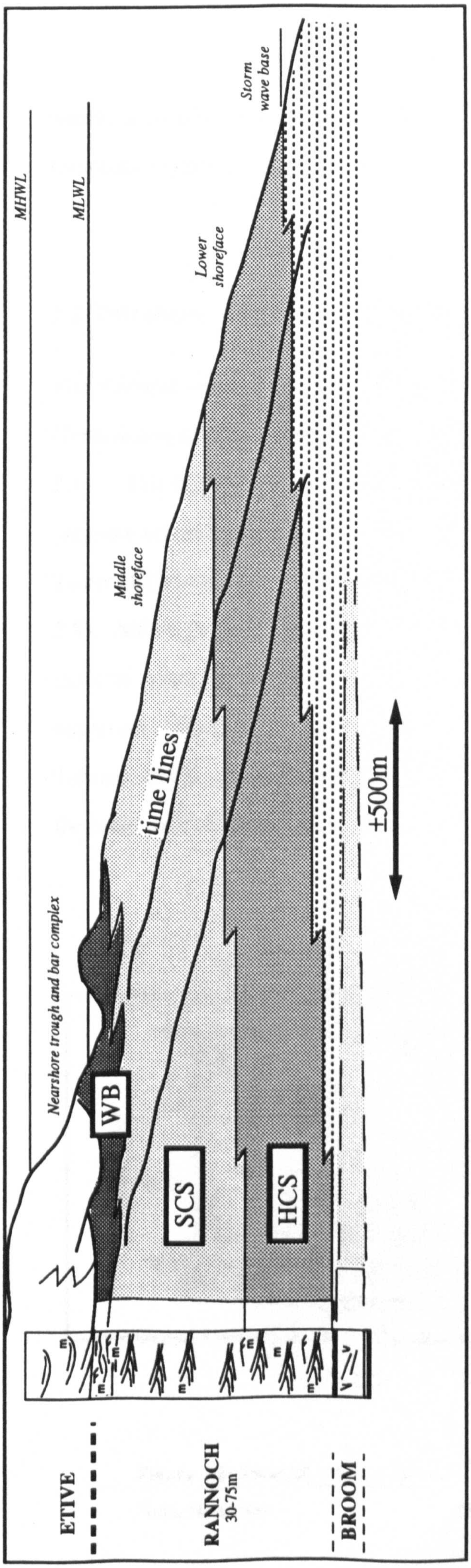

Figure 2.7: A depositional model for the Rannoch Formation showing the distribution of lamination types and associated bedforms in a storm-dominated shoreface. (Redrawn, with minor modifications, from Scott, 1992). The beach/shoreface is shown migrating from left to right in this figure.

within a relatively narrow age range (Mitchener *et al.*, 1992), implying that a reasonable degree of reservoir continuity can be expected.

2.2 Petroleum Engineering Challenges in the Rannoch Formation

The Rannoch-Etive unit of the Middle Jurassic, Brent Group in the U.K. northern North Sea is a major oil-bearing and oil-producing horizon in a number of fields (Fig. 2.1). The Rannoch-Etive section generally forms a single flow unit with good pressure communication throughout. This is illustrated by the Repeat Formation Tester (RFT) data from a water injector on the western flank of Statfjord Field (Fig. 2.8). Although the up-dip production has been from the Rannoch interval only, the uniform water gradient over the Rannoch-Etive intervals records uniform pressure depletion. Similar data have been published from the Thistle Field (Bayat and Tehrani, 1985), although in this field some pressure discontinuities were observed in the lower part of the Rannoch section.

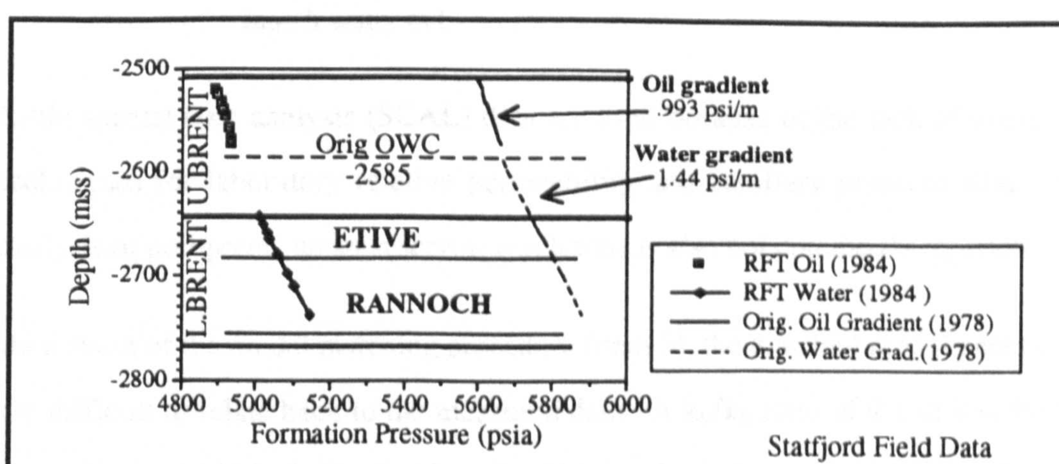

Figure 2.8: Pressure data for the Rannoch-Etive flow unit from the Statfjord Field, North Sea

The production performance of the Rannoch-Etive flow unit has been routinely modelled in the fields in which it produces. The interval generally produces oil under a waterflood process. There have been several publications outlining the reservoir simulation approach to the Rannoch-Etive unit. These include field-specific studies: Thistle (Bayat and Tehrani, 1985); Dunlin (Braithwaite *et al.*, 1989); Cormorant (Grant *et al.*, 1990); and, more recently, a Rannoch-specific study (Thomas and Bibby, 1991).

The common approach in the published papers, is to use the following simulation parameters :

1. Absolute horizontal permeability from core plugs.

2. Vertical permeability (k_v) as a fixed ratio (initially, usually 10%) of horizontal permeability (k_h).

3. Power-law relative permeability curves.

4. Zero capillary pressure.

5. Arbitrary adjustments to k_v/k_h and/or transmissibilities to history match water cut.

Little special core analysis (SCAL) data are used because of the lack of averaging techniques for laboratory relative permeability and capillary pressure data. The analysis of poroperms under reservoir conditions is also not commonly reported.

As a result of the model matching procedure (item 5), the matched model parameters are difficult to relate back to the measured data. A k_v/k_h ratio of 0.1 or less for the 3m or larger grid blocks is significantly different from the average indicated by the core plugs in a typical Rannoch well (Fig. 2.9). Up to the present time there has been no systematic investigation of scale-up procedure for critical parameters such as k_v/k_h ratio from core plugs to the grid block scale.

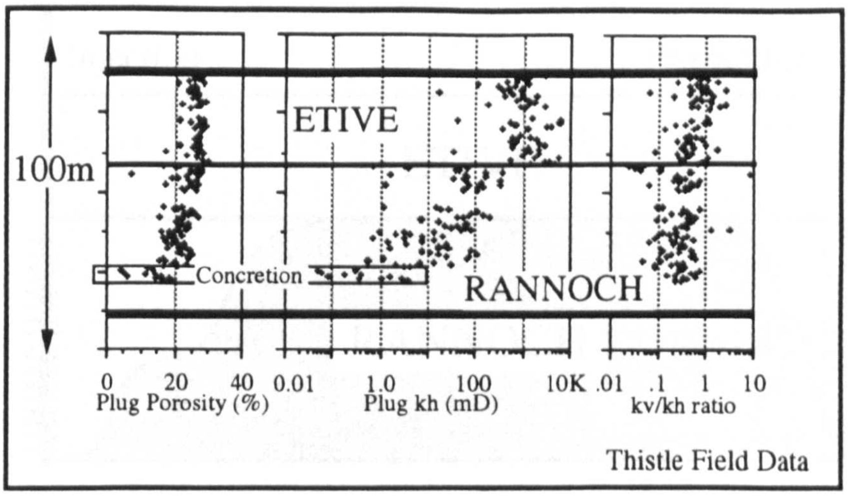

Figure 2.9: Core plug data for a typical lower Brent, Rannoch-Etive sequence. Porosity and permeability increase upward through the Rannoch shoreface. Significantly higher permeabilities are encountered in the Etive Formation. These data are from Thistle Field.

Typical cross-sectional well models (*i.e.*, an injection-production well pair at either end of a modelled cross-section through part of the field) tend to show the over-riding of water through the high permeability Etive and bypassing of Rannoch oil (Fig. 2.10). This is contrary to what might be expected. In a waterflood of a flow unit with a high permeability zone at the top, gravitational effects on the heavier water would be expected to produce an efficient sweep of the low permeability zone at the base. The conclusions of the models, however, history matched by adjusting the input parameters, have been seen to be misleading. Recent experience of infill drilling has not found the large volumes of by-passed Rannoch oil that have been generally predicted by these models (BP Thistle Group, personal communication). This has driven some operators to further investigate the reservoir management of the Rannoch-Etive unit and has resulted in the acquisition of additional data which forms the basis for this current study.

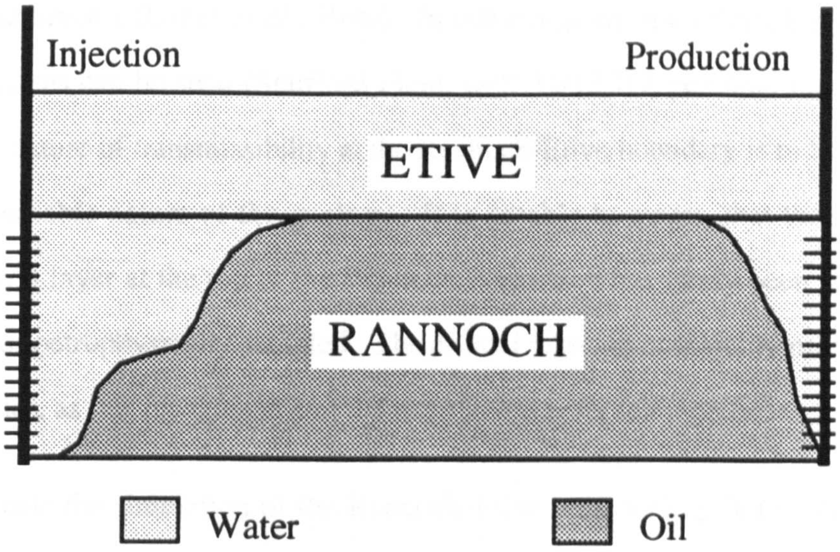

Figure 2.10: Schematic of Rannoch-Etive production performance as suggested by previous simulation studies. Water over-riding the Rannoch suggests bypassed oil. (After Thomas and Bibby, 1991).

In these model studies, the significance of the Rannoch-Etive boundary (in effect the top few metres of the Rannoch) has become apparent. In addition to investigating the field-scale production performance, two detailed studies have attempted to measure the transmissibility at the boundary using local pressure differences induced by well testing or production (Dake, 1982; Bunn and Yaxley, 1986). In these studies, various permeabilities (5mD in Dake and a variable 10 - 0.03mD in Bunn and Yaxley) were determined for this horizon. These values tend to be less, however, than the average vertical permeability of the interval, as measured in core plugs (Fig. 2.9), although in neither study were detailed geological descriptions or core plug data presented. Similarly, by studying the water infiltration into the Rannoch from the overlying Etive by gravity and capillary forces (sudation) in the Dunlin Field, Braithwaite *et al.* (1989) were able to determine a vertical permeability of 5-10mD for the interval.

The boundary between the Etive and Rannoch is geologically very variable, due mainly to the variable nature of the overlying Etive (Scott, 1992). Sharp, erosive boundaries occur where distributary or tidal channels, at the base of the Etive, erode

Rannoch sediments (Grant *et al.*, 1990). In other regions, interdigitating Etive and Rannoch facies can be seen (Statfjord Field, well 33/12-B9, personal observation). A variable nature of transmissibility at the Rannoch-Etive boundary is to be expected from the variable nature of the geology. It is notable however, that the thin, very variable, WB layer at the top of the Rannoch Formation has rarely been adequately described or petrophysically sampled. The critical ±3m are commonly preserved for future studies, as it is recognised that the interval has reservoir significance.

To complicate the simulation of the Rannoch-Etive unit, sealing faults, due to clay smearing, have been recognised in some fields (*e.g.*, Thistle Field: Bayat and Tehrani, 1985; Cormorant Field: Bentley and Barry, 1991). In addition, the injection of cold water is thought to induce thermal fracturing in the near-well region. These natural and man-made structural phenomena, while possibly very important in specific cases, are not considered further in this study. Here, we concentrate on the characterisation of the depositional variability of the Rannoch, which is present in all fields. For other reasons, the diagenetic concretions described from the Rannoch have also been ignored. Where the effects of concretions have been considered (Braithwaite *et al.*, 1989), they have been shown to be relatively unimportant to fluid flow. The prime concern of this study was to focus on the primary depositional fabric the Rannoch Formation.

The challenges faced in this integrated geoengineering study of the Rannoch Formation are threefold: Firstly, to characterise the permeability distribution more effectively than past efforts. Secondly, to incorporate the pervasive lamination in a geologically-reasonable way in the reservoir simulation models. Thirdly, to explain the larger scale flow performance. If this can be achieved in an integrated fashion, a major step forward in the understanding of the flow behaviour of Rannoch Formation reservoirs will have been made.

CHAPTER 3

CORE PLUG AND PROBE PERMEABILITY MEASUREMENT

In this chapter, the measurement of permeability by core plug and probe methods is considered with specific reference to the Rannoch Formation in the studied wells. Traditional petrophysical sampling of the Rannoch Formation by core plugs is discussed prior to introducing the newly acquired data. The measurement of permeability usually presents a greater challenge than the measurement of porosity. Permeability varies over a greater range, is sensitive to the type and scale of measurement and its estimation has a major impact on fluid flow prediction. In this work, we concentrate on the permeability description of the Rannoch Formation, with reference to porosity where appropriate.

In particular, the limitations of the traditional sampling by core plugs are considered which, in keeping with industry-standard practice, imply a fixed volume and interval spacing. In contrast, the probe permeameter sampling scheme is more exploratory, no recommended practice having yet been adopted by industry (Sutherland, 1991). To study the many aspects of probe measurement, a flexible approach to sampling was required. Prior to a discussion of the sample schemes, the physics of measurement is considered.

3.1 The Physics of Core Plug Permeability Measurements

The physics and procedure for permeability measurement on core plugs is well established in the oil industry (API, 1960). Core plugs are usually cut by drilling horizontally or vertically (with respect to bedding) in whole, unslabbed, core material. Plugs are then trimmed, to give a cylindrical sample one-inch in diameter and one-inch in length, and cleaned. In some cases, larger 1.5in plugs are used. The core plugs are encased in a compliant sleeve within a steel cylinder (Archer and Wall, 1986). This type of measurement device (sleeve and cylinder) is often referred to as a Hassler Cell. Pressure on the sleeve ensures that the sample is sealed on faces parallel to the flow direction. Dry gas, usually nitrogen, is injected into the upstream end of the core, flows quasi-linearly through the plug, and vents to the atmosphere. The permeability is determined by Darcy's Law from the measurement of stable flow rate (Q), pressure drop (ΔP), area (A) and length (L) of the sample cylinder (Fig. 3.1).

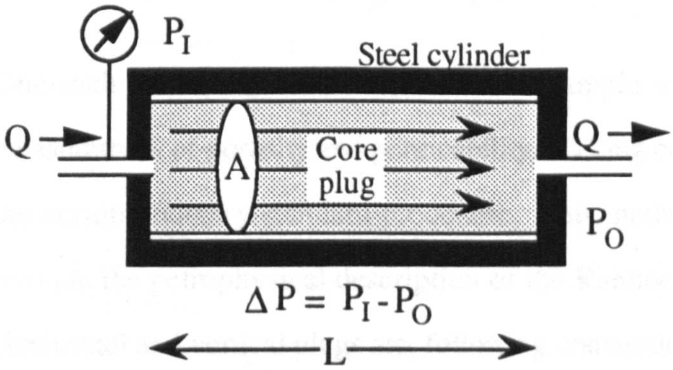

Darcy's Law

$$k = \frac{Q\, 2\, \mu\, L\, P_O}{A\,(P_I^2 - P_O^2)}$$

Figure 3.1: Core plug permeability measurement

The relationship between permeability and flow rate is generally linear, as described by Darcy's Law. In regions of high flow rate or low permeability, however, non-linear effects are apparent. At high flow rates, non-linear flow results from inertia leading to, at very high rates, turbulence. These effects can be corrected for (Firoozabadi and Katz, 1979) but, where possible (i.e., unless the permeability is very high), these flow regimes should be avoided by maintaining as low a pressure drop as practical on the sample.

In low permeability media, a second non-linear phenomena occurs. Gas slippage is the term given to the increased flow of gas relative to that expected from a liquid. The sample has an effective higher permeability to gas because a) gas molecules are loosely bonded and can travel easily before encountering neighbours and b) there is no zero-velocity boundary layer (as found with liquids), increasing the effective diameter of the pores. The effects of slippage can, however, be corrected for and equivalent liquid permeabilities determined (Archer and Wall, 1986).

In summary, the physics of core plug measurements is well understood and the techniques are well accepted by industry. There are, however, limitations and these are discussed in the following section.

3.2 Traditional Core Plug Sample Scheme

One-inch core plugs are the traditional sample volume (1.3×10^{-5} m^3) for the measurement of porosity and permeability. Taking core plugs at a one-foot spacing is the current industry-standard procedure. This method has been used extensively to provide the petrophysical description of the Rannoch Formation prior to this study. Horizontal and vertical plugs are, following convention, taken at one-foot intervals on which horizontal and vertical permeabilities, porosities and grain densities are measured.

The limitations of this traditional form of petrophysical sampling and measurement include the following (refer to Fig. 3.2):

1. The one-foot sample interval is rarely followed rigourously. The quality of core recovery and competency does not always allow such sampling (3.2a). There is also a tendency for operator bias towards the more permeable zones.

2. Horizontal and vertical measurements are made on adjacent but different material (3.2b). In very heterogeneous formations, these can lead to selective sampling a misleading quantification of anisotropy at the plug-scale.

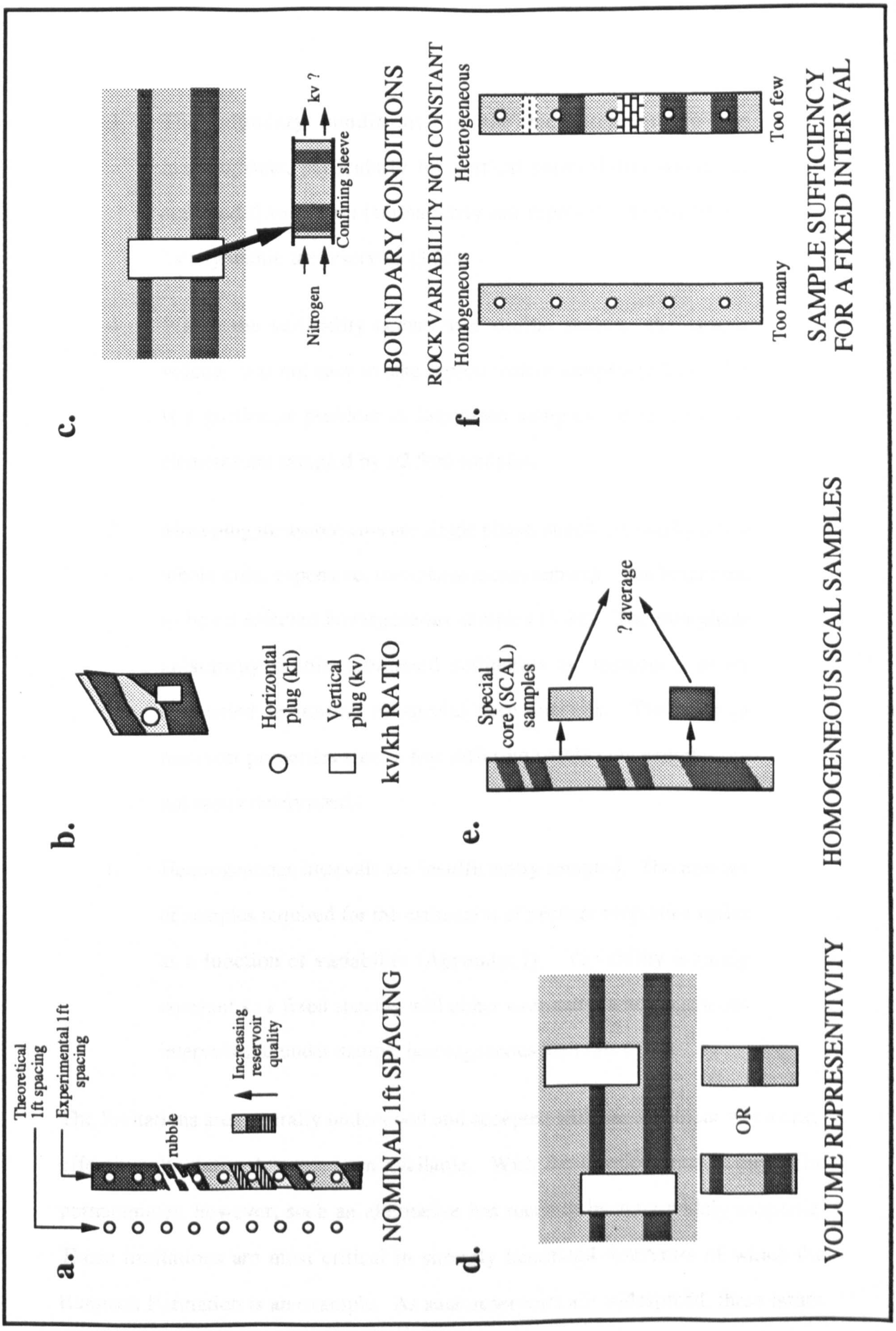

Figure 3.2: Limitations of core plug and whole core sample volumes and spacings. Refer to text for explanations

3. The boundary conditions for the measurement may be inappropriate, particularly for vertical permeability where the confined flow across laminae may not represent the conditions locally within the reservoir (3.2c).

4. Where the variability occurs at a similar scale to the sample volume, it is not easy to take representative samples (3.2d). This is a particular problem in laminated samples where cm-scale elements are sampled by ±2.5cm samples.

5. Most plug measurements are single phase, supplemented by a few whole-core, expensive, two-phase measurements. The latter tend to be on selected homogeneous samples (3.2e). The two-phase anisotropy within laminated sediments is, therefore, never quantified in routine or special core analysis. The average reservoir properties from a few differing whole core samples are not easily determined.

6. Heterogeneous intervals are insufficiently sampled. The number of samples required for the estimation of average properties varies as a function of variability (Appendix I). Variability is rarely constant so a fixed spacing will either over-sample homogeneous intervals and under-sample heterogeneous intervals (3.2f).

The limitations are generally understood and accepted with the argument that a cost-effective alternative has not been available. With the development of the probe permeameter, however, such an alternative has recently become widely available. These limitations are most critical in strongly laminated reservoirs of which the Rannoch Formation is an example. As such reservoirs are widespread, these issues imply a serious shortcoming of the standard petrophysical practise. Core plugs are, therefore, an inappropriate primary method for the petrophysical characterisation of laminated sediments.

Core plugs, however, are the only currently available means whereby petrophysical measurements can be made at overburden conditions. In the Rannoch Formation, significant (30-40%) differences have been noticed when such measurements have been made and compared to surface conditions (Stiles and Valenti, 1990). The need for special core analysis is not, therefore, in question. The selection of the few "representative" samples from which such overburden-corrected properties could be determined is the issue here.

3.3 The Development of the Probe Permeameter

Probe permeameters have undergone significant development since the technique was first described by Dykstra and Parsons (1950). Until the early 1980's, only Shell, applying the technique to unconsolidated sands (Eijpe and Weber, 1971; Weber *et al.*, 1972) and aeolian sediments (van Veen, 1975) appear to have considered the application further. Development of the modern generation of probe permeameters followed with work at Heriot-Watt (Cadman, 1984; Clelland, 1984; Martin and Evans, 1988; Robertson and McPhee, 1990), the University of Texas at Austin (Goggin, 1988; Goggin *et al.*, 1988; Kittridge *et al.*, 1990), Imperial College (Daltaban *et al.*, 1989; Lewis *et al.*, 1990) and Statoil (Hurst and Rosvoll, 1989; Halvorsen and Hurst, 1990; Halvorsen, 1991; Gibbons *et al.*, 1991). Other recent studies show the increasingly widespread acceptance of the technique within the industry (Dreyer *et al.*, 1990; Daws and Prosser, 1992, Hartkamp-Bakker, 1991; Prosser and Maskall, 1993). At the time of this study, the most sophisticated laboratory device has been developed by Statoil (Halvorsen and Hurst, 1991). In this study, most of the data were measured by this device (Fig. 3.3).

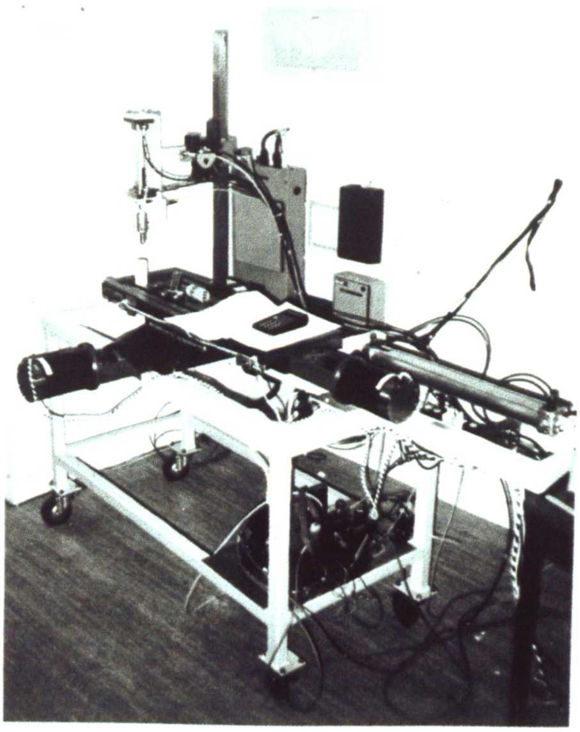

Figure 3.3: Statoil's laboratory probe permeameter (courtesey of Christian Halvorsen). Automated table, controlled by computer-driven stepping motors, ensures an accuracy of measurment location to 0.01mm (Halvorsen and Hurst, 1991).

The probe permeameter allows quick, relatively cheap, non-destructive, detailed (almost exhaustive) sampling of permeability, from which small-scale distribution maps of permeability can be derived. A characteristic of such sampling programs is the ability to closely correlate permeability with geological features.

There has been a rapid expansion of published probe permeameter studies in recent years as the field and laboratory devices have been developed. Most of the recent studies have been outcrop studies (Goggin *et al.*, 1988; Dreyer *et al.*, 1990; Kittridge *et al.*, 1990; Lewis *et al.*, 1990), but a significant number of core studies have also been published (Martin and Evans, 1988; Hurst and Rosvoll, 1989; Halvorsen, 1991; Gibbons *et al.*, 1991). These studies have lead to an improved understanding of the relationship between geology and permeability variation (Goggin, 1991; Lake, 1992). In particular, the probe has been able to measure the permeability of individual laminae, for the first time, and this development will be exploited in the scale-up for reservoir simulation in this study.

3.4 The Physics of Probe Permeameter Measurements

The physics of the probe permeameter (also previously called the minipermeameter) is reasonably simple (Fig. 3.4). Gas (usually nitrogen) is injected into the surface of the rock through a nozzle, venting to the atmosphere.

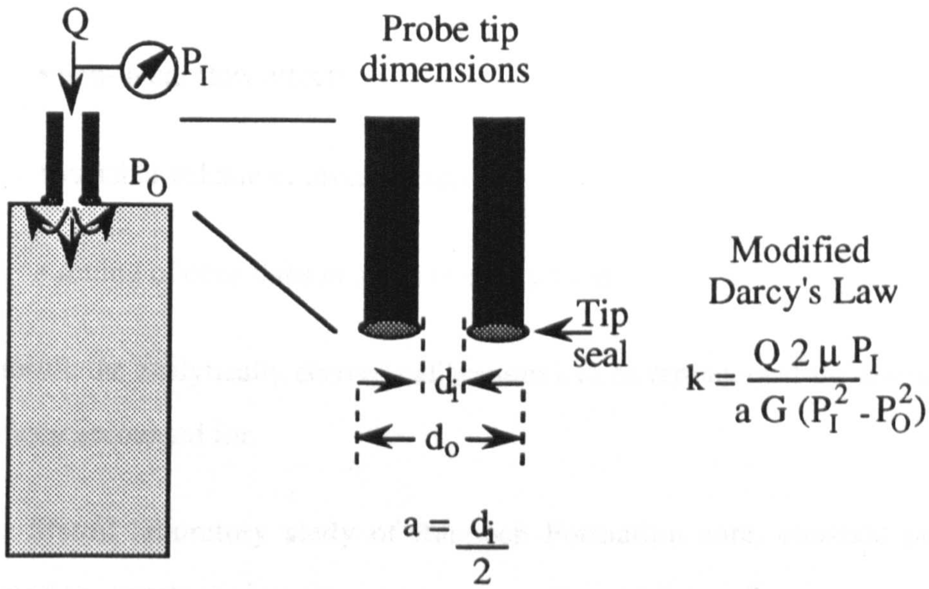

Figure 3.4: Probe permeability measurement on a core plug. Probe tip inner (d_i) and outer (d_o) diameters are used to determine the geometrical factor (G) which is a function of tip seal width relative to the aperture (refer to Goggin, 1988).

A linear relationship for pseudo-spherical flow for injected nitrogen through a probe tip has been derived from Darcy's Law (Goggin, 1988). This relationship holds well under ideal conditions and is commonly used to determine probe permeability (Dreyer *et al.*, 1990). The relatively simple physics, however, is complicated by a number of operational practicalities:

- variable deformation of the tip seal (dependent on the application pressure)
- quality of the tip seal (function of tip seal material, application pressure and surface rugosity)
- surface preparation (damage, fines)
- presence of additional phases (moveable water, oil, residual oil)
- heterogeneity of the sample
- temperature fluctuations
- non-linear flow effects
- variable volume of investigation
- setting of core slabs in a bed of epoxy resin

As a result, the analytically derived calibrations can be erroneous if the above are not rigorously accounted for.

In the Statoil laboratory study of Rannoch Formation core, constant probe tip deformation, constant viscosity, good seal quality and linear flow were ensured by careful equipment design and operating procedures (Halvorsen and Hurst, 1990). Moveable fluids were not a problem in this study due to the use of dried core. The effects of residual fluids, resin imbibition and surface damage are discussed further in the following sections.

The determination of permeability from the probe can be achieved either analytically or empirically. In this study, various empirical calibrations were determined by a number of regression methods employing measurements on uniform plugs of known permeability. These are discussed fully in Appendix II. In general, a fair to good comparison between empirical and analytical calibration constants (Goggin, 1988) was found and calibration was not considered a major issue in this study.

The volume investigated by a probe is the subject of much interest and speculation. Many probe permeameter operators have considered the depth of investigation. The depth of investigation will be influenced by the operating conditions and the nature of the sampled material. Empirical observations (Halvorsen and Hurst, 1991) and numerical simulation results (Goggin, 1988; Winterbottom, 1990) point towards a limited depth of investigation. The depth of investigation has been considered during this study and the results of a numerical simulation study are discussed in Appendix III.

The above work suggests the probe permeameter depth of investigation, at 50% pressure drop, to be of order two times the internal probe (aperture) diameter (2 to 8 x 10^{-7} m^3). As such, the volume of investigation is 2-7% the volume of a one-inch core plug for typical laboratory probe sizes (0.3 - 0.6cm internal radius). Comparison of probe with core plug measurements is often good, with systematic differences due to sample treatments or the effects of local heterogeneity occurring. The systematic differences are discussed more fully in later sections.

3.5 Probe Permeameter Sampling Scheme

In this study, various sampling schemes were adopted for a variety of applications. Cores from two Rannoch Formation wells were made available for this probe permeameter study. An initial pilot study on 8m of Rannoch material from two intervals in a Statfjord Field (Fig. 3.5) well was followed by a more comprehensive study of a 40m interval from a Thistle Field well (Fig. 3.6). The location of the fields is given in Fig. 2.1. All the probe measurements in this study were taken by Christian Halvorsen with the Statoil probe permeameter (Halvorsen and Hurst, 1990). Three probes were used, the characteristics of which are as follows:

- Large Probe 1 (LP1): $d_i = 5.9mm$, $d_o = 10.5mm$

- Small Probe 1 (SP1): $d_i = 3.6mm$, $d_o = 7.9mm$

- Small Probe 2 (SP2): $d_i = 3.4mm$, $d_o = 10.2mm$

The cores from each well had been plugged, slabbed and resinated prior to the study.

In the Thistle well, additional unresinated core material was also available. In this material, three types of probe measurement were taken:

- on the trimmed ends of cleaned core plugs,

- on the surface of resinated, uncleaned core,

- on cut, cleaned and uncleaned, unresinated core.

The probes, sample spacings, objectives and results of these measurements are discussed in the following sections.

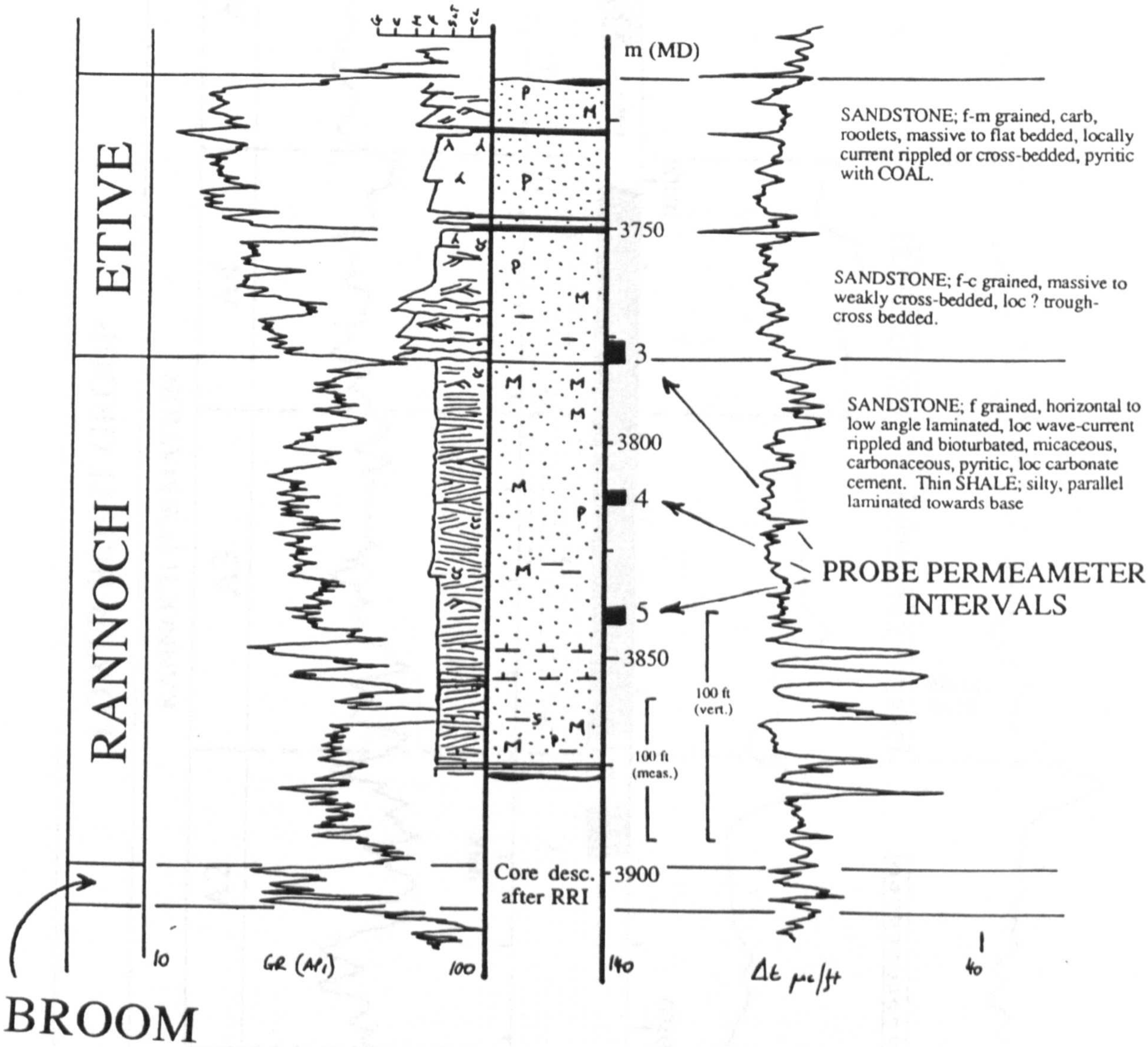

Figure 3.5: Statfjord well 33/12-B9 showing location of intervals of cores 4 and 5 on which the initial probe permeability study of the Rannoch Formation was carried out.

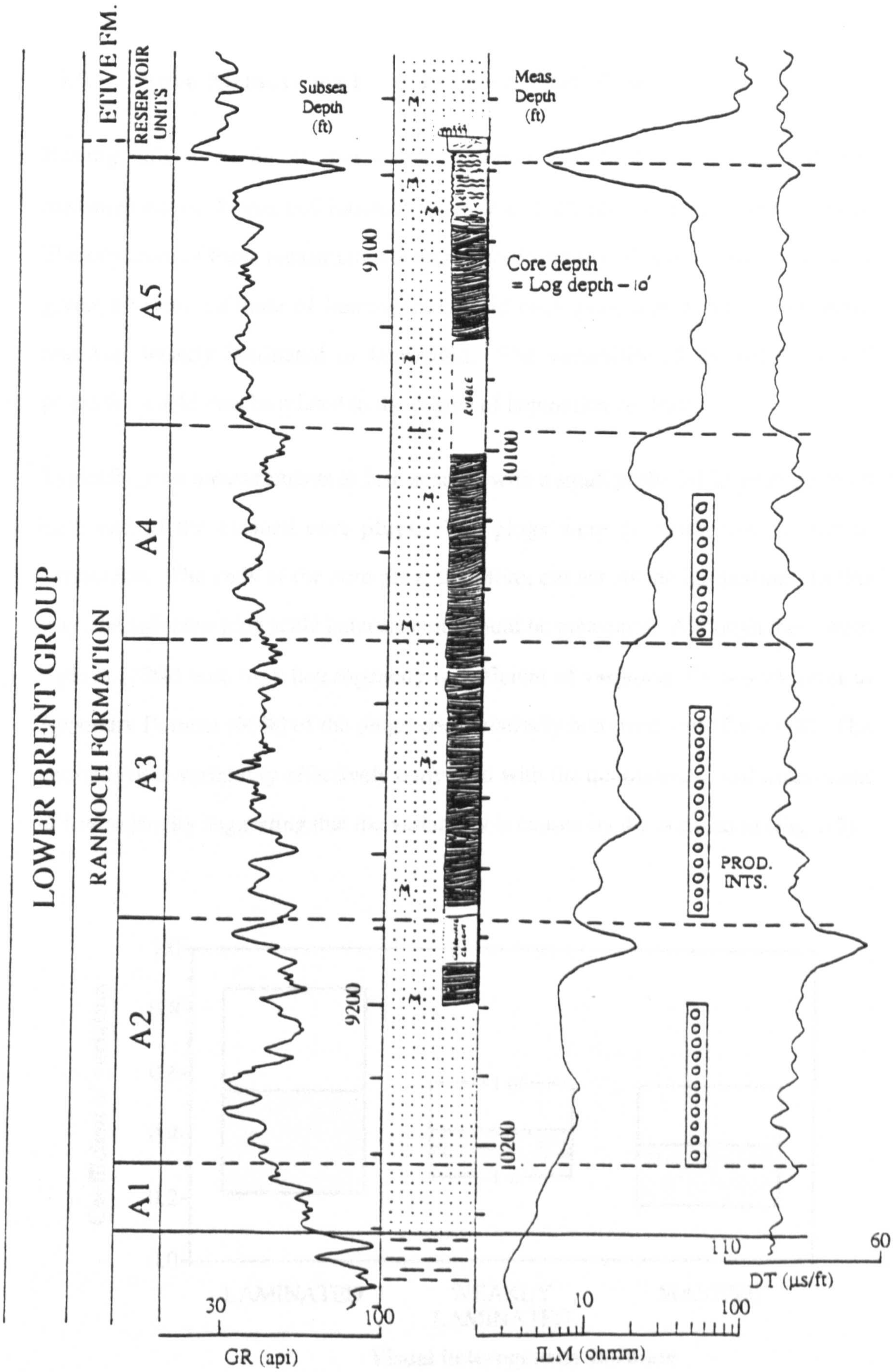

Figure 3.6: Thistle well A31 showing interval of cores which the more comprehensive probe permeability study of the Rannoch was carried out.

3.5.1 Probe Measurements on Rannoch Core Plugs

Having calibrated the probes using methods discussed in Appendix II, the measurement of the cleaned Rannoch cores from a Thistle Field well were sampled. The objective of these measurements was to confirm the calibration. The plugs were given a visual estimate of heterogeneity and each plug was described as either massive, weakly laminated or laminated. The variability of the petrophysical properties could thus be related to the degree of lamination contrast.

Typically, four measurements at 1cm spacing with a small probe (SP2) were taken on each end of the cleaned core plugs. The plugs were generally cut parallel to lamination. The ends of the core plug, therefore, cut across the lamination. In this way, the sub-core plug scale heterogeneity could be measured. Although there were 9 plugs (10%) with high heterogeneity (coefficient of variation: $Cv > 0.75$, refer to Appendix I), most (66%) of the plugs were relatively homogeneous ($Cv < 0.5$). The petrophysical variability effectively correlated with the qualitative visual assessment of heterogeneity suggesting that the variability is caused by the lamination (Fig. 3.7).

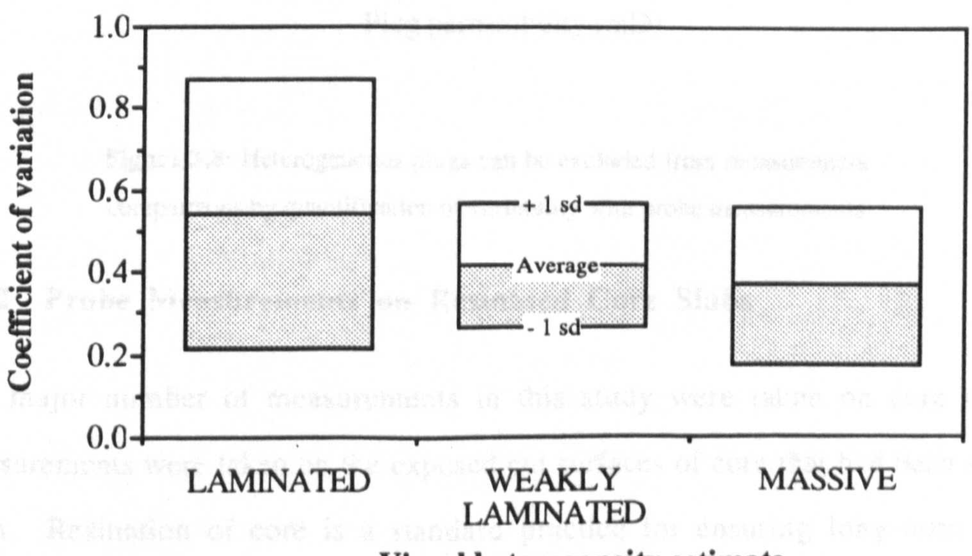

Figure 3.7: Quantification of visual assessments of heterogeneity with the probe permeameter for a set of Rannoch Formation core plugs.

When the average probe permeability measurements are compared with the core plug permeabilities, a clear relationship can be seen (Fig. 3.8 left). For the homogeneous plugs (*i.e.*, those with Cv < 0.3, taking into account the fact that these Cv's were based on only 8 samples) the correlation between measurements is even clearer (Fig. 3.8 right). From these data we confirm that the probe and plug measurements of permeability on the same, cleaned, relatively homogeneous core plugs is the same. It is noteable that most of the Rannoch core plugs are relatively uniform despite the laminated nature. The variability of probe measurements on core plugs proved to be an effective method for screening homogeneous core plugs.

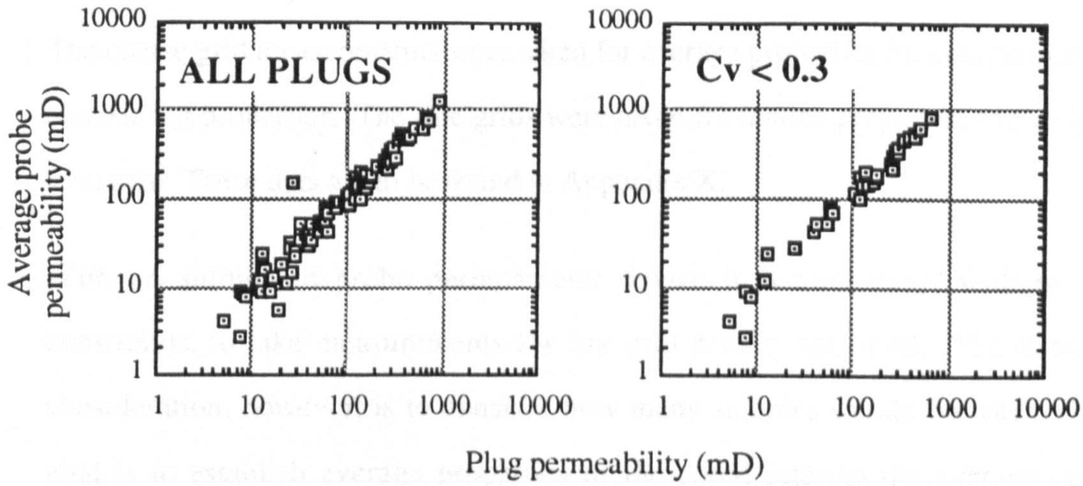

Figure 3.8: Heterogeneous plugs can be excluded from measurement comparisons by quantification of variability with probe measurements

3.5.2 Probe Measurements on Resinated Core Slabs

The major number of measurements in this study were taken on core slabs. Measurements were taken on the exposed cut surfaces of core that had been set in resin. Resination of core is a standard practice for ensuring long term core preservation. Core slabs (representing approximately metre intervals) are carefully aligned and partially embedded in epoxy resin. The resinated material is perfect for probe permeametry as less handling of material is required and the geometry is fixed.

The automated probe permeameter can detect the breaks in the core and areas with excessive surface rugosity (Halvorsen and Hurst, 1990). Metre-lengths of core slab can, therefore, be sampled without supervision.

In the initial Statfjord well programme, two sample schemes were adopted (Fig. 3.9):

- Large probe (LP1), coarse, 1cm (vertical down core) by 2cm (lateral across core) grid over the length of the core (approx. 3000 measurements)

- Small probe (SP1), fine, 2 x 2mm or 5 x 5mm grids over selected intervals (approx. 5000 measurements)

The coarse grid measurements were taken for average properties for comparison with electric log properties. The fine grids were taken for lamina properties over selected intervals. These data are to be found in Appendix X.

With an automated probe permeameter device it is very easy, with no time constraints, to take measurements for any grid density specified. The important consideration, however, is to consider how many samples should be taken. If the goal is to establish average properties of the cored interval the average can be determined from subsets of the data and the variability in estimates to sample spacing investigated. A range of statistical parameters can also be calculated for the subsets.

A systematic study of sampling was carried out on the core from the Statfjord well. The results of this study are discussed for one of the studied intervals (interval Core 5 in Fig. 3.5). As it is the sampling strategy independent of the geology we are concerned with here, we can for the time being ignore the geological setting of the selected interval.

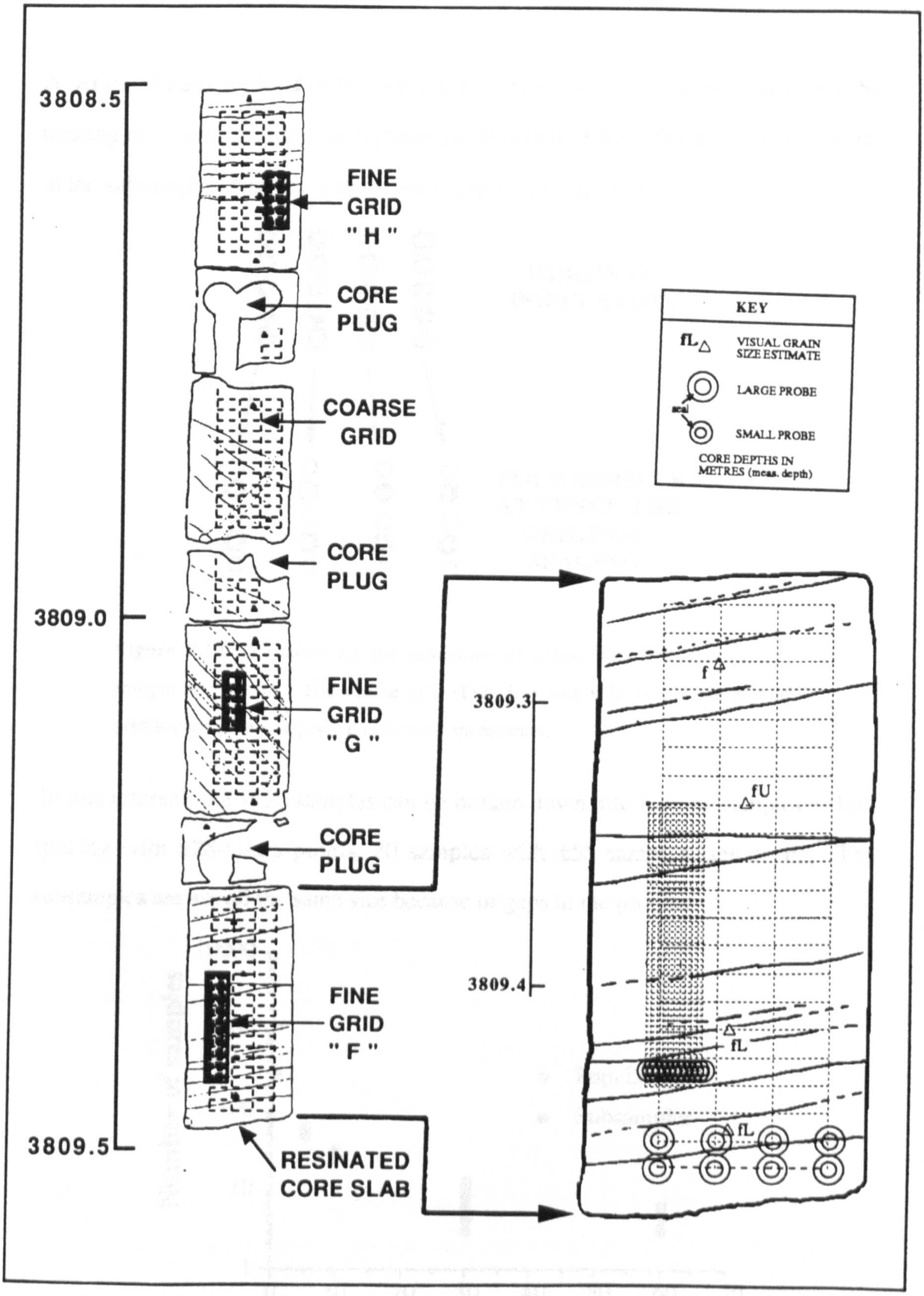

Figure 3.9: Coarse and fine grid sampling scheme for the Statfjord core study. Details of a metre interval of core 4 shown (refer Fig. 3.5).

A series of subsamples can be generated from the original sample population by treating the coarse grid as four separate profiles (Fig. 3.10). The number of samples in the subsamples declines with increasing spacing (Fig. 3.11).

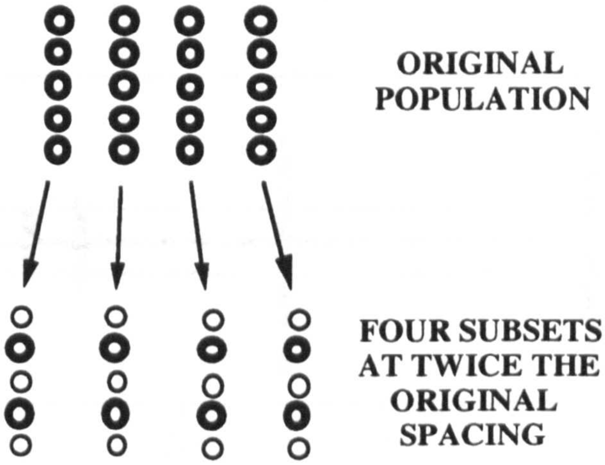

Figure 3.10: Procedure for the generation of subsamples from the original sample population. The coarse grid (Fig. 3.9) was split into a number of profiles and points skipped at increasing increments.

In this interval, the 1120 samples can be broken down into four subsamples at 1cm spacing with ±280 data points, 20 samples with ±56 samples, and so on. The subsamples are not all the same size because of gaps in the profiles.

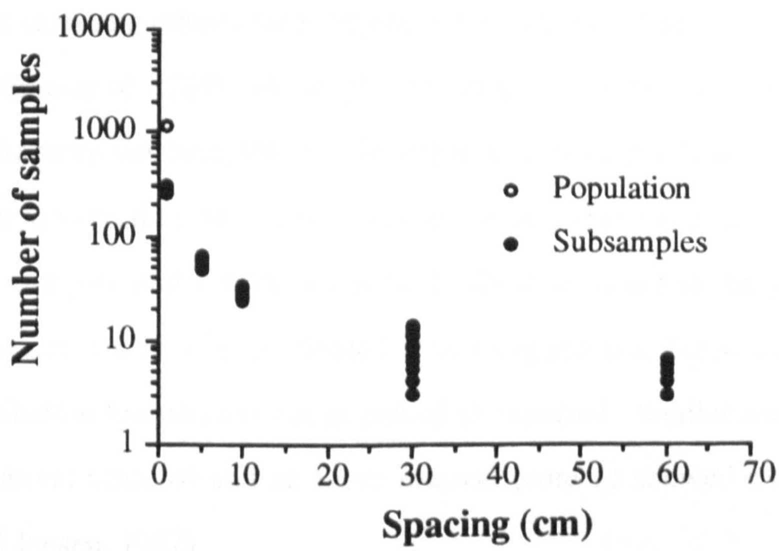

Figure 3.11: Number of samples for each subsample generated by the procedure illustrated in Fig. 3.10.

The arithmetic average was determined for each of the subsamples. The variability increases as the sample spacing increases and the number of data points in each subsample declines (Fig. 3.12).

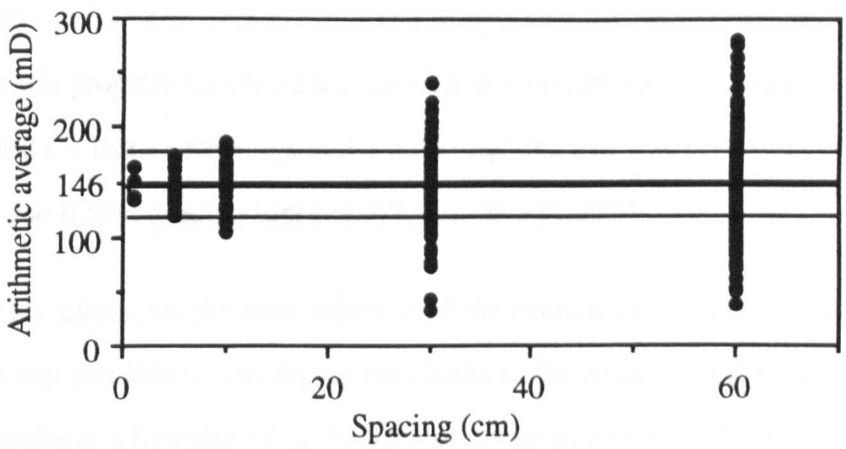

Figure 3.12: Arithmetic average for each subsample generated by the procedure illustrated in Fig. 3.10. The average permeability of the complete data set (the population in this case) is 146mD. Lines ±20% of the arithmetic average are shown.

Fig. 3.12 suggests that a ±5cm sample interval would be appropriate for this interval if the average ±20% is desired. The Cv of the investigated interval is 0.86. Using the optimum sampling criteria (see Appendix I) of Hurst and Halvorsen (1991) for the same tolerance of ±20%, 74 samples are required for this level of variability ($[10Cv]^2$). Seventy-four samples over 4m suggests a spacing of 5.4cm which agrees well with the observed result. This study shows that Hurst and Rosvoll's criteria can be used as a powerful sample design tool. The data from this study interval are approximately root-normally distributed which suggest that Hurst and Rosvoll's normal distribution limitation is not as critical as expected. Similar analysis for the Rannoch interval (core 4) and an Etive interval (core 3) showed similar results (Corbett and Jensen, 1992).

From the above, the additional information gained from the four profiles at the coarse spacing was very minor. This is despite the fact that each of the profiles sample different geological elements because the grid is not aligned to the geology (Fig. 3.9). Three of the four profiles provide redundant data. Following this analysis of the pilot study, the coarse grid was reduced to a single vertical profile for the Thistle study. The Thistle programme called for samples at a maximum 2cm spacing, based on the estimated Cv from core plugs and a 20% required tolerance. In the event, data was acquired at 0.5cm spacing (approx. 6200 measurements).

With grids taken over the same intervals of the resinated core with two different probe sizes, it was possible to investigate the effects of the resin. The depth of investigation of the probe is a function of probe aperture diameter (Appendix III). Different size probes should therefore have different depths of investigation. A comparison of the arithmetic averages for large (LP1) and small (SP1) probe measurements over comparable areas shows no systematic differences (Fig. 3.13). These data show that neither probe measurement is affected by the resin. In the fine grained Rannoch, the imbibition of resin is relatively shallow. The thickness of unresinated core available generally exceeds two aperture diameters. For this study, the resination is not going to present a problem.

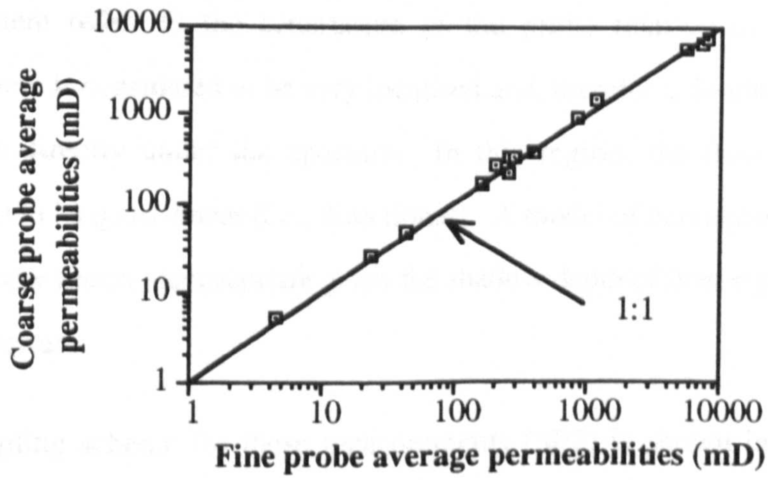

Figure 3.13: Comparison of large and small probe measurements over selected core intervals.

permeameter that were not possible on resinated slabs. In particular, it was possible to investigate the affects of core cleaning, surface damage and probe orientation.

These criteria on which blocks were selected included:

- representativity of typical Rannoch facies
- correspondance with intervals of slabbed core
- previously sampled by horizontal and vertical core plugs

Three blocks were finally selected (core depths given refer to Fig. 3.6):

A1-2	WB facies	10055.5-.8ft
B1-2	SCS facies	10112.6-3.3ft
B1-3	HCS facies	10125.0-.3ft

A series of measurements were completed on prepared and unprepared surfaces by Christian Halvorsen. On typical core slab surfaces normal to the bedding surfaces "horizontal" probe (k_h) measurements were taken. On surfaces cut parallel to bedding "vertical" probe (k_v) measurements were taken. The orientation of the measurement refers to the orientation of the probe relative to bedding. The measurement is considered to be very localised and, therefore, dominated by the first few pores directly under the aperture. In this region, the flow of nitrogen is considered to be quasi-linear (*i.e.*, directional). A model of hemispherical flow from a point source seems inappropriate given the shallow depth of investigation relative to a broad aperture.

The sampling scheme for these measurements (SP2) is shown in Fig. 3.14 and includes (Appendix X):

- probe k_h grids orientated parallel and normal to bedding surfaces,

• probe k_v grids on surfaces sub-parallel to bedding,

• measurements at 45^o to the bedding surfaces.

These measurements were taken to study the effects of grain fabric anisotropy at the measurement volume for the probe permeameter. Some of these grids were repeated before and after cleaning and before and after cutting to investigate the effects of surface damage and residual fluids. The location of grids was such that averaging and scale-up of probe measurements could be investigated at the core plug scale, using the available core plug data on each block.

3.6 Discussion of Sample Volume and Spacing

The limitations of core plugs for heterogeneous laminated resevoirs have been described. A third of the Rannoch Formation core plugs showed significant internal heterogeneity. The small volume of the probe (1/15 - 1/60th of a one-inch core plug for LP1 and SP1, respectively) is expected to be more uniform.

A variety of probe permeameter sampling schemes has been demonstrated on plugs, unresinated and resinated core. Whilst it is possible with automated probe devices to collect exhaustive data for each sample, the additional information gained by such an approach can be rather limited. In this study, the following were found to be adequate:

1. Core plugs. Four measurements on each end.

2. Blocks. Grids orientated parallel and normal to the bedding.

3. Resinated slab. A single 2cm spaced profile.

The analysis of these data is fully explored in the following chapter.

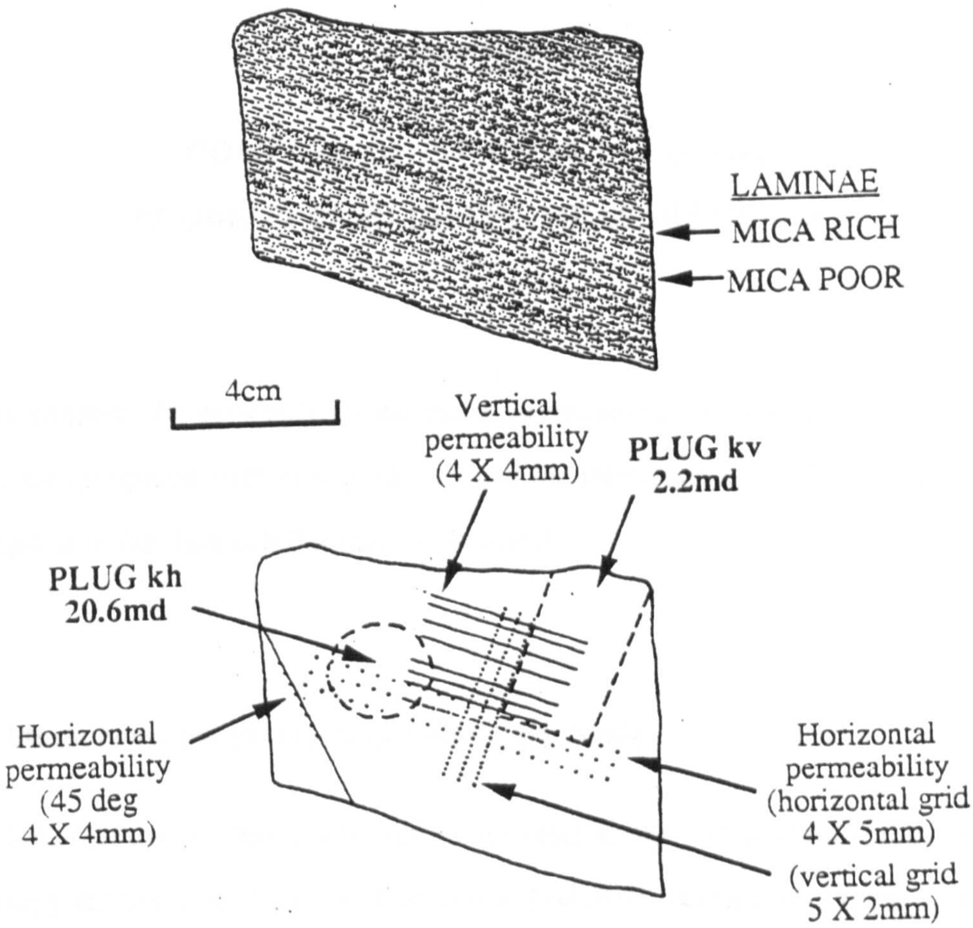

Figure 3.14: Typical probe permeameter sample programme for an unresinated block (B1-3) of the Rannoch in the Thistle Field. Grids are orientated with respect to bedding. After measurements were made on the slab surface (for k_h horizontal and vertical grids), the block was cut along one inclined (45^o) surface and eight bed-parallel surfaces. Measurements were taken on these surfaces.

CHAPTER 4

COMPARISON OF CORE PLUG AND PROBE PERMEABILITY MEASUREMENTS

In this chapter, the results from the probe permeameter measurements at various scales are compared with core plug data and the implications for the petrophysical description of the Rannoch Formation discussed.

4.1 Measurements at the Sub-Core Plug Scale

A major objective of this study was to investigate the small scale (probe-scale) anisotropy measured by the ratio of vertical to horizontal permeability (k_v/k_h). Three samples were used; two from the low contrast facies (B1) with clearly defined sub-cm laminae, and one from the wavy bedded facies (A1) with thicker laminae/beds (up to 2cm).

The resulting permeability profiles for the three sampled blocks are shown in Figures 4.1 (blocks B1.3, B1.2) and 4.2 (A1.2). At each level, the average permeabilities and ±1 standard deviation error bars are shown. The averages are determined from 3, 20, 4 and 24 data points for vertical k_h, horizontal k_h, inclined and k_v grids, respectively.

The three samples are clearly laminated and the pattern of permeability variation reflects the sedimentary lamination. There is a good correlation between geology and petrophysics. High permeability layers consistently correspond with low mica intervals.

Comparing the measurements on the inclined 45^o surface (Fig. 4.1 top) with measurements on a surface normal to bedding, we see that similar permeabilities are measured, particularly in the more uniform mica-bearing interval -5.0 to -5.6cm. This suggests that the impact of mica platelets oblique to the probe orientation is not significant for the size of probe used. This probe is not able to show grain fabric anisotropy, the mica platelets being dispersed and significantly smaller than the area of the aperture. This is in keeping with the size of the mica platelets seen in the thin section analysis (Fig. 2.4). Differences at -4.0, -4.7 and -6.0cm occur where the horizontal measurement cannot resolve the low permeability laminae.

The averages of probe k_h measurements are identical for the vertical and horizontal grids (open circles and black circles) for each of the investigated blocks. Indeed, given the low variability of the three adjacent measurements along a lamina on the vertical k_h grid, a single measurement within a lamina is considered sufficient to characterise its permeability. Laminae are defined as being texturally homogeneous. It appears that they are also homogeneous in terms of permeability, at least over a limited (5cm) length. Note that the additional variability in the interval 0 to -2.5cm in Fig. 4.1 (bottom) is attributable to orientation of the grid at an angle to the lamination above a laminaset bounding surface.

In all three blocks the probe-scale anisotropy has been measured at a number of locations. Over a wide range of permeabilities (5-1200mD), the probe k_v/k_h approaches unity. Exceptions (*e.g.*, B1-3 at -2.5, -2.9 and -4.1cm; B1-2 at -3.8 and -5.4cm) can be attributed to shoulder bed effects (*i.e.*, where permeability changes rapidly, k_h measurements will not resolve thin layers). A cubic Hassler Cell, with face dimensions of 1 x 1cm, was cut from the wavy-bedded sandstone (block A1-2 at 6.5cm) and also found to be isotropic (Halvorsen, pers. com.). It was, however, not possible to find homogeneous micaceous intervals of sufficient volume to test the apparent probe isotropy.

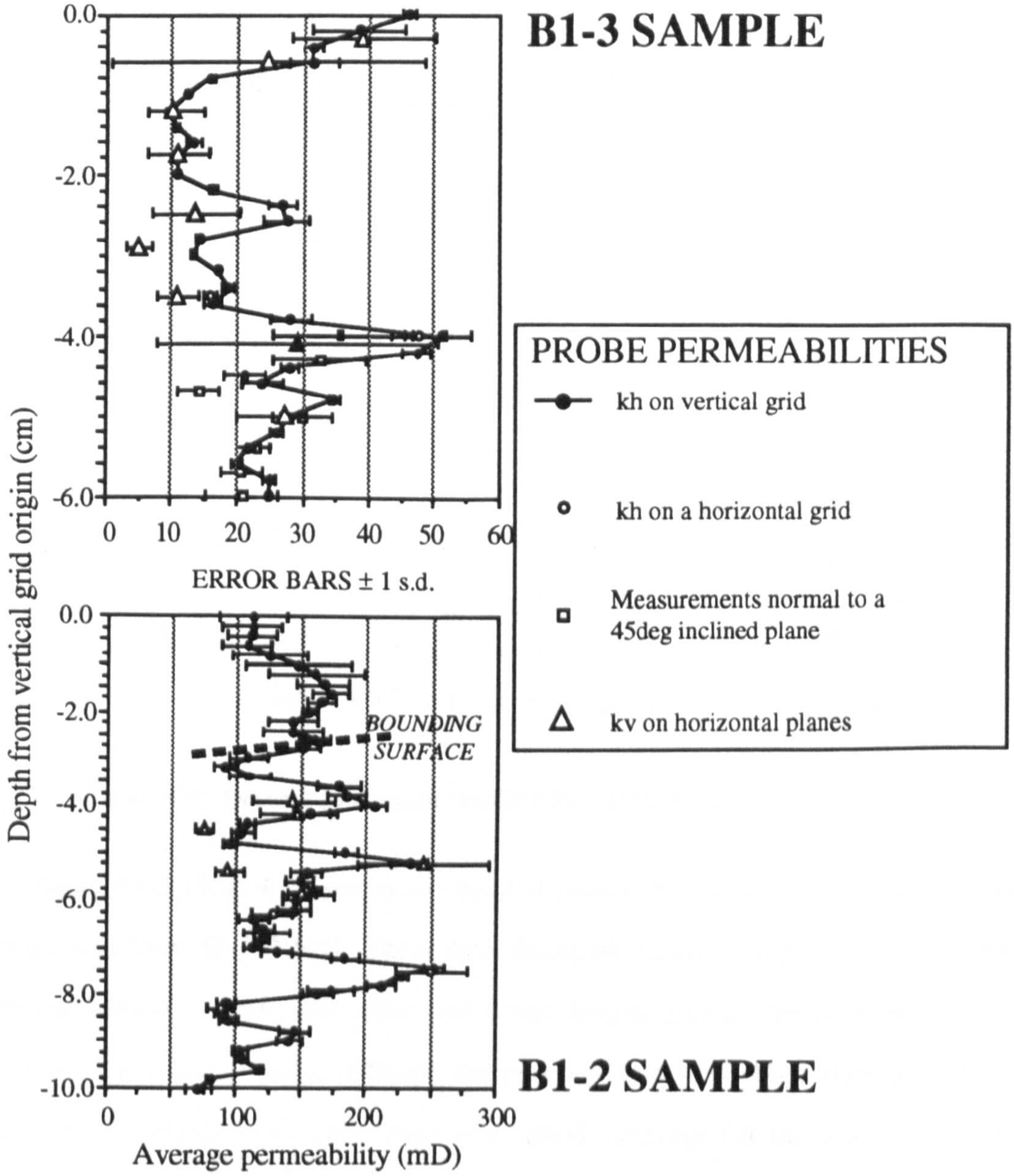

Figure 4.1: Detailed permeability profiles for samples B1-3 (above) and B1-2 (below). Higher variability in measurements above bounding surface because the grid is orientated parallel to bedding below this surface.

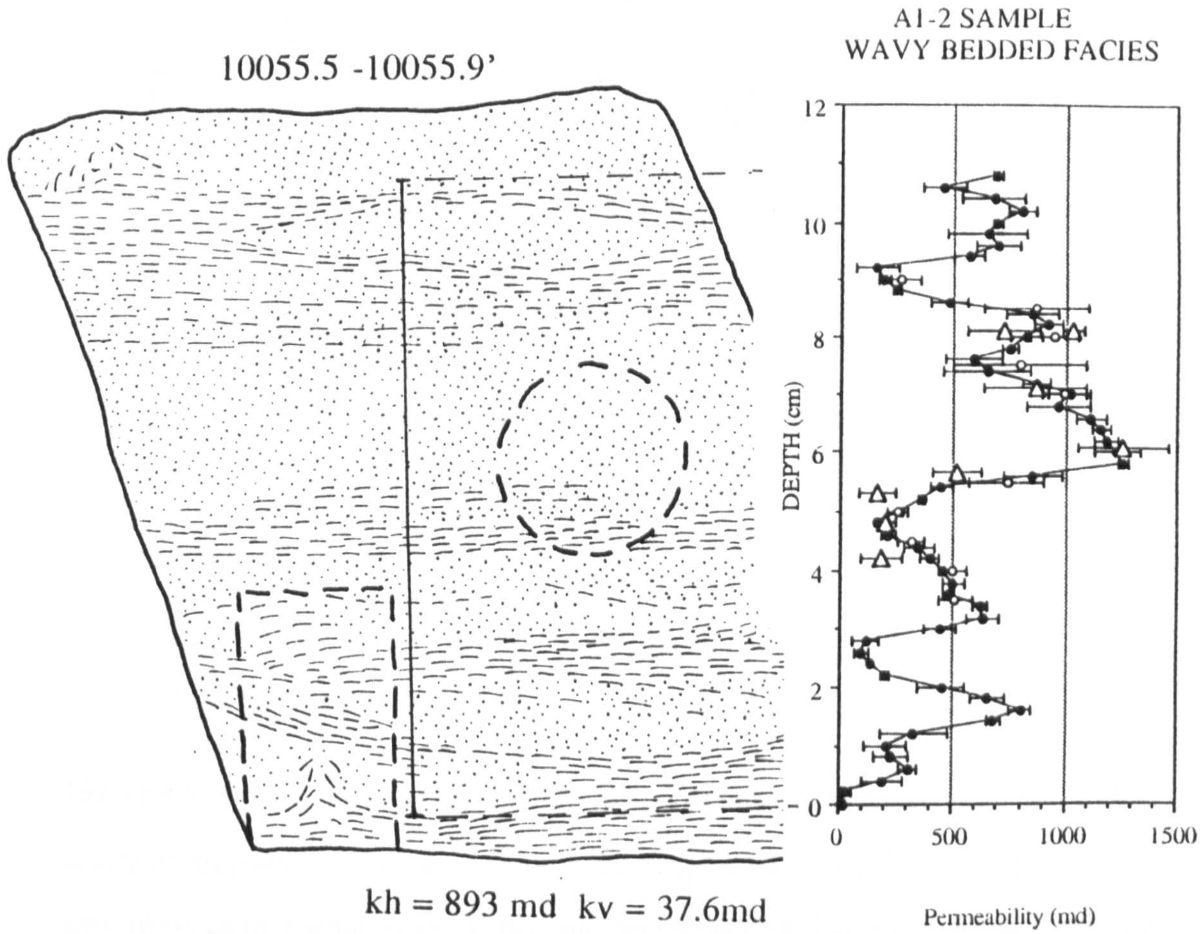

Figure 4.2: Detailed permeability profiles for sample A1-2.

In sample A1-2 (Fig. 4.2), the wavy-bedded facies, permeabilities in the (10+cm) profile vary from 50-1250mD. These data, therefore, reflect a degree of permeability heterogeneity (Cv = 0.6) over short centimetre length scales. The core plugs fail to represent the heterogeneity, although the plug k_v/k_h ratio (0.04) certainly indicates anisotropy. Whether this anisotropy is a "good" average for the block is another matter. Certainly, the different locations for k_h and k_v plugs has helped capture the anisotropy due to the lamination, but the plug volume is wholly inadequate to capture the average anisotropy of this cored interval. If the vertical plug had been cut in the same lamina as the horizontal plug, the k_v/k_h ratio would have been closer to unity.

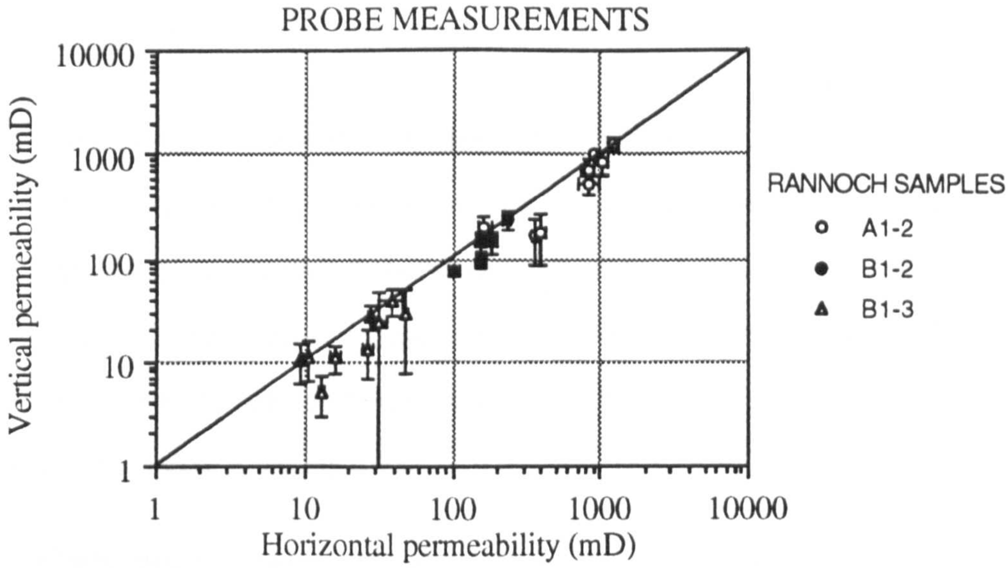

Figure 4.3: Probe scale k_v:k_h relationship for the Rannoch Formation. (Error bars ±1s.d.).

The probe-scale k_v/k_h ratio for the Rannoch is summarised in Fig. 4.3. Over three orders of magnitude the data lie close to the diagonal ($k_v = k_h$) line. The probe scale anisotropy as measured by the k_v/k_h ratio lies between 0.5 and 1.0. From these data we conclude that lamina permeabilities tend to be isotropic and that the anisotropy in sediments commonly seen in core plugs results largely from lamination rather than grain fabric. The micaceous Rannoch has a strong fabric anisotropy so this result is surprising. The probe volume is generally above the microscopic/macroscopic (Haldorsen, 1986) threshold for these laminae and therefore gives a representative measurement of the properties of the stratal element.

From these detailed probe data from three blocks, representing two subfacies (A1 and B1) and a wide range of permeabilities (2-1250mD), we observe that:

•No extra information is provided by extended profiles along laminae ("horizontal" grids) over the limited vertical grid. In these laminated sediments, a single profile provides a good estimate of lamina permeability. The variability observed along laminae over the 5cm width of these core samples is very limited: $0.07 < Cv < 0.15$ in B1.3 and $0.1 < Cv < 0.37$ in A1.2.

•Measurements inclined at 45 degrees to the bedding and, therefore, to the ubiquitous mica platelets in this formation, are comparable with measurements normal to bedding. The mica platelets (up to 0.3mm) are small relative to the probe injection area (3.8mm diameter). The probe does not, therefore, resolve fabric anisotropy which may exist from the mica at certain scales of measurement.

•Probe measurements normal to the bedding planes ("k_v") are generally comparable to horizontal ("k_h") measurements suggesting the formation is isotropic at the probe scale (even with the grain fabric of mica-rich sediments). Notable exceptions indicate planes that cut adjacent laminae at a very low angle (<10 degrees), exposing very thin (<2mm), low permeability laminae not resolved with "horizontal" probe measurements. These data highlight a limitation of the probe. Probe measurements on a slabbed core surface (or outcrop face) will not "see" the thin low permeability laminae that may control the vertical permeability. Such sample programmes are thus insufficient for defining all the permeability variation within laminated sediments.

4.2 Bounding Surface Permeability Measurement

Laminaset bounding surfaces are very prominent in Rannoch Formation core material. The surfaces mark the discordant boundary between concordant packages of laminae (for further discussion refer to Appendix VII). As these features are widespread within the Rannoch Formation, a detailed study was carried out to determine their petrophysical properties. Sample B1.2 included a bounding surface (Fig. 4.1 bottom) showing an apparent truncation angle of 27 degrees. A plane BB2 was cut at a low angle to this bounding surface (Fig. 4.4 top). The grid of probe measurements acquired on this plane was aligned to the strike of laminae beneath the bounding

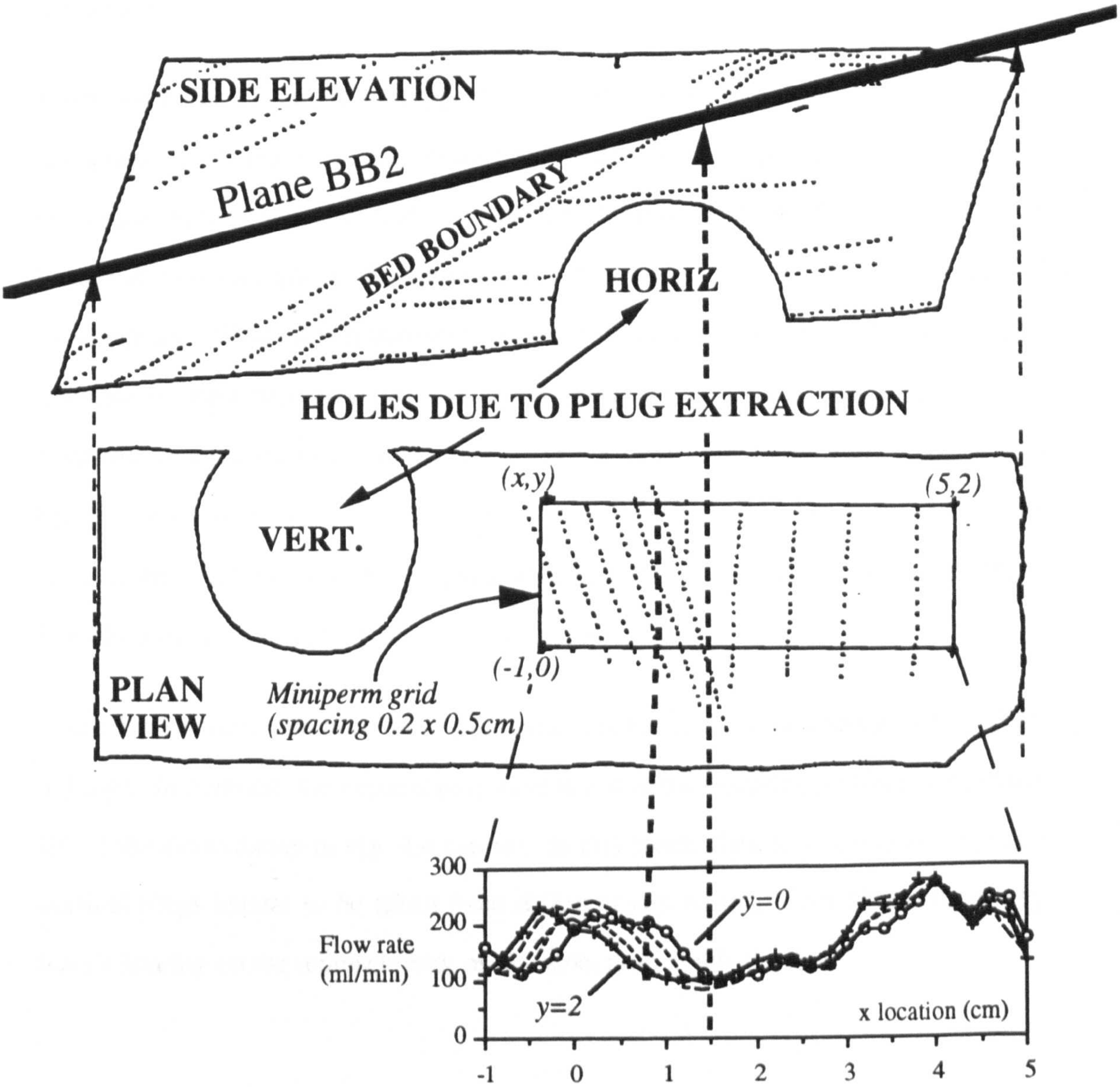

Minipermeameter profiles on plane cut obliquely to bounding surface

Figure 4.4: Detailed permeability mapping of a bounding surface, sample B1-2. The upper sketch shows the sampled block from the side with the top of the core to the top. The centre sketch shows the lower surface exposed along the sectioned plane BB2 in the upper sketch. The lower graph shows the 5 probe permeameter profiles at 0.5cm spacing from the grid outlined on the surface in the centre sketch.

surface (Fig. 4.4 centre). From the resulting profiles the offset of the transition to a higher permeability lamina immediately above the bounding surface is apparent (Fig. 4.4 bottom).

From these data, there is no suggestion of any significant permeability reduction associated with the laminaset boundary. The observed permeability profile is consistant with erosion followed by rapid deposition without time for fines to settle or bioturbation to take place. This is as expected from the storm origin interpretation of these events. While it is possible to cut plugs through the laminaset boundaries and investigate their permeability, this is not generally done in a systematic way in reservoir characterisation. Whilst the Rannoch laminaset boundaries appear not to have flow significance, this will not necessarily be true in other formations/environments. As a significant element in reservoir sediments, laminaset bounding surfaces deserve systematic investigation.

In the B1.2 sample the horizontal plug hole lies beneath the bounding surface (Fig. 4.4 top). In contrast, the vertical plug hole is above the bounding surface (*i.e.*, to the left of the discordancy in Fig. 4.4 centre). In this block, therefore, the horizontal and vertical plugs appear to be taken from different laminasets. This observation may have a bearing on the representivity of the k_v/k_h ratio at this depth.

4.3 Plug-scale Permeability Measurements

The probe permeameter sample volume represents approximately 1/60th (SP2) of the one-inch core plug volume. It is reasonable to expect the core plug permeability could be estimated as an average of many smaller measurements over the same total volume. The scale-up from probe to core plug measurement was investigated using the block sample data described above.

The blocks selected had previously been plugged in the horizontal and vertical directions. We make comparisons between the arithmetic and harmonic averages (refer to Appendix I) of the probe data with plug k_h and k_v measurements (Table 4.1). In each case, the probe intervals have been depth matched as carefully as possible with plug intervals. We note that because the plugs are trimmed after being cut, it is very difficult to ascertain the exact interval represented by the plug measurement. This uncertainty is more critical to the vertical plug intervals.

The arithmetic average is appropriate to flow along layers (*i.e.*, comparable with a horizontal plug measurement) and the harmonic to flow across layers (vertical plug). If all the layers present in the core plug have been sampled with the probe, and the layers are relatively uniform the respective averages will estimate horizontal and vertical permeability.

	HORIZ. PERM.			VERT. PERM.		
	B1-3	B1-2	A1.1	B1-3	B1-2	A1.1
PROBE HORIZ.	23.8	140.6	550	19.4	129.8	200
PROBE VERT.	18.0	142.3	577	10.7	120.5	268
CORE PLUG	20.6	150	893	2.2	59	37.6

Table 4.1: Comparison of core and probe estimates of horizontal and vertical permeability. (N.B., Probe horizontal = arithmetic average; probe vertical = harmonic average)

These data, bearing in mind the concerns over depth matching, suggest:

- that the arithmetic average of closely spaced probe data provides a reasonable estimate (±6-15% for B1-2 and B1-3; within 35-40% in A1-1) of horizontal plug permeability in these laminated facies, and,

- that the harmonic average of closely spaced probe measurements consistently overestimates the vertical permeability by 2-5 times. In these laminated facies, it is not possible to resolve thin low permeability layers with probe spacings of 2mm. The preparation of more bed-parallel planes may have improved the resolution, but there are practical limitations to this approach.

In making these comparisons, we should also bear in mind the tendency for the probe to read lower permeabilities on uncleaned material (particularly for plugs above 100mD). These differences are further discussed in the following section.

The fundamental differences in both flow geometry and scale of plug and probe measurements have been described previously. These differences suggest that only in the most homogeneous of media can the plug and probe measurements be expected to be identical. Nevertheless, carrying out a systematic comparison of the two measurements is a recommended procedure in any study for several reasons:

- to highlight potential problems with either measurement,
- to understand the effects of sample treatment and preservation,
- to understand the effects of sub-core plug scale heterogeneity.

In this current study, probe permeameter measurements were taken on the ends of a series of core plugs from the Rannoch Formation. Using calibration factors empirically determined on homogeneous (non-Rannoch) core plugs, the probe measurements were compared with plug permeabilities (Fig. 4.5). The variablity in permeability seen in the core plugs, as measured by Cv, could be related to the degree of lamination. The more strongly laminated, heterogeneous plugs had Cv > 0.75 and could then be excluded from the comparisons. A good comparison for probe and plug measurements, with probe permeabilities tending to be slightly higher at high permeabilities, was observed.

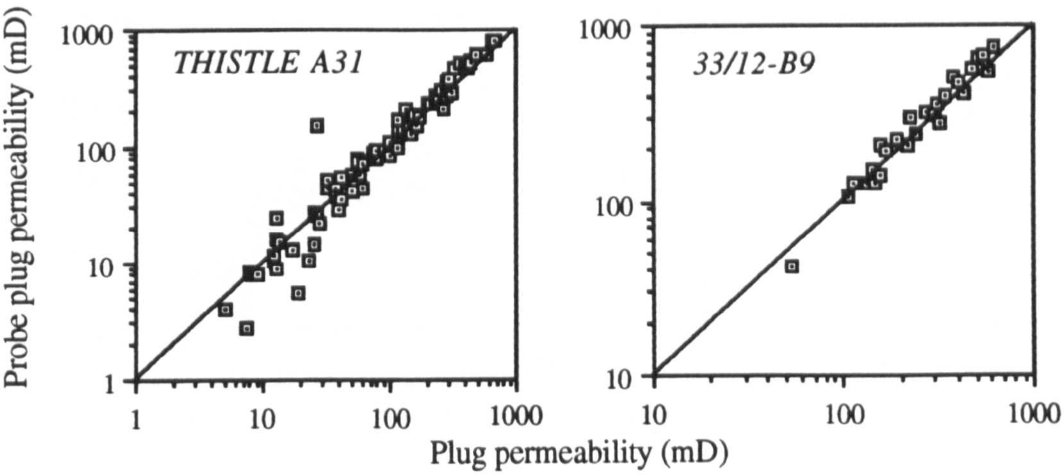

Figure 4.5: Comparison of probe and Hassler cell permeabilities on cleaned homogeneous plugs.

The minor differences between cleaned probe and cleaned plug measurements (Fig. 4.5) may be due to heterogeneity in the Rannoch plugs that wasn't present in the calibration plugs. An alternative calibration, using these Rannoch core plugs, could correct for these minor effects.

There were significant differences, however, for both the Statfjord and Thistle wells when probe permeabilities measured on core slab surfaces in the immediate region of the plugs were compared with the plug permeabilities (Fig. 4.6). The probe permeabilities can be seen to be both consistently lower above 100mD (core plug) and higher below 2mD. This conflicts with the probe measurements directly on the cleaned Rannoch core plugs (Fig. 4.5).

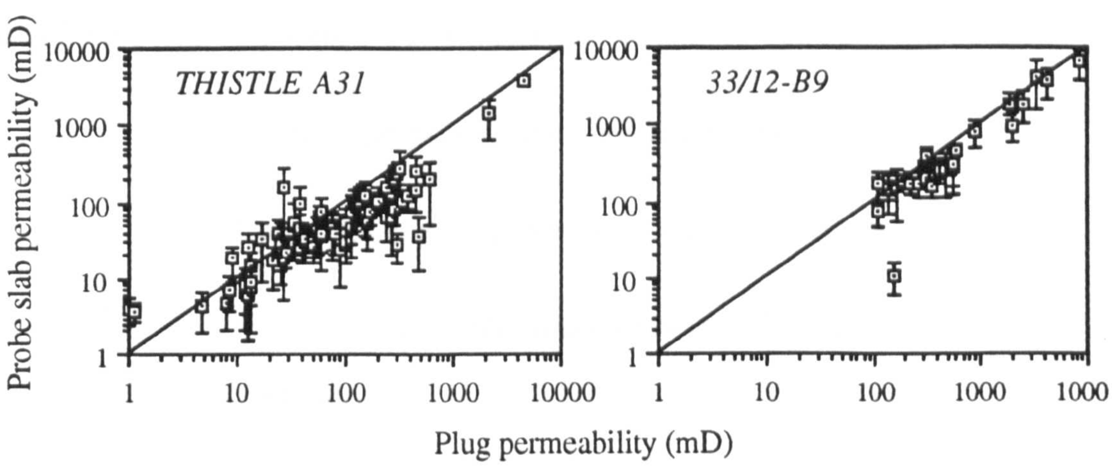

Figure 4.6: Comparison of arithmetically averaged probe permeabilities on uncleaned slabbed core with cleaned plug permeabilities. Note tendency for probe permeabilities to be less than plug above 100mD (plug) in both wells and greater than plug below 2mD in the Thistle well. Error bars ±1s.d.

The discrepency at lower permeabilities can be explained by the lower limit of the operating conditions for the selected probe tip. For the designed range of pressures and injection rates for the probe used (SP2), 2mD represents a practical lower limit. The differences at higher permeabilities are attributed to differences in the treatment of core plugs and core slabs (*i.e.*, the preparation, cleaning, or preservation). For reasons previously discussed (section 3.5.2), that the resin is not considered to be a significant factor. The effects of cleaning were systematically investigated and are described in the following section.

4.4 Treatment Effects Affecting Core Plug and Core Slab Measurements

Systematic differences were recognised (Fig. 4.6) between probe measurements on cleaned core plugs and uncleaned core slabs. To investigate the effects of different treatments, a series of probe measurements over the same grid (on block B1.2) were taken for the following sequence of treatments:

1. with no preparation (i.e., before cleaning),
2. after cleaning by immersion in methanol and toluene solvents,
3. after cutting a fresh surface a few mm parallel to the original surface,
4. after repeating step 3.

By comparing probe permeabilities, measured after each of the above steps, with those measured on the resinated core and the core plug k_h measurement (Fig. 4.7) it can be shown that:

- Block surfaces show less surface damage than the resinated core. (This possibly results from the practise geologists have of wetting the core surface during core description).
- Cleaning the (oil stained) blocks results in a marginal increase (± 10%) in permeability.
- Preparing a fresh surface increases the permeability.
- The variability, as measured by the coefficient of variation, appears relatively unaffected by the treatment for this sample.
- Cleaning the core and preparing fresh surfaces has resulted in probe permeabilities that are more comparable with those measured on the cleaned core plug. These data suggest that surface damage through ageing is primarily responsible for the permeability impairment observed on the core slab surfaces.

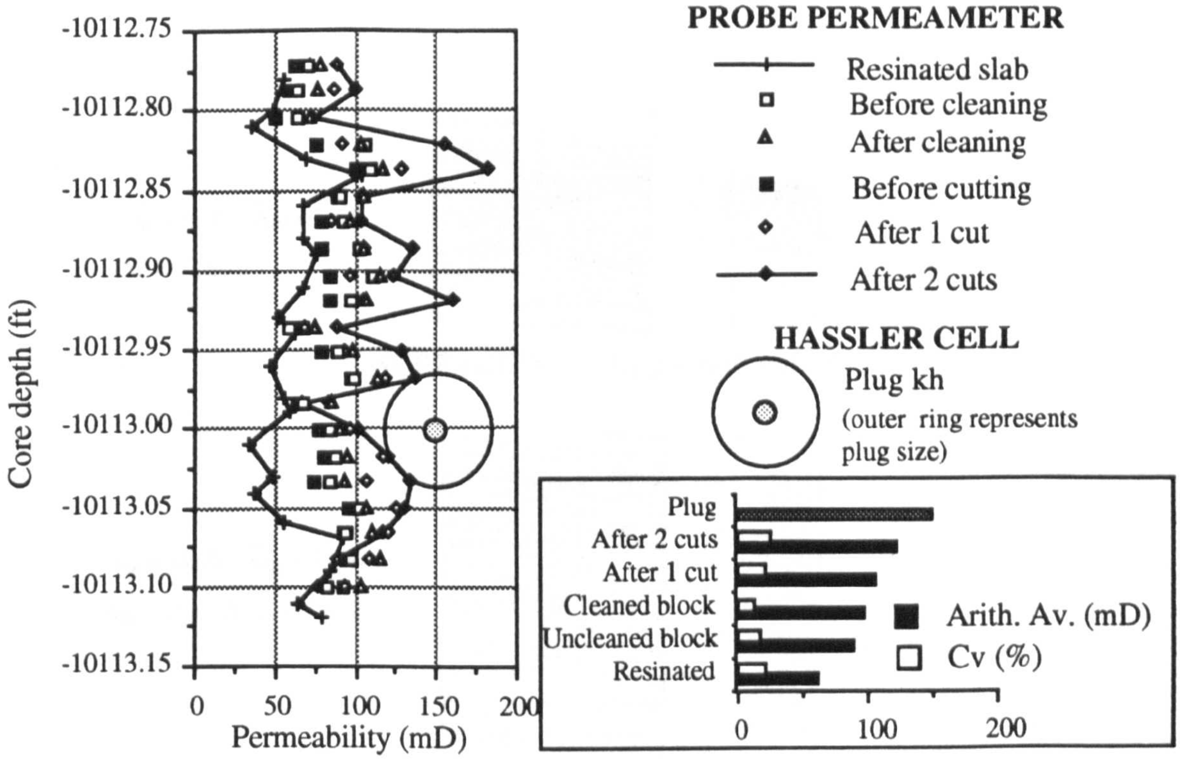

Figure 4.7: Comparison of probe measurements after various treatments. Location and scale of core plug shown for reference.

4.5. Lamina and Laminaset Scale Measurement of Permeability

Detailed grids at 2 x 2mm spacing were measured on representative Rannoch laminasets from the Statfjord well. Permeability variation in the three main laminaset types, low mica lamination, high mica lamination and ripple lamination, was mapped out using the probe permeameter (Fig. 4.8). The lamination types were distinguished by mica content and laminar structure. The permeability showed a close relationship to both.

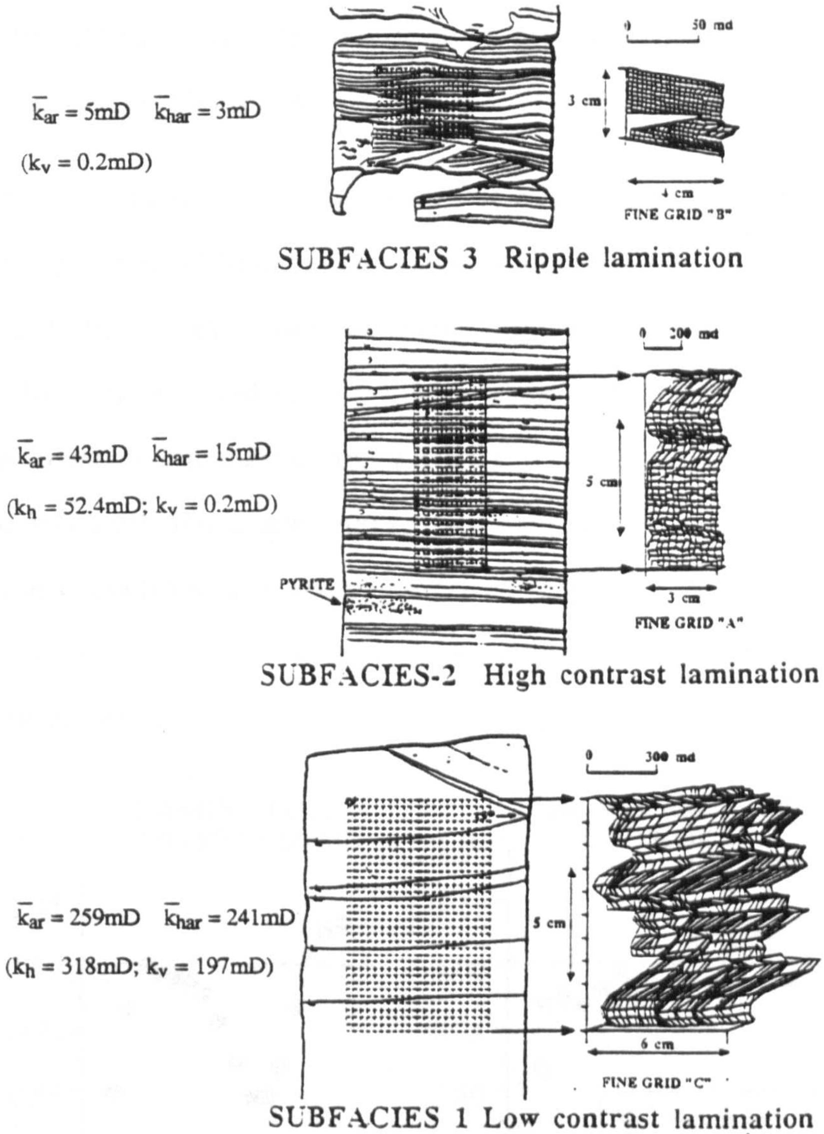

Figure 4.8: Probe permeability maps of the three main Rannoch laminaset types. Nearby plug k_v and k_h measurements are shown for comparison. High and low contrast lamination refer to the relative mica content of adjacent laminae and the resulting contrast in visual appearance.

The comparison between arithmetic probe averages and plug k_h permeabilities is reasonably good. Plug k_v values, however, tend to be over-estimated by the probe harmonic averages (as noted above), suggesting that all the low permeability micaceous laminae have not been measured. Nevertheless, the probe permeability maps show permeability structure effectively unseen by the core plugs.

A fourth facies type, the wavy-bedded facies was mapped in the Thistle well (block A1, Fig. 4.2). This facies is usually confined to the upper ±3m of the Rannoch Formation and is considered significant to the modelling of flow between the Rannoch and the overlying Etive.

The laminated nature of these sediments is reflected in the semivariogram (see Appendix I) generated from the 2mm spaced data (Fig 4.9). Along the lamination (*i.e.*, within the texturally uniform laminae) in the high mica laminaset (Fig. 4.8 centre), low variance and relatively long correlation lengths are seen. Across bedding, however, cm-scale correlation lengths and periodicity are characteristic. These short correlation lengths and regular statistical structures were unseen (and possibly unsuspected by the geostatisticians and engineers) prior to the development of the probe permeameter. They have been found to be characteristic of most, if not all, laminated sediments.

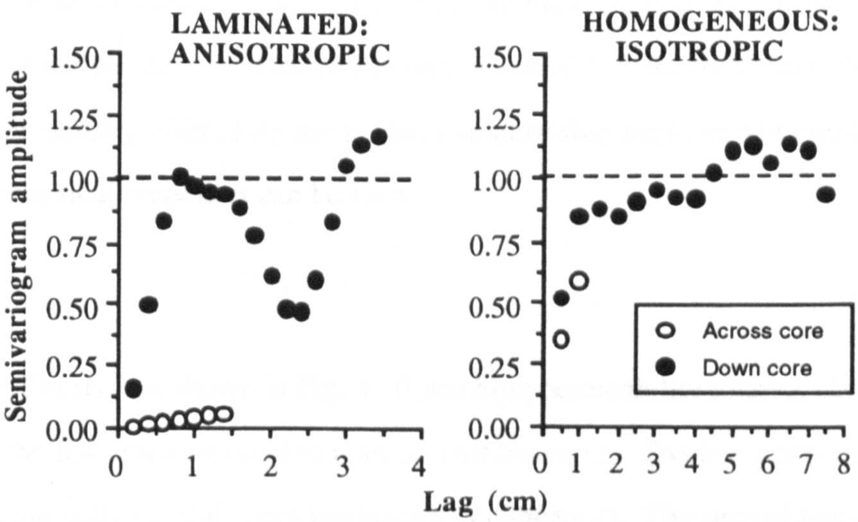

Figure 4.9: Comparison of a semivariogram in a high mica, anisotropic, Rannoch laminaset with one from a relatively homogeneous (Etive) sediment. The former shows the characteristic short correlation lengths and hole effects (periodic) structure associated with a laminated sediment. The high permeability correlated features responsible for the hole at 2.25cm can be seen in Fig. 4.8 (centre). The semivariogram function (γ - Appendix I) has been normalised by dividing by the variance to give a semivariogram amplitude.

One should note that the features responsible for the hole in the vertical (*i.e.*, down core) semivariogram on the left of Fig. 4.9 can be seen in Fig. 4.8 (centre). These are not the fine mm-scale laminae that are shown in the accompanying sketch (which are not resolved by the probe) but a larger scale periodicity that can be seen in the photograph of this interval (Fig. 2.3b). This periodicity, possibly related to bedform migration, is also seen in Rannoch material from Cormorant (Fig. 3a left in Scott, 1992). The semivariogram shows no indication of the finer scale lamination.

4.6. Laminaset and Bed Scale Variability

The core plug data can be used to provide some measure of variability at this scale. The one-foot core plugs, however, undersample the bed-scale variability and fail to reveal the well defined permeability structure that is typically associated with individual laminasets (Fig. 4.10). Bed thicknesses, typically a few feet, require a greater sample density than is traditionally available from core plugs. With the greater sample density offered by the probe, a relationship between sedimentary fabric and petrophysical properties can be seen.

In the 2m section shown in Fig. 4.10, the high permeability interval closely correlates with the low mica lamination interval (subfacies 1). The low permeability intervals correlate with the high mica lamination (subfacies 2). The rippled laminated material (subfacies 3) has the lowest permeabilities. The probe data, therefore, show a close relationship between permeability and lamination type suggesting that the permeability distribution in this interval of the Rannoch Formation is related to depositional structure.

Comparing the probe permeabilities with the 6 core plugs in this interval we note the broad similarity. The low permeability rippled interval (subfacies 3), however, was not sampled by the horizontal plugs, probably because of problems associated with cutting the plug. This omission could lead to poor estimates of the vertical permeability in this interval.

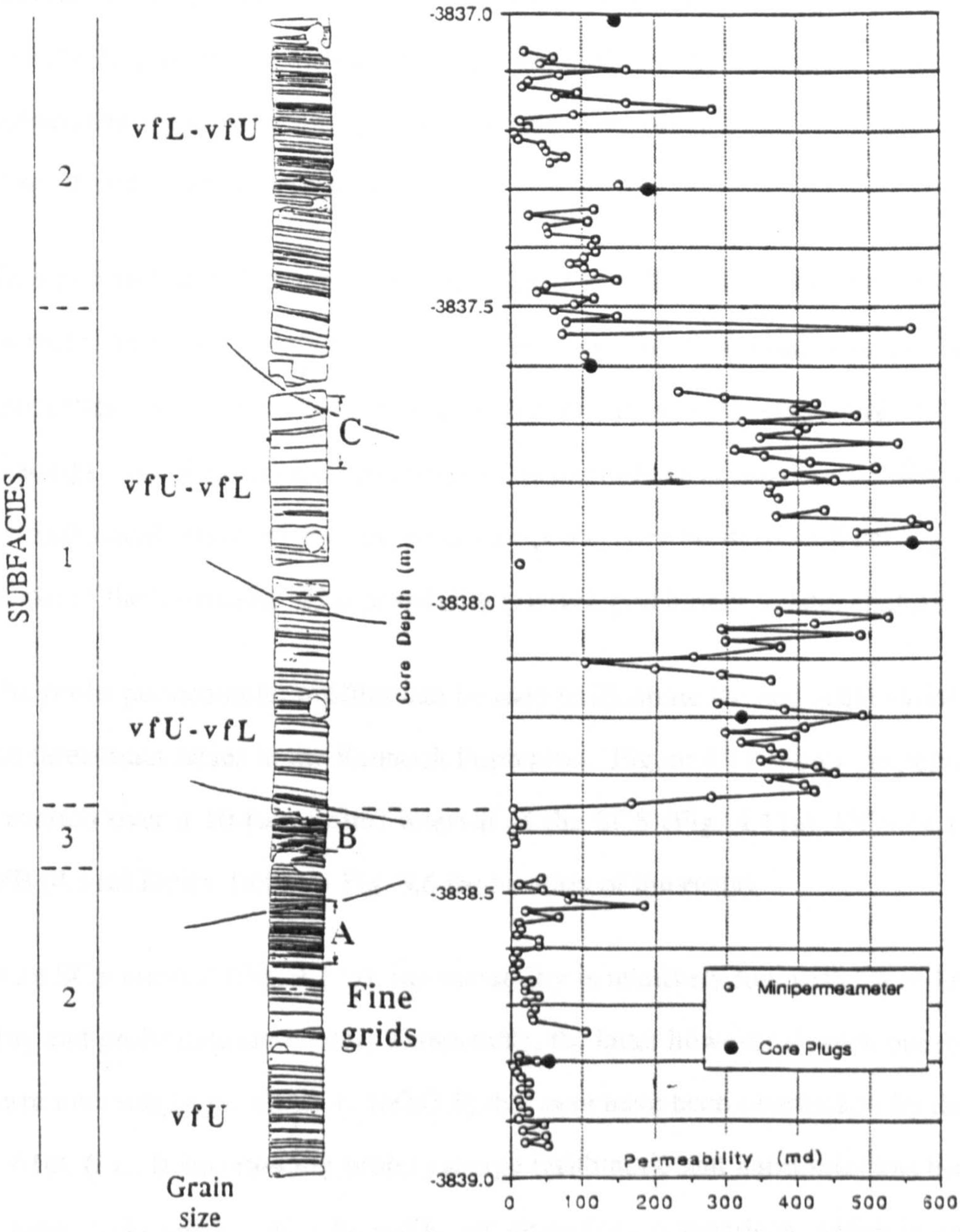

Figure 4.10: Pattern of probe permeabilities showing distribution within a single bed. Note the location of the three detailed laminaset grids (Fig. 4.8) within a one-metre interval. Refer to Fig. 3.5 for location of interval (core 5).

It is interesting to consider the variability of the subfacies intervals in Fig. 4.10. The low mica lamination (subfacies 1) has Cv = 0.31 and, despite the apparent variability in the profile, is relatively homogeneous. The upper and lower high mica lamination (subfacies 2) intervals have comparable Cv's of 0.83 and 0.99, respectively. This lamination is petrophysically heterogeneous (Corbett and Jensen, 1992b). The ripple lamination (subfacies 3) has Cv = 1.52 and is very heterogeneous. The probe data, therefore, supply information on the variability of petrophysical properties. In subsequent chapters, we will try to establish how important this variability is to the flow of hydrocarbons in this reservoir.

This example from the Rannoch Formation shows the scale of typical hierarchies of elements in clastic reservoirs. These elements and, their associated petrophysical properties, invariably occur at scales poorly sampled by core plugs at one-foot spacings. If a depositional control over the petrophysical data can be identified, the petrophysical model of the reservoir can potentially be derived from a geological model of the formation. This possibility is developed further in later chapters.

The probe permeameter profiles can be used to illustrate the bed-scale variability for the three main facies in the Rannoch Formation. Figure 4.11 shows the permeability variation over a 10-foot (±3m) interval of the SCS (Fig. 4.11a), HCS (4.11b) and WB (4.11c) facies (refer to Fig. 3.6 for location of intervals).

In an SCS interval (Fig. 4.11a), the variability is relatively low with Cv = 0.63. The plug and probe data are broadly comparable, the latter however do pick out some low perm intervals (*e.g.*, 10061.1, 10063.8) that may have been overlooked by the plugs. A 61pt. (*i.e.*, 0.3m) running probe average (arithmetic and harmonic) has been used to estimate k_h and k_v. Plug k_h and k_v are given for a comparison, which is very good at 10063, 10067 and 10068. These averages become uniform over zones (*e.g.*, 10061-68ft) where 0.3m-intervals provide representative

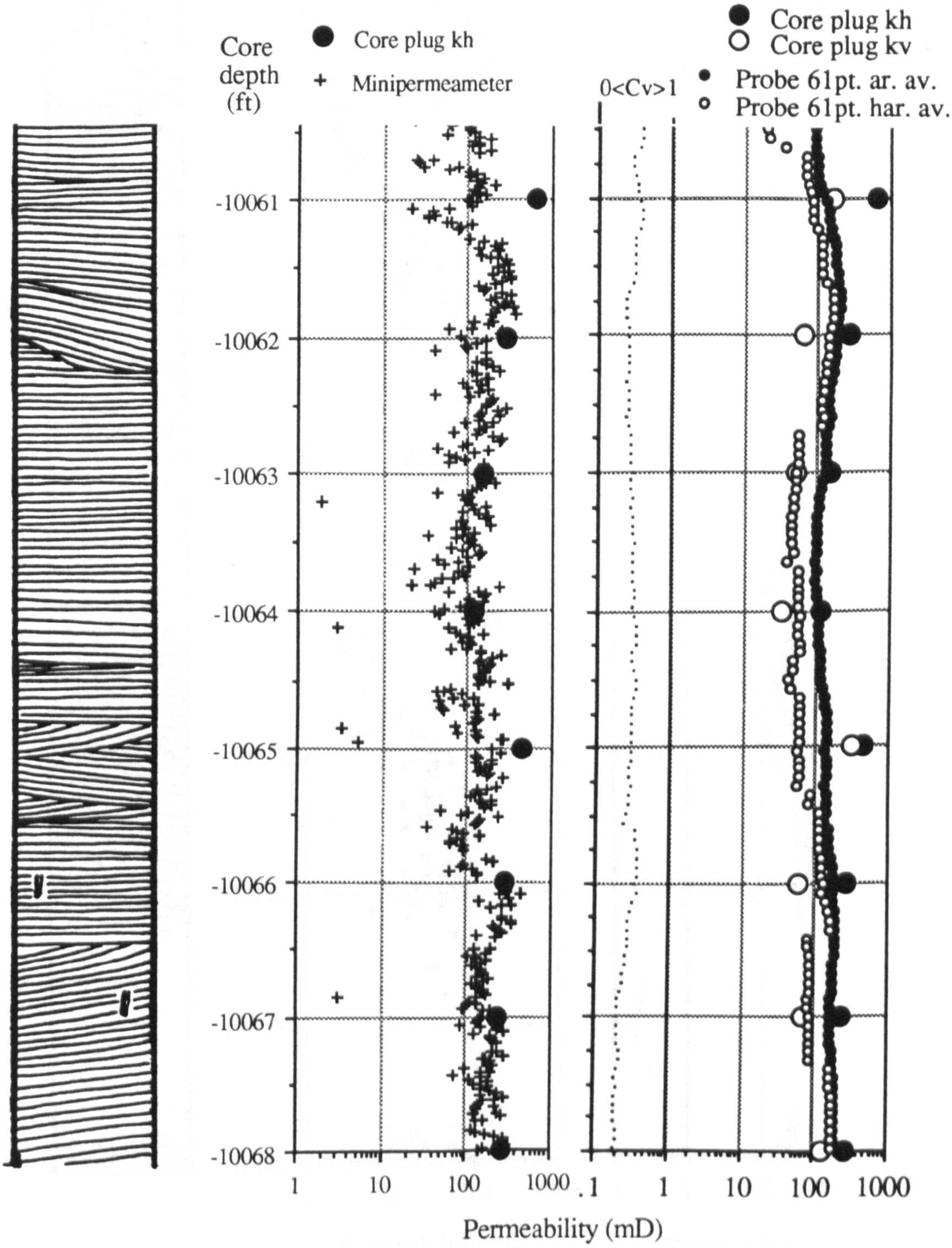

Figure 4.11a: Permeability variation within the SCS facies, Rannoch Formation, Thistle Field.

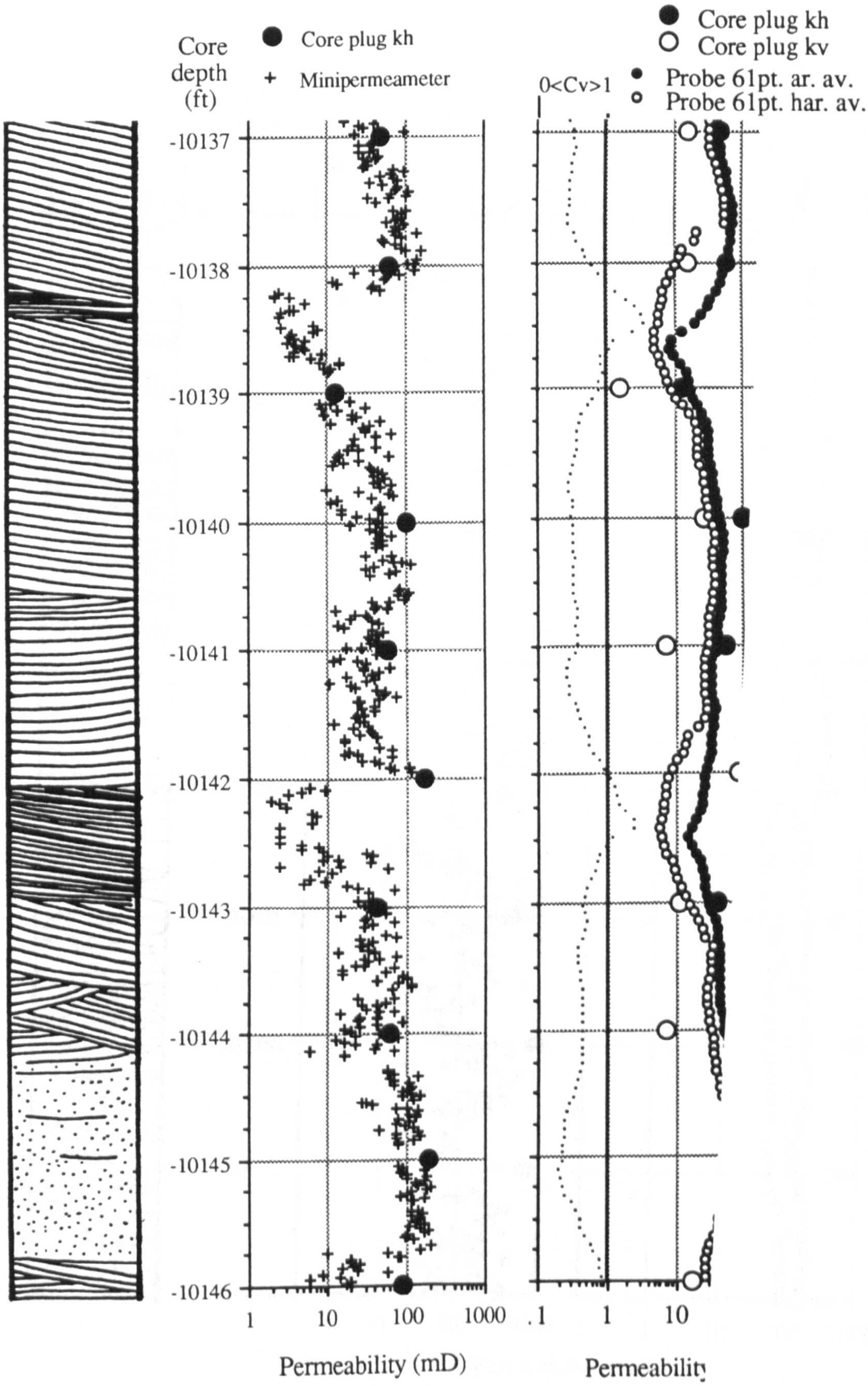

Figure 4.11b: Permeability variation within the HCS facies, Rannoch Formation, Thistle Field.

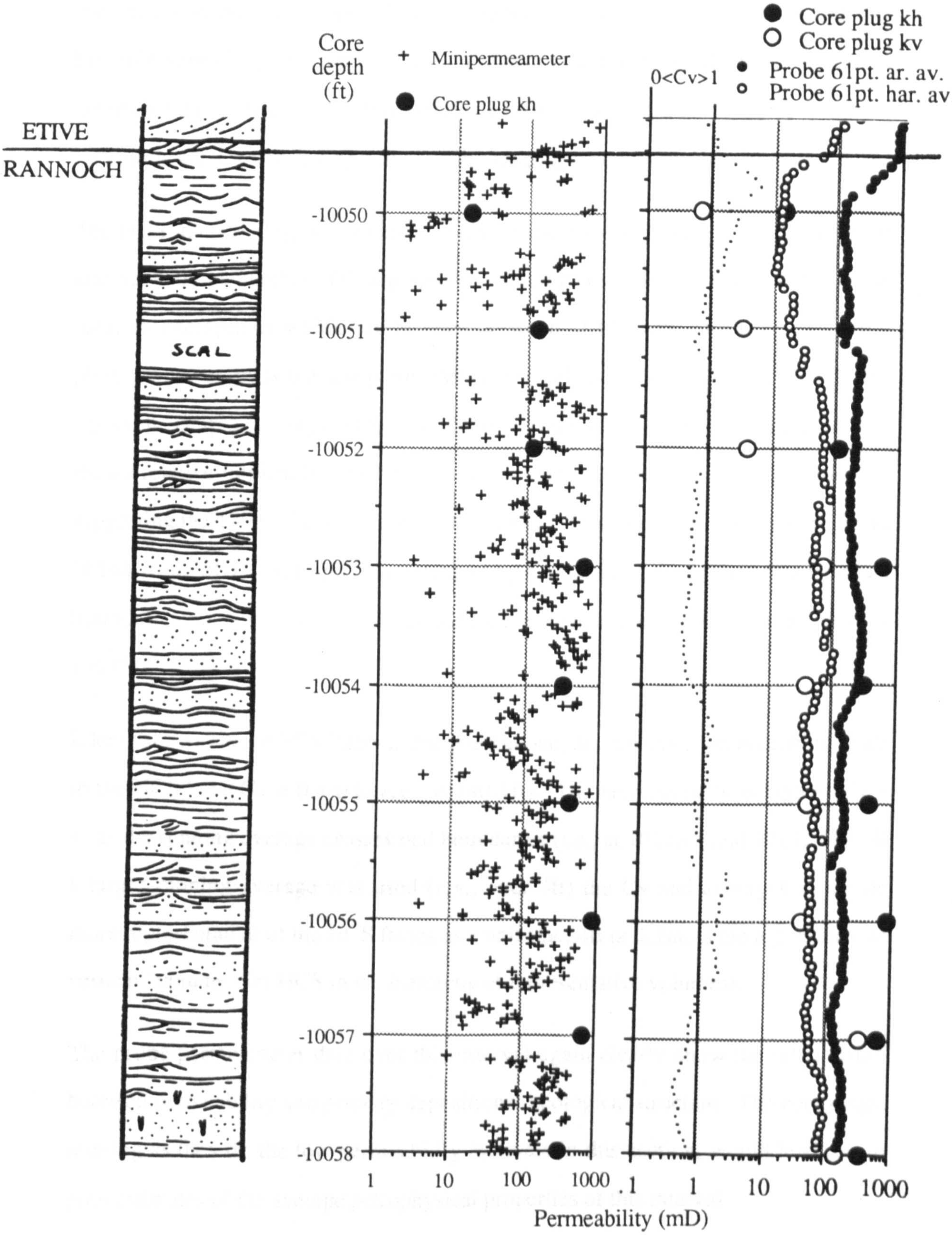

Figure 4.11c: Permeability variation within the WB facies, Rannoch Formation, Thistle Field.

volumes of these facies. The Cv in this latter interval varies between 0.4 and 0.6. For this variability, 36 samples (*i.e.*, a spacing of ±8cm) would be sufficient to determine the average permeability of this ±3m interval within ±20% (refer to section on sample sufficiency in Appendix I). The ten plugs are insufficient for this purpose.

The HCS interval (Fig. 4.11b) has a greater variability with a Cv = 0.93. The ±3m interval shows a number of fining-up (*i.e.*, reducing permeability) cycles in the probe data, an example of which can be seen between 10142 and 10138.2ft. The core plugs, however, miss the low permeability intervals at 10142.0-.8 and 10138.2-.8ft. Optimum sample spacing for this interval would be ±3cm. The 61pt. running average shows relative uniformity over the low mica lamination intervals (*e.g.*, 10140-1ft) suggesting the ±30cm intervals are representative. That the more massive sand (from 10144.25-5.75ft) is isotropic, is confirmed by similarity of the probe arithmetic and harmonic averages over the interval and by the vertical and horizontal core plugs at 10145ft.

Like those within the SCS interval discussed above, the low mica lamination intervals in the HCS have Cv = 0.4-0.6 (*e.g.*, 10140-1ft). The heterogeneity is higher (Cv > 1) as the running average crosses bed boundaries (*i.e.*, at 10138.5 and 10142.5ft). If a larger running average was used (*e.g.*, over 4ft) the Cv and averages would be more representative of the HCS facies as a unit (*i.e.*, 4ft or 1.2m, is the representative vertical "volume" for HCS in the hierarchy of representative volumes).

The probe permeameter data over this interval again clearly show the relationship between permeability and primary depositional geological structure. The core plugs, missing as they do the low permeability intervals in this section, would lead one to poor estimates of the average petrophysical properties of this interval.

It is in the WB interval (Fig. 4.11c), however, that the probe permeameter proves most useful. This interval is only ±3m thick and is almost completely represented by the 8.5ft interval shown in Fig. 4.11b. The variability of this interval (Cv = 0.99) is similar to that of the previous HCS interval. In this WB facies, however, the variability occurs at the lamination scale. The 61pt. running average shows relatively uniform properties, suggesting that ±30cm is a representative sample spacing for averages.

A Cv = 0.99 suggests 100 samples are sufficient (this equates to a ±3cm spacing). Ten core plugs are clearly insufficient. The horizontal plugs tend to be preferentially located in the high permeability layers; the 10056ft plug can be seen to come from 10055.5ft in Fig. 4.11c by detailed correlation of the detailed probe profile in Fig. 4.2. As a result of this preferential and insufficient sampling, the estimate of arithmetic average permeability for the WB interval from the plugs (390mD) is significantly higher than that derived from the probe data (172mD). Because the latter is made from >100 data points, we can be confident that the population mean lies between 138 and 206mD. Whilst the probe arithmetic and harmonic averages show relative anisotropy, the absolute values of k/k_h may be over-estimated because of the problems previously discussed concerning the probe resolution of thin low permeability laminae. For this thinly (±3m) developed, heterogeneous interval, the probe permeameter provides the only effective measurement device.

Providing sufficient closely spaced samples have been taken, the permeability structure can be revealed by the semivariogram (Appendix I). Periodicity in sediments gives rise to repetitive permeability patterns and these result in "holes" where the variance at certain lag distances is significantly reduced (*i.e.*, pairs of data points at this spacing are likely to be more similar than those at a fraction of the spacing). Holes are commonly seen in variograms generated from probe data (Goggin *et al.*, 1988) and these commonly represent average bed thicknesses. Their significance is often overlooked by the fitting of a spherical model. In the Rannoch Formation, the variogram is particularly useful for determining average HCS bed thicknesses. In the Statfjord well, a significant hole (Fig 4.12) suggested a bed thickness of ±1.4m. Hole lags could therefore be used to suggest a representative sample volume.

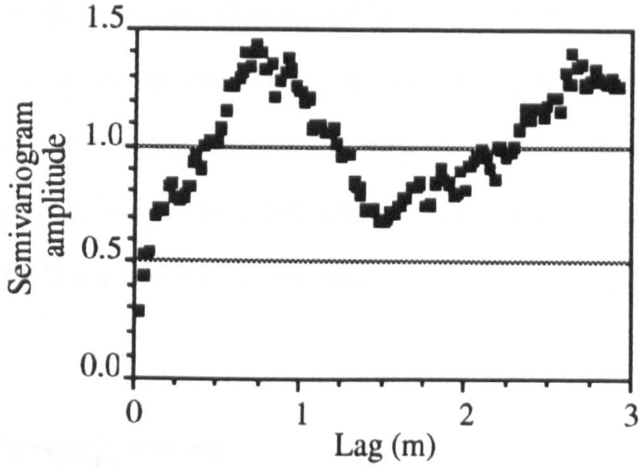

Figure 4.12: Permeability semivariogram for the probe data from the Statfjord Field Rannoch interval shown in part by Fig. 4.10. Semivariogram has been normalised by dividing by the sample variance.

Note, however, that the identification of the hole seems to require a sample spacing that is a fraction (1/10th appears to be a reasonable rule-of-thumb) of the hole lag. The semi-variogram for the same interval from core plugs at the 1ft (±30cm) interval fails to identify the hole structure (Fig. 4.13).

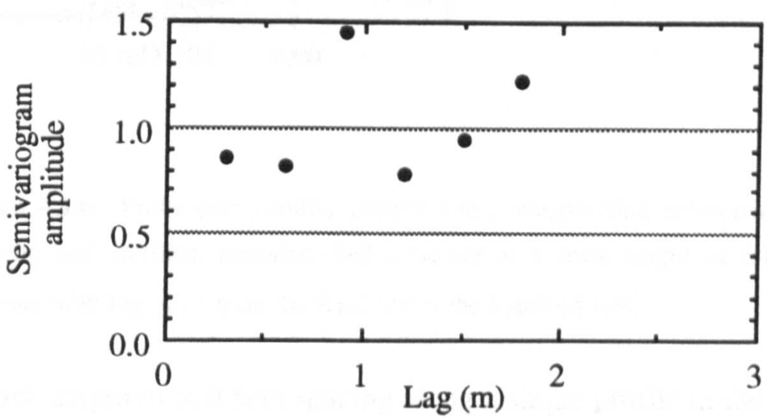

Figure 4.13: Permeability semivariogram from 1ft spacing core plugs for the same interval as shown in Fig. 4.12. Semivariogram has been normalised by dividing by the sample variance.

An interval in the Thistle well shows a variogram with a hole at a similar spacing (1.3m in Fig. 4.14). In this case the sedimentary structure (a 1.14m-thick HCS bed) can be clearly seen in the permeability profile (Fig. 4.14 left, between 10142 and 10138.25ft). More work on the statistical interpretation of the more complex semivariograms that are typical of sedimentary rocks is needed. The geological control, however, on the variogram structure has been clearly illustrated here and a petrophysical sampling significance suggested.

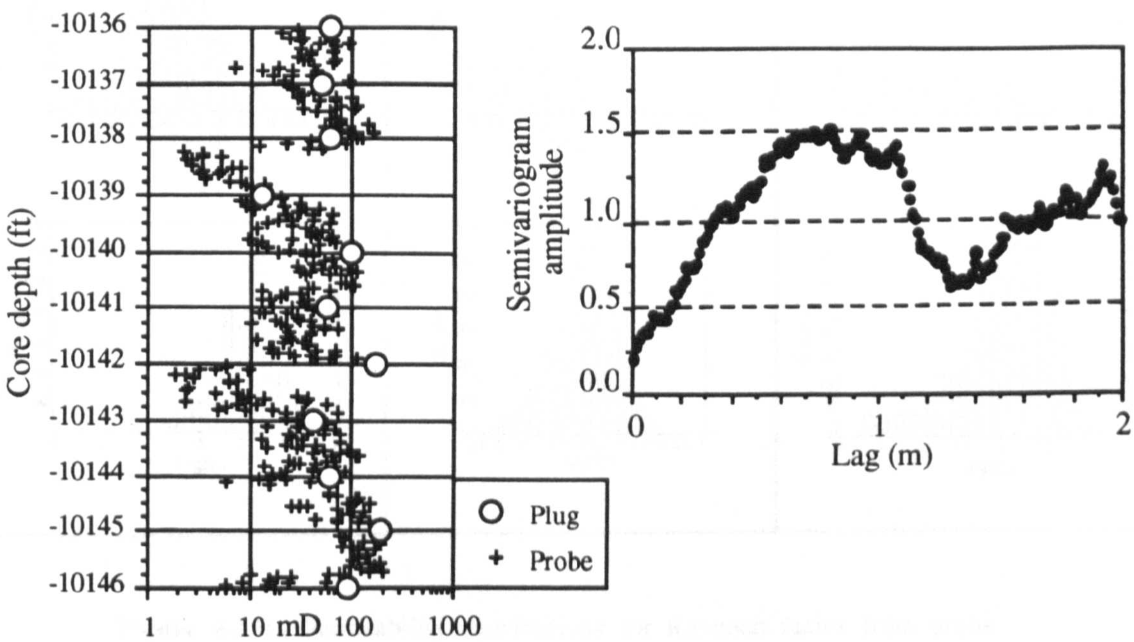

Figure 4.14: Probe permeability pattern and corresponding semivariogram showing well defined, repeated, bed structure at a scale-length of ±1.2m. Compare with Fig. 4.12 from the Rannoch in the Statfjord well.

The probe data, acquired at 0.5cm spacing along a single profile in the Thistle well, also allows the distribution type for the different facies to be determined (Fig. 4.15). Power transformation values (p-values, Appendix I) of 0.4, 0.1 and 0.3 were determined for the SCS, HCS and WB facies, respectively. The Rannoch facies, therefore, have distributions that lie between root- and log-normal pdf's (Appendix I).

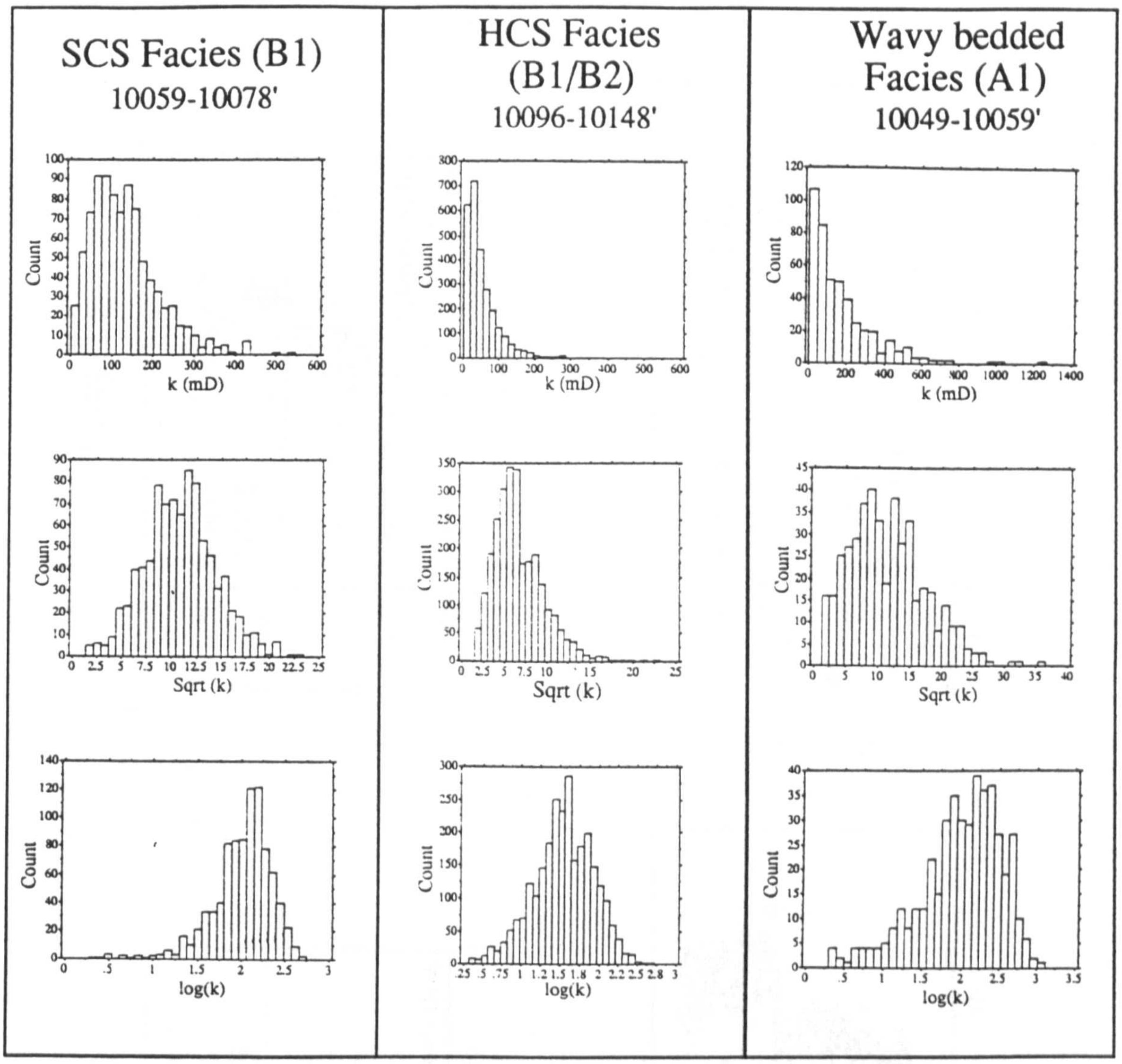

Figure 4.15: Permeability distributions for Rannoch facies from probe permeameter measurements.

4.7. Formation Scale Measurement of Permeability

To complete the review of the petrophysical description of the Rannoch Formation at various scales, we consider the porosity/permeability description of the Rannoch at the formation (or parasequence, Fig. 1.2) scale. The coarsening-up shoreface sequence is reflected in the upward-increasing permeability and porosity trends. In the Thistle Field, where the overall level of permeability is lower, the trend in the plug data is more dramatic (Fig. 4.16a) than in Statfjord Field (Fig. 4.16b).

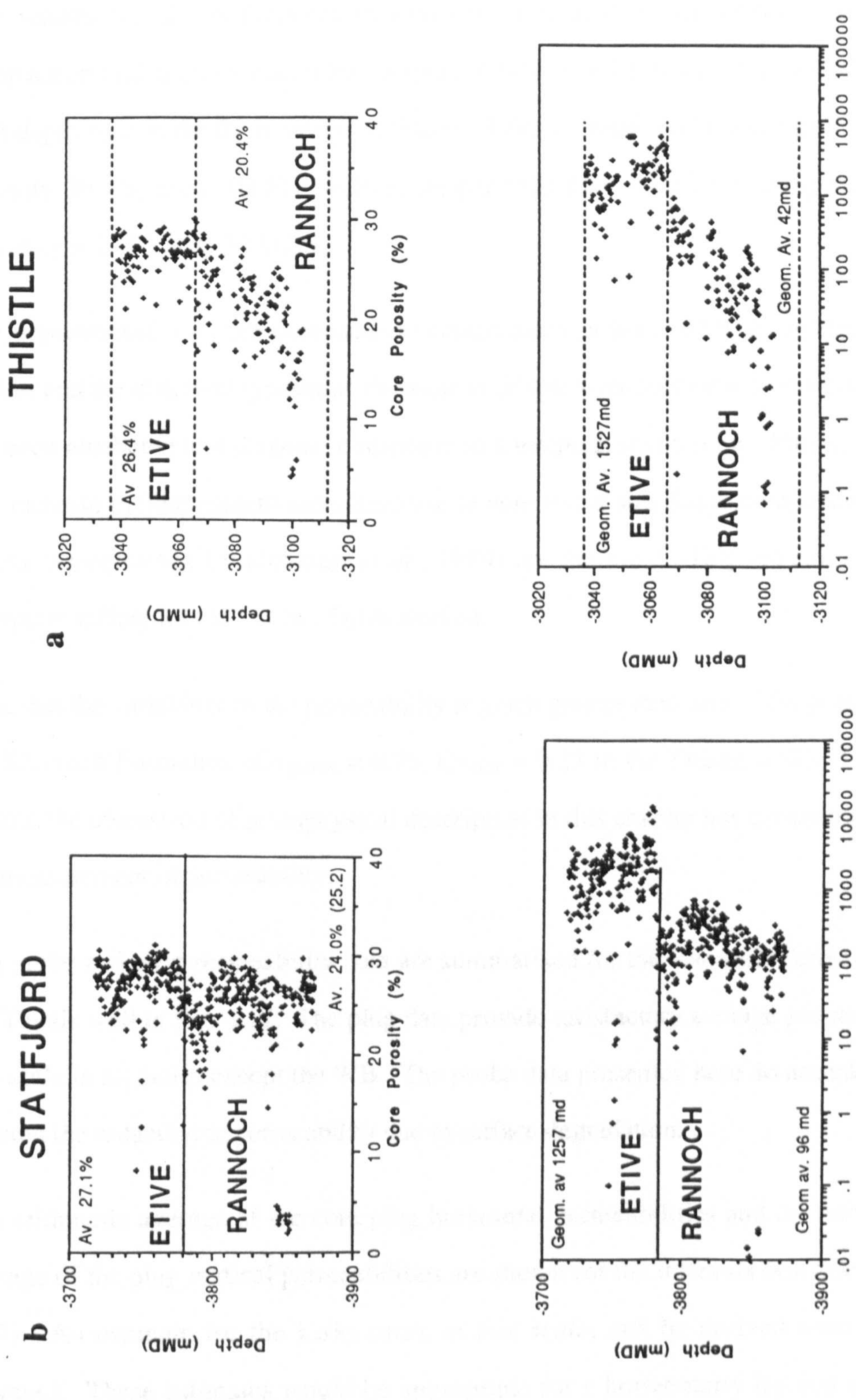

Figure 4.16: Permeability/porosity trends for the Rannoch Formation; **a**, Thistle Field (total vertical thickness, TVT, of the interval shown = ±70m) and **b**, Statfjord Field (TVT = ±100m).

The reason for the differences in porosity is related to the post-depositional compaction and is consistent with regional trends of reduction of primary porosity with depth seen in the Brent province (Harris, 1992). Thistle Field (average Rannoch porosity 20.4% in the studied well) is deeper (±2800mss) than the Statfjord Field (porosity = 24%) at ±2590mSS.

The depositional (*i.e.*, pre-compaction) composition in both fields is thought to be similar and the observed systematic decrease in felspar with depth and increase in illite has been attributed to a diagenetic response to a temperature increase (Harris, 1992). The increase in illite content and a decrease in pore throat size due to compaction and quartz overgrowths (Scotchman *et al.*, 1989) are the most likely reasons for the poroperm differences in the two fields studied.

Note that the variability of the permeability is much greater than that of the porosity in the Rannoch Formation ($Cv_{perm} = 0.76$, $Cv_{por} = 0.23$ in the Thistle well). For this reason, the discussion of petrophysical description in this chapter has concentrated on the measurement of permeability.

The probe and plug permeability data are summarised for the Rannoch Formation in the Thistle well in Fig. 4.17. The plug data provide satisfactory average properties at this scale in all facies except the WB. The probe data presented here do not take into account the reduction in permeability due to surface degradation.

The arithmetic average of the core plug horizontal permeabilities and the harmonic average of the plug vertical permeabilities are shown for the intervals described (Fig 4.17). An estimate for the k_v/k_h ratio, *at this scale*, can be derived from these averages. These estimates would be appropriate for a horizontally layered model. The k_v/k_h ratios generated by averaging plug data over intervals are significantly lower than the average core plug k_v/k_h ratio (0.65) or the probe k_v/k_h ratio (±1.0). We examine in the following section how the k_v/k_h ratio declines systematically in the Rannoch Formation with increasing scale of measurement volume. This behaviour is expected for all layered sedimentary rocks. The problems associated with the determination of appropriate grid block k_v/k_h ratios stem from an incomplete understanding of this behaviour.

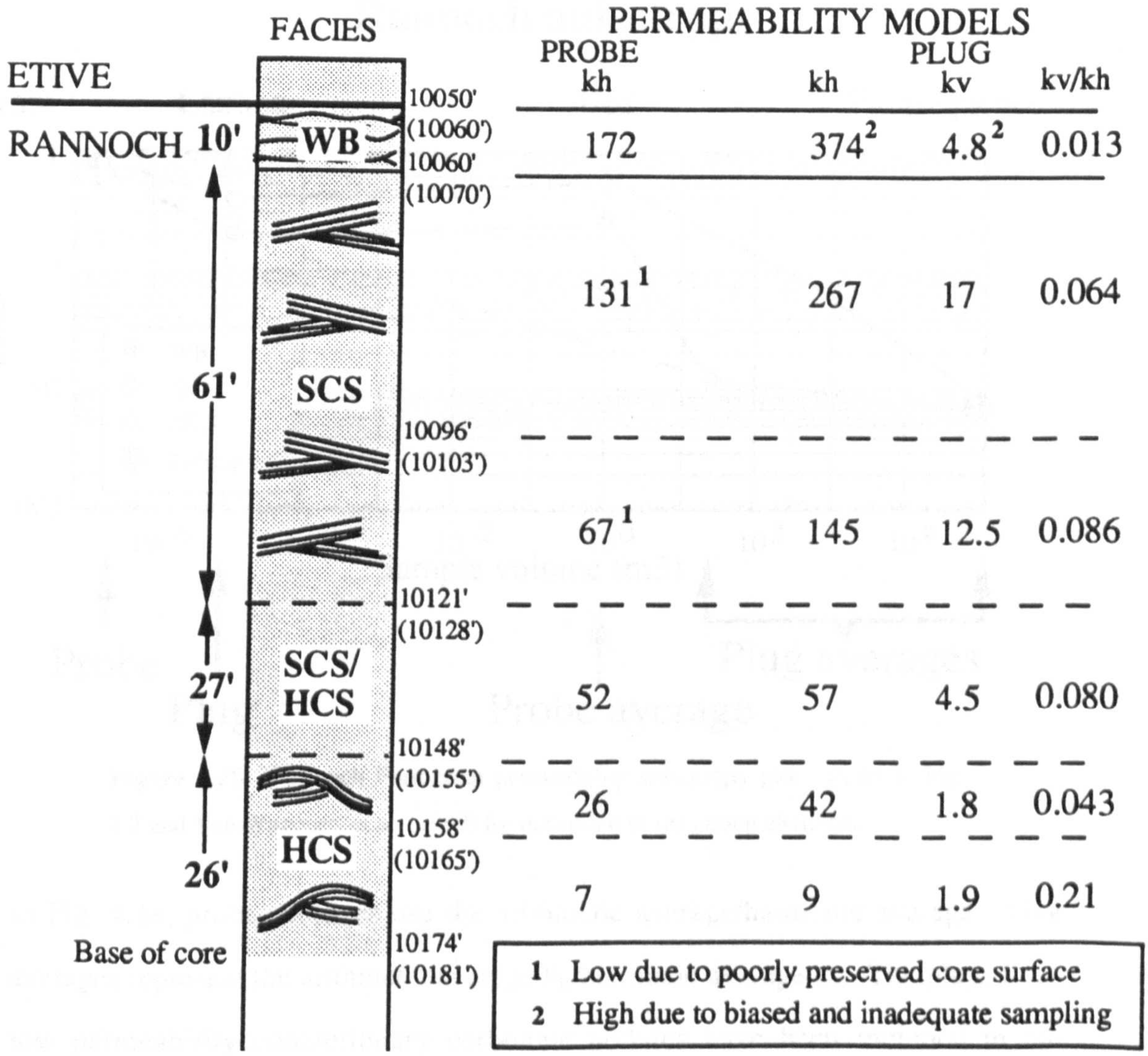

Figure 4.17: Plug and probe permeability summary for the Rannoch Formation, Thistle Field. Core depths shown (log depths in parenthesis).

4.8 Anisotropy (kv/kh ratio) Measured at Different Scales.

Permeability anisotropy (*i.e.*, k_v/k_h ratio) is a traditional input into reservoir simulators. Data are generally taken from k_v/k_h ratios determined from core plugs. The k_v/k_h ratio, however, is a function of the volume of rock sampled. In Section 4.1 the probe volumes of rock were shown to be relatively isotropic. The anisotropy systematically increases (*i.e.*, lower k_v/k_h ratio) in the Rannoch Formation with increasing volume sampled (Fig. 4.18).

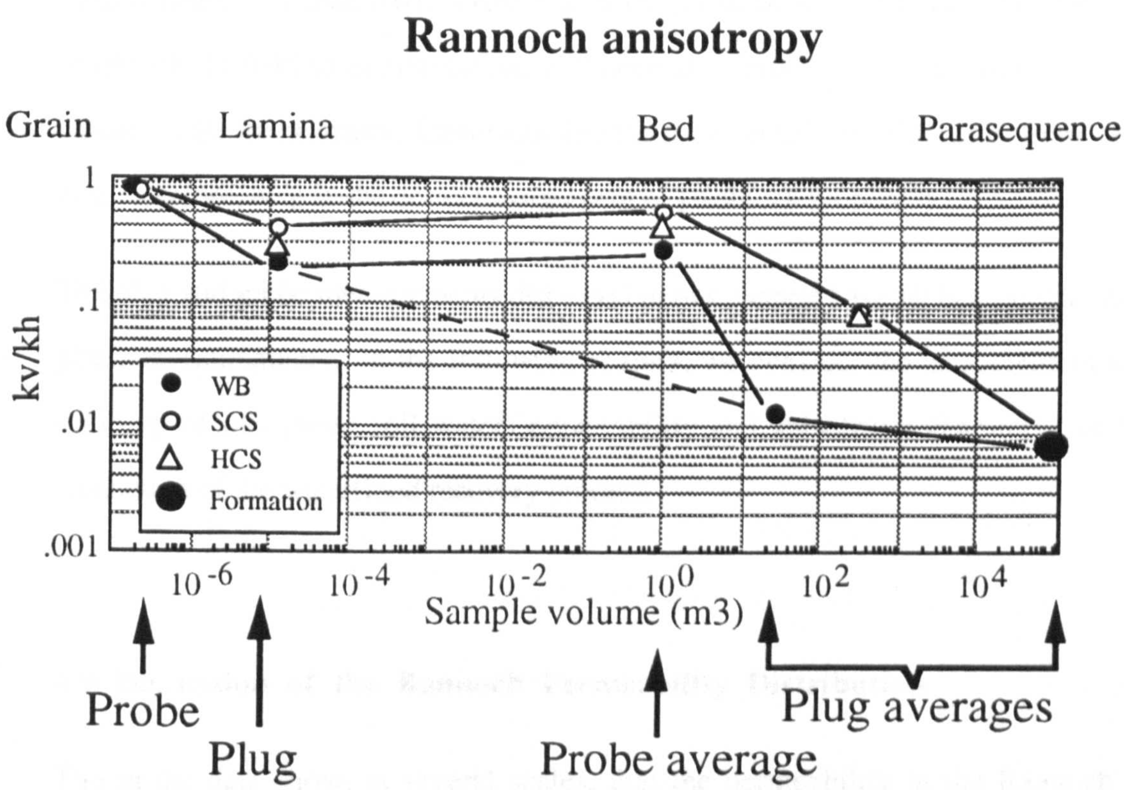

Figure 4.18: Rannoch Formation permeability anisotropy plot. Refer to Fig 1.2 and Van Wagoner, et al. (1990) for definition of the stratal elements.

In Fig. 4.18, probe averages use the arithmetic average/harmonic average. Plug averages represent the arithmetic average k_h/harmonic average k_v. The plugs from low permeability concretionary carbonate nodules have been included in the determination of the formation scale estimate.

At the probe scale the degree of anisotropy (k_v/k_h) is equally low in all facies. In the core plugs the WB facies has higher anisotropy than the HCS, which is in turn higher than the SCS. At the bed scale, the SCS and HCS have similar anisotropy. The averaged plug data suggest that the WB should have a higher anisotropy at this scale and probe harmonic averages have been shown to be a poor k_v estimator. Formation properties are dominated by the inclusion of the low permeability carbonate concretions. If these are considered not continuous (as has been shown for the Cormorant Field by Braithwaite *et al.*, 1989) then they can be legitimately excluded from the averaging. When the carbonates are excluded, the formation anisotropy ratio is nearer 0.1 than 0.01. From Fig. 4.18, it can be seen that the k_v/k_h ratio for gridblocks in field-scale simulations will need to be much lower than such ratios for smaller-scale assessments. Understanding the scale sensitivity of the anisotropy ratio can, therefore, help in the correct assignment of gridblock properties.

The plug and probe measurements discussed in this chapter have all been single (gas) phase measurements. In the following chapter, we consider the measurement and scale-up of two-phase (oil-water) permeability and anisotropy charcteristics for simulation of the waterflood recovery process.

4.9 Discussion of the Rannoch Permeability Distribution

The probe data show, at several scales, that the permeability in the Rannoch is strongly controlled by the primary depositional structure of mica-rich and mica-poor sandstones. Clear relationships between permeability patterns and laminae, laminasets and beds have been identified. Many of these elements are highly variable.

The core plugs samples are sufficient to characterise the permeability of the Rannoch shoreface as a whole. The section is greater than 58ft so the optimum sampling criteria ($[10 \cdot 0.76]^2$) is satisfied by 1ft samples. However, certain intervals (*e.g.*, the WB) are poorly characterised by the plugs alone. The permeability patterns and variability are well described by the probe data although the absolute values are lower (attributed to surface damage of the slab surface). The permeability patterns identify the stratal elements and assist in the scale-up of scale dependent properties (*i.e.*, k_v/k_h).

The data presented here show that the permeability description in the laminated Rannoch Formation is best achieved by a combination of the probe permeameter (patterns and variability) together with selected core plugs (absolute values). The core plugs are optimumly selected from intervals shown by the probe to be relatively homogeneous. It is not advised that the probe permeameter device be used as the sole instrument of permeability measurement.

CHAPTER 5

TWO-PHASE FLOW PROPERTIES OF LAMINASET ELEMENTS

In the previous chapter, a clear relationship between sedimentary facies and permeability distribution for the Rannoch Formation has been demonstrated. Despite the subsequent diagenetic changes due to compaction and temperature increases, the patterns of permeability are clearly related to primary depositional fabric. The limitations of traditional core plugs (failure to capture small scale variation, volume dependency of plug k_v/k_h ratios, important intervals missed, key facies undersampled, etc.) were also highlighted. The core plug data alone are insufficient for the permeability description. Measurements with the probe at a different scale provide the description of the variability and characteristics of thin facies that was previously unobtainable with plugs. The supplementary probe data also provide further description of the anisotropy.

In chapter 4 we also showed that the appropriate or representative averaging volumes are related to the stratal elements. The properties of these natural building blocks of reservoirs can be determined from probe (and selected plug) measurements. Average properties for large scale grid blocks in reservoir simulators are then derived from the distribution of sub-gridblock stratal elements.

The production mechanism for the Rannoch Formation is waterflood (edge-water drive and water injection). Waterflood requires grid block scale estimates of average two-phase properties, not traditionally provided by core plugs. In this chapter, reservoir simulation of very detailed small-scale permeability fields is used to determine two-phase flow properties for the smallest representative groups of stratal elements (*i.e.*, laminasets).

5.1 Introduction to Two-Phase Flow

Recent work on the flow response to small scale geological features and scaling their effects to field scale models (Ringrose *et al.*, 1991) has shown that:

- •small scale geological structure (*e.g.*, cross-bedded laminae) influence flow performance through localised capillary effects, and
- •these effects remain at larger scales when the aggregated small scale structure is taken into account.

In this study, influence of small scale lamination, present throughout the Rannoch Formation in varying degrees of contrast, on flow performance at the larger scales is studied. In this study, the effects are the lamination are quantified by numerical simulation rather than laboratory experiment.

The average or effective relative permeabilities of each phase are commonly determined by pseudofunctions (Appendix VI). The scaling-up of flow characteristics by the use of pseudofunctions or "pseudos" is widely advocated for reservoir simulations (Kyte and Berry, 1975; Lasseter *et al.*, 1986; Lake *et al.*, 1990; Kossack *et al.*, 1990; Muggeridge, 1991). "Small scale" simulations are used to determine the properties for coarser scale simulations ("pseudo-properties") so that the small scale performance is accounted for. However, in many instances, the pseudofunction technique has been poorly applied because of:

- •starting at a scale that includes heterogeneity and implies the use of a pseudo rather than a rock curve (1ft in Kossack *et al.*, 1990)
- •choosing to ignore the variation in capillary pressure with rock type because there is generally no sensitivity to capillary pressure for large grid blocks (Kossack *et al.*, 1990; Muggeridge, 1991)

•failing to account for the aggregation of strongly structured (laminated) rocks in the scaling-up process, thus failing to incorporate the effects of small-scale sedimentary structure

Local capillary effects are important at low rates (*i.e.*, less than 1m/day, Fig. 5.1) and are thus likely to be manifest where interwell rates are of order 0.3m/day (1ft/day), considered by many (Kortekaas, Tehrani, personal communication) to be appropriate for the Rannoch Formation in many North Sea fields (Thistle and Statfjord Fields included).

In this study, we combine permeability data at the smallest measureable scale (*i.e.*, probe measurements at 2mm spacing over centimetre-scale grids) with "rock" capillary pressure and relative permeability curves to generate pseudos (for porosity, permeability, relative permeability and capillary pressure) for the representative laminasets. The following chapter will consider how these effects can be scaled for input into conventional (metre-scale gridblock) reservoir simulations using knowledge of the hierarchical structure of stratal elements.

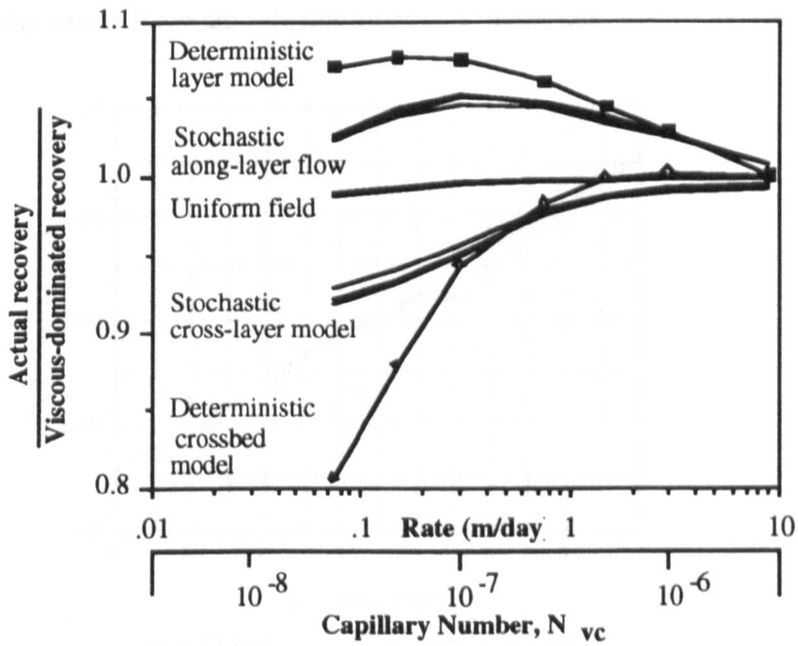

Figure 5.1: Rate dependancy of recovery for cross layer and along layer waterflooding. Differences in recovery with flow orientation, due to local capillary forces, disappear in the viscous- dominated region. (From Ringrose *et al.*, 1992).

5.2. Single-Phase Laminaset Properties

The permeability variation in the Rannoch Formation is closely related to the primary depositional fabric at the lamina (Figs. 4.1, 4.2, and 4.8) and bed scale (Fig. 4.10, 4.11). The (horizontal) permeability fields in various laminasets have been measured by detailed probe permeameter grids in geologically-representative intervals (Figs. 4.2, and 4.8). Vertical permeability approximates horizontal permeability (Fig. 4.3) at the scale of probe measurement. The inability of the probe to measure the properties of very thin laminae has previously been discussed (p. 61). It is considered, however, that the variability and the extreme values have been reasonably well characterised even if some thin low (or high) permeability laminae have been overlooked.

At present, no device exists for the simultaneous measurement of porosity and permeability at the probe scale. In the Rannoch, however, there is a strong linear relationship between average probe log permeability and core plug porosity for the more homogeneous core plugs (Fig. 5.2). This suggests a good relationship between porosity and permeability exists for relatively homogeneous materials.

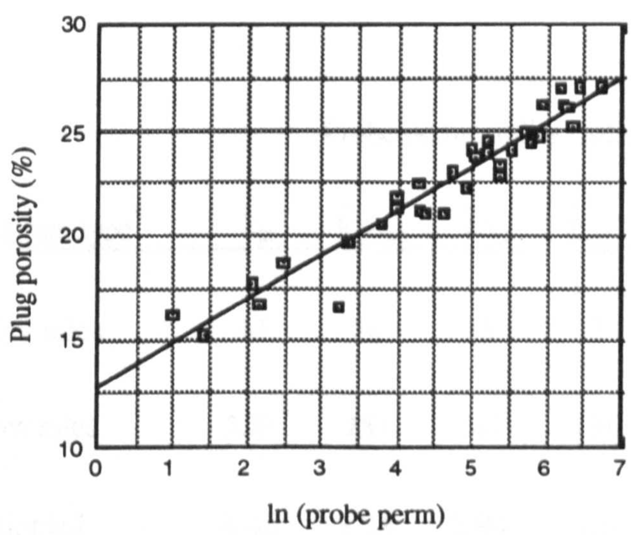

y = 12.698 + 2.1100x   R^2 = 0.930

Figure 5.2: Probe permeability (arithmetic average of 4 measurements at each end of the plug) versus plug porosity for the homogeneous Rannoch Formation plugs (Cv < 0.3).

Lamina are texturally uniform in nature and effectively homogeneous so one can expect good poroperm relationships within laminae. Poor relationships between core plug porosity and permeability can be expected when there is sub-core plug scale heterogeneity. In the Rannoch, there are many relatively homogeneous plugs and a good relationship can be seen between core plug porosity and permeability. With the plug data alone, however, there is no systematic way to eliminate outliers with sub-plug heterogeneity.

Using the relationship in Fig 5.2, porosity can be easily determined for the permeability field. For the four recognised Rannoch laminaset types, the probe poroperm summary is presented in Table 5.1. Note that the permeability heterogeneity is consistently higher than the porosity heterogeneity.

For comparison, the plug values from the same intervals are shown in Table 5.2. Comparisons between 1) probe arithmetic average and plug horizontal and 2) plug and "probe" porosity show that reasonable characterisation of these parameters (k within 40%, and ϕ within 15%) have been achieved with the probe.

	Probe permeability (mD)					Porosity (%)	
Laminaset type	$\overline{k}_{ar}$	$\overline{k}_{geom}$	$\overline{kh}_{ar}$	k_{min}	Cv	$\overline{\phi}_{ar}$	Cv
High mica	43	26	15	2	1.06	19.6	0.11
Low mica	259	251	241	136	0.26	24.4	0.02
Rippled	4.46	3.38	2.94	1.6	1.28	15.3	0.08
Wavy bedded	550	422	234	30	0.60	25.5	0.07

Table 5.1: Rannoch laminaset probe poroperm properties.

The vertical permeability is, for reasons previously discussed, generally overestimated by the harmonic average of probe measurements. In the rippled and wavy bedded laminasets the probe estimate of vertical permeability is out by a factor of 10 (*i.e.*, one order of magnitude). In the low and high mica laminasets, vertical permeability was estimated within 40%.

The probe poroperm grids for the high and low mica laminasets therefore adequately describe the petrophysical variation. Thin low permeability lamina in all but the rippled laminasets have been identified (see k_{min}) and the potential of k_{min} as an estimator of k_v could be further investigated.

Laminaset type	k_h (mD)	k_v (mD)	ϕ (%)
High mica	52	11.9	22.5
Low mica	318	197	27.6
Rippled	n/a	0.2	14.6
Wavy bedded	893	37.6	28.0

Table 5.2: Rannoch laminaset plug poroperm properties for equivalent intervals to Table 5.1.

5.3. Determination of Two-Phase Properties

5.3.1 Capillary pressure

A family of capillary pressure curves have been derived from drainage rock capillary pressure data for the Rannoch Formation in the Thistle Field (Appendix IV). The derived curves cover the range of permeability values encountered in the above grids (Fig. 5.3).

These data are taken from volumes of rock (*i.e.*, core plugs) that are significantly larger than the grid blocks or individual laminae within the laminasets. Assuming that the selected core plugs are reasonably uniform (the criteria on which such samples are conventionally selected), the curves should also be applicable to smaller volumes of homogeneous rock. Until the development of small scale capillary pressure devices that would allow the capillary pressures of lamina to be directly measured, there is no means of validating this assumption. Lamina capillary pressure data, together with porosity and permeability data, would show less scatter than is traditionally seen with core plugs if smaller scale devices were available.

The shape and spread of the curves, is consistent with those expected from reasonably well sorted, fine grained material. The similar shape to the curves suggest the pore distribution is consistent over a range of permeabilities. Although these curves are not imbibition curves, they are thought to be reasonable approximations, and their use in models is thought to represent the appropriate physics. Further discussion of Rannoch drainage and imbibition curves can be found in Appendix IV. At the present time there are insufficient imbibition data for our purposes. In future studies, however, a more systematic collection of imbibition data is called for.

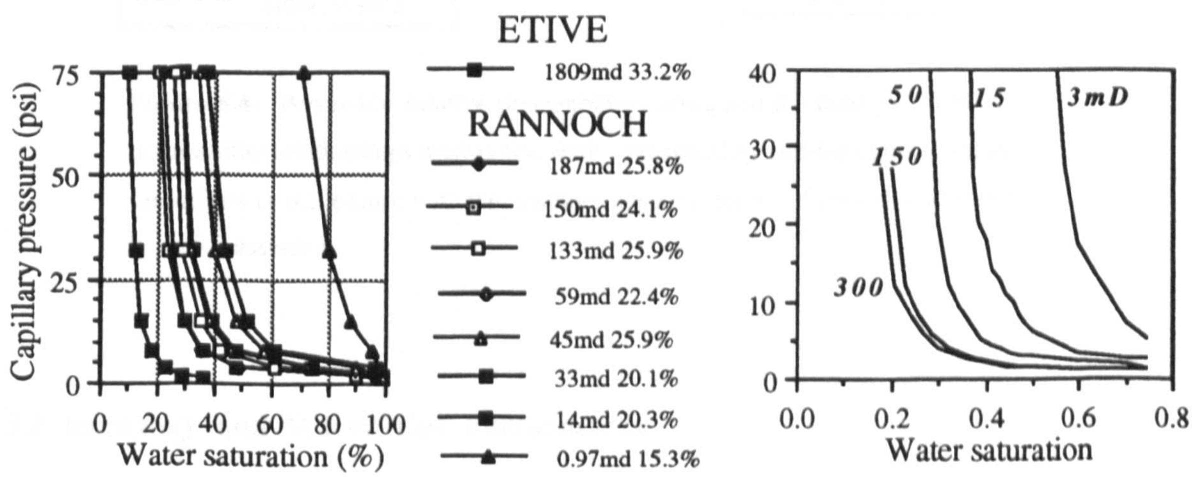

Figure 5.3: Capillary pressure curves for the Rannoch Formation from Thistle A33 and the family of curves selected for this study.

5.3.2 Relative permeability

Power-law relationships between relative permeabilities to oil (k_{ro}) and water (k_{rw}) with water saturation (p. 113 in Archer and Wall, 1986; Muggeridge, 1990) have been adapted to the varying connate water saturations (S_{wc}) indicated by the capillary pressure curves (Fig. 5.4). The residual oil saturation (S_{or}) has been assumed constant (25%). No experimental relative permeability data have been used in this study. The power-law relationships are traditionally used to provide relative permeability curves in Rannoch field simulations (Thomas and Bibby, 1991) and this practice is followed here (refer to Appendix V). The issue of wettability has, by selecting numerical curves of a moderately water-wet character, been avoided in this study.

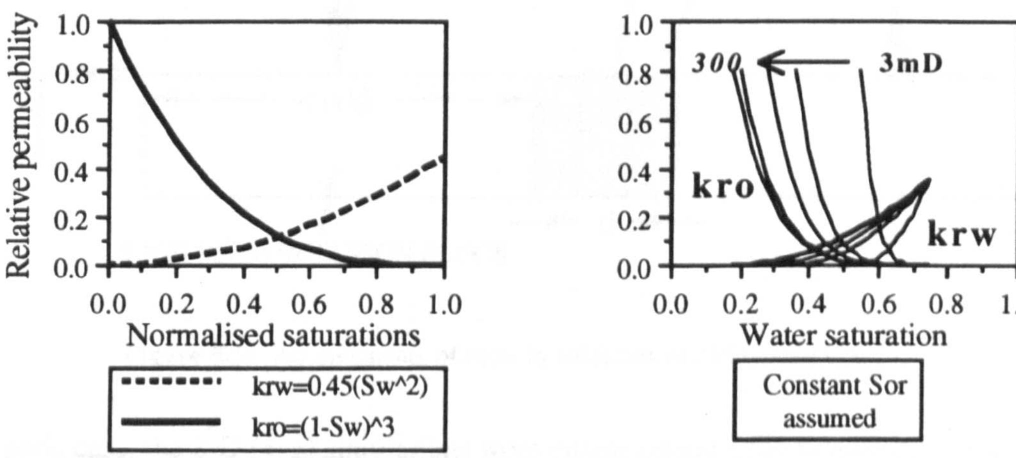

Figure 5.4: Power-law relative permeability curves and the family of relative permeability relationships used in this study, generated by shifting connate water saturations in accordance with the capillary pressure curves. Constant end-point k_{or} = 0.8 assumed.

5.3.3 Recovery and Water Cut Performance

To determine the two-phase flow characteristics of the Rannoch laminasets, detailed simulations were carried out on each of the permeability fields (Figs. 4.2 and 4.8) using the ECLIPSE (ECL, 1988) black oil simulator. The measured permeabilities (a single profile for grids A, C and WB repeated to form the layered structure and grid B in entirety) were assigned to 2x2mm or 3x3mm grid blocks, preserving the scale and geometry of the measurement grids. Each grid block was considered isotropic at this scale ($k_x = k_y = k_z$) and initially flooded parallel to the bedding (*i.e.*, x-direction). Each subject grid (laminaset) was embedded in identically-constructed blocks before and after (with reference to the flooding direction). These two blocks acted as "buffers" between the subject block and the injection/production blocks (Fig. 5.5). These latter blocks were ten times the length of the subject block to ensure calculation of consistent pseudofunctions (Kossack *et al.*, 1990). An example ECLIPSE input file (EXFGA003.DATA) is included in Appendix VIII.

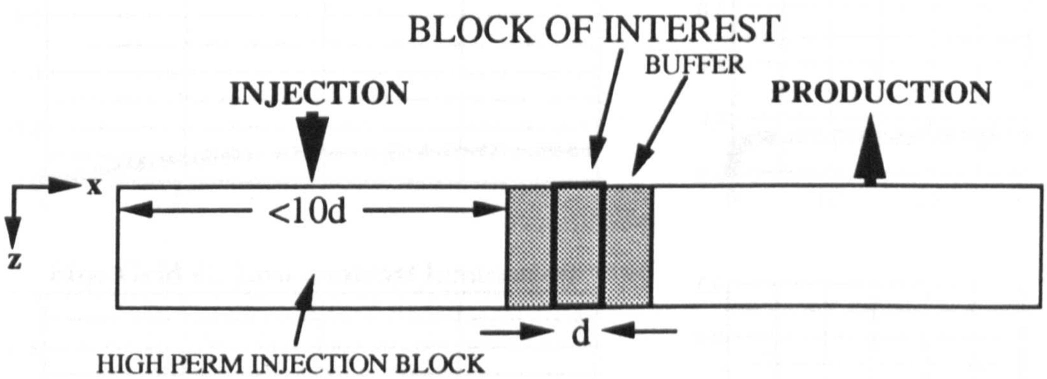

Figure 5.5: Arrangements of cells in subfacies model simulations

In each case, the 2-D (x, z) simulations were characterised a favourable mobility ratio (M = 0.63) waterflood with constant frontal advance rate (0.24m/day). The constant advance rate was maintained by altering the y-dimension of the various models to maintain a constant pore cross-sectional area. These constraints are thought to represent "typical" North Sea Rannoch conditions. Recovery from the subject block was monitored as a function of grid volumes throughput for the three HCS subfacies (Fig.5.6) and the wavy bedded facies (Fig. 5.7). For these two responses, the high contrast lamination and the wavy bedded subfacies showed considerable anisotropy while the other two subfacies were nearly isotropic. Whilst the ultimate recovery is best for the more uniform grid (grid C) the pore volumes throughput required to achieve that recovery is significantly higher than in the more structured fields.

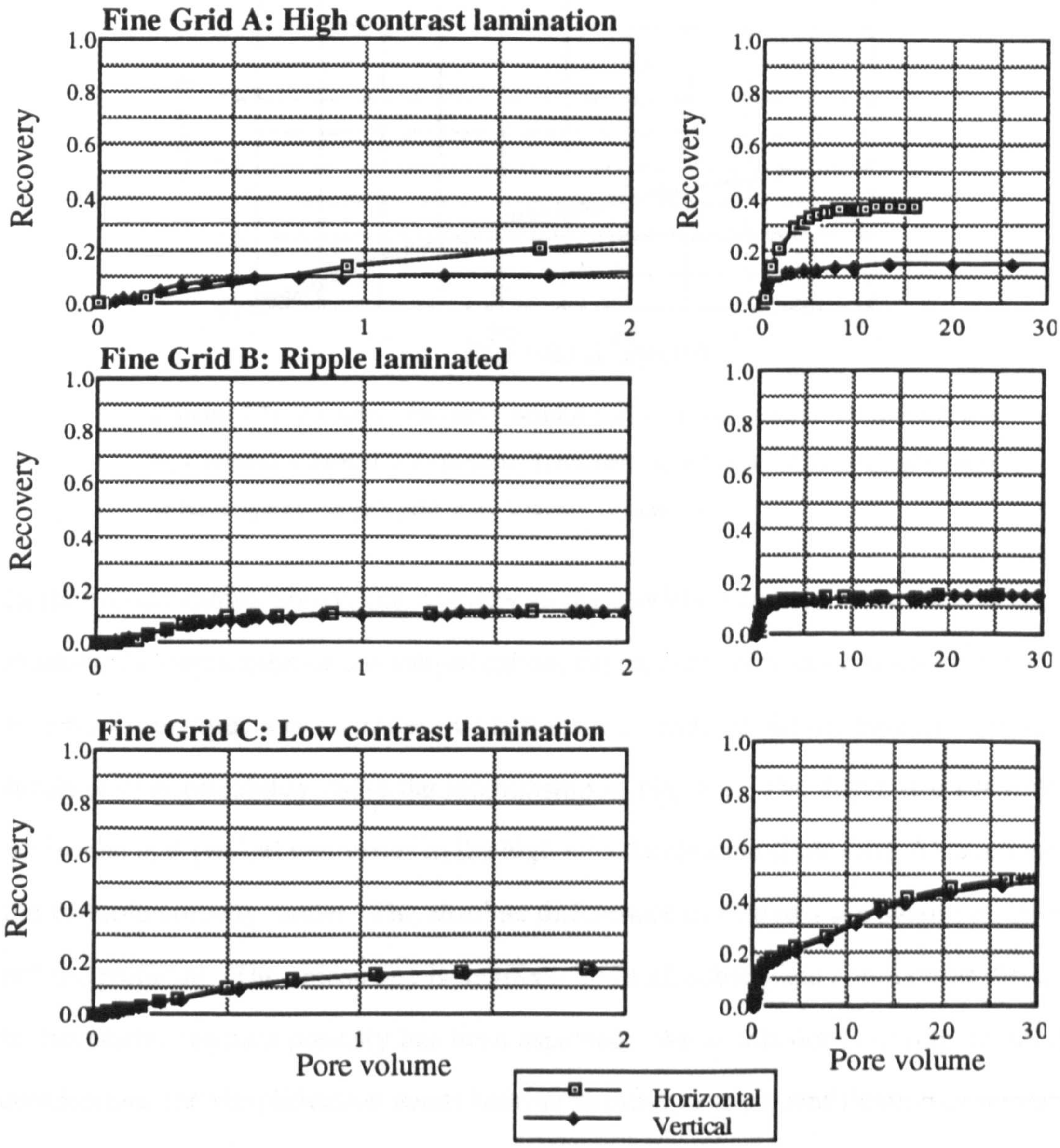

Figure 5.6: Recovery performance for waterflood simulation in HCS subfacies, Rannoch Formation. Bed parallel (horizontal) and bed normal (vertical) direction shown. Recovery is fraction of pore volume within the subject grid; pore volume is the volume injected in units of subject grid pore volumes. Expanded scale of plots on the left allow the early time behaviour to be more clearly seen.

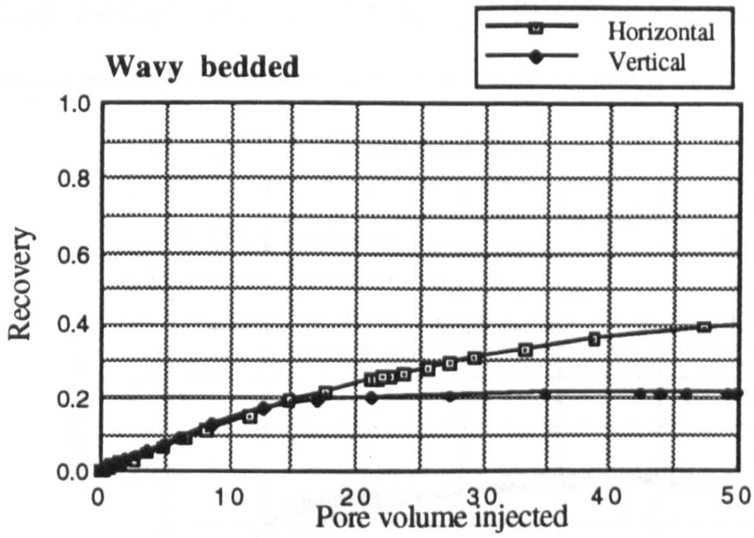

Figure 5.7: Recovery for wavy bedded facies in bed parallel (horizontal) and bed normal (vertical) directions. Recovery as fraction of subject grid pore volume against subject grid pore volumes injected.

In the floods shown above, the porosity in the models was held constant at 15%. To examine the implication of this simplification, the recovery of total oil-in-place at one pore volume throughput was compared with that for a model in which porosity varied as a function of permeability using the relationship in Fig. 5.2. The difference between the horizontal and vertical recoveries in the high mica lamination (Fine Grid A) is reduced in the variable porosity model. The absolute differences in recovery are small (4-11%) but not insignificant. The anisotropy is unaffected. In all subsequent simulations discussed in this study, constant porosity has been assumed. While this does not impact the flow conclusions, the simplification needs bearing in mind in any quantification of remaining hydrocarbons.

5.3.4 Pseudo Relative Permeabilities and Capillary Pressures

The pseudofunctions were determined using the Kyte and Berry (1975) equations in the ECLIPSE option *PSEUDO*. Back substitution of the rock curves in a coarse grid with pseudo permeabilities, pseudo relative permeabilities, and pseudo capillary pressures gave the same flow performance as the detailed grid (Fig. 5.8). In contrast, substitution by the arithmetic average and the corresponding rock capillary and relative permeability curves did not, however, produce the same flow performance.

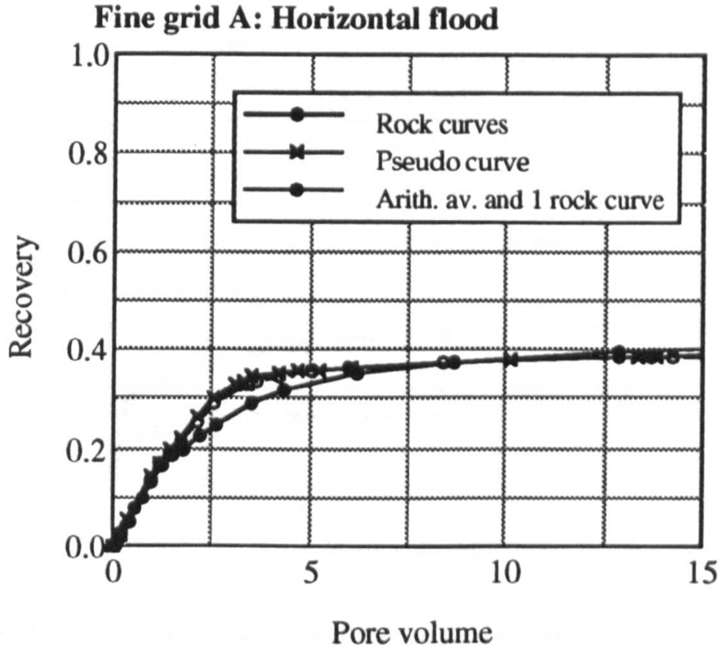

Figure 5.8: Comparison of detailed layered model performance (using permeability-determined capillary pressure and relative permeability curves), uniform model with "pseudos", and uniform model with arithmetic average permeability and corresponding capillary pressure and relative permeability curves. High contrast lamination.

To determine pseudofunctions for flow in the vertical (z) direction, the permeability fields were rotated and flooded normal to the laminae. The gravitational field would not thus be correctly represented, however, its effects at this scale are considered negligible. The performance of the pseudos and the detailed simulation in comparison with the harmonic average permeability again showed that the latter fails to match the performance of the detailed simulations (Fig. 5.9).

Figure 5.10 shows the horizontal and vertical pseudos for each laminaset. The geopseudos for the laminasets are also listed in Appendix IX. The least and most variable laminasets (low contrast mica lamination Cv = 0.26, and ripple lamination, 1.26) behave isotropically. The high contrast mica lamination and WB lamination (Cv's = 1.06 and 0.6, respectively) are, in comparison, strongly anisotropic.

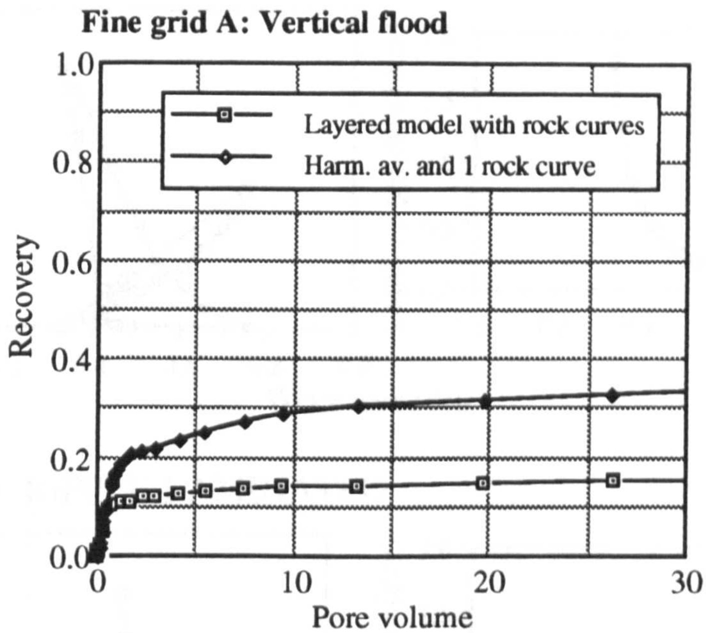

Figure 5.9: Comparison of detailed layered model with uniform model. High contrast lamination; vertical waterflood direction

The anisotropy in the anisotropic laminasets increase as the water saturation increases. At a certain saturation, the flow of oil decreases almost to zero whilst a reasonable relative permeability to water continues. The saturation cannot increase as the oil is trapped by the laminated structure. The end point k_{or} is reduced and S_{or} increased.

In the pseudos generated by the ECLIPSE option *PSEUDO* (Fig. 5.10) the average absolute permeability is always determined as the arithmetic average. This is not consistent with the Kyte and Berry (1975) procedure which called for the harmonic average for layer series flow. The effective oil permeability is given by the kk_{ro} product and is required in the Darcy two-phase flow equation. The anisotropy can be associated with the absolute permeability (*i.e.*, by the k_v/k_h ratio) or by the anisotropic relative permeabilities. Ideally both single-phase and two-phase anisotropies should be captured. This requires a pseudoisation technique that takes into account the orientation and nature of the permeability field. In this work, the anisotropy is captured by the pseudo relative permeabilities and not by the absolute k_v/k_h ratio. We have seen earlier how sensitive the latter is to the scale of measurement.

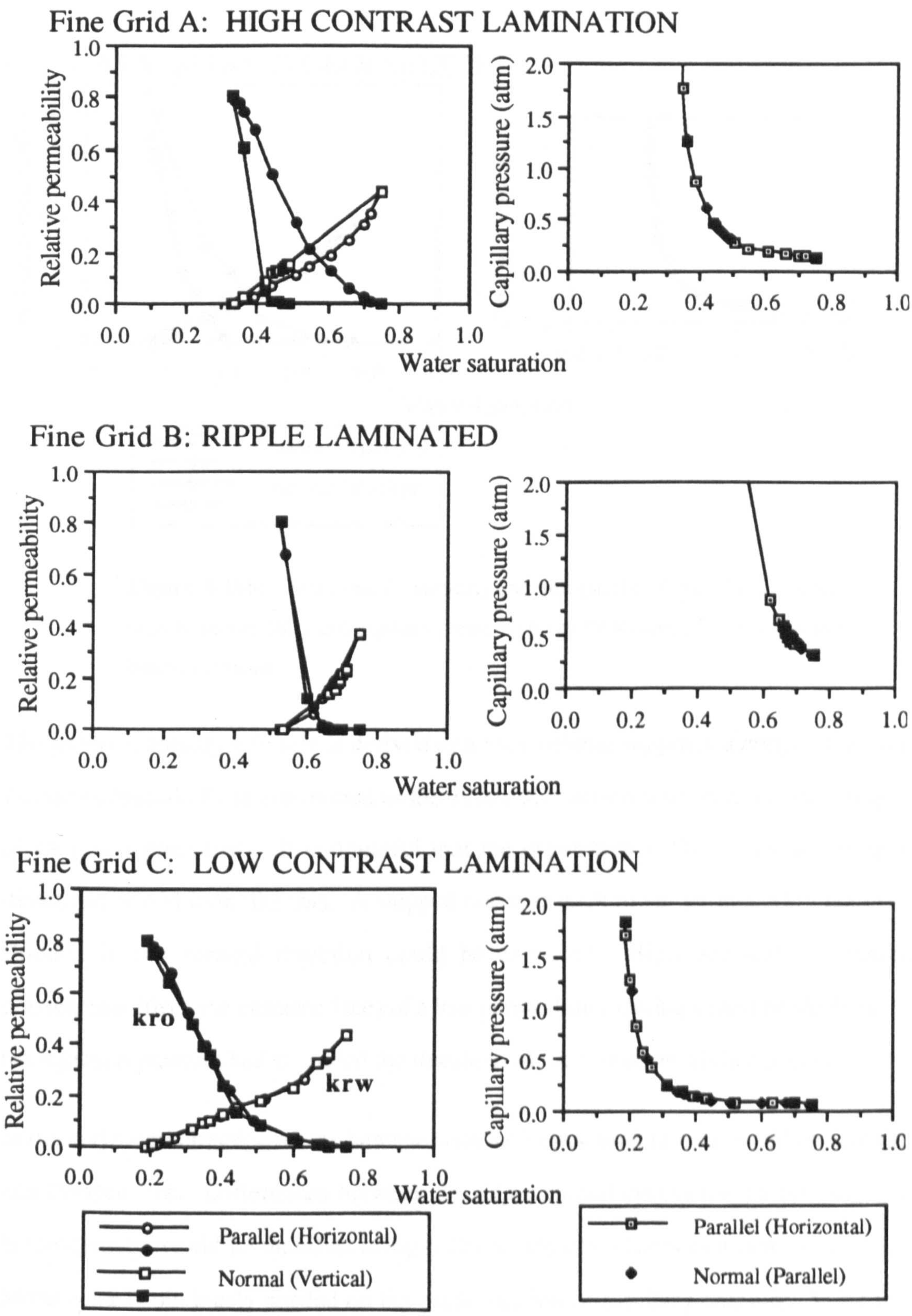

Figure 5.10a: Bed-normal (vertical) and bed-parallel (horizontal) pseudo relative permeability and capillary pressure curves for Rannoch Formation HCS/SCS laminasets.

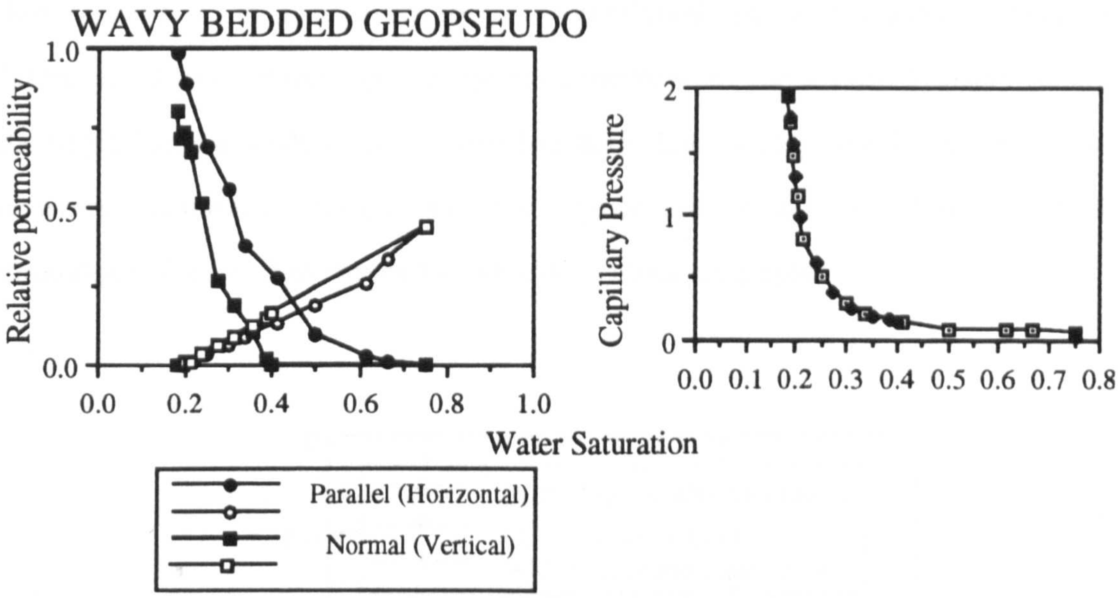

Figure 5.10b: Bed-normal (vertical) and bed-parallel (horizontal) pseudo relative permeability and capillary pressure curves for Rannoch Formation wavy bedded laminaset

The pseudo capillary pressure is derived as a pore volume weighted average of the input Pc curves (pseudo Pc is determined as the differences between the pore volume weighted block phase pressures). It is doubtful that the experimental Pc curves in orthogonal directions would look like this. A stepped curve as each lower permeability laminae is flooded in the vertical direction could be expected. High permeability laminae downstream (from the entrance face) of a low permeability lamina would be shielded until the injection pressure had exceeded the threshold of the low permeability lamina.

In the horizontal direction *all* the laminae with the largest pore throats would be accessible and flooded first. Differences between the experimental curves due to sub-plug scale heterogeneity would be manifest using different injection faces in a laminated sample. More work is obviously needed on the pseudoisation of capillary pressure. What is the appropriate physics during the waterflood that should be captured in the average property of a large grid block? In this study, however, we continue with the pore volume weighted pseudo Pc curves, having flagged some concerns over their physical meaning.

Contrasting the horizontal flow performance of the laminasets (Fig. 5.11), we can see that the most efficient recovery (with the combined benefit of viscous and capillary forces) is achieved in the high contrast mica lamination. The poorest recovery occurs in the ripple laminaset where oil is trapped in the isolated high permeability zones. Good recovery is achieved in the isotropic low contrast mica lamination, although for greater throughput of water than required in the high contrast lamination.

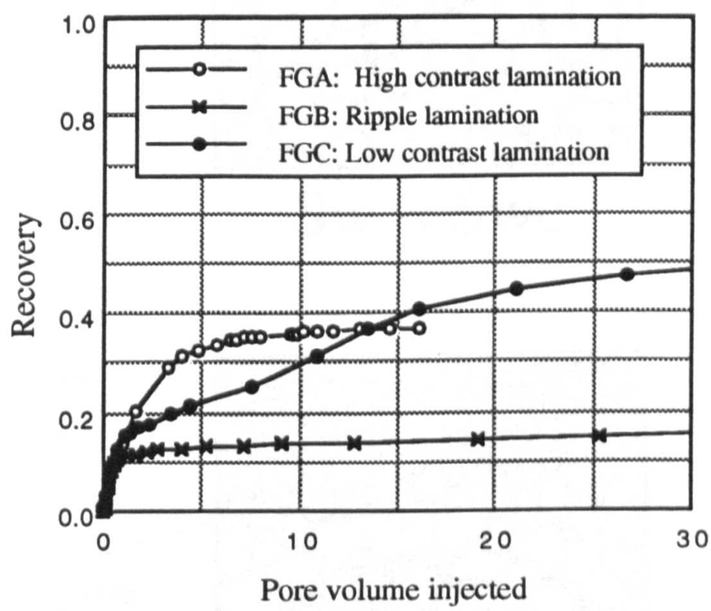

Figure 5.11: Horizontal flow performance of three Rannoch Formation laminasets.

At the pore scale, the trapping mechanism is represented schematically in Fig. 5.12. Significant trapping of oil in the centre of the large pores occurs in the high permeability, high porosity laminae, when impeded by smaller pores at residual oil saturation (in a water-wet reservoir). This occurs in vertical flow through horizontally laminated rocks, when isolated high permeability zones (*e.g.*, ripples) are present or in cross-laminated systems under horizontal flow (Van der Graaf and Ealey, 1989).

The trapping at the lamina-scale is the reason behind the differences seen in Fig. 5.11. This is, therefore, a different capillary-trapping mechanism from that which might occur in individual or dead-end pores. Oil trapped in this semi-continuous state (*i.e.*, as a continuous phase within laminae) is potentially more significant than data from laboratory studies on "homogeneous" plugs, or whole core samples, might suggest.

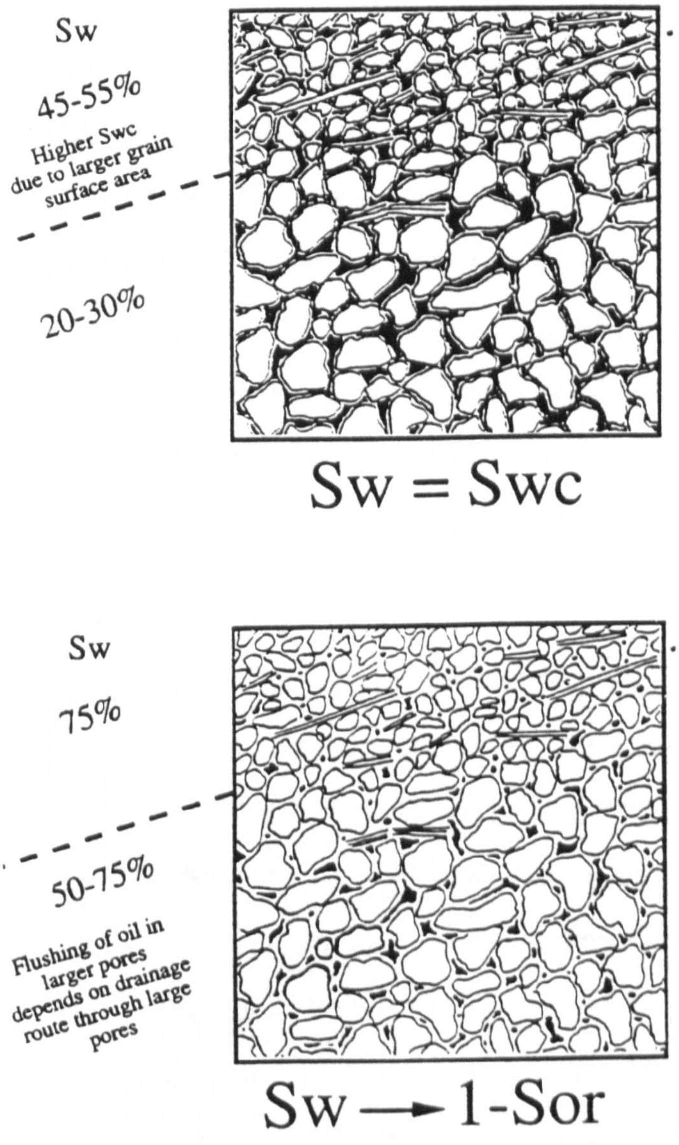

Figure 5.12: Schematic representation of capillary trapping at the lamina-scale. The oil phase is trapped (by capillary forces) in the large pores in a water-wet system.

The pseudos for the Rannoch laminasets represent the effective two-phase flow properties for cm-scale grid blocks. The vertical/horizontal anisotropy is captured by different pseudos. These laminasets have been shown to be both statistically and geologically representative of the cm-scale variability seen within the Rannoch Formation. The Rannoch two-phase properties are effectively characterised at this scale. The cm-scale grid blocks (i.e., four different laminasets) can be used in larger scale simulations, the pseudos capturing both the intrablock variability and capillary flow effects. This simulation of the representative laminasets therefore represents the first stage of a geologically-reasonable, stratal element based, scale-up procedure that has been called the *geopseudo* method. The geopseudo method is defined as the use of pseudo-properties obtained at a hierarchy of geologically-representative, stratal element scales. The mm-scale simulation is necessary to capture the significant lamina variability and capillary pressure effects of the Rannoch Formation. Simulations at larger scale cannot adequately capture either the inter-lamina variability or the flow physics of waterfloods in laminated sediments. In the next chapter, we examine the scale-up of these laminaset elements to the reservoir scale.

These mm-scale simulations could be replaced with carefully acquired experimental data on blocks the same scale as the laminaset grids (*i.e.*, representative heterogeneous samples). These experiments, however, may be expensive and beyond the capabilities of many laboratories. The geopsuedo simulations, therefore, potentially provide an error free, well controlled, numerical alternative to establishing the petrophysical properties of laminated sediments. The accuracy of these simulations will, however, depend on the quality of input data. Whilst the probe permeameter is a significant development in the characterisation of lamina, further smal scale measurement devices are required for porosity, capillary pressure and relative permeability. In addition, new pseudoisation techniques are needed to adequately describe the anisotropy of relative permeability and capillary pressure in laminated sediments for a variety of boundary conditions.

5.4 Rannoch Laminaset Two-phase Properties

The effective two-phase properties of the Rannoch laminasets have been determined by a series of numerical experiments. The low contrast laminaset showed the characteristic performance of a uniform rock. The suggests that the variability described (Cv = 0.26) is not significant. The rippled laminaset, with high variability (Cv = 1.28), showed isotropic properties dominated by the poor quality matrix leading to a high S_{or}. The high contrast laminaset and WB laminaset (Cv = 1.02 and 0.6) showed a high degree of anisotropy.

Three of the laminasets described occur within a metre interval in the Rannoch (fine grids A, B and C in Fig. 4.10). The imposition of a single relative permeability function, Pc function and S_{or} for the Rannoch Formation, when they can be seen to vary with the geological structure at such small scales, is clearly a gross oversimplification. In the next chapter the "averaging" of these results is determined by scaling-up these laminaset pseudos for metre-scale grid blocks. Clearly relative permeability curves cannot be averaged but have to be scaled-up as a function of the geology.

CHAPTER 6

SCALE-UP OF LAMINASET PROPERTIES FOR CROSS-SECTIONAL WELL MODELS

The effective properties of centimetre scale reservoir elements for the Rannoch Formation has been determined in the last chapter. In cross-sectional well models in practical field simulations, however, the grid blocks are metre to decametre scale. A further scale-up and pseudoisation stage is needed to get the effective properties of these larger grid blocks. The scale-up from laminaset to the bed scale is discussed in this chapter.

6.1 Stratal Elements and the Geopseudo Concept

As discussed in Chapter 2, the natural building blocks of sedimentary reservoirs are widely recognised to be the stratal elements: lamina, laminaset, bed and bedset (Fig. 2.2). The scale of these elements is not universally defined by geologists. Lamina, for example, are commonly defined as elements less than 1cm thick (Pettijohn *et al*, 1972, p.100), however, some consider elements up to 25cm to be laminae (Campbell, 1967). There is, however, general agreement that laminae should be texturally uniform. A better limiting length scale for the purposes of reservoir characterisation would be 5cm: laminae would then be capillary sensitive and beds not (Fig. 5.1).

In the Rannoch laminasets, there are certainly laminae that are uniform in permeability (with inferred textural uniformity) and sufficient contrasts exist between laminae to induce capillary effects at the low rates expected away from the production/injection wells. The flow effects of these laminasets are appropriately captured (Chapter 5) by numerical simulation.

In the stratal element concept of sequence stratigraphy, the laminasets aggregate in specific stacking arrangements within sand bodies. Therefore, the numerical scale-up needs to represent the aggregation of stratal elements. Simply enlarging the dimensions of the grid blocks is wholly inappropriate as it reduces the variability, induces longer correlation lengths (particularly in the vertical) and reduces the strength of the capillary pressure gradients. The correct scale-up procedure is to aggregate the cm-scale laminaset blocks (or their pseudo flow properties) in a realistic geological stacking pattern. The pseudoisation, or determination of effective flow properties, at the hierarchical scale of the stratal elements is the geopseudo approach.

6.2 Geopseudos for the Laminaset Elements

The estimation of average porosities, absolute permeabilities, pseudo relative permeabilities and pseudo capillary pressures for the represenative Rannoch laminaset elements at the centimetre scale was discussed in Chapter 5. These pseudos (Appendix IX) are the pseudo properties for the laminaset elements at this scale. The geopseudos represent the effective flow properties of a *given volume* (8 x 8 x 8cm) of the representative laminasets. If laminaset properties are required for significantly larger gridblocks, the pseudo volume must also incorporate additional laminae. Pseudos are linked to specific grid block dimensions. The laminaset block sizes are appropriate to capture lamina-driven capillary effects. If the sediment is homogeneous (*i.e.*, $Cv < 0.5$) at this scale, lamina effects are likely to be less significant. Beds, therefore, in the absence of significant lamination, will tend to have isotropic pseudo properties for cubic cells.

6.3 Geological Model for the Arrangement of Laminasets Within the Rannoch Formation

There is no outcrop of the Rannoch Formation. The laminaset and bed geometries are, therefore, not directly measurable. Outcrop analogues can, however, be used to provide laminaset and bed geometries. For the Rannoch Formation, the Oxfordian Bencliff Grit on the Dorset Coast and the Upper Cretaceous Kennilworth member in Utah have been proposed as suitable analogues. Data have been collected from the former and compared with other workers' data from the latter (discussed further in Appendix VIII). From these data, the average dimensions of HCS laminaset geometries has been determined. In the outcrop data, most of the laminasets are of similar character. The lensoid groupings of laminae are bounded by laminaset bounding surfaces.

In any single profile or core section, it is not always possible to distinguish between the order of bounding surfaces. Some bounding surfaces can have the same laminasets above and below (*i.e.*, first order). Other bounding surfaces clearly separate different laminasets (*i.e.*, second order). In core, however, where the bounding surface cannot be examined over the entire length it is impossible to be rigorous and apply a more sophisticated hierarchy of bounding surfaces consistently. In this respect, the matching of core and analogue data is not as comprehensive as the sedimentologist might be seeking.

In this work, groupings of different laminasets in the Rannoch are termed beds, consistent with the spirit of the stratal terminology. For this reason, the laminasets in the outcrops may be different in scale from the beds in the Rannoch. Whilst more work is needed, relating the petrophysical patterns between outcrop and the Rannoch, the pervasive nature of the laminasets in the outcrop support the concept of aggregation of stratal elements in the shallow marine environment.

The Rannoch laminasets described in previous chapters are grouped in beds. When the beds are not tabular, it is common to refer to these scale elements as bedforms. The bedform reflects the depositional character of the sea bed which in the case of HCS, was undulatory. A simplified representation of a 2-D section through an HCS bedform is shown in Fig. 6.1a (derived from Fig. 3.5). For the simulation at the HCS bedform scale, 8 x 8cm grid blocks were assigned laminaset geopseudos in the arrangement shown in Fig. 5.1b. An example ECLIPSE input file for bedform scale simulation is included in Appendix VIII.

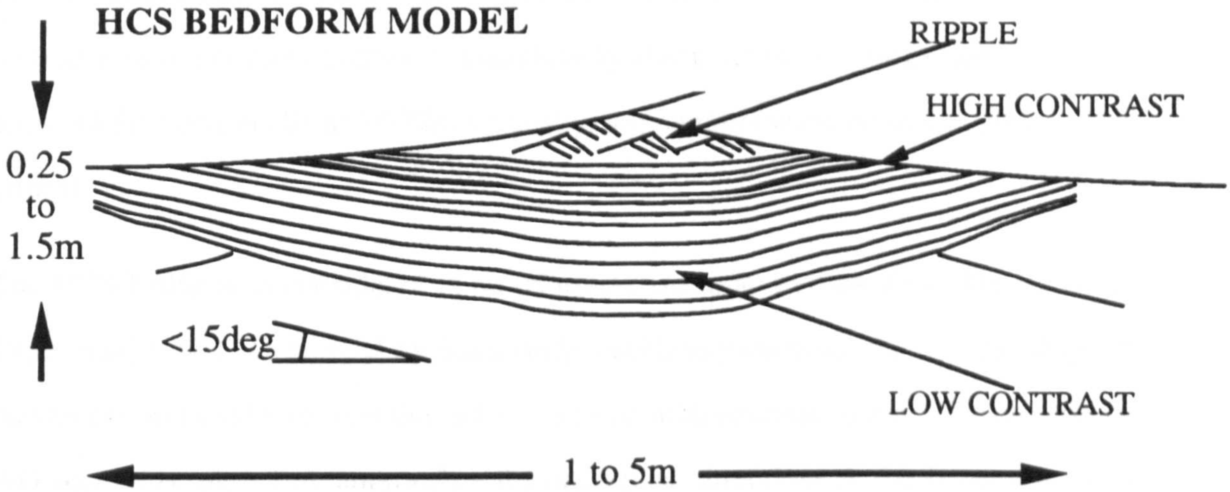

Figure 6.1a: Two-dimensional HCS bedform model showing internal arrangement of laminaset styles: ripple, high contrast and low contrast.

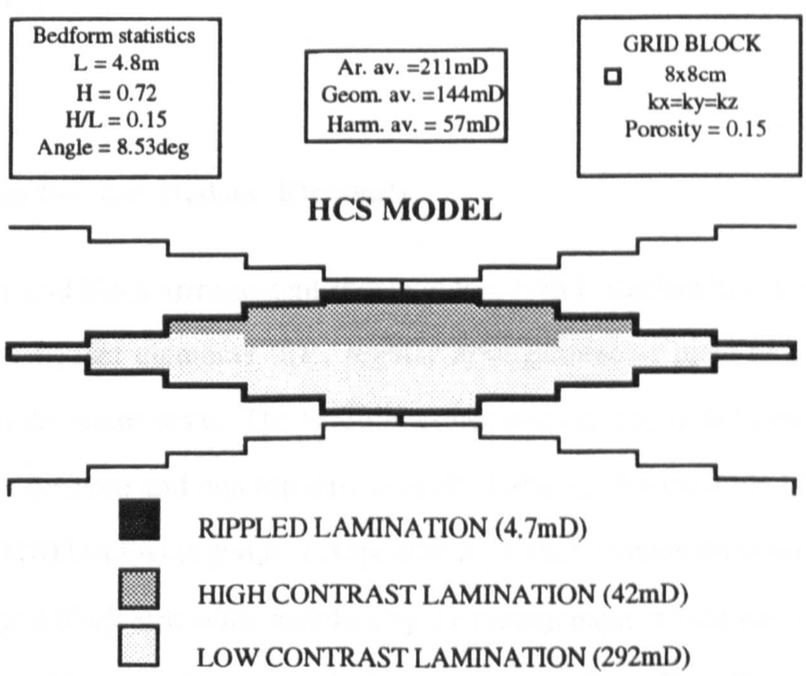

Figure 6.1b: Two-dimensional gridblock representation of HCS bedform model shown in Fig. 6.1a, embedded in similar bedforms.

The modelled HCS bedform geometry (length, 4.8m; height, 0.72m; aspect ratio 0.15) is larger than the laminaset geometry measured at outcrop (2.5, 0.2, 0.08m). In this study, a need for orthogonal grids and cubic blocks presented great limitations on the possible modelled bedform geometries. The discretised bounding surfaces in the model are a coarse simplification of the curvilinear surfaces found in nature. Further work and improved modelling techniques for the representation of such surfaces is needed before the full sensitivity to bed geometry can be explored. Providing the next scale of homogenisation or pseudoisation is significantly above the largest dimensions discussed above (4.8m horizontally and 0.72m vertically) this simplification is not thought to be too critical.

The HCS bedform is considered to be relatively isotropic in plan view (Harms *et al.*, 1975; Sun, 1990). Generated by dominantly oscillatory currents, the circular shape of hummocks and swales reflects the lack of a strong unidirectional current. This simplified 2-D section is, therefore, appropriate for orthogonal directions in the simulator. This greatly simplifies the bedform modelling as a full 3-D model is not required. This simplification would not be appropriate for a more directional bedform (*e.g.*, trough cross-bedding).

6.4 Geopseudos for Bedset Elements

The bedform grid block arrangement shown in Fig. 6.1b is stacked in a regular pattern to represent the bedset elements (*i.e.*, regular arrangement of beds or bedforms), for simulation at the metre-scale. The bedform dimensions in this model approximate those suggested by the core and outcrop data described above. An example ECLIPSE input file (HCS2D010.DATA) is given in Appendix X. Other geometries were evaluated (by altering the grid block size while maintaining the arrangement of subfacies) but the model appears reasonably insensitive to small changes in geometry. The effect of the bedform structure, when aggregated (Fig. 6.2), is to effectively layer the reservoir (relative to a uniform medium). The bedset pseudos (Fig. 6.3) reflect this anisotropy and give the appropriate two-phase permeabilities for flow parallel with and normal to the bedding direction. The anisotropy arises from 1) the bedform geometry and 2) the two-phase flow properties for the laminaset elements.

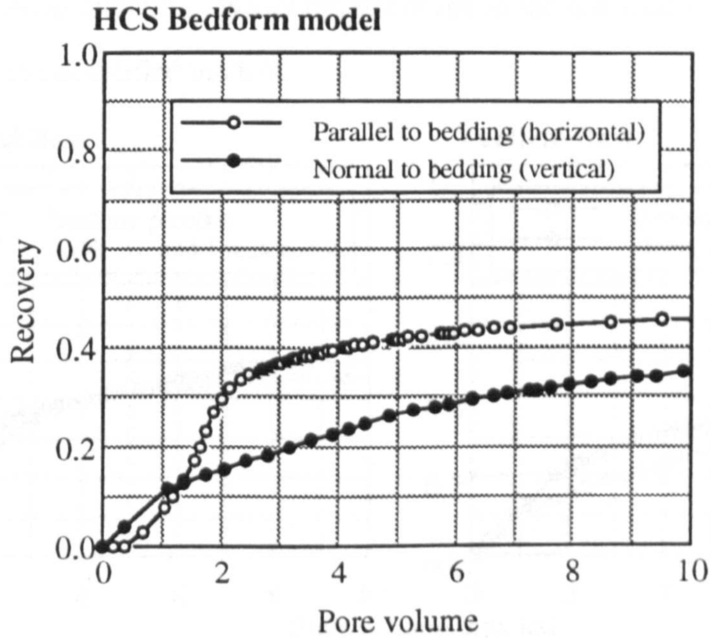

Figure 6.2: Anisotropic flow performance in Rannoch Formation HCS bedform model

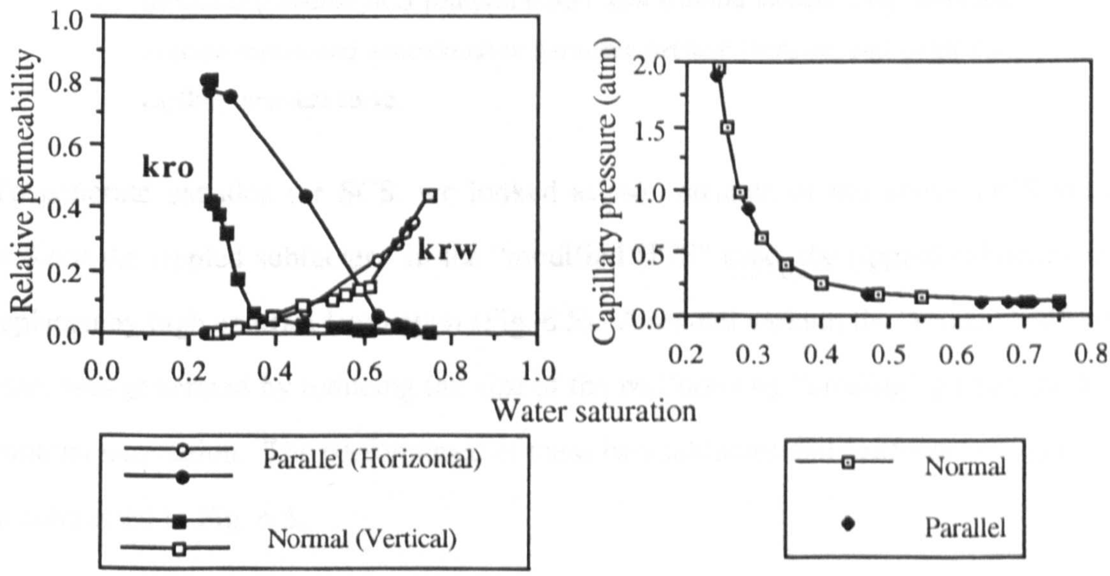

Figure 6.3: Bed-normal (vertical) and bed-parallel (horizontal) pseudo relative permeability and capillary pressure curves for the Rannoch Formation HCS bedsets.

Arithmetic or harmonic averages and the corresponding single rock curves (*i.e.*, ignoring the effects of the lamination, but maintaining the geometry) do not show a similar behaviour for two-phase flow through the model (Fig. 6.4). At 2.5 pore volumes injected, recovery is underestimated by 3% in the horizontal direction and overestimated by 10% in the vertical direction. Water breakthrough in the horizontal flood direction is slightly earlier in the simplified models.

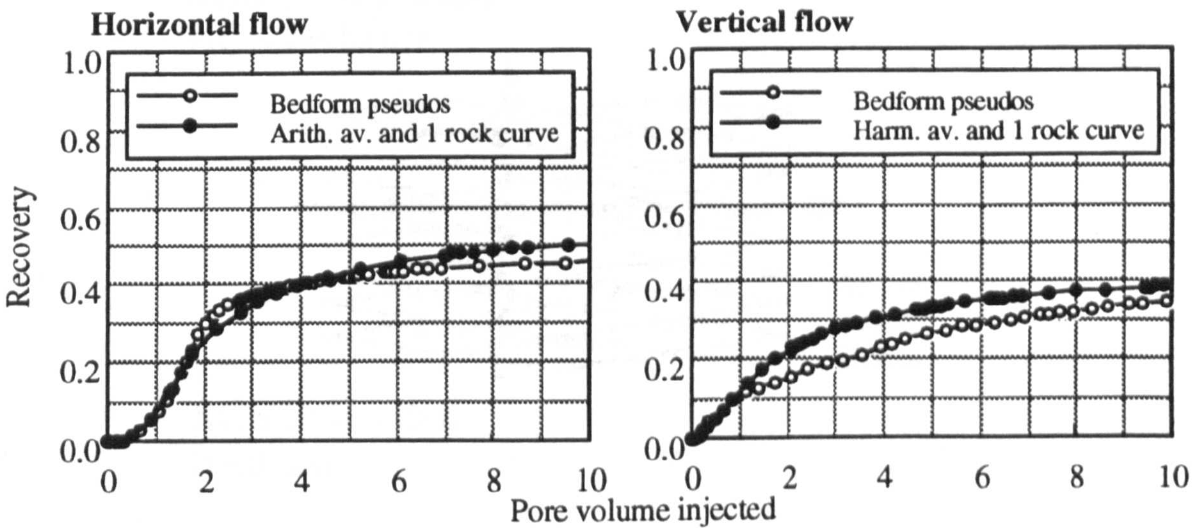

Figure 6.4: Comparison of recovery performance for the geopseudo (*i.e.*, with laminaset pseudos) HCS bedform model with uniform models using arithmetic average (horizontal waterflood) or harmonic average (vertical) and single rock capillary pressure curve.

To generate pseudos for SCS, we looked at two variants of the above HCS model without the rippled subfacies. In the "modified HCS" case, the rippled subfacies was replaced by high contrast lamination (Fig. 6.5). A second variant, the "eroded bedform" case, was generated by reducing the size of the bedforms by "eroding" part of the high contrast lamination. The performance of these two subfacies and bedform arrangements is contrasted in Fig. 6.5.

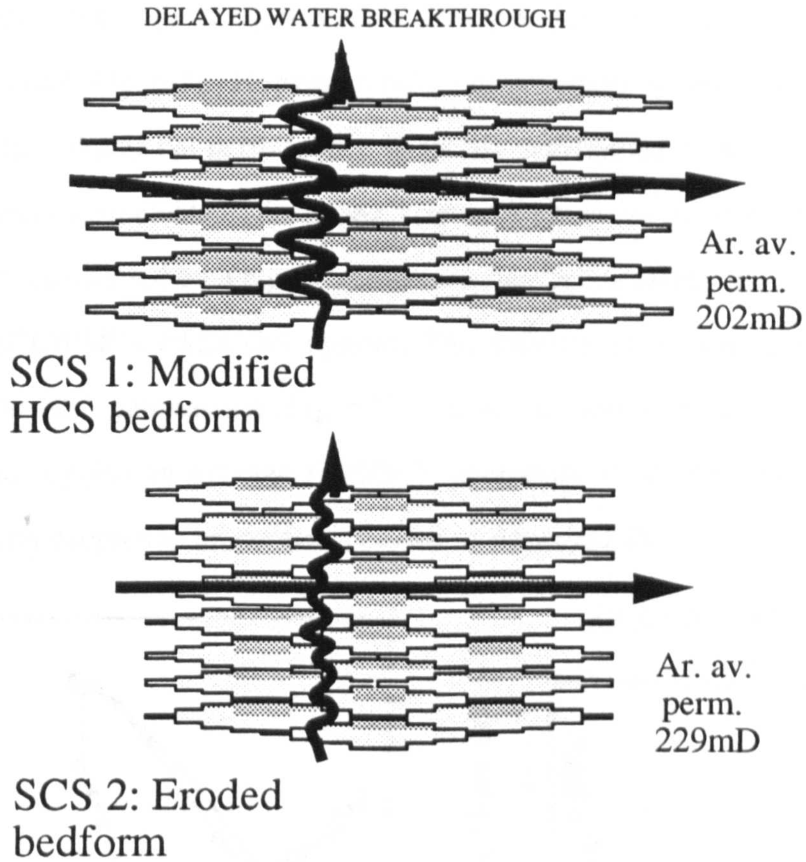

Figure 6.5: Flow through SCS stacked bedforms; modified HCS bedform and eroded SCS bedform.

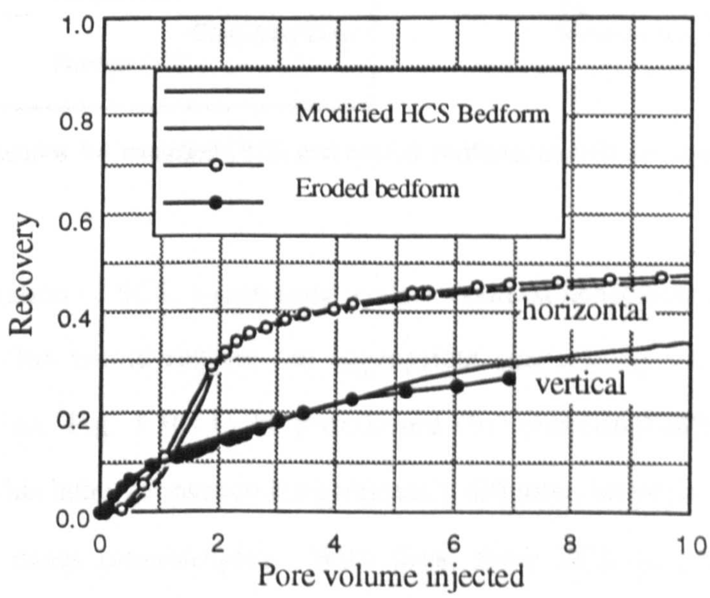

Figure 6.6: Flow performance for modified HCS and eroded bedform models of amalgamated SCS.

Recovery versus pore volume injected show similar performance for each case (and also to the HCS model, Fig. 6.3). Horizontal recovery is slightly accelerated in the eroded bedform model. Water cut performance is greatly accelerated in the eroded bedform model and this is attributable to the reduced tortuosity over the modified HCS bedform (Fig. 6.6) and represented by a higher pseudo absolute permeability (*i.e.*, the arithmetic average in ECLIPSE's *PSEUDO* option). The differences in flow perfomance are captured in the SCS geopseudos (Fig. 6.7). These are similar to the HCS geopseudo (Fig. 6.3) and suggest an average HCS/SCS geopseudo could be adopted for these facies. Bedform geopseudo properties are listed in Appendix IX.

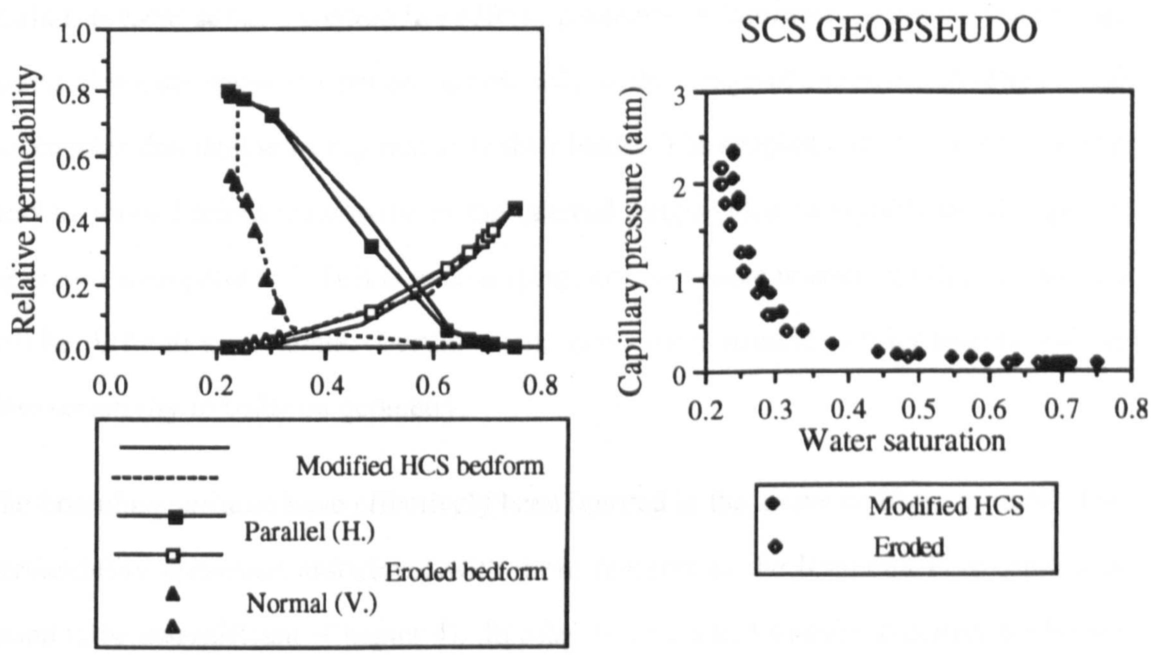

Figure 6.7: Geopseudos for modified HCS, and eroded bedform, models for amalgamated SCS bedforms.

A third representation of SCS, where only the low contrast lamination is preserved, can be envisaged. This would require the appropriate subfacies geopseudo (low mica contrast lamination, Fig. 5.10) to be pseudoised (for numerical effects only) at the bedform scale. This latter geopseudo is significantly different (isotropic) when compared with other SCS cases (anisotropic). With these three SCS geopseudos, the flow performance across the transition from HCS to amalgamated SCS can be correctly represented in the cross-sectional well model.

6.5 Discussion of Bed Scale Simulations

In the above bedform model, many assumptions and simplifications have had to be made, due to the lack of Rannoch outcrop, differences between average shoreface laminaset and Rannoch assumed bedform geometries, model bedform dimensions, the requirement for orthogonal grid blocks, and the very regular stacking pattern resulting in a very simplified geological model. This variability could be captured by further stochastic simulations, and assigning variable geopseudos to a regular grid block framework. These pseudos could represent subtle variation in bedform geometry or laminaset patterns. In outcrop, stratal elements show variability (albeit only in the range of metres) and lengths and thicknesses that tend to be log-normally distributed. The simplistic models studied above tend to show limited sensitivity in the derived geopseudos to significant changes in laminaset arrangement. This is encouraging, because more realistic geological models will be difficult to simulate. Further work, however is needed to fully understand the flow sensitivity to bedform geometry.

The bounding surfaces have effectively been ignored in the above bedform models. The permeability reduction associated with these features in the Rannoch Formation was found to be insignificant (Chapter 4). In other formations, however, this may not be the case. Correct representation of these features, however, in relatively coarse models will require further study.

The regular bedform patterns observed in the permeability profiles in certain Rannoch intervals (Fig. 4.11b) suggest that more tabular beds may develop in certain Rannoch intervals. Tabular beds are a feature of the Kennilworth shorface unit (Brenchley *et al.*, 1992) and may also be present in the Rannoch. Tabular beds will further emphasise the layered nature of the Rannoch Formation indicated by the stacked bedform model presented above.

CHAPTER 7

CROSS-SECTIONAL SIMULATION STUDY OF THE RANNOCH

The objective of this chapter is to apply the geopseudos for the HCS, SCS and WB bedforms in a field scale cross-sectional model. The upscaling approach that is presented in this study involves numerical simulation at additional smaller scales. This is potentially time consuming and, therefore, engineers need to know the impact of the small scale geology in the field scale models. This understanding will allow field simulation practitioners to assess the relative importance of the small scale petrophysics to waterflood field performance.

The objective in this chapter is to apply the upscaling approach discussed previously in this work - the geopseudo method - to the large scale modelling of waterflooding in the Rannoch in the three fields. The petrophysical data discussed in previous chapters comes from the Thistle and Statfjord Fields. In this section the effective properties are applied in those fields and another where the Rannoch is depositionaly the same but has petrophysical (poroperm) differences. In this way, the transportability of the geopseudo method can be appraised.

The geopseudo properties generated in the previous chapter have been generated for a specific suite of input parameters:

- an absolute permeability and related range of capillary curves
- an assumed wettability
- a single grid block dimension

For the pseudo properties to be transported for a different range of conditions, careful consideration to each of these parameters must be given. Petrophysical differences, most importantly differences in the level and contrast of lamina permeabilities, will result in different capillary effects. In this study, these effects have not been systematically determined for the various laminaset and bedform geometries. This work will need to be done in any further field-specific studies. Whilst wettability differences may exist between fields, this work assumes these to be constant in the studied fields in the lack of any data to suggest otherwise. The fields studied require different sized grid blocks in the cross-sectional models, because of significant size differences between fields. These, numerical, differences have been accounted for in this work.

The cross-sectional well models aim to show how the use of geologically-realistic relative permeability curves can give significantly different water cut and recovery predictions over commonly used rock curves. Relative permeability curves are the measure of the two-phase flow properties of rock and are therefore logically dependent on geological structure. This structure needs to be captured, either by numerical simulation following the method presented here, or by careful experimental work. The selection of the correct relative permeability curve is a crucial factor in building a geologically-realistic reservoir simulation model.

This study attempts to show, however, that deterministic modelling at the natural scale lengths present in sediments (geopseudo method) gives a more geologically-realistic solution to the overall field performance. The construction of a more geologically appropriate simulation model from such an approach does, of course, require additional levels of data and simulation calculation. These additional data come from (a) the detailed reservoir description provided by the probe permeameter and (b) ancillary knowledge of the sedimentary architecture. The predictions of such a model should, therefore, be treated with more confidence by both geoscientists and engineers alike.

7.1 Variability of the Rannoch in North Sea Fields

The Rannoch Formation is an important oil bearing reservoir unit in many North Sea fields. In this study, three fields across the basin where the Rannoch is a major producing interval have been studied, namely, Cormorant, Thistle and Statfjord, the locations of which are shown in Fig. 7.1.

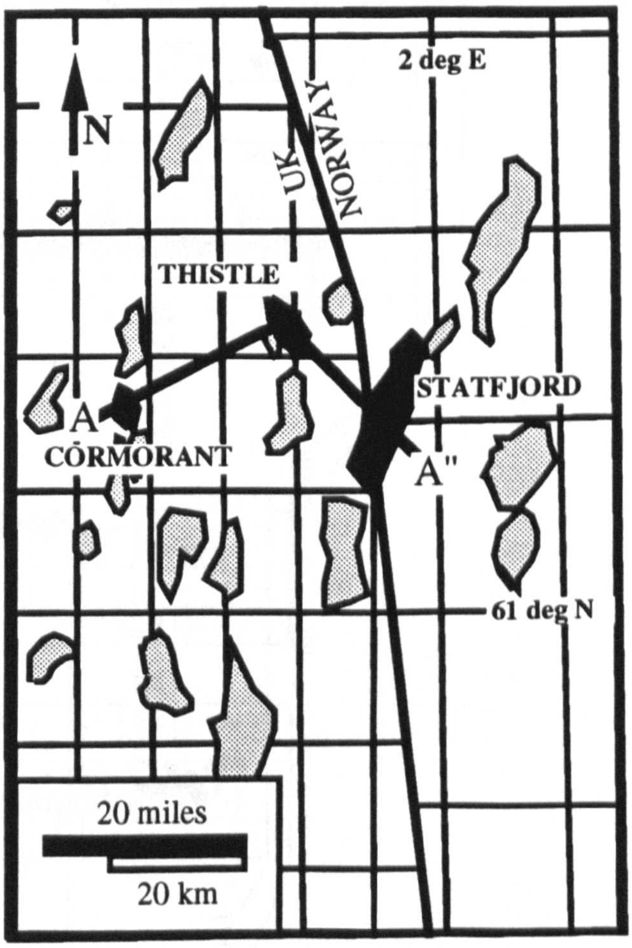

Figure 7.1: Location map of North Sea Rannoch-producing fields discussed in this chapter

There is a regional improvement in Rannoch reservoir quality from Cormorant in the west to Statfjord in the east as indicated by the poroperm differences shown in Fig. 7.2. This improvement arises as a result of reduced compaction due to shallower burial and increased overpressuring towards the axis of the basin. The depositional setting of the Rannoch is thought to be reasonably consistent in the three fields. The Rannoch shoreface is a regionally mappable, continuous unit (Mitchener *et al.*, 1992) overlain by the Etive barrier system. The Broom Formation which underlies the Rannoch, however, is part of a different depositional system (Mitchener *et al.*, 1992) and shows a dramatic thining from west to east.

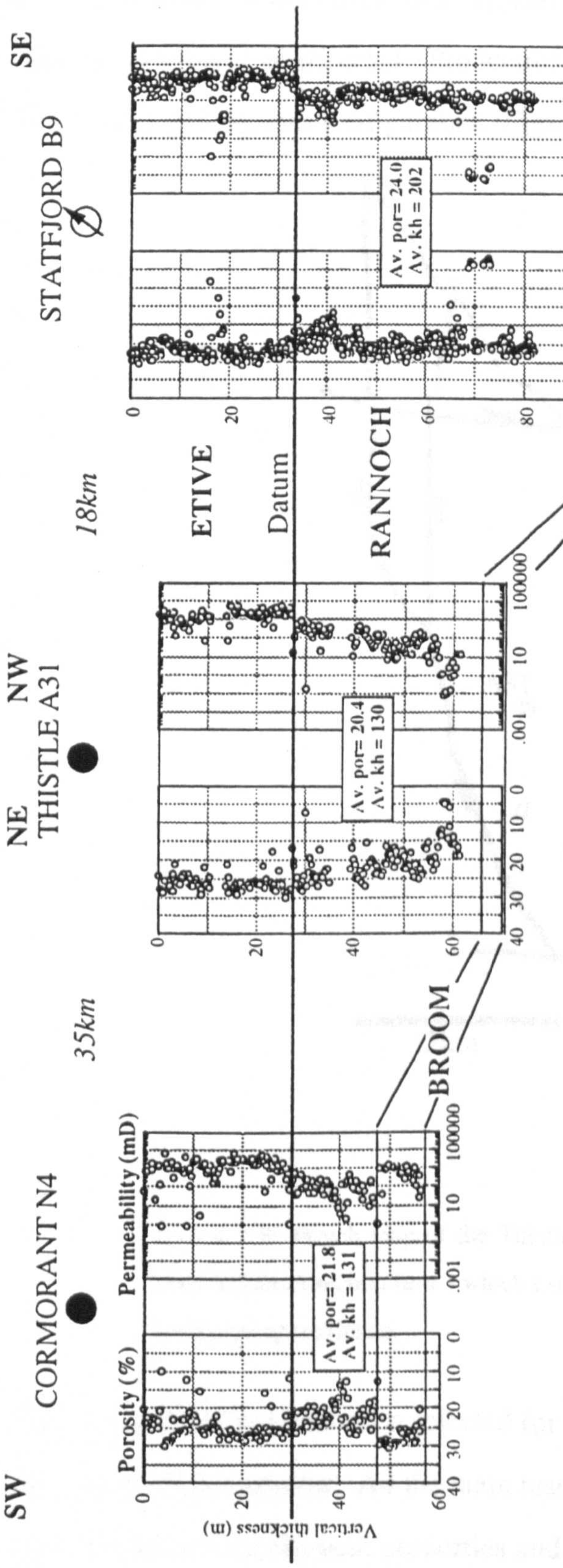

Figure 7.2: Cross-section through lower Brent Group in the northern North Sea showing the west to east thickening and poroperm improvement in the Rannoch reservoir. (Refer to Fig. 7.1 for location of section).

7.2 Cross-Sectional Well Modelling in Thistle Field (Operator: BP Exploration)

To examine the waterflooding at the interwell (megascopic; Haldorsen, 1986) scale, a 2-D cross sectional model based on a "typical producer" well in Thistle Field (Bayat and Tehrani, 1985) was constructed. Production data from Thistle A33 were modelled in a simple producer-injector configuration (Figs. 7.3 and 7.4).

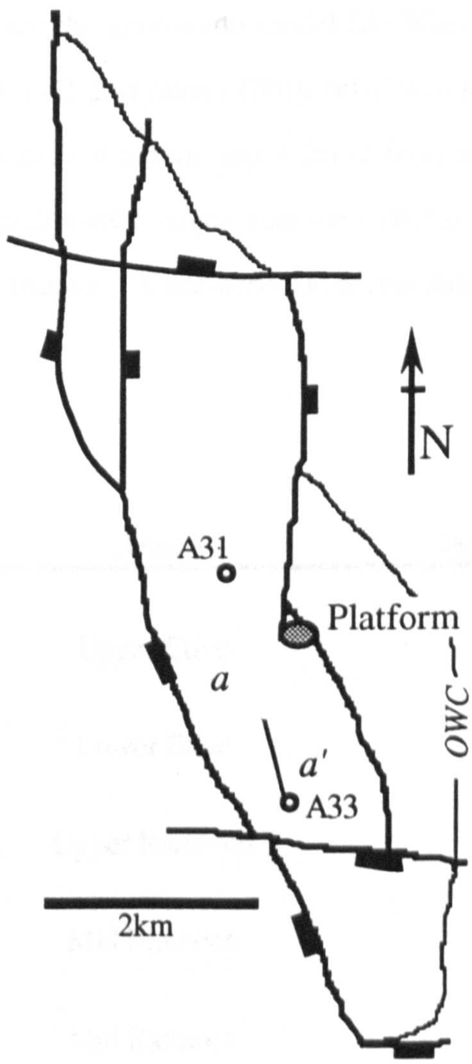

Figure 7.3: Sketch map of the Thistle Field showing locations of wells and modelled cross section (*a-a'*) which extends 585m from well A33 towards A31. Scale only approximate.

This arrangement had also been selected for a cross-sectional well model in an internal study by the field operator. All the main reservoir, numerical and scheduling data (*e.g.*, grid, formation petrophysical properties and completions) in the operator's study have been replicated in this study. Only the relative permeability and capillary pressure curves were changed, the rock curves being substituted with the bedform geopseudos in our work. The traditional modelling approach of the operator follows standard industry practice for the Rannoch Formation (Thomas and Bibby, 1991); this principally involves altering the transmissibility multipliers between gridblocks to match the watercut performance.

The ECLIPSE input file for the geopseudo model (A33GEOP2.DATA) is included in Appendix VIII. A 48 x 1 x 42 grid model (2016 cells) was built with a Rannoch block size of 12.2m (40 feet) in the x-direction and 1.5m (5 feet) in the z-direction (Fig. 7.4). The grid block size is significantly larger than the dimensions of the stratal elements discussed in the previous chapter. "Core-derived" permeability values were assigned as follows (Table 7.1):

Layer	Unit	Permeability (mD)
1	Upper Etive	1500
2	Lower Etive	3000
3-12	Upper Rannoch	270
13-22	Mid Rannoch	200
23-32	Mid Rannoch	50
33-42	Lower Rannoch	20

Table 7.1: Thistle model layer permeabilities. Layers 1 & 2 are 10.7m (35 feet) in the z-direction.

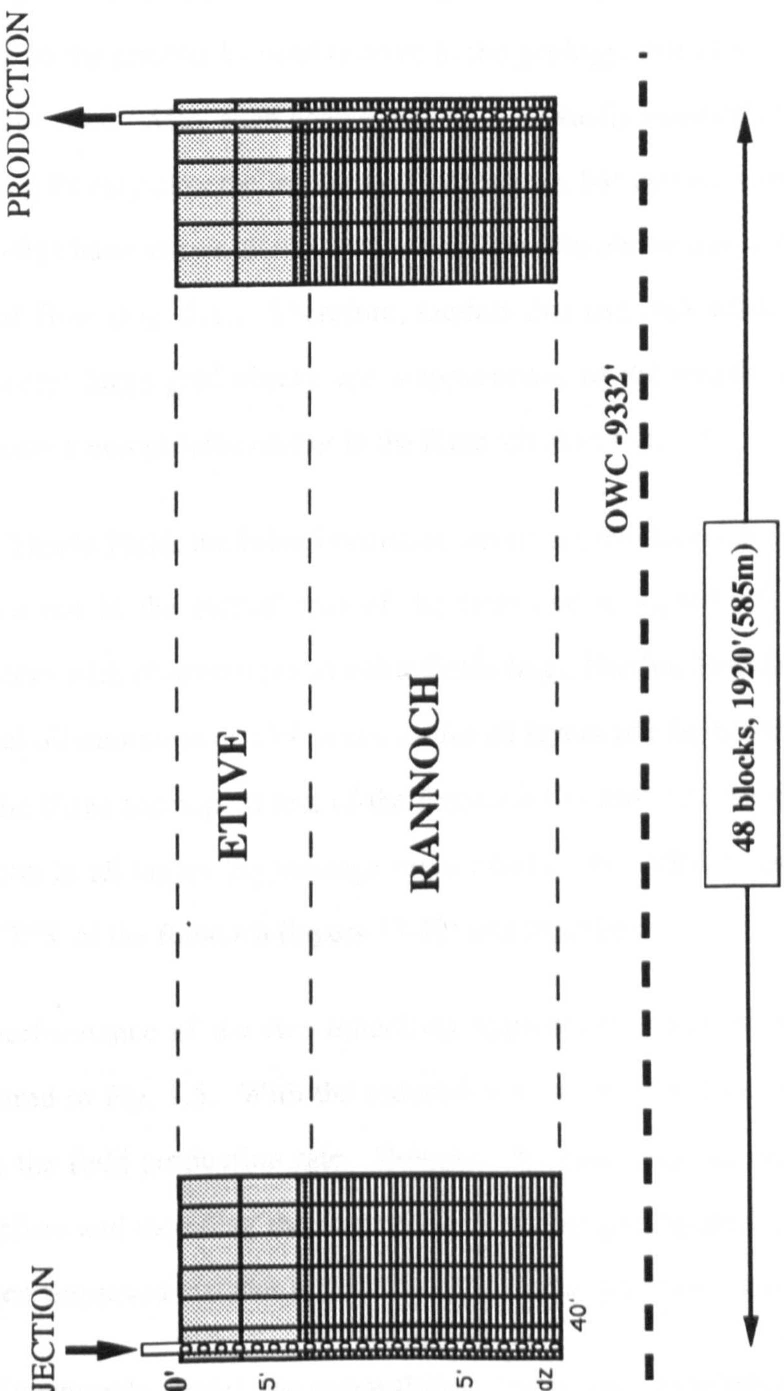

Figure 7.4: Thistle Field cross-sectional well model.

Traditional engineering practice is to employ rock relative permeabilities at this scale since such a grid is usually considered as being sufficiently "fine". It is likely, however, given the size of the gridblocks used relative to the geology, that some form of pseudo curves should be used. Also, such coarse models, are usually insensitive to capillary pressure; changing Pc may alter the in-place oil saturations, but will not impact flow. Ringrose *et al.*, (1991) have shown that 5 feet is considerably above the scale length at which Pc impacts flow (Fig. 5.1). Therefore, models that use rock relative permeabilities and (relatively) large grid blocks are inappropriate to the length scales at which some significant heterogeneities occur in the Rannoch reservoir.

In the Thistle Field, the Etive Formation overlying the Rannoch is thought to be largely watered-out in the central part of the field due to significant production. This is consistent with observations in other fields (*e.g.*, Dunlin, Braithwaite *et al.*, 1989). A residual oil saturation of 25% was used for all layers and the model initialised, therefore, with the Etive and top 10 feet of the Rannoch flooded (*i.e.*, Sw = 75% for layers 1-4). Injection in all layers (by voidage replacement) controlled by production through the lower 75% of the Rannoch (layers 13-42) was modelled.

The performance of the two modelling approaches - traditional and geopseudo - is compared in Fig. 7.5. With the reduced transmissibility data, the model is unable to match the field production rate. However, by removing the imposed transmissibility multipliers and including the appropriate bedform geopseudos, whilst making no other changes, improved matches to production and water cuts were achieved.

In the geopseudo model, the permeabilities in the top 3m of the Rannoch were reduced from 270 to 150mD, recognising the inadequate sampling by core plugs and reduced probe measurements. This was the case in well Thistle A31 (Fig. 4.11c), however, the same critical interval in Thistle A33 had been "preserved" for special core analysis and no routine core analysis carried out.

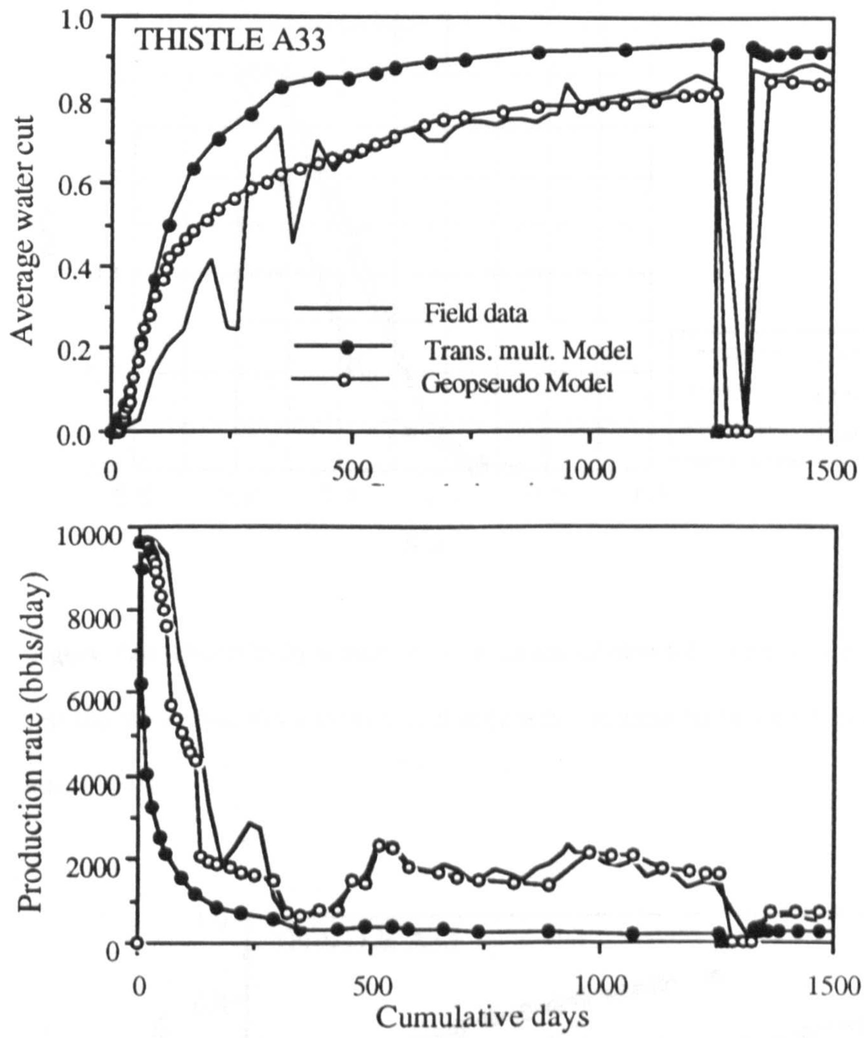

Figure 7.5: Comparisons of model water cuts and production rates. Differences at 250 days are due to a scale treatment which was not explicitly modelled.

A comparison was also made with the rock relative permeability curves, correctly scaled for numerical effects (Fig. 7.6) but without the geologically-induced anisotropy. The water-cut match of the uniform scaled-up model is also bettered by the geopseudo model (Fig. 7.7).

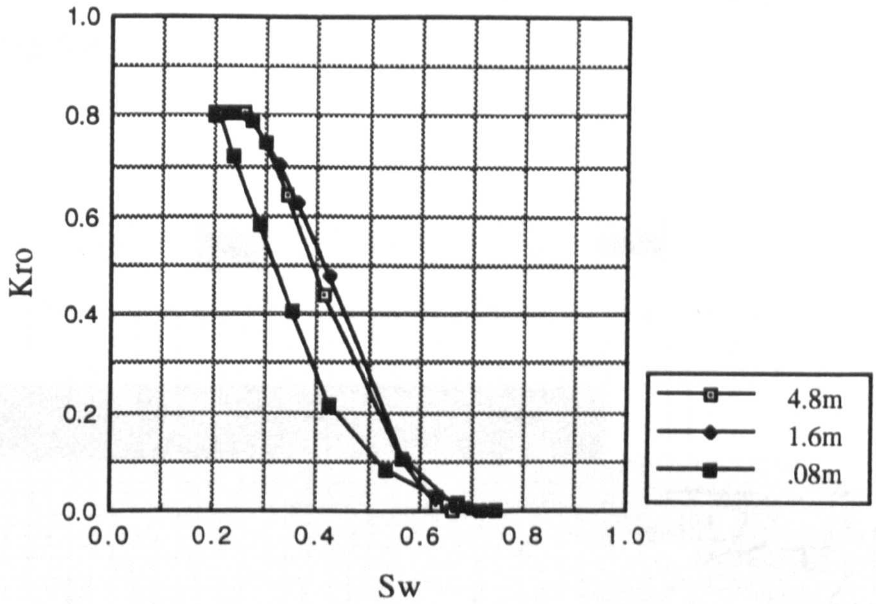

Figure 7.6: Numerically scaled kro rock curves suitable for a 8cm square grid cell and for horizontally and vertical directions in a rectangular (4.8 x 1.6m) grid block.

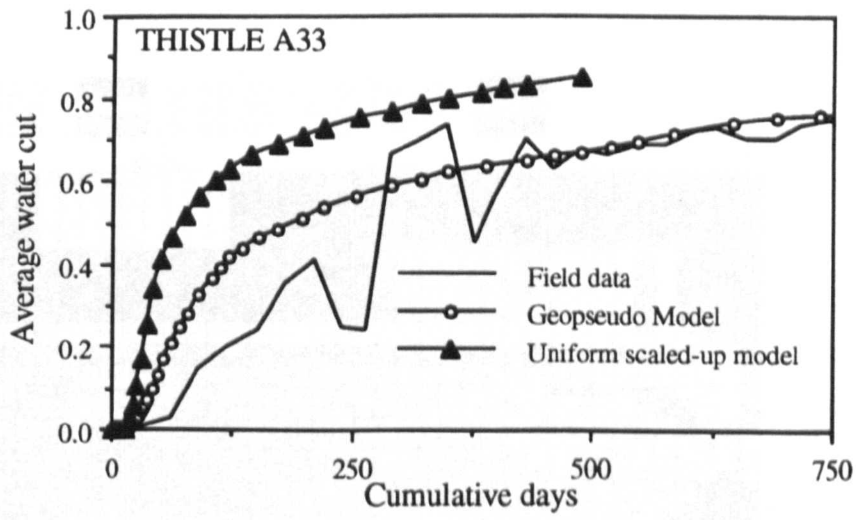

Figure 7.7: Comparison of water cut performance for correctly scaled-up rock curves.

Whilst the geopseudo model is seen to be an improvement, in that water cut and production rates can be more easily matched with the geological description included, there is still room for improvement in the early (up to 250 days) water cut and rate behaviour. The distribution of water saturations predicted by the geopseudo model can be seen in Fig. 7.8.

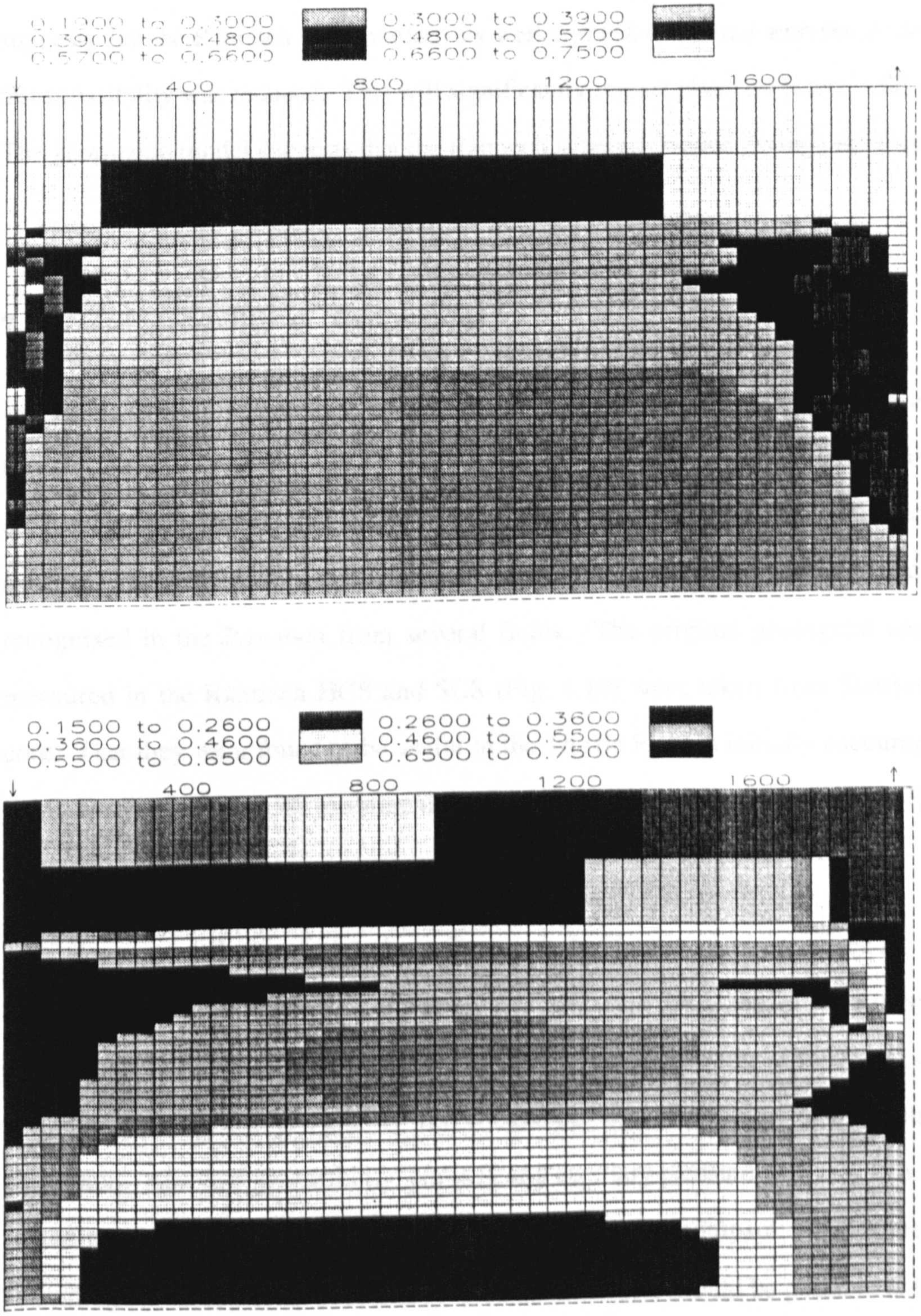

Figure 7.8: Thistle Field cross sectional model saturation distributions; **top**, after 290 days; **lower**, after 1472 days.

In this model, the oil displaced from the Rannoch into the Etive resaturates the latter with time in the region of the producing well. This is not thought to happen in reality as the oil moves updip away from the producing well location. This trapping of oil in the Etive leads to spurious reduced water cuts late in the model life. The geopseudo model also suggests that the Rannoch will be relatively well drained, compared with the model where transmissibility was reduced. This will significantly impact plans for future infill drilling. The geopseudo model suggests that the Rannoch is being drained through the Etive.

7.3 Transportability of Geopseudos

For the Rannoch geopseudos generated in this study to be widely useful, some degree of transportability between fields within the same depositional unit needs to be demonstrated. This is also important for the broader application of the geopseudo method. The sedimentary structures at the small scale (i.e., HCS, SCS, WB) have been recognised in the Rannoch from several fields. The original geological laminasets measured in the Rannoch HCS and SCS (Fig. 4.10) were taken from Statfjord Field core. That they were found to be useful in the Thistle Field is initially encouraging. In the following sections, we examine the performance of geopseudos in the Statfjord and Cormorant Fields.

The flow parameters of the three Rannoch bedforms (*i.e.*, geopseudo relative permeability) are characteristic of a geological structure for a certain scale of simulator grid block. They not only incorporate the effect of the small scale sedimentary structure and the viscous/capillary/gravity force balance, but also the effects of numerical dispersion. Absolute permeability, porosity and capillary pressure will vary as a function of the mean pore throat size since they are sensitive to compaction, diagenesis, etc. Providing variations in the pore sizes can be quantified, it should be possible to transport the Rannoch geopseudos from field to field allowing for changes in grid block scale. Regional compaction trends are present in the Rannoch Fields (Fig. 7.2) and the performance of the geopseudos in matching field data in the Statfjord and Cormorant Fields is evaluated below.

7.3.1 Statfjord Field (Operator: Statoil)

The Statfjord Field (Kirk, 1980; Buza and Unneberg, 1987; Roberts *et al.*, 1987) lies 18km south-east of the Thistle Field and straddles the UK/Norway median line (Fig. 7.1). The north-westerly flank of the NE-SW tilted fault block is structurally simple as shown in Fig. 7.9. This flank of the field, provides an ideal area for examining the component of the waterflood performance which is primarily depositionally controlled. In this area of the field, the movement of the waterflood front between down dip water injector and up dip oil producer has been monitored by observation wells located in the area between them (Fig. 7.8).

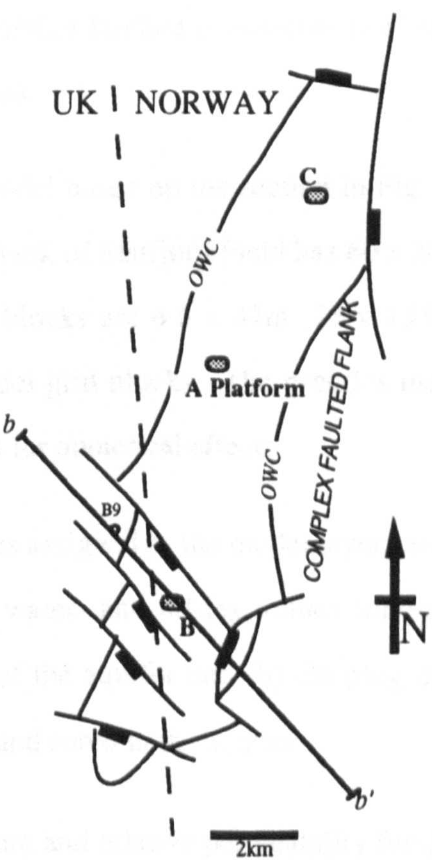

Figure 7.9: Simplified sketch map of the Statfjord Field. Scale approximate. Location of studied well (B9) shown and line of section *b-b'*.

These observation wells are the water injection wells to the underlying Statfjord Formation (Triassic), which can be periodically used for monitoring water saturations in the Rannoch-Etive section by cased hole electric logs. The western flank of Statfjord, therefore, provides an excellent opportunity for the testing of models of the Etive/Rannoch displacement mechanism.

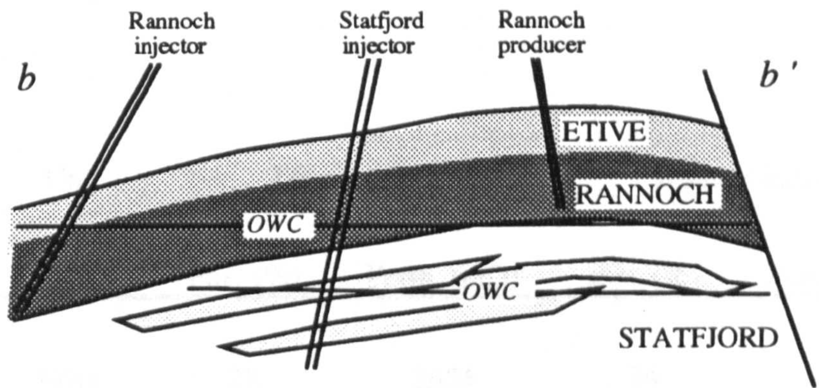

Figure 7.10: Simplified Statfjord cross-section (*b-b'* in Fig. 7.9) showing geometry of wells on the w. flank

The 2-D cross-sectional model based on the section in Fig. 7.10 is shown in Fig. 7.11. The model of the western flank of Statfjord Field has 60 x 20 x 20 cells in the x, y and z directions. Rannoch grid blocks are 4.6 x 47m (15 x 155ft) and are therefore much larger than the Thistle model grid blocks. The pseudos used in this model, therefore, have to be scaled to account for numerical effects.

The petrophysical properties assigned to the model layers are shown in Table 7.2. Note that (a) the differences in water- and oil-leg values follow the operator's model and represent reduced quality of the aquifer and (b) the plug data in Fig. 7.2 comes from water injection well drilled and cored in the aquifer.

The pseudo capillary pressure and relative permeability for the various bed types (HCS, SCS and WB) have to be determined for the larger scale grid blocks (Fig. 7.12). The anisotropy is enhanced as the scale of grid block increases. This is consistent with the observed scale dependency of k_v/k_h (Fig. 4.18). It is noticeable that the permeabilities within the field are significantly higher than those for which the geopseudos were determined. It is expected, therefore, that the Swc will be too high in the Statfjord oil zone. Obviously the input rock Pc curves can be changed, however, in this initial study we wish to compare the performance of the *same* geopseudos, accounting only for grid block scale changes. The input file for the Statfjord Field simulations (STAT001.DATA) can be found in Appendix X.

Layer	Unit	Oil column		Water column	
		Por. (%)	Perm. (mD)	Por. (%)	Perm. (mD)
1	Etive	28	2654	24	454
2,3	Etive	31	6766	26	831
4,5,6	Etive	30	4548	26	736
7	Rannoch	28	590	27	419
8	Rannoch	30	1551	27	685
9,10,11	Rannoch	32	2446	27	384
12	Rannoch	33	3330	28	659
13-17	Rannoch	30	1551	27	685
18	Rannoch	28	1259	23	106
19, 20	Rannoch	22	36	21	25

Table 7.2: Statfjord model layer permeabilities. (Refer to Fig. 7.11)

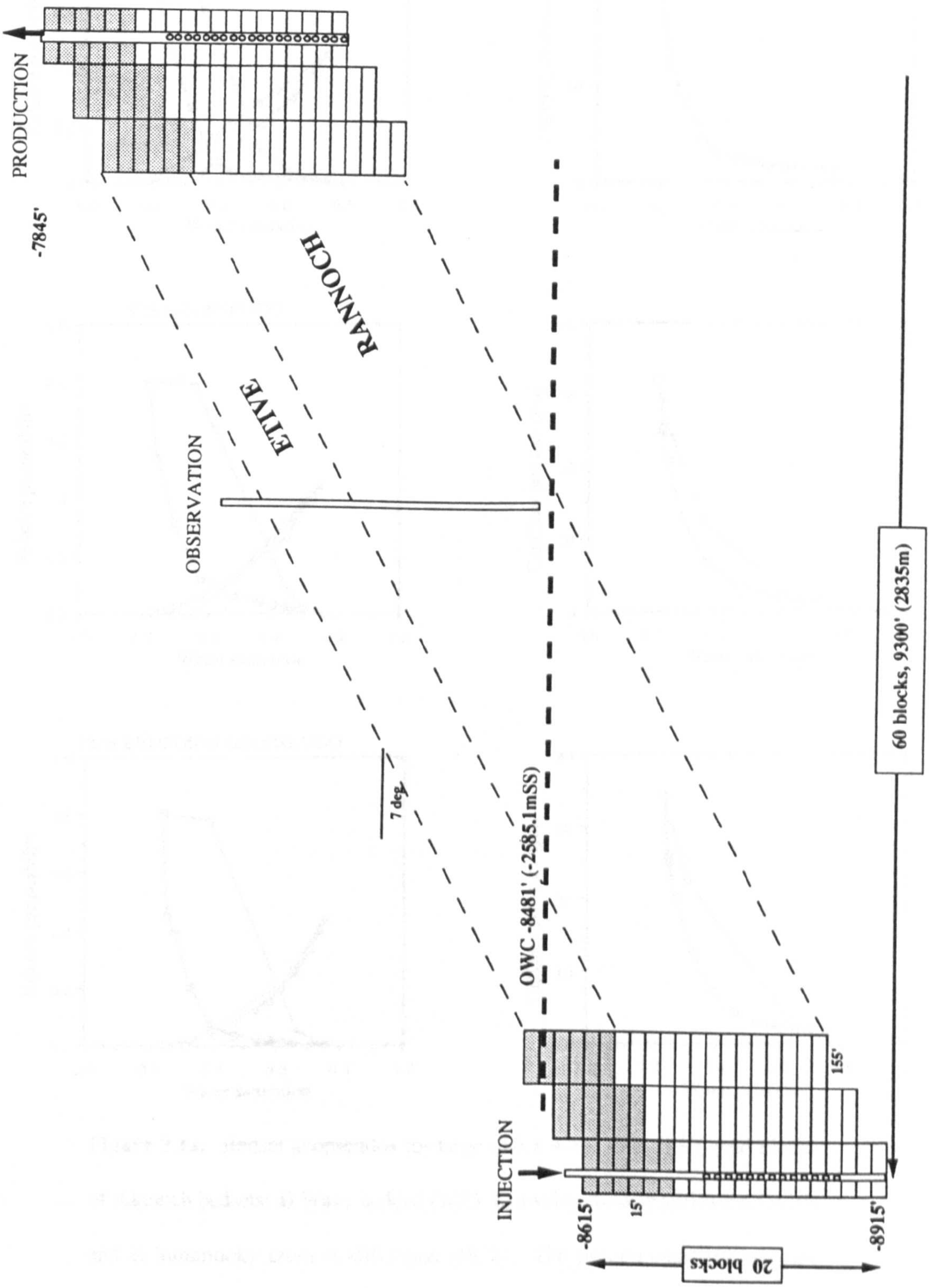

Figure 7.11: Statfjord cross-sectional well model. (Refer to Fig. 7.10 for location of section).

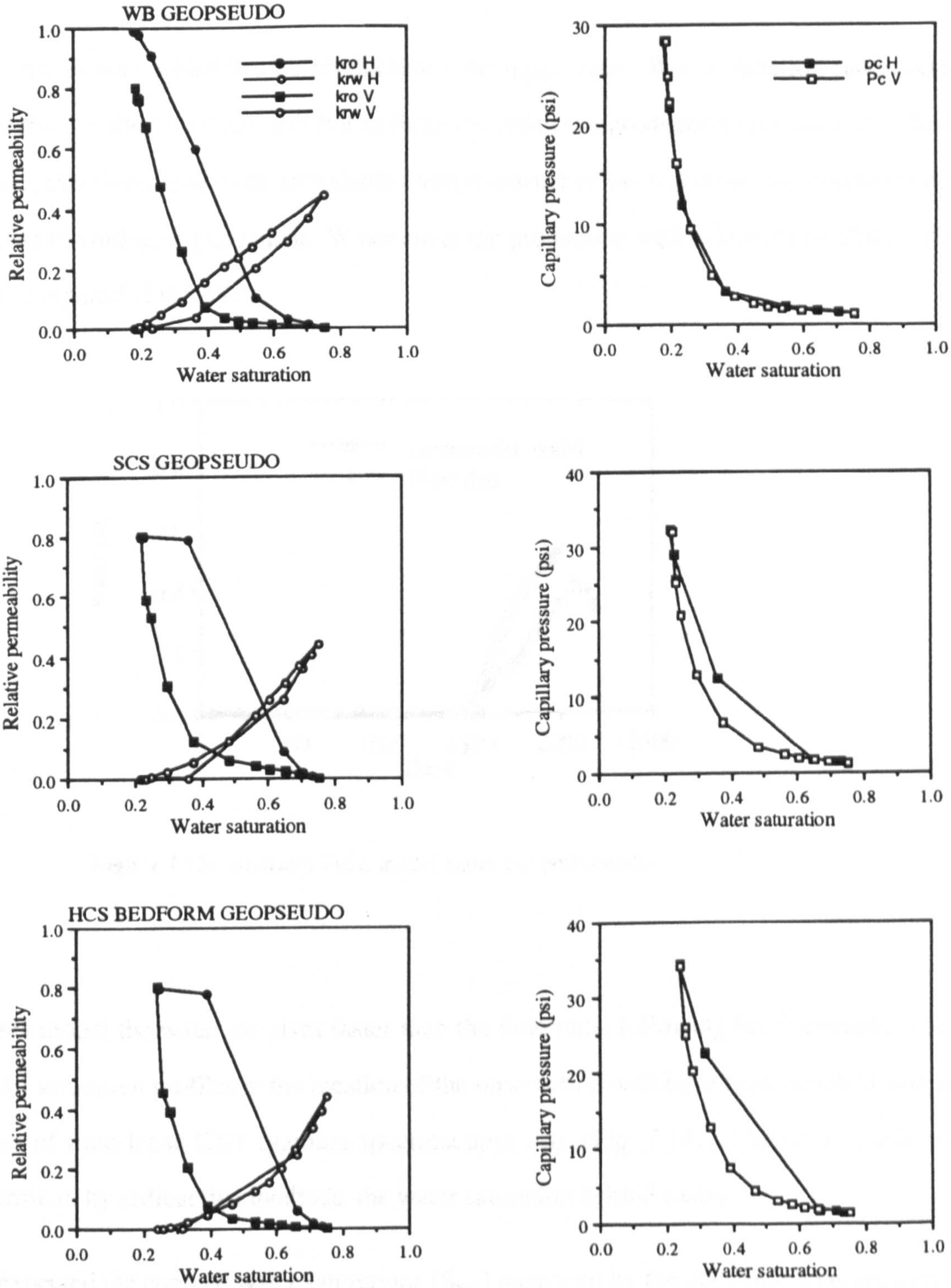

Figure 7.12: Bedset geopseudos for large (4.6 x 47m, 15 x 155ft) grid blocks of Rannoch bedsets: **a)** Wavy bedded (WB); **b)** swaley cross stratification (SCS); and **c)** hummocky cross stratification (HCS). The pseudo capillary pressure curves for HCS and SCS suggest anisotropic capillary pressure curves. This is not nescessarily physical but a possible function of pseudo block aspect ratio. Pseudo capillary pressure curves require additional work but at this scale the effects of Pc in the model are negligible.

The model was controlled by production total liquid rate. Water injection rates were available for the down dip well but as these exceeded the production rate and if matched would, therefore, lead to an unrealistic overpressuring of the reservoir, the injection rate was set to voidage replacement. Water cut at the production well following breakthrough was compared (Fig. 7.13).

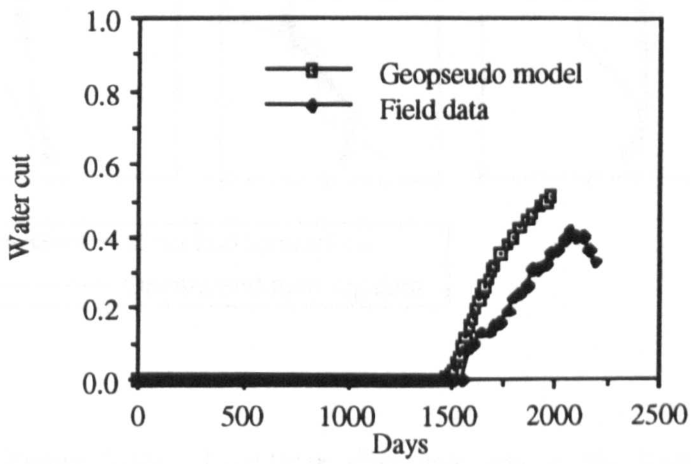

Figure 7.13: Statfjord Field model water cut performance

In this model the water cut rises faster than the field data, following breakthrough. The model saturation profiles at the location of the observation well have been matched with a series of time-lapse GST (gamma spectroscopy) logs (Fig. 7.14). The GST is able to determine, by radioactive methods, the water saturation behind casing.

As expected the connate water saturations (S_{wc}) measured by the open hole logs are over-estimated by the model saturations because of the (Thistle) Pc curves used in the Etive and Rannoch sections. The higher permeability of the Rannoch oil column in Statfjord Field would be associated with Pc curves with lower S_{wc}.

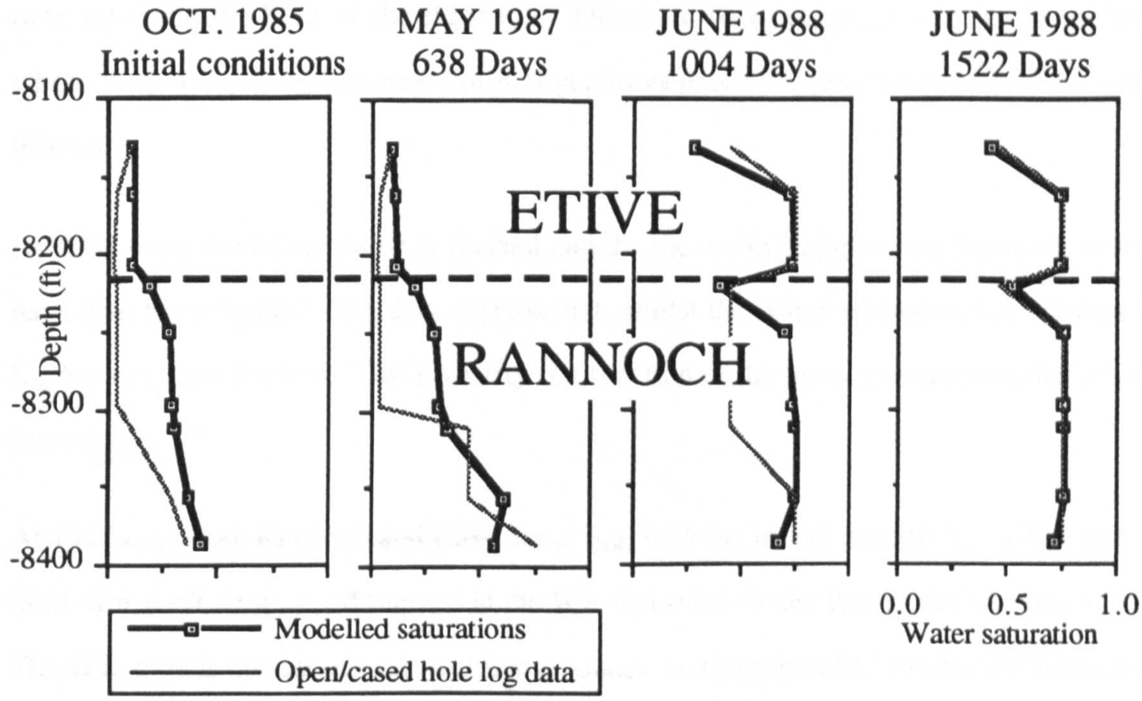

Figure 7.14: Time-lapse saturation logs in the Rannoch Formation, compared with modelled saturations (refer to Fig. 7.11 for location of observation well.

Bearing in mind these differences in original S_{wc}, we can concentrate on the changes in water stauration that occur with time in the field data and the model. At 638 days, the saturation changes in model and field data are limited to the lower part of the Rannoch. At 1004 days, however, the Etive has watered-out. This match between model and field data is to be expected, as the breakthrough time at the well has been matched (Fig. 7.13) by altering the model y dimensions. If the breakthrough time has been matched, the passage of the water front through the Etive has also been determined by the selected model size. In other words, this match says nothing about the quality of the model.

The Rannoch in the model at 638 days shows greater increase in Sw than seen in field data in the upper part. In the lower part of the Rannoch, however, the model shows an appropriate reduction in Sw at 638 days. The field data support the model that water is running along the base of the Rannoch. This is to be expected in the Statfjord Field running along the base of the Rannoch. This is to be expected in the Statfjord Field where the good quality Rannoch Formation allows gravity to play a part in sweeping the Rannoch.

At 1004 days, the Etive has been flushed and the the model suggests the Rannoch would have also been flushed. The data suggest that, whilst the water saturation has increased, S_{or} has not been reached. This disparity is a function of the initial conditions selected for this model.

At 1522 days both Rannoch and Etive are at S_{or}, with the model pseudo S_{or} matching the field data, including the oil trapped in the WB facies below the Rannoch/Etive boundary. The WB zone is not completed in either producer or injector wells. Production from this unit is, therefore, limited to vertical flooding as water moves across the Rannoch\Etive boundary. The high permeability contrasts seen in the WB facies are expected to trap oil within the laminae. These Statfjord data suggest that lamina-trapping of oil by capillary forces can occur at the field-scale. Because the WB unit here is thin, however, the trapped oil in this facies is a relatively insignificant percentage in the field.

Both model and field data suggest that the Rannoch oil is displaced from the base upwards and that the flood front passes though the Etive and Rannoch in fairly close succession. In the Rannoch, however, the small scale capillary forces, accurately represented in the upscaled geopseudo model, delay the under-running of the water as can be seen in Fig. 7.15a (*c.f.* Fig. 7.15b).

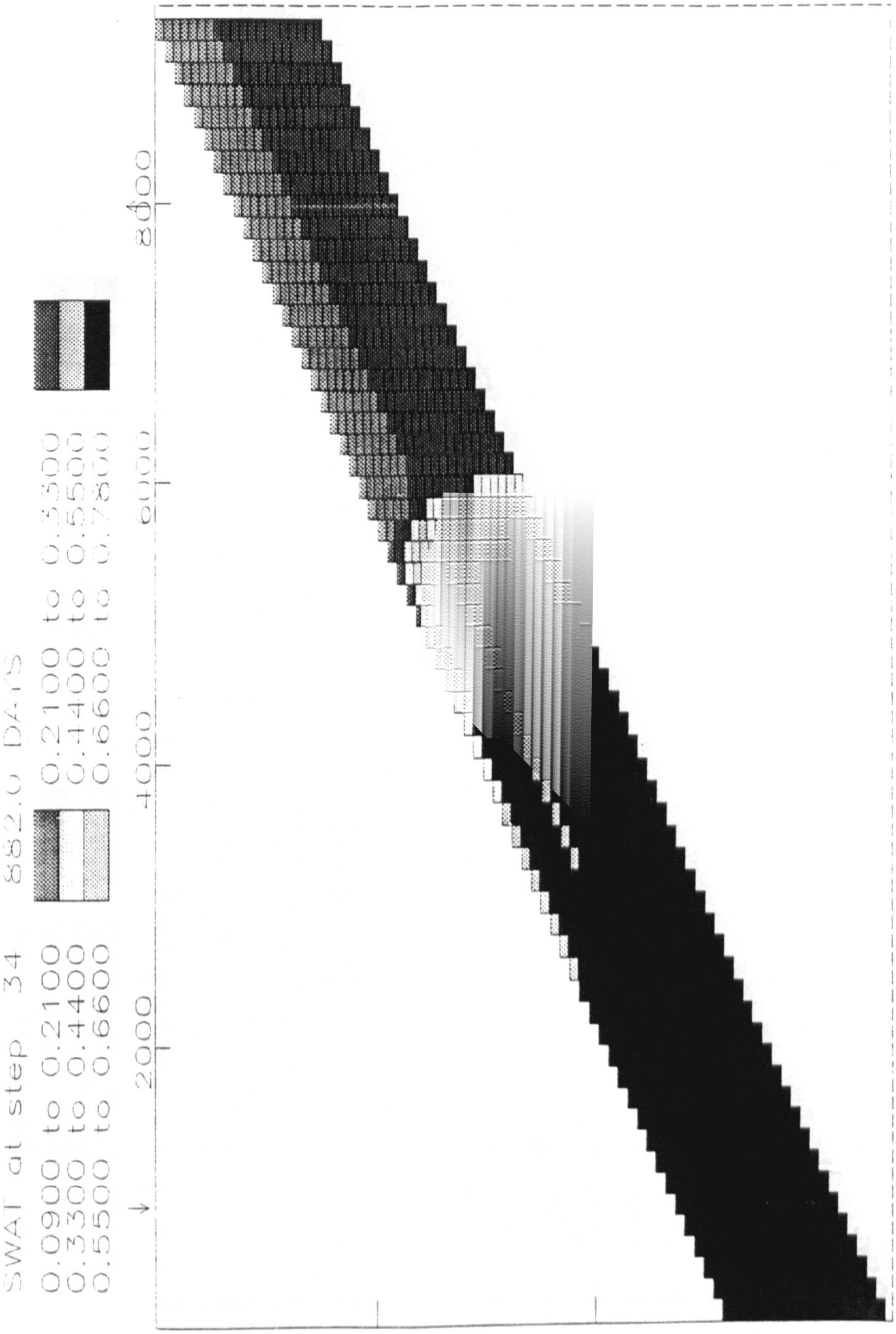

Figure 7.15a: Water Saturation in the Statfjord model at 882 days: geopseudo model.

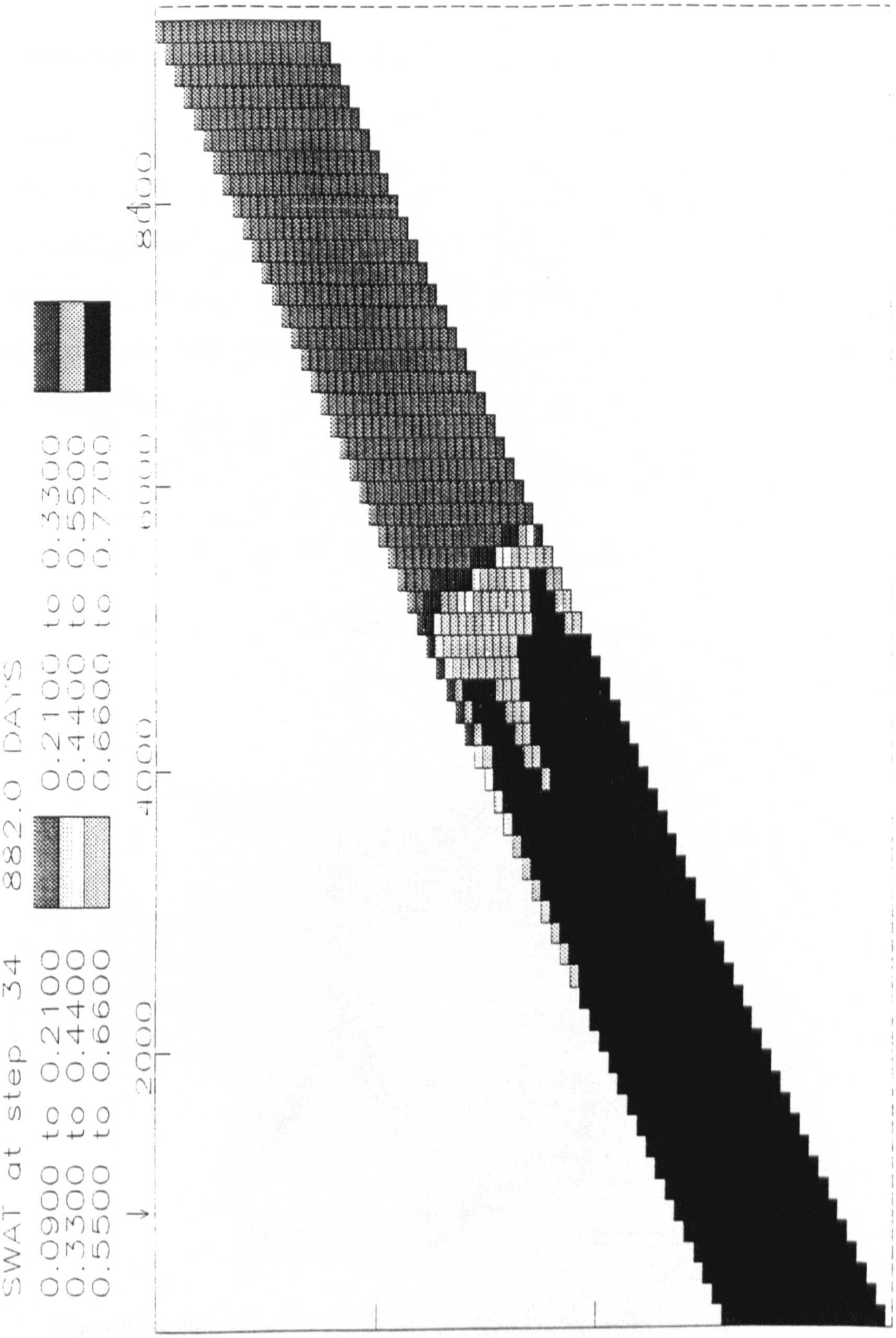

Figure 7.15b: Water Saturation in the Statfjord model at 882 days: rock curve model.

7.3.2 Cormorant Field (Operator: Shell Exploration and Prooduction)

The Cormorant Field (Budding and Inglin, 1981; Bunn and Yaxley, 1986; Bentley and Barry, 1991; Scott, 1992) lies 35km southwest of the Thistle Field (Fig. 7.1). A cross-sectional model in the northern fault block of the Cormorant Field (line c-c' in Fig. 7.16) was constructed to investigate the geopseudo scale-up procedure in this field (Fig 7.17). Rock properties were taken from well N4 and formation dip (14°) from the area down flank to the north-west of N4.

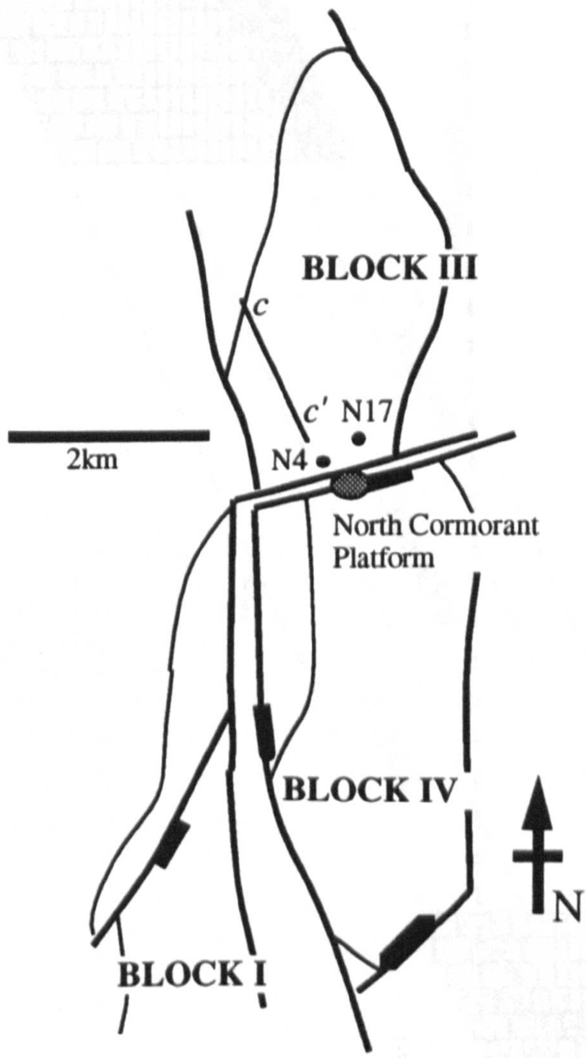

Figure 7.16: Sketch map of the northern Cormorant Field showing location of modelled section (*c-c'*) in Fault Block III. Scale approximate. (Adapted from Styles and Valenti, 1990)

Permeabilities in the Cormorant are significantly lower than those in Thistle and published corrections for the effects of connate water and overburden pressure have to be taken into account (Styles and Valenti, 1990). These corrections are significant (*e.g.*, 100mD reduces to 38mD), however, no such corrections were considered for the Thistle core plug data on which the Thistle model was based. The 17-layer model corrected permeabilities are shown in Table 7.3.

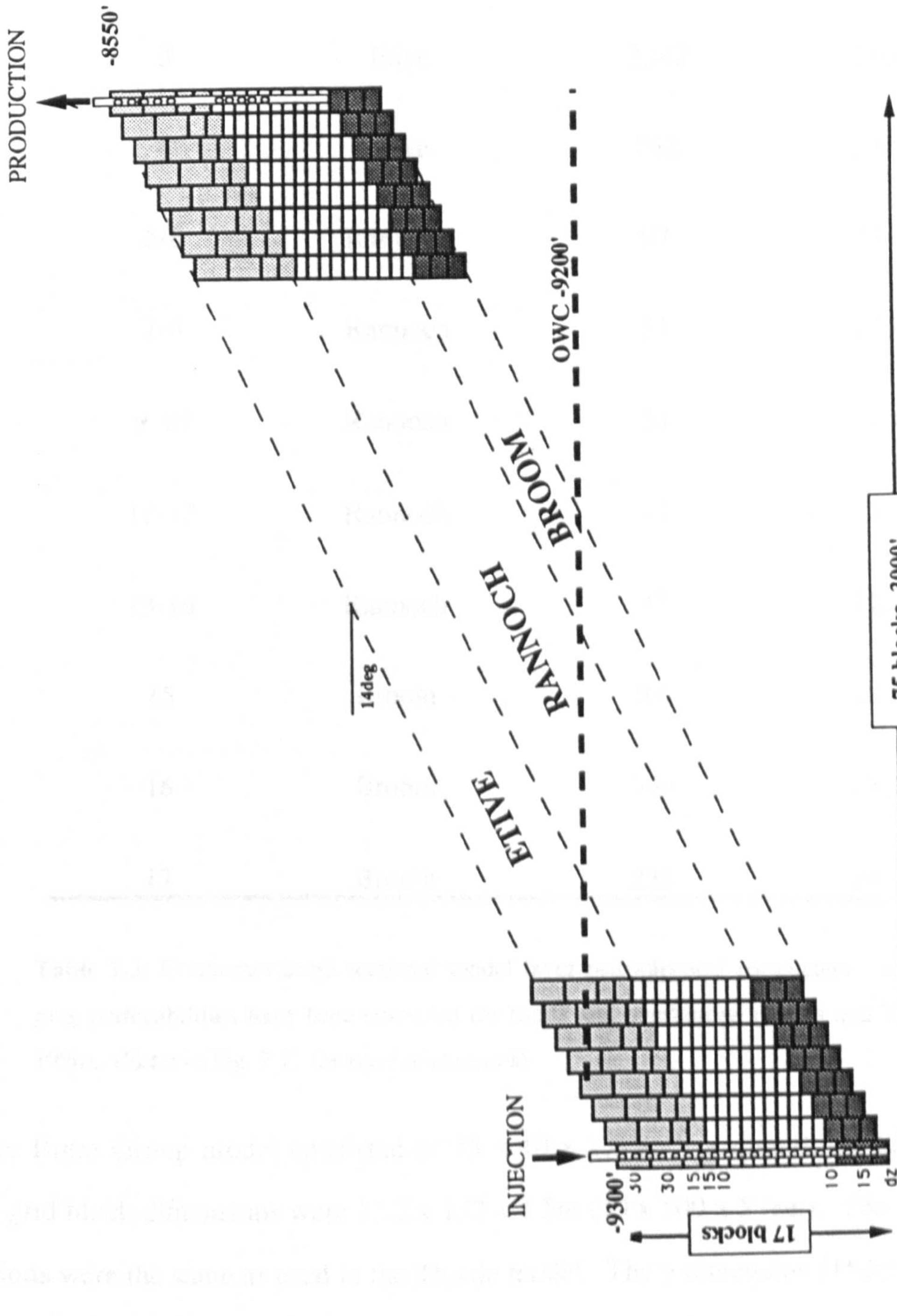

Figure 7.17: Cormorant Field cross-sectional model showing arrangement of blocks, layers and wells. (For location of section refer to Fig. 7.16).

Layer	Unit	Permeability (mD)	Porosity (%)
1	Etive	921	24.3
2	Etive	1388	25.4
3	Etive	2382	26.4
4	Etive	762	25.8
5-6	Rannoch	97	23.1
7-8	Rannoch	51	22.0
9-10	Rannoch	54	22.6
11-12	Rannoch	17	18.5
13-14	Rannoch	47	22.6
15	Broom	209	23.8
16	Broom	590	28.8
17	Broom	238	26.2

Table 7.3: Cormorant cross sectional model layer petrophysical parameters. Average plug permeabilities have been corrected for fluids and overburden (Styles and Valenti, 1990). (Refer to Fig. 7.17 for layer thicknesses)

The lower Brent Group model consisted of 75 x 10 x 17 (x, y, z directions) blocks. Rannoch grid block dimensions were 12.2 x 152 x 1.5m (40 x 500 x 5 feet). The x and z dimensions were the same as used in the Thistle model. The y dimension (152m) was adjusted in the model to match water breakthrough. This is an unavoidable limitation of cross-sectional modelling where the effective lateral volume between wells is not known.

Although full field 3-D modelling would have to be used to match this parameter correctly, altering the Δy within realistic limits is one way to build a cross-sectional model of the correct volume. Average core plug porosities for each layer were also used (Table 7.3). Water breakthrough in cross-sectional modelling is not considered a diagnostic parameter for judging model results unless used in conjunction with Δy.

In the model (CORM001.DATA in Appendix X), the production well was completed in the upper Etive (layers 1 and 2) together with the middle Rannoch (layers 7 to 11). Water injection was to all layers. The model was controlled by liquid rate (total rate based on nearby well N17) at the producer and voidage replacement at the injector (Fig. 7.18).

The water cut performance is compared, as with previous models, for the geopseudo and rock curves (Fig. 7.19). In this model the differences due to different relative permeability curves are less marked. Both models suggest that the Rannoch is being swept. In the Cormorant Field, the WB facies seen in Fault Block I in the southern part of the field (Fig. 15a in Scott, 1992) may not be developed in Fault Block III to the north (D. Schwartz, personal communication). The modelling in Cormorant Field is less conclusive as there is little data available to confirm the sweep of the Rannoch.

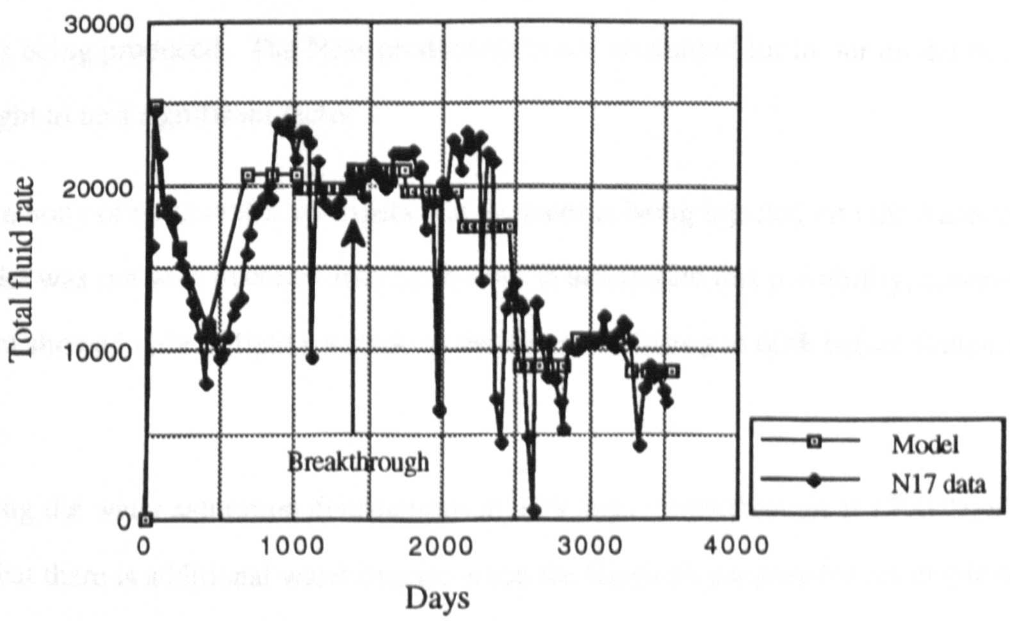

Figure 7.18: Total fluid injected; field data and model control input.

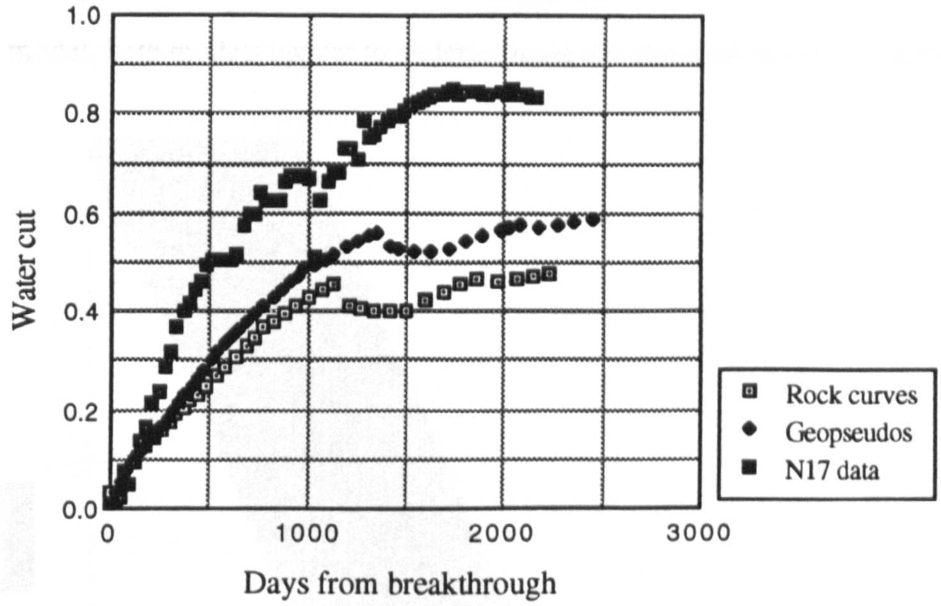

Figure 7.19: Water cut performance of rock curve model and geopseudo model after breakthrough.

Percentages of the total production entering the well bore in the model (4% from the Rannoch), compare reasonably with production log data. The well (N17) was completed and perforated on 2/4/82. On 12/6/82, no flow was detected from the Rannoch. On 9/11/86, 2% of the total well flow was coming from the Rannoch. The well is also completed in the Lower Ness (the unit overlying the Etive) from which 11-12% of the fluid was being produced. The Ness production is not accounted for in our model but is not thought to be a significant factor.

There is a body of opinion that considers that no water is being injected into the Rannoch. The model was run with injection into Etive only to investigate this possibility, however, the model showed only a slight response to the water cut (rising to 60% before flattening out).

Comparing the water saturation distributions at 639 days (breakthrough at 1300 days) it is clear that there is additional water overide when the Rannoch geopseudos are employed (Fig. 7.20). These simulation results suggest the Rannoch oil is being produced indirectly through the Etive Formation. Although the water cut rises faster in the geopseudo model, both models appear to underestimate the observed water cut increase.

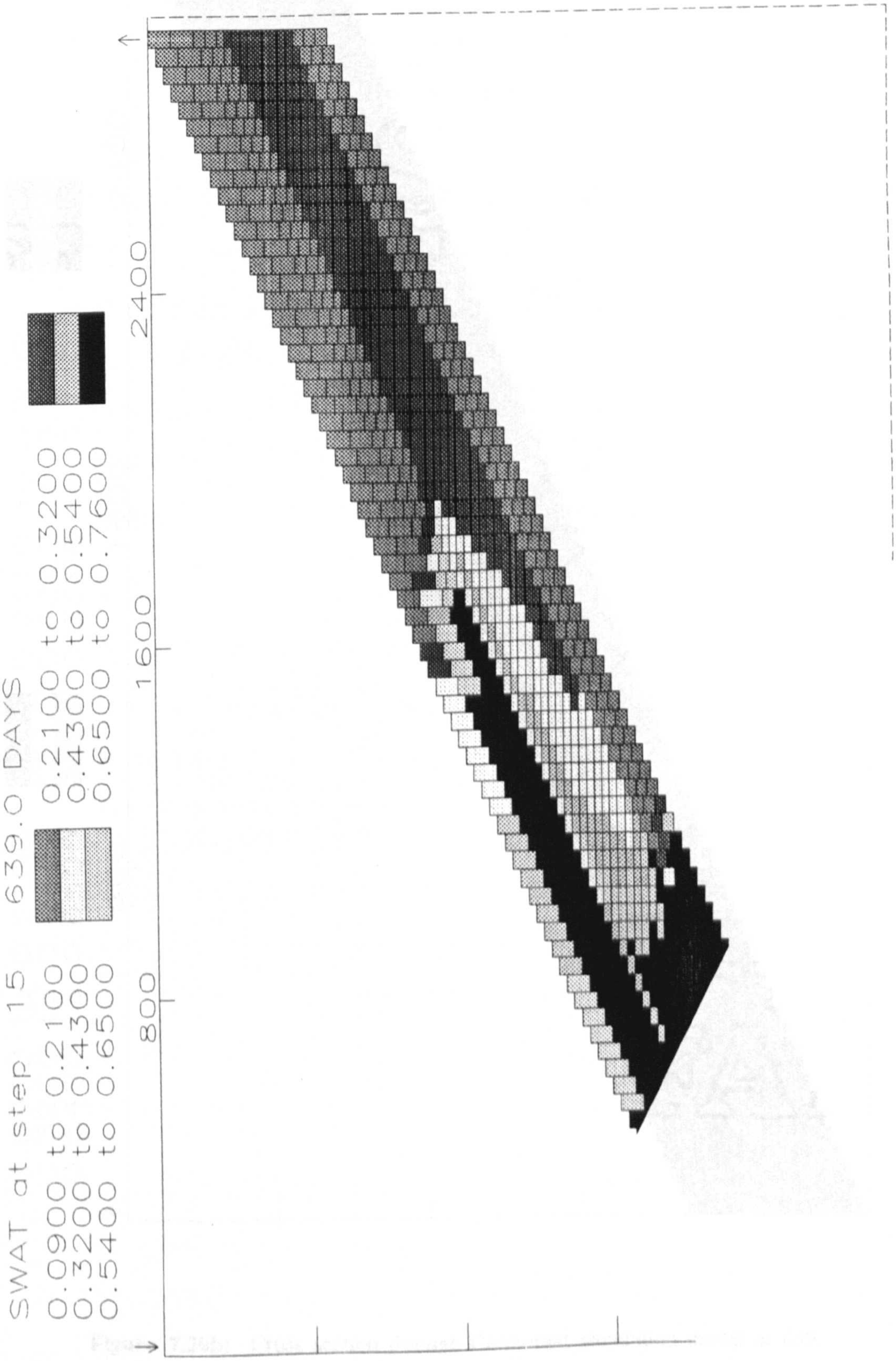

Figure 7.20a: Cross-section through Cormorant simulation model at 639 days; geopseudo model.

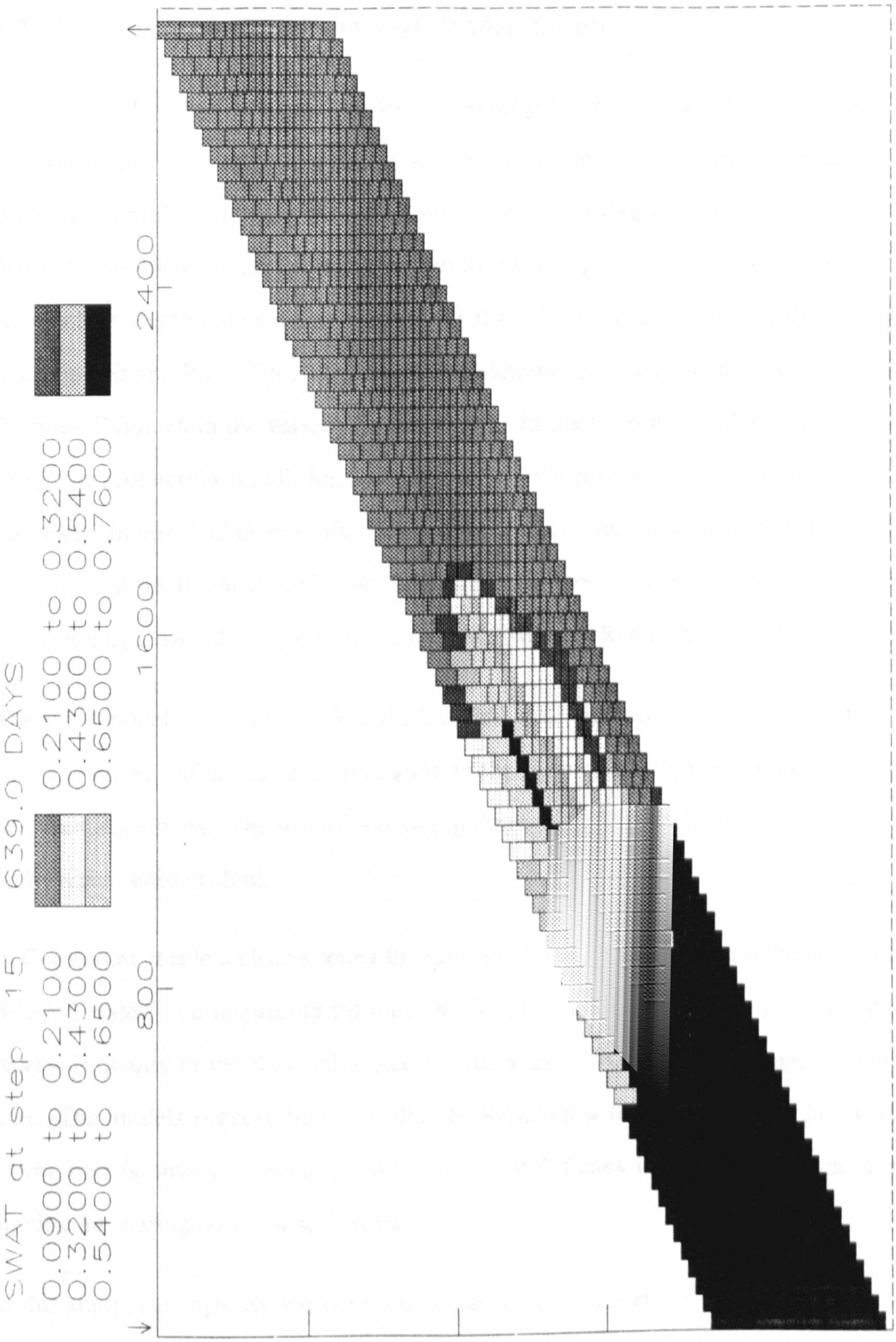

Figure 7.20b: Cross section through Cormorant simulation model at 639 days; rock curve model.

7.4 Discussion of Cross-Sectional Model Results.

The aim of the cross-sectional modelling exercise has been to attempt to evaluate the significance of the lamination on the field performance of the Rannoch Formation. In principle, a well correlated shoreface sequence containing pervasive lamination and historical production data should have been the ideal place to consider the problem. The Rannoch production, however, is complicated by the presence of the highly permeable overlying Etive. It is difficult in the fields to determine exactly what is being produced from the Rannoch in the various studied fields. In Statfjord the model is supported by excellent production (GST) logs which confirm the production mechanism from the Rannoch. In this field there is also evidence of lamina trapped oil in the WB facies. The remainder of the Rannoch (SCS and HCS) are being produced by "horizontal" flood in a "horizontally" layered reservoir. Good ultimate sweep of Rannoch oil can be expected.

The same model appears to work in the Thistle Field. The water cut and production can be matched by building in the lamination in the form of geologically-realistic relative permeability curves. The waterflood sweep through the Rannoch appears to be backed up by recent infill drilling.

In Cormorant, it is less clear whether the same model for the Rannoch production (lateral, delayed waterflood displacing oil into the Etive) is appropriate. The greatly reduced reservoir quality of the Rannoch suggests little water is being directly injected into the unit. The models suggest, however, that the Rannoch is being swept. Further work in Cormorant is obviously needed. Whether the WB facies is present in Block III is a significant starting point for such work.

In this study, the objective has not been to match the field performance on a well by well basis. That is beyond the scope of this study, limited as it is by available data and to cross-sectional models. It is felt, however, that the attempt to view the modelling of the Rannoch with a common geoengineering approach has been instructive. Insights into the general production characteristics of the Rannoch production across the basin have been gained. As far as we are aware, this is the first study of the Rannoch to consider comparisons between fields operated by different companies. The study has approached the problem with a consistent geological model and engineering approach.

During the study, the potential for the geopseudo method for the scale-up of small scale geological heterogeneities has been demonstrated. Also, the transportability of geopseudos for particular sedimentary structures has been investigated. The prospects for the success of the geopseudo method look encouraging, however, more work on the transportability is clearly needed.

CHAPTER 8

CONCLUSIONS AND RECOMMENDATIONS FOR FURTHER WORK

In this chapter, the conclusions are drawn under each of the main areas of study that have been undertaken during this work. In each section, the areas that need additional work are also highlighted.

8.1. The Use of the Probe Permeameter in Laminated Reservoirs

The major data collection and interpretation phase of this study concentrated on the acquisition and interpretation of probe permeameter data from two Rannoch Formation wells. The data were collected by Christian Halvorsen, while the interpretation and comparisons with other data were carried out in this research project. The sample requirements and programme for the Thistle well were determined following the interpretation of the initial Statfjord study.

The main conclusions are as follows:

- The probe permeameter device is an excellent development for the measurement of the petrophysical properties of laminae. The small volume of investigation is often limited to a single lamina. Used in conjunction with an automated positioning device, the probe is capable of measuring detailed grids from which permeability maps of various laminated facies can be made.

- In the Rannoch Formation, adjacent laminae with up to two orders of magnitude difference in permeability were seen (2-200mD and 16-1300mD).

- Measurement of lamina properties by core plugs is often inappropriate because of the relatively large sample volume.

• Permeability in laminae that are thicker than the probe aperture tend to be isotropic.

• The probe is unable to effectively resolve the properties of laminae that are less than the aperture diameter.

• The effective depth of investigation of the probe approximates to two aperture diameters.

• A relationship for porosity from probe permeability measurements has been derived for the Rannoch Formation.

• The variability of permeability is closely related to the primary depositional fabric in the Rannoch Formation.

• Anisotropy in vertical and horizontal plug permeability measurements is largely due to lamination rather than grain fabric.

• Permeability correlation lengths are closely related to the length scales of stratal elements. There are a hierarchy of correlation lengths in a sedimentary sequence. Careful sampling schemes (domain length and sample spacing) are required to measure these correlation lengths.

• The appropriate number of samples to estimate the arithmetic average permeability to within ±20% tolerance is a simple function of the coefficient of variation $[(10Cv)^2]$. This simple rule of thumb (extended from the original work of Hurst and Rosvoll, 1989, by the adoption here of a more realistic tolerance) holds for permeability distributions that are either normal or skewed. Rannoch permeability distributions are generally root- to log-normal.

• Probe permeabilities measured on slabbed Rannoch core material (above 100mD) appear to be reduced due to surface damage or ageing. Probe measurements, in this study, appear to be relatively unaffected by either the imbibed resin or residual (dry) fluids.

• Laminaset bounding surfaces in the Rannoch appear to be relatively free of permeability impairment.

• Published analytical solutions and empirically derived relationships give consistent calibration curves for the probe permeameter *if* careful procedures are followed.

Areas in which the probe methodolgy needs further investigation or care in usage are relatively limited, the main concern being the accurate measurement of thin low permeability laminae.

In general, the probe permeameter has as a result of recent studies, including this one, become an accepted measurement device. The advantages discussed in this report are largely self-evident. That there will potentially be differences between probe and plug measurements is now widely accepted and understood. The conclusions of this report, however, emphasise that those differences should be systematically examined and understood where possible. Accepted as *bona fide* measurements of permeability, new scale-up procedures for the comparison of probe measurements with plug, electric log, well test and simulator grid block values are needed.

8.2. The Geopseudo Methodology and Implications for Petrophysics

Sedimentary rocks are commonly made up of a hierarchy of stratal elements. The probe data in the Rannoch Formation show that the permeability variability is very closely correlated with primary depositional structure. This relationship can be exploited in the scale-up. The hierarchy of stratal elements is visible in the nested correlation structure of the probe permeability data as seen in the variograms. Homogenisation should ideally occur at scales above the correlation length. To capture the appropriate physics which may be more sensitive to one length scale than another (*e.g.*, capillary pressure effects) the pseudoisation of properties at various length scales is appropriate. A scale-up procedure based on the pseudoisation of the properties of representative laminasets at the fine scale, followed by pseudoisation of the laminaset groupings in representative bed elements has been developed to exploit the geological knowledge. This procedure has been termed the geopseudo method.

The geopseudo method has implications for petrophysical measurements. A volume compatable porosity and capillary pressure device needs to be developed to determine the properties of representative laminae. For numerical simulation, instead of saturating the available core with permeability measurements, recognition of the representative elements can lead to a more selective sampling programme. If the subject reservoir is strongly laminated, carefully selected laminated blocks can give more representative SCAL results. Understanding the geometry and stacking of the stratal elements in the reservoir can also provide a significant basis for the description of the inter-well region. Measurements of unrepresentative elements, as can happen with core plugs, will lead to "noisy" data and confuse the interpretation.

8.3. Rannoch Formation Average Reservoir Properties and the Location of Remaining Oil

Core plugs are adequate for the porosity description of the Rannoch. They are also sufficient for the description of absolute horizontal permeability over most of the interval. There are, however, thin and very variable intervals of facies that are significant to the formation flow characteristics that are not adequately sampled by core plugs. Furthermore, the k_v/k_h ratio from adjacent horizontal and vertical core plugs are a volume-specific measurement. The appropriate k_v/k_h for large grid blocks cannot be determined as a simple average of the core plug data.

The permeability description by core plugs in the Rannoch is supplemented by probe permeameter data. These data provide an improved sampling of the variable wavy bedded facies from which appropriate average absolute horizontal permeabilities can be determined. The patterns revealed by the probe permeameter allow the selection of representative laminasets. The appropriate average relative permeabilities and capillary pressures can be determined by numerical simulation of these elements. The averages of the dynamic two-phase properties are appropriately determined by pseudoisation.

Numerical models containing the small scale geology suggests that the primary flooding mechanism for the Rannoch is by bed-parallel flow. The expected residual oil over most of the Rannoch will be low. Trapping of oil, however, is likely to occur in the laminae within the wavy bedded facies. The volumetric significance of this, however, is low. The progress of the waterflood in the Rannoch is slowed (relative to the overlying Etive) by the absolute permeability differences and the strong capillary effects. These capillary effects suggest that there will be a lateral transition zone in advance of the flood front. The petrophysical description of the sediments below the Rannoch/Etive boundary show that the boundary is more complicated than a single tight zone. The interval requires a more comprehensive petrophysical analysis than has been traditionally available.

NOMENCLATURE

a	Probe aperture radius (cm)
A	Core plug area (sq.cm.)
Cv	Coefficient of variation
d_i	Probe internal diameter (cm)
d_o	Probe external diameter (cm)
ECLIPSE	Black oil numerical simulation package
FGA	Fine grid A: Low contrast lamination
FGB	Fine grid B: Ripple lamination
FGC	Fine grid C: High contrast lamination
G	Goggin's geometrical factor
GR	Gamma Ray Log (API)
GST	Gamma spectroscopy tool
h	Lag distance
HCS	Hummocky cross stratification
k	Permeability (mD)
$\bar{k}_{ar}$	Arithmetic average permeability (mD)
$\bar{k}_{geom}$	Geometric average permeability (mD)
k_h	Horizontal permeability (mD)
$\bar{k}_{har}$	Harmonic average permeability (mD)
k_{ro}	Relative permeability to oil (fraction)
k_{rw}	Relative permeability to water (fraction)
k_v	Vertical permeability (mD)
k_v/k_h	Vertical to horizontal permeability ratio
k_x, k_y, k_z	Permeability in x, y, z, directions
L	Core plug length (cm)
LP1	Large probe 1 (d_i = 0.59cm, d_o = 10.5cm)
MHWL	Mean high water level
MLWL	Mean low water level
OOIP	Original oil-in-place
p	Transformation exponent ($-1 \leq p \leq 1$)
Pc	Capillary pressure (atm)
Pct	Threshold capillary pressure
Po	Oil phase pressure
Pw	Water phase pressure
P_I	Injection pressure (atm)
P_O	Outlet pressure (atm)
PSEUDO	Option within the ECLIPSE program

PV, pv	Pore volumes throughput (total system)
Q	Flow rate (ml/min)
RFT	Repeat formation tester
SCS	Swaley cross stratification
S_n	Normalised saturation ($S_n = 1 - S_{wc} - S_{or}$)
S_{nwr}	Non-wetting residual saturation (fraction)
S_o	Oil saturation (fraction)
S_{or}	Residual oil saturation (fraction)
SP1	Small probe 1 ($d_i = 0.36cm$, $d_o = 0.79cm$)
SP2	Small probe 2 ($d_i = 0.34cm$, $d_o = 1.02cm$)
S_w	Water saturation (fraction)
S_{wirr}	Irreduceable water saturation (fraction)
S_{wc}	Connate water saturation (fraction)
TVT	True vertical thickness
WB	Wavy bedded lamination
x, y, z	Orthogonal coordinate axes (x flow direction, y transverse, z vertical)

Greek letters

Δt	Sonic Log ($\mu s/ft$)
ϕ	Porosity (%)
$\overline{\phi}_{ar}$	Arithmetic average porosity (%)
μ	Viscosity (cp)

REFERENCES

Amyx, J. W., D. M. Bass Jr. and R. L. Whiting, 1960, Petroleum Reservoir Engineering, McGraw-Hill, New York, 610p.

API., 1960, Recommended practice for core analysis procedure, American Petroleum Institute, Report 40, Dallas, Texas.

Allen, J. R. L., 1970, Physical Processes of Sedimentation, Unwin University Books, London, 272p.

Allen, J. R. L., 1985, Principles of Physical Sedimentology, George Allen and Unwin, London, 248p.

Allen, P. A., 1989, Hummocky cross-stratification is not produced under progressive gravity waves, Nature, 313, p. 562-564.

Allen, P. A., and J. R. Underhill, 1989, Swaley cross-stratification produced by unidirectional flows, Bencliff Grit (U. Jurassic) Dorset, U.K., Jour. Geol. Soc. Lond., 146, p. 241-252.

Anderson, W. G., 1987, Wettability Literature Survey - Part 4: Effects of wettability on capillary pressure. Journal of Petroleum Technology, p. 1283-1300.

Archer, J. S., and C. G. Wall, 1986, Petroleum Engineering: Principles and Practice, Graham and Trotman, Newcastle, 362p.

Ashley, G. M., 1990, Classification of large-scale subaqueous bedforms: a new look at an old problem, Jour. Sed. Pet., 60, p. 160-172.

Bayat, M. G., and D. H. Tehrani, 1985, The Thistle Field - Analysis of its past performance and optimisation of its future development. Presented at Offshore Europe 85 Conference, Aberdeen, UK.

Bentley, M. R., and J. J. Barry, 1991, Representation of a fault sealing in a reservoir simulation: Cormorant Block IV, UK North Sea, SPE 22667, presented at 66th Ann. Tech. Conf. & Exhib., Dallas, Texas, October 6-9th.

Berthois, L., 1962, Etude du comportement hydraulic du mica, Sedimentology, 1, p. 40-49.

Braithwaite, C. I. M., J. D. Marshall and T. C. Holland, 1989, Improving recovery from the Dunlin Field, U.K. Northern North Sea, SPE 19878, presented at 64th Ann. Tech. Conf. & Exhib., San Antonio, Texas, Oct. 8th-11th.

Brenchley, P.J., 1989, Storm Sedimentation, Geology Today, p. 133-137.

Brenchley, P.J., S. S. Flint and S. G. Stromberg, 1992, Quantitative facies discrimination and the application of sequence stratigraphy to bed length modelling af shallow marine heterolithic facies, in Subsurface reservoir characterisation from outcrop observation, M. Montadert and R. Eschard (eds.), Editions Technip (in press).

Brooks, R. H., and A. T. Carey, 1964, Hydraulic properties of porous media, Hydrol Paper 3 Civil Engineering Department, Colorado State University, Fort Collins.

Brown, S., P. C. Richards and A. R. Thomson, 1987, Patterns in the deposition of the Brent Group (Middle Jurassic), U.K. North Sea, in J. Brooks and K. Glennie (eds.), Petroleum Geology of Northwest Europe, Graham and Trotman, London.

Brown, S., and P. C. Richards, 1989, Facies and development of the Middle Jurassic Brent Delta near the northern limit of its progradation, U.K. North Sea, in Whateley, M. K. G., and K. T. Pickering, (eds.), Deltas: Sites and Traps for Fossil Fuels, Geol. Soc. Spec. Publ. No 41, p. 253-267.

Budding, M. C., and H. F. Inglin, 1981, A reservoir geological model of the Brent Sands in Southern Cormorant, in L. V. Illing and G. D. Hobson (eds.), Petroleum Geology of the Continental Shelf of N. W. Europe, Inst. of Petroleum, London.

Bunn, G. F., and L. M. Yaxley, 1986, Design, Implementation, and Interpretation of a "Three-Dimensional Well Test" in the Cormorant Field, North Sea., SPE 15858, presented at the SPE European Petroleum Conference, London, 20-22 October.

Buza, J. W., and A. Unneberg, 1987, Geological and Reservoir Engineering aspects of the Statfjord Field, in J.Kleppe et. al. (eds), North Sea Oil and Gas Reservoirs, Graham and Trotman, London.

Cadman, M., 1984, Non-destructive permeability measurement, Unpubl. M. Eng. Thesis, Heriot-Watt University, Edinburgh.

Campbell, C. V., 1967, Lamina, laminaset, bed and bedset. Sedimentology, 8, p. 7-26.

Cheel, R. J., 1991, Grain fabric in hummocky cross-stratified storm beds: genetic implications. Journal of Sedimentary Petrology, 61, p. 102-110.

Clelland, W., 1984, Measurement and analysis of small scale permeability distributions in sandstones, Unpubl. Phd thesis, Heriot-Watt Univ., Edinburgh.

Corbett, P. W. M., and J. L. Jensen, 1992a, Variation of reservoir statistics according to sample spacing and measurement type for some intervals in the Lower Brent Group, Log Analyst, 33, p. 22-41.

Corbett, P. W. M., and J. L. Jensen, 1992b, Estimating the mean permeability: How many measurements do you need?, First Break, 10, p. 89-94.

Corey, A.T., and C. H. Rathjens, 1956, Effect of stratification on relative permeability, Pet. Trans., AIME, 207, p. 358-360.

Craig, F.F., 1971, The Reservoir Engineering Aspects of Waterflooding, SPE Monograph No. 3.

Dake, L., 1982, Application of repeat formation tester in vertical and horizontal pulse testing in the Middle Jurassic Brent Sands, EUROPEC, London, 25-28th October.

Daltaban, T. S., J. J. M. Lewis and J. S. Archer, 1989, Field minipermeameter measurements - their collection and interpretation, Proc. 5th European Symp. on Improved Oil Rec., Budapest, 25-27th April.

Davies, J.C., 1973, Statistics and data analysis in geology, John Wiley and Sons, New York, 550p.

Daws, J. A., and D. J. Prosser, 1992, Scales of permeability heterogeneity within the Brent Group, Journal of Petroleum Geology, 15(4), p. 397-418.

Dott, R. H. and J. Bourgeois, 1982, Hummocky stratification - significance of its variable bedding sequences, Bulletin Geological Society of America, 93, p. 663-680.

Dreyer, T., A. Scheie and O. Walderhaug, 1990, Minipermeameter-based study of permeability trends in channel sand bodies, AAPG Bull., 74, p. 359-374.

Duke, W. L., 1985, Hummocky cross-stratification, tropical hurricanes and intense winter storms, Sedimentology, 32, p. 167-194.

Duke, W. L., 1987, Reply: Hummocky cross-stratification, tropical hurricanes and intense winter storms, Sedimentology, 34, p. 344-359.

Duke, W. L., R. C. W. Arnott and R. J. Cheel, 1991, Shelf sandstones and hummocky-cross stratification: New insights on a stormy debate. Geology, 19, p. 625-628.

Dykstra, H. and R. L. Parsons, 1950, The prediction of oil recovery by waterflood, in Secondary Recovery in the U.S.A., Am. Pet. Inst.

ECL, 1988, Eclipse reference manual, Version 88/09, Exploration Consultants Limited, Henley-on-Thames.

Eijpe, R., and K. J. Weber, 1971, Minipermeameter for consolidated rock and unconsolidated sand, American Association of Petroleum Geologists Bulletin, 55, p. 307-309.

Ezeudembah, A.S., and P. M. Dranchuk, 1982, Flow mechanism of Forcheimer's cubic equation in high-velocity radial gas flow through porous media, SPE 10979, presented at 57th Ann. Tech. Conf. & Exhib., New Orleans, Louisiana, 26-29th September.

Firoozabadi, A., and D. L. Katz, 1979, An analysis of high-velocity gas flow through porous media, Journal of Petroleum Technology, p. 211-216.

Goggin, D.J., 1988, Geologically-sensible modelling of the spatial distribution of permeability in eolian deposits: Page Sandstone (Jurassic), Northern Arizona, Unpubl. Phd thesis, University of Texas, Austin, Texas.

Goggin, D. J., M. A. Chandler, G. Kocurek, and L. W. Lake, 1988, Patterns of permeability in eolian deposits: Page Sandstone (Jurassic), NE Arizona, SPEFE, June.

Goggin, D. J., R. L. Thrasher and L. W. Lake, 1988, A theoretical and experimental analysis of minipermeameter response including gas slippage and high velocity flow effects, In-situ, 12, p. 79-116.

Goggin, D.J., 1991, Minipermeametry. Is it worth the effort?. Presented at Petroleum Science and Technology Institute Advances in Minipermeametry Conference, June 27th.

Gibbons, K., C. Halvorsen and E. Siring, 1991, Vertical and horizontal permeability variation within a sandstone reservoir based on minipermeameter data, Presented at Petroleum Science and Technology Institute Advances in Minipermeametry Conference, June 27th.

Graff, W. J. E. van de, and P. J. Ealey, 1989, Geological modeling for simulation studies, American Association of Petroleum Geologists Bulletin, 73, p. 1436-1444.

Grant, I., J. D. Marshall, P. Dietvorst, and J. Hordijk, 1990, Improved reservoir management by integrated study: Cormorant Field, Block 1, SPE 20891, presented at Europec 90, The Hague, Netherlands, 22-24th October.

Graue, E., W. Helland-Hansen, J. Johnsen, L. Lomo, A. Nottvedt, K. Ronning, A. Ryseth and R. Steel, 1987, Advance and retreat of the Brent Delta system, Norwegian North Sea, in J. Brooks and K. Glennie, (eds.), Petroleum Geology of Northwest Europe, Graham and Trotman, London.

Haldorsen, H. H., 1986, Simulator parameter assignment and the problem of scale in reservoir engineering, in L. W. Lake and H. B. Carroll, (eds.); Reservoir Characterization, Academic Press, Orlando.

Halvorsen, C., 1991, Probe permeametry applied to a highly laminated sandstone reservoir, Presented at Petroleum Science and Technology Institute Advances in Minipermeametry Conference, June 27th.

Halvorsen, C., and A. Hurst, 1990, Principles, practice and applications of laboratory minipermeametry, in P.F. Worthington (ed.), Advances in Core Evaluation Accuracy and Prediction, Gordon and Breach Science Publishers, London, p. 521-549.

Harms, J. C., J. B. Southard, D. R. Spearing and R. G. Walker, 1975, Depositional environments as interpreted from primary sedimentary structures and stratification sequences, SEPM short course no. 2, Dallas, Texas.

Harris, N. B., 1992, Burial diagenesis of Brent Sandstones: A study of Statfjord, Hutton and Lyell Fields, in A. C. Morton, R. S. Hazeldine, M. R. Giles and S. Brown (eds.), Geology of the Brent Group, Geol. Soc. Spec. Publ., 61, p. 289-327.

Hartkamp-Bakker, C. A., 1991, Capillary oil entrapment in crossbedded sedimentary structures of fluvial sandstone reservoirs, SPE 22761, 66th Annual Technical Conference and Exhibition of the Society of Petroleum Engineers, Dallas, Tx, October 6-9th.

Hearn, C. L., 1971, Simulation of stratified waterflooding by pseudo relative permeability curves, Journal of Petroleum Technology, July, p. 805-813.

Hoimyr, O, A. Kleppe and J. P. Nystuen, 1993, Effects of heterogeneities in a braided stream channel sandbody on the simulation of oil recovery: A case study from the Lower Jurassic Statfjord Formation, Snorre Field, North Sea, from M. Ashton (ed.) Advances in Reservoir Geology, Geol. Soc. Special Publ., 69, p. 105-134.

Honarpour, M., L. Koederitz, and A. H. Harvey, 1986, Relative Permeability of Petroleum Reservoirs, CRC Press, Florida, 143p.

Hunter, R. E., and H. E. Clifton, 1982, Cyclic deposits and hummocky cross-stratification of probable storm origin in Upper Cretaceous rocks of Cape Sebastian Area, Southwestern Oregon, Journal of Sedimentary Petrology, 52, p. 127-143.

Hurst, A., and K. Rosvoll, 1989, Permeability variations in sandstones and their relationship to sedimentary structures, NIPER/DOE 2nd International Reservoir Characterisation Tech. Conf., June 25-28th, Dallas.

Jacks, H. H., O. J. E. Smith and C. C. Mattax, 1973, The modelling of a three-dimensional reservoir with a two dimensional simulator - The use of dynamic pseudo functions, Society of Petroleum Engineers Journal, June, p. 175-185.

Jarvis, M., P. W. M. Corbett and J. J. M. Lewis, 1992, Operator Manual for the Heriot-Watt Laboratory Minipermeameter, Unpubl. Internal Report.

Jensen, J. L., 1991, Use of the geometric average for effective permeability estimation, Mathematical Geology, 23, p. 833-840.

Jensen, J. L., D. V. Hinkley and L. W. Lake, 1987, A statistical study of reservoir permeability: Distributions, correlations and averages, SPEFE, December.

Johnson, N. L., and S. Kotz, 1970, Continuous univariate distributions - 1, MacMillan Publ. Co., New York, 300p.

Journal, A. G. and C. J. Huijbregts, 1978, Mining Geostatistics, Academic Press, London, 600p.

Kirk, R. H., 1980, Statfjord Field - A North Sea Giant, in M. T. Halbouty (ed.), Giant Oil and Gas Fields of the Decade 1968-1978, AAPG Memoir 30, Tulsa, Oklahoma.

Kittridge, M. G., L. W. Lake, F. J. Lucia and G. E. Fogg, 1990, Outcrop/Subsurface Comparisons of heterogeneity in the San Andres Formation, SPEFE, September.

Kortekaas, T. F. M., 1985, Water-oil displacement characteristics in cross-bedded reservoir zones. Society of Petroleum Engineers Journal, December, p. 917-926.

Kossack, C. A., J. O. Aasen and S. T. Opdal, 1990, Scaling heterogeneities with pseudofunctions, SPEFE, September, p. 226-232.

Kreisa, R. D., 1981, Storm generated sedimentary structures in subtidal marine facies with examples from Middle and Upper Ordovician of Southwestern Virginia, Journal of Sedimentary Petrology, 51, p. 823-848.

Krumbein, W. C., and G. D. Monk, 1942, Permeability as a function of the size parameters of unconsolidated sand, Petroleum Technology, AIME Tech. Publ., 1492 (5), p. 1-11.

Klein, G. de V., and K. M. Marsaglia, 1987, Discussion: Hummocky cross-stratification, tropical hurricanes and intense winter storms, Sedimentology, 34, p. 333-338.

Kyte, J. R., and D. W. Berry, 1975, New pseudofunctions to control numerical dispersion, Society of Petroleum Engineers Journal., p. 269-276.

Lake, L. W., 1989a, Preface to Reservoir Characterisation-1, SPE Reprint Series No.27, Society of Petroleum Engineers, Richardson, Texas, 272p.

Lake, L. W., 1989b, Enhanced Oil Recovery, Prentice Hall, New Jersey, 550p.

Lake, L.W., 1992, What we've learned about permeability from all those outcrop studies, abstract presented at the EAPG workshop Characterisation and modelling of lateral heterogeneity in reservoirs, Paris, 30th May.

Lake, L. W., E. Kasap and M. Shook, 1990, Pseudofunctions - The key to practical use of reservoir description, in A. T. Buller, E. Berg, O. Hjelmeland, J. Kleppe, O. Torsaeter and J. O. Aasen (eds.), North Sea Oil and Gas Reservoirs II, Norwegian Institute of Technology, Graham and Trotman, London.

Lasseter, T. J., J. R. Waggoner and L. W. Lake, 1986, Reservoir heterogeneities and their influence on ultimate recovery, in L. W. Lake and H. B. J. Carroll (eds) Reservoir Characterisation, Academic Press, Orlando, Florida.

Lemouzy, P., 1992, Upscaling and pseudoisation, abstract presented at the EAPG workshop Characterisation and modelling of lateral heterogeneity in reservoirs, Paris, 30th May.

Leverett, M. C., 1941, Capillary behaviour in porous solids. Trans. AIME, 142, p. 152-169.

Lewis, J. J. M., B. Lowden and A. Hurst, 1990, Permeability distribution and measurement of reservoir-scale sedimentary heterogeneities in subsurface exposures of a shallow marine sand-body, Fieltrip A11 Guide, 13th IAS Congress, Nottingham.

Lowry, P., and T. Jacobsen, 1990, Sedimentological and reservoir characteristics of a fluvial-dominated delta-front sequence, Ferron Sandstone Member (Turonian), East Central Utah, (abstract), Advances in Reservoir Geology '90 Conf., Geol. Soc., London.

Macdonald, A. M. (ed.), 1977, Chambers Twentieth Century Dictionary, Chambers, Edinburgh, 1652p.

Martin, J. H., and P. F. Evans, 1988, Reservoir modelling of marginal aeolian/sabkha sequences, Southern North Sea (U.K. Sector), SPE 18155, presented at 63rd Ann. Tech. Conf. & Exhib., Houston, Texas, 2-5th October.

Mitchener, B. C., D. A. Lawrence, M. A. Partington, M. B. J. Bowman and J. Gluyas, 1992, Brent Group: sequence stratigraphy and regional implications in A. C. Morton, R. S. Hazeldine, M. R. Giles and S. Brown (eds.), Geology of the Brent Group, Geol. Soc. Spec. Publ., 61, p. 45-80.

Muggeridge, A. H., 1991, Generation of effective relative permeabilities from detailed simulation of flow in heterogeneous porous media, in Lake, L. W., H. B. J. Carroll and T. C. W. Wesson (eds.), Reservoir characterisation II, Academic Press, Orlando, Florida.

Nottvedt, A., and R. D. Kriesa, 1987, Model for the combined flow origin of hummocky cross stratification, Geology, 15, p. 357-361.

Noman, R., and J. S. Archer, 1987, The effect of pore structure on non-Darcy gas flow in some low permeability reservoir rocks, SPE/DOE 16400, presented at SPE/DOE Low Permeability Reservoirs Symposium, Denver, Colorado, 18-19th May.

Pettijohn, F. J., P. E. Potter and R. Siever, 1972, Sand and Sandstone, Springer-Verlag, New York, 553p.

Prosser, D. J., and R. Maskall, 1993, Small scale permeability variation within aeolian sandstone: a case study using core cut sub-parallel to slipface bedding, the Auk Field, UKCNS, in C. P. North and D. J. Prosser (eds.), The Geological Society, London, (in press).

Reynolds, A. D., 1992, Storm, wave and tide-dominated sedimentation in the Dinantian Middle Limestone Group, Northumbrian Basin, Proc. Yorks. Geol. Soc., 49, p. 135-148.

Richards, P.C., and S. Brown, 1986, Shoreface storm deposits in the Rannoch Formation (Middle Jurassic), Northwest Hutton oil field. Scottish Journal of Geology, 22, p. 367-75.

Richards, P. C., S. Brown, J. M. Dean and R. Anderton, 1988, A new palaeogeographic reconstruction for the Middle Jurassic of the Northern North Sea, Jour. Geol. Soc. Lond., 146, p. 883-886.

Ringrose, P. S., K. S. Sorbie, P. W. M. Corbett and J. L. Jensen, 1992, Immiscible flow behaviour in laminated and cross-bedded sandstones, Jour. Petroleum Science and Engineering, 9(2), in press.

Roberts, J. D., A. S. Mathieson and J. M. Hampson, 1987, Statfjord, in A. M. Spenser *et. al.* (eds.) Geology of the Norwegian Oil and Gas Fields, Graham and Trotman, London, p. 319-340.

Robertson, G. M. and C. A. McPhee, 1990, High resolution probe permeability: An aid to reservoir description, paper presented at EURCAS, 21st-23rd May, London.

Robertson, R. W., and B. H. Caudle, 1971, Permeability continuity of laminae in the Calvin Sandstone. Journal of Petroleum Technology, p. 661-70.

Scotchman, I. C., Johnes, L. H., and Millar, R. S., 1989, Clay diagenesis and oil migration in Brent Sandstones of NW Hutton Field, UK North Sea, Clay minerals, 24, p. 339-374.

Scott, E. S., 1992, The palaeoenvironments and dynamics of the Rannoch-Etive nearshore and coastal succession, Brent Group, Northern North Sea, in A. C. Morton, R. S. Hazeldine, M. R. Giles and S. Brown (eds.), Geology of the Brent Group, Geol. Soc. Spec. Publ., 61, p. 129-147.

Size, W.B., 1987, Use of representative samples and sampling plans in describing geologic variability and trends, in Use and abuse of statistical methods in the earth sciences, by W.B.Size (ed.), Oxford University Press, 169p.

Southard, J. B., J. M. Lambie, D. C. Frederico, H. T. Pile and C. R. Weidman, 1990, Experiments on bed configurations in fine sands under bidirectional purely oscillatory flow, and the origin of hummocky cross-stratification, Journal of Sedimentary Petrology, 60, p. 1-17.

Stone, H. L., 1991, Rigorous black oil pseudo functions, SPE paper 21207 prepared for the 11th SPE Symposium on Reservoir Simulation, Anaheim, California, February 17-20th.

Stoneley, R., and Selley, R. C., 1991, A field guide to the Petroleum Geology of the Wessex Basin, Imperial College, London, 49p.

Styles, J. H. Jr., and N. S. Valenti, 1990, Investigating completion strategies - Cormorant Field, U.K. North Sea, SPEFE, March, p. 23-30.

Sun, S.Q., 1990, Discussion on swaley cross-stratification produced by unidirectional flows, Bencliff Grit (Upper Jurassic), Dorset, U.K., Jour. Geol. Soc., Lond., 147, p. 396-400.

Sutherland, W. J., C. Halvorsen, A. Hurst, C. A. McPhee, G. Robertson, P. R. Whattler and P. F. Worthington, 1991, Recommended practice for probe permeametry, paper presented at Minipermeametry in Reservoir Studies Conference, Edinburgh, 27th June.

Swift, D. J. P., and D. Nummendal, 1987, Discussion: Hummocky cross-stratification, tropical hurricanes and intense winter storms, Sedimentology, v.34, p. 338-344.

Thomas, J. M. D., and R. Bibby, 1991, The depletion of the Rannoch-Etive sand unit in Brent Sand reservoirs in the North Sea. Proceedings of the Third International Reservoir Technical Conference, sponsored by U.S. Department of Energy and National Institute for Petroleum and Energy Research, Paper 3RC-28. 39p.

Timmerman, E. H., 1982, Practical Reservoir Engineering, Pennwell Books, Tulsa, Oklahoma, 365p.

Van Wagoner, J. C., R. M. Mitchum, K. M. Campion and V. D. Rahmanian, 1990, Siliclastic sequence stratigraphy in Well Logs, Cores and Outcrops, AAPG Methods in Exploration Series, No. 7, American Association of Petroleum Geologists, Tulsa, Oklahoma, 55p.

Veen, F. R. van, 1975, Geology of the Leman Gas Field, in A. W. Woodland (ed.), Petroleum and the continental shelf of North-west Europe, Appl. Sci. Publ., Barking, Essex.

Walker, R. G., W. L. Duke and D. A. Leckie, 1983, Hummocky cross-stratification: significance of its variable bedding sequences: discussion and a reply, Bull. Geol. Soc. Am., 94, p. 1245-1251.

Walker, R. G., 1985, Ancient examples of tidal sand bodies formed in open shallow seas, in R. W. Tillman, D. J. P. Swift and R. G. Walker (eds.), Shelf sands and sandstone reservoirs, SEPM Short Course Notes 13.

Wardlaw, N. C., and J. P. Cassan, 1978, Estimation of recovery efficiency by visual observation of pore systems in reservoir rocks, Bull. Canadian Petroleum Geology, 24, p. 572-585.

Weber, K. J., 1986, How heterogeneity affects oil recovery, in L. W. Lake and H. B. Carroll (eds.), Reservoir Characterization, Academic Press, Orlando.

Weber, K. J., R. Eijpe, D. Leijnse and C. Moens, 1972, Permeability distribution in a Holocene distributary channel fill near Leerdam (The Netherlands), Geologie en Mijnbouw, 51, p. 53-62.

Winterbottom, F. A., 1990, Numerical modelling of a minipermeameter, Unpubl. M. Eng. Thesis, Heriot-Watt University, Edinburgh.

Yokokawa, M. and F. Masuda, 1991, Grain fabric of hummocky cross-stratification, Journal of Geological Society of Japan, 97, p. 909-916.

APPENDIX I

STATISTICAL METHODS

In this section, we review the statistical methods used in reservioir characterisation that are encountered in the main text. Reservoir characterisation, in the definition of Lake (1989a), "seeks to define quantitatively the input data needed to undertake predictions of flow through permeable media". Thus the obvious need for statistics in the summary petrophysical properties and understanding the spatial description of the reservoir for numerical simulation.

As the basis of any discussion of statistics, some terminology needs to be clearly understood. The reservoir unit for which the geologist or engineer is required to infer (or estimate or guess) values can be considered a population. This population may be the entire reservoir (*e.g.*, the Brent reservoir in the North Sea), a subdivision of the Brent (*e.g.*, the Etive, Rannoch) or even a sedimentological entity within the reservoir (*e.g.*, a bedform or lamina type). In each case, the estimate of the population parameter (*e.g.*, mean) by the process of statistical inference will be different.

The geologist usually estimates the population parameter by an appropriate descriptive statistic (*e.g.*, arithmetic average) from a sample. The sample can be a small set of measurements (*e.g.*, core plugs) taken from the reservoir or population of interest. The confidence with which the sample statistic can be taken as an estimate of the population parameter can be quantified.

In the petroleum industry, the samples that are available are generally very small and not necessarily representative. It is common to infer the parameters for an entire reservoir (order 10^{8}-10^{10} m^3) from a few cores (10-10^2 m^3) from which limited samples are taken (10^{-2}-10^{-3} m^3). The wells that are cored are often those drilled in "unrepresentative" field areas. Commonly, only the exploration and appraisal wells (under non-optimum conditions of interval, recovery or mud chemistry) and the first few development wells are cored. These wells are generally located in the crestal areas of the field which, possibly because of variable diagenesis in the hydrocarbon column, are often not representative of the reservoir population as a whole. Cores are rarely taken in the water-legs beneath hydrocarbon accumulations, but aquifer parameter estimation can be as important as parameters for the reservoir and the diagenesis is often different for aquifers.

It is important to recognise that the estimates of the core population parameters (*i.e.,* average horizontal permeability or porosity) should be based on sufficient samples taken from that core. If the core properties are poorly estimated, one can only expect the reservoir properties to be poorly estimated. Geologists and engineers should at least provide good estimates of core populations. The more variable a parameter is, the more samples are required to estimate it - permeability is commonly very variable and therefore most difficult to estimate.

I.1. Measures of Central Tendency

The most commonly used descriptive statistics that are determined from a sample are the measures of central tendency. By 'central tendency' we mean the tendency of the observations (measurements) in a sample to centre around a particular value rather than spread themselves across the range. When required to produce a set of summary numbers that describe our available set of variables, the average is the most easily determined.

The various measures of central tendency are defined and the relative merits of the measures for reservoir characterisation are considered. In this text, mean is the population parameter and average the sample statistic (used as an estimator of the population mean).

APPENDIX I: Statistical methods

I. 1.1. The Arithmetic Average

The arithmetic average of N data is obtained by adding the quantities and dividing by the number of data in the sample. This is commonly expressed mathematically as:

$$\overline{k}_{ar} = \frac{1}{N}\sum_{i=1}^{N} k_i$$

where k represents permeability.

The arithmetic mean is equally sensitive to all values. The practice of core analysis contractors to optimise the sampling of the "sands" can tend to produced unrepresentative biassed (*i.e*, systematically erroneous), high values for the arithmetic average.

I. 1. 2. The Geometric Average

The geometric average is determined as the Nth root of the product of N data and is usually written as:

$$\overline{k}_{geom} = \left(\prod_{i=1}^{N} k_i\right)^{1/N}$$

The geometric average of permeability can also be considered as the exponential of the arithmetic average of the natural log of permeability. This is easier to compute, as the product term in the above expression rapidily exceeds the capacity of most computers. It can be written in this form as:

$$\overline{k}_{geom} = \exp\left[\frac{1}{N}\sum_{i=1}^{N} \log_e(k_i)\right]$$

The geometric average is indeterminate in the presence of zero data values and this can cause problems for a sandstone matrix containing shales.

I. 1. 3. The Harmonic Average

The harmonic average for N permeability data is given by:

$$\overline{k}_{har} = N\left(\sum_{i=1}^{N} \frac{1}{k_i}\right)^{-1}$$

Like the geometric average, the harmonic average is also indeterminate in the presence of zero values.

The inverse of permeability (k^{-1}) can be considered as resistance to flow. The harmonic average is therefore the permeability that corresponds to the arithmetic average resistance to flow. It follows that the harmonic mean is sensitive to low values (*i.e.*, large values of k^{-1}). We have also seen that low permeability, fine grained material commonly occurs in much thinner layers (*e.g.*, micaceous or carbonaceous laminae) than high permeability, coarse grained material (*e.g.*, channel fill sandstones). As a result, even the harmonic average tends to produce an overestimate of vertical permeability.

I. 1. 4. Differences between Measures of Central Tendency

For a "perfectly" normal distribution all the above measures of central tendency will overlie (Fig. I-1). Differences become increasingly marked as the distributions become more skewed. In this latter situation which measure should be used? Skewed distributions (Fig. 4.15) are commonplace in permeability data and estimating a single average measure may not be appropriate.

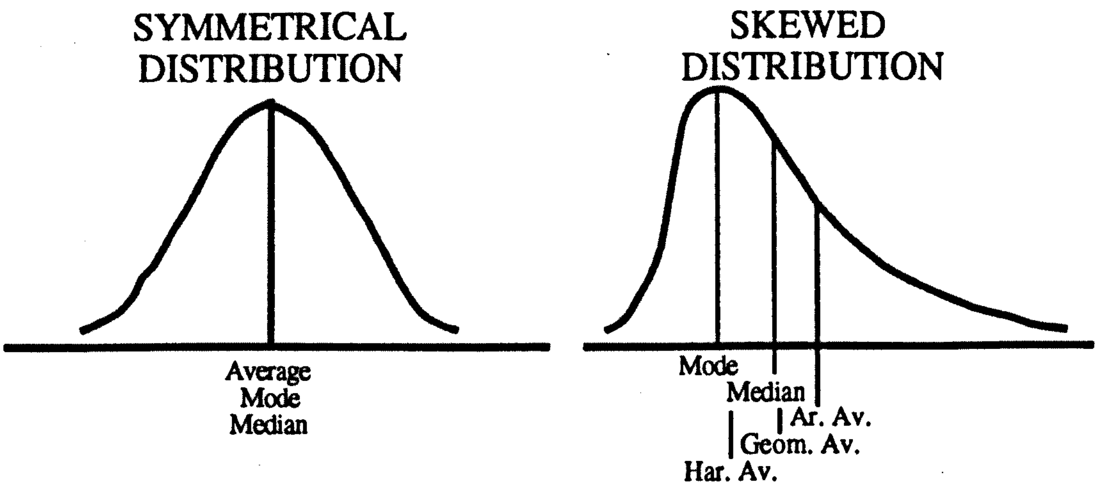

Figure I.1: Distibutions of measures of central tendency.

Differences in the arithmetic ($\bar{k}_{ar}$), geometric ($\bar{k}_{geom}$), and harmonic ($\bar{k}_{har}$) averages are a function of the sample heterogeneity, and are commonly observed in permeability datasets. The differences are such that always:

$$\bar{k}_{har} \leq \bar{k}_{geom} \leq \bar{k}_{ar}$$

The differences can be exploited for permeability as each average is appropriate for different flow conditions (refer to Archer and Wall, 1986):

$\bar{k}_{ar}$	bed parallel, single phase flow (*i.e.*, horizontal flow in a horizontally layered, bounded system)
$\bar{k}_{har}$	bed series, single phase flow (*i.e.*, vertical flow in a horizontally layered, bounded system)
$\bar{k}_{geom}$	single phase flow in a random, 2-D field

The use of the various averages to estimate mean permeability is appropriate only for the specific flow conditions described. Often the averages are used as (poor) estimators under the wrong flow conditions (*e.g.*, two phase flow, wrong dimensions, wrong boundary conditions, etc.), so extreme care is needed here to select the appropriate average. If the medium is homogeneous, the various averages will be very close in value.

I.2. Measures of Variability

In the previous section we reviewed measures of central tendency. The second class of descriptive statistics that can be used to describe a sample are measures of variability or dispersion. These are commonly used in other areas of data analysis but tend, traditionally, to be overlooked in petroleum engineering (particularly by geologists). As we will see in this and subsequent sections, the measures of variability of permeability can:

- define the level of heterogeneity
- determine the number of samples required
- indicate likely recovery process
- suggest likely flow performance

Because of these reasons, we feel that measures of variability can be equally (if not more) useful than averages. Every estimate of central tendency (of permeability) should be accompanied by a measure of variability.

I.2.1. The Standard Deviation

In statistics, a deviation is a distance from the mean. The mean deviation is thus the average deviation for a sample. The standard deviation (or root mean square difference if the assumed mean in the determination of the latter is the true mean) is given as the positive square root of variance:

$$s = \left(\sum_{i=1}^{N} \frac{(k_i - \bar{k})^2}{N} \right)^{0.5}$$

or

$$s = \left(\sum_{i=1}^{N} \frac{k_i^2}{N} - \bar{k}^2 \right)^{0.5}$$

Standard deviation has the units of measurement (e.g., mD in the case of permeability).

The lower the standard deviation the less the dispersion or spread of a distribution about the mean. 68% of all the observations in a normal distribution lie within one standard deviation (SD) either side of the mean (±2SD and ± 3SD include 95% and 99.7% of the observations, respectively).

I. 2. 2. The Coefficient of Variation

The standard deviation often tends to increase as the mean increases. An S.D. of 80mD is a high dispersion for a mean of 100mD, but a low dispersion if the mean is 1000mD. A more useful (in reservoir characterisation) absolute measure of dispersion is given by the coefficient of variation, or normalised standard deviation:

$$Cv = S.D. / \bar{k}_{ar}$$

For small samples ($N < 10$), the standard deviation needs to be multiplied by a correction factor (Johnson and Kotz, p. 63, 1970):

$$\left[1+\frac{1}{4(N-1)}\right]$$

The coefficient of variation is becoming more widely encountered in reservoir description, particularly in probe permeameter studies (Fig. I-2).

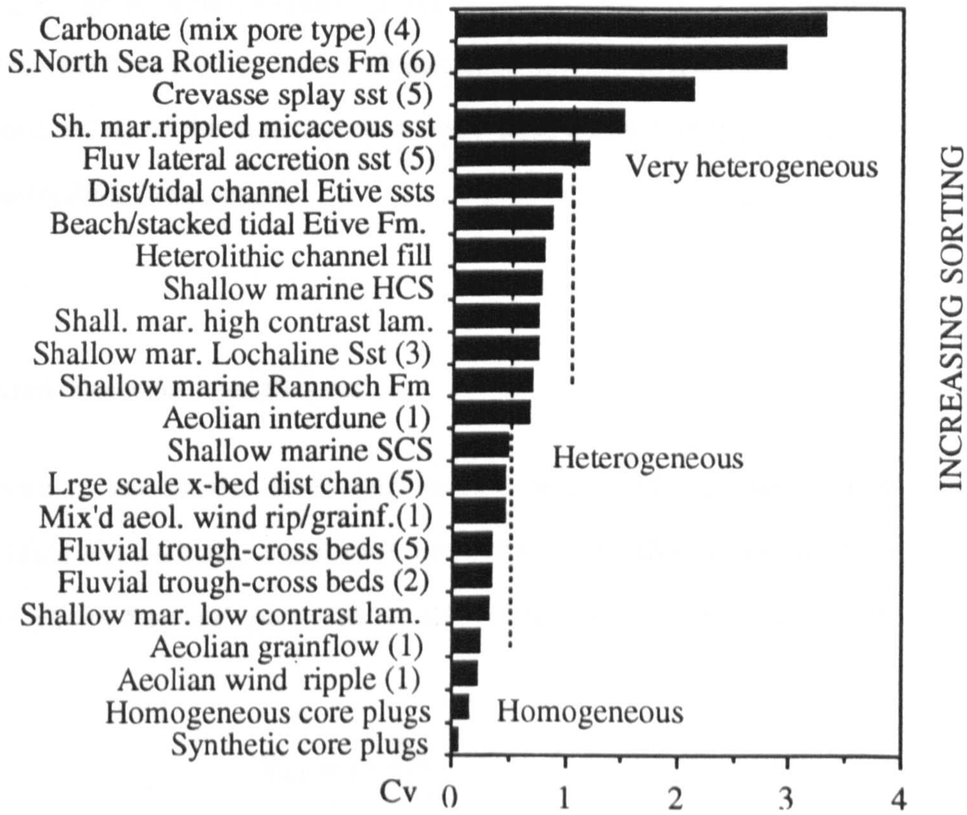

Figure I.2: Coefficient of variation for a range of geological materials. Sources of data for this plot are shown (1) Goggin *et al.*, 1988; (2) Dreyer *et al.*, 1990; (3) Lewis *et al.*, 1990; (4) Kittridge *et al.*, 1991; (5) Jacobsen *et al.*, 1991; (6) Rosvoll, pers.comm.

The Cv has been used to quantify various levels of heterogeneity, widespread use of which will undoubtedly lead to better communication of heterogeneity levels:

$0.0 < Cv < 0.5$	Homogeneous
$0.5 < Cv < 1.0$	Heterogeneous
$1.0 < Cv$	Very heterogeneous

The comparison of formation by variability and consistent definition of heterogeneity is recommended in reservoir characterisation. Normal distributions have $Cv < 0.5$ (Size, 1987); for $Cv > 0.5$ the distributions become increasingly skewed. Even under the latter conditions, the Cv appears to be a useful statistic. The y-axis on Fig. I-2, a list of geological nomenclature generally increasing in scale, can be deconvolved into combinations of stratal elements at various scales. The further systematic understanding of the hiearchy of stratal elements, their length scales and variability is reserved for future study.

I. 2. 3. Dykstra-Parsons Coefficient

A further measure of variability, developed by the oil industry, recognises that permeability is often log normally distributed. For permeability that is log-normally distributed, the Dykstra-Parsons coefficient is defined (Dykstra and Parsons, 1950) as:

$$V_{DP} = 1 - \frac{k_\sigma}{k_{0.5}}$$

where k_σ is the permeability one standard deviation below the median permeability ($k_{0.5}$) for a distribution of the logarithm (usually base 10) of permeability. These parameters are best determined by plotting a probability plot for log(k) and reading off the 50 and 16th percentiles. This graphical procedure for the determination of V_{DP} (for which probability paper is required) is illustrated in Fig. I-3.

V_{DP} is useful because of correlations with waterflood performance (Dykstra and Parsons, 1950) and EOR and common occurence in the petroleum engineering literature.

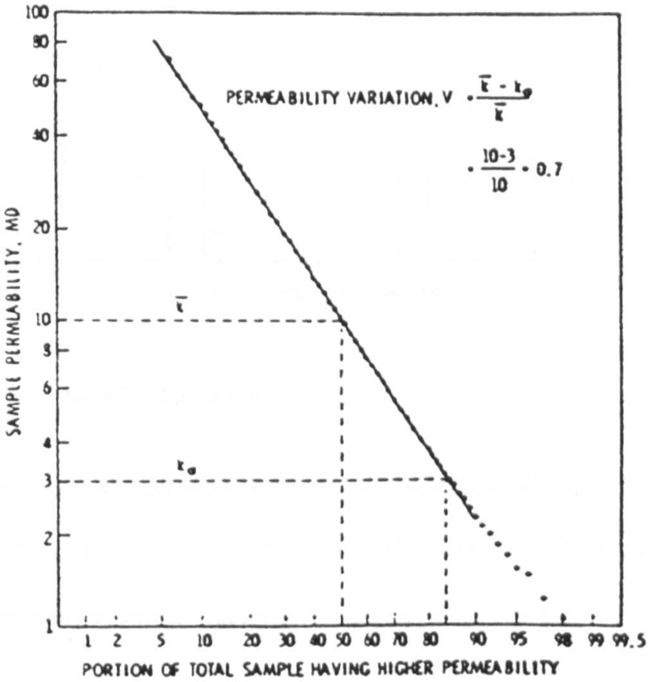

Figure I-3: Graphical solution of the Dykstra-Parsons coefficient (after Craig, 1971)

The Rannoch Formation in the Statfjord well has $V_{DP} = 0.54$ (Cv = 0.7) from core plugs. The Rannoch in Thistle, however, because of the carbonate nodules, has $V_{DP} = 0.72 - 0.996$ (Cv = 1.26 - 1.48). Neither measure of variability gives any measure of spatial variation.

I. 3. Distributions

A distribution is a graphical representation of a set of frequencies (observed distribution) or probabilities (theoretical distribution). Frequencies are presented on a bar chart (histogram) in which the width of the bars are proportional to the class interval and the height of the bars is proportional to the frequency it represents (Fig. I-4).

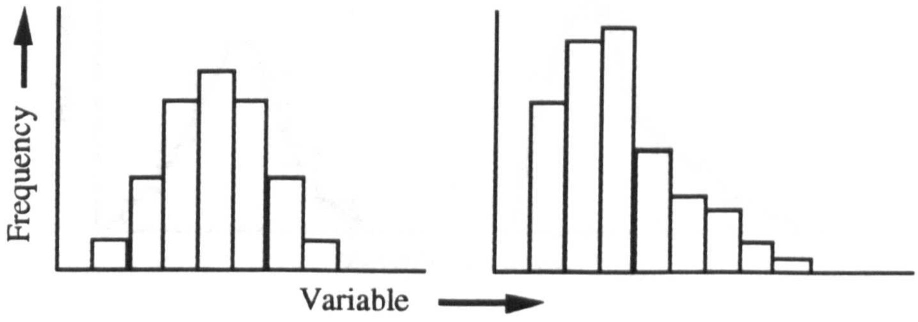

Figure I-4: Simple histograms

The class interval is the interval between boundaries selected to subdivide the range into a number of (usually equal) "windows". Points falling at the boundaries are systematically included in the class interval below or above.

Probability is a measure of the relative frequency of occurrence of an event. Probability (P) is a number between 0 and 1. Probability 0 means impossibility, 1 is certainty. Values can be derived from a theoretical distribution or by observation.

For a discrete distribution, probability is defined as:

$$\frac{\text{number of required outcomes}}{\text{total number of possible outcomes}}$$

Thus the probability of picking a spade from a pack of cards is $\frac{13}{52}$.

For a continuous variable, the probability is the relevant area under the graph of its prob-ability density function (pdf). The total area under the graph is 1, *i.e.*, a random variable is certain to lie within the range of its pdf. The pdf's for the variables in the sample hist-ograms above can be derived as the sample size approaches infinity and the class interval approaches zero (Fig. I-5).

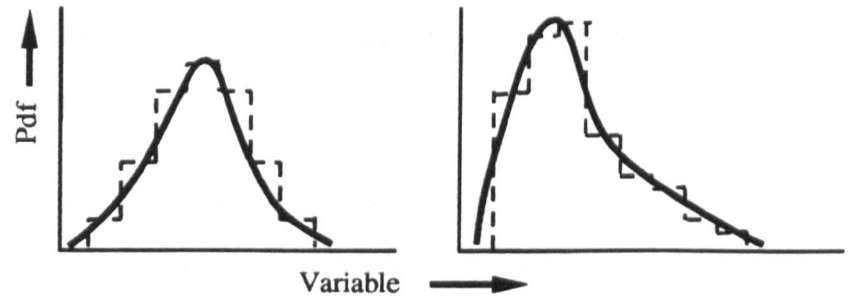

Figure I-5: Probability distribution functions underlying the sample histograms

If there are sufficient observations in the sample, the sample histogram can be thought of as an estimate (or approximation) to the underlying variable pdf. For this reason, sample histograms are often referred to as pdf's (strictly, pdf is a population parameter).

The function that gives the cumulative probability or cumulative frequency (*i.e.*, the frequency with which a varible has a value less than or equal to a particular value) of the random variable is known as the cumulative distribution function (cdf) (Fig. I-6).

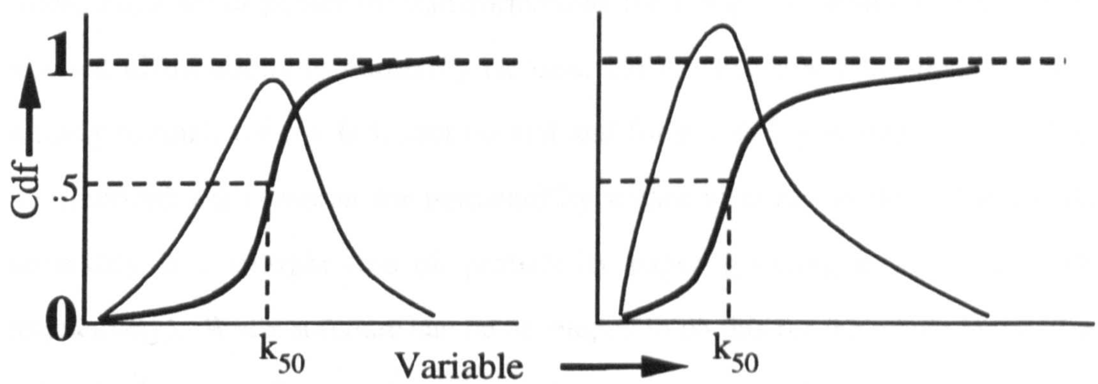

Figure I.6: Cumulative distribution functions associated with the above pdf's

Cdf's are the form of distributions that are commonly used as the input to Monte Carlo simulation. Random numbers between 0 and 1 are used to derive a number of realisations of the variable cdf (*e.g.*, for porosity, volume, shale length, channel width, etc.). The pdf of the random variable will, with enough realisations, assume the sample pdf. This procedure is the basis for stochastic (random) simulation.

There are major benefits in identifying the form of underlying pdf:

- the pdf is a statistical function that defines the extreme values and the probability of their occurrence.

- non-normal distributions can be transformed to normality if the underlying distribution is known. Parametric methods are appropriate and regression is enhanced for normally distributed variables.

- parametric (*i.e.*, sensitive to the underlying distribution) statistical tests are more powerful. Procedures where we don't know the form of the pdf are called non-parametric.

Distibutions that are not symmetrical are known as skewed. Consider the two pdf's in Fig. I-5, the one on the left is symmetrical whereas the one on the right is positively skewed (i.e., tail - queue in French - to the positive side of the mode). There are a set of power (p) transformations for $1 > p > -1$ which will transform skewed distributions to normality (Jensen, 1987). For $p = 1$ the distribution is already normal, for $p = 0.5$, root normal and for $p = 0$, log normal. These three distributions are common for permeability within reservoir rocks. The test for normality is a straight line on probability paper (plotting k, $k^{0.5}$ and log(k) respectively). While software can be developed to do this for the whole range of p-values to determine the straightest line and p to 3 significant figures, recognising that permeability is normal, root normal or log normal is sufficient in most cases.

How far the points can deviate from a straight line will depend on the number of data. For 10 -15 points, the allowable variation can be large. For 100 - 200 points the variation about the line should be small. For these reasons a lot of data are required to distinguish between normal and log normal for $Cv < 0.5$. With increasing skewness, the curvature on probability plots is more apparent and straight lines for the p-transformed variable easier to determine (Fig. I-7).

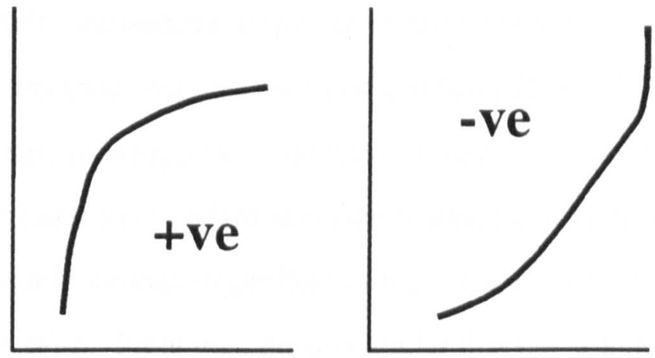

Figure I-7: Skewness as it appears in normal probability plots.

I. 4. Sample Sufficiency

The issue of sample sufficiency is not usually covered in basic statistical texts or even considered in petroleum engineering. Core plugs, for example, are taken every foot, regardless - because that's the way it has always been done! In fairness to the core contractors, geologists and engineers, this has, historically, been the practical (in terms of cost, core preservation, etc.) sample limit. With the development of probe permeameters, however, we are able to reconsider sample sufficiency and, because probe measurements are relatively cheap and non-destructive, ensure that sufficient samples for our requirements are obtained. This is one of the key advancements with the development of this device.

It is important to realise that the sample requirements for descriptive statistics (*i.e.*, estimating population parameters within specified tolerances) varies with the paramater estimated. For example, the arithmetic average can be much less data hungry than the harmonic average or pdf. Also, we will see that the sample requirements for other statistics measures that depend on spatial position may be quite different.

APPENDIX I: Statistical methods

How do we determine the number or spacing of sufficient samples? A useful concept is the N-zero (N_0) method proposed by Hurst and Rosvoll (1990). The central limit theorem states that, if independent samples of size n are drawn from a parent population with mean μ and standard deviation σ, then the distribution of their means will be approximately normal (regardless of the population pdf) with mean μ and standard deviation $\sigma/\sqrt{n}$. From this, the probability that the sample mean ($\bar{k}_s$) of N observations lies within a certain range of the population mean (μ) can be determined for a given confidence interval. For a 95% confidence level (i.e., only a maximum of five times in 100 will the population mean lie outside that range) the range is given by $\pm t \bullet SE$, where the standard error (SE) is given by S.D./$\sqrt{N}$. (The greater the sample number, N, the more confident we can be about estimates of the mean).

Standard error (SE) is the standard deviation of the sample mean, drawn from a parent population, and is a measure of the difference between sample and population means. Student's t is a measure of the difference between estimated mean, for a single sample, and the population mean, normalised by the SE. For normal distributions the t value varies with size of sample and confidence level, and these values are well known (standard t tables in any basic statistics text). The above can be expressed, mathematically, as:

$$\text{Prob} \left(\bar{k}_s = \mu \pm t \bullet \frac{SD}{\sqrt{N_s}} \right) = 95\%$$

For a sample such that $\bar{k}_0 \pm P\%$ tolerance satisfies the predetermined confidence interval, or:

$$\text{Prob} \left(\bar{k}_0 = \mu \pm \frac{P \bullet \bar{k}_0}{100} \right) = 95\%$$

So when this condition is satisfied, $N_s = N_0$, and:

$$\frac{P \bullet \bar{k}_0}{100} = t \bullet \frac{SD}{N_0}.$$

Rearranging this gives an expression for the optimum number of specimens, N_0:

$$N_0 = \left(\frac{t \bullet SD \bullet 100}{P \bullet \bar{k}_0}\right)^2$$

Now, for N > 30, t = 2 and with a 20% tolerance (*i.e.*, the sample mean will be within ±20% of the parent mean, which is considered to be an acceptable limitation), the expression reduces to:

$$N_0 = \left(\frac{2 \bullet Cv \bullet 100}{20}\right)^2 \qquad \text{where } Cv = S.D. / \bar{k}_0$$

$$N_0 = (10 \bullet Cv)^2$$

This rule of thumb is a very simple way of determining sample sufficiency. Although derived for the estimate of the arithmetic mean from uncorrelated samples by normal theory, we have found it useful in designing sample programs in a range of core and outcrop studies. Having determined the optimum number of samples, the domain length (D) will determine the optimum sample spacing (D_0) as:

$$D_0 = D / N_0$$

An initial sample of 25 measurements, evenly spaced over the domain, which can be a lamina, bedform, formation, outcrop, etc is recommended. If the Cv, determined from this sample, is less than 0.5, sufficient samples have been collected. If more are required, infilling the original with 1, 2 or n samples, will give 50, 75 or 25n samples. In this way, sufficient samples can be collected.

The appropriate level of sampling therefore varies as the variability differs. Because formations contain facies of differing variability, some facies will be adequately sampled with 1ft core plugs, but some thin, highly variable and, possibly, significant facies can be under-sampled. This happens in the Rannoch Formation (Fig. 4.11c) where the critical facies at the Rannoch/Etive boundary in some wells is only 10ft thick with Cv = 1. Over 100 samples, therefore, are needed in such an interval and

10 core plugs are obviously insufficient. The core plugs are, however, sufficient over the remainder of the Rannoch.

I. 5. Linear Regression

Linear regression is a statistical technique that is commonly used to explore relationships between two variables. It is most commonly used in reservoir characterisation in the area of petrophysics, where parameters measured in core are related to electric log readings. Linear regression in petrophysics is used for:

- tool calibration (*e.g.*, probe permeameter)
- log calibration (*e.g.*, matrix determination from intercept)
- electric log - core parameter predictors (*e.g.*, density-permeability)

Linear regression is so called because the regression parameters (a, b, c, etc.) are applied as a linear function, *i.e.*:

$$y = a + bx + cx^2 + dx^3 + ...mx^n$$

Obviously, such an expression (unless the x^2 term and higher powers are zero) is not necessarily a straight line. In the above equation y is known as the response and x the predictor.

Linear regression is generally used to relate measurements (*e.g.*, probe permeameter flow rates or log densities) to known data (*e.g.*, in both cases, core plug permeabilities) which may themselves be measurements. Both measurements are likely to contain errors giving rise to a scatter when y (ordinate) is plotted against x (absissa) (Fig. I-8). Additionally the relationship between response and predictor may not be a good one.

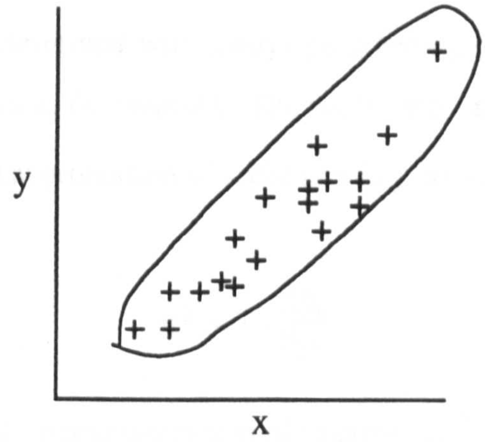

Figure I-8: Two variables that show a positive correlation.

A linear model would be fitted to this data by a least squares procedure, to give a relationship of the form:

$$\hat{y}_i = a \bullet x_i + b$$

where a is the slope and b, the intercept, of the fitted linear model. The best fit is defined by minimising the sum of squares of the residuals ($d = \hat{y}_i - y_i$) (Fig. I-9, also refer to Montgomery and Peck, 1982). Confidence intervals for the slope can be calculated (Jensen, 1991) and help identify outliers. Significance tests of slope and intercept are also available (Montgomery and Peck, 1982).

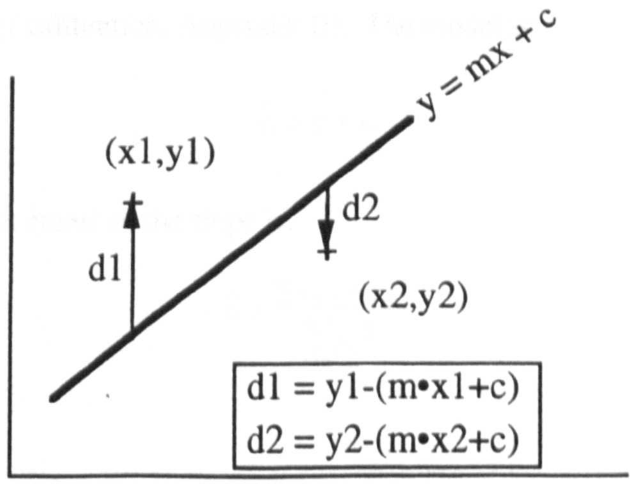

Figure I-9: Method of least squares for y on x regression

APPENDIX I: Statistical methods

The regression line determined will always pass through the means of the data ($\bar{x}$, $\bar{y}$), the point known as the centroid. The coefficient of determination (R^2) can be determined to see what proportion of variability in y is explained by the model. It is defined by:

$$R^2 = 1 - \frac{SS_e}{S_{yy}}$$

where: SS_{reg} = regression sum of squares $= \sum (\hat{y}_i - \bar{y})^2$

S_{yy} = total sum of squares in y $= \sum (y_i - \bar{y})^2$

SS_e = residual sum of squares $= \sum (\hat{y}_i - y)^2$

and $S_{yy} = SS_{reg} + SS_e$.

Note that the magnitude of R^2 increases with the steepness of the cloud of points, and R^2 neither measures the slope of the regression line nor the appropriateness of the model (Jensen, 1991). R^2 only determines the proportion of variability in y explained by the model. Also, R^2 should only be used with care to compare different models.

Sometimes it is appropriate to determine a zero-intercept model (has been used for probe permeameter calibration, Appendix II). The model is:

$$\hat{y}_i = a \bullet x_i$$

The least squares estimate of the slope is:

$$\hat{a} = \frac{\sum(y_i \bullet x_i)}{\sum x_i^2}$$

with

$$R^2 = 1 - \frac{\sum(\hat{y}_i - y_i)^2}{\sum y_i^2}$$

Note, the no-intercept R^2 (which has the sum of squares about the origin in the denom-inator) and with-intercept model R^2 (sum of squares about mean in the denominator) are not comparable.

The residuals between the observed values (y_i) and the predicted responses ($\hat{y}_i$) should always be plotted for a regression to see the quality of the model. Each of the regressions in Fig. I-10 would give similar R^2 values but clearly the right one is a poor model.

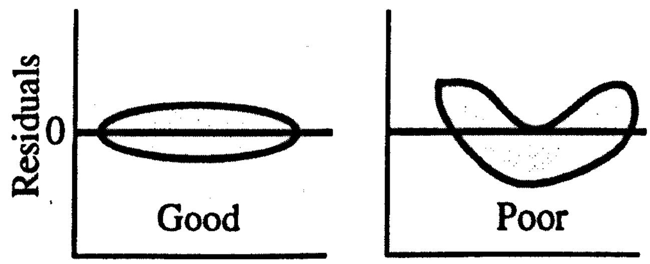

Figure I-10: Residuals demonstrate the quality of the regression model

I. 6. Spatial Correlation

In reservoir engineering, two autocorrelation functions, the correlogram and the semivariogram, are commonly encountered (Fig. I-11). The former tends to be used to measure the degree of similarity between neighbouring grid blocks in a numerical simulation and the latter to examine the spatial behaviour of permeability in outcrop or core studies. The latter is also used in a mapping procedure known as kriging which has been adopted from the mining industry and has been used (with some success) in the petroleum industry.

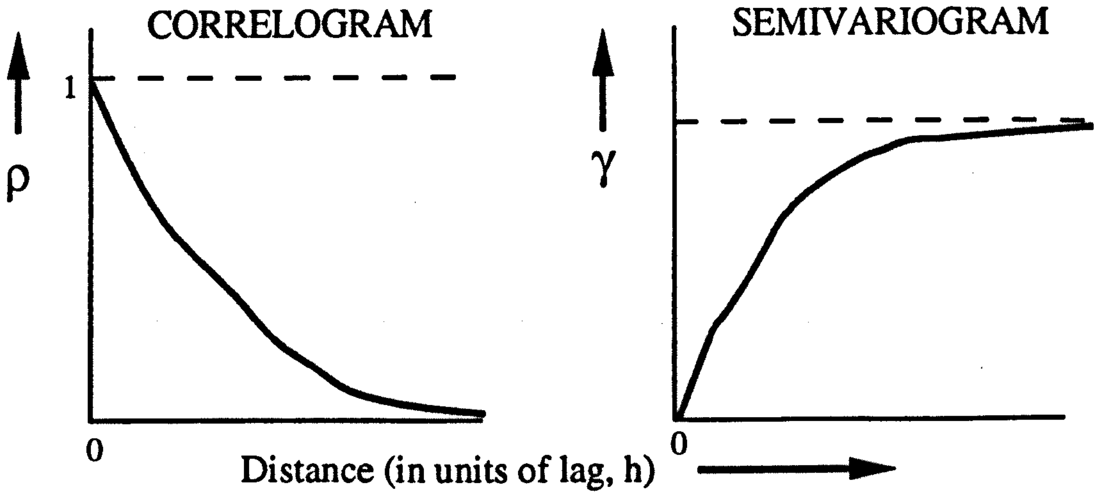

Figure I-11: Characteristic shapes of autocorrelation funcions in the presence of correlation.

The autocorrelation function (ρ) is given by:

$$\rho(h) = \frac{1}{(N-h) \bullet (SD)^2} \sum [(k(x) - \bar{k})(k(x+h) - \bar{k})]$$

where k(x) and k(x+h) are the permeabilities of any two points seperated by lag h and N is the number of pairs of points. As h tends to zero the correlation function tends to unity. A plot of the function against lag is the correlogram.

For comparison, the semivariogram function (γ, referred hereafter as the variogram) is given by:

$$\gamma(h) = \frac{1}{2N} \sum [k(x) - k(x+h)]^2$$

at a lag distance h. As h approaches zero the variogram (*i.e.*, variance) approaches zero. Note that the variogram doesn't require an estimate of the mean and is, therefore, more precise than the correlogram.

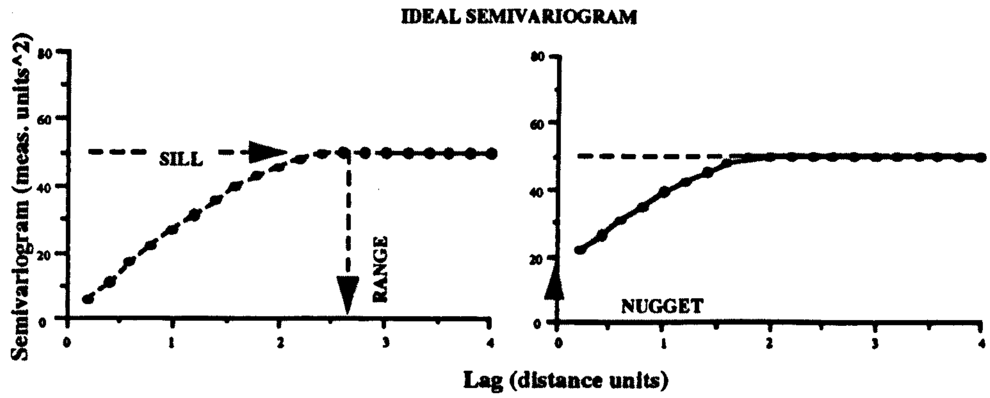

Figure I-12: Variogram terminology. (From Journal and Huijbregts, 1978).

The variogram has some additional features (Fig. I-12). At some separation (the range) the variogram often approaches the variance of the domain (the sill) and the correlation between points at this separation is zero. If the variogram at the closest separation is away from the origin, a nugget is said to exist, often indicative of measurement inaccuracy. If the variogram at the closest separation approaches the sill, the data are said to be uncorrelated (Fig. I-13, right). On a correlogram, uncorrelated data show the correlation function at or near zero from the shortest separation.

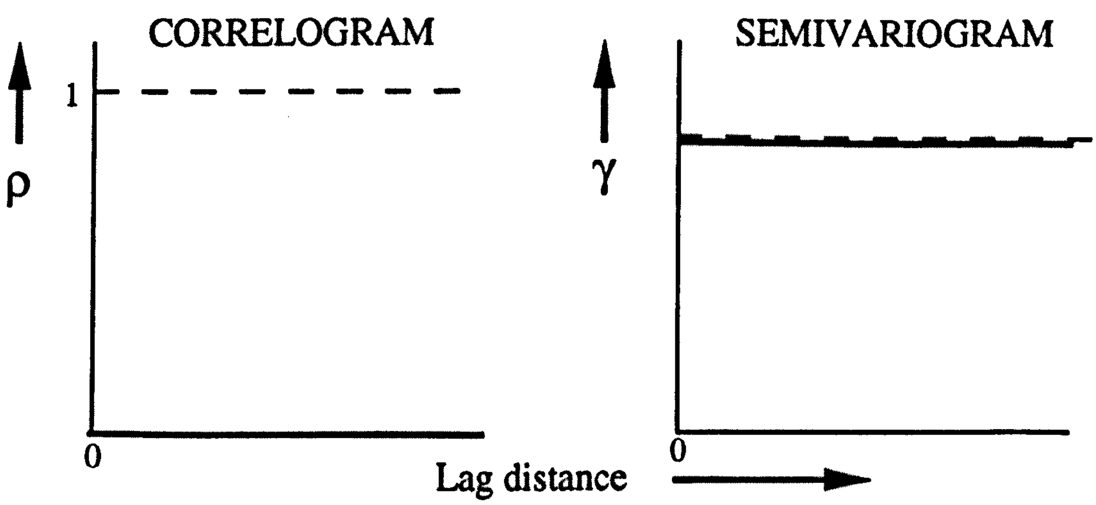

Figure I-13: Characteristic shapes of autocorrelation functions for random samples

It is important to determine the correlation in a data set, as correlation effectively reduces the amount of information carried by each observation. This can result in additional samples being required. There is a paradox here, because we have seen earlier that N_0 samples (derived for uncorrelated samples) can give appropriate estimates of mean properties, even though permeability measurements can be seen to be correlated. Although the reason for this paradox is not clear at the present time, it can be demonstrated that correlation in sedimentary rocks exists at several scales. These scales are marked by significant decreases of the variogram at some positive lag distance (holes).

The semivariogram can sometimes reveal "average" periodicities that are represented by a significant reduction in variance at some lag separation greater than the range. Two example variograms from the Rannoch (Fig. I-14) in two different wells show a periodicity at 1.2 - 1.4m (4 - 4.5ft). This periodicity is similar to that clearly seen in other minipermeameter intervals and is thought to be related to the (hummocky cross-stratified) bedform thickness. This periodicity in sediment can impact fluid flow (Chapters 5, 6) and that the holes, therefore, might be used as a diagnostic tool. The significance and value of the detailed semivariogram structure in geology and reservoir engineering requires further study.

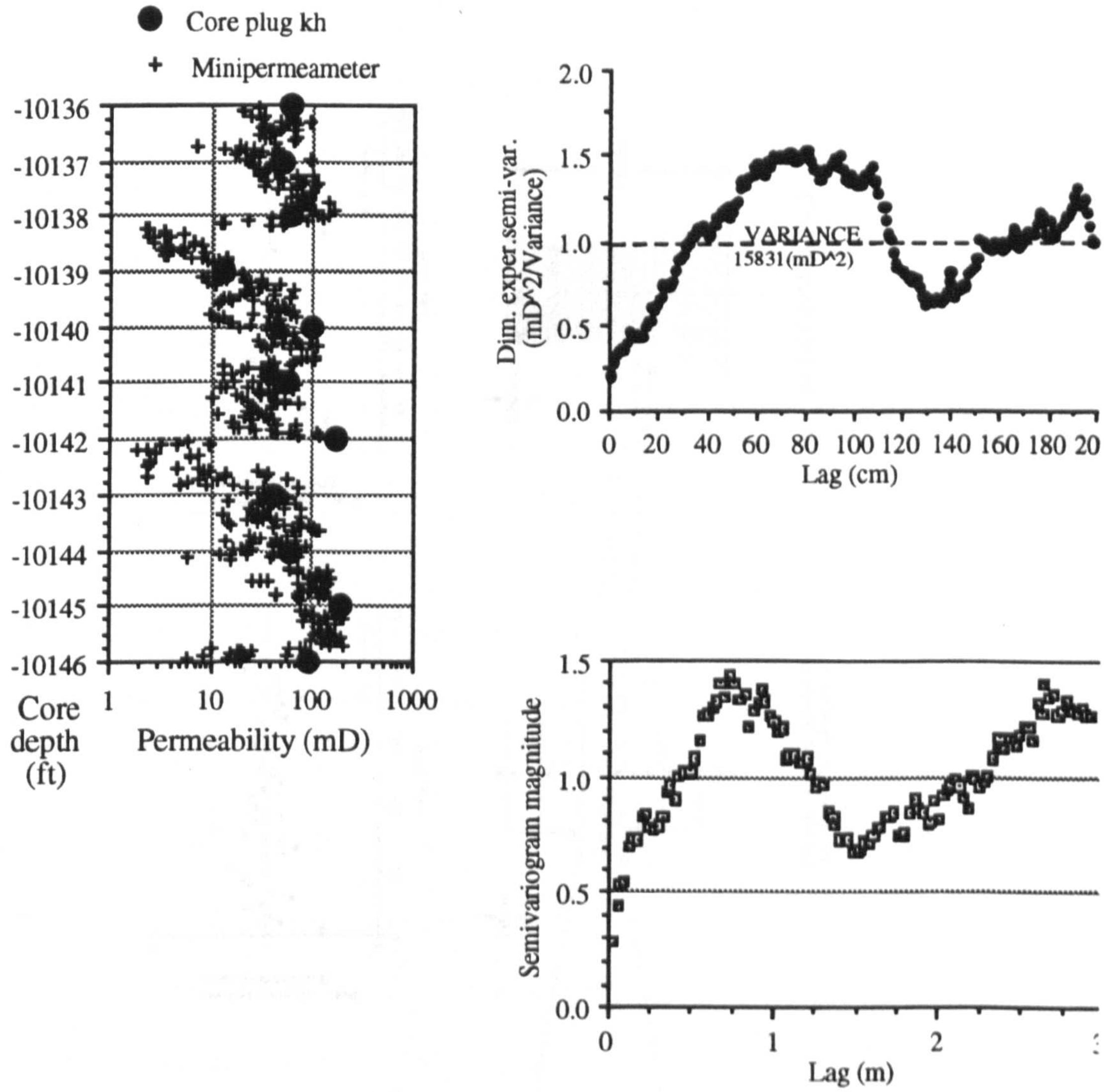

Figure I-14: Periodicity in sedimentary rocks and their variograms

This decrease in variance at certain separations reflects increased correlation and corresponds to the "wavelength" of a lamina or bedform. In this situation, where adjacent measurements come from different laminae (or may be separated by several laminae, each marking a geological event) it is difficult to see how they can be "correlated" despite the shape of the variogram!

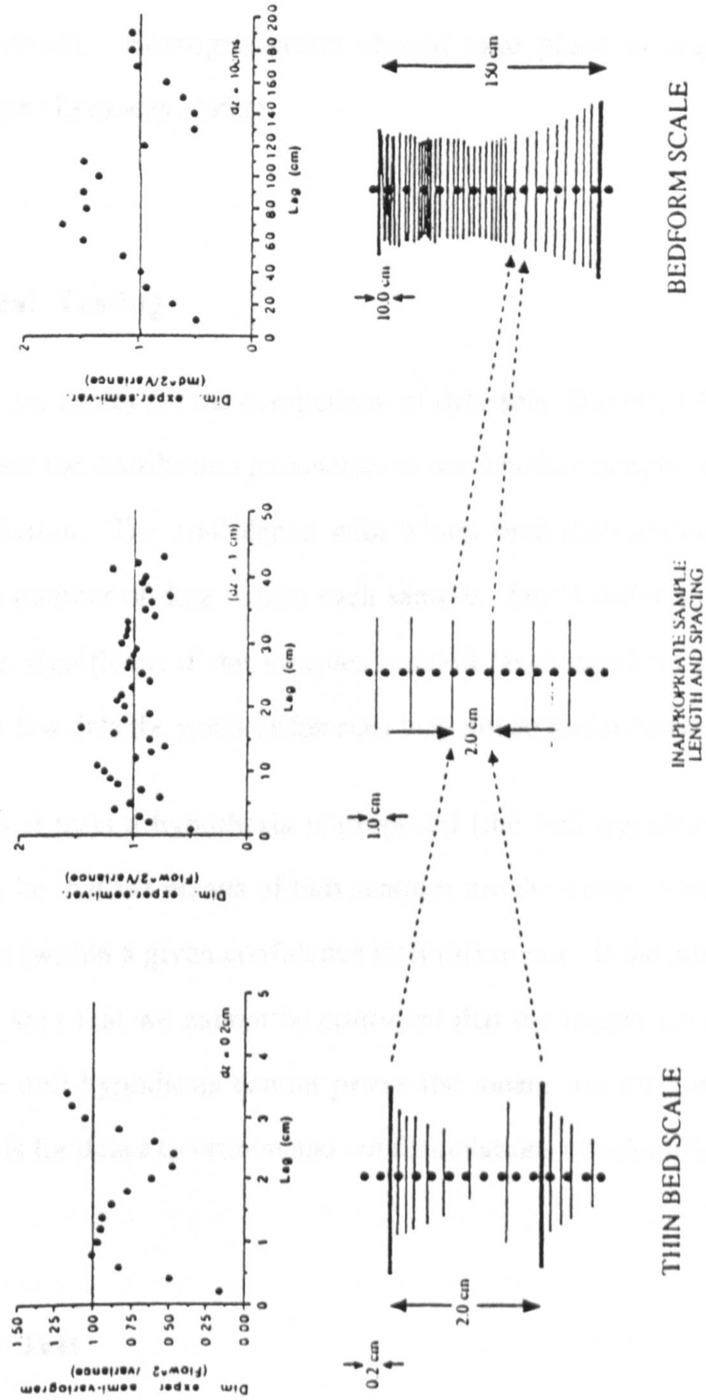

Figure I-15: Multiple correlation scales in sedimentary rocks, as shown by the variograms

It can also be seen in Fig. I-15 that each of these scales requires a tailor-made sampling plan, which may require more than N_0 samples. The presence of multiple correlation lengths in sediments, calls for homogenisation at various scales (i.e, the geopseudo method). Homogenisation should take place at scales above *the* correlation length (Lemouzy, 1992).

I. 7. Statistical Testing

Statistical tests are useful for the comparison of data sets (Davies, 1973). It is often useful to compare the distribution parameters to see whether samples are drawn from the same population. The confidence with which such distinctions can be made depends on the number of data within each sample. Small differences (*e.g.*, in the means) may be significant if the samples contain large numbers of data. If the samples contain few data the small differences may not be statistically different.

In most statistical tests a hypothesis is proposed (the null hypothesis). The null hypothesis may be that the means of two samples are the same. The statistical test can confirm this (within a given confidence interval) or not. If the null hypothesis is rejected it only says that we cannot be confident that the means are not the same - rejection of the null hypothesis cannot *prove* the means are different. Statistical methods are tools for data exploration and not formulations of scientific laws.

I. 7. 1. The t-Test

The t-test is used to test the equality of means. The null hypothesis is:

$$H_0: \mu_1 = \mu_2$$

versus the alternative,

$$H_1: \mu_1 \neq \mu_2$$

The test statistic is determined as:

$$t = \frac{(\bar{x}_1 - \bar{x}_2)}{s_p\sqrt{(1/n_1 + 1/n_2)}}$$

where the pooled estimate of polulation standard deviation (s_p) is given by:

$$s_p^2 = \frac{(n_1-1)s_1^2 + (n_2-1)s_2^2}{n_1 + n_2 - 2}$$

If the t value exceeds the value for the appropriate confidence level and degrees of freedom (given by $v = n_1 + n_2 - 2$) the null hypothesis can be rejected (the means are not the same). If the t value is less than the critical value there is *no evidence* that the samples are from populations having different means.

The t-test is most efficient for the normal distribution. It is appropriate, therefore, to transform the sample data using the power transformation and carrying out the test on the transformed data

I. 7. 2. The F-Test

The equality of the variances can be tested by the F-test (Davies, 1973). The t-test uses a null hypothesis of equal means whereas the F-test uses a null hypothesis of equal variances. The F-test and t-test are therefore both needed for the comparison of distributions. The F-value is calculated by:

$$F = \frac{s_1^2}{s_2^2}$$

where s_1^2 is the larger variance and s_2^2 is the smaller. The null hypothesis is now,

$$H_0: s_1^2 = s_2^2$$

and the alternative,

$$H_1: s_1^2 \neq s_2^2$$

If the calculated F-value is less than critical value given in statistical tables for a given level of significance (usually 5% or 95% confidence) we would have no evidence for concluding the variances are different. In this study, the t-test and F-test are used to compare measurements of stratal elements from different outcrops (Appendix VII).

APPENDIX II

PROBE PERMEAMETER CALIBRATION

The steady-state probe permeameter measures a stable injection rate of nitrogen at a given pressure. To determine permeability the rate needs to be calibrated for the specific injection pressure. A fixed injection rate limits the operating range of the instrument. In the initial Statfjord study measurements were taken at three injection pressures: 10, 90 and 400mbar. Each of two probes required calibration at these injection pressures. A series of measurements on homogeneous plugs (from a reference collection) were taken as the basis for these empirical calibrations (Halvorsen and Hurst, 1990). These empirical calibrations are discussed and compared with a published analytical model (Goggin, 1988). These empirical calibrations appear to work well over a single order of magnitude permeability variation.

In the Thistle study, a more sophisticated probe operating method was employed. The operating pressure was allowed to vary so that the injection rate settled within the "linear" regime (*i.e.*, at rates above the region of slippage and below the region of non-linear effects). The optimum injection rate of between 10 and 500ml/min was selected (C. Halvorsen, personal communication). In this case, a Statoil calibration curve, in which the effects of pressure changes were accounted for, provides a single k - Q/P relationship. This seems a pragmatic solution to the practical problems associated with core permeabilities varying over two or more orders of magnitude. The method is very amenable to automated control.

The published analytical solution (Goggin, 1988) has been noted by several authors to give similar results to the empirical calibration curves (Halvorsen and Hurst, 1990: Robertson and McPhee, 1990), however, care must be taken to ensure that the tip geometry is carefully measured for the relevant application pressure.

At the present time, the recommended calibration procedure is by measurement of homogeneous plugs of known permeability (Sutherland *et al.*, 1990). This study would confirm that careful calibration and care in the determination of permeability are time-consuming but unavoidable practices. The depth rationalisation and permeability determination for the Statfjord pilot study took several months.

I.1 Empirical Calibration

A number of regression models (Appendix I) were considered for the calibration of the Statfjord probe data using measurements for constant injection pressure on homogeneous plugs (Appendix X.1.a). A free regression linear model, a linear model fixed at the origin (no intercept), a power law and a quadratic model were all considered. The linear no intercept model was considered to give the most appropriate fit (Fig. II-1).

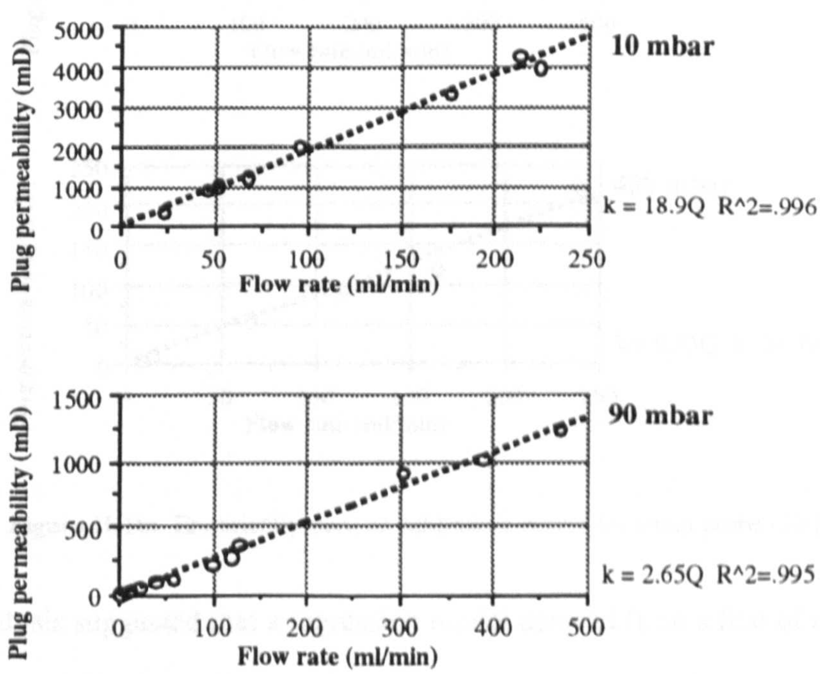

Figure II-1a: Empirically-derived calibration curves for the large probe (LP1).

There were no significant deviations from a linear relationship to suggest that the linear Q:k Darcy relationship did not hold. There were also no significant intercepts on the free regression lines. The calibration lines were used to derive the permeability data listed in Appendix X.

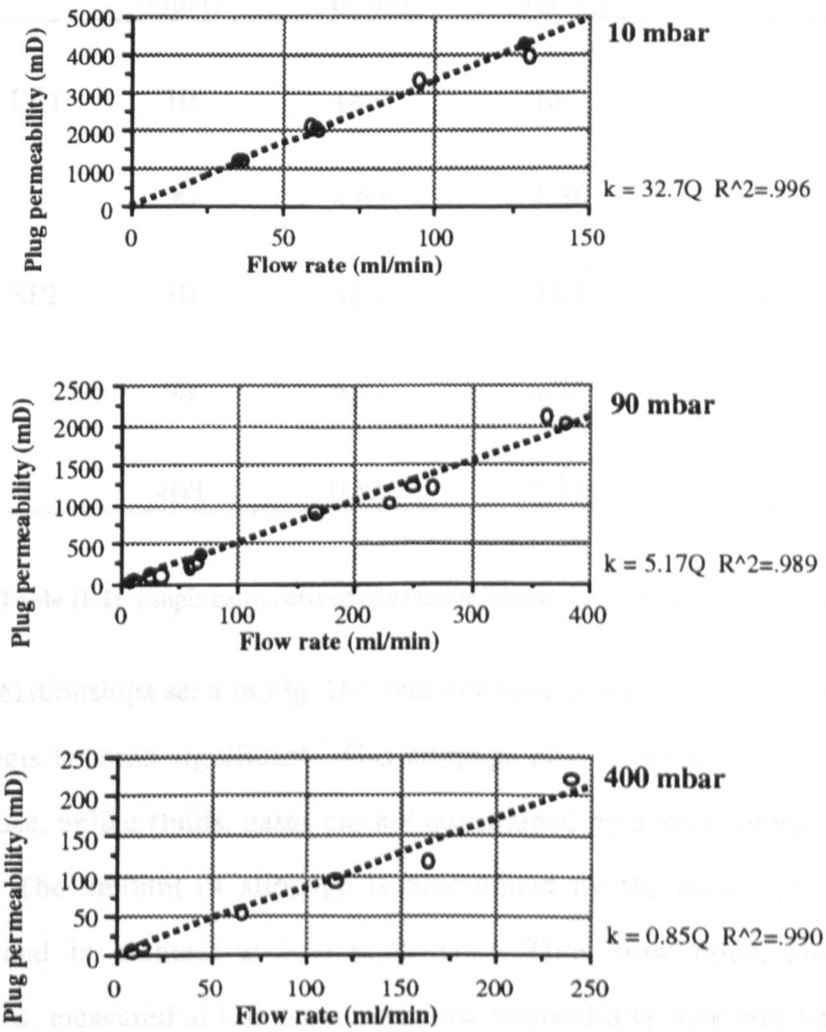

Figure II-1b: Empirically-derived calibration curves for small probe (SP1).

Further analysis suggested that a regression model derived from a line of unit slope on a log-log plot would give a linear relationship with a more uniform error model. The conversion factors derived from the two empirical methods are compared in Table II-1. Differences between the two approaches are less than 15%. Conversion factors derived from these empirical methods are compared in the following section with the analytical solution.

Probe	Pressure (mbar)	Factor (lin-lin)	Factor (log-log)	Percent. Difference
LP1	10	18.9	18.7	+1
	90	2.65	2.36	+12
SP1	10	32.7	33.5	-2
	90	5.17	4.53	+14
	400	0.85	0.77	+10

Table II-1: Empirically-derived conversion factors for probe flow rates to permeabilities.

The linear relationships seen in Fig. II-1 will not hold in regions where gas slippage or inertial effects become significant. Gas slippage effects occur in low permeability media because, unlike fluids, gases are not constrained by a zero velocity layer at the pore wall. The amount of slippage is determined by the mean free path of the molecules and is greatest at low pressures. Thus flow rates, and hence air permeabilities, measured at low pressure in low permeability rock will be higher than those measured at higher gas pressures or those obtained with liquids. The Statoil probe permeameter operates at lower pressures (< 1 bar) than is usual in the Hassler cell plug apparatus (> 1 bar). On a plot of probe permeameter flow rate versus Hassler cell permeability, the data would plot below a straight line through the origin at low rates particularly for low pressures (e.g. 10 mbar) if significant slippage effects were present. This does not appear to be the case in Fig II-1. If slippage effects are identified the appropriate Klinkenberg correction for liquid permeability at the operating pressure must be employed. By operating outside the region of slippage, the gas permeabilities should be close to liquid permeabilities.

At increasing flow rates, non-laminar, non-Darcy flow may become important. These non-laminar effects are a result of the complex geometry of the pore network (in addition to "true turbulence" that will occur in smooth straight pipes at high flow rates) in reservoir rocks and a function of porosity, permeability, pore shape, pore connectivity, pore roughness and heterogeneity (Noman and Archer, 1987). Inertial effects can be apparent prior to the onset of true, eddying, turbulent flow (Firoozabadi and Katz, 1979; Ezeudembah and Dranchuk, 1982) and are most likely to occur at high velocities and/or small pore radii. The effect of non-laminar flow is seen as a reduced flow rate, compared to that expected for laminar flow, for a given pressure and permeability. A series of measurements taken at increasing pressures on the same homogeneous plug should demonstrate where non-laminar flow effects become a significant factor.

In considering high velocity effects and calibration, it is important to bear in mind the velocity of the injected gas. At 550 ml/min, the velocity of injected gas at the probe/rock interface is approximately 35 to 90cm/s for the large and small probes respectively. Data from the department's core analysis manual suggests the velocities in a Hassler cell plug are often lower (20 cc/s is equivalent to an injection rate of 4 cm/s into a 1" plug). Non-laminar flow is then potentially more likely to be encountered with the probe permeameter. Calibration curves derived from real plugs have high velocity flow effects "built-in", at least over the range of measured flow rates. Providing the nature of the pores (porosity, tortuosity, etc.) in the rock under investigation is similar to the calibration plugs, reasonable determination of permeability can be expected.

In the Thistle study, the greater quantity of sampled core meant that the selection of specific injection pressures would not be practical. Instead, the device was programmed to select a variable injection pressure that ensured a reasonable flow rate

(10-500ml/min). This operating mode required a different calibration curve. A relationship was derived for the probe (SP2) from calibration data (Appendix X.2.a) on a plot of normalised permeability against flow rate (Fig. II-2). In this way, the effects of varying pressure could be incorporated. This method is similar to a procedure used in the department where k is plotted against Q/P (Jarvis *et al.*, 1992).

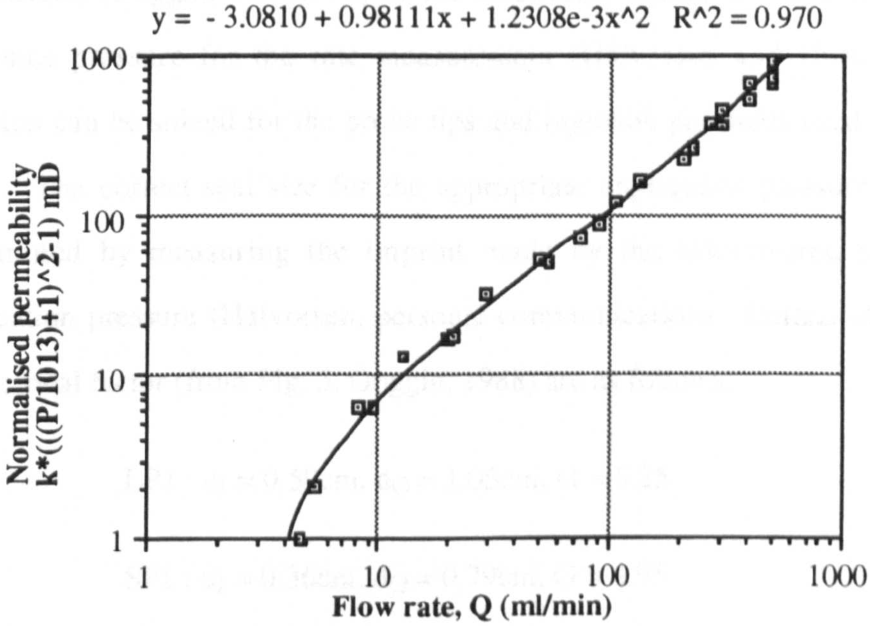

Figure II-2: Empirically-derived calibration curves for small probe (SP1). After Christian Halvorsen (personal communication).

In these data, there is non-linearity for flow rates below 10ml/min and above 500ml/min suggesting that flow rates within this range follow the linear Darcy relationship. The curve shown was used to determine the permeabilities in the Thistle study.

II.2. Analytical calibration

The analytical solution proposed by Goggin (1988), which has been derived from the Darcy equation, has also been used to calculate permeability from the flow rates, pressures and tip geometries. In the formulation:

$$k = \frac{2\,Q\,\mu\,P_I}{a\,G\,(P_I^2 - P_O^2)}$$

k is the permeability (m^2), Q is the flow rate (m^3/s), μ is the nitrogen viscosity (Pa s), P_I is the injection pressure (Pa), P_O is the atmospheric pressure (Pa), a is the internal tip-seal radius (m) and G is the geometrical factor appropriate for the tip and sample dimensions (Goggin, 1988). P_I in the numerator occurs in this formulation as the reference pressure for the rate measurement (Halvorsen and Hurst, 1990). This equation can be solved for the probe tips and injection pressures used in the Statfjord study. The correct seal size for the appropriate application pressure (0.5 atm) was determined by measuring the imprint made by the ink-covered seal under that application pressure (Halvorsen, personal communication). Details of geometry and geometrical factor (from Fig. 5, Goggin, 1988) are as follows:

LP1 : $d_I = 0.59$cm, $d_O = 1.05$cm, $G = 5.25$

SP1 : $d_I = 0.36$cm, $d_O = 0.79$cm, $G = 4.95$

The Goggin (1988) analytical solution simplifies to $k = F.Q$ (where the conversion factor, $F = \frac{2\,\mu\,P_I}{a\,G\,(P_I^2 - P_O^2)}$) for comparison with the factors derived by regression (Table II-2). In this simplification of Goggin's model, the injection pressure has been assumed constant and non-linear corrections ignored.

In general, the empirical and analytical conversion factors are in close agreement for the lower pressure rating, but diverge at higher pressures. This suggests that some non-linear effects may be present in the data acquired at higher pressure. The steeper slope seen in the calibration data can, therefore, be explained by non-laminar effects that are not accounted for the above simplification of Goggin's model.

Probe	Pressure (mbar)	Regression *F* (lin-lin)	Regression *F* (log-log)	Goggin *F*	%age Diff. (lin-lin)	%age Diff. (log-log)
LP1	10	18.9	18.7	18.7	+1	0
	90	2.65	2.36	2.00	+33	+18
SP1	10	32.7	33.5	32.6	<+1	+3
	90	5.17	4.53	3.48	+49	+30
	400	0.85	0.77	0.68	+17	+13

Table II-2: Comparison of empirical and calculated conversion factors.

A maximum 50% difference between the empirically- (linear-linear regression) and theoretically-derived probe permeameter permeabilities may not be significant when order of magnitude variations are being measured. The closer agreement between the log-log regression and theoretically-derived coefficients (maximum difference 30%) supports the use of this approach, and, for this data set, would result in lower probe permeabilities and increased differences with the core plug data. Calibration is not responsible for the differences between probe and plug discussed in Chapter 4 (Section 4.3).

APPENDIX III

THE PROBE VOLUME OF INVESTIGATION

The volume of investigation of the probe is a subject of much interest to all involved in the interpretation of probe data. Numerical studies show this to be limited to a few aperture diameters (Goggin, 1988). The limited volume of investigation appears to conflict with the experimental observation of "bubbles" exiting a (water saturated) block a large distance (several centimetres) from the injection point. In this study, numerical simulations (using ECLIPSE) black oil simulator were carried out to investigate the volume of investigation further. In particular, the effects of a no permeability boundary (*i.e.*, resin) a short distance from the tip were an initial concern.

III.1. ECLIPSE Model Study

Two previous computer model studies have considered the depth of investigation of the probe permeameter under various boundary conditions and tip geometries (Goggin, 1988; Daltaban and Lewis, 1989). This present study was initiated to see whether an "industry standard" simulation package could be used to model the probe permeameter and, in particular, to evaluate the depth of investigation and the effects of an impermeable boundary layer a short distance into the rock beneath the probe (*i.e.*, under the appropriate boundary conditions for the data acquisition in this study). The core slab on which our probe permeameter measurements were taken had previously been resinated to preserve the core and only *ca.* 0.75 - 1.0 cm of the slab remained unimpregnated. It was observed that the impregnation was significantly greater in the coarse grained, high permeablity Etive material. Impregnation into the fine grained Rannoch was generally 2mm or less.

III.1.1 Model Construction and Operation

A two-dimensional, radial model was constructed using ECLIPSE (ECL, 1988). For the purpose of this study, a single phase fluid and an homogeneous, isotropic medium were considered sufficient to model the effects of a zero-permeability layer at a non-zero distance below the injection surface.

Grid dimensions were varied during the development of the model and an intermediate, simplified grid construction is shown in Fig. III-1. The ECLIPSE input file can be referred to in Appendix VIII. The final model (which included additional cells to model the probe) has 294 blocks. Gas injection into an inner boundary cell, with adjacent radial cells set to zero porosity and zero permeability, was used to simulate the permeameter probe. The injected flow was thus constrained to enter the "core" and escape to the "atmosphere" from the "core" surface outside the area of the tip seal. The "atmosphere" was drained by a "producer" at distance from the "core" and the volume injected balanced with the volume produced to simulate steady state conditions.

To ensure the injection pressure was uniform over the injected surface, the injection cell was further subdivided into 5 cells with radii chosen to normalise the flux, using the curve published by Goggin *et al.* (1988, their Fig. 4). High transmissibility from the injected cell to the top layer of the "core" ensured that the pressure drop from injector to the "core" (at the core surface) was minimal.

Operation of the model was controlled by varying injection rates and "core" permeabilities and monitoring the resulting pressure in the injection cell.

III.1.2 Model Results

A series of model runs using the injection rate and permeability data for the large probe (LP1) were used to validate the model. For the flow rates and corresponding permeabilities measured, the model was used to predict the injection pressure. The

ECLIPSE model pressures were then matched against the probe permeameter operating pressures (10 and 90mbar gauge) and values calculated from the Darcy equation (Fig. II-2). In the ECLIPSE model, the rates measured at atmospheric pressure were corrected to the operating pressure ($P_O Q_O = P_I Q_I$).

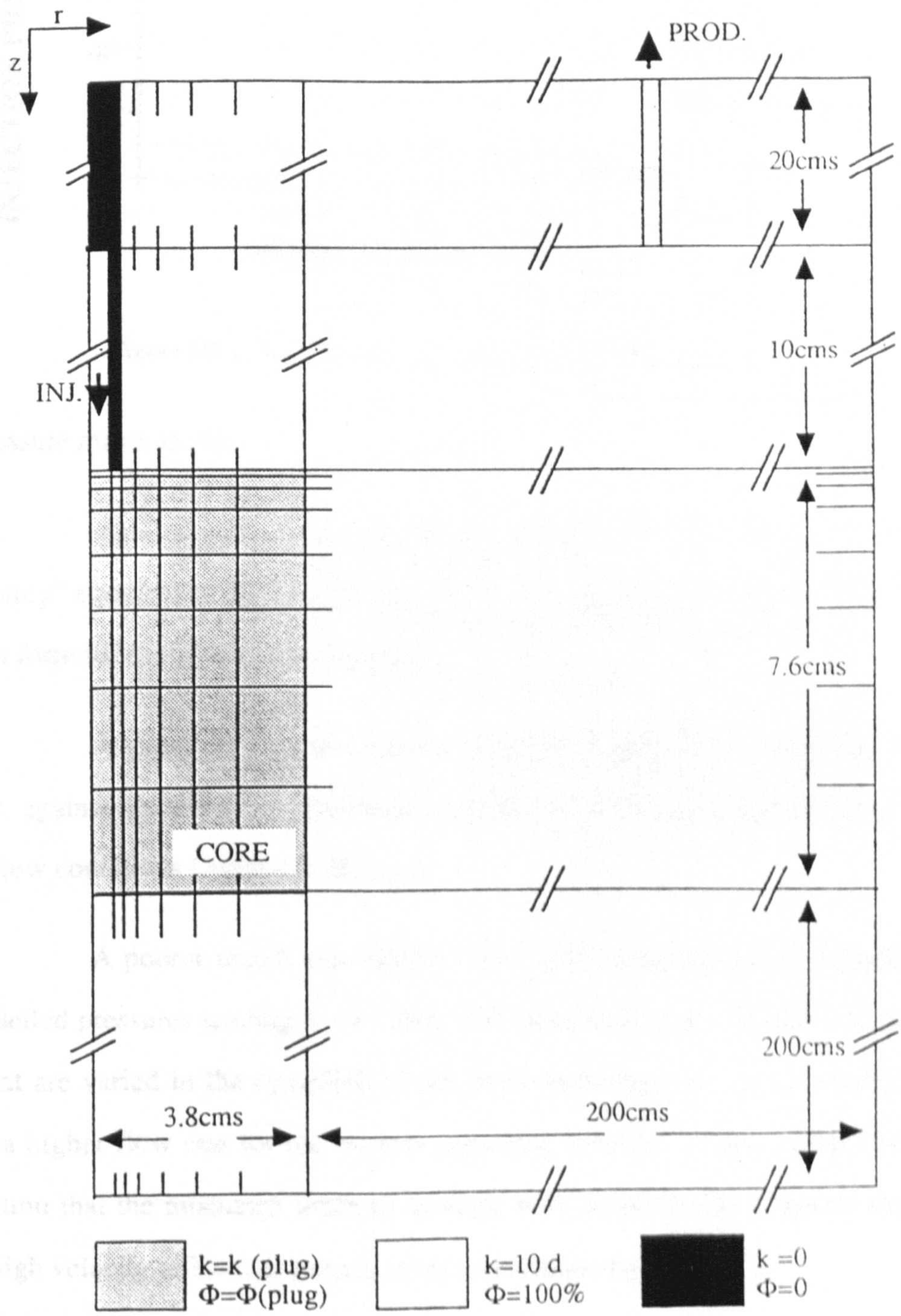

Figure III-1: Schematic illustration of the ECLIPSE probe permeameter model grid.

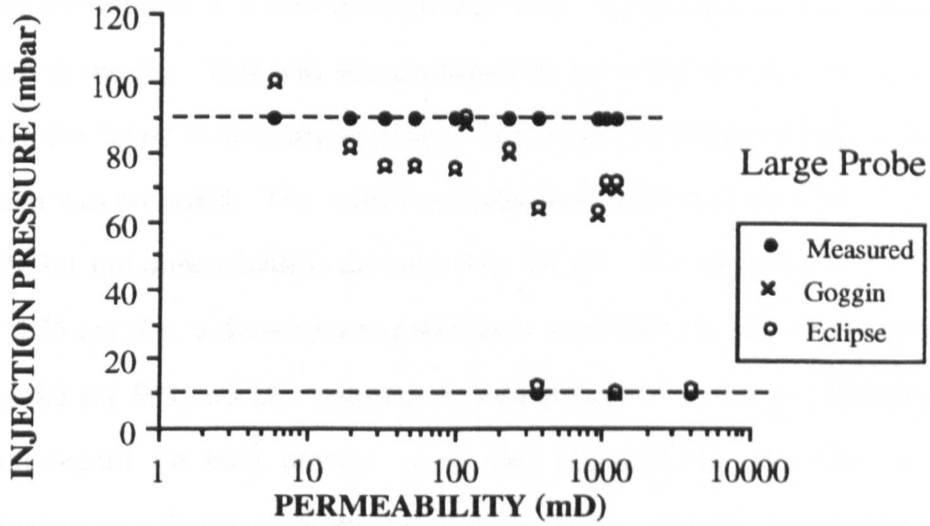

Figure III-2: ECLIPSE probe permeameter model pressure match

The pressure match shows:

1. As expected, a close match was obtained between the ECLIPSE model and "Darcy" equation of Goggin (1988). This was expected since the ECLIPSE model is also a formulation of the Darcy equation.

2. A good match was obtained between measured and simulated data at 10mbar, again supporting the observation that those data were acquired under linear, Darcy flow conditions (Appendix II, p. vi).

3. A poorer match was obtained with the measured data at 90mbar, with the modelled pressures tending to be lower than those measured. In fact it is the flow rates that are varied in the operation of the probe permeameter, so the model would predict a higher flow rate for the 90mbar operating pressure. This, coupled with the observation that the mismatch tends to increase with permeability, suggests that non-linear, high velocity effects are present in the calibration data.

The validation study concluded that the ECLIPSE model was a good representation of the linear flow regime and could be used to examine the effects of core resination and pobe depth of investigation. The main purpose of this modelling exercise was to examine the effects of a zero-permeability layer, within the "core", a short distance from the probe tip. This was accomplished by progressively setting the lowest grid blocks in the "core" to zero permeability. The respective change in injection pressure at each step was recorded. The results are presented both in terms of absolute distance (Fig. III.3a) and dimensionless distance (Fig. III.3b). It is apparent from these figures that at 0.75 cm (*i.e.,* a dimensionless thickness normalised to the inner probe radius of 2.5 and 4.2 for SP1 and LP1 respectively) the effects of a zero permeability layer are minimal (<5%) for both probes. It is also apparent that the effective depth of investigation is a function of the inner probe radius, with the larger probe having a deeper investigation. These model results predict that there should be minimal effects caused by the resin and, if apparent at all, should be seen as a relatively lower permeability by the larger probe in comparison to the small probe, as a result of the former's deeper investigation.

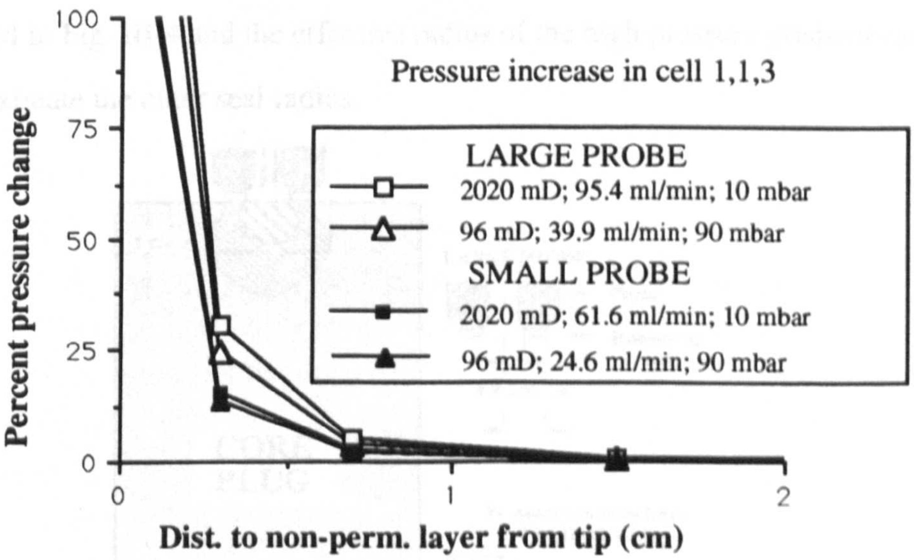

Figure III-3a: Modelled probe permeameter response to an impermeable boundary at an absolute distance from the probe tip

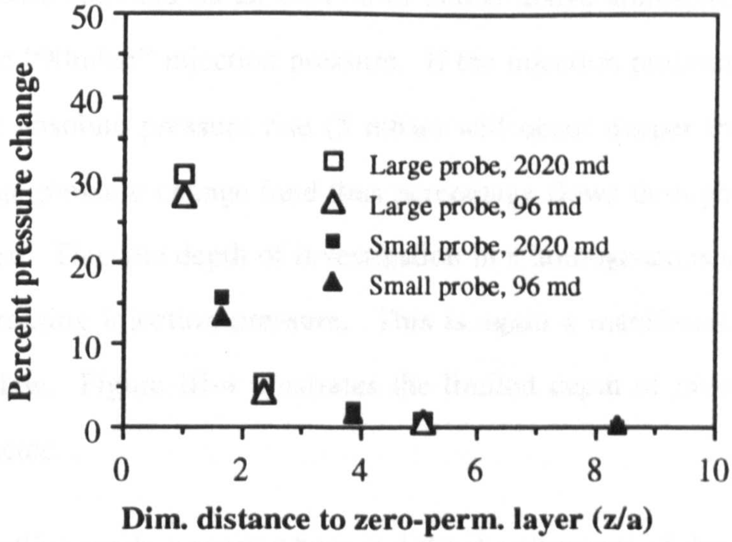

Figure III-3b: Modelled probe permeameter response to an impermeable boundary at a dimensionless distance from the probe tip.

These model results also suggest that the effective depth of investigation, in an homogeneous system, is somewhat less than the four-times inner probe radius quoted by Goggin *et al.* (1988). The pressure disturbance around the probe permeameter is illustrated in Fig. III-4 and the effective radius of the high pressure gradient can be seen to approximate the outer seal radius.

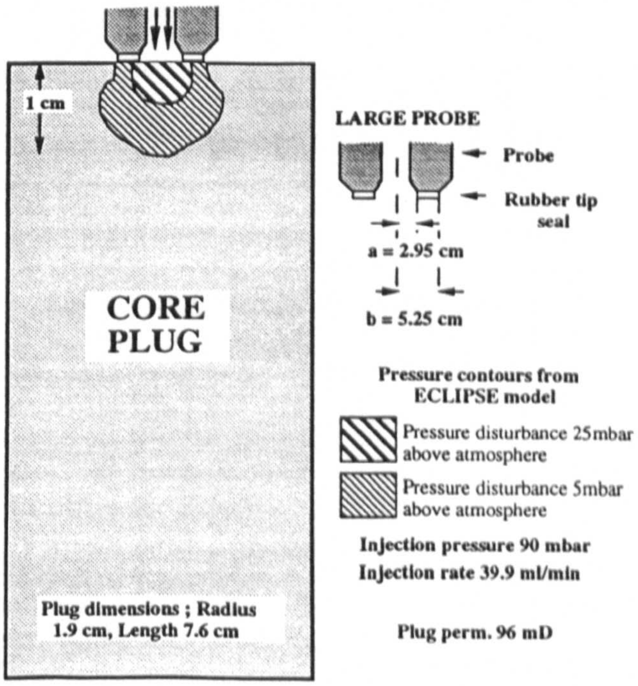

Figure III-4: Pressure disturbance around the probe permeameter tip.

The pressure contours (at an interval of 5mbar above atmospheric) are approximately 5% of the "90mbar" injection pressure. If the injection pressure is increased ten-fold, the same absolute pressure rise (5 mbar) will occur deeper into the "core", but the percentage pressure change (and thus percentage flows through the plug) will remain unchanged. Thus the depth of investigation in a homogeneous system will not change with increasing injection pressure. This is again a manifestation of the linearity of Darcy's law. Figure III-4 illustrates the limited depth of investigation of the probe permeameter.

The modelling work presented here and the development of this study (Winterbottom, 1990) conclude that the effective (or significant) volume of investigation is a small factor (two times) of the internal aperture diameter. The bubbles exiting the core at some distance from the injection point, that were discussed at the start of this appendix, represent a small volume of the nitrogen injected. The minimum pressure drop as the gas exits the core will not be registered by the probe. The majority of the gas vents to the atmosphere in the immediate region of the tip seal.

APPENDIX IV

CAPILLARY PRESSURE

The measurement of capillary pressure in reservoir rocks is one of the few direct measurements of the system that contains the reservoir fluids (*i.e.*, the pores and pore throats). It is very rare, however, that systematic capillary pressure characterisation of a reservoir is carried out. There is a widely held belief in the engineering community (various practicing reservoir engineers, personal communication) that capillary pressure is not significant to the quantification of reservoir fluid flow in waterflooding of unfractured reservoirs.

Historically, therefore, because capillary pressure measurements are expensive and time consuming to make, only a few samples are measured. In this study, only one of the fields described (Thistle) had a reasonable range of capillary pressure curves for the Rannoch Formation. These were drainage curves (see the following section), imbibition curves were even rarer, however, three were available from Cormorant Field. Interestingly, drainage capillary pressure curves are also a primary tool of the sedimentologist, however, the data acquired by the different disciplines are rarely integrated.

In this section, the capillary pressure data for the Rannoch Formation are interpreted in the light of a wider appreciation of a fundamental geological control. All the data discussed in this section are for core plugs. Whilst these are assumed to be from homogeneous plugs (following the industry convention), no systematic analysis or measurement of sub-core plug capillary pressure heterogeneity was possible because of the lack of a suitable device.

IV.1 Definition of Drainage and Imbibition Capillary Pressure Curves

The displacement of an occupying fluid in a pore space by a second (immiscible) fluid will be controlled by the relative wettabilities of the two fluids to the rock. The pressure required to displace the wetting fluid in the largest pores is equivalent to the threshold capillary pressure. A plot of saturation versus the pressure required to displace fluid from ever decreasing pore sizes is known as a capillary pressure (Pc) curve (Fig. IV-1). If this curve describes a decrease in wetting phase saturation it is known as a drainage curve.

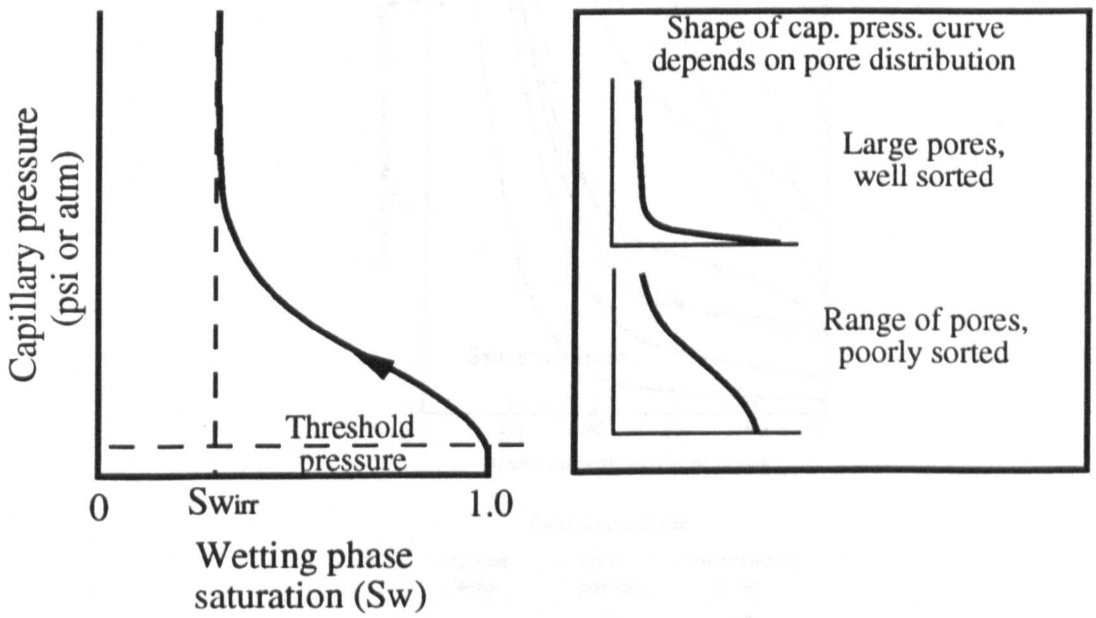

Figure IV-1: A capillary pressure curve. This curve represents the injection pressure required for a non-wetting phase (*e.g.*, oil) to invade a 100% water-bearing interval (*e.g.*, as a reservoir fills with oil over geological time) which is water-wet. The inset shows how the shape of the capillary pressure curve depends on the distribution of pore sizes.

The pressure required to displace the wetting phase (*i.e.*, the liquid phase that for reasons of fluid or rock chemistry is preferentially attracted to the rock surface) increases as the pore and pore throat sizes decrease. The Pc curve in a rock with a uniform pore distribution shows a sharp bend in the region of the threshold pressure for the respective pore thoat size. A range of pores and, hence, pore throats and threshold pressures in a rock gives rise to a more gentle curve. This curve is typically measured in the laboratory by air displacing brine or mercury displacing air. The Rannoch Formation, like most reservoirs is not uniquely water-wet, but generally thought to be moderately water wet (K. Sorbie, personal communication). A series of drainage Pc curves for a range of reservoir rocks is shown in Fig. IV-2.

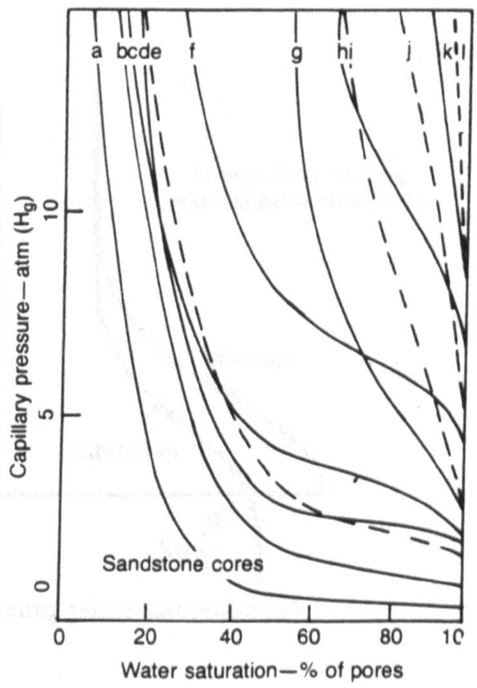

Sandstone cores

Curve letter	Total porosity %	Permeability to air, md
a	17	285
b	12	8
c	19	13
d	14	3
e	32	30
f	20	1
g	12	0.5
h	11	0.3
i	28	2
j	25	0.4
k	15	0.3
l	25	0.1

Figure IV-2: Capillary pressure curves for typical reservoir rock types (from Timmerman, 1982).

These curves show a range of curve forms; the higher permeability rocks tend to be better sorted than the low permeability rocks. These curves are not from a single reservoir, however, a similar range of curves can be expected from a single heterogeneous reservoir.

As the measurement process is reversed, the wetting phase is imbibed, however some of the displacing fluid remains trapped in individual, small pores and the capillary pressure curve displays hysteresis (Fig. IV-3). The residual oil trapped in the pores is a measure of the microcopic sweep efficiency.

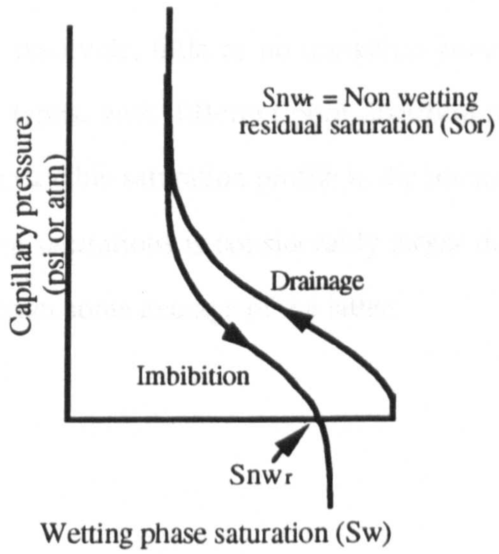

Figure IV-3: Capillary pressure hysteresis. After a displacing fluid has entered the pores it is not possible to completely flush the invading fluid out. A residual saturation (Snw_r) will remain trapped in the smaller pores.

As the original water filling the reservoir is displaced by migrating oil, drainage of the water phase is said to occur. In this situation, the water is known as the wetting phase and remains as a coating of the grain surfaces. The reversal of this process, as water displaces oil (*e.g.*, during a waterflood) is considered an imbibition process, because water saturation increases. Oil, in this situation, is the non-wetting phase and is located in the centre of the pores.

IV.2. Capillary Pressure Distribution in Reservoirs

In a reservoir containing oil and water, the buoyancy of the oil gives rise to a pressure difference between the oil and water phases (Fig. IV-4). This pressure, at equilibrium conditions, is equal to the capillary pressure (Pc). The saturation can also be plotted against depth (*i.e.*, a function of Pc and the density difference between the liquids). Reservoir rock close to the oil-water contact that is not at connate (*i.e.*, immoveable) water saturation is considered to be in a transition zone ($1\text{-}S_{nwr} < Sw < Sw_{irr}$). In poor quality reservoirs, this transition zone can be of a significant thickness, whereas, in a very good quality reservoir, little or no transition zone is seen. In reservoirs, several interbedded rock types, with different pore distributions and different Pc curves, can give rise to a more variable saturation profile in the transition zone (Fig. IV-4). The scale of these electric log saturations is considerably larger than the core plug measurements and therefore represent some average of the latter.

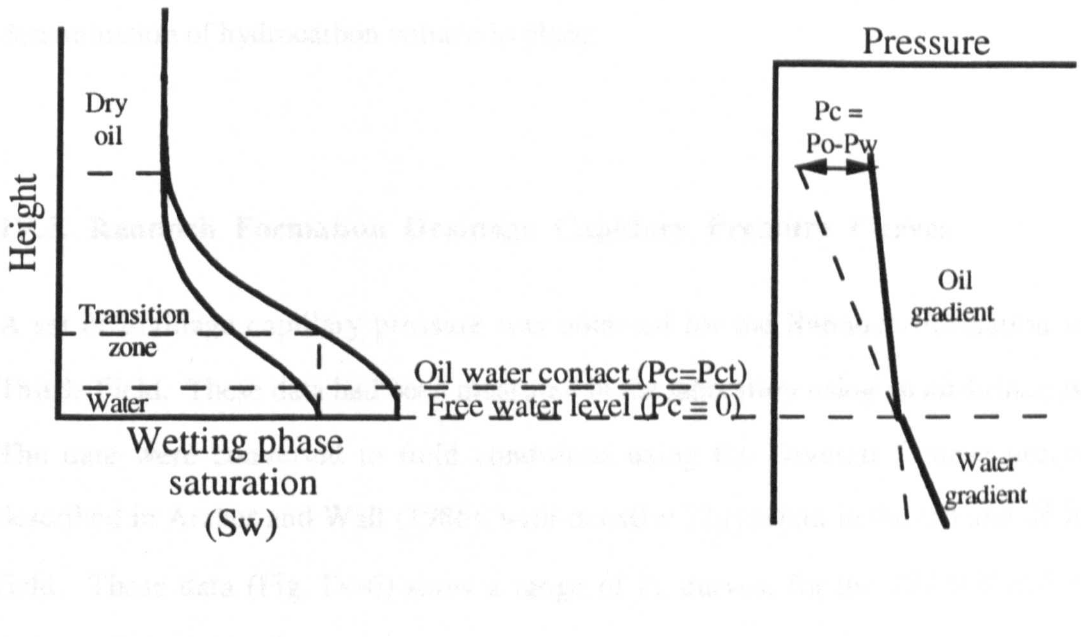

Figure IV-4: Static water saturation distribution in a homogeneous reservoir. Pressure gradients shown.

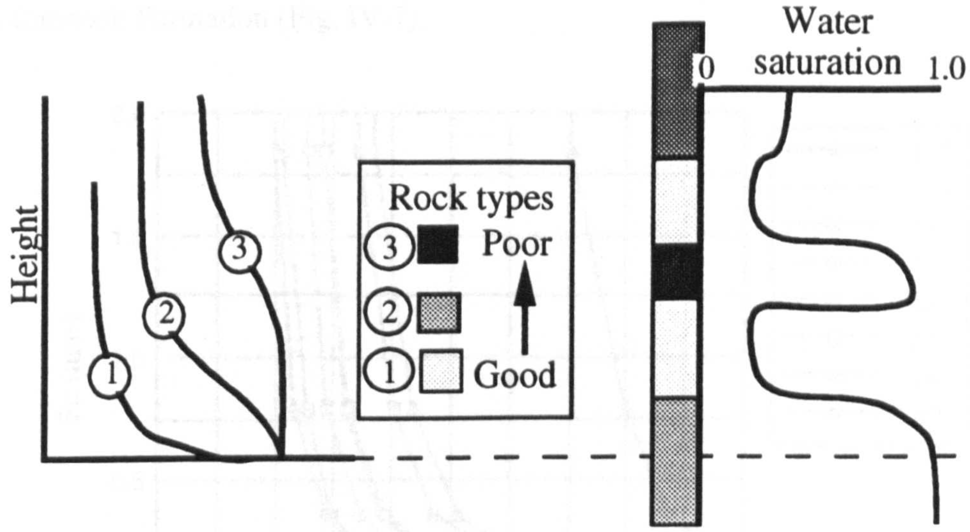

Figure IV-5: Static water saturation distribution in a layered reservoir, where the capillary pressures of the interbedded reservoir rocks varies.

In reservoir simulators, the initial hydrocarbon saturations and, hence, hydrocarbons-in-place, are determined from the height above the hydrocarbon-water contact. Choosing the correct "average" capillary pressures can, therefore, have a major impact on the determination of hydrocarbon volume in place.

IV.3. Rannoch Formation Drainage Capillary Pressure Curves

A set of drainage capillary pressure was obtained for the Rannoch Formation in the Thistle Field. These data had been measured in the laboratory using an air-brine system. The data were converted to field conditions using the Leverett J-curve procedure described in Archer and Wall (1986), with $\sigma\cos\theta$ = 72dyne/cm in the lab and 26 in the field. These data (Fig. IV-6) show a range of Pc curves, for the 187-0.97mD plugs measured, describing a systematic variation in pore throat geometry.

The Leverett J-function can also be used to scale a Pc curve for a measured k/ϕ to another k/ϕ. However, the form of the J-curves generated from the above data show differences, suggesting the simple capillary bundle modelled by the Leveret J-function is too simple for the Rannoch Formation (Fig. IV-7).

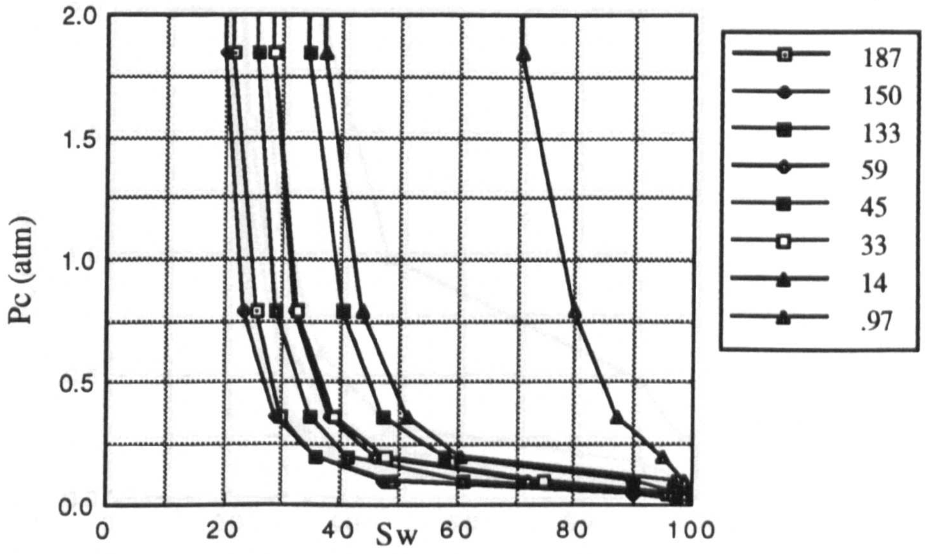

Figure IV-6: Laboratory drainage Pc measurements for a series of Rannoch Formation (Thistle Field) core plugs, transformed to field units using the Leverett J-curve. Figures in key are permeabilities (mD).

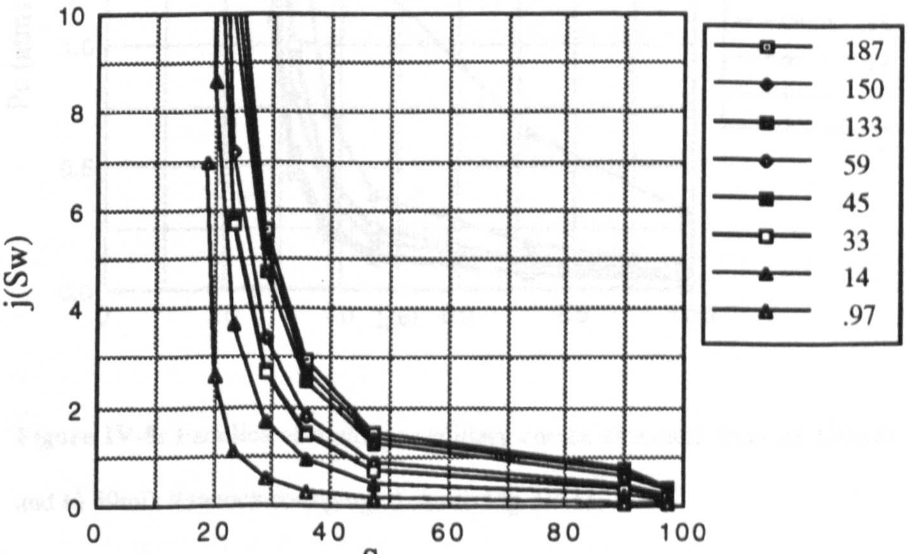

Figure IV-7: J-curves generated from the Rannoch laboratory data shown in Figure IV-6.

As a result of this, a family of curves generated from one of these J-curves does not fully represent the lab data (Fig. IV-8).

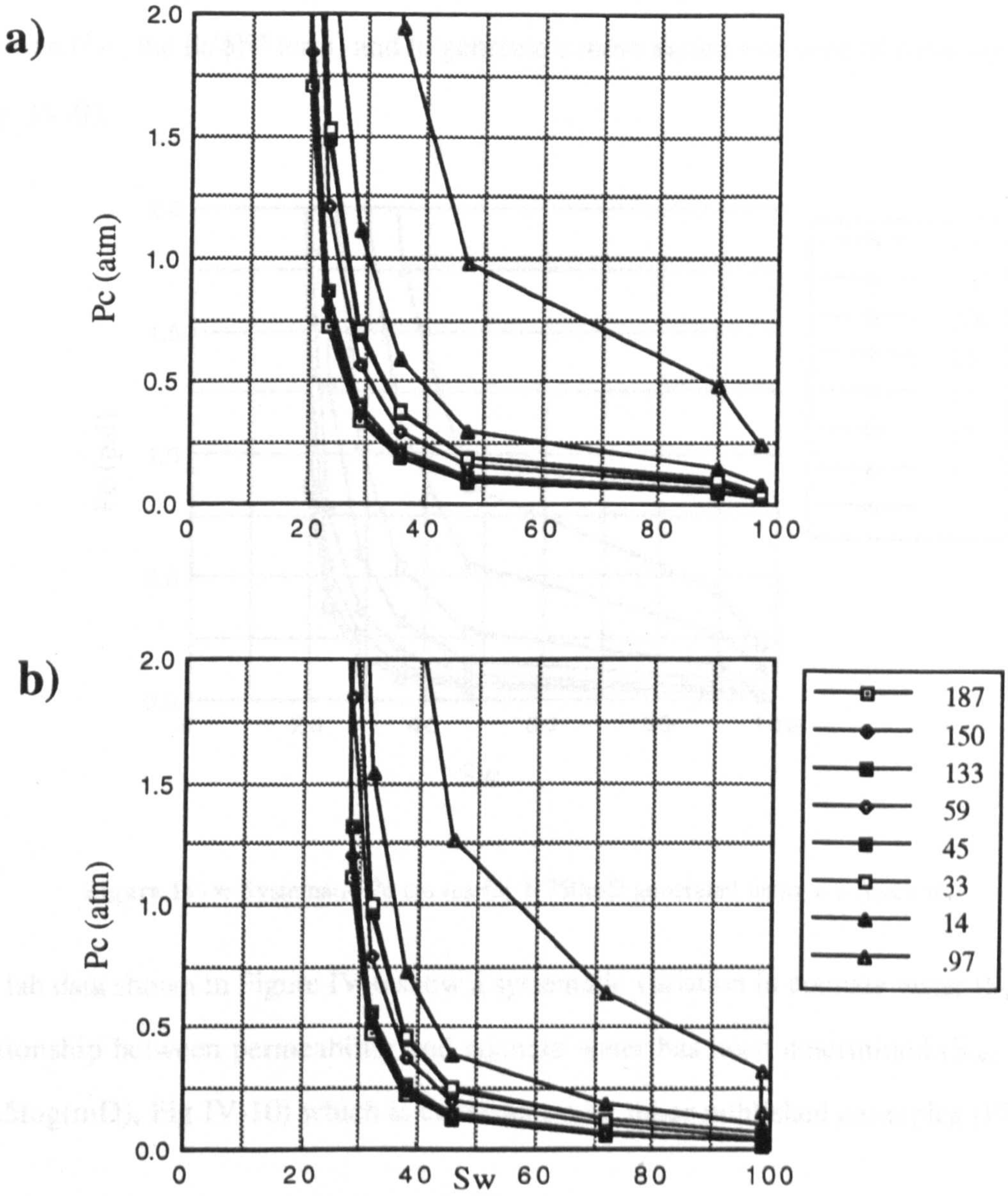

Figure IV-8: Families of drainage capillary curves generated from **a)** 150mD and **b)** 59mD Rannoch core plugs (refer to Fig. IV-6).

The J-curve models show that the J-curve does not, in the simplest form (Archer and Wall, 1986), account for systematic variations in connate water saturation. The clustering of Pc curves, however, for permeabilities above 100mD suggests that capillary contrasts in relatively high permeable rocks are not severe.

From the probe permeameter and core plug data in the Rannoch Formation, a relationship between k and ϕ has been determined (ϕ (%) = 12.698 + 2.11ln(k(mD)), refer to Fig. 5.2). This relationship can be used to reduce the number of variables in the Leveret J-function (*i.e.*, the $[k/\phi]^{0.5}$ term) and to generate a more systematic suite of capillary curves (Fig. IV-9).

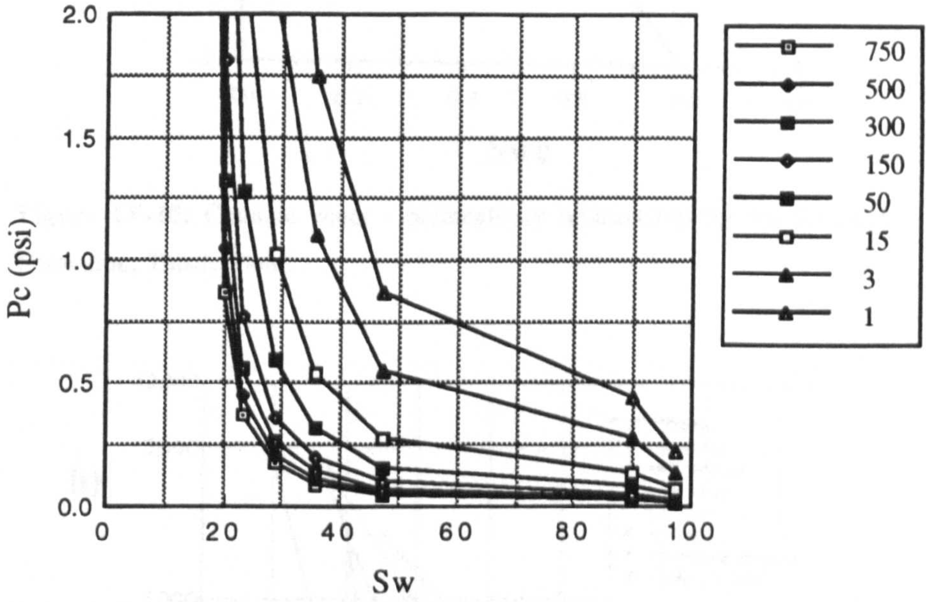

Figure IV-9: Systematic Pc curves for 1-750mD generated using a J-function.

The lab data shown in Figure IV-6 show a systematic variation in connate water (S_{wc}). A relationship between permeability and connate water has been determined (S_{wc} = 0.6-0.165log(mD), Fig IV-10) which is consistent with other published examples (Fig. IV-11).

This relationship has been used to generate a set of curves for appropriate permeabilities for use in the Rannoch simulation studies (Fig. IV-12). The drainage curves have been truncated at a residual oil (S_{or}) of 25%, the implications of which will be discussed later. There is further potential for parameterising the J-curve function for the Rannoch and combining with the ϕ/k and S_{wc}/k relationships to develop an improved set of Pc curves. This work is beyond the scope of the current study and has been reserved for future work following the acquisition of additional Rannoch data sets.

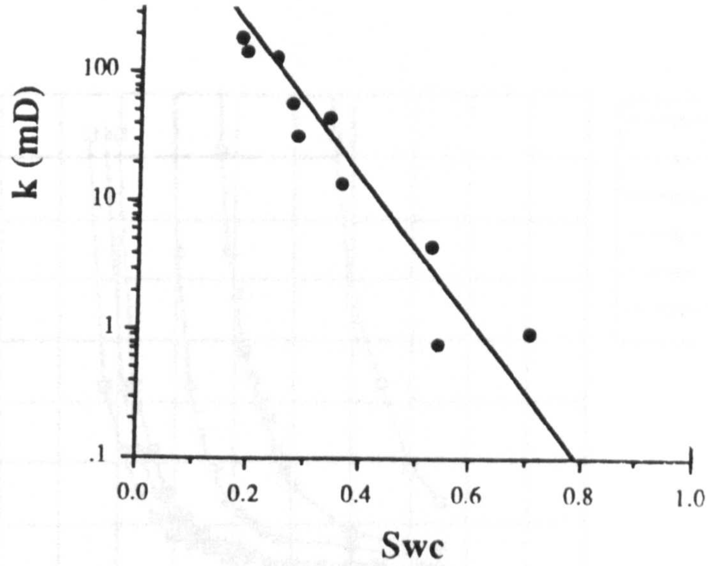

Figure IV-10: Connate water - permeability relationship for the Rannoch Formation, Thistle Field.

b)

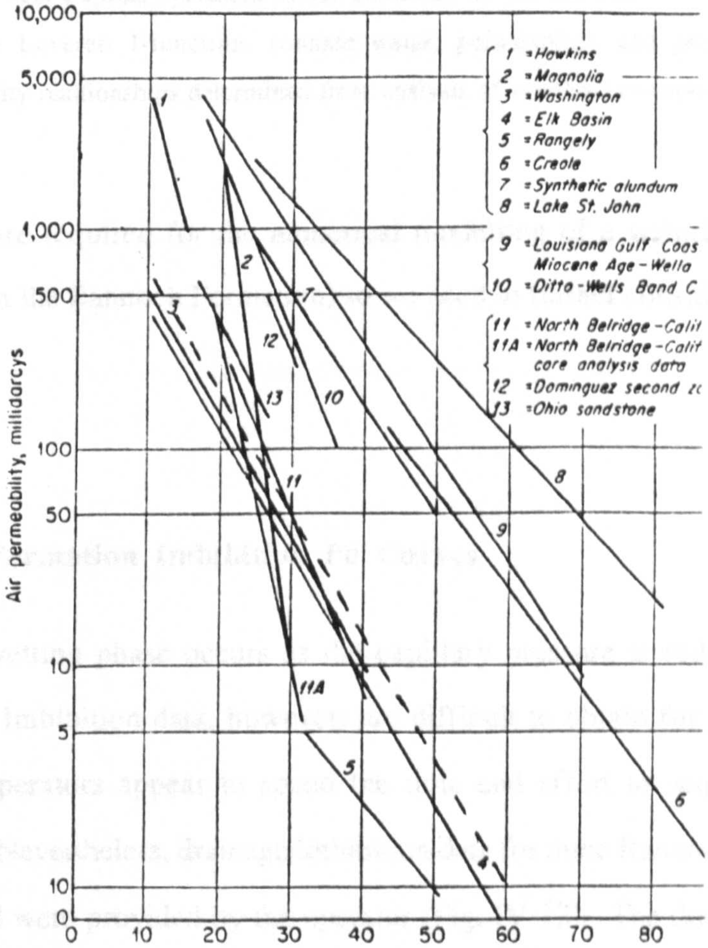

Figure IV-11: Connate water - permeability relationships for various formations. (After Amyx *et al.*, 1960). Dashed line is relationship shown in IV-10.

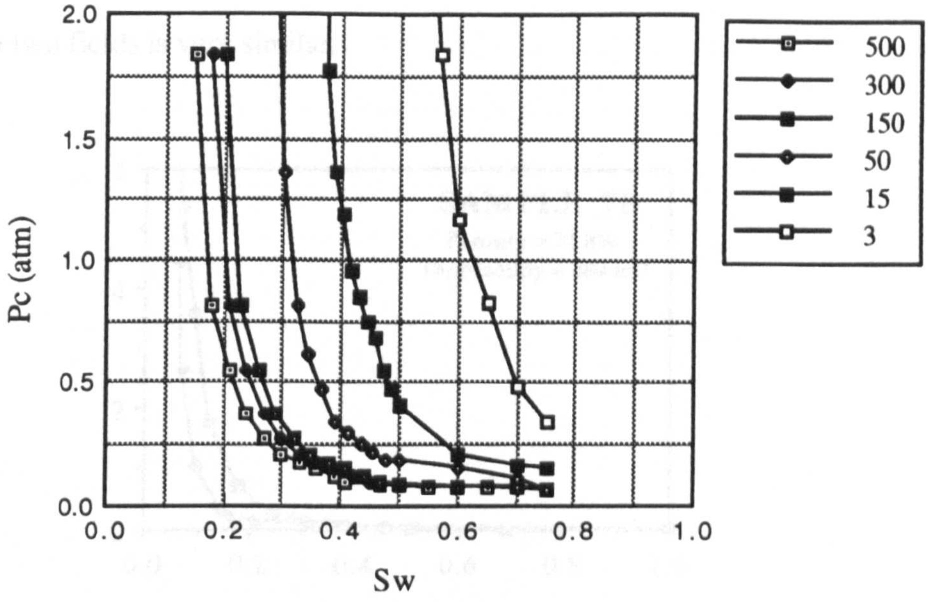

Figure IV-12: Capillary pressure curves generated for the Rannoch Formation using the Leverett J-function, connate water, permeability and porosity permeability realtionships determined from analysis of available petrophysical data.

Imbibition curves are required for the numerical modelling of a waterflood (*i.e*, an imbibition process in the Rannoch Formation) so we need to further consider imbibition Pc data.

IV. 4. Rannoch Formation Imbibition Pc Curves

Imbibition of the wetting phase occurs as the capillary pressure is reduced to zero (Anderson, 1987). Imbibition data, however, are difficult to obtain for the Rannoch Formation. Few operators appear to spend the time and effort to acquire useable imbibition Pc data. Nevertheless, drainage/imbibition data for three Rannoch samples in the Cormorant Field were provided by the operator (Fig. IV-13). The drainage curves are compatible for the similar reservoir quality rock described in the above drainage data from Thistle Field, indicating transportability of capillary curves within the Rannoch

Formation (Fig. IV-14). In Fig. IV-14 the drainage curves measured for the Rannoch at 133mD in two fields is very similar.

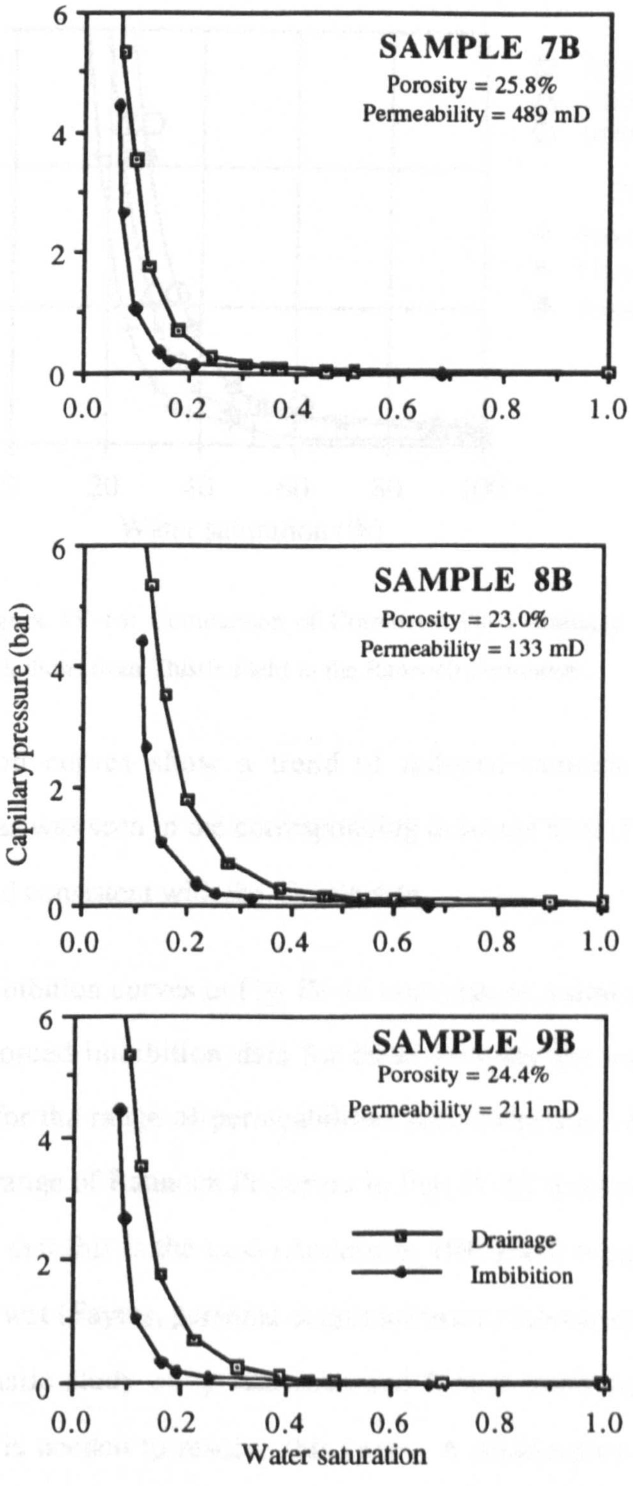

Figure IV-13: Rannoch drainage/imbibition capillary pressure curves from Cormorant Field

Further work is needed to show how variable, in terms of Pc, rock of the same permeability is in the same reservoir unit. With the data currently to hand, a single suite of capillary curves for the Rannoch Formation seems appropriate.

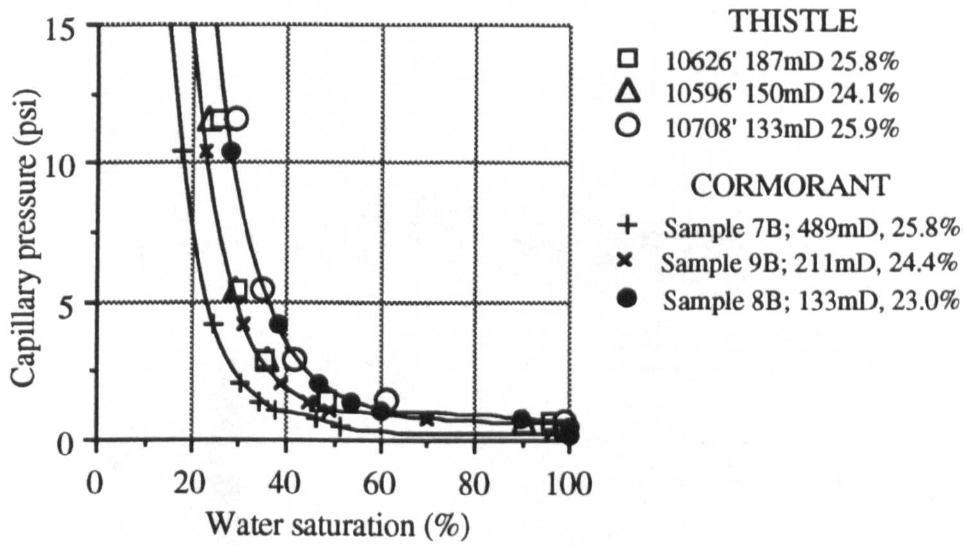

Figure IV-14: Comparison of Cormorant Field drainage capillary pressures with those from Thistle Field in the Rannoch Formation.

The imbibition curves show a trend of reduced connate water with increasing permeability, as was seen in the corresponding drainage data (Fig. IV-15), the latter also showing a trend consistent with the Thistle data.

Each of the imbibition curves in Fig. IV-15 converge to a similar non-wetting saturation at zero Pc. Forced imbibition data for these samples are not available. These data indicate that, for the range of permeabilities seen (which is very limited, 133-489mD, given the full range of Rannoch Pc curves in Fig: IV-6), a constant S_{or} can be expected. It is not likely that this is the case (Anderson, 1987) and suggests that the data reflect strongly water wet (Fayers, personal communication) laboratory conditions. A need for a more systematic study of spontaneous and forced imbibition for a wider range of permeabilities is needed to resolve this issue. A relationship for S_{or} with S_{wc} (Lake 1989b, p. 53) needs to be determined for the Rannoch Formation.

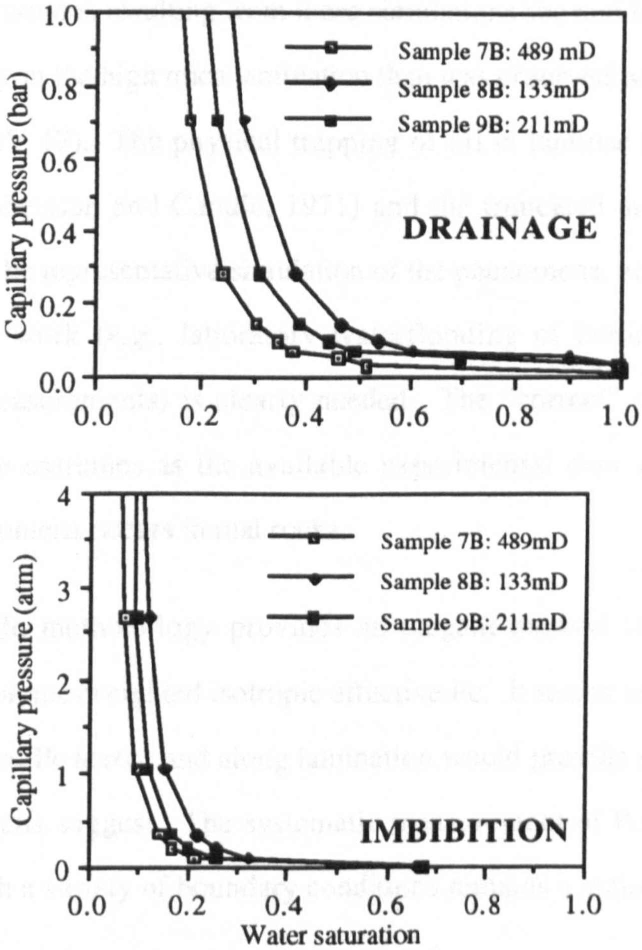

Figure IV-15: Comparison of drainage and imbibition capillary curves for Cormorant Field Rannoch Formation.

The situation under study here (*i.e.*, waterfloods of laminated sediments) is the trapped non-continuous, oil phase remaining in the relatively high permeability laminae as the Pc in the low permeability laminae goes to zero (oil-phase largely disconnected). This capillary-trapped oil, by the laminae, is thought to be more significant in some stongly laminated than the capillary-trapped oil in individual dead-end pores.

The "correct" Pc curves (*i.e.*, those within the appropriate Sw at zero Pc on the imbibition cycle) for use in the waterflood simulations cannot be determined from the available experimental data. The truncated drainage curves, however, are thought to represent the correct trapping mechanism at the lamina scale. Simulated waterfloods in the laminated sediments were therefore conducted using a suite of curves generated from the above imbibition data from the J-curve scaling procedure and a constant S_{or} (Figs. IV-16). The pseudos resulting from these simulations showed less capillary trapping and less anisotropy in the high mica lamination than was observed with the truncated drainage curves (Fig. IV-17). The physical trapping of oil in laminae has been experimentally observed (Robertson and Caudle, 1971) and the truncated drainage curve results are considered to be representative simulation of the phenomena, although additional careful experimental work (*e.g.*, laboratory waterflooding of laminated sediments, forced imbibition measurements) is clearly needed. The "correct" curves are thought to lie between these extremes as the available experimental data suggests that the lamina trapping phenomena occurs in real rocks.

The geopseudo methodology provides an elegant method for averaging Pc curves, providing a volume-weighted isotropic effective Pc. It seems unlikely that experimental measurement of Pc across and along lamination would provide such isotropic data as the numerical results suggest. The systematic measurement of Pc, however, in laminated sediments with a variety of boundary conditions remains a major undertaking for further sudy.

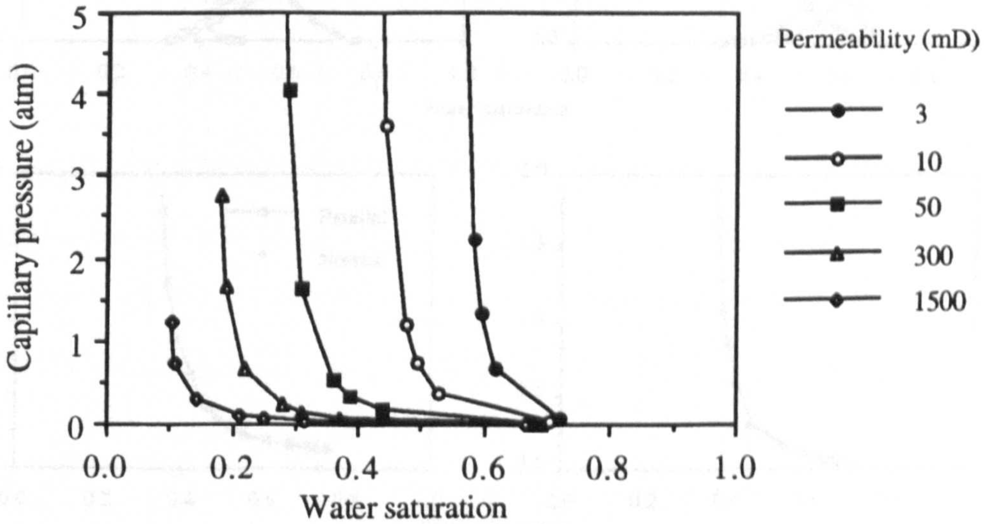

Figure IV-16: Family of J-curved derived imbibition capillary pressure curves for a range of Rannoch permeabilities.

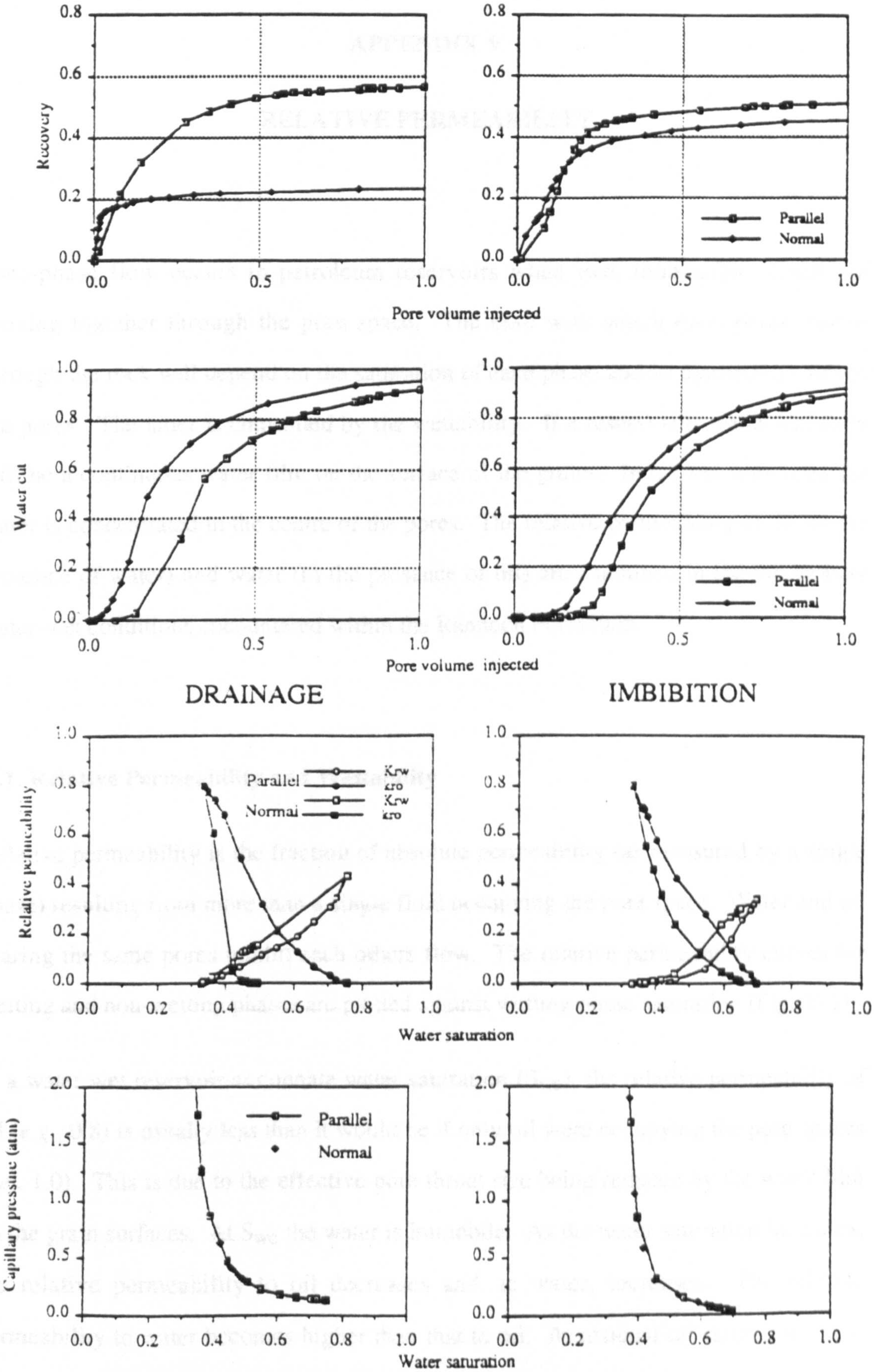

Figure IV-17: Performance and pseudos for high-mica lamination (fine grid A, Fig. 4.8, middle) using truncated drainage and scaled imbibition Pc curves. (Refer to Chapter 5 for details of the method of generation of these data).

APPENDIX V

RELATIVE PERMEABILITY

Two-phase flow occurs in petroleum reservoirs when two, immiscible, fluids are moving together through the pore space. The ease with which each phase moves through the rock will depend on the saturation of each phase and its distribution within the pores. The latter is controlled by the wettability. If a reservoir is water-wet there will be a continuous water film on the surface of the grains. In oil wet reservoirs the water is concentrated in the centre of the pores. The relative permeability to oil (in the presence of water) and water (in the presence of oil) are examined in the moderately water-wet conditions encountered within the Rannoch Formation.

V.1. Relative Permeability and Wettability

Relative permeability is the fraction of absolute permeability (as measured by a single phase) resulting from more than a single fluid occupying the pore space. Water and oil sharing the same pores inhibit each others flow. The relative permeability curves for wetting and non-wetting phases are plotted against wetting phase saturation (Fig. V-1).

In a water wet reservoir at connate water saturation (S_{wc}), the relative permeability of oil (*e.g.*, 0.8) is usually less than it would be if only oil were occupying the pore spaces (*i.e.*, 1.0). This is due to the effective pore throat size being reduced by the water film on the grain surfaces. At S_{wc} the water is immobile. As the water saturation increases, the relative permeability to oil decreases and, to water, increases. The relative permeability to water becomes higher than that to oil. At residual oil saturation (S_{or}), the permeability to oil becomes zero but, because the oil remains in the centre of the pores (Fig. V-2, Fig. 5.12), the relative permeability to water is significantly reduced from the absolute permeability.

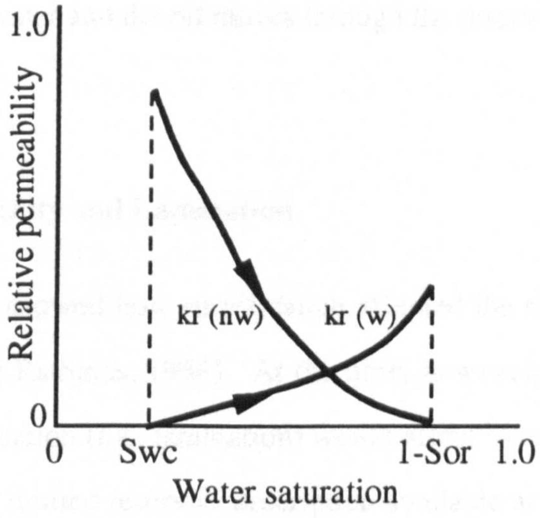

Figure V-1: Relative permeability curves: kr (nw) is the non-wetting (oil) phase relative permeability curve, kr (w), the wetting (water) phase curve.

In a water-wet rock, the presence of residual oil in the centre of the larger pores reduces the relative permeability to water when compared to an oil-wet rock (Fig. V-2).

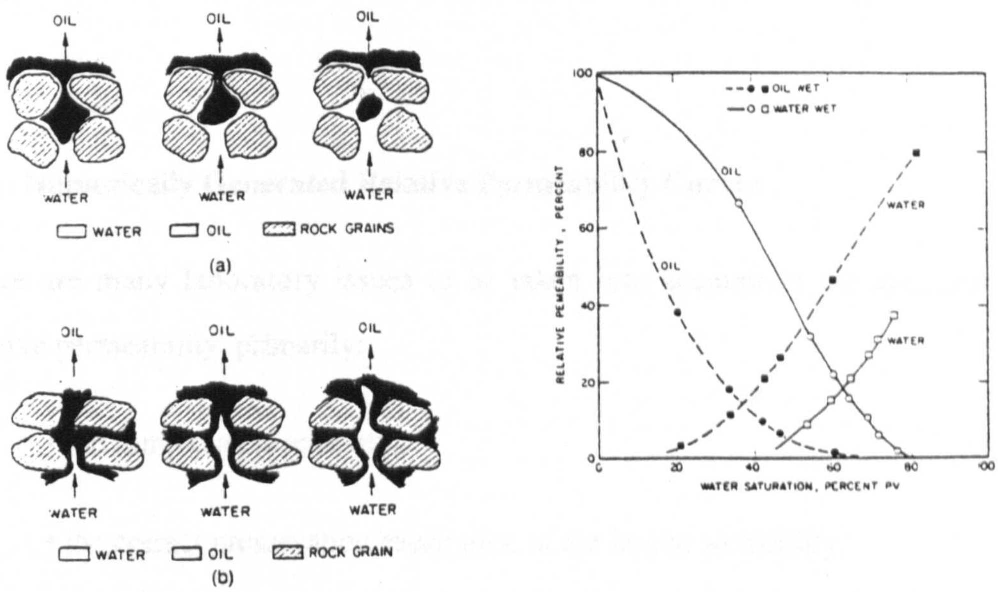

Figure V-2: Water displacing oil from a pore during a waterflood and the appropriate relative permeability curves for **a)** strongly water-wet rock and **b)** strongly oil-wet rock (from Anderson, 1990).

The relative permeability curves map the changes in permeability of each phase as the fractional saturation of each phase changes. This change in saturation occurs as the interface between the water and the oil moves through the reservoir.

V.2. Relative Permeability and Lamination

Early laboratory work showed how stratification affected the relative permeability of gas and oil (Corey and Rathjens, 1956). At the time, however, it was not possible to predict how the stratification (*i.e.*, lamination) would affect over-all performance of an oil field because of the limited reservoir description available at the time. Thirty years later, these experiments remain the only notable published study of the affect of lamination on relative permeability (Hornapour *et al.*, 1986). The affects on the large scale reservoir remain to be investigated. No effective description, however, of the lamination within reservoirs has been available until the development of the probe permeameter. This study investigates the field scale effects of lamination for the first time.

V.3. Numerically Generated Relative Permeability Curves

There are many laboratory issues to be taken into account in the measurement of relative permeability, primarily:

- the sample representivity,
- the correct preservation/restoration of the in-situ wettability,
- the measurement of bulk saturations during the flooding experiment.

Most relative permeability experiments are carried out on whole core samples that are judged to be homogeneous. Strongly laminated samples are avoided. The inevitable presence of weak lamination within whole core samples, however, will affect the relative permeability experiment. For these reasons, it is unlikely that a single experiment will suffice to characterise the reservoir. The cost and selection of average relative permeability curves from many experiments means that few samples are ever investigated.

For these reasons the industry tends to use numerical approximations for what are considered to be the appropriate wettability conditions. Corey and Rathjens (1956) parameterised the relative permeability curves in a number of experiments and their relationships are commonly used (Muggeridge, 1991). The Corey-Rathjens exponents are commonly used to generate the so called "rock" curves for simulation studies (Thomas and Bibby, 1991). In this study, the following relative permeability relationships were used (refer to Fig. 5.4):

$$k_{rw} = 0.45(Sw^2),\ k_{ro} = (1\text{-}Sw)^3$$

These are considered appropriate for a moderately water wet reservoir. The wettability of the Rannoch, however, has not been specifically investigated during this study.

APPENDIX VI

PSEUDOISATION

The term *pseudo* is defined in the dictionary as meaning false, sham as an adjective or pretender as a noun (Macdonald, 1977). Pseudo properties in petroleum engineering are false properties that used in numerical simulation to simulate average properties. Not necessarily physically correct or meaningful in themselves, pseudo properties are, nevertheless, used to simulate the effective properties of volumes of reservoir material that are not directly measureable.

The permeabilities, relative permeabilities and capillary pressures for relative large volumes of reservoir rock (*e.g.*, 10m vertically by 100m horizontally) are not directly measureable. These parameters are, however, fundamental to the understanding and modelling of a two-phase (*e.g.*, waterflood) process. The way in which these properties are traditionally derived is by assembling a finer scale model of units for which measurements (*e.g.*, core plugs) are available. From the fine models, the effective relative permeabilities for a larger block can be derived by analytical methods or by numerical simulation of the refined grid (Fig. VI-1).

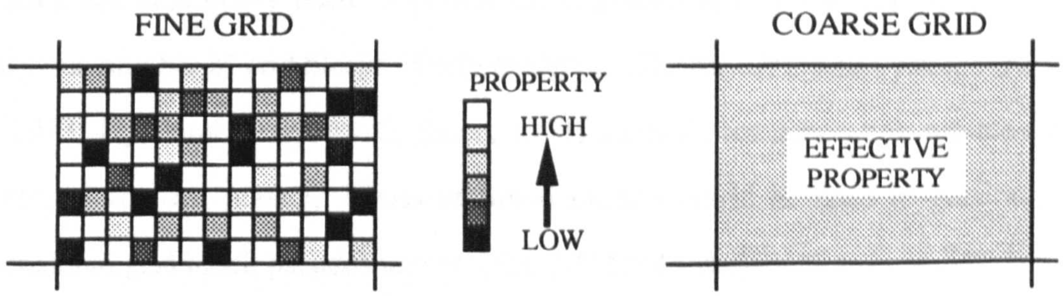

Figure VI-1: Sketch illustrating the determination of effective properties for a large block from the simulation of many smaller blocks. The effective property of the block on the right is determined from pseudoisation of the fine grid properties on the left.

Simple statistical averages can be used for certain properties, boundary conditions and flow processes. For example, the arithmetic average is the appropriate estimator for average permeability for single-phase, layer parallel flow. For more complex geometries and processes, fine scale numerical simulation is the only option. Effective properties of large grid blocks determined from fine scale simulations are known as pseudos and pseudoisation is the process whereby they are calculated.

The effectiveness of pseudos are usually tested by the back-substitution of the large grid block (with pseudos) for the refined grid (with rock properties) in the numerical experiment. Pseudos should reproduce the flows from the fine grid model for the coarse grid model. Large grid blocks and their pseudos properties together *pretend* to be fine grid block models and rock data. Pseudos are, therefore, the appropriate average dynamic properties (*i.e.*, they can vary with time or saturation) for large grid blocks of specific dimensions and under specific physical assumptions. Pseudos for a specified block dimension and process may be incorrect for significantly different sized blocks and different processes.

Because laboratory measurements are carried out on finite blocks (*e.g.*, core plugs and whole-core samples) which can include heterogeneities, the resulting laboratory measurements are effectively pseudos. Whether they are *representative* pseudos for that specific volume within the reservoir is another issue.

Pseudos are commonly used in petroleum engineering in numerical simulation to reduce the number of grid blocks. Early analytical (Hearn, 1971) and dynamic (Jacks *et al.*, 1973; Kyte and Berry, 1975; Stone, 1991) methods for generating pseudos were developed for this reason. Cross-sectional models could be used to generate one dimensional grid block pseudos and enabled 3-D field simulations to be reduced to a 2-D areal model.

VI.1. Pseudo Relative Permeability and Capillary Pressure

Relative permeability relationships can be measured on core samples. In reservoir simulations at the field scale, gridblocks are significantly larger than the samples so scale-up and averaging of relative permeability is required. Pseudoisation is the process by which the scale-up of relative permeabilities is most commonly achieved.

Hearn's (1971) method considers the vertical section to comprise several uniform layers which can be differing in permeability and non-communicating. In such reservoirs, the vertical sweep is primarily controlled by permeability variation. In each layer a piston-like displacement takes place. The pseudo relative permeability is determined by a simple porosity/thickness weighted average saturations and thickness weighted permeabilities. Such analytical methods have rather limited application to stratified reservoirs with non-communicating layers.

Dynamic pseudos are produced by numerical simulation by a number of methods (*e.g.*, Jacks *et al.*, 1973; Kyte and Berry, 1975; Stone, 1991). The Kyte and Berry procedure (Kyte and Berry, 1975), for example, follows a number of steps:

- Calculate pseudo absolute permeability as the harmonic average of stack permeabilities (arithmetic average) between coarse grid block centres.

- Calculate pseudo water saturation as pore volume weighted average of cross sectional blocks (*i.e.*, fine grid).

- Calculate pseudo flow rates for water and oil as the total flow across the coarse block boundaries.

- Calculate dynamic pseudo phase pressures (at the coarse grid block centre) as the average pressures for a stack of fine blocks through the coarse grid block centre.

- Calculate the pseudo relative permeabilities using the Darcy equation, pseudo flow rates, pseudo phase pressures and pseudo absolute permeability.

- Calculate the pseudo capillary pressure as the difference between the pseudo phase pressures.

In one of the examples that Kyte and Berry discuss (their Case 2 in Kyte and Berry, 1975), the pseudo capillary pressure curves are negative over part of the saturation range (*i.e.,* unphysical for a typical wetting:non-wetting system) to account for different pressures in different layers of the cross-sectional model.

Stone's (1991) method, for comparison, follows a similar procedure but uses total flow rate weighted average of the fine grid fractional flows to determine coarse grid phase flows. Transmissibility weighted averages of the phase pressures are then used to determine pseudo capillary pressure curves. This method has a stated advantage when poor vertical permeability prevents vertical equilibrium (an assumption of the Kyte and Berry method).

The ECLIPSE black oil simulation code that has been extensively used in this study incorporates a modified Kyte and Berry method in the determination of the pseudo relative permeability and capillary pressure (ECLIPSE option *PSEUDO*, ECL, 1988). The pseudo absolute permeability is calculated as the arithmetic average of the fine grid permeabilities. In a vertically layered reservoir (*i.e.*, if flowing across a series of beds as in the vertical floods of the laminasets - Chapter 5) the harmonic average of the layers gives a more appropriate, single (moveable) phase permeability. ECLIPSE, however, uses the arithmetic average and captures the effect of the layers in the pseudo relative permeability curve. As the kk_r product appears in the two-phase flow equations the net effect is the same. Providing the large grid block flows like the fine scale grid block and produces the same effect, the pseudoisation can be considered the most appropriate procedure for determining effective properties. The boundary conditions for the numerical simulation of the fine grid need to be the same as for the coarse grid.

This can be difficult to achieve when the coarse grid is close to the system size (*i.e.*, when the number of grid blocks available is similar to the number of blocks required for the detailed description of the coarse grid). In this case, realistic boundary conditions (*i.e.*, coarse grid blocks surrounded by other coarse grid blocks) can be difficult to represent. Other methods of pseudoisation (tensors) may be required in these cases.

The numerical simulator, ECLIPSE, does not use directional capillary pressure curves and the pseudo capillary pressure curves are the same in each direction. The appropriate pseudo Pc curve and the degree of anisotropy in Pc is an issue that needs further study. The pseudo Pc curves that are generated by ECLIPSE and presented in this study are pore voulme weighted. The correct scale-up and pseudoisation of Pc is an important issue as it controls the average in-place hydrocarbon saturations and, therefore, estimates of oil-in-place.

Whilst further work on the pseudoisation of relative permeability and capillary pressure to take account of the geological structure is needed, the technique lends itself well to the variety of geology encountered. Pseudoisation allows the dynamic effects of forces to be built in. Carefully constructed pseudos provide the appropriate combined rock and fluid flow properties at any required scale.

APPENDIX VII

AN OUTCROP STUDY FOR STRATAL ELEMENT GEOMETRIES

In this geoengineering study of the Rannoch Formation, the geometry of the stratal elements was an important consideration in the scale-up procedure. The laminaset, bed and bedset geometries in the Rannoch Formation are not readily determined in core because of the limited sample available. An outcrop study of a reservoir analogue was, therefore, required. Unfortunately, the Rannoch Formation or equivalent shoreface deposits within the Middle Jurassic do not outcrop. Other shoreface sequences, however, including the Oxfordian Bencliff Grit on the Dorset Coast and the Kennilworth Member of the Cretaceous Blackhawk Formation in Utah, have been proposed as Rannoch analogues (Allen and Underhill, 1989; Scott, 1992).

In this study, looking at the stratal elements as the basic building blocks of reservoirs, it is the similarity of these small scale stratal elements (*i.e.*, laminae, laminasets and beds) that is important. The form of these stratal elements is largely controlled by grain size and current processes and is less sensitive to subtle characteristics of the environmental or sequence stratigraphic setting. The appropriateness of the Bencliff Grit and the Kennilworth Member as analogues for Rannoch *stratal elements*, therefore, depends on a detailed comparison of the available geometrical data from cores and outcrop.

VII.1 Stratal Element Terminology

Recent developments in sequence stratigraphic concepts (Campbell, 1967; van Wagoner, 1990) have provided the formal terminology for the sequence of hierarchical stratal elements (Fig. 2.2). The small scale sedimentary structures, of a primary depositional origin, can now be identified as lamina, laminaset, bed or bedset members of the hierarchy. Stratal elements are bounded by surfaces defined by:

- changes in texture,
- stratal terminations, and
- paraconformities marked by burrow horizons.

The surfaces that bound laminasets (*i.e.*, relatively conformable succession of genetically related laminae) are defined here as *laminaset bounding surfaces*. These surfaces define the geometries of beds and are the subject of this study. It has not been possible to distinguish consistently between laminaset and bed bounding surfaces, so all surfaces defined by the criteria listed above are initially considered to be laminaset bounding surfaces.

VII. 2. Background to the Studied Outcrop Sections

The Upper Jurassic Bencliff Grit (Osmington Mills, Dorset Coast) is a relatively limited, two-dimensional, outcrop of fine grained sandstone. Sandwiched betweeen ooid grainstones and open marine clays, the 4m-thick section (Fig. VII-1) is interpreted as being shallow marine with an estuarine influence (Allen and Underhill, 1989). Amalgamated lenticular beds within the Bencliff Grit have been interpreted as HCS (Sun, 1990). From a series of photomosaics, the lenticular beds have been mapped throughout this sequence and their geometries measured for comparison with the Rannoch Formation and the Kennilworth Member.

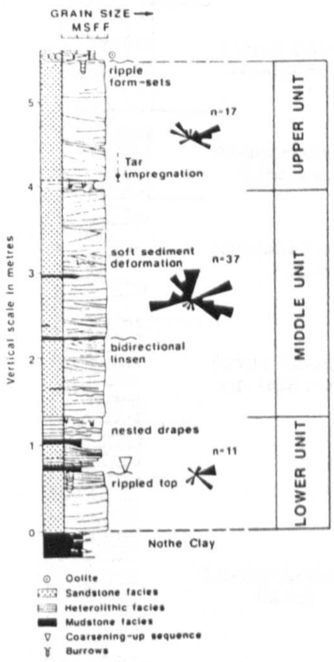

Figure VII-1: Sedimentary log from the Bencliff Grit section at Osmington. (From Allen and Underhill, 1989).

The Upper Cretaceous Blackhawk Formation (Book Cliffs, Utah) provides an extensive outcrop of prograding shoreface sequences (van Wagoner, 1990; O'Byrne and Flint, 1992). From a detailed study of shorefaces, which included these outcrops, Brenchley, Flint and Stromberg (Brenchley *et al.*, 1992) have developed a model for the facies sequence in a storm-influenced parasequence (Fig. VII-2). In a "definitive" shoreface section of the Kennilworth Member in Woodside Canyon, detailed maps of HCS bedforms from photomosaics were made by Simon Stromberg. Data from these maps were provided for comparison with the Rannoch Formation and Bencliff Grit data.

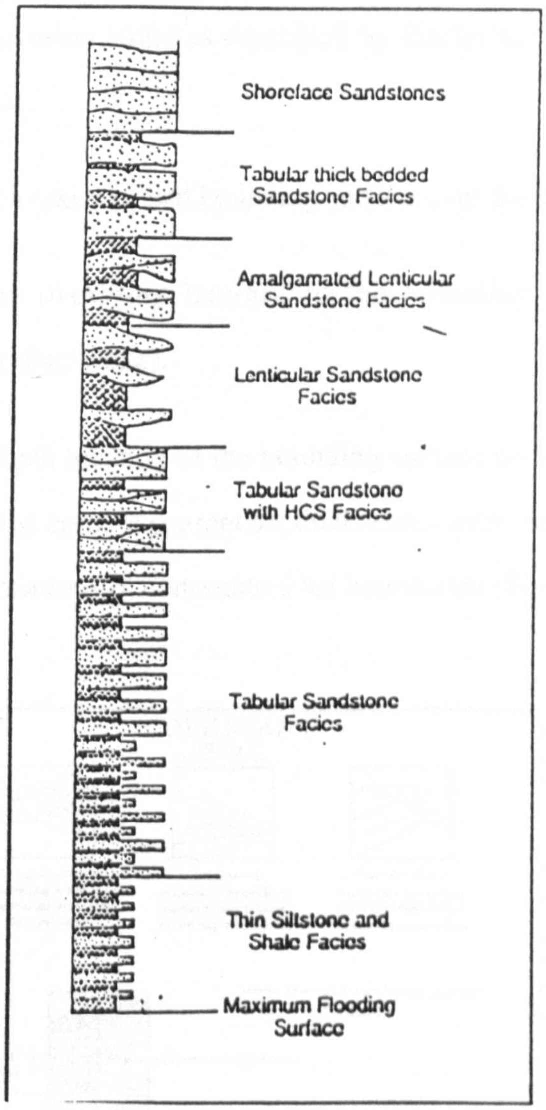

Figure VII-2: A model facies succession in a storm-influenced parasequence. (From Brenchley *et al.*, 1992)

VII.3. Quantification of Laminaset Geometry

In quantifying the geometry of laminasets, we have considered those features that are recognisable in core. When presented with a narrow, approximately 10cm-wide, section of a formation, slabbed in an inconsistent and indeterminate orientation, the quantitative data that can be detected are limited to (Fig. VII-3a):

- Depth location of bed bounding surface;
- Apparent truncation angle as described by discordant lamination on the slabbed surface;
- Qualitative convexity of bed bounding surface over the width of the core;
- Nature of the overlying laminae to the bounding surface (whether concordant or discordant).

Where recognised, the depth location of the bounding surface was measured (±5cm) along the central axis of the core. Apparent set thicknesses were determined from the separation between the locations of consecutive set boundaries (Fig. VII-3b).

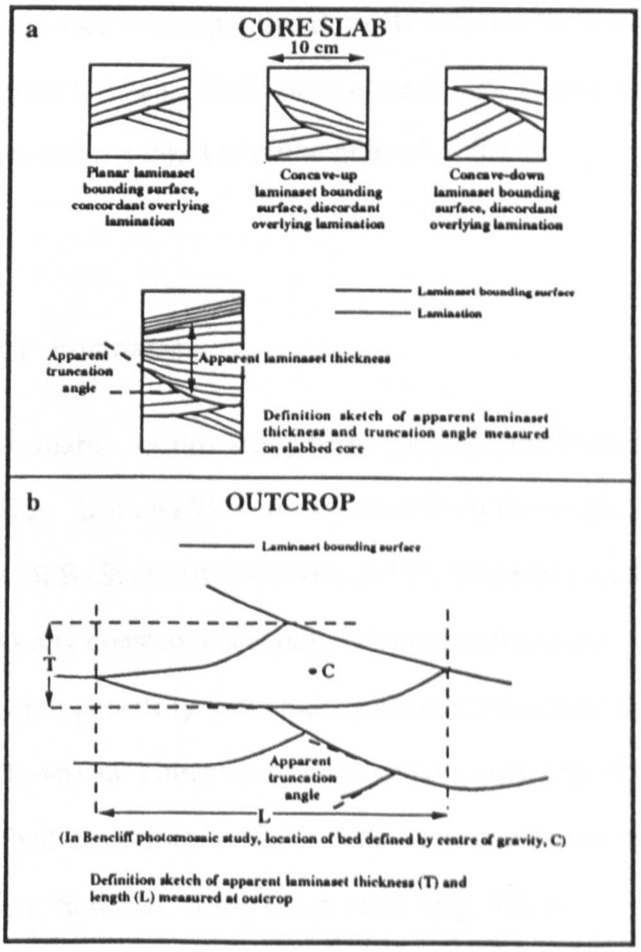

Figure VII-3: Definition sketch for laminaset bounding surface features measured in this study of **a)** core slabs and **b)** outcrop faces.

Bed bounding surfaces could not be recognised where no angularity occurred between laminae (although this is likely to occur). Exceptions to this can be seen when bounding surfaces can be clearly identified on other core faces. As a result, the average thickness of "beds" measured in core is likely to be larger than measured at outcrop. Apparent truncation angles were measured (to within 1°) and the concavity/convexity of surfaces recorded. Lengths and thicknesses (*i.e.*, bed aspect ratios) were measured at outcrop and defined as the maximum vertical and horizontal distances with respect to the depositional horizon.

VII.4 Data Aquisition

Laminaset bounding surface data was collected from two cored wells in the Rannoch Formation and from two outcrops: the Bencliff Grit on the Dorset Coast and the Kennilworth Member in Utah. Collection of such data in core and outcop requires different techniques and is subject to different level of detail.

VII.4.1 Rannoch Formation

Two wells were available for this study from the Rannoch Formation in two North Sea producing fields. Both wells were deviated from the vertical; Well A (Thistle A31) at 22° and Well B (Statfjord 33/12-B9) at 58°. In neither well had the core been orientated, nor was any consistant slabbing orientation followed. Features measured in the two wells were generally low angle, planar, concordant laminaset bounding surfaces (Fig. VII-4a) or concave-up, discordant surfaces (Fig. VII-4b). The character of the bed bounding surfaces was very similar in the two wells, the concave-up surfaces, however, being much rarer (Fig. VII-5).

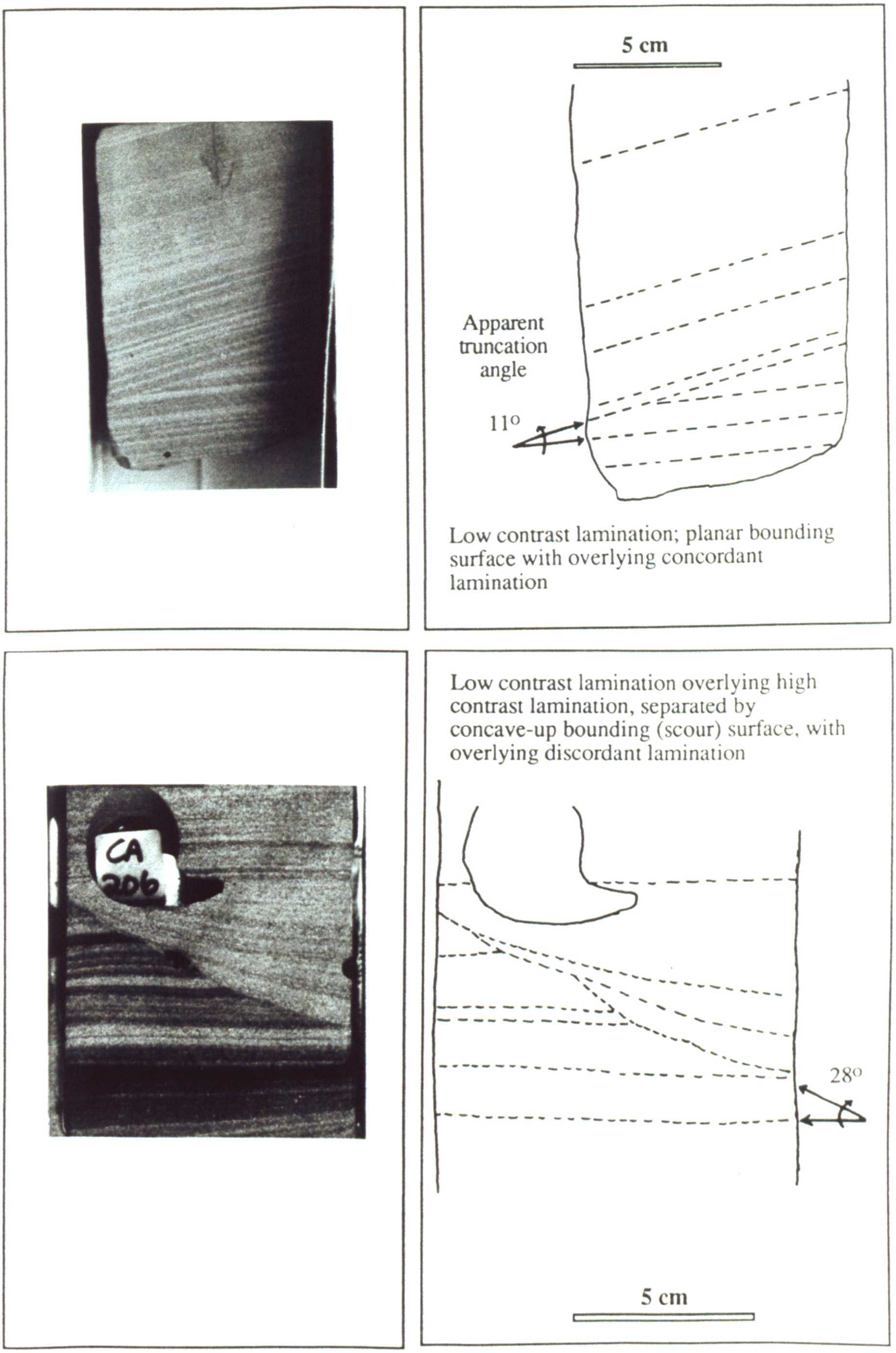

Figure VII-4: Examples of Rannoch Formation laminaset bounding surfaces as seen in slabbed core.

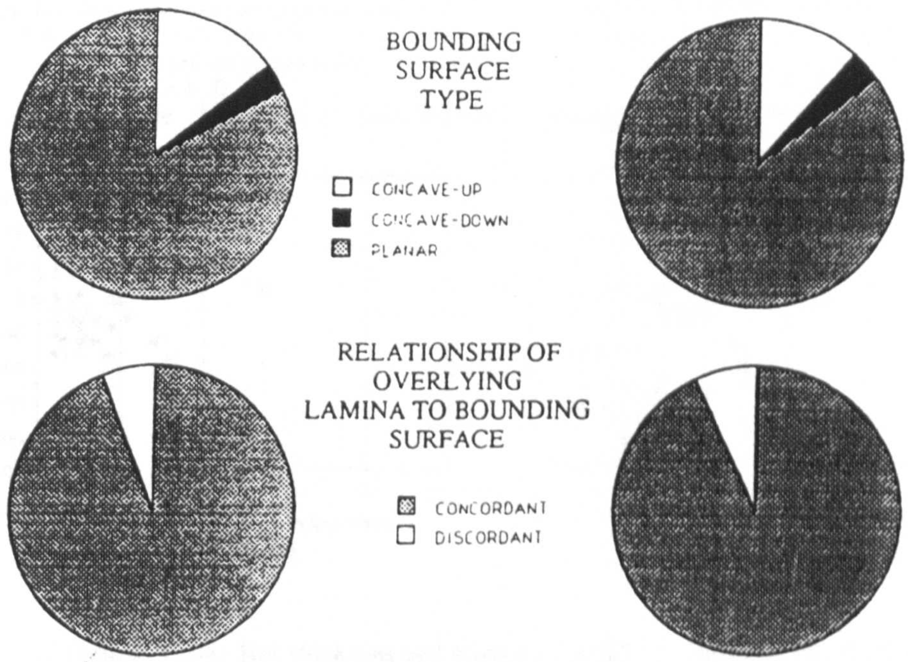

Figure VII-5: Bounding surface type and lamina relationships for low-angle cross lamination in Rannoch wells A (left) and B (right).

The location of the laminaset bounding surfaces in each of the two wells, the average thickness for the bed overlying the bounding surface and the angle of truncation below the bounding surface are shown for the two wells at comparable (vertical) depth scales. Subtle trends, of decreasing set thickness and increasing truncation angle up through the Rannoch Formation can be discerned in these data (Fig. VII-6).

The average (deviation corrected) laminaset thickness of 0.24 and 0.19m for wells A and B, respectively, is considered reasonably comparable. The differences between truncation angles (7.4 and 12.1°) appear, at first sight, to be more significant. The differences and similarities are discussed further below.

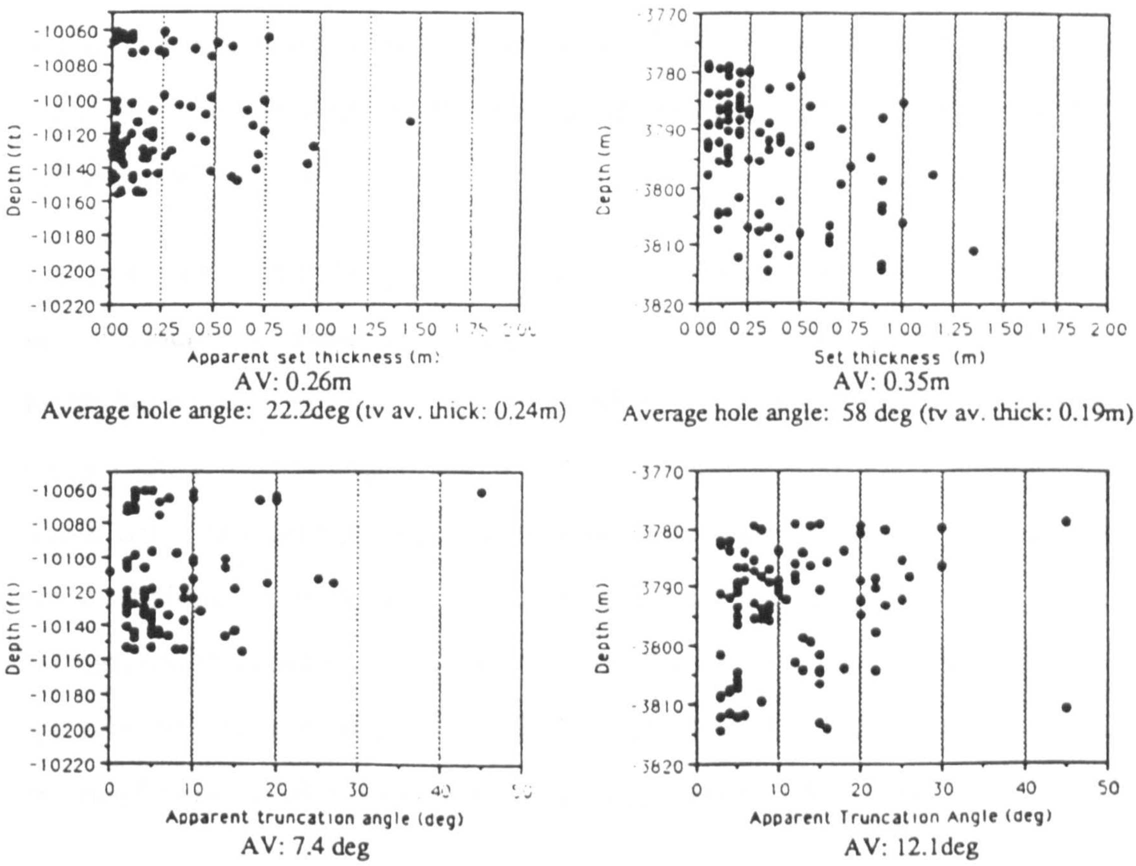

Figure VII-6: Bed thickness and truncation angle vs. depth for the Rannoch wells A (left) and B (right).

VII.4.2 Bencliff Grit

The Bencliff Grit outcrop studied occurs on the Dorset Coast to the east of Osmington. The section (4m maximum thickness) is exposed over a distance of approximately 140m before dipping below beach level. Although not a producing reservoir, the section is characterised by active oil seepage (Stoneley and Selley, 1991). The Bencliff Grit has a more contentious origin than the Kennilwoth but, most recently, is thought to be of a storm-influenced estuarine origin (Allen and Underhill, 1989). In a pilot study, an initial small representative selection of beds was sampled (number, N = 12; average length, L = 3.8m; average thickness, T = 0.37m and aspect ratio, R = L/T = 12.3) before a more complete mapping from photomosaics (Fig. VII-7) was completed (N = 224; L = 4.1; T = 0.34 and R = 12.9) in a similar fashion to those in the Kennilworth. The pilot sample and the mapping of the entire section produced similar results supporting the representivity of the pilot bed selection.

It appears that, within the upper unit recognised by Allen and Underhill, the aspect ratio (R) increases towards to top (Fig. VII-8). The base of the unit is characterised by thicker beds. What is also apparent on the the photomosaics is the grouping of some of these beds in larger, sigmoidal features, representing a bed element (Fig. VII-9, 10). These latter features indicate downlapping laminae to the base and these are the unidirectional features noted by Allen and Underhill (1989, Underhill, personal communication). The dominant lenticular laminasets, on the other hand, do appear to be similar to the Kennilworth HCS, and their 3-D geometry has been well described by Sun (1990) from the large exposed nodules on the beach.

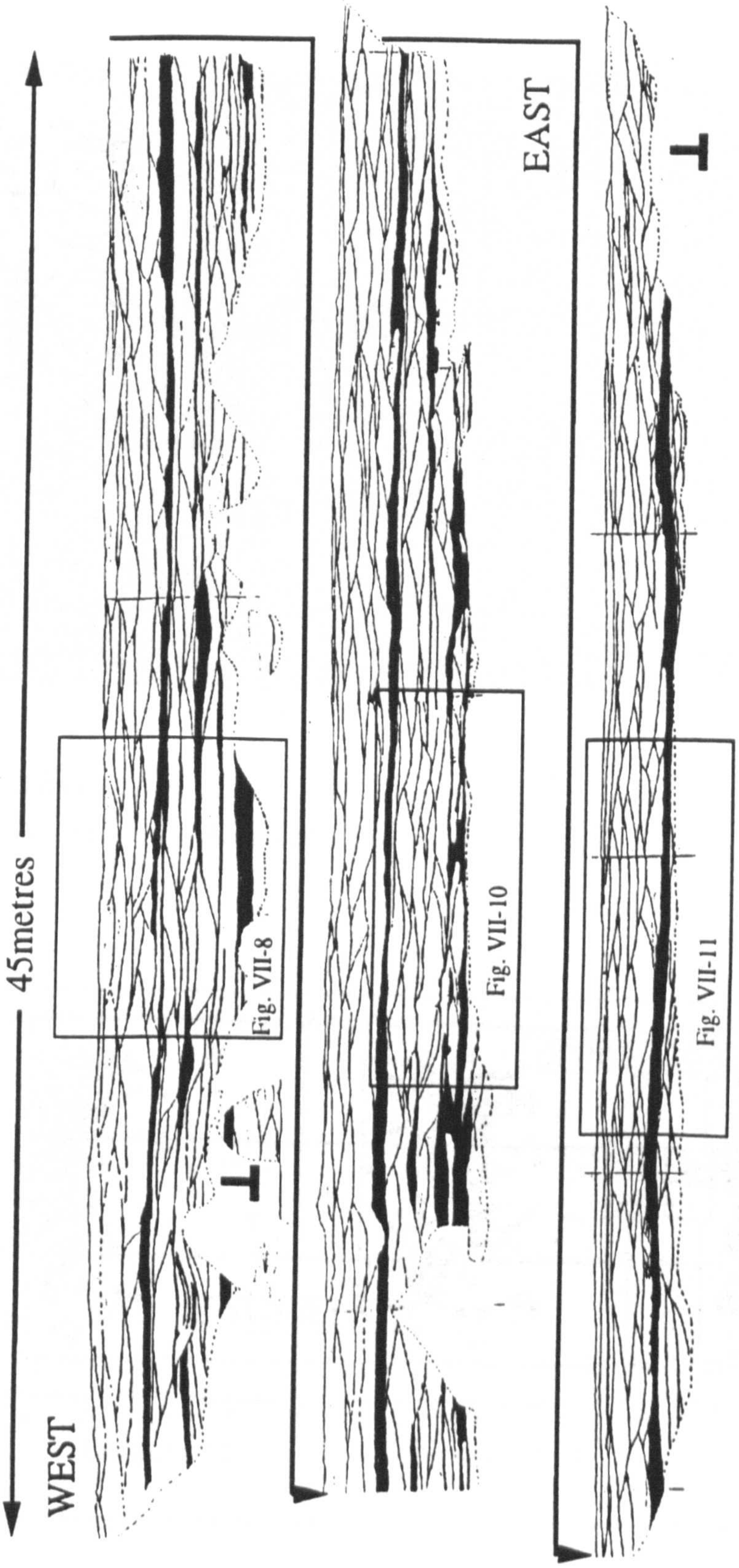

Figure VII-7: Laminaset elements in the Bencliff Grit at Osmington. (Scale bars are 1metre).

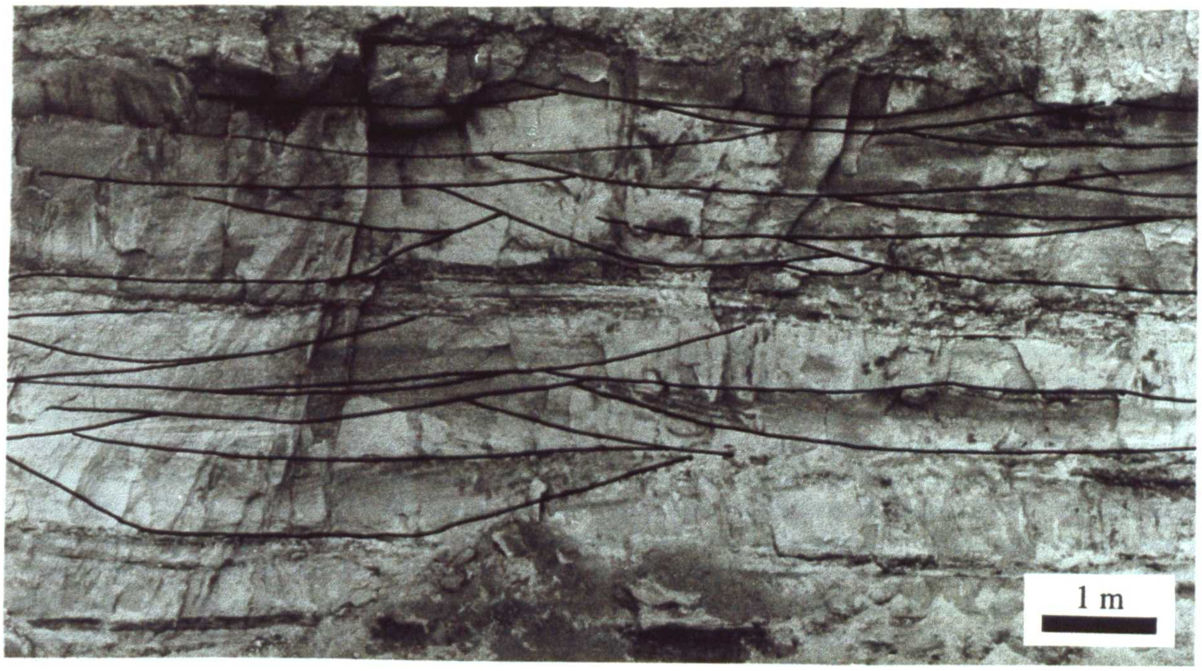

Figure VII-8: Example of HCS laminaset elements in the Bencliff outcrop. Scale bar = 1m. Refer to Fig. VII-7 for location.

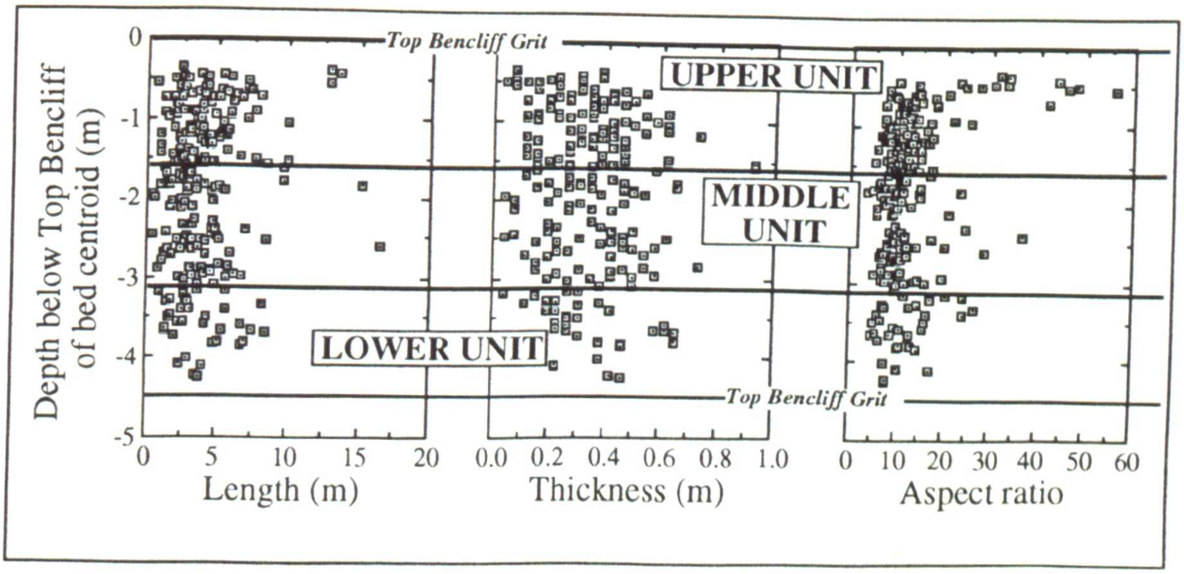

Figure VII-9: Variation of bed length, thickness and aspect ratio with depth through the Bencliff Grit outcrop. Units refer to those defined by Allen and Underhill (1989), refer to Fig. VII-1.

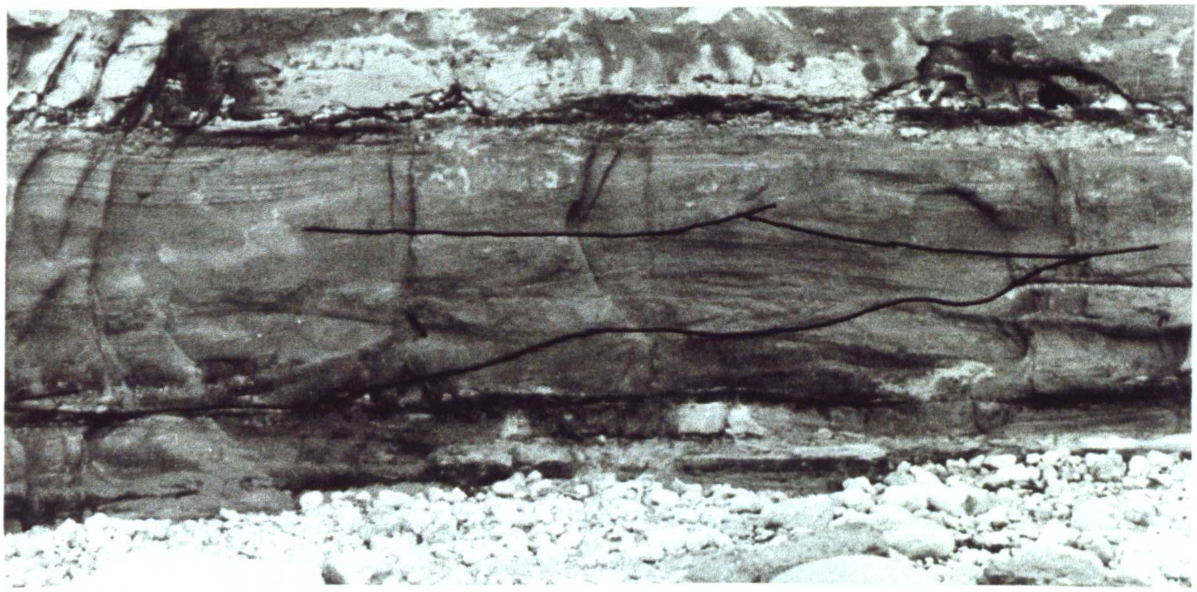

Figure VII-10: Example of larger scale bed elements in the Bencliff outcrop showing downlapping lamination overlying the basal scour. Scale as Fig. VII-11. Refer to Fig. VII-7 for location.

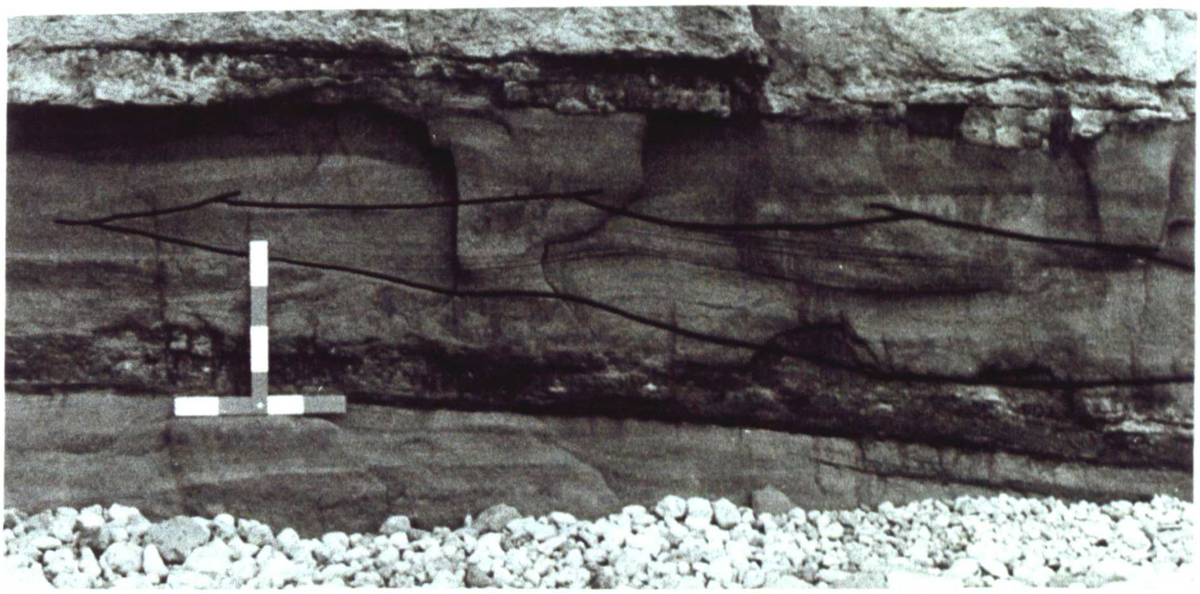

Figure VII-11: Antiformal lamination over undulating bank or erosional scour in a larger scale scale element. Scale bar = 1m. Refer to Fig. VII-7 for location.

VII.4.3 Kennilworth Member

HCS has been mapped by Simon Stromberg (Fig. VII-12) in a well exposed shoreface section in the Kennilworth Member (Blackhawk Formation) in Woodside Canyon (Utah). To quantify the geometry of the bed bounding surfaces, measurements were made along a series of transects. Data collection followed methods described above. In addition to these data, the length of the HCS bed that underlies and overlies the bounding surface was also recorded.

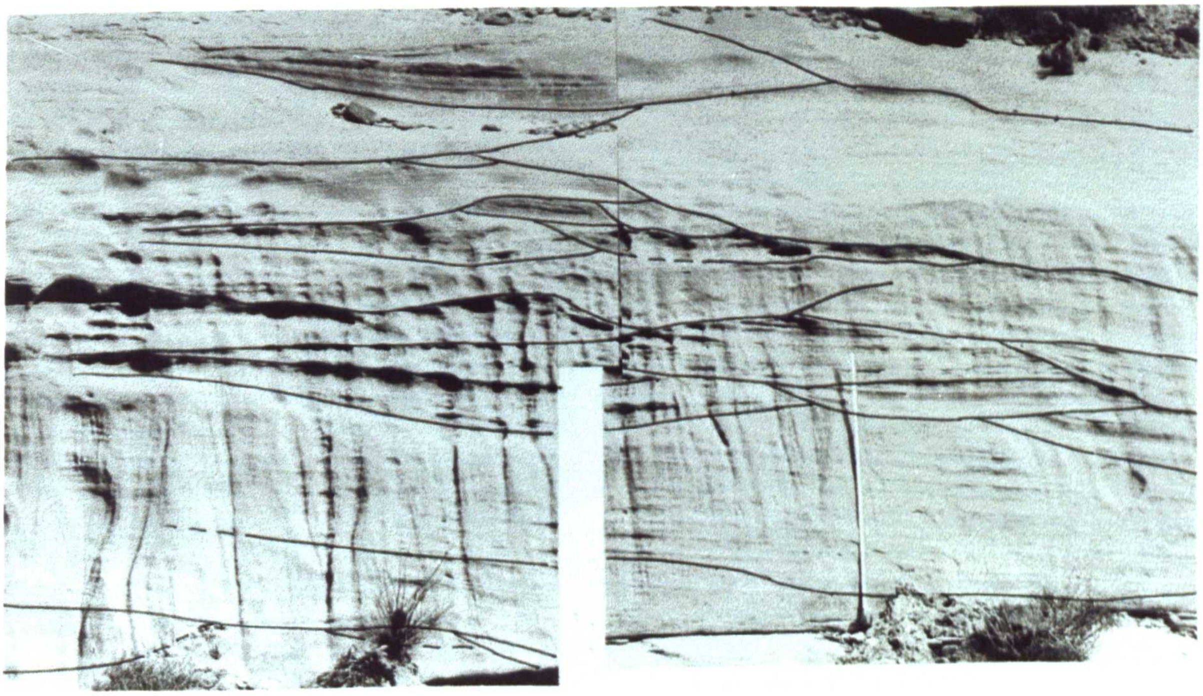

Figure VII-12: Example of HCS laminaset elements in the Kennilworth outcrop. Tape measure in the foreground = 1m. (Photograph courtesy of S. Stromberg)

The bed bounding surfaces are predominantly planar concordant (Fig. VII-13), consistent with the Rannoch Formation observations. This conflicts with the observations of Scott (1992), also from the Blackhawk, where laminae were seen to generally downlap. The dip of bounding surfaces was recorded (average 5.8°). Assuming a dominant concordant fill, the truncation angles were determined from the dip of successive bounding surfaces (9.6°).

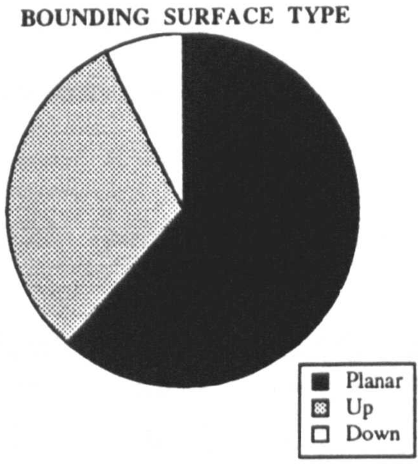

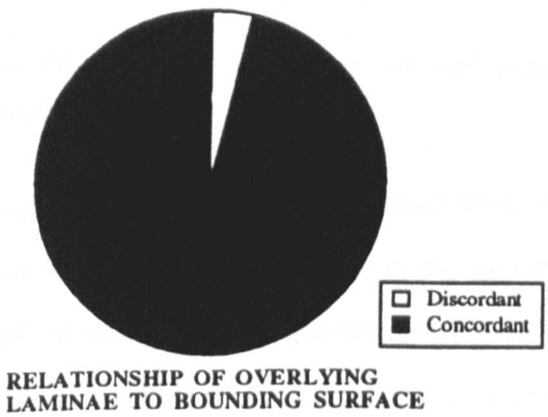

Figure VII-13: Laminaset bounding surface types and lamina relationships for HCS in Kennilworth Member outcrop at Woodside.

VII.5. Statistical Laminaset Data Comparison

In this section, the data are compared and discussed using statistical analyses. The dip and truncation angle comparisons are useful in establishing the geological similarities between outcrops and between the wells and possible outcrop analogues.

We can compare dip data from the outcrops (Table VII-1). Mean bedform dips range from 5.8° (Kennilworth) to 8.6° (Bencliff) with the maximum dips of 24° (Kennilworth) to 32° (Bencliff). From these data it is appropriate to consider these sediments as *low angle* cross lamination.

	Bencliff (pilot)		Kennilworth		Rannoch	
					Well A	Well B
Angle	Truncation	Dip	Truncation	Dip	Truncation	Truncation
Number	103	102	69	85	83	94
Min.	1	0	1	0	0	3
Max.	39	32	30	24	45	45
Mean	13.4	8.6	9.6	5.8	7.2	12.1
Variance	53.4	34.0	44.3	33.4	48.7	72.6
Coeff. var.	0.55	0.68	0.69	1.00	0.97	.70

Table VII-1: Comparison of Truncation and Dip Angles for Rannoch, Kennilworth and Bencliff Grit.

Mean truncation angles range from 7.2° (Rannoch Well A) to 13.4° (Bencliff). Maximum truncation angles of 45° were seen in the two Rannoch wells. This is greater than the angle of repose for fine quartz sand, 32-43° depending on packing (Allen 1985, p.36), as the angle is measured relative to a plane that may be dipping (up to 32°) in the opposite sense. Maximum dips of 30-39° in the outcrops are comparable with expected angle of repose. The steep dips in HCS sediments have been interpreted as evidence of very rapid cut and fill of unconsolidated sediment (Hunter and Clifton, 1982; Reynolds, 1992).

The distributions of dip and truncation angles are positively skewed. Square-root transformed distributions are also positively skewed, however, log-normal transformations tend to be slightly negatively skewed. This suggests that a log-normal distribution for these data can be used as an approximation of a gaussian transformation. We have, therefore, used parametric statistical tests (those which assume normal distributions) on the natural logarithms of the dip and truncation angle data to test the statistical significance of the observed differences (Appendix I). The F-test (Davies, 1973) is used to test the equality of variances. The low values for the ratio of ln(dip) and ln(truncation) variances for the samples (shown below the diagonals in Tables VII-2 and VII-3) show no evidence that the samples are drawn from different populations. Having passed the F-test, it is appropriate to compare the equality of the means by the t-test (Davies, 1973). There is no evidence that the mean dip samples come from populations having different means (Table VII-2).

F-value/t-value	Bencliff (Pilot)	Kennilworth
Bencliff (Pilot)	XXX	1.00(1.96)
Kennilworth	1.28(1.39)	XXX

Table VII-2: Significance values (F-values, below diagonal; t-values, above diagonal) for the natural log of dip angle (assuming dip log-normally distributed). Significance value at the 95% confidence interval shown in parenthesis, significant values shown with*.

The statistical inference from the truncation data is less clear (Table VII-3). The mean of the Kennilworth data lies between the mean truncation angle seen in the two Rannoch wells. There is no statistical evidence, however, that the population means are the same.

F-value/t-value	Bencliff (Pilot)	Kennilworth	Rannoch Well A	Rannoch Well B
Bencliff (Pilot)	XXX	5.09*(1.96)	9.55*(1.96)	2.23*(1.96)
Kennilworth	1.38(1.39)	XXX	3.01*(1.96)	3.13*(1.96)
Rannoch Well A	1.23(1.39)	1.12(1.39)	XXX	7.21*(1.96)
Rannoch Well B	1.04(1.39)	1.32(1.39)	1.18(1.39)	XXX

Table VII-3: Significance values (F-values, below diagonal; t-values, above diagonal) for the natural log of truncation angle (log-normally distributed). Significance value at the 95% confidence interval shown in parenthesis, significant values shown with*.

Bed geometries, required for use in the reservoir model, were compared by apparant thickness and length, the latter for the outcrop studies alone. Mean lengths ranged from 2.3m (Kennilworth) to 4.1m (Bencliff) (Table VII-4). Mean thicknesses ranged from 0.18m (Rannoch well B) to 0.34m (Bencliff). Beds in the Bencliff tend to be bigger (longer and thicker) than those observed in the Kennilworth.

	Bencliff (Pilot)		Bencliff (Photo.)		Ben. (Pr.)	Kennil.		Rannoch A	Rannoch B
metres	L	T	L	T	*T*	L	*T*	*T*	*T*
Number	12	12	224	224	88	64	64	81	97
Min.	1	0.1	0.4	0.04	0.05	0.3	0.03	0.01	0.05
Max.	8.9	1.0	16.5	0.9	0.7	6	0.8	1.4	2.35
Mean	3.83	0.37	4.05	0.34	0.28	2.29	0.24	0.24	0.18
Variance	5.23	0.08	6.14	0.03	0.03	2.24	0.03	0.067	0.04
Coeff. var.	0.60	0.77	0.61	0.48	0.59	0.65	0.66	1.09	1.03

Table VII-4: Comparison of laminaset geometries (apparent thickness, *T*, maximumum thickness, T, and length, L in metres) for Rannoch (wells A and B), Kennilworth and Bencliff Grit.

Comparing the statistical tests for the bed length, the pilot study and photomosaic study are indistinguishable. There are, however, statistically significant differences between the mean lengths of Kennilworth and Bencliff (Table VII-5).

F-value/t-value	Bencliff (Pilot)	Bencliff (Photo)	Kennilworth
Ben. (Pilot)	XXX	0.50(1.96)	3.30*(1.96)
Ben. (Photo)	1.11(2.4)	XXX	9.88*(1.96)
Kennilworth	1.36(1.99)	1.50*(1.39)	XXX

Table VII-5: Significance values (F-values, below diagonal; t-values, above diagonal) for the natural log of length (assuming dip log-normally distributed). Significance value at the 95% confidence interval shown in parenthesis, significant values shown with*.

Thickness data were also collected at Bencliff along a series of randomly chosen profiles to simulate the data collection in the Rannoch cores and to be consistent with the Kennilworth data (*i.e.*, apparent thickness) (Table VII-4).

	Bencliff (Pilot)	Bencl. (Photo)	Bencl. (Prof.)	Kennil-worth	Ran. A	Ran. B
Ben. (Pilot)	XXX	0.44(1.96)	1.54(1.96)	2.23*(1.96)	1.77(1.96)	3.27*(1.96)
Ben.(Photo)	1.74(1.75)	XXX	5.80*(1.96)	7.91*(1.96)	7.32*(1.96)	14.9*(1.96)
Ben.(Prof.)	1.30(1.90)	1.33(1.39)	XXX	1.94(1.96)	2.01*(1.96)	6.4*(1.96)
Kennilworth	1.14(1.92)	1.53*(1.39)	1.15(1.39)	XXX	1.05(1.96)	4.05*(1.96)
Rannoch A	2.84*(1.92)	4.94*(1.25)	3.70*(1.25)	3.23*(1.25)	XXX	0.05(1.96)
Rannoch B	1.50(1.92)	2.61*(1.25)	1.95*(1.25)	1.71*(1.25)	1.90*(1.25)	XXX

Table VII-6: Significance values (F-values, below diagonal; t-values, above diagonal) for the natural log of thickness (log-normally distributed). Significance value at the 95% confidence interval shown in parenthesis, significant values shown with*.

The means of the Bencliff profiles and the Kennilworth data are statistically indistinguishable, however, with the larger Bencliff sample there is evidence that the population means are different (Table VII-6). The statistical analysis appear to suggest that large samples are needed to distinguish populations of significantly different geometry. Despite the statistical analysis, the differences discussed here may not be geologically significant but there are no similar quantitative studies with which to judge.

The aspect ratios in both outcrops show a scatter about the average ratios (Fig. VII-14). The thickest beds are seen in the two Rannoch wells (1.4 - 2.4m), possibly reflecting the problems associated with recognising bed boundaries in cores with concordant, low angle lamination. As far as an analogue for the Rannoch stratal geometries, these data sets suggest that the Kennilworth beds are most appropriate of the two sections studied.

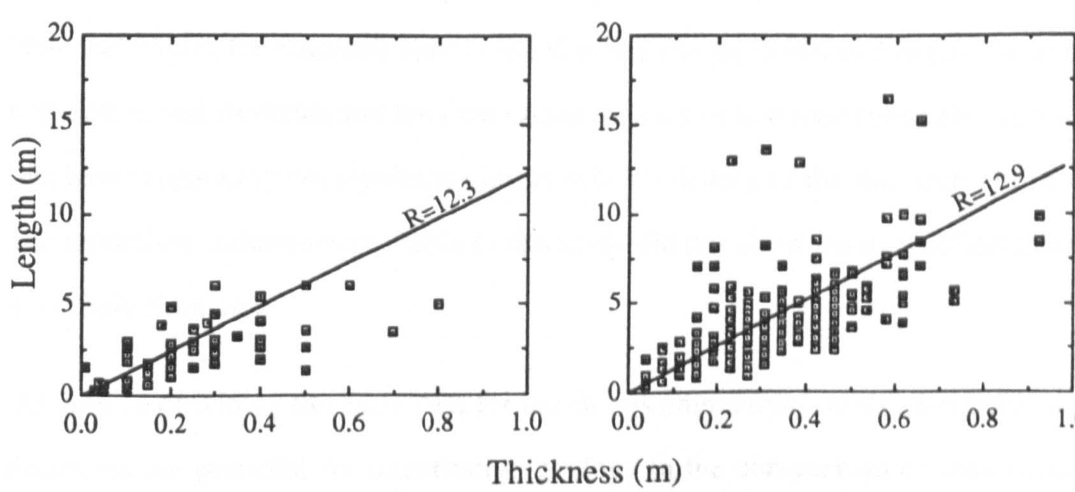

Figure VII-14: Length-thickness relationships for HCS laminasets in the Kennilworth Member (left) and the Bencliff Grit (right).

VII. 6. Lenticular shoreface laminaset geometries for engineering studies

From this study, an "average" geometry can be determined for the lenticular beds observed in shoreface sandbodies, by averaging the above data:

Bed Length	2.5m
Bed Height	0.2m
Dip angle	5.8°
Truncation angle	9.6°

These beds will have a circular plan view. For deterministic reservoir models, a stacking of units with these dimensions would be an appropriate first approximation. A more sophisticated stochastic model would employ the observed variability. At the present time, the flow sensitivity to bed geometry is not well established and is the subject of ongoing research. Whether the observed statistical differences prove to be of either geological or engineering significance, requires additional systematic data collection following the methods presented here and additional numerical simulation. New techniques for reservoir simulation also need to be developed to cope with the non-orthogonal elements and the flow characteristics of laminaset bounding surfaces (the latter apparantly not significant in the flow modelling of the Rannoch, Fig. 4.4). The modelling techniques available to this study did not allow the data collected here to be fully simulated.

As well as providing the basic data for use in this engineering study, this field work illustrates the potential for quantitative geology in the comparison of sedimentary structures. Quantitative techniques are amenable to statistical analysis and appropriate for the selection of reservoir analogues. Despite the relatively large number of laminasets and laminaset boundaries measured in this study, the sample set is rather small given the many storm-dominated shorefaces not measured. It is hoped that the work presented here will stimulate the collection and comparison of data from a wide range of analogues. In this way, the true variability of lenticular beds in shoreface sediments can be determined. It is felt, however, that some conclusions from these data are appropriate and these are summarised as follows:

- Systematic determination of stratal element thicknesses and lamina truncation angles in core can be used quantitatively in the selection of suitable reservoir analogue in low angle cross-laminated shoreface sediments.
- Of the outcrops studied, the Kennilworth is the most appropriate laminaset analogue for the North Sea Rannoch Formation, supporting the storm-influenced shoreface origin for the latter.
- The "average" geometry of Rannoch laminaset elements is estimated to be length 2.5m and thickness 0.2m.
- Average dip of bed bounding surfaces in the most appropriate Rannoch analogue is 5.8°.
- The geometries of beds studied are consistent with the defined scale of HCS laminasets.
- Relationships between laminaset length and laminaset height are poor.
- Laminaset dips, thicknesses and lengths are approximately log-normally distributed.
- Steep scours (up to 32°) can occur in these low-angle cross-laminated sediments, although their occurence is rare.

APPENDIX VIII: ECLIPSE Input Files

VIII. 1 2-D Radial Probe Permeameter Model (MINIKMOD3C.DATA)

```
--
--                  Model 3c    294 active blocks
--                    One injector, one producer
--                 5 Cells over inner injection radius
--                    Injection in outer cell only
--       Cell radii determined from Goggin's normalised flux
--                      (refer to ECL, 1988)
--
RUNSPEC
2-D Probe model (LP1) R=3.8cm z= 7.6cm
= NDIVIR  NDIVITHETA NDIVZ  QRDIAL NUMRES QNNCON
      21          1          14        T        1        T    /
= OIL    WATER    GAS
   F        F        T   /
= UNIT CONVENTION
    'LAB'  /
= NRPVT
     1   /
=  NSSFUN
    /
=  NDRXVD
      /
= NTVIP
     /
= NWMAXZ   NCWMAX    NGMAXZ   NWGMAX
       2          1              1          2    /
=  QIMCOL
    /
=  MXMFLO
    /
= MXSFLO
    /
= NANAQU
   /
=  DAY   MONTH  YEAR
     1       'JAN'     1990        /
=  QSOLVE
     /
--=====================================
GRID
--
INRAD
  0.01  /
--   PLUG RADIUS     3.8CM         LENGTH  7.6CM
--   LARGE PROBE  .295  .23CM     SMALL PROBE  .18  .215CM
DRV
   0.19175  0.05015  0.02065   0.00885   0.236
   5*0.046  5*0.055 0.1  0.2  0.4  0.8  1.5  2000     /
--
DTHETAV
   360 /
--
DZ
    21 *20
    21 *10
    21 *0.001
    21 *0.05
    21 *0.1
    21 *0.15
    21 *0.2
    21 *0.4
    21 *0.8
```

```
   21 *1.0
   21 *1.4
   42 *1.85
   21 *200  /
--
NNC
   5,1,2     1,1,3     515263    /
   5,1,2     2,1,3     515224    / To connect injection cell 5,1,2
   5,1,2     3,1,3     515122    / to cells within inner radius
   5,1,2     4,1,3     514885    /
   /
--    R1   R2   THETA1   THETA2   Z1   Z2
BOX
      1    10     1         1        1    1  /
PORO
   10*0.01  /
PERMR
    10*0.0  /
PERMZ
     5*0.0  /
BOX
      5    5      1         1        2    2  /
PORO
   0.99     /
PERMR
    100000  /
PERMZ
     100000  /
BOX
      1    4      1         1        2    2  /
PORO
   4*0.01    /
PERMR
    4*0.0    /
PERMZ
     4*0.0   /
BOX
      6    10     1         1        2    2  /
PORO
   5*0.01    /
PERMR
    5*0.0    /
PERMZ
     5*0.0   /
BOX
      11   21     1         1        1    2  /
PORO
   22*0.999     /
PERMR
    22*100000    /
PERMZ
    22*100000    /
--
BOX
      1    20     1         1        3    13  /
PORO
   220*0.18     /
PERMR
    220*96     /
PERMZ
    220*96     /
--
BOX
```

```
      21   21    1       1     3   13  /
PORO
   11*0.999   /
PERMR
   11*100000   /
PERMZ
   11*100000   /
--
BOX
      1   21    1       1     14   14  /
PORO
   21*0.999   /
PERMR
   21*100000   /
PERMZ
   21*100000   /
--
BOX
      1   21    1       1     1   1  /
--
TOPS
 21*0.0  /
--
MULTIPLY
   'PERMR'  1   1   20   1  1    8   13   /
   'PERMZ'  1
   'PORO'   1
   /
ENDBOX
--
OLDTRAN
--
-- RPTGRID
-- 6*1 3*0  1 0 1 /
--
--==================================
EDIT
--
--   R1  R2  THETA1  THETA2  Z1  Z2
BOX
      5   5    1       1     2   2  /
TRANZ
 515165  /
TRANR
  0 /
BOX
      1   5    1       1     1   1  /
TRANZ
 5*0  /
BOX
      1   4    1       1     2   2  /
TRANZ
 4*0  /
BOX
      6   10    1       1     2   2  /
TRANZ
 5*0  /
--=========================================
PROPS
--          OIL      WAT       GAS
GRAVITY
            0.7      1.0       0.9672   /
--        P    COMPRESSIBILITY
```

```
ROCK
          1.0           1.0E-6
--       P          Z          VIS
PVDG
        1.0    0.99971      1.727E-2
        2.0    0.99970      1.728E-2
--
--==============================================
SOLUTION
--
--     DATUM      Pi@DATUM
EQUIL
        10.0          1.01325   /
--
RPTSOL
  1 0 0 1 /
--==============================================
SUMMARY
--
WBHF
   'PROD'   'INJ'   /
--
WPI
   'INJ'  /
--
WGIR
   'INJ'  /
--
WGPR
    'PROD'   'INJ'   /
--
BPR
 21   1  1 /   PROD
  1   1  2 /   INJ
  1   1  3 /
  2   1  3 /
  3   1  3 /
  4   1  3 /
  5   1  3 /
 /
--
RPTSMRY
  1 /
--
RUNSUM
--=====================================
SCHEDULE
--
RPTSCHED
 1 0 0 1 0 0 2 0 1 10*0 /
--
-- WELL    WELL    LOCATION      BHP     PREF.
-- NAME   GROUP   I          J   DATUM   PHASE
--
WELSPECS
  'PROD'     'G'    21         1       10.0      'GAS'   /
  'INJ'      'G'     1         1       10.0      'GAS'   /
   /
--
-- WELL    LOCATION      INTERVAL     STATUS      WELL
-- NAME  I          J      K1      K2     O OR S        ID
COMPDAT
  'PROD'  21        1       1       1       'OPEN'   2*   0.25  /
```

```
   'INJ'      5       1        2        2       'OPEN'   2*   0.015  /
   /
-- WELL      STATUS    CONTROL     TARG   OR UP  LIMIT
-- NAME                 MODE              RATE
WCONPROD
   'PROD'    'OPEN'      'BHP'       5*   1.01325    /
   /
-- WELL      FLUID    STATUS    CONTROL     TARG   OR UP  LIMIT
-- NAME      TYPE                MODE              RATE
WCONINJ
   'INJ'      'GAS'    'OPEN'    'RATE'      23940     3*    /
   /
--
--
TSTEP
  3*0.0001    /
--
--
--==========================================
END
```

VIII. 2 Subfacies Scale; Fine Grid A (EXFGA003.DATA)

```
--
--          LAMINATED SAND SIMULATION
--
--       BASED ON STATFJORD PROBE PERMEAMETER DATA
--
--           FINE GRID A HORIZONTAL DIRECTION
--                 (extended model)
--
--        (With entrance and exit blocks >4times sample block length.
--      With identical sample block as buffer before and after subject block
--              see Kossack, Aasen and Opdal, 1990)
--
--==========================================================
RUNSPEC
RANNOCH LAMINATION SIMULATION
= NDIVIX NDIVIY NDIVIZ
  194   1   41 /
= OIL WAT GAS
  T  T  F /
= UNIT CONVENTION
  'LAB' /
=  NRPVT
   1 /
= NSSFUN  NTSFUN
   35    5 /
= NDRXVD
   /
=  NTFIP
   5 /
= NWMAXZ NCWMAX NGMAXZ NWGMAX
  2    42   1    2 /
= QIMCOL
   /
= MXMFLO
   /
= MXSFLO
   /
= NANAQU
   /
=  DAY  MONTH  YEAR
   1   'JAN'  1990  /
= QSOLVE  NSTACK
   T     25 /
--
--==============================================================
GRID
--
EQUALS
       'DX'    300      1    1    1 1     1 41  /
       'DX'    1        2  193    1 1     1 41  /
       'DX'    300    194  194    1 1     1 41  /
       'DY'  5          1  194    1 1     1 41  /
       'DZ'    0.2      1  194    1 1     1 41  /
       'TOPS' 30000     1  194    1 1     1  1     /
/
EQUALS
       'PORO'  0.15     1 1      1 1     1  41   / Injection block
       'PERMX'          1500     /
--
--**********************************************************
--                 FINE GRID A
--**********************************************************
```

```
--
'PORO' 0.15    2 193   1 1    1 1   / Lamina
'PERMX'         17     /
'PORO' 0.15    2 193   1 1    2 2   / Lamina
'PERMX'         50     /
'PORO' 0.15    2 193   1 1    3 3   / Lamina
'PERMX'         106    /
'PORO' 0.15    2 193   1 1    4 4   / Lamina
'PERMX'         141    /
'PORO' 0.15    2 193   1 1    5 5   / Lamina
'PERMX'         174    /
'PORO' 0.15    2 193   1 1    6 6   / Lamina
'PERMX'         174    /
'PORO' 0.15    2 193   1 1    7 7   / Lamina
'PERMX'         96     /
'PORO' 0.15    2 193   1 1    8 8   / Lamina
'PERMX'         35     /
'PORO' 0.15    2 193   1 1    9 9   / Lamina
'PERMX'         7      /
'PORO' 0.15    2 193   1 1    10 10   / Lamina
'PERMX'         19     /
'PORO' 0.15    2 193   1 1    11 11   / Lamina
'PERMX'         13     /
'PORO' 0.15    2 193   1 1    12 12   / Lamina
'PERMX'         17     /
'PORO' 0.15    2 193   1 1    13 13   / Lamina
'PERMX'         26     /
'PORO' 0.15    2 193   1 1    14 14   / Lamina
'PERMX'         35     /
'PORO' 0.15    2 193   1 1    15 15   / Lamina
'PERMX'         75     /
'PORO' 0.15    2 193   1 1    16 16   / Lamina
'PERMX'         101    /
'PORO' 0.15    2 193   1 1    17 17   / Lamina
'PERMX'         92     /
'PORO' 0.15    2 193   1 1    18 18   / Lamina
'PERMX'         69     /
'PORO' 0.15    2 193   1 1    19 19  / Lamina
'PERMX'         24     /
'PORO' 0.15    2 193   1 1    20 20   / Lamina
'PERMX'         4      /
'PORO' 0.15    2 193   1 1    21 21   / Lamina
'PERMX'         11     /
'PORO' 0.15    2 193   1 1    22 22   / Lamina
'PERMX'         12     /
'PORO' 0.15    2 193   1 1    23 23   / Lamina
'PERMX'         10     /
'PORO' 0.15    2 193   1 1    24 24   / Lamina
'PERMX'         9      /
'PORO' 0.15    2 193   1 1    25 25   / Lamina
'PERMX'         11     /
'PORO' 0.15    2 193   1 1    26 26  / Lamina
'PERMX'         16     /
'PORO' 0.15    2 193   1 1    27 27  / Lamina
'PERMX'         14     /
'PORO' 0.15    2 193   1 1    28 28   / Lamina
'PERMX'         20     /
'PORO' 0.15    2 193   1 1    29 29   / Lamina
'PERMX'         16     /
'PORO' 0.15    2 193   1 1    30 30   / Lamina
'PERMX'         2      /
'PORO' 0.15    2 193   1 1    31 31   / Lamina
'PERMX'         6      /
```

```
        'PORO' 0.15    2 193   1 1    32  32  / Lamina
        'PERMX'         14     /
        'PORO' 0.15    2 193   1 1    33 33  / Lamina
        'PERMX'         31     /
        'PORO' 0.15    2 193   1 1    34 34  / Lamina
        'PERMX'         49     /
        'PORO' 0.15    2 193   1 1    35 35  / Lamina
        'PERMX'         45     /
        'PORO' 0.15    2 193   1 1    36  36  / Lamina
        'PERMX'         20     /
        'PORO' 0.15    2 193   1 1    37  37  / Lamina
        'PERMX'         33     /
        'PORO' 0.15    2 193   1 1    38  38  / Lamina
        'PERMX'         46     /
        'PORO' 0.15    2 193   1 1    39  39  / Lamina
        'PERMX'         33     /
        'PORO' 0.15    2 193   1 1    40 40  / Lamina
        'PERMX'         31     /
        'PORO' 0.15    2 193   1 1    41  41  / Lamina
        'PERMX'         24     /
--
        'PORO' 0.15     194  194      1 1     1  41  / Production block
        'PERMX'        1500    /
/
COPY
        'PERMX'         'PERMY' 1  194 1 1   1   41 /
        'PERMX' 'PERMZ'        /
/
ENDBOX
--
PSEUDOS
--
--==================================================================
PROPS
--      OIL    WAT    GAS
DENSITY
        0.81   1.0    0.08  /
--
--   P    Bo    Vis
PVDO
    65.0   1.187   0.88
   476.0   1.1     1.1
  /
--    (DATA FROM THISTLE A31 DST INTERPRETATION PARAMETERS)
--   P       Bw      Cw       Vis    Viscosibility
PVTW
   412.0      1.02    3.0D-06   0.88    0.0 /
--
--
--   P          Cr
ROCK
   412.0     5.0D-06   /
--
--***************************************************
--              ROCK CURVES
--***************************************************
--     So    Kro
--                        15mD
SOF2
        0.25     0.00
        0.3      0.005
        0.4      0.064
        0.5      0.143
```

```
        0.514   0.154
        0.528   0.37
        0.542   0.424
        0.556   0.478
        0.57    0.532
        0.584   0.585
        0.598   0.639
        0.612   0.693
        0.626   0.746
        0.64    0.800
/
--                      50mD
        0.25    0.0
        0.3     0.004
        0.4     0.044
        0.5     0.11
        0.522   0.124
        0.544   0.24
        0.566   0.310
        0.588   0.38
        0.61    0.45
        0.632   0.52
        0.654   0.59
        0.676   0.66
        0.698   0.73
        0.72    0.8
/
--                      150md
        0.25    0.0
        0.30    0.004
        0.4     0.03
        0.5     0.086
        0.53    0.103
        0.56    0.147
        0.59    0.229
        0.62    0.311
        0.65    0.392
        0.68    0.474
        0.71    0.555
        0.74    0.637
        0.77    0.718
        0.8     0.8
/
--                      1500md
        0.25    0.0
        0.36    0.016
        0.575   0.112
        0.8     0.8
/
--                      3md
        0.25    0.0
        0.30    0.0008
        0.33    0.0082
        0.35    0.0250
        0.37    0.0622
        0.39    0.1345
        0.4     0.1898
        0.41    0.2621
        0.43    0.4724
        0.44    0.6190
        0.45    0.8
/
--
```

APPENDIX VIII: ECLIPSE Input Files

```
--      Sw      Krw                 Pc
SWFN
--                  15md
        0.36    0.0                 3.741
        0.374   0.012               1.769
        0.388   0.025               1.361
        0.402   0.037               1.190
        0.416   0.05                0.952
        0.430   0.062               0.85
        0.444   0.075               0.748
        0.458   0.087               0.68
        0.472   0.1                 0.544
        0.486   0.124               0.476
        0.5     0.133               0.408
        0.6     0.201               0.204
        0.7     0.318               0.17
        0.75    0.44                0.156
/
--                  50md
        0.28    0.0                 2.721
        0.302   0.016               1.361
        0.324   0.033               0.816
        0.346   0.049               0.612
        0.368   0.065               0.476
        0.39    0.081               0.34
        0.412   0.098               0.293
        0.434   0.114               0.252
        0.456   0.13                0.218
        0.478   0.15                0.19
        0.5     0.162               0.184
        0.6     0.218               0.15
        0.7     0.339               0.109
        0.75    0.44                0.068
/
--                  150md
        0.2     0.0                 1.837
        0.23    0.019               0.816
        0.26    0.038               0.544
        0.29    0.057               0.374
        0.32    0.076               0.272
        0.35    0.095               0.211
        0.38    0.114               0.177
        0.41    0.133               0.15
        0.44    0.152               0.122
        0.47    0.168               0.095
        0.5     0.183               0.092
        0.6     0.231               0.082
        0.7     0.354               0.075
        0.75    0.44                0.068
/
--                  1500md
        0.2     0.0                 0.2
        0.425   0.096               0.1
        0.64    0.2                 0.05
        0.75    0.35                0.02
/
--                                          3 md
        0.55    0.0                 2.72
        0.57    0.0036              1.84
        0.6     0.0225              1.16
        0.65    0.09                0.82
        0.7     0.2025              0.48
        0.75    0.36                0.34
```

```
        /
--
--======================================================================
REGIONS
--
--        SUBJECT BLOCK REGION 3
--
FIPNUM

        1*1     64*2    64*3    64*4    1*5
        1*1     64*2    64*3    64*4    1*5
        1*1     64*2    64*3    64*4    1*5
        1*1     64*2    64*3    64*4    1*5
        1*1     64*2    64*3    64*4    1*5
        1*1     64*2    64*3    64*4    1*5
        1*1     64*2    64*3    64*4    1*5
        1*1     64*2    64*3    64*4    1*5
        1*1     64*2    64*3    64*4    1*5
        1*1     64*2    64*3    64*4    1*5
        1*1     64*2    64*3    64*4    1*5
        1*1     64*2    64*3    64*4    1*5
        1*1     64*2    64*3    64*4    1*5
        1*1     64*2    64*3    64*4    1*5
        1*1     64*2    64*3    64*4    1*5
        1*1     64*2    64*3    64*4    1*5
        1*1     64*2    64*3    64*4    1*5
        1*1     64*2    64*3    64*4    1*5
        1*1     64*2    64*3    64*4    1*5
        1*1     64*2    64*3    64*4    1*5
        1*1     64*2    64*3    64*4    1*5
        1*1     64*2    64*3    64*4    1*5
        1*1     64*2    64*3    64*4    1*5
        1*1     64*2    64*3    64*4    1*5
        1*1     64*2    64*3    64*4    1*5
        1*1     64*2    64*3    64*4    1*5
        1*1     64*2    64*3    64*4    1*5
        1*1     64*2    64*3    64*4    1*5
        1*1     64*2    64*3    64*4    1*5
        1*1     64*2    64*3    64*4    1*5
        1*1     64*2    64*3    64*4    1*5
        1*1     64*2    64*3    64*4    1*5
        1*1     64*2    64*3    64*4    1*5
        1*1     64*2    64*3    64*4    1*5
        1*1     64*2    64*3    64*4    1*5
        1*1     64*2    64*3    64*4    1*5
        1*1     64*2    64*3    64*4    1*5
        1*1     64*2    64*3    64*4    1*5
        1*1     64*2    64*3    64*4    1*5
        1*1     64*2    64*3    64*4    1*5
        1*1     64*2    64*3    64*4    1*5  /
--
SATNUM
        1*4 192*1 1*4
        1*4 192*2 1*4
        1*4 192*3 1*4
        1*4 192*3 1*4
        1*4 192*3 1*4
        1*4 192*3 1*4
        1*4 192*2 1*4
        1*4 192*2 1*4
        1*4 192*1 1*4
        1*4 192*1 1*4
        1*4 192*1 1*4
```

```
        1*4 192*1 1*4
        1*4 192*1 1*4
        1*4 192*2 1*4
        1*4 192*2 1*4
        1*4 192*3 1*4
        1*4 192*2 1*4
        1*4 192*2 1*4
        1*4 192*1 1*4
        1*4 192*5 1*4
        1*4 192*1 1*4
        1*4 192*1 1*4
        1*4 192*1 1*4
        1*4 192*1 1*4
        1*4 192*1 1*4
        1*4 192*1 1*4
        1*4 192*1 1*4
        1*4 192*1 1*4
        1*4 192*1 1*4
        1*4 192*5 1*4
        1*4 192*1 1*4
        1*4 192*1 1*4
        1*4 192*1 1*4
        1*4 192*2 1*4
        1*4 192*2 1*4
        1*4 192*1 1*4
        1*4 192*1 1*4
        1*4 192*2 1*4
        1*4 192*1 1*4
        1*4 192*1 1*4
        1*4 192*1 1*4        /
--
--===========================================================
SOLUTION
--
--  DATUM  Pi@DATUM  WOC   Pc@WOC   GOC Pc@GOC
EQUIL
   30004   313   40004   0    27000   0  2* 0/
--
--    Pb Sob Swb       Pob@Datum
RPTSOL
     1  0  1   12*0 1 /
--===========================================================
SUMMARY
--
WWCT
 'PROD'
 /
--
FOIP
--
FWIP
--
ROIP
        3 /
--
RWIP
        3  /
--
RWFT
        2  3
        3  4
/
--
```

```
ROFT
        2 3
        3 4
/
--
RPTSMRY
 1 /
--
RUNSUM
--=================================================================
SCHEDULE
--
RPTSCHED
 1 0 1 0 0 0 2 2 1 6*0 1 0 0 /
--
--    WELL  WELL  LOCATION  BHP    PREF.
--    NAME  GROUP  I   J   DATUM  PHASE
WELSPECS
     'PROD' 'G'  194  1   30004  'OIL' /
--
     'INJ'  'G'  1    1   30004  'WAT' /
       /
--
--    WELL  LOCATION  INTERVAL  STATUS      WELL
--    NAME  I   J   K1  K2   O or S       ID
COMPDAT
     'PROD' 194  1    1  41   'OPEN'  2*   1.5 /
     'INJ'    1  1    1  41   'OPEN'  2*   1.5 /
       /
--
--    WELL  STATUS  CONTROL  TARGET RATES or UPPER LIMITS
--    NAME          MODE   OIL  WAT  GAS  LIQ RV  BHP(atm)
WCONPROD
     'PROD'  'OPEN'  'BHP'   5*          313.0 /
       /
--
--    WELL  FLUID  STATUS  CONTROL  RATE        BHP TAR
--    NAME  TYPE           MODE     cc/hr       (atm)
WCONINJ
     'INJ'  'WAT'  'OPEN'  'RATE'   6   3*    500   /
       /
--
TUNING
/
/
20 1  25 1  20 /
--
--    DAYS
TSTEP
  1 2 4 6 9 20 30 30 50 100 250 500 /
--=================================================================
END
```

VIII. 3 Facies Scale; HCS Bedform (HCS2D010.DATA)

```
--          HCS2D010.DATA
--
--             HCS/SCS SIMULATION
--
--        BASED ON STATFJORD MINIPERMEAMETER DATA
--
--          FINE GRIDS:
--                B - HETEROLITHIC
--          A - HIGH CONTRAST LAMINATED
--          c - LOW CONTRAST LAMINATED
--
-- (With extra entrance and exit blocks >4times sample block length
--  With identical sample block as buffer before and after subject block
--        see Kossack, Aasen and Opdal, 1990)
--
--*****************************************************************
RUNSPEC
RANNOCH LAMINATION SIMULATION
= NDIVIX NDIVIY NDIVIZ
  184  1   30 /
= OIL WAT GAS
  T  T  F /
= UNIT CONVENTION
  'LAB' /
=  NRPVT
   1 /
= NSSFUN  NTSFUN QDIRKR  QREVKR
  35    8     T     T  /
= NDRXVD NTEQUL
   /
=  NTFIP
  5 /
= NWMAXZ NCWMAX NGMAXZ NWGMAX
  2    30   1    2 /
= QIMCOL
  /
= MXMFLO
  /
= MXSFLO
  /
= NANAQU
  /
=  DAY  MONTH  YEAR
  1   'JAN'  1990  /
= QSOLVE  NSTACK
  T     50 /
--
--================================================================
GRID
--
EQUALS
        'DX'    5000    1   1   1 1      1 30  /
        'DX'    250     2   2   1 1      1 30  /
        'DX'    8       3   182 1 1    1 30  /
        'DX'    250  183   183 1  1    1 30  /
        'DX'    5000 184   184 1  1    1 30  /
        'DY'  5         1  184  1 1      1 30  /
        'DZ'    8       1  184  1 1      1 30  /
        'TOPS' 300      1  184  1 1      1 1      /
/
PERMX
--
```

```
--   INJECTION BLOCKS
         1500  500
--   BUFFER              SUBJECT BLOCK          BUFFER
24*292 12*4.7 24*292     24*292 12*4.7 24*292     24*292 12*4.7 24*292
--   PRODUCTION BLOCKS
         500  1500
--       ditto for subsequent layers
     1500  500
18*292 24*42 18*292      18*292 24*42 18*292      18*292 24*42 18*292
           500
         1500 1500  500
12*292 36*42 12*292      12*292 36*42 12*292      12*292 36*42 12*292
           500
         1500  1500 500
18*292 24*42 18*292      18*292 24*42 18*292      18*292 24*42 18*292
           500
         1500 1500  500
         180*292
           500
         1500 1500  500
6*4.7 48*292 6*4.7       6*4.7 48*292 6*4.7       6*4.7 48*292 6*4.7
           500
         1500  1500 500
12*42 36*292 12*42       12*42 36*292 12*42       12*42 36*292 12*42
           500
         1500  1500 500
18*42 24*292 18*42       18*42 24*292 18*42       18*42 24*292 18*42
           500
         1500 1500  500
12*42 36*292 12*42       12*42 36*292 12*42       12*42 36*292 12*42
           500
         1500 1500  500
180*292
           500
--
         1500 1500  500
24*292 12*4.7 24*292     24*292 12*4.7 24*292     24*292 12*4.7 24*292
           500
         1500  1500 500
18*292 24*42 18*292      18*292 24*42 18*292      18*292 24*42 18*292
           500
         1500 1500  500
12*292 36*42 12*292      12*292 36*42 12*292      12*292 36*42 12*292
           500
         1500 1500  500
18*292 24*42 18*292      18*292 24*42 18*292      18*292 24*42 18*292
           500
         1500 1500  500
         180*292
           500
         1500  1500 500
6*4.7 48*292 6*4.7       6*4.7 48*292 6*4.7       6*4.7 48*292 6*4.7
           500
         1500  1500 500
12*42 36*292 12*42       12*42 36*292 12*42       12*42 36*292 12*42
           500
         1500  1500 500
18*42 24*292 18*42       18*42 24*292 18*42       18*42 24*292 18*42
           500
         1500  1500 500
12*42 36*292 12*42       12*42 36*292 12*42       12*42 36*292 12*42
           500
         1500 1500  500
```

```
        180*292
          500
--
        1500 1500  500
 24*292 12*4.7 24*292     24*292 12*4.7 24*292     24*292 12*4.7 24*292
          500
        1500  1500 500
 18*292 24*42 18*292      18*292 24*42 18*292      18*292 24*42 18*292
          500
        1500  1500 500
 12*292 36*42 12*292      12*292 36*42 12*292      12*292 36*42 12*292
          500
        1500 1500  500
 18*292 24*42 18*292      18*292 24*42 18*292      18*292 24*42 18*292
          500
        1500 1500  500
        180*292
         500
        1500  1500  500
6*4.7 48*292 6*4.7        6*4.7 48*292 6*4.7       6*4.7 48*292 6*4.7
          500
        1500 1500  500
 12*42 36*292 12*42       12*42 36*292 12*42       12*42 36*292 12*42
          500
        1500  1500 500
 18*42 24*292 18*42       18*42 24*292 18*42       18*42 24*292 18*42
         500
        1500  1500  500
 12*42 36*292 12*42       12*42 36*292 12*42       12*42 36*292 12*42
          500
        1500 1500  500
        180*292
         500  1500
       /
--
EQUALS
        'PORO'  0.15      1  184    1  1      1  30  /
        /
--
COPY
        'PERMX'           'PERMY'  1   184  1  1    1    30 /
        'PERMX' 'PERMZ'          /
/
ENDBOX
--
PSEUDOS
--
--==================================================================
PROPS
--      OIL     WAT     GAS
DENSITY
       0.81    1.0     0.08  /
--
--    P    Bo    Vis
PVDO
    65.0   1.187   0.88
   476.0   1.1     1.1
  /
--    (DATA FROM THISTLE A31 DST INTERPRETATION PARAMETERS)
--    P        Bw       Cw        Vis    Viscosibility
PVTW
   412.0      1.02     3.0D-06   0.88    0.0 /
--
```

```
--
--   P        Cr
ROCK
    412.0     5.0D-06  /
--
--*********************************************
--          LAMINA GEOPSEUDOS
--*********************************************
--  So        Kro
SOF2
--   RIPPLED (Fine grid B)       4.7mD   KROX,Y
--
   0.250000     0.000000 -- Lower end point
   0.304270     0.000827 -- Generated point
   0.312878     0.001074 -- Generated point
   0.317877     0.001306 -- Generated point
   0.321754     0.001610 -- Generated point
   0.327173     0.002545 -- Generated point
   0.334108     0.005341 -- Generated point
   0.342488     0.008989 -- Generated point
   0.352660     0.014486 -- Generated point
   0.380120     0.083819 -- Generated point
   0.460026     0.675495 -- Generated point
   0.472421     0.800013 -- Upper end point
/
--            ditto          KROZ
--
   0.250000     0.000000 -- Lower end point
   0.304270     0.000827 -- Generated point
   0.312878     0.001074 -- Generated point
   0.317877     0.001306 -- Generated point
   0.321754     0.001610 -- Generated point
   0.327173     0.002545 -- Generated point
   0.334108     0.005341 -- Generated point
   0.342488     0.008989 -- Generated point
   0.352660     0.014486 -- Generated point
   0.380120     0.083819 -- Generated point
   0.460026     0.675495 -- Generated point
   0.472421     0.800013 -- Upper end point
/
--        HIGH CONTRAST LAMINATED (Fine grid A)      42mD  KROX,Y
--
   0.250000     0.000000 -- Lower end point
   0.270818     0.010191 -- Generated point
   0.286327     0.028645 -- Generated point
   0.314071     0.062037 -- Generated point
   0.371862     0.151121 -- Generated point
   0.450080     0.233102 -- Generated point
   0.496912     0.340494 -- Generated point
   0.566993     0.502644 -- Generated point
   0.620186     0.679683 -- Generated point
   0.646477     0.742377 -- Generated point
   0.663949     0.776434 -- Generated point
   0.672210     0.789297 -- Generated point
   0.679014     0.800004 -- Upper end point
/
--           ditto          KROZ
--
   0.250000     0.000000 -- Lower end point
   0.353819     0.003249 -- Generated point
   0.369623     0.005668 -- Generated point
   0.380290     0.010750 -- Generated point
   0.394429     0.021220 -- Generated point
```

```
   0.430593     0.046092 -- Generated point
   0.465080     0.071618 -- Generated point
   0.479659     0.082510 -- Generated point
   0.508721     0.107421 -- Generated point
   0.586236     0.427022 -- Generated point
   0.648131     0.708908 -- Generated point
   0.679025     0.799998 -- Upper end point
/
--        LOW CONTRAST LAMINATION (Fine grid C) 292mD KROX,Y
--
   0.250000     0.000000 -- Lower end point
   0.311442     0.008028 -- Generated point
   0.383459     0.028204 -- Generated point
   0.511960     0.105553 -- Generated point
   0.578874     0.221427 -- Generated point
   0.618287     0.327397 -- Generated point
   0.647260     0.395714 -- Generated point
   0.696341     0.524623 -- Generated point
   0.748311     0.676054 -- Generated point
   0.779523     0.764485 -- Generated point
   0.797308     0.781502 -- Generated point
   0.812444     0.799979 -- Generated point
   0.814697     0.799979 -- Upper end point
/
--              ditto          KROZ
--
   0.250000     0.000000 -- Lower end point
   0.299639     0.003949 -- Generated point
   0.327358     0.010520 -- Generated point
   0.398226     0.030120 -- Generated point
   0.491454     0.084667 -- Generated point
   0.556015     0.138640 -- Generated point
   0.594750     0.241173 -- Generated point
   0.633068     0.357365 -- Generated point
   0.650185     0.396573 -- Generated point
   0.683616     0.479555 -- Generated point
   0.748701     0.642662 -- Generated point
   0.795331     0.748251 -- Generated point
   0.814706     0.799997 -- Upper end point
/
--                   ROCK CURVE   500mD   KROX,Y,Z
         0.25     0.0
         0.3      0.004
         0.4      0.030
         0.5      0.086
         0.550    0.114
         0.58     0.202
         0.61     0.283
         0.64     0.365
         0.67     0.446
         0.7      0.528
         0.73     0.61
         0.76     0.691
         0.79     0.773
         0.82     0.8
/
--                   ROCK CURVE   1500mD   KROX,Y,Z
         0.25     0.0
         0.36     0.016
         0.575    0.112
         0.8      0.8
/
--
```

```
--  Sw        Krw          Pc
SWFN
--
--  RIPPLED (Fine grid B)        4.7mD  KRWX,Y
--
 0.527579    0.000000     2.823417 -- Lower end point
 0.531533    0.000305     2.558716 -- Initial state point
 0.539974    0.000955     2.198792 -- Generated point
 0.619880    0.060518     0.850647 -- Generated point
 0.647340    0.115738     0.663818 -- Generated point
 0.657512    0.134495     0.592865 -- Generated point
 0.665892    0.150921     0.535583 -- Generated point
 0.672827    0.165700     0.492126 -- Generated point
 0.678246    0.176362     0.469116 -- Generated point
 0.682123    0.184493     0.456696 -- Generated point
 0.687122    0.195740     0.442139 -- Generated point
 0.695730    0.215086     0.417084 -- Generated point
 0.750013    0.369056     0.318154 -- Upper end point
/
--          ditto         KRWZ
--
 0.527579    0.000000     2.823417 -- Lower end point
 0.531533    0.000305     2.558716 -- Initial state point
 0.539974    0.000955     2.198792 -- Generated point
 0.619880    0.060518     0.850647 -- Generated point
 0.647340    0.115738     0.663818 -- Generated point
 0.657512    0.134495     0.592865 -- Generated point
 0.665892    0.150921     0.535583 -- Generated point
 0.672827    0.165700     0.492126 -- Generated point
 0.678246    0.176362     0.469116 -- Generated point
 0.682123    0.184493     0.456696 -- Generated point
 0.687122    0.195740     0.442139 -- Generated point
 0.695730    0.215086     0.417084 -- Generated point
 0.750013    0.369056     0.318154 -- Upper end point
/
--  HIGH CONTRAST LAMINATED (Fine grid A)     42mD    KRWX,Y
--
 0.320986    0.000000     3.260144 -- Lower end point
 0.327772    0.002449     2.392487 -- Generated point
 0.336051    0.006015     1.735016 -- Generated point
 0.353523    0.013713     1.243591 -- Generated point
 0.379814    0.028161     0.859924 -- Generated point
 0.433007    0.067394     0.466339 -- Generated point
 0.503088    0.110213     0.268036 -- Generated point
 0.549920    0.138770     0.197723 -- Generated point
 0.628138    0.186231     0.169403 -- Generated point
 0.685929    0.264334     0.144867 -- Generated point
 0.713673    0.316661     0.134064 -- Generated point
 0.729182    0.353725     0.130280 -- Generated point
 0.750021    0.440008     0.123807 -- Upper end point
/
--          ditto               KRWZ
--
 0.320975    0.000000     3.284751 -- Lower end point
 0.326862    0.004463     2.485779 -- Initial state point
 0.351869    0.023419     1.258118 -- Generated point
 0.413764    0.079223     0.581421 -- Generated point
 0.491279    0.156597     0.294037 -- Generated point
 0.520341    0.178306     0.235626 -- Generated point
 0.534920    0.187891     0.208862 -- Generated point
 0.569407    0.225552     0.189545 -- Generated point
 0.605571    0.264986     0.176239 -- Generated point
 0.619710    0.281531     0.171082 -- Generated point
```

```
    0.630377    0.296075    0.167572 -- Generated point
    0.646181    0.329088    0.162292 -- Generated point
    0.749997    0.439998    0.123804 -- Upper end point
/
--        LOW CONTRAST LAMINATION (Fine grid C) 292mD        KRWX,Y
--
    0.185303    0.000000    1.837008 -- Lower end point
    0.187556    0.000000    1.758514 -- Generated point
    0.202692    0.003185    1.244507 -- Generated point
    0.220477    0.008621    0.774414 -- Generated point
    0.251689    0.028687    0.503510 -- Generated point
    0.303659    0.063696    0.268951 -- Generated point
    0.352740    0.093620    0.182709 -- Generated point
    0.381713    0.109343    0.161652 -- Generated point
    0.421127    0.134643    0.126038 -- Generated point
    0.488040    0.167099    0.100983 -- Generated point
    0.616541    0.243676    0.081512 -- Generated point
    0.688558    0.333735    0.080597 -- Generated point
    0.750013    0.439994    0.067998 -- Upper end point
/
--            ditto                 KRWZ
--
    0.185294    0.000000    1.836995 -- Lower end point
    0.204669    0.004760    1.177460 -- Generated point
    0.251299    0.031702    0.509796 -- Generated point
    0.316384    0.072205    0.249573 -- Generated point
    0.349815    0.094896    0.194580 -- Generated point
    0.366932    0.104459    0.175446 -- Generated point
    0.405250    0.129684    0.140717 -- Generated point
    0.443985    0.154588    0.105225 -- Generated point
    0.508546    0.183398    0.091156 -- Generated point
    0.601774    0.232572    0.081909 -- Generated point
    0.672642    0.326765    0.076874 -- Generated point
    0.700361    0.360512    0.074677 -- Generated point
    0.750000    0.439998    0.068000 -- Upper end point
/
--          ROCK CURVE   500mD KRWX,Y,Z
          0.18    0.0       1.837
          0.21    0.006     0.816
          0.24    0.025     0.544
          0.27    0.044     0.374
          0.30    0.063     0.272
          0.33    0.082     0.211
          0.36    0.101     0.177
          0.39    0.120     0.15
          0.42    0.139     0.122
          0.45    0.159     0.095
          0.5     0.183     0.092
          0.6     0.231     0.082
          0.7     0.354     0.075
          0.75    0.44      0.068
/
--          ROCK CURVE  1500mD  KRWX,Y,Z
          0.2     0.0       0.2
          0.425   0.096     0.1
          0.64    0.2       0.05
          0.75    0.35      0.02
/
--
--=====================================================================
REGIONS
--
--        SUBJECT BLOCK REGION 3
```

```
--
FIPNUM

        2*1    60*2    60*3    60*4    2*5
        2*1    60*2    60*3    60*4    2*5
        2*1    60*2    60*3    60*4    2*5
        2*1    60*2    60*3    60*4    2*5
        2*1    60*2    60*3    60*4    2*5
        2*1    60*2    60*3    60*4    2*5
        2*1    60*2    60*3    60*4    2*5
        2*1    60*2    60*3    60*4    2*5
        2*1    60*2    60*3    60*4    2*5
        2*1    60*2    60*3    60*4    2*5
        2*1    60*2    60*3    60*4    2*5
        2*1    60*2    60*3    60*4    2*5
        2*1    60*2    60*3    60*4    2*5
        2*1    60*2    60*3    60*4    2*5
        2*1    60*2    60*3    60*4    2*5
        2*1    60*2    60*3    60*4    2*5
        2*1    60*2    60*3    60*4    2*5
        2*1    60*2    60*3    60*4    2*5
        2*1    60*2    60*3    60*4    2*5
        2*1    60*2    60*3    60*4    2*5
        2*1    60*2    60*3    60*4    2*5
        2*1    60*2    60*3    60*4    2*5
        2*1    60*2    60*3    60*4    2*5
        2*1    60*2    60*3    60*4    2*5
        2*1    60*2    60*3    60*4    2*5
        2*1    60*2    60*3    60*4    2*5
        2*1    60*2    60*3    60*4    2*5
        2*1    60*2    60*3    60*4    2*5
        2*1    60*2    60*3    60*4    2*5
        2*1    60*2    60*3    60*4    2*5
/
--
--   SATURATION REGIONS IDENTIFIED BY PERMEABILITY (mD)
-- 1=4.7H 2=4.7V 3=42H 4=42V 5=292H 6=292V 7=1500H&V 8=500H&V
--
SATNUM

        8 7
        24*5 12*1 24*5  24*5 12*1 24*5  24*5 12*1 24*5
        7 8
        8 7
        18*5 24*3 18*5  18*5 24*3 18*5  18*5 24*3 18*5
        7 8 8
        7
        12*5 36*3 12*5  12*5 36*3 12*5  12*5 36*3 12*5
        7 8 8
        7
        18*5 24*3 18*5  18*5 24*3 18*5  18*5 24*3 18*5
        7 8 8
        7
        180*5
        7 8 8
        7
        6*1 48*5 6*1    6*1 48*5 6*1    6*1 48*5 6*1
        7 8 8
        7
        12*3 36*5 12*3  12*3 36*5 12*3  12*3 36*5 12*3
        7 8 8
        7
        18*3 24*5 18*3  18*3 24*5 18*3  18*3 24*5 18*3
```

```
7 8 8
7
12*3 36*5 12*3   12*3 36*5 12*3   12*3 36*5 12*3
7 8 8
7
180*5
7 8 8
--
7
24*5 12*1 24*5   24*5 12*1 24*5   24*5 12*1 24*5
7 8 8
7
18*5 24*3 18*5   18*5 24*3 18*5   18*5 24*3 18*5
7 8 8
7
12*5 36*3 12*5   12*5 36*3 12*5   12*5 36*3 12*5
7 8 8
7
18*5 24*3 18*5   18*5 24*3 18*5   18*5 24*3 18*5
7 8 8
7
180*5
7 8 8
7
6*1 48*5 6*1     6*1 48*5 6*1     6*1 48*5 6*1
7 8 8
7
12*3 36*5 12*3   12*3 36*5 12*3   12*3 36*5 12*3
7 8 8
7
18*3 24*5 18*3   18*3 24*5 18*3   18*3 24*5 18*3
7 8 8
7
12*3 36*5 12*3   12*3 36*5 12*3   12*3 36*5 12*3
7 8 8
7
180*5
7 8 8
--
7
24*5 12*1 24*5   24*5 12*1 24*5   24*5 12*1 24*5
7 8 8
7
18*5 24*3 18*5   18*5 24*3 18*5   18*5 24*3 18*5
7 8 8
7
12*5 36*3 12*5   12*5 36*3 12*5   12*5 36*3 12*5
7 8 8
7
18*5 24*3 18*5   18*5 24*3 18*5   18*5 24*3 18*5
7 8 8
7
180*5
7 8 8
7
6*1 48*5 6*1     6*1 48*5 6*1     6*1 48*5 6*1
7 8 8
7
12*3 36*5 12*3   12*3 36*5 12*3   12*3 36*5 12*3
7 8 8
7
18*3 24*5 18*3   18*3 24*5 18*3   18*3 24*5 18*3
7 8 8
```

```
        7
        12*3 36*5 12*3   12*3 36*5 12*3   12*3 36*5 12*3
        7 8 8
        7
        180*5
        7 8
/
KRNUMX

        8 7
        24*5 12*1 24*5   24*5 12*1 24*5   24*5 12*1 24*5
        7 8 8
        7
        18*5 24*3 18*5   18*5 24*3 18*5   18*5 24*3 18*5
        7 8 8
        7
        12*5 36*3 12*5   12*5 36*3 12*5   12*5 36*3 12*5
        7 8 8
        7
        18*5 24*3 18*5   18*5 24*3 18*5   18*5 24*3 18*5
        7 8 8
        7
        180*5
        7 8 8
        7
        6*1 48*5 6*1     6*1 48*5 6*1     6*1 48*5 6*1
        7 8 8
        7
        12*3 36*5 12*3   12*3 36*5 12*3   12*3 36*5 12*3
        7 8 8
        7
        18*3 24*5 18*3   18*3 24*5 18*3   18*3 24*5 18*3
        7 8 8
        7
        12*3 36*5 12*3   12*3 36*5 12*3   12*3 36*5 12*3
        7 8 8
        7
        180*5
        7 8 8
--
        7
        24*5 12*1 24*5   24*5 12*1 24*5   24*5 12*1 24*5
        7 8 8
        7
        18*5 24*3 18*5   18*5 24*3 18*5   18*5 24*3 18*5
        7 8 8
        7
        12*5 36*3 12*5   12*5 36*3 12*5   12*5 36*3 12*5
        7 8 8
        7
        18*5 24*3 18*5   18*5 24*3 18*5   18*5 24*3 18*5
        7 8 8
        7
        180*5
        7 8 8
        7
        6*1 48*5 6*1     6*1 48*5 6*1     6*1 48*5 6*1
        7 8 8
        7
        12*3 36*5 12*3   12*3 36*5 12*3   12*3 36*5 12*3
        7 8 8
        7
        18*3 24*5 18*3   18*3 24*5 18*3   18*3 24*5 18*3
```

```
        7 8 8
        7
        12*3 36*5 12*3   12*3 36*5 12*3   12*3 36*5 12*3
        7 8 8
        7
        180*5
        7 8 8
--
        7
        24*5 12*1 24*5   24*5 12*1 24*5   24*5 12*1 24*5
        7 8 8
        7
        18*5 24*3 18*5   18*5 24*3 18*5   18*5 24*3 18*5
        7 8 8
        7
        12*5 36*3 12*5   12*5 36*3 12*5   12*5 36*3 12*5
        7 8 8
        7
        18*5 24*3 18*5   18*5 24*3 18*5   18*5 24*3 18*5
        7 8 8
        7
        180*5
        7 8 8
        7
        6*1 48*5 6*1     6*1 48*5 6*1     6*1 48*5 6*1
        7 8 8
        7
        12*3 36*5 12*3   12*3 36*5 12*3   12*3 36*5 12*3
        7 8 8
        7
        18*3 24*5 18*3   18*3 24*5 18*3   18*3 24*5 18*3
        7 8 8
        7
        12*3 36*5 12*3   12*3 36*5 12*3   12*3 36*5 12*3
        7 8 8
        7
        180*5
        7 8
/
KRNUMZ

        8 7
        24*6 12*2 24*6   24*6 12*2 24*6   24*6 12*2 24*6
        7 8 8
        7
        18*6 24*4 18*6   18*6 24*4 18*6   18*6 24*4 18*6
        7 8 8
        7
        12*6 36*4 12*6   12*6 36*4 12*6   12*6 36*4 12*6
        7 8 8
        7
        18*6 24*4 18*6   18*6 24*4 18*6   18*6 24*4 18*6
        7 8 8
        7
        180*6
        7 8 8
        7
        6*2 48*6 6*2     6*2 48*6 6*2     6*2 48*6 6*2
        7 8 8
        7
        12*4 36*6 12*4   12*4 36*6 12*4   12*4 36*6 12*4
        7 8 8
        7
```

```
        18*4 24*6 18*4   18*4 24*6 18*4   18*4 24*6 18*4
        7 8 8
        7
        12*4 36*6 12*4   12*4 36*6 12*4   12*4 36*6 12*4
        7 8 8
        7
        180*6
        7 8 8
--
        7
        24*6 12*2 24*6   24*6 12*2 24*6   24*6 12*2 24*6
        7 8 8
        7
        18*6 24*4 18*6   18*6 24*4 18*6   18*6 24*4 18*6
        7 8 8
        7
        12*6 36*4 12*6   12*6 36*4 12*6   12*6 36*4 12*6
        7 8 8
        7
        18*6 24*4 18*6   18*6 24*4 18*6   18*6 24*4 18*6
        7 8 8
        7
        180*6
        7 8 8
        7
        6*2 48*6 6*2     6*2 48*6 6*2     6*2 48*6 6*2
        7 8 8
        7
        12*4 36*6 12*4   12*4 36*6 12*4   12*4 36*6 12*4
        7 8 8
        7
        18*4 24*6 18*4   18*4 24*6 18*4   18*4 24*6 18*4
        7 8 8
        7
        12*4 36*6 12*4   12*4 36*6 12*4   12*4 36*6 12*4
        7 8 8
        7
        180*6
        7 8 8
--
        7
        24*6 12*2 24*6   24*6 12*2 24*6   24*6 12*2 24*6
        7 8 8
        7
        18*6 24*4 18*6   18*6 24*4 18*6   18*6 24*4 18*6
        7 8 8
        7
        12*6 36*4 12*6   12*6 36*4 12*6   12*6 36*4 12*6
        7 8 8
        7
        18*6 24*4 18*6   18*6 24*4 18*6   18*6 24*4 18*6
        7 8 8
        7
        180*6
        7 8 8
        7
        6*2 48*6 6*2     6*2 48*6 6*2     6*2 48*6 6*2
        7 8 8
        7
        12*4 36*6 12*4   12*4 36*6 12*4   12*4 36*6 12*4
        7 8 8
        7
        18*4 24*6 18*4   18*4 24*6 18*4   18*4 24*6 18*4
```

```
        7 8 8
        7
        12*4 36*6 12*4   12*4 36*6 12*4   12*4 36*6 12*4
        7 8 8
        7
        180*6
        7 8
/
--
--==============================================================
SOLUTION
--
--  DATUM  Pi@DATUM  WOC   Pc@WOC   GOC Pc@GOC
EQUIL
    304    313    10304   0     0   0  2* 0 /
--
--   Pb Sob Swb       Pob@Datum
RPTSOL
     1  0   1   12*0 1 /
--==============================================================
SUMMARY
--
WWCT
 'PROD'
 /
--
FOIP
--
FWIP
--
ROIP
        3 /
--
RWIP
        3  /
--
RWFT
        2  3
        3  4
/
--
ROFT
        2  3
        3  4
/
--
RPTSMRY
1  /
--
RUNSUM
--==============================================================
SCHEDULE
--
RPTSCHED
1 0 1 0 0 0 2 2 1 6*0 1 0 0  /
--
--    WELL WELL  LOCATION  BHP   PREF.
--    NAME GROUP  I   J  DATUM  PHASE
WELSPECS
     'PROD' 'G'  184   1   304   'OIL' /
--
     'INJ'  'G'  1   1   304   'WAT' /
       /
```

```
--
--    WELL  LOCATION INTERVAL STATUS      WELL
--    NAME  I  J  K1 K2  O or S       ID
COMPDAT
     'PROD' 184  1   1 30  'OPEN'  2*  3.0 /
     'INJ'  1  1   1 30  'OPEN'  2*  3.0 /
       /
--
--    WELL  STATUS  CONTROL  TARGET RATES or UPPER LIMITS
--    NAME          MODE   OIL  WAT  GAS  LIQ RV  BHP
WCONPROD
     'PROD'  'OPEN'  'BHP'   5*          311.9 /
       /
--
--**************************************************************
-- MODEL CONTROLLED BY INJECTION RATE (=.24m/day)
--**************************************************************
--    WELL  FLUID  STATUS  CONTROL RATE       BHP TAR
--    NAME  TYPE           MODE   cc/hr       (atm)
WCONINJ
     'INJ'  'WAT'  'OPEN'  'RATE'  180   3*    500   /
       /
--
TUNING
/
/
20 1  50 1  25 /
--
--    DAYS
TSTEP
 1 2 4 6 9 20 30 30 50 100 250 500 7*1000 /
--
--=====================================================================
END
```

VIII. 4 Formation Scale; Thistle Field (A33GEOP2.DATA)

```
--
--        THISTLE FIELD SIMULATION
--
--   BASED ON A331C.DATA (BP MODEL)
--
--************************************************
--      WITH FACIES GEOPSEUDOS
--************************************************
--
--
--==========================================
RUNSPEC
THISTLE A33 SIMULATION
= NDIVIX NDIVIY NDIVIZ
  48   1    42 /
= OIL WAT GAS
  T  T  F /
= UNIT CONVENTION
  'FIELD' /
=  NRPVT
   1 /
= NSSFUN NTSFUN   QDIRKR
  35    7       T  /
= NDRXVD
   /
=  NTFIP
  2 /
= NWMAXZ NCWMAX NGMAXZ NWGMAX
  2    42   1    2 /
= QIMCOL
   /
= MXMFLO
   /
= MXSFLO
   /
= NANAQU
   /
=  DAY  MONTH  YEAR
   1    'JAN'  1990  /
= QSOLVE  NSTACK
   T     25 /
--
--=============================================================
GRID
--
EQUALS
        'DX'     40        1 48     1 1      1 42  /
        'DY'   2000        1 48     1 1      1 42  /
        'DZ'     35        1 48     1 1      1  2  /
        'DZ'      5        1 48     1 1      3 42  /
        'TOPS'  9000       1 48     1 1      1 1       /
/
EQUALS
        'PORO'  0.25       1 48     1 1      1  1  /ETIVE
        'PERMX'            1500     /
        'NTG'    1.0       /
/
EQUALS
        'PORO'  0.28       1 48     1 1      2  2  /ETIVE
        'PERMX'            3000     /
        'NTG'    1.0       /
/
```

```
--***********************************************************
-- WAVY BEDDED FACIES (LAYERS 3 & 4) PERMEABILITY REDUCED
--***********************************************************
EQUALS
        'PORO' 0.23    1 48    1 1     3  4  / RANNOCH
        'PERMX'        150     /
        'NTG'   1.0    /
/
EQUALS
        'PORO' 0.23    1 48    1 1     5  12  / RANNOCH
        'PERMX'        270     /
        'NTG'   1.0    /
/
EQUALS
        'PORO' 0.22    1 48    1 1     13  22  / RANNOCH
        'PERMX'        200     /
        'NTG'   0.8    /
/
EQUALS
        'PORO' 0.22    1 48    1 1     23  32  / RANNOCH
        'PERMX'         50     /
        'NTG'   0.9    /
/
EQUALS
        'PORO' 0.18    1 48    1 1     33  42  / RANNOCH
        'PERMX'         20     /
        'NTG'   1.0    /
/
COPY
        'PERMX'        'PERMY' 1 48 1 1  1  42 /
        'PERMX' 'PERMZ'        /
/
--*****************************************************************
--      PERM AND TRANSMISSABILITY MULTIPLIERS DISABLED
--*****************************************************************
--    PERM MULTIPLIER TO MATCH A33 PI
--          (FROM BP MODEL)
--
--MULTIPLY
--      'PERMX' 1.25   1  48 1 1   1   42 /
--      'PERMZ' 1.25 /
--/
--
--=================================================================
EDIT
--
--      TRANSMISSABILITY MULTIPLIER TO MATCH EARLY WATER CUT BEHAVIOUR
--              (FROM BP CROSS-SECTIONAL MODEL)
--
--TRANX
--      96*1.0  1920*0.06 /
--TRANZ
--      96*1.0   1920*0.006 /
--
--=================================================================
PROPS
--      OIL    WAT    GAS
DENSITY
      53.0   63.0    0.08  /
--
--   P    Bo    Vis
PVDO
    959.0   1.187   0.88
```

```
    7000.0   1.1    1.1
   /
--   (DATA FROM A31 DST INTERPRETATION PARAMETERS)
--    P       Bw      Cw      Vis   Viscosibility
PVTW
    6060.0      1.02    3.0D-06   0.88    0.0 /
--
--
--    P        Cr
ROCK
    6060.0     5.0D-06  /
--*************************************************
--    (REL.PERM. AND CAP.PRESS. GEOPSEUDOS)
--*************************************************
SOF2
--
--          WAVY BEDDED GEOPSEUDO       X,Y
--
--   So        Kro
   0.250000     0.000000 -- Lower end point
   0.332957     0.012786 -- Generated point
   0.387468     0.029031 -- Generated point
   0.501143     0.095281 -- Generated point
   0.591481     0.275656 -- Generated point
   0.663656     0.373504 -- Generated point
   0.703076     0.556966 -- Generated point
   0.749369     0.693772 -- Generated point
   0.803574     0.888859 -- Generated point
   0.817758     0.986956 -- Upper end point
/
--               ditto         Z
--
   0.250000     0.000000 -- Lower end point
   0.601541     0.001743 -- Generated point
   0.616147     0.013926 -- Generated point
   0.646199     0.106492 -- Generated point
   0.690970     0.188545 -- Generated point
   0.725616     0.264941 -- Generated point
   0.762166     0.516398 -- Generated point
   0.790764     0.672023 -- Generated point
   0.800958     0.715714 -- Generated point
   0.808200     0.733293 -- Generated point
   0.814481     0.768330 -- Generated point
   0.817395     0.800002 -- Upper end point
/
--
--          SCS GEOPSEUDO          X,Y
--
   0.249985     0.000000 -- Lower end point
   0.291101     0.008696 -- Generated point
   0.299401     0.011532 -- Generated point
   0.311386     0.016067 -- Generated point
   0.332722     0.025567 -- Generated point
   0.375119     0.050044 -- Generated point
   0.514721     0.316330 -- Generated point
   0.703423     0.722668 -- Generated point
   0.751478     0.781592 -- Generated point
   0.771826     0.782944 -- Generated point
   0.778083     0.783141 -- Generated point
   0.780777     0.799984 -- Upper end point
/
--             ditto          Z
--
```

```
   0.250000      0.000000 -- Lower end point
   0.531093      0.051628 -- Generated point
   0.572827      0.066315 -- Generated point
   0.648960      0.088682 -- Generated point
   0.685041      0.124961 -- Generated point
   0.711230      0.216053 -- Generated point
   0.729548      0.363551 -- Generated point
   0.747085      0.457992 -- Generated point
   0.766559      0.509208 -- Generated point
   0.777202      0.535628 -- Generated point
   0.778470      0.800001 -- Upper end point
/
--
--        HCS GEOPSEUDO            X,Y
--
   0.249983      0.000000 -- Lower end point
   0.286625      0.008376 -- Generated point
   0.293850      0.011116 -- Generated point
   0.304648      0.015592 -- Generated point
   0.323113      0.024696 -- Generated point
   0.360948      0.048618 -- Generated point
   0.521270      0.422794 -- Generated point
   0.704209      0.744517 -- Generated point
   0.750837      0.763881 -- Generated point
   0.757073      0.799983 -- Upper end point
/
--        ditto                Z
--
   0.250000      0.000000 -- Lower end point
   0.387693      0.008625 -- Generated point
   0.411325      0.010700 -- Generated point
   0.438967      0.013638 -- Generated point
   0.474678      0.018596 -- Generated point
   0.538747      0.028044 -- Generated point
   0.608132      0.043055 -- Generated point
   0.651378      0.061517 -- Generated point
   0.687310      0.174610 -- Generated point
   0.713630      0.319381 -- Generated point
   0.732610      0.373898 -- Generated point
   0.748107      0.410305 -- Generated point
   0.752627      0.415168 -- Generated point
   0.754629      0.799993 -- Upper end point
/
--         ROCK CURVE  1500mD
--
         0.25    0.0
         0.35    0.004
         0.46    0.030
         0.53    0.086
         0.58    0.114
         0.61    0.202
         0.64    0.283
         0.67    0.365
         0.73    0.446
         0.76    0.528
         0.79    0.61
         0.82    0.691
         0.85    0.773
         0.9     0.8
/
--
--     Sw   Krw                Pc
SWFN
```

```
--
--              WAVY BEDDED GEOPSEUDO            X,Y
--
   0.182242     0.000000     28.486124
   0.186541     0.000873     25.296415
   0.194172     0.002840     21.442125
   0.203680     0.005290     16.891787
   0.214801     0.008062     11.971890
   0.250631     0.030110     7.498693
   0.296924     0.057581     4.430153
   0.336344     0.084313     3.098137
   0.408519     0.124124     2.128510
   0.498857     0.188109     1.399721
   0.612532     0.253604     1.236918
   0.667043     0.332530     1.164717
   0.749999     0.440001     1.046340
/
--              ditto               Z
--
   0.182605     0.000000     28.486610
   0.185519     0.000608     25.989788
   0.191800     0.003361     22.802387
   0.199042     0.006517     19.183100
   0.209236     0.011317     14.400449
   0.237834     0.033631     8.939224
   0.274384     0.062657     5.595311
   0.309030     0.088021     3.905418
   0.353801     0.121952     2.828157
   0.383853     0.148372     2.445591
   0.398459     0.162765     2.291312
   0.750000     0.439996     1.046355
/
---
--              SCS GEOPSEUDO               X,Y
--
   0.219223     0.000000     32.225315
   0.220608     0.000000     29.680822
   0.221917     0.000000     29.333700
   0.228174     0.000003     26.525280
   0.248522     0.000892     18.979488
   0.296577     0.013652     9.086331
   0.485279     0.109329     2.082320
   0.624881     0.245073     1.485384
   0.667278     0.297837     1.425292
   0.688614     0.332036     1.393901
   0.700599     0.352828     1.375957
   0.708899     0.367741     1.365200
   0.750014     0.440000     1.204337
/
--              ditto               Z
--
   0.221530     0.000000     32.125484
   0.222786     0.000000     29.660643
   0.233441     0.000691     23.156693
   0.252915     0.005295     15.916327
   0.270452     0.013923     12.467029
   0.288770     0.024031     8.911875
   0.314959     0.034716     6.423225
   0.351040     0.051745     4.451668
   0.427173     0.076623     2.785994
   0.468907     0.094763     2.256335
   0.750000     0.439025     1.237330
/
```

```
--
--              HCS GEOPSEUDO                X,Y
--
   0.242927    0.000000    34.310970
   0.249162    0.000223    28.374683
   0.295791    0.003360    12.702032
   0.478730    0.069170     2.542026
   0.639052    0.229303     1.602437
   0.676887    0.279646     1.540552
   0.695352    0.311219     1.514540
   0.706150    0.331185     1.494804
   0.713375    0.346178     1.480005
   0.750012    0.437091     1.413491
/
--                ditto                  Z
--
   0.245371    0.000000    34.141262
   0.247366    0.000000    30.536541
   0.251893    0.000000    27.760406
   0.267390    0.001884    20.002945
   0.286370    0.006026    14.745336
   0.312690    0.018123     9.780584
   0.348622    0.036151     6.180594
   0.391868    0.054426     4.137291
   0.461253    0.082635     2.923240
   0.525322    0.105130     2.418682
   0.561033    0.120739     2.200270
   0.588675    0.133876     2.046448
   0.612307    0.145473     1.924000
   0.750000    0.435907     1.451024
/
--               ROCK CURVE      1500md
        0.10    0.0          27.0
        0.13    0.006        12.0
        0.16    0.025        8.0
        0.19    0.044        5.5
        0.22    0.063        4.0
        0.25    0.082        3.1
        0.28    0.101        2.6
        0.31    0.120        2.2
        0.34    0.139        1.8
        0.37    0.159        1.4
        0.42    0.183        1.35
        0.5     0.231        1.2
        0.6     0.354        1.1
        0.75    0.44         1
/
--
--==================================================================
REGIONS
FIPNUM
--    ETIVE  RANNOCH
        96*1  1920*2  /
--
SATNUM
--   ETIVE  WB  SCS  HCS
       96*7 96*1 240*3 1584*5  /
KRNUMX
       96*7 96*1 240*3 1584*5  /
KRNUMZ
       96*7 96*2 240*4 1584*6  /
--
--==================================================================
```

```
SOLUTION
--
SWAT
        192*0.75  1824*0.20  /
PRESSURE
    2016*4600  /
--
--
--  DATUM  Pi@DATUM  WOC  Pc@WOC  GOC Pc@GOC
--EQUIL
--   9200    4600   9332   0    8500   0 /
--
--   Pb Sob Swb       Pob@Datum
RPTSOL
     1  0  1  12*0 1 /
--=================================================================
SUMMARY
--
ROFT
        1        2        /
/
RWFT
        1        2        /
/
WBHP
 'PROD' 'INJ' /
--
WWCT
 'PROD'
 /
--
FOIP
--
FWIP
--
FOPR
--
FWPR
--
FWIR
--
FOPT
--
FWPT
--
FPR
--
--
RPTSMRY
1 /
--
RUNSUM
--=================================================================
SCHEDULE
--
RPTSCHED
1 0 1 0 0 0 2 2 1 6*0 1 0 0 /
--
--    WELL WELL  LOCATION  BHP   PREF.
--    NAME GROUP  I   J  DATUM  PHASE
WELSPECS
    'PROD' 'G'  48  1   9200   'OIL' /
--
```

```
     'INJ'  'G'  1   1   9200   'WAT' /
      /
--
--   WELL  LOCATION INTERVAL STATUS      WELL
--   NAME   I  J   K1 K2  O or S        ID
COMPDAT
     'PROD'  48  1   13 42  'OPEN'   2*   0.66667 /
     'INJ'   1  1    1 42  'OPEN'   2*   0.66667 /
      /
--
--   WELL  STATUS  CONTROL   TARGET RATES or UPPER LIMITS
--   NAME          MODE   OIL  WAT  GAS  LIQ RV  BHP
WCONPROD
     'PROD'  'OPEN'  'LRAT'     3*     9604  1* 1500.0 /
      /
--
--   WELL  FLUID  STATUS  CONTROL      BHP TAR
--   NAME  TYPE           MODE
WCONINJ
     'INJ'   'WAT'  'OPEN'  'RESV'  1* 0.0  1.0  'FVDG'   /
      /
--*****************************************************************
-- PRODUCTION WELL BHP INCREASED TO 1500psi IN LINE WITH BP TARGET
--*****************************************************************
--   DAYS
TSTEP
 1 9 20 31 /
--
--
--   WELL  STATUS  CONTROL   TARGET RATES or UPPER LIMITS
--   NAME          MODE   OIL  WAT  GAS  LIQ RV  BHP
WCONPROD
     'PROD'  'OPEN'  'LRAT'     3*     7508  1* 1500.0 /
      /
--
--
--   DAYS
TSTEP
 30  30 /
---
---
--   WELL  STATUS  CONTROL   TARGET RATES or UPPER LIMITS
--   NAME          MODE   OIL  WAT  GAS  LIQ RV  BHP
WCONPROD
     'PROD'  'OPEN'  'LRAT'     3*     3694  1* 1500.0 /
      /
--
--
--   DAYS
TSTEP
 50 50 69 /
---
---
--   WELL  STATUS  CONTROL   TARGET RATES or UPPER LIMITS
--   NAME          MODE   OIL  WAT  GAS  LIQ RV  BHP
WCONPROD
     'PROD'  'OPEN'  'LRAT'     3*     1746  1* 1500.0 /
      /
--
--
--   DAYS
TSTEP
 61  /
```

```
---
---
--    WELL  STATUS CONTROL  TARGET RATES or UPPER LIMITS
--    NAME         MODE   OIL  WAT  GAS  LIQ RV  BHP
WCONPROD
     'PROD'  'OPEN'  'LRAT'    3*     2197  1* 1500.0 /
       /
--
--
--    DAYS
TSTEP
 79 /
---
---
--    WELL  STATUS CONTROL  TARGET RATES or UPPER LIMITS
--    NAME         MODE   OIL  WAT  GAS  LIQ RV  BHP
WCONPROD
     'PROD'  'OPEN'  'LRAT'    3*     4315  1* 1500.0 /
       /
--
--
--    DAYS
TSTEP
 59 /
---
---
--    WELL  STATUS CONTROL  TARGET RATES or UPPER LIMITS
--    NAME         MODE   OIL  WAT  GAS  LIQ RV  BHP
WCONPROD
     'PROD'  'OPEN'  'LRAT'    3*     7404  1* 1500.0 /
       /
--
--
--    DAYS
TSTEP
 57 /
---
---
--    WELL  STATUS CONTROL  TARGET RATES or UPPER LIMITS
--    NAME         MODE   OIL  WAT  GAS  LIQ RV  BHP
WCONPROD
     'PROD'  'OPEN'  'LRAT'    3*    6384  1* 1500.0 /
       /
--
--
--    DAYS
TSTEP
 39 150  150 /
---
---
--    WELL  STATUS CONTROL  TARGET RATES or UPPER LIMITS
--    NAME         MODE   OIL  WAT  GAS  LIQ RV  BHP
WCONPROD
     'PROD'  'OPEN'  'LRAT'    3*     10027  1* 1500.0 /
       /
--
--
--    DAYS
TSTEP
 183 /
---
---
--    WELL  STATUS CONTROL  TARGET RATES or UPPER LIMITS
```

```
--    NAME        MODE   OIL  WAT  GAS  LIQ RV  BHP
WCONPROD
     'PROD'  'OPEN'  'LRAT'    3*    8807  1* 1500.0 /
       /
--
--
--    DAYS
TSTEP
 188 /
---
---
--    WELL  STATUS  CONTROL   TARGET RATES or UPPER LIMITS
--    NAME        MODE   OIL  WAT  GAS  LIQ RV  BHP
WCONPROD
     'PROD'  'SHUT'  'LRAT'    3*    0  1* 1500.0 /
       /
--
--
--    DAYS
TSTEP
 68 /
---
---
--    WELL  STATUS  CONTROL   TARGET RATES or UPPER LIMITS
--    NAME        MODE   OIL  WAT  GAS  LIQ RV  BHP
WCONPROD
     'PROD'  'OPEN'  'LRAT'    3*    4413  1* 1500.0 /
       /
--
--
--    DAYS
TSTEP
 148  200 /
---
---
---
--==========================================================
END
```

VIII. 5 Formation Scale; Statfjord Field (STAT001.DATA)

```
--
--        STATFJORD FIELD SIMULATION
--
--   WEST FLANK 3-D CROSS-SECTIONAL MODEL
--
--
--
--
--=============================================
RUNSPEC
STATFJORD SIMULATION
= NDIVIX NDIVIY NDIVIZ
  60   20   20 /
= OIL WAT GAS
  T  T  F /
= UNIT CONVENTION
  'FIELD' /
=  NRPVT
   1 /
= NSSFUN NTSFUN   QDIRKR
  35    7      T /
= NDRXVD
   /
=  NTFIP
   2 /
= NWMAXZ NCWMAX NGMAXZ NWGMAX
  2    20   1    2 /
= QIMCOL
  /
= MXMFLO
  /
= MXSFLO
  /
= NANAQU
   /
=  DAY  MONTH  YEAR
   1   'JAN' 1990  /
= QSOLVE  NSTACK
   T    25 /
--
--==============================================================
GRID
--
EQUALS
        'DX'    155     1 60    1 20    1 20  /
        'DY'    125     1 60    1 20    1 20  /
        'DZ'     15     1 60    1 20    1 20  /
--
--
--
        'TOPS'  8701.5   1  1   1 20    1  1    /
        'TOPS'  8684     2  2   1 20    1  1    /
        'TOPS'  8666.5   3  3   1 20    1  1    /
        'TOPS'  8649     4  4   1 20    1  1    /
        'TOPS'  8631.5   5  5   1 20    1  1    /
        'TOPS'  8614     6  6   1 20    1  1    /
        'TOPS'  8596.5   7  7   1 20    1  1    /
        'TOPS'  8579     8  8   1 20    1  1    /
        'TOPS'  8561.5   9  9   1 20    1  1    /
        'TOPS'  8544    10 10   1 20    1  1    /
        'TOPS'  8526.5  11 11   1 20    1  1    /
        'TOPS'  8509    12 12   1 20    1  1    /
```

```
        'TOPS'  8491.5  13  13  1 20    1 1    /
        'TOPS'  8474    14  14  1 20    1 1    /
        'TOPS'  8456.5  15  15  1 20    1 1    /
        'TOPS'  8439    16  16  1 20    1 1    /
        'TOPS'  8421.5  17  17  1 20    1 1    /
        'TOPS'  8404    18  18  1 20    1 1    /
        'TOPS'  8386.5  19  19  1 20    1 1    /
        'TOPS'  8369    20  20  1 20    1 1    /
        'TOPS'  8351.5  21  21  1 20    1 1    /
        'TOPS'  8334    22  22  1 20    1 1    /
        'TOPS'  8316.5  23  23  1 20    1 1    /
        'TOPS'  8299    24  24  1 20    1 1    /
        'TOPS'  8281.5  25  25  1 20    1 1    /
        'TOPS'  8264    26  26  1 20    1 1    /
        'TOPS'  8246.5  27  27  1 20    1 1    /
        'TOPS'  8229    28  28  1 20    1 1    /
        'TOPS'  8211.5  29  29  1 20    1 1    /
        'TOPS'  8194    30  30  1 20    1 1    /
        'TOPS'  8176.5  31  31  1 20    1 1    /
        'TOPS'  8159    32  32  1 20    1 1    /
        'TOPS'  8141.5  33  33  1 20    1 1    /
        'TOPS'  8124    34  34  1 20    1 1    /
        'TOPS'  8106.5  35  35  1 20    1 1    /
        'TOPS'  8089    36  36  1 20    1 1    /
        'TOPS'  8071.5  37  37  1 20    1 1    /
        'TOPS'  8054    38  38  1 20    1 1    /
        'TOPS'  8036.5  39  39  1 20    1 1    /
        'TOPS'  8019    40  40  1 20    1 1    /
        'TOPS'  8001.5  41  41  1 20    1 1    /
        'TOPS'  7984    42  42  1 20    1 1    /
        'TOPS'  7966.5  43  43  1 20    1 1    /
        'TOPS'  7949    44  44  1 20    1 1    /
        'TOPS'  7931.5  45  45  1 20    1 1    /
        'TOPS'  7914    46  46  1 20    1 1    /
        'TOPS'  7896.5  47  47  1 20    1 1    /
        'TOPS'  7879    48  48  1 20    1 1    /
        'TOPS'  7861.5  49  49  1 20    1 1    /
        'TOPS'  7844    50  50  1 20    1 1    /
        'TOPS'  7826.5  51  51  1 20    1 1    /
        'TOPS'  7809    52  52  1 20    1 1    /
        'TOPS'  7791.5  53  53  1 20    1 1    /
        'TOPS'  7774    54  54  1 20    1 1    /
        'TOPS'  7756.5  55  55  1 20    1 1    /
        'TOPS'  7739    56  56  1 20    1 1    /
        'TOPS'  7721.5  57  57  1 20    1 1    /
        'TOPS'  7704    58  58  1 20    1 1    /
        'TOPS'  7686.5  59  59  1 20    1 1    /
        'TOPS'  7669    60  60  1 20    1 1    /
/
--
--
--              ETIVE LAYERS
--
--
EQUALS
        'PORO'  0.24     1 15    1 20    1 1  /ETIVE 1 WATER
        'PERMX'          454     /
        'NTG'   1.0      /
--
        'PORO'  0.28     16 60   1 20    1 1  /ETIVE 1 OIL
        'PERMX'          2654    /
        'NTG'   1.0      /
--
```

```
        'PORO' 0.26    1 15    1 20    2  2  / ETIVE 2 WATER
        'PERMX'         831    /
        'NTG'    1.0   /
--
        'PORO' 0.31    16 60   1 20    2  2  / ETIVE 2 OIL
        'PERMX'        6766    /
        'NTG'    1.0   /
--
        'PORO' 0.26    1 16    1 20    3  3  / ETIVE 3 WATER
        'PERMX'         831    /
        'NTG'    1.0   /
--
        'PORO' 0.31    17 60   1 20    3  3  / ETIVE 3 OIL
        'PERMX'        6766    /
        'NTG'    1.0   /
--
        'PORO' 0.26    1 16    1 20    4  4  / ETIVE 4 WATER
        'PERMX'         736    /
        'NTG'    1.0   /
--
        'PORO' 0.30    17 60   1 20    4  4  / ETIVE 4 OIL
        'PERMX'        4548    /
        'NTG'    1.0   /
--
        'PORO' 0.26    1 17    1 20    5  5  / ETIVE 5 WATER
        'PERMX'         736    /
        'NTG'    1.0   /
--
        'PORO' 0.30    17 60   1 20    5  5  / ETIVE 5 OIL
        'PERMX'        4548    /
        'NTG'    1.0   /
--
        'PORO' 0.26    1 17    1 20    6  6  / ETIVE 6 WATER
        'PERMX'         736    /
        'NTG'    1.0   /
--
        'PORO' 0.30    18 60   1 20    6  6  / ETIVE 6 OIL
        'PERMX'        4548    /
        'NTG'    1.0   /
/
--
--            RANNOCH LAYERS
--
EQUALS
        'PORO' 0.27    1 17    1 20    7  7  / RANNOCH 1 WATER
        'PERMX'        419     /
        'NTG'    1.0   /
--
        'PORO' 0.28    18 60   1 20    7  7  / RANNOCH 1 OIL
        'PERMX'        590     /
        'NTG'    1.0   /
--
        'PORO' 0.27    1 18    1 20    8  8  / RANNOCH 2 WATER
        'PERMX'        685     /
        'NTG'    1.0   /
--
        'PORO' 0.30    19 60   1 20    8  8  / RANNOCH 2 OIL
        'PERMX'        1551    /
        'NTG'    1.0   /
--
        'PORO' 0.27    1 18    1 20    9  9  / RANNOCH 3 WATER
        'PERMX'        384     /
        'NTG'    1.0   /
```

```
--
        'PORO' 0.32     19 60   1 20    9  9  / RANNOCH 3 OIL
        'PERMX'         2446    /
        'NTG'   1.0     /
--
        'PORO' 0.27     1 19    1 20    10 10 / RANNOCH 4 WATER
        'PERMX'         384     /
        'NTG'   1.0     /
--
        'PORO' 0.32     20 60   1 20    10 10 / RANNOCH 4 OIL
        'PERMX'         2446    /
        'NTG'   1.0     /
--
        'PORO' 0.27     1 19    1 20    11 11 / RANNOCH 5 WATER
        'PERMX'         384     /
        'NTG'   1.0     /
--
        'PORO' 0.32     20 60   1 20    11 11 / RANNOCH 5 OIL
        'PERMX'         2446    /
        'NTG'   1.0     /
--
        'PORO' 0.28     1 20    1 20    12 12 / RANNOCH 6 WATER
        'PERMX'         659     /
        'NTG'   1.0     /
--
        'PORO' 0.33     21 60   1 20    12 12 / RANNOCH 6 OIL
        'PERMX'         3330    /
        'NTG'   1.0     /
--
        'PORO' 0.27     1 20    1 20    13 13 / RANNOCH 7 WATER
        'PERMX'         685     /
        'NTG'   1.0     /
--
        'PORO' 0.30     21 60   1 20    13 13 / RANNOCH 7 OIL
        'PERMX'         1551    /
        'NTG'   1.0     /
--
        'PORO' 0.27     1 21    1 20    14 14 / RANNOCH 8 WATER
        'PERMX'         685     /
        'NTG'   1.0     /
--
        'PORO' 0.30     22 60   1 20    14 14 / RANNOCH 8 OIL
        'PERMX'         1551    /
        'NTG'   1.0     /
--
        'PORO' 0.27     1 21    1 20    15 15 / RANNOCH 9 WATER
        'PERMX'         685     /
        'NTG'   1.0     /
--
        'PORO' 0.30     22 60   1 20    15 15 / RANNOCH 9 OIL
        'PERMX'         1551    /
        'NTG'   1.0     /
--
        'PORO' 0.27     1 22    1 20    16 16 / RANNOCH 10 WATER
        'PERMX'         685     /
        'NTG'   1.0     /
--
        'PORO' 0.30     23 60   1 20    16 16 / RANNOCH 10 OIL
        'PERMX'         1551    /
        'NTG'   1.0     /
--
        'PORO' 0.27     1 22    1 20    17 17 / RANNOCH 11 WATER
        'PERMX'         685     /
```

```
        'NTG'   0.25    /
--
        'PORO'  0.30    23 60   1 20    17  17  / RANNOCH 11 OIL
        'PERMX'         1551    /
        'NTG'   0.25    /
--
        'PORO'  0.23    1 23    1 20    18  18  / RANNOCH 12 WATER
        'PERMX'         106     /
        'NTG'   0.25    /
--
        'PORO'  0.28    24 60   1 20    18  18  / RANNOCH 12 OIL
        'PERMX'         1259    /
        'NTG'   0.25    /
--
        'PORO'  0.21    1 23    1 20    19  19  / RANNOCH 13 WATER
        'PERMX'         25      /
        'NTG'   0.25    /
--
        'PORO'  0.22    24 60   1 20    19  19  / RANNOCH 13 OIL
        'PERMX'         36      /
        'NTG'   0.25    /
--
        'PORO'  0.21    1 24    1 20    20  20  / RANNOCH 14 WATER
        'PERMX'         25      /
        'NTG'   0.25    /
--
        'PORO'  0.22    25 60   1 20    20  20  / RANNOCH 14 OIL
        'PERMX'         36      /
        'NTG'   0.25    /
--
/
--
COPY
        'PERMX'         'PERMY' 1 60 1 20  1  20 /
        'PERMX' 'PERMZ'         /
/
--
--
--==================================================================
PROPS
--      OIL   WAT    GAS
DENSITY
        53.0  63.0   0.08  /
--
--   P    Bo    Vis
PVDO
    959.0   1.187   0.88
   7000.0   1.1     1.1
  /
--   (DATA FROM A31 DST INTERPRETATION PARAMETERS)
--    P       Bw      Cw       Vis   Viscosibility
PVTW
   6060.0     1.02    3.0D-06  0.88    0.0 /
--
--
--    P        Cr
ROCK
   6060.0     5.0D-06  /
--*****************************************************
--    (REL.PERM. AND CAP.PRESS. GEOPSEUDOS)
--*****************************************************
SOF2
--
```

```
--          WAVY BEDDED GEOPSEUDO          X,Y
--
--   So          Kro
  0.250000      0.000000 -- Lower end point
  0.332957      0.012786 -- Generated point
  0.387468      0.029031 -- Generated point
  0.501143      0.095281 -- Generated point
  0.591481      0.275656 -- Generated point
  0.663656      0.373504 -- Generated point
  0.703076      0.556966 -- Generated point
  0.749369      0.693772 -- Generated point
  0.803574      0.888859 -- Generated point
  0.817758      0.986956 -- Upper end point
/
--              ditto          Z
--
  0.250000      0.000000 -- Lower end point
  0.601541      0.001743 -- Generated point
  0.616147      0.013926 -- Generated point
  0.646199      0.106492 -- Generated point
  0.690970      0.188545 -- Generated point
  0.725616      0.264941 -- Generated point
  0.762166      0.516398 -- Generated point
  0.790764      0.672023 -- Generated point
  0.800958      0.715714 -- Generated point
  0.808200      0.733293 -- Generated point
  0.814481      0.768330 -- Generated point
  0.817395      0.800002 -- Upper end point
/
--
--          SCS GEOPSEUDO          X,Y
--
  0.249985      0.000000 -- Lower end point
  0.291101      0.008696 -- Generated point
  0.299401      0.011532 -- Generated point
  0.311386      0.016067 -- Generated point
  0.332722      0.025567 -- Generated point
  0.375119      0.050044 -- Generated point
  0.514721      0.316330 -- Generated point
  0.703423      0.722668 -- Generated point
  0.751478      0.781592 -- Generated point
  0.771826      0.782944 -- Generated point
  0.778083      0.783141 -- Generated point
  0.780777      0.799984 -- Upper end point
/
--              ditto          Z
--
  0.250000      0.000000 -- Lower end point
  0.531093      0.051628 -- Generated point
  0.572827      0.066315 -- Generated point
  0.648960      0.088682 -- Generated point
  0.685041      0.124961 -- Generated point
  0.711230      0.216053 -- Generated point
  0.729548      0.363551 -- Generated point
  0.747085      0.457992 -- Generated point
  0.766559      0.509208 -- Generated point
  0.777202      0.535628 -- Generated point
  0.778470      0.800001 -- Upper end point
/
--
--          HCS GEOPSEUDO          X,Y
--
  0.249983      0.000000 -- Lower end point
```

```
  0.286625      0.008376 -- Generated point
  0.293850      0.011116 -- Generated point
  0.304648      0.015592 -- Generated point
  0.323113      0.024696 -- Generated point
  0.360948      0.048618 -- Generated point
  0.521270      0.422794 -- Generated point
  0.704209      0.744517 -- Generated point
  0.750837      0.763881 -- Generated point
  0.757073      0.799983 -- Upper end point
/
--       ditto                  Z
--
  0.250000      0.000000 -- Lower end point
  0.387693      0.008625 -- Generated point
  0.411325      0.010700 -- Generated point
  0.438967      0.013638 -- Generated point
  0.474678      0.018596 -- Generated point
  0.538747      0.028044 -- Generated point
  0.608132      0.043055 -- Generated point
  0.651378      0.061517 -- Generated point
  0.687310      0.174610 -- Generated point
  0.713630      0.319381 -- Generated point
  0.732610      0.373898 -- Generated point
  0.748107      0.410305 -- Generated point
  0.752627      0.415168 -- Generated point
  0.754629      0.799993 -- Upper end point
/
--        ROCK CURVE  1500mD
--
          0.25      0.0
          0.35      0.004
          0.46      0.030
          0.53      0.086
          0.58      0.114
          0.61      0.202
          0.64      0.283
          0.67      0.365
          0.73      0.446
          0.76      0.528
          0.79      0.61
          0.82      0.691
          0.85      0.773
          0.9       0.8
/
--
--     Sw   Krw                 Pc
SWFN
--
--             WAVY BEDDED GEOPSEUDO              X,Y
--
   0.182242     0.000000     28.486124
   0.186541     0.000873     25.296415
   0.194172     0.002840     21.442125
   0.203680     0.005290     16.891787
   0.214801     0.008062     11.971890
   0.250631     0.030110      7.498693
   0.296924     0.057581      4.430153
   0.336344     0.084313      3.098137
   0.408519     0.124124      2.128510
   0.498857     0.188109      1.399721
   0.612532     0.253604      1.236918
   0.667043     0.332530      1.164717
   0.749999     0.440001      1.046340
```

```
/
--              ditto            Z
--
  0.182605    0.000000    28.486610
  0.185519    0.000608    25.989788
  0.191800    0.003361    22.802387
  0.199042    0.006517    19.183100
  0.209236    0.011317    14.400449
  0.237834    0.033631     8.939224
  0.274384    0.062657     5.595311
  0.309030    0.088021     3.905418
  0.353801    0.121952     2.828157
  0.383853    0.148372     2.445591
  0.398459    0.162765     2.291312
  0.750000    0.439996     1.046355
/
---
--         SCS GEOPSEUDO                    X,Y
--
  0.219223    0.000000    32.225315
  0.220608    0.000000    29.680822
  0.221917    0.000000    29.333700
  0.228174    0.000003    26.525280
  0.248522    0.000892    18.979488
  0.296577    0.013652     9.086331
  0.485279    0.109329     2.082320
  0.624881    0.245073     1.485384
  0.667278    0.297837     1.425292
  0.688614    0.332036     1.393901
  0.700599    0.352828     1.375957
  0.708899    0.367741     1.365200
  0.750014    0.440000     1.204337
/
--              ditto            Z
--
  0.221530    0.000000    32.125484
  0.222786    0.000000    29.660643
  0.233441    0.000691    23.156693
  0.252915    0.005295    15.916327
  0.270452    0.013923    12.467029
  0.288770    0.024031     8.911875
  0.314959    0.034716     6.423225
  0.351040    0.051745     4.451668
  0.427173    0.076623     2.785994
  0.468907    0.094763     2.256335
  0.750000    0.439025     1.237330
/
--
--         HCS GEOPSEUDO                    X,Y
--
  0.242927    0.000000    34.310970
  0.249162    0.000223    28.374683
  0.295791    0.003360    12.702032
  0.478730    0.069170     2.542026
  0.639052    0.229303     1.602437
  0.676887    0.279646     1.540552
  0.695352    0.311219     1.514540
  0.706150    0.331185     1.494804
  0.713375    0.346178     1.480005
  0.750012    0.437091     1.413491
/
--              ditto            Z
--
```

```
    0.245371     0.000000     34.141262
    0.247366     0.000000     30.536541
    0.251893     0.000000     27.760406
    0.267390     0.001884     20.002945
    0.286370     0.006026     14.745336
    0.312690     0.018123     9.780584
    0.348622     0.036151     6.180594
    0.391868     0.054426     4.137291
    0.461253     0.082635     2.923240
    0.525322     0.105130     2.418682
    0.561033     0.120739     2.200270
    0.588675     0.133876     2.046448
    0.612307     0.145473     1.924000
    0.750000     0.435907     1.451024
/
--                ROCK CURVE      1500md
          0.10   0.0          27.0
          0.13   0.006        12.0
          0.16   0.025        8.0
          0.19   0.044        5.5
          0.22   0.063        4.0
          0.25   0.082        3.1
          0.28   0.101        2.6
          0.31   0.120        2.2
          0.34   0.139        1.8
          0.37   0.159        1.4
          0.42   0.183        1.35
          0.5    0.231        1.2
          0.6    0.354        1.1
          0.75   0.44         1
/
--
--=================================================================
REGIONS
FIPNUM
--    ETIVE  RANNOCH
        7200*1  16800*2        /
--
SATNUM
--   ETIVE   HCS
       7200*7 16800*5  /
KRNUMX
       7200*7 16800*5  /
KRNUMZ
       7200*7 16800*6  /
--
--=================================================================
SOLUTION
--
--
--  DATUM  Pi@DATUM  WOC   Pc@WOC   GOC Pc@GOC
EQUIL
   8100    4767   8473   0     7500   0 /
--
--    Pb Sob Swb       Pob@Datum
RPTSOL
    1  0  1   12*0 1 /
--=================================================================
SUMMARY
--
FPR
--
WBHP
```

```
 'PROD' 'INJ' /
--
WWCT
 'PROD'
 /
--
FOIP
--
FWIP
--
FOPR
--
FWPR
--
FWIR
--
FOPT
--
FWPT
--
RPTSMRY
 1 /
--
RUNSUM
--==========================================================
SCHEDULE
--
RPTSCHED
 1 0 1 0 0 0 2 2 1 6*0 1 0 0 /
--
--    WELL  WELL  LOCATION  BHP   PREF.
--    NAME  GROUP  I  J  DATUM  PHASE
WELSPECS
     'PROD' 'G'  52  1   8100   'OIL' /
--
     'INJ'  'G'  6   1   9200   'WAT' /
       /
--
--    WELL  LOCATION  INTERVAL  STATUS      WELL
--    NAME   I  J   K1  K2   O or S        ID
COMPDAT
    'PROD'  52  10   8  20  'OPEN'   2*   0.66667 /
    'INJ'    6  10  12  18  'OPEN'   2*   0.66667 /
       /
--
--    WELL  STATUS  CONTROL   TARGET RATES or UPPER LIMITS
--    NAME          MODE   OIL  WAT  GAS  LIQ RV  BHP
WCONPROD
     'PROD'  'OPEN'  'LRAT'    3*    30000  1* 1500.0 /
       /
--
--    WELL  FLUID  STATUS  CONTROL       BHP TAR
--    NAME  TYPE          MODE
WCONINJ
     'INJ'  'WAT'  'OPEN'  'RESV'  1* 0.0  1.0  'FVDG'   /
       /
--
--   DAYS
TSTEP
 1 9 20 30 30 100 200 300 500 800 /
--
--==========================================================
END
```

VIII. 6 Formation Scale; Cormorant Field (CORM001.DATA)

```
--
--        CORMORANT FIELD SIMULATION
--
--   WEST FLANK 3-D CROSS-SECTIONAL MODEL
--
--==========================================
RUNSPEC
CORMORANT SIMULATION
= NDIVIX NDIVIY NDIVIZ
  75   10    17 /
=OIL WAT GAS
  T  T  F /
= UNIT CONVENTION
  'FIELD' /
=  NRPVT
   1 /
= NSSFUN  NTSFUN   QDIRKR
    35   ·7        T  /
= NDRXVD
   /
= NTFIP
  6 /
= NWMAXZ NCWMAX NGMAXZ NWGMAX
   2    17   1    2 /
= QIMCOL
   /
= MXMFLO
   /
= MXSFLO
   /
= NANAQU
   /
=  DAY  MONTH  YEAR
   1   'JAN'  1993  /
= QSOLVE  NSTACK
    T     25 /
--
--==============================================================
GRID
--
EQUALS
        'DX'     40      1 75    1 10     1 17  /
        'DY'     40      1 75    1 10     1 17  /
        'DZ'     30      1 75    1 10     1  2  /
        'DZ'     15      1 75    1 10     3  4  /
        'DZ'     10      1 75    1 10     5 14  /
        'DZ'     15      1 75    1 10    15 17  /
--
        'TOPS'  9250     1   5   1 10    1  1     /
        'TOPS'  9200     6   10  1 10  1  1       /
        'TOPS'  9150    11   15         1 10    1  1     /
        'TOPS'  9100    16   20         1 10    1  1     /
        'TOPS'  9050    21   25         1 10    1  1     /
        'TOPS'  9000    26   30         1 10    1  1     /
        'TOPS'  8950    31   35         1 10    1  1     /
        'TOPS'  8900    36   40         1 10    1  1     /
        'TOPS'  8850    41   45         1 10    1  1     /
        'TOPS'  8800    46   50         1 10    1  1     /
        'TOPS'  8750    51   55         1 10    1  1     /
        'TOPS'  8700    56   60         1 10    1  1     /
        'TOPS'  8650    61   65         1 10    1  1     /
        'TOPS'  8600    66   70         1 10    1  1     /
```

```
        'TOPS'  8550     71   75          1 10    1  1      /
/
--
--              ETIVE LAYERS
--
EQUALS
        'PORO'  0.243    1 75     1 10    1  1  / ETIVE 1
        'PERMX'          1435     /
        'NTG'    1.0     /
--
        'PORO'  0.254    1 75     1 10    2  2  / ETIVE 2
        'PERMX'          1901     /
        'NTG'    1.0     /
--
        'PORO'  0.264    1 75     1 10    3  3  / ETIVE 3
        'PERMX'          2702     /
        'NTG'    1.0     /
--
        'PORO'  0.258    1 75     1 10    4  4  / ETIVE 4
        'PERMX'          1254     /
        'NTG'    1.0     /
--
--              RANNOCH LAYERS
--
--
        'PORO'  0.231    1 75     1 10    5  6  / RANNOCH 1,2
        'PERMX'          235      /
        'NTG'    1.0     /
--
        'PORO'  0.22     1 75     1 10    7  8  / RANNOCH 3,4
        'PERMX'          133      /
        'NTG'    1.0     /
--
        'PORO'  0.226    1 75     1 10    9  10  / RANNOCH 5,6
        'PERMX'          140      /
        'NTG'    1.0     /
--
        'PORO'  0.185    1 75     1 10    11  12  / RANNOCH 7,8
        'PERMX'          47.4     /
        'NTG'    1.0     /
--
        'PORO'  0.226    1 75     1 10    13  14  / RANNOCH 9,10
        'PERMX'          122      /
        'NTG'    1.0     /
--
--              BROOM LAYERS
--
        'PORO'  0.238    1 75     1 10    15  15  / BROOM 1
        'PERMX'          458      /
        'NTG'    1.0     /
--
        'PORO'  0.288    1 75     1 10    16  16  / BROOM 2
        'PERMX'          1040     /
        'NTG'    1.0     /
--
        'PORO'  0.262    1 75     1 10    17  17  / BROOM 3
        'PERMX'          511      /
        'NTG'    1.0     /
/
--
COPY
        'PERMX'          'PERMY'  1 75  1  10   1   17 /
        'PERMX' 'PERMZ'           /
```

```
/
--=========================================================
PROPS
--      OIL    WAT    GAS
DENSITY
        36.0   63.0    0.08  /
--
--    P       Bo    Vis
PVDO
     1050.0   1.19   1.00
     5500.0   1.15   1.25
   /
--   (DATA FROM A31 DST INTERPRETATION PARAMETERS)
--    P        Bw       Cw       Vis    Viscosibility
PVTW
    6060.0       1.02    3.0D-06   0.88     0.0 /
--
--
--    P          Cr
ROCK
    6060.0      5.0D-06   /
--*************************************************
--    (REL.PERM. AND CAP.PRESS. GEOPSEUDOS)
--*************************************************
SOF2
--
--          WAVY BEDDED GEOPSEUDO       X,Y
--
--   So          Kro
   0.250000      0.000000 -- Lower end point
   0.332957      0.012786 -- Generated point
   0.387468      0.029031 -- Generated point
   0.501143      0.095281 -- Generated point
   0.591481      0.275656 -- Generated point
   0.663656      0.373504 -- Generated point
   0.703076      0.556966 -- Generated point
   0.749369      0.693772 -- Generated point
   0.803574      0.888859 -- Generated point
   0.817758      0.986956 -- Upper end point
/
--                ditto          Z
--
   0.250000      0.000000 -- Lower end point
   0.601541      0.001743 -- Generated point
   0.616147      0.013926 -- Generated point
   0.646199      0.106492 -- Generated point
   0.690970      0.188545 -- Generated point
   0.725616      0.264941 -- Generated point
   0.762166      0.516398 -- Generated point
   0.790764      0.672023 -- Generated point
   0.800958      0.715714 -- Generated point
   0.808200      0.733293 -- Generated point
   0.814481      0.768330 -- Generated point
   0.817395      0.800002 -- Upper end point
/
--
--          SCS GEOPSEUDO          X,Y
--
   0.249985      0.000000 -- Lower end point
   0.291101      0.008696 -- Generated point
   0.299401      0.011532 -- Generated point
   0.311386      0.016067 -- Generated point
   0.332722      0.025567 -- Generated point
```

```
   0.375119      0.050044 -- Generated point
   0.514721      0.316330 -- Generated point
   0.703423      0.722668 -- Generated point
   0.751478      0.781592 -- Generated point
   0.771826      0.782944 -- Generated point
   0.778083      0.783141 -- Generated point
   0.780777      0.799984 -- Upper end point
/
--           ditto            Z
--
   0.250000      0.000000 -- Lower end point
   0.531093      0.051628 -- Generated point
   0.572827      0.066315 -- Generated point
   0.648960      0.088682 -- Generated point
   0.685041      0.124961 -- Generated point
   0.711230      0.216053 -- Generated point
   0.729548      0.363551 -- Generated point
   0.747085      0.457992 -- Generated point
   0.766559      0.509208 -- Generated point
   0.777202      0.535628 -- Generated point
   0.778470      0.800001 -- Upper end point
/
--
--       HCS GEOPSEUDO            X,Y
--
   0.249983      0.000000 -- Lower end point
   0.286625      0.008376 -- Generated point
   0.293850      0.011116 -- Generated point
   0.304648      0.015592 -- Generated point
   0.323113      0.024696 -- Generated point
   0.360948      0.048618 -- Generated point
   0.521270      0.422794 -- Generated point
   0.704209      0.744517 -- Generated point
   0.750837      0.763881 -- Generated point
   0.757073      0.799983 -- Upper end point
/
--       ditto                    Z
--
   0.250000      0.000000 -- Lower end point
   0.387693      0.008625 -- Generated point
   0.411325      0.010700 -- Generated point
   0.438967      0.013638 -- Generated point
   0.474678      0.018596 -- Generated point
   0.538747      0.028044 -- Generated point
   0.608132      0.043055 -- Generated point
   0.651378      0.061517 -- Generated point
   0.687310      0.174610 -- Generated point
   0.713630      0.319381 -- Generated point
   0.732610      0.373898 -- Generated point
   0.748107      0.410305 -- Generated point
   0.752627      0.415168 -- Generated point
   0.754629      0.799993 -- Upper end point
/
--       ROCK CURVE  1500mD
--
         0.25    0.0
         0.35    0.004
         0.46    0.030
         0.53    0.086
         0.58    0.114
         0.61    0.202
         0.64    0.283
         0.67    0.365
```

```
        0.73    0.446
        0.76    0.528
        0.79    0.61
        0.82    0.691
        0.85    0.773
        0.9     0.8
/
--
--    Sw   Krw                  Pc
SWFN
--
--              WAVY BEDDED GEOPSEUDO           X,Y
--
   0.182242     0.000000     28.486124
   0.186541     0.000873     25.296415
   0.194172     0.002840     21.442125
   0.203680     0.005290     16.891787
   0.214801     0.008062     11.971890
   0.250631     0.030110      7.498693
   0.296924     0.057581      4.430153
   0.336344     0.084313      3.098137
   0.408519     0.124124      2.128510
   0.498857     0.188109      1.399721
   0.612532     0.253604      1.236918
   0.667043     0.332530      1.164717
   0.749999     0.440001      1.046340
 /
--              ditto                Z
--
   0.182605     0.000000     28.486610
   0.185519     0.000608     25.989788
   0.191800     0.003361     22.802387
   0.199042     0.006517     19.183100
   0.209236     0.011317     14.400449
   0.237834     0.033631      8.939224
   0.274384     0.062657      5.595311
   0.309030     0.088021      3.905418
   0.353801     0.121952      2.828157
   0.383853     0.148372      2.445591
   0.398459     0.162765      2.291312
   0.750000     0.439996      1.046355
 /
---
--            SCS GEOPSEUDO                X,Y
--
   0.219223     0.000000     32.225315
   0.220608     0.000000     29.680822
   0.221917     0.000000     29.333700
   0.228174     0.000003     26.525280
   0.248522     0.000892     18.979488
   0.296577     0.013652      9.086331
   0.485279     0.109329      2.082320
   0.624881     0.245073      1.485384
   0.667278     0.297837      1.425292
   0.688614     0.332036      1.393901
   0.700599     0.352828      1.375957
   0.708899     0.367741      1.365200
   0.750014     0.440000      1.204337
 /
--            ditto                  Z
--
   0.221530     0.000000     32.125484
   0.222786     0.000000     29.660643
```

```
 0.233441    0.000691    23.156693
 0.252915    0.005295    15.916327
 0.270452    0.013923    12.467029
 0.288770    0.024031     8.911875
 0.314959    0.034716     6.423225
 0.351040    0.051745     4.451668
 0.427173    0.076623     2.785994
 0.468907    0.094763     2.256335
 0.750000    0.439025     1.237330
/
--
--          HCS GEOPSEUDO                X,Y
--
 0.242927    0.000000    34.310970
 0.249162    0.000223    28.374683
 0.295791    0.003360    12.702032
 0.478730    0.069170     2.542026
 0.639052    0.229303     1.602437
 0.676887    0.279646     1.540552
 0.695352    0.311219     1.514540
 0.706150    0.331185     1.494804
 0.713375    0.346178     1.480005
 0.750012    0.437091     1.413491
/
--            ditto               Z
--
 0.245371    0.000000    34.141262
 0.247366    0.000000    30.536541
 0.251893    0.000000    27.760406
 0.267390    0.001884    20.002945
 0.286370    0.006026    14.745336
 0.312690    0.018123     9.780584
 0.348622    0.036151     6.180594
 0.391868    0.054426     4.137291
 0.461253    0.082635     2.923240
 0.525322    0.105130     2.418682
 0.561033    0.120739     2.200270
 0.588675    0.133876     2.046448
 0.612307    0.145473     1.924000
 0.750000    0.435907     1.451024
/
--            ROCK CURVE       1500md
       0.10   0.0          27.0
       0.13   0.006        12.0
       0.16   0.025         8.0
       0.19   0.044         5.5
       0.22   0.063         4.0
       0.25   0.082         3.1
       0.28   0.101         2.6
       0.31   0.120         2.2
       0.34   0.139         1.8
       0.37   0.159         1.4
       0.42   0.183         1.35
       0.5    0.231         1.2
       0.6    0.354         1.1
       0.75   0.44          1
/
--
--==================================================================
REGIONS

EQUALS
       'FIPNUM'  1 1  74 1 10  1  4 /
```

```
        'FIPNUM'  2 75 75 1  10  1  4 /
        'FIPNUM'  3 1  74 1  10  5 14 /
        'FIPNUM'  4 75 75 1  10  5 14 /
        'FIPNUM'  5 1  74 1  10 15 17 /
        'FIPNUM'  6 75 75 1  10 15 17 /
/
--
SATNUM
--   ETIVE   WB   HCS   BROOM
        3000*7 750*1  6750*5  2250*7 /
KRNUMX
        3000*7 750*1  6750*5  2250*7 /
KRNUMZ
        3000*7 750*2  6750*6  2250*7 /
--
--=====================================================================
SOLUTION
--
---
--  DATUM  Pi@DATUM  WOC   Pc@WOC   GOC Pc@GOC
EQUIL
    8690    4824  9200   0    7500   0 /
--
--    Pb Sob Swb        Pob@Datum
RPTSOL
      1  0   1   12*0 1 /
--=====================================================================
SUMMARY
--
FPR
--
WBHP
'PROD' 'INJ' /
--
WWCT
 'PROD'
  /
--
FOIP
--
FWIP
--
FOPR
--
FWPR
--
FWIR
--
ROFT
        1 2 /
        3 4 /
/
--
RPTSMRY
 1  /
--
RUNSUM
--=====================================================================
SCHEDULE
--
RPTSCHED
 1 0 1 0 0 0 2 2 1 6*0 1 0 0 /
--
```

```
--    WELL WELL  LOCATION  BHP   PREF.
--    NAME GROUP  I   J  DATUM  PHASE
WELSPECS
      'PROD' 'G'  75  1   8100  'OIL' /
--
      'INJ'    'G'  1   1   9200  'WAT' /
        /
--
--    WELL  LOCATION INTERVAL STATUS      WELL
--    NAME   I   J   K1 K2  O or S       ID
COMPDAT
     'PROD'  75  5   1  2  'OPEN'  2*  0.66667 /
      'PROD'  75  5   7  11  'OPEN'  2*  0.66667 /
      'INJ'     1  5   1  17  'OPEN'  2*  0.66667 /
        /
--
--    WELL  STATUS CONTROL  TARGET RATES or UPPER LIMITS
--    NAME          MODE  OIL WAT GAS LIQ RV BHP
WCONPROD
      'PROD' 'OPEN' 'BHP'      5*        3440.0 /
        /
--
--    WELL  FLUID  STATUS CONTROL             BHP TAR
--    NAME  TYPE          MODE
WCONINJ
      'INJ' 'WAT' 'OPEN' 'RESV' 1* 0.0 1.0 'FVDG' 10000  /
        /
--
--   DAYS
TSTEP
  1 2 3 5 10 10 31 18*62 /
--==================================================================
END
```

APPENDIX IX: Rock Curves and Geopseudos

IX.1 Rock Relative Permeability and Capillary Pressure Curves

```
--          So      Kro
--                                3mD
           0.25    0.0
           0.30    0.0008
           0.33    0.0082
           0.35    0.0250
           0.37    0.0622
           0.39    0.1345
           0.4     0.1898
           0.41    0.2621
           0.43    0.4724
           0.44    0.6190
           0.45    0.8
/
--                                15mD
           0.25    0.00
           0.3     0.005
           0.4     0.064
           0.5     0.143
           0.514   0.154
           0.528   0.37
           0.542   0.424
           0.556   0.478
           0.57    0.532
           0.584   0.585
           0.598   0.639
           0.612   0.693
           0.626   0.746
           0.64    0.800
/
--                                50mD
           0.25    0.0
           0.3     0.004
           0.4     0.044
           0.5     0.11
           0.522   0.124
           0.544   0.24
           0.566   0.310
           0.588   0.38
           0.61    0.45
           0.632   0.52
           0.654   0.59
           0.676   0.66
           0.698   0.73
           0.72    0.8
/
--                                150mD
           0.25    0.0
           0.30    0.004
           0.4     0.03
           0.5     0.086
           0.53    0.103
           0.56    0.147
           0.59    0.229
           0.62    0.311
           0.65    0.392
           0.68    0.474
           0.71    0.555
           0.74    0.637
           0.77    0.718
           0.8     0.8
```

```
            0.25    0.0                 300mD
            0.3     0.004
            0.4     0.030
            0.5     0.086
            0.550   0.114
            0.58    0.202
            0.61    0.283
            0.64    0.365
            0.67    0.446
            0.7     0.528
            0.73    0.61
            0.76    0.691
            0.79    0.773
            0.82    0.8
/           --                          750/500mD
            0.25    0.0
            0.333   0.004
            0.43    0.030
            0.53    0.086
            0.58    0.114
            0.61    0.202
            0.64    0.283
            0.67    0.365
            0.70    0.446
            0.73    0.528
            0.76    0.61
            0.79    0.691
            0.81    0.773
            0.85    0.8
/           --                          1500mD
            0.25    0.0
            0.35    0.004
            0.46    0.030
            0.53    0.086
            0.58    0.114
            0.61    0.202
            0.64    0.283
            0.67    0.365
            0.73    0.446
            0.76    0.528
            0.79    0.61
            0.82    0.691
            0.85    0.773
            0.9     0.8
/
--
--            Sw    Krw                 Pc
SWFN
--                                              3mD
            0.55    0.0                 2.72
            0.57    0.0036              1.84
            0.6     0.0225              1.16
            0.65    0.09                0.82
            0.7     0.2025              0.48
            0.75    0.36                0.34
            /
--
--                                            15mD
            0.36    0.0                 3.741
            0.374   0.012               1.769
            0.388   0.025               1.361
            0.402   0.037               1.190
            0.416   0.05                0.952
            0.430   0.062               0.85
            0.444   0.075               0.748
            0.458   0.087               0.68
```

```
          0.472    0.1             0.544
          0.486    0.124           0.476
          0.5      0.133           0.408
          0.6      0.201           0.204
          0.7      0.318           0.17
          0.75     0.44            0.156
/
--                                       50mD
          0.28     0.0             2.721
          0.302    0.016           1.361
          0.324    0.033           0.816
          0.346    0.049           0.612
          0.368    0.065           0.476
          0.39     0.081           0.34
          0.412    0.098           0.293
          0.434    0.114           0.252
          0.456    0.13            0.218
          0.478    0.15            0.19
          0.5      0.162           0.184
          0.6      0.218           0.15
          0.7      0.339           0.109
          0.75     0.44            0.068
/
--                                       150mD
          0.2      0.0             1.837
          0.23     0.019           0.816
          0.26     0.038           0.544
          0.29     0.057           0.374
          0.32     0.076           0.272
          0.35     0.095           0.211
          0.38     0.114           0.177
          0.41     0.133           0.15
          0.44     0.152           0.122
          0.47     0.168           0.095
          0.5      0.183           0.092
          0.6      0.231           0.082
          0.7      0.354           0.075
          0.75     0.44            0.068
/
--                                       300mD
          0.18     0.0             1.837
          0.21     0.006           0.816
          0.24     0.025           0.544
          0.27     0.044           0.374
          0.30     0.063           0.272
          0.33     0.082           0.211
          0.36     0.101           0.177
          0.39     0.120           0.15
          0.42     0.139           0.122
          0.45     0.159           0.095
          0.5      0.183           0.092
          0.6      0.231           0.082
          0.7      0.354           0.075
          0.75     0.44            0.068
/
--                                       500/750mD
          0.15     0.0             1.837
          0.18     0.006           0.816
          0.21     0.025           0.544
          0.24     0.044           0.374
          0.27     0.063           0.272
          0.30     0.082           0.211
          0.33     0.101           0.177
          0.36     0.120           0.15
          0.39     0.139           0.122
          0.41     0.159           0.095
```

```
        0.47    0.183           0.092
        0.55    0.231           0.082
        0.65    0.354           0.075
        0.75    0.44            0.068
/
--                                     1500mD
        0.10    0.0             1.837
        0.13    0.006           0.816
        0.16    0.025           0.544
        0.19    0.044           0.374
        0.22    0.063           0.272
        0.25    0.082           0.211
        0.28    0.101           0.177
        0.31    0.120           0.15
        0.34    0.139           0.122
        0.37    0.159           0.095
        0.42    0.183           0.092
        0.5     0.231           0.082
        0.6     0.354           0.075
        0.75    0.44            0.068
/
```

IX.2 Geopseudo Relative Permeability and Capillary Pressure Curves

IX..2.1 Ripple, high contrast, low contrast, wavy bedded - 8 x 8cm

	HORIZONTAL						VERTICAL					
	Sw	So	krw	kro	Pc(atm)	Pc(psi)	Sw	So	krw	kro	Pc(atm)	Pc(psi)
RIPPLE LAMINATION	0.5276	0.4724	0.0000	0.8000	2.8234	41.4928	0.5310	0.4690	0.0000	0.8000	2.8050	41.2228
Ar.Av.=4.7mD	0.5315	0.4685	0.0003		2.5587	37.6028	0.5348	0.4652	0.0038	0.1191	2.5658	37.7072
	0.5400	0.4600	0.0010	0.6755	2.1988	32.3133	0.6677	0.3323	0.1326	0.0084	0.5943	8.7338
	0.6199	0.3801	0.0605	0.0838	0.8506	12.5011	0.6846	0.3154	0.1579	0.0036	0.5078	7.4619
	0.6473	0.3527	0.1157	0.0145	0.6638	9.7554	0.6923	0.3077	0.1767	0.0020	0.4700	6.9071
	0.6575	0.3425	0.1345	0.0090	0.5929	8.7127	0.6975	0.3025	0.1910	0.0013	0.4464	6.5604
	0.6659	0.3341	0.1509	0.0053	0.5356	7.8709	0.7048	0.2952	0.2103	0.0007	0.4214	6.1936
	0.6728	0.3272	0.1657	0.0025	0.4921	7.2323	0.7117	0.2883	0.2247	0.0005	0.4019	5.9056
	0.6782	0.3218	0.1764	0.0016	0.4691	6.8941	0.7159	0.2841	0.2318	0.0004	0.3905	5.7384
	0.6821	0.3179	0.1845	0.0013	0.4567	6.7116	0.7500	0.2500	0.3676	0.0000	0.3214	4.7236
	0.6871	0.3129	0.1957	0.0011	0.4421	6.4977						
	0.6957	0.3043	0.2151	0.0008	0.4171	6.1294						
	0.7500	0.2500	0.3691	0.0000	0.3182	4.6756						
HIGH CONTRAST LAMINATION	0.3303	0.6697	0.0000	0.8000	3.2103	47.1789	0.3302	0.6698	0.0000	0.8000	3.2330	47.5126
Ar.Av = 42mD	0.3368	0.6632	0.0024	0.7905	2.4005	35.2771	0.3359	0.6641	0.0040		2.4858	36.5309
	0.3453	0.6547	0.0058	0.7755	1.7556	25.8009	0.3607	0.6393	0.0216	0.6054	1.2750	18.7368
	0.3628	0.6372	0.0135	0.7402	1.2549	18.4417	0.4195	0.5805	0.0829	0.0505	0.6219	9.1397
	0.3894	0.6106	0.0281	0.6793	0.8681	12.7576	0.4437	0.5563	0.1159	0.0121	0.4654	6.8398
	0.4432	0.5568	0.0675	0.5059	0.4683	6.8820	0.4525	0.5475	0.1239	0.0057	0.4245	6.2389
	0.5073	0.4927	0.1138	0.3199	0.2843	4.1776	0.4610	0.5390	0.1307	0.0043	0.3956	5.8137
	0.5493	0.4507	0.1427	0.2133	0.2226	3.2717	0.4722	0.5278	0.1396	0.0028	0.3636	5.3441
	0.6078	0.3922	0.1910	0.1272	0.1888	2.7752	0.4812	0.5188	0.1467	0.0017	0.3406	5.0060
	0.6581	0.3419	0.2485	0.0628	0.1611	2.3675	0.4860	0.5140	0.1507	0.0012	0.3296	4.8432
	0.7031	0.2969	0.3089	0.0286	0.1458	2.1433	0.4901	0.5100	0.1541	0.0007	0.3196	4.6965
	0.7205	0.2795	0.3463	0.0104	0.1421	2.0881	0.4937	0.5063	0.1571	0.0003	0.3112	4.5741
	0.7500	0.2500	0.4361	0.0000	0.1328	1.9514	0.7500	0.2500	0.4361	0.0000	0.1328	1.9513
LOW CONTRAST LAMINATION	0.1853	0.8147	0.0000	0.8000	1.8370	26.9966	0.1853	0.8147	0.0000	0.8000	1.8370	26.9964
Ar.Av. = 292mD	0.1876	0.8124		0.8061			0.2047	0.7953	0.0048	0.7483	1.1775	17.3039
	0.1890	0.8110	0.0000		1.7020	25.0129	0.2513	0.7487	0.0317	0.6427	0.5098	7.4919
	0.2019	0.7981	0.0025		1.2700	18.6641	0.3164	0.6836	0.0722	0.4796	0.2496	3.6677
	0.2027	0.7973		0.7815			0.3498	0.6502	0.0949	0.3966	0.1946	2.8595
	0.2183	0.7817	0.0069		0.8220	12.0804	0.3669	0.6331	0.1045	0.3574	0.1754	2.5783
	0.2205	0.7795		0.7645			0.4053	0.5948	0.1297	0.2412	0.1407	2.0680
	0.2407	0.7593	0.0184		0.5849	8.5952	0.4440	0.5560	0.1546	0.1386	0.1052	1.5464
	0.2517	0.7483		0.6761			0.5085	0.4915	0.1834	0.0847	0.0912	1.3396
	0.2671	0.7329	0.0365		0.4171	6.1294	0.6018	0.3982	0.2326	0.0301	0.0819	1.2037
	0.3037	0.6963		0.5246			0.6726	0.3274	0.3268	0.0105	0.0769	1.1297
	0.3153	0.6847	0.0678		0.2515	3.6955	0.7004	0.2996	0.3605	0.0039	0.0747	1.0974
	0.3527	0.6473		0.3957			0.7500	0.2500	0.4400	0.0000	0.0680	0.9993
	0.3630	0.6370	0.0984		0.1914	2.8133						
	0.3817	0.6183		0.3274								
	0.3957	0.6043	0.1188		0.1588	2.3330						
	0.4211	0.5789		0.2214								
	0.4352	0.5648	0.1435		0.1188	1.7464						
	0.4880	0.5120		0.1056								
	0.5205	0.4795	0.1841		0.0872	1.2818						
	0.6165	0.3835		0.0282								
	0.6356	0.3644	0.2620		0.0794	1.1665						
	0.6886	0.3114		0.0080								
	0.6967	0.3033	0.3460		0.0815	1.1984						
	0.7500	0.2500	0.4400	0.0000	0.0680	0.9993						
WAVY BEDDED	0.1822	0.8178	0.0000	0.9870	1.9384	28.4860	0.1826	0.8174	0.0000	0.8000	1.9384	28.4865
Ar. Av. = 508mD	0.1865	0.8135	0.0009		1.7213	25.2963	0.1855	0.8145	0.0006	0.7333	1.7685	25.9897
	0.1942	0.8058	0.0028	0.8889	1.4590	21.4421	0.1918	0.8082	0.0034	0.7183	1.5516	22.8023
	0.2037	0.7963	0.0053		1.1494	16.8917	0.1990	0.8010	0.0065	0.7157	1.3053	19.1830
	0.2148	0.7852	0.0081		0.8146	11.9718	0.2092	0.7908	0.0113	0.6720	0.9799	14.4004
	0.2506	0.7494	0.0301	0.6938	0.5103	7.4987	0.2378	0.7622	0.0336	0.5164	0.6083	8.9392
	0.2969	0.7031	0.0576	0.5570	0.3015	4.4301	0.2744	0.7256	0.0627	0.2649	0.3807	5.5953
	0.3363	0.6637	0.0843	0.3735	0.2108	3.0981	0.3090	0.6910	0.0880	0.1885	0.2657	3.9054
	0.4085	0.5915	0.1241	0.2757	0.1448	2.1285	0.3538	0.6462	0.1220	0.1065	0.1924	2.8281
	0.4989	0.5011	0.1881	0.0953	0.0952	1.3997	0.3839	0.6161	0.1484	0.0139	0.1664	2.4456
	0.6125	0.3875	0.2536	0.0290	0.0842	1.2369	0.3985	0.6015	0.1628	0.0017	0.1559	2.2913
	0.6670	0.3330	0.3325	0.0128	0.0793	1.1647	0.7500	0.2500	0.4400	0.0000	0.0712	1.0464
	0.7500	0.2500	0.4400	0.0000	0.0712	1.0463						

IX..2.2 HCS, SCS - 1.5 x 12m (5 x 40ft)

	HORIZONTAL						VERTICAL					
	Sw	So	krw	kro	Pc(atm)	Pc(psi)	Sw	So	krw	kro	Pc(atm)	Pc(psi)
HUMMOCKY CROSS-STRAT.	0.2374	0.7626	0.0000	0.8000	2.2764	33.4537	0.2445	0.7555	0.0000	0.8000	2.0779	30.5364
Ar.Av. = 210mD	0.2435	0.7565	0.0001	0.7727	1.9042	27.9834	0.2454	0.7546	0.0000		2.0779	30.5364
	0.2907	0.7093	0.0035	0.7533	0.8454	12.4235	0.2464	0.7536	0.0000	0.4235	1.9648	28.8748
	0.4686	0.5314	0.0690	0.4362	0.1728	2.5398	0.2603	0.7397	0.0010	0.4057	1.4788	21.7318
	0.6356	0.3644	0.2339	0.0499	0.1071	1.5733	0.2811	0.7189	0.0037	0.3497	0.9834	14.4515
	0.6748	0.3252	0.2862	0.0261	0.1026	1.5083	0.3105	0.6895	0.0195	0.2062	0.6198	9.1087
	0.6944	0.3056	0.3189	0.0165	0.1006	1.4782	0.3499	0.6501	0.0360	0.0683	0.3954	5.8106
	0.7055	0.2945	0.3387	0.0117	0.0995	1.4621	0.3998	0.6002	0.0539	0.0461	0.2586	3.8009
	0.7130	0.2870	0.3530	0.0088	0.0984	1.4459	0.4828	0.5172	0.0854	0.0293	0.1714	2.5182
	0.7500	0.2500	0.4371	0.0000	0.0939	1.3799	0.5471	0.4529	0.1088	0.0192	0.1420	2.0873
							0.7500	0.2500	0.4359	0.0000	0.0987	1.4510
SWALEY CROSS STRAT.	0.2192	0.7808	0.0000	0.8000	2.1928	32.2252	0.2215	0.7785	0.0000	0.8000	2.1860	32.1254
Ar.Av. = 202mD	0.2206	0.7794	0.0000		2.0197	29.6807	0.2228	0.7772	0.0000	0.5356	2.0183	29.6605
	0.2219	0.7781	0.0000	0.7831	1.9960	29.3336	0.2334	0.7666	0.0007	0.5092	1.5757	23.1566
	0.2282	0.7718	0.0000	0.7829	1.8049	26.5252	0.2529	0.7471	0.0053	0.4580	1.0830	15.9163
	0.2485	0.7515	0.0009	0.7816	1.2915	18.9794	0.2705	0.7295	0.0139	0.3636	0.8483	12.4670
	0.2966	0.7034	0.0137	0.7227	0.6183	9.0863	0.2888	0.7112	0.0240	0.2161	0.6064	8.9118
	0.4853	0.5147	0.1093	0.3163	0.1417	2.0823	0.3150	0.6850	0.0347	0.1250	0.4371	6.4232
	0.6249	0.3751	0.2451	0.0500	0.1011	1.4854	0.3510	0.6490	0.0517	0.0887	0.3029	4.4517
	0.6673	0.3327	0.2978	0.0256	0.0970	1.4253	0.4272	0.5728	0.0766	0.0663	0.1896	2.7860
	0.6886	0.3114	0.3320	0.0161	0.0948	1.3939	0.4689	0.5311	0.0948	0.0516	0.1535	2.2563
	0.7006	0.2994	0.3528	0.0115	0.0936	1.3760	0.7500	0.2500	0.4390	0.0000	0.0842	1.2373
	0.7089	0.2911	0.3677	0.0087	0.0929	1.3652						
	0.7500	0.2500	0.4400	0.0000	0.0820	1.2043						

APPENDIX X: Probe permeameter data sets

X. 1. Statfjord

X. 1. a Statfjord Study Calibration Data

SMALL PROBE (SP1)

PERMEABILITY (mD)	FLOW RATE (10 mbar) (ml/min)	FLOW RATE (90 mbar) (ml/min)	FLOW RATE (400 mbar) (ml/min)
5.9			9.4
10.6			14.4
34.2		7.6	
50		10.4	
53			67.1
96		24.6	116
118		33.2	164
221		58.6	240
228		60.7	
265		66.2	
368		67.8	
904		165	
1015		230	
1205	36.8	266	
1232	35.4	249	
2020	61.6	378	
2070	60.4		
2100	58.6	362	
3320	95		
3950	131		
4250	129		

LARGE PROBE (LP 1)

PERMEABILITY (mD)	FLOW RATE (10 mbar) (ml/min)	FLOW RATE (90 mbar) (ml/min)
5.9		3.3
19.1		8.6
32.3		13.6
53		22.2
96		39.9
118		58.2
221		101
228		101
265		121
368	22.8	128
904	46.9	305
1015	52.5	389
1232	68.1	470
2020	95.4	
3320	177	
3950	225	
4250	213	

X. 1. b 33/12-B9 - Detailed Grids A-H

MINIPERMEAMETER PERMEABILITIES (mD)

CORE 5
3838.52-.600 m

Fine grid "A"

Profile No.	1	2	3	4	5	6	7	8	9	10	11	12	13	14	15	16
Fine grid offset (m)	0.000	0.002	0.004	0.006	0.008	0.010	0.012	0.014	0.016	0.018	0.020	0.022	0.024	0.026	0.028	0.030
Coarse grid offset (m	-0.003	-0.001	0.001	0.003	0.005	0.007	0.009	0.011	0.013	0.015	0.017	0.019	0.021	0.023	0.025	0.027
Core Depth (mMD)																
3838.520	17	16	16	16	17	15	15	17	18	20	25	28	28	33	35	36
3838.522	50	55	64	65	70	69	74	81	85	82	82	82	85	88	93	88
3838.524	106	102	110	111	113	112	118	118	119	132	131	136	145	139	134	133
3838.526	141	148	145	157	170	168	175	182	183	191	188	183	176	169	158	148
3838.528	174	184	198	217	223	225	224	218	206	209	202	192	171	154	134	121
3838.530	174	167	160	176	186	169	169	142	111	113	128	125	115	95	84	77
3838.532	96	96	90	90	81	81	80	73	65	59	57	59	64	65	64	63
3838.534	35	45	45	33	25	19	17	17	18	18	18	22	26	27	28	24
3838.536	7	8	7	8	7	8	9	9	7	6	6	6	6	6	5	5
3838.538	19	20	20	21	22	21	21	20	20	19	19	19	19	19	19	18
3838.540	13	14	13	16	16	17	14	15	10	14	15	18	17	17	19	19
3838.542	17	15	17	17	17	18	20	20	20	20	21	21	21	21	20	19
3838.544	26	26	26	27	27	31	33	36	38	39	36	35	33	31	28	27
3838.546	35	36	32	35	37	44	39	49	48	47	39	37	37	35	34	31
3838.548	75	73	72	67	71	73	77	73	70	69	63	66	61	59	59	59
3838.550	101	97	92	90	95	97	98	97	97	97	93	90	94	88	89	92
3838.552	92	91	88	87	88	94	93	92	93	98	92	93	91	96	95	95
3838.554	69	66	69	70	69	71	77	75	80	86	81	78	78	82	82	77
3838.556	24	22	25	22	24	25	31	30	32	35	37	32	28	34	35	33
3838.558	4	4	4	4	4	4	4	4	4	5	5	5	5	5	5	5
3838.560	11	12	12	12	12	11	11	10	11	12	12	12	12	11	11	10
3838.562	12	12	12	13	12	11	12	11	11	11	12	12	12	11	11	10
3838.564	10	11	11	11	11	11	11	11	10	10	10	11	11	10	11	10
3838.566	9	10	10	10	11	10	10	10	9	9	9	10	12	11	11	11
3838.568	11	11	11	10	9	8	8	8	7	7	8	9	8	8	8	8
3838.570	16	16	15	15	14	15	15	16	17	16	16	16	15	15	15	14
3838.572	14	14	13	11	12	12	14	15	16	16	15	16	14	15	14	16
3838.574	20	21	21	21	22	21	20	18	17	16	15	14	13	13	13	13
3838.576	16	19	21	22	21	20	19	19	18	16	17	15	14	13	14	15
3838.578	2	2	2	2	2	2	2	2	2	2	4	2	2	3	4	2
3838.580	6	6	5	5	5	5	4	4	4	4	3	3	3	3	3	3
3838.582	14	14	14	14	13	14	13	12	11	10	9	8	8	8	8	8
3838.584	31	30	28	29	28	29	26	21	17	16	16	14	12	13	14	13
3838.586	49	47	46	46	46	48	47	44	39	38	36	37	39	44	44	37
3838.588	45	37	39	47	47	52	49	52	48	49	50	51	57	58	57	54
3838.590	20	20	20	20	20	20	22	22	23	23	22	23	25	27	27	32
3838.592	33	32	30	28	30	29	29	29	31	31	28	30	30	30	33	32
3838.594	46	44	36	34	36	34	33	34	37	33	32	30	33	34	37	32
3838.596	33	35	33	32	35	37	37	36	36	38	37	39	45	48	48	48
3838.598	31	30	29	30	35	37	37	38	38	45	51	48	52	57	55	55
3838.600	24	22	20	20	22	20	24	26	27	30	31	28	28	28	32	30

MINIPERMEAMETER PERMEABILITIES (mD)

CORE 5
3838.391-.421 m

Fine grid "B"

Profile No.	1	2	3	4	5	6	7	8	9	10	11	12	13	14	15	16	17	18	19	20	21
Fine grid offset (m)	0.000	0.002	0.004	0.006	0.008	0.010	0.012	0.014	0.016	0.018	0.020	0.022	0.024	0.026	0.028	0.030	0.032	0.034	0.036	0.038	0.040
Coarse grid offset (n	-0.003	-0.001	0.001	0.003	0.005	0.007	0.009	0.011	0.013	0.015	0.017	0.019	0.021	0.023	0.025	0.027	0.029	0.031	0.033	0.035	0.037
Core Depth (mMD)																					
3838.391	2.9	2.8	2.7	2.4	2.3	2.3	2.3	2.6	3.0	2.6	2.6	2.9	4.2	5.4	6.2	6.9	7.6	6.1	4.8	3.8	2.9
3838.393	2.5	2.4	2.4	2.6	2.7	2.9	3.1	3.4	3.0	2.9	2.4	2.2	2.3	2.3	2.4	2.5	2.8	3.0	4.7	3.8	3.6
3838.395	2.7	2.8	2.8	2.8	2.9	2.9	2.8	3.0	3.4	3.1	2.8	3.0	3.3	3.6	3.3	2.9	2.9	3.1	3.4	3.7	3.9
3838.397	2.1	2.3	2.4	2.3	2.4	2.3	2.2	2.1	2.1	2.0	2.1	2.4	2.9	3.2	3.2	3.2	2.8	2.5	2.5	2.7	3.0
3838.399	2.2	2.3	2.3	2.3	2.5	2.5	2.3	2.0	1.9	1.8	1.7	1.8	1.8	2.0	2.0	2.1	2.1	2.0	2.1	2.3	2.5
3838.401	2.5	2.5	2.4	2.6	2.7	2.5	2.4	2.4	2.3	2.1	2.0	1.9	2.0	2.1	2.2	2.2	2.2	2.2	2.1	2.2	2.5
3838.403	1.9	1.9	2.1	2.4	2.2	2.2	2.4	2.5	2.6	2.7	2.6	2.7	2.8	2.8	2.8	2.5	2.3	2.1	2.0	1.9	2.0
3838.405	1.6	1.8	1.8	2.0	2.1	2.2	2.4	2.5	3.2	3.3	3.4	4.1	4.3	4.0	2.5	2.1	1.9	1.7	1.7	1.7	1.7
3838.407	1.6	1.6	1.6	1.6	1.6	1.7	1.8	2.1	2.6	3.0	3.3	4.2	5.2	8.5	8.0	10.4	18.9	13.4	6.5	10.3	8.7
3838.409	2.1	2.1	4.7	4.9	4.2	4.0	4.3	6.2	5.1	2.5	2.1	2.0	2.2	2.2	2.8	6.6	16.1	9.9	16.1	21.6	19.9
3838.411	56.3	48.8	14.0	6.7	5.6	5.5	5.5	7.5	6.7	3.8	2.7	2.5	2.3	2.2	2.4	2.2	2.2	2.3	2.2	2.0	2.0
3838.413	53.7	39.5	12.1	8.2	7.0	4.9	3.8	3.2	2.8	2.2	2.0	2.1	1.9	1.9	2.0	2.1	2.1	2.2	2.0	2.0	2.1
3838.415	4.1	4.7	4.7	4.4	4.3	3.8	3.7	3.5	2.9	3.0	2.7	2.3	2.0	2.1	2.2	2.4	2.1	2.4	2.4	2.4	2.5
3838.417	4.2	3.8	3.9	4.0	3.8	3.8	4.0	4.3	4.4	4.7	4.2	3.5	3.6	3.6	4.5	6.8	7.7	7.3	6.1	4.4	3.8
3838.419	4.2	3.6	3.4	3.8	5.5	6.5	9.1	9.7	8.6	8.1	8.9	9.6	9.8	9.5	9.9	10.0	9.1	7.8	6.7	5.1	3.8
3838.421	3.1	3.0	3.3	4.1	5.7	6.9	9.4	9.4	9.8	9.0	9.9	12.1	12.0	12.2	11.1	11.7	11.8	11.4	8.8	7.1	4.3

MINIPERMEAMETER PERMEABILITIES (mD)

CORE 5
3837.647-.746 m

Fine grid "C"

Profile No.	1	2	3	4	5	6	7	8	9	10	11	12	13	14	15	16	17	18	19	20	21
Fine grid offset (m)	0.000	0.003	0.006	0.009	0.012	0.015	0.018	0.021	0.024	0.027	0.030	0.033	0.036	0.039	0.042	0.045	0.048	0.051	0.054	0.057	0.060
Coarse grid offset (m	0.004	0.007	0.010	0.013	0.016	0.019	0.022	0.025	0.028	0.031	0.034	0.037	0.040	0.043	0.046	0.049	0.052	0.055	0.058	0.061	0.064
Core Depth (mMD)																					
3837.647	185	203	194	221	219	190	195	208	224	218	231	205	220	211	162	158	173	172	173	159	167
3837.650	207	221	241	237	263	260	242	233	260	278	257	265	248	207	182	185	172	159	163	163	150
3837.653	216	226	239	230	260	273	274	257	247	248	257	252	261	239	224	198	193	202	191	184	178
3837.656	237	242	254	268	296	310	299	292	291	283	298	290	277	274	256	223	231	196	184	170	178
3837.659	293	304	314	327	310	311	327	323	309	295	319	313	294	306	279	247	235	221	190	233	197
3837.662	272	266	268	326	329	341	344	387	387	422	463	390	396	386	299	240	201	189	211	201	227
3837.665	352	377	391	401	405	393	363	379	414	409	380	370	354	344	275	214	181	158	169	181	196
3837.668	357	372	376	345	390	349	368	357	354	352	343	344	368	304	265	201	193	180	201	199	202
3837.671	300	302	326	327	334	340	307	339	329	325	341	344	318	309	242	199	165	153	168	174	199
3837.674	285	268	305	281	300	335	319	311	301	310	335	334	313	296	206	204	163	158	168	183	210
3837.677	303	305	339	322	329	329	334	334	318	352	313	341	316	278	248	244	215	203	191	232	262
3837.680	337	336	336	333	358	348	360	353	363	380	366	328	331	288	258	240	196	202	194	197	252
3837.683	370	405	366	376	398	393	337	347	347	326	336	300	282	282	258	249	230	230	239	250	271
3837.686	352	349	345	375	384	389	378	413	409	399	401	397	346	311	287	233	220	186	187	184	167
3837.689	379	402	366	356	371	370	335	336	332	281	268	276	237	218	188	155	147	135	152	172	149
3837.692	279	284	262	247	275	265	232	228	207	216	186	171	160	170	140	159	138	139	163	151	150
3837.695	262	244	219	228	252	211	212	184	151	163	150	163	153	131	140	160	164	153	160	150	171
3837.698	272	261	248	236	218	217	222	185	161	191	172	215	212	188	190	206	220	223	208	186	190
3837.701	315	343	328	315	304	290	278	262	244	219	225	240	229	237	200	223	203	215	226	192	192
3837.704	314	320	294	282	276	258	230	235	203	173	170	171	193	215	222	203	228	232	240	227	240
3837.707	312	301	299	291	276	266	259	283	264	257	274	239	290	304	320	297	292	291	281	260	290
3837.710	379	351	354	364	346	291	318	334	358	352	334	324	299	314	320	290	272	254	254	267	269
3837.713	309	294	285	237	249	222	250	221	231	262	241	253	252	270	290	280	293	282	280	301	292
3837.716	257	276	269	289	261	242	273	233	221	252	261	226	239	250	239	250	269	254	236	246	268
3837.719	235	209	272	222	224	241	224	212	223	286	286	241	227	235	250	296	327	285	309	319	273
3837.722	248	249	262	246	229	222	222	193	227	243	249	220	200	207	196	230	293	259	248	242	260
3837.725	238	243	234	228	226	213	186	191	194	181	201	184	178	193	205	216	253	256	272	247	268
3837.728	260	278	266	268	225	232	252	213	214	197	236	233	224	229	244	252	281	279	303	277	287
3837.731	298	363	327	360	389	348	354	335	314	295	345	347	295	322	313	328	361	333	329	341	364
3837.734	409	420	356	382	394	382	341	346	319	346	358	278	281	286	262	315	309	266	269	277	320
3837.737	387	396	325	325	322	346	282	277	279	259	247	246	232	220	227	259	263	210	208	228	252
3837.740	294	269	258	215	234	218	236	208	221	175	183	205	189	172	203	189	179	171	179	221	226
3837.743	237	215	202	207	213	172	192	186	205	183	168	160	168	175	169	161	172	167	162	178	198
3837.746	187	217	186	166	178	140	155	161	144	149	133	140	166	177	161	177	166	157	143	165	173

MINIPERMEAMETER PERMEABILITIES (mD)

CORE 5
3835.855-.905 m

Fine grid "D"

Profile No.	1	2	3	4	5	6	7	8	9	10	11	12	13
Fine grid offset (m)	0.000	0.002	0.004	0.006	0.008	0.010	0.012	0.014	0.016	0.018	0.020	0.022	0.024
Coarse grid offset (m	0.008	0.010	0.012	0.014	0.016	0.018	0.020	0.022	0.024	0.026	0.028	0.030	0.032
Core Depth (mMD)													
3835.855	52	50	48	41	36	27	20	18	21	21	28	37	48
3835.857	32	36	40	46	46	46	47	40	36	33	31	26	21
3835.859	6	6	7	7	8	22	33	38	38	47	48	46	41
3835.861	9	7	6	5	6	6	6	6	6	11	23	32	37
3835.863	31	28	22	19	15	10	8	6	6	5	5	5	6
3835.865	47	40	40	39	37	35	32	29	22	16	11	8	6
3835.867	23	32	36	41	46	48	51	54	52	41	38	36	29
3835.869	7	7	7	7	12	13	26	31	48	49	53	51	48
3835.871	8	8	7	6	6	6	6	6	6	8	16	27	33
3835.873	9	8	7	7	6	6	5	6	6	6	5	5	6
3835.875	9	8	7	6	6	6	7	7	6	6	6	6	5
3835.877	10	7	7	6	6	6	7	7	7	7	7	6	6
3835.879	17	14	11	9	8	8	7	7	6	7	6	6	6
3835.881	34	33	31	31	27	24	15	13	11	10	8	7	7
3835.883	35	36	37	40	39	36	33	30	28	26	20	15	13
3835.885	23	25	27	29	31	35	37	37	34	33	32	33	32
3835.887	12	14	18	18	21	22	22	25	23	23	28	32	34
3835.889	7	7	7	9	9	8	10	13	13	17	19	21	21
3835.891	18	16	13	12	9	7	7	7	7	8	10	10	12
3835.893	26	23	21	18	17	14	11	10	9	7	7	7	7
3835.895	33	30	27	26	27	23	19	19	19	17	15	13	10
3835.897	35	34	34	33	33	27	25	27	28	26	23	21	18
3835.899	58	48	39	34	36	33	34	31	31	28	26	28	26
3835.901	112	99	96	81	67	54	46	37	32	28	33	30	32
3835.903	116	113	116	114	111	97	88	85	74	60	40	35	29
3835.905	64	69	79	96	105	97	103	108	97	84	78	69	58

Profile No.	14	15	16	17	18	19	20	21	22	23	24	25	26
Fine grid offset (m)	0.026	0.028	0.030	0.032	0.034	0.036	0.038	0.040	0.042	0.044	0.046	0.048	0.050
Coarse grid offset (m	0.034	0.036	0.038	0.040	0.042	0.044	0.046	0.048	0.050	0.052	0.054	0.056	0.058
Core Depth (mMD)													
3835.855	49	48	48	50	50	53	55	52	48	47	35	33	31
3835.857	20	19	21	27	33	39	40	38	39	37	34	34	34
3835.859	38	35	31	25	22	16	17	18	18	23	22	27	28
3835.861	40	45	47	46	39	36	34	28	25	19	16	16	16
3835.863	6	6	26	28	34	37	37	35	33	31	29	28	25
3835.865	5	5	5	5	5	6	6	11	17	20	21	23	28
3835.867	22	17	13	8	6	5	5	5	5	5	5	5	7
3835.869	37	36	33	29	22	18	15	10	8	7	6	5	6
3835.871	35	40	41	40	38	36	34	31	25	21	19	16	12
3835.873	9	14	20	24	29	32	35	34	33	32	32	32	29
3835.875	5	5	5	5	6	7	8	12	19	17	25	32	33
3835.877	6	6	6	6	5	5	5	5	6	6	6	11	14
3835.879	7	7	6	6	6	6	5	6	6	6	6	6	6
3835.881	6	6	6	6	6	6	6	6	6	6	6	6	6
3835.883	12	9	8	7	7	7	7	6	6	6	6	7	7
3835.885	32	31	22	19	14	12	11	9	8	8	8	7	7
3835.887	38	37	35	33	30	27	23	19	17	14	12	10	10
3835.889	23	27	33	31	31	33	32	34	29	25	25	22	21
3835.891	14	17	20	21	20	22	24	30	29	30	29	31	32
3835.893	8	8	8	10	11	12	14	15	18	21	23	24	26
3835.895	9	7	6	6	6	7	7	8	10	10	12	11	13
3835.897	13	12	9	9	8	7	8	6	6	6	7	7	9
3835.899	25	19	16	15	14	12	11	11	10	10	9	8	8
3835.901	29	25	26	29	25	20	21	18	16	15	14	14	13
3835.903	29	28	33	35	32	30	30	28	25	24	23	21	20
3835.905	51	56	51	36	30	32	30	29	31	33	31	28	28

APPENDIX X: Probe permeameter data sets

MINIPERMEAMETER PERMEABILITIES (mD)

CORE 4
3811.270-.320 m

Fine grid "E"

Profile No.	1	2	3	4	5	6	7	8	9	10	11
Fine grid offset (m)	0.000	0.002	0.004	0.006	0.008	0.010	0.012	0.014	0.016	0.018	0.020
Coarse grid offset (m)	0.009	0.011	0.013	0.015	0.017	0.019	0.021	0.023	0.025	0.027	0.029
Core Depth (mMD)											
3811.270	490	506	423	376	385	397	327	365	379	364	304
3811.272	507	451	437	385	329	302	300	252	289	283	284
3811.274	434	395	381	357	323	291	296	272	295	348	359
3811.276	416	407	439	430	395	326	315	321	358	398	334
3811.278	540	519	462	487	439	410	315	370	396	328	332
3811.280	577	436	361	371	369	388	316	334	376	302	301
3811.282	460	473	469	367	341	368	322	321	310	291	221
3811.284	402	431	399	300	293	317	224	223	239	237	219
3811.286	327	347	339	238	312	291	240	237	227	183	204
3811.288	392	332	305	237	347	286	329	343	301	271	232
3811.290	407	337	280	273	393	437	383	385	414	424	341
3811.292	405	376	349	371	416	437	381	427	510	450	470
3811.294	376	428	429	430	407	339	397	415	468	408	466
3811.296	402	431	450	458	401	347	323	372	371	333	335
3811.298	396	371	400	410	355	317	311	280	231	237	215
3811.300	359	315	332	343	316	314	363	287	199	190	164
3811.302	296	286	243	235	268	235	236	172	135	116	107
3811.304	211	214	176	168	130	123	125	112	97	99	89
3811.306	151	118	116	106	96	100	94	82	86	89	75
3811.308	116	115	103	88	83	79	74	68	72	72	75
3811.310	110	103	96	86	72	72	78	74	75	73	74
3811.312	92	93	90	85	84	84	89	86	74	73	74
3811.314	91	89	93	89	81	91	94	95	87	75	81
3811.316	91	86	86	87	86	94	90	93	85	81	83
3811.318	97	88	75	81	89	86	86	87	89	78	77
3811.320	95	95	80	75	81	79	74	88	84	82	98

CORE 4
3809.335-.435 m

Fine grid "F"

Profile No.	1	2	3	4	5	6	7	8	9	10	11
Fine grid offset (m)	0.000	0.002	0.004	0.006	0.008	0.010	0.012	0.014	0.016	0.018	0.020
Coarse grid offset (m)	-0.004	-0.002	0.000	0.002	0.004	0.006	0.008	0.010	0.012	0.014	0.016
Core Depth (mMD)											
3809.335	129	141	128	136	144	136	119	114	106	114	118
3809.337	148	134	145	145	162	146	137	113	114	113	114
3809.339	155	134	147	164	159	143	144	135	126	126	134
3809.341	163	164	189	174	149	159	141	142	144	145	161
3809.343	161	154	187	176	148	139	155	150	146	160	149
3809.345	156	148	149	163	150	140	140	165	178	194	190
3809.347	171	173	179	182	155	142	161	168	215	233	214
3809.349	189	187	198	185	192	204	189	220	286	246	217
3809.351	196	196	203	202	229	231	216	222	205	236	232
3809.353	195	202	223	237	246	222	241	233	218	209	212
3809.355	240	245	241	231	226	226	205	228	227	193	204
3809.357	239	241	220	223	206	201	179	189	179	174	175
3809.359	248	230	223	206	181	183	178	144	144	158	177
3809.361	189	200	177	165	145	138	132	153	133	155	161
3809.363	169	166	172	165	167	164	166	208	166	147	145
3809.365	192	184	181	175	173	164	151	143	155	142	119
3809.367	180	168	166	172	149	140	145	143	137	133	122
3809.369	171	147	155	176	174	172	156	141	142	143	139
3809.371	194	169	170	176	179	175	145	132	120	129	129
3809.373	184	176	175	201	188	164	143	127	108	111	127
3809.375	193	184	185	181	188	146	142	130	126	131	140
3809.377	196	191	183	168	181	153	136	140	147	138	141
3809.379	207	195	175	179	190	147	136	141	135	154	160
3809.381	220	214	187	167	185	176	150	142	142	154	153
3809.383	191	194	172	144	160	148	141	131	126	112	103
3809.385	163	140	136	133	142	131	119	115	110	107	112
3809.387	130	121	134	134	127	126	130	128	110	100	109
3809.389	124	124	142	143	120	123	128	125	112	115	119
3809.391	125	125	137	136	134	147	139	127	136	133	142
3809.393	181	172	174	192	181	184	178	171	149	157	145
3809.395	216	227	223	204	206	170	171	172	142	139	134
3809.397	245	223	194	194	197	162	150	159	140	145	133
3809.399	248	229	192	148	160	150	138	125	130	124	113
3809.401	190	181	152	134	123	124	127	123	124	111	121
3809.403	150	154	139	147	128	127	150	147	134	135	132
3809.405	146	173	175	162	149	156	161	174	165	146	130
3809.407	160	211	201	189	178	192	193	188	190	173	154
3809.409	196	240	203	205	220	210	188	176	179	181	168
3809.411	241	228	221	214	217	184	171	163	172	181	164
3809.413	241	237	203	209	201	187	175	182	199	183	183
3809.415	223	228	229	202	202	197	184	197	203	164	157
3809.417	229	232	216	193	205	192	181	188	177	205	158
3809.419	220	215	187	185	172	195	193	183	190	185	199
3809.421	217	191	201	185	187	194	179	171	172	159	158
3809.423	224	214	203	171	148	156	156	145	132	131	126
3809.425	194	149	162	147	123	137	132	116	100	95	112
3809.427	149	140	141	133	119	123	124	114	113	113	110
3809.429	147	141	144	132	122	124	117	110	109	107	108
3809.431	158	124	114	104	108	105	96	103	94	94	100
3809.433	125	107	108	100	99	100	110	111	107	107	113
3809.435	125	108	107	114	105	112	122	131	117	121	142

MINIPERMEAMETER PERMEABILITIES (mD)

CORE 4
3809.052-.100 m

Fine grid "G"

Profile No.	1	2	3	4	5	6	7	8	9	10	11
Fine grid offset (m)	0.000	0.002	0.004	0.006	0.008	0.010	0.012	0.014	0.016	0.018	0.020
Coarse grid offset (m)	0.007	0.009	0.011	0.013	0.015	0.017	0.019	0.021	0.023	0.025	0.027
Core Depth (mMD)											
3809.052	179	190	187	180	190	175	148	152	161	177	180
3809.054	189	214	227	179	153	180	179	153	154	176	189
3809.056	193	212	214	185	154	175	192	140	134	149	175
3809.058	193	206	176	174	163	160	154	144	136	128	125
3809.060	199	209	186	168	176	148	134	148	155	150	136
3809.062	218	217	208	198	165	169	147	145	177	173	132
3809.064	210	202	212	172	150	166	167	155	165	166	139
3809.066	275	226	203	150	150	161	179	202	173	150	145
3809.068	247	219	202	212	206	187	184	205	175	136	126
3809.070	216	339	254	226	199	185	178	188	168	163	145
3809.072	240	338	346	216	186	190	185	166	187	192	155
3809.074	245	232	238	299	220	192	179	186	188	193	160
3809.076	232	217	242	286	244	248	187	193	181	187	162
3809.078	221	242	290	211	245	294	222	192	188	197	186
3809.080	213	243	244	187	182	221	244	218	209	214	180
3809.082	190	206	237	217	205	210	240	253	221	207	187
3809.084	216	212	224	252	246	199	218	300	247	216	190
3809.086	199	240	206	229	249	209	218	245	225	231	199
3809.088	232	221	197	190	232	237	233	208	206	240	229
3809.090	313	206	197	213	191	218	216	209	223	236	289
3809.092	340	240	174	202	195	172	192	208	211	202	231
3809.094	308	314	242	244	204	198	193	224	230	223	209
3809.096	237	239	240	288	192	208	212	219	210	235	201
3809.098	240	212	224	223	202	213	209	216	193	210	196
3809.100	285	203	216	280	313	308	211	220	166	175	185

MINIPERMEAMETER PERMEABILITIES (mD)

CORE 4
3808.582-.632 m

Fine grid "H"

Profile No.	1	2	3	4	5	6	7	8	9	10	11
Fine grid offset (m)	0.000	0.002	0.004	0.006	0.008	0.010	0.012	0.014	0.016	0.018	0.020
Coarse grid offset (m)	0.042	0.044	0.046	0.048	0.050	0.052	0.054	0.056	0.058	0.060	0.062
Core Depth (mMD)											
3808.582	448	475	458	477	520	562	569	636	599	542	554
3808.584	469	484	517	482	482	559	572	601	588	601	604
3808.586	442	454	451	476	474	520	573	545	515	585	612
3808.588	404	445	462	509	539	570	583	571	621	579	605
3808.590	502	529	518	558	633	596	590	609	624	601	706
3808.592	609	598	595	630	707	632	646	658	629	718	781
3808.594	570	651	614	629	687	627	599	621	664	731	694
3808.596	546	573	546	512	549	532	530	571	548	541	571
3808.598	496	453	465	487	516	502	627	596	492	483	504
3808.600	479	542	538	505	548	625	693	679	630	666	606
3808.602	536	624	575	597	634	562	673	672	662	675	652
3808.604	578	574	554	557	561	551	576	507	477	511	555
3808.606	602	628	591	550	573	603	596	593	555	558	618
3808.608	679	593	578	542	583	581	543	566	541	541	581
3808.610	458	367	365	368	385	391	367	352	340	361	378
3808.612	247	238	197	181	213	216	221	206	216	224	219
3808.614	175	189	192	190	197	183	186	194	204	186	197
3808.616	164	178	186	194	197	178	194	202	196	190	237
3808.618	171	173	175	174	193	170	179	210	204	259	248
3808.620	154	159	157	181	185	176	150	199	214	225	291
3808.622	160	150	140	170	186	172	167	175	188	203	244
3808.624	161	153	142	161	181	163	183	170	182	210	242
3808.626	138	150	132	132	143	180	180	177	201	212	229
3808.628	127	117	120	141	129	134	162	176	185	190	205
3808.630	126	136	139	141	146	144	153	156	158	163	191
3808.632	119	130	141	145	146	138	150	153	153	160	189

X. 1. c 33/12-B9 - Coarse Grids - Cores 4, 5

MINIPERMEAMETER PERMEABILITIES (md)

CORE 4
3808.526-3809.456 m

Profile offset (m) / Core Depth(m)	0.00	0.02	0.06	0.08
3808.526	585	499	424	404
3808.536	401	419	330	319
3808.546	522	458	360	388
3808.556	559	523	485	653
3808.566	659	507	428	496
3808.576	664	573	445	491
3808.586	678	522	394	545
3808.596	691	533	479	505
3808.606	799	795	730	510
3808.616	198	159	165	227
3808.626	169	135	125	190
3808.636	172	149	133	170
3808.646	185	154	160	201
3808.656	205	174	183	209
3808.666				
3808.676				
3808.686				
3808.696				
3808.706				
3808.716				168
3808.726				164
3808.736			153	181
3808.746			194	187
3808.756				
3808.766				
3808.776				
3808.786	269			
3808.796	194	198	159	187
3808.806	199	173	176	158
3808.816	196	188	167	179
3808.826	181	176	158	175
3808.836	195	165	166	171
3808.846	200	170	131	175
3808.856	207	162	160	165
3808.866	206	183	131	186
3808.876	196	181	133	172
3808.886	216	151	131	195
3808.896	193	162	133	213
3808.906	178	185	208	218
3808.916	181	195		255
3808.926				
3808.936				
3808.946	182			
3808.956	275			
3808.966	164	191	182	
3808.976	183	156	217	
3808.986	240	171	220	306
3808.996	289	289		
3809.006				
3809.016				
3809.026	203	233	188	169
3809.036	245	209	169	192
3809.046	303	206	182	190
3809.056	337	205	178	163
3809.066	313	257	153	171
3809.076	379	262	133	184
3809.086	338	240	222	177
3809.096	211	261	234	191
3809.106	288	287	199	229
3809.116	396	226	266	277
3809.126	333	232	233	244
3809.136	292	241	202	303
3809.146	299	246	276	347
3809.156	311	290	264	344
3809.166	363	375	479	467
3809.176	453			581
3809.186				
3809.196				
3809.206	447			
3809.216				
3809.226				
3809.236			278	
3809.246				
3809.256				
3809.266	233	155	120	187
3809.276	197	195	181	191
3809.286	223	184	129	201
3809.296	219	204	188	215
3809.306	287	196	107	91
3809.316	129	93	86	110
3809.326	153	117	81	98
3809.336	121	115	102	155
3809.346	188	236	191	201
3809.356	278	208	126	150
3809.366	194	124	115	121
3809.376	195	131	118	121
3809.386	144	111	130	179
3809.396	239	122	103	153
3809.406	205	166	195	194
3809.416	246	182	173	123
3809.426	174	105	111	170
3809.436	168	167	218	223
3809.446	232	176	182	184
3809.456	128	161	222	207

MINIPERMEAMETER PERMEABILITIES (md)

CORE 4
3809.514-3810.404 m

Profile offset (m) / Core Depth(m)	0.00	0.02	0.04	0.06
3809.52			105	
3809.53	170			158
3809.54				154
3809.55				72
3809.56				209
3809.57				198
3809.58				171
3809.59				161
3809.60				292
3809.61				
3809.62				
3809.63	207	162	149	118
3809.64	133	175	148	167
3809.65	248	230	210	167
3809.66	202	215	163	213
3809.67	293	223	138	192
3809.68	194	202	166	159
3809.69	227	169	141	163
3809.70	206	239	171	210
3809.71	147	187	147	146
3809.72	297	163	248	235
3809.73	275	277	218	193
3809.74	228	215	159	188
3809.75	293	200	149	152
3809.76	216	259	228	231
3809.77	235	242	237	251
3809.78	173	282	318	314
3809.79				
3809.80				
3809.81				
3809.82			192	147
3809.83			299	
3809.84				182
3809.85				171
3809.86				214
3809.87				
3809.88		191		
3809.89		151		
3809.90				
3809.91				
3809.92				
3809.93				
3809.94			249	
3809.95			328	
3809.96	239	171	323	369
3809.97	183	256	349	395
3809.98				
3809.99				
3810.00				
3810.01				
3810.02	213	200	169	165
3810.03	228	225	173	165
3810.04	216	153	168	165
3810.05	252	199	178	208
3810.06	199	173	167	214
3810.07	170	143	126	184
3810.08	176	127	126	181
3810.09	168	149	164	177
3810.10	144	171	163	198
3810.11	172	216	204	225
3810.12				
3810.13				
3810.14				
3810.15				
3810.16		386		
3810.17	398			
3810.18	289			
3810.19				
3810.20				
3810.21				
3810.22				
3810.23	326	199	207	245
3810.24	363	183	208	236
3810.25	348	227	193	109
3810.26	384	217	123	203
3810.27	291	115	118	215
3810.28	258	116	171	237
3810.29	236	244	323	219
3810.30	337	313	325	187
3810.31	368	284	166	209
3810.32	392	219	207	211
3810.33	240	191	243	178
3810.34	237	250	152	245
3810.35	346	203	166	166
3810.36	259	162	157	218
3810.37	215	183	162	195
3810.38	230	160	200	201
3810.39	240	218	231	170
3810.40		258	255	255

APPENDIX X: Probe permeameter data sets

MINIPERMEAMETER PERMEABILITIES (md)

CORE 4
3810.565-3811.465 m

Profile offset (m) / Core Depth(m)	0.00	0.02	0.04	0.06
3810.565				164
3810.575				159
3810.585	166			226
3810.595				
3810.605				
3810.615	123	109	118	
3810.625	196	128	125	160
3810.635	192	117	121	120
3810.645	196	154	110	126
3810.655	260	215	179	213
3810.665	269	197	167	222
3810.675	215	156	127	192
3810.685	237	171	128	198
3810.695	204	169	172	209
3810.705	222	172	188	218
3810.715	197	130	165	192
3810.725	205	152	157	185
3810.735	204	173	160	198
3810.745	196	210	195	192
3810.755	196	175	178	204
3810.765	226	183	129	252
3810.775	258	215	229	327
3810.785				
3810.795				254
3810.805	292		222	214
3810.815	239	233	209	222
3810.825	216	244	208	167
3810.835			276	196
3810.845				189
3810.855				328
3810.865				
3810.875				
3810.885	226	195	149	283
3810.895	326	340	231	341
3810.905	313	288	227	386
3810.915	330	269	186	283
3810.925	326	237	157	264
3810.935	272	192	250	348
3810.945	401	281	211	344
3810.955	282	253	260	452
3810.965	163	255		437
3810.975				
3810.985		658	600	
3810.995	397	359	491	527
3811.005				
3811.015				
3811.025				
3811.035				
3811.045				
3811.055				
3811.065				
3811.075				
3811.085				
3811.095	300	330		
3811.105	169	283	193	281
3811.115		403		322
3811.125				402
3811.135				406
3811.145				
3811.155				
3811.165			190	242
3811.175		191	309	284
3811.185	264	220	383	277
3811.195	255	200	328	385
3811.205	354	282	311	314
3811.215	314	220	252	322
3811.225	347	257	409	572
3811.235	531	319	356	480
3811.245	529	414	357	350
3811.255	428	363	413	358
3811.265	467	320	460	339
3811.275	408	297	281	284
3811.285	317	349	288	86
3811.295	315	117	76	73
3811.305	117	85	83	
3811.315	96	90	191	101
3811.325	160	411	111	117
3811.335	123	114	96	114
3811.345	155	99	103	105
3811.355	112	103	103	100
3811.365	122	112	94	126
3811.375	105	94	165	163
3811.385			195	171
3811.395				
3811.405				
3811.415				
3811.425				
3811.435				
3811.445	183			124
3811.455	266			165
3811.465	281			172

MINIPERMEAMETER PERMEABILITIES (md)

CORE 4
3811.528-3812.428 m

Profile offset (m) / Core Depth(m)	0.00	0.02	0.04	0.06
3811.528	191	162	148	117
3811.538	160	117	98	95
3811.548	214	188	145	146
3811.558	268	272	157	165
3811.568	284	233	171	171
3811.578	150	145	107	116
3811.588	217	154	190	179
3811.598	149	142	123	151
3811.608	177	166	159	191
3811.618	215	227	273	239
3811.628	105	123	147	170
3811.638	179	235	281	387
3811.648				216
3811.658				
3811.668			195	198
3811.678		173	207	287
3811.688	347	384	333	292
3811.698	272	301		
3811.708				
3811.718	173	149	173	135
3811.728	250			170
3811.738	258			211
3811.748	492			273
3811.758	236			302
3811.768	238	285	266	784
3811.778	194	208	202	
3811.788				
3811.798		119		
3811.808	173	166	126	158
3811.818	294	193	112	149
3811.828	235	154	126	195
3811.838	321	158	107	187
3811.848	256	219	156	205
3811.858	216	235	123	111
3811.868	172	158	121	103
3811.878	164	101	109	183
3811.888	173	121	115	168
3811.898	123	173	230	161
3811.908				
3811.918				
3811.928			163	
3811.938				
3811.948		151		
3811.958		469	365	
3811.968	377	401		
3811.978	279	292		
3811.988	482	572		
3811.998				
3812.008				
3812.018	238	153	170	185
3812.028	284	200	206	194
3812.038	252	197	189	193
3812.048	211	175	220	189
3812.058	201	98	97	84
3812.068	190	115	120	94
3812.078	155	110	101	89
3812.088	210	164	153	148
3812.098	183	204	175	146
3812.108	167	188	160	153
3812.118	120	207	202	197
3812.128	114	115	142	116
3812.138	84	122	167	118
3812.148	87	115	116	163
3812.158	109	146	165	156
3812.168	109	115	124	125
3812.178	181	126	155	208
3812.188	137	122	226	211
3812.198	29	54	77	94
3812.208	26	29	41	48
3812.218		14	18	40
3812.228				
3812.238				
3812.248				
3812.258				
3812.268				
3812.278				
3812.288				
3812.298				
3812.308	193	229		
3812.318	243	195	270	224
3812.328	360	263	221	156
3812.338	323	218	218	207
3812.348	305	233	242	201
3812.358	234	166	176	210
3812.368	420	304	311	266
3812.378	295	250	226	189
3812.388	258	220	222	277
3812.398	319	231	226	289
3812.408	244	167	188	217
3812.418	263	171	175	206
3812.428	109	180	144	181
3812.438	138	175	192	196
3812.448	84	118	145	162
3812.458	90	95	96	119

APPENDIX X: Probe permeameter data sets

MINIPERMEAMETER PERMEABILITIES (md)

CORE 5
3835.027-3835.957 m

Profile offset (m) / Core Depth(m)	0.00	0.02	0.04	0.06
3835.027	90	96	77	88
3835.037	207	191	113	122
3835.047	331	350	310	400
3835.057	144	101	86	94
3835.067	176	116	100	121
3835.077	236	169	143	199
3835.087	174	118	100	155
3835.097	100	91	88	94
3835.107	99	94	96	103
3835.117	78	83	90	96
3835.127	149	146	169	173
3835.137	114	149	164	176
3835.147				
3835.157				
3835.167	197	181		
3835.177	241	192		
3835.187	74	70		
3835.197	145	119	112	255
3835.207		239	156	262
3835.217		162	191	
3835.227				139
3835.237		243	178	164
3835.247		115	118	120
3835.257	120	146	117	99
3835.267	117	158	169	160
3835.277	202	255	251	181
3835.287	253	196	108	86
3835.297	164	202	151	147
3835.307	237	153	121	106
3835.317	181	92	78	99
3835.327	151	108	103	110
3835.337	202	154	111	113
3835.347	154	101	100	196
3835.357	223	147	112	177
3835.367	148	99	101	163
3835.377	138	117	156	206
3835.387	177	125	178	197
3835.397	183	112	145	145
3835.407	108	108	173	190
3835.417	153	235	336	370
3835.427	227	287		
3835.437				
3835.447	164	169		
3835.457	239	251		
3835.467	251	271		
3835.477	168	179		
3835.487	332	342	268	
3835.497	406	341	305	368
3835.507	210	173	165	153
3835.517	199	141	156	122
3835.527	143	104	124	123
3835.537	224	241	243	251
3835.547	116	114	168	154
3835.557				
3835.567				
3835.577				
3835.587	227	236	198	169
3835.597	180	189	185	165
3835.607	163	155	106	92
3835.617	175	175	117	104
3835.627	239	253	154	144
3835.637	219	244	197	220
3835.647	200	176	164	207
3835.657	153	143	141	166
3835.667	78	167	175	224
3835.677	68	222	232	242
3835.687	63	170	197	162
3835.697	176	199	214	186
3835.707	252	222	204	237
3835.717	277	231	239	265
3835.727	194	239	245	287
3835.737				
3835.747	249			
3835.757	187	202	180	179
3835.767	121	137	118	122
3835.777	285			
3835.787	227			
3835.797				
3835.807			162	179
3835.817			255	272
3835.827				
3835.837				
3835.847	50			
3835.857	24	35	41	39
3835.867	22	36	13	24
3835.877	23	7	6	26
3835.887	15	27	31	11
3835.897	71	31	11	16
3835.907	33	85	80	38
3835.917	34	17	23	28
3835.927	19	41	55	30
3835.937	73	34	24	28
3835.947	113	113	110	56
3835.957	31	41	76	100

MINIPERMEAMETER PERMEABILITIES (md)

CORE 5
3836 012-3836 972 m

Profile offset (m) / Core Depth(m)	0.00	0.02	0.04	0.06
3836.012	124			
3836.022	144	127		
3836.032				
3836.042	90	68	46	30
3836.052	60	64	58	65
3836.062	140	92	39	32
3836.072		79	74	103
3836.082			54	55
3836.092			18	17
3836.102		44	52	69
3836.112		106	115	88
3836.122	58	66	63	76
3836.132	108	117	91	83
3836.142	109	112	99	80
3836.152	169			
3836.162				
3836.172	166	169	174	163
3836.182	96	59	62	72
3836.192	116	144	114	93
3836.202	103	111	111	109
3836.212	166	182	176	164
3836.222	204	242	216	181
3836.232	98	80	98	143
3836.242	119	148	122	167
3836.252	184	146	90	83
3836.262	79	55	38	73
3836.272	44	30	29	33
3836.282	54	65	80	104
3836.292	121	114	106	123
3836.302	87	83	71	68
3836.312	56	76	108	125
3836.322	211	188	187	198
3836.332	110	85	104	121
3836.342	149	176	193	286
3836.352	260	285		302
3836.362				
3836.372	75		58	66
3836.382	78	68	55	68
3836.392	120	99	77	87
3836.402	222	144	96	72
3836.412				
3836.422				
3836.432			55	84
3836.442				
3836.452				
3836.462				
3836.472			284	237
3836.482		284	237	153
3836.492		236	206	152
3836.502		207	200	141
3836.512		191	124	74
3836.522		66	93	94
3836.532		100	140	158
3836.542		218	101	94
3836.552		86	145	168
3836.562		150	187	224
3836.572		189	155	107
3836.582		100	173	
3836.592				
3836.602				
3836.612				
3836.622		202	179	166
3836.632		105	105	151
3836.642		227	199	168
3836.652				
3836.662				
3836.672		10	8	9
3836.682			17	17
3836.692				
3836.702				
3836.712				
3836.722				
3836.732		14	17	16
3836.742		6	5	5
3836.752		4	4	5
3836.762		47	61	51
3836.772		74	81	87
3836.782		260	250	252
3836.792		52	19	15
3836.802		7	11	11
3836.812		61	64	70
3836.822		115	99	136
3836.832		229	226	
3836.842		398	400	399
3836.852			369	316
3836.862		41	54	53
3836.872		192	210	
3836.882		302	201	156
3836.892		195	123	121
3836.902		191	232	251
3836.912		123	109	143
3836.922		191	188	143
3836.932	188	230	188	
3836.942	190	122	174	
3836.952	140	125	154	
3836.962	141	124	153	
3836.972	144	137	154	

APPENDIX X: Probe permeameter data sets

MINIPERMEAMETER PERMEABILITIES (md)

CORE 5
3837.025-3837.935 m

Profile offset (m) / Core Depth(m)	0.00	0.02	0.04	0.06
3837.025				
3837.035				
3837.045				
3837.055				
3837.065	19	11	8	
3837.075	62	62	60	46
3837.085	42	30	40	40
3837.095	162	175	174	152
3837.105	70	110	160	143
3837.115	27	31	27	27
3837.125	15	11	25	46
3837.135	96	87	81	77
3837.145	64	63	65	72
3837.155	162	166	152	111
3837.165	279	313	338	269
3837.175	89	144	154	108
3837.185	13	11	4	7
3837.195	24	24	25	14
3837.205	5	5	6	8
3837.215	11	16	19	14
3837.225	43	35	18	13
3837.235	51	43	36	34
3837.245	80	63	53	48
3837.255	56	48	52	55
3837.265		218	183	143
3837.275				215
3837.285				
3837.295	152	175	217	
3837.305				
3837.315				
3837.325				
3837.335	116	107	93	58
3837.345	25	19	19	34
3837.355	108	97	71	50
3837.365	49	32	25	49
3837.375	52	36	36	57
3837.385	120	105	72	67
3837.395	114	156	115	107
3837.405	119	138	103	77
3837.415	104	116	94	68
3837.425	84	47	49	52
3837.435	103	86	97	83
3837.445	117	104	78	80
3837.455	149	118	97	92
3837.465	49	39	37	54
3837.475	36	39	43	44
3837.485	118	84	46	32
3837.495	90	175	121	81
3837.505	62	60	43	72
3837.515	147	51	30	54
3837.525	78	116	114	85
3837.535	558	94	77	67
3837.545	72	77	111	107
3837.555			88	76
3837.565				
3837.575				
3837.585	104			
3837.595				
3837.605				
3837.615				
3837.625				
3837.635		260	176	122
3837.645	231	242	231	162
3837.655	297	355	329	280
3837.665	425	495	430	313
3837.675	395	432	363	348
3837.685	481	488	409	328
3837.695	320	278	202	229
3837.705	409	344	347	360
3837.715	399	365	348	392
3837.725	347	287	301	364
3837.735	540	492	377	424
3837.745	310	252	249	259
3837.755	353	256	278	332
3837.765	416	387	393	386
3837.775	509	525	461	478
3837.785	379	397	353	422
3837.795	451	401	405	476
3837.805	359	342	366	475
3837.815	356	454	386	571
3837.825	370	592	547	679
3837.835				
3837.845	434		478	
3837.855	367	407		
3837.865	557	513		
3837.875	583	394		
3837.885	480	321		
3837.895				
3837.905				
3837.915				
3837.925				
3837.935	10	365		

MINIPERMEAMETER PERMEABILITIES (md)

CORE 5
3838.017-3838.947 m

Profile offset (m) / Core Depth(m)	0.00	0.02	0.04	0.06
3838.017	370	350	235	
3838.027	526	433	272	246
3838.037	422	393	333	356
3838.047	290	205	177	195
3838.057	485	395	307	355
3838.067	296	241	225	259
3838.077	374	363	404	422
3838.087				
3838.097	252	217	174	195
3838.107	103	110	96	99
3838.117	198	163	184	175
3838.127	290	271	271	277
3838.137	361	370	351	319
3838.147			498	544
3838.157				
3838.167				
3838.177	285	259		
3838.187	380	374		
3838.197	489	493		
3838.207				
3838.217	407	378	257	
3838.227	295	233	180	148
3838.237	394	296	280	247
3838.247	317	241	281	264
3838.257	360	300	281	226
3838.267	378	303	286	217
3838.277	345	321	286	235
3838.287	424	375	329	231
3838.297	449	337	246	270
3838.307	358	310	346	359
3838.317	408	280	326	303
3838.327	421	433	475	405
3838.337	276	401	451	398
3838.347	167	283	233	260
3838.357	3	2	5	81
3838.367			3	2
3838.377				
3838.387	14	33	14	51
3838.397	3	3	6	8
3838.407	2	4	16	10
3838.417	5	5	5	4
3838.427				5
3838.437				
3838.447				
3838.457				
3838.467				
3838.477	42	59		
3838.487	12	11	15	17
3838.497	46	43	33	34
3838.507	86	72	64	54
3838.517	82	73	65	64
3838.527	183	196	151	74
3838.537	18	17	15	14
3838.547	67	65	58	43
3838.557	11	10	14	14
3838.567	13	14	13	10
3838.577	9	13	10	10
3838.587	39	42	43	34
3838.597	38	37	45	35
3838.607	9	3	3	3
3838.617	2	2	3	3
3838.627	10	10	9	8
3838.637	3	3	2	3
3838.647	6	6	5	5
3838.657	28	32	21	21
3838.667	19	17	15	16
3838.677	19	17	23	23
3838.687	38	35	26	32
3838.697	20	19	17	19
3838.707	34	28	25	22
3838.717	27	24	24	28
3838.727	30	27	28	31
3838.737				
3838.747	106	90	74	65
3838.757		20	21	22
3838.767			25	23
3838.777				
3838.787	10	9	8	7
3838.797	36	29	16	13
3838.807	3	4	19	36
3838.817	9	7	7	7
3838.827	14	15	12	8
3838.837	25	17	14	11
3838.847	13	13	15	33
3838.857	26	24	26	28
3838.867	12	13	13	12
3838.877	13	12	10	9
3838.887	26	28	28	27
3838.897	11	11	10	12
3838.907	49	42	36	33
3838.917	17	14	18	19
3838.927	51	42	43	57
3838.937	20	19	21	32
3838.947	53	47	46	42

X. 1. Thistle

X. 2. a Thistle study calibration data

Hassler cell permeability (md)	Minipermeameter injection pressure (mbar)	Minipermeameter flow rate (cc/min)
280	30	20
879	30	49.8
1225	30	73.4
2020	30	104
4300	30	231
33.7	90	8.1
94	90	21
280	90	54.4
879	90	135
1225	90	209
2020	90	271
1.04	400	4.6
2.16	400	5.4
6.8	400	9.5
13.7	400	12.9
33.7	400	29.1
94	400	91.1
280	400	226
879	232	300
1225	140	300
2020	108	300
4300	41.7	300
879	334	400
1225	195	400
2020	155	400
4300	60.2	400
879	419	500
1225	250	500
2020	203	500
4300	80.4	500

X. 2. b Thistle A31 - Blocks

A.1.2 Profile

Spacing (cm)	Vertical Profile Perm. (mD)	S.D. (mD)
0.00	17	15
0.20	31	21
0.40	192	89
0.60	304	38
0.80	228	78
1.00	204	92
1.20	327	151
1.40	682	34
1.60	800	52
1.80	654	81
2.00	449	105
2.20	200	21
2.40	132	5
2.60	92	33
2.80	115	60
3.00	440	74
3.20	636	73
3.40	619	34
3.60	480	28
3.80	501	48
4.00	448	10
4.20	394	40
4.40	346	66
4.60	211	30
4.80	166	16
5.00	263	12
5.20	357	17
5.40	446	50
5.60	850	132
5.80	1260	21
6.00	1233	108
6.20	1185	57
6.40	1161	40
6.60	1116	68
6.80	969	144
7.00	1018	96
7.20	867	59
7.40	650	194
7.60	591	126
7.80	748	37
8.00	820	74
8.20	923	63
8.40	850	116
8.60	479	84
8.80	245	18
9.00	189	24
9.20	155	96
9.40	566	70
9.60	698	101
9.80	647	178
10.00	691	19
10.20	804	60
10.40	675	138

10.60	456	92
10.80	691	19
	Horizontal profile	
3.50	508	75
4.00	498	66
4.50	313	61
5.00	251	44
5.50	737	166

B.1.2 Profile

Vertical Profile	
Spacing (cm)	Perm. (mD)
0.00	87
0.50	102
1.00	99
1.50	109
2.00	89
2.50	93
3.00	88
3.50	71
4.00	104
4.50	94
5.00	62
5.50	102
6.00	118
6.50	108
7.00	98
7.50	96
8.00	114
8.50	112
9.00	68
9.50	67
10.00	75

B.1.3 Profile

	Vertical Profile	
Spacing (cm)	Perm. (mD)	S.D. (mD)
0.00	46	1.0
0.20	39	6.9
0.40	32	1.4
0.60	32	3.8
0.80	16	0.4
1.00	12	0.2
1.20	9	0.3
1.40	11	0.4
1.60	13	1.2
1.80	11	0.2
2.00	11	0.1
2.20	16	0.6
2.40	27	2.2
2.60	28	3.4
2.80	14	0.3
3.00	13	0.5
3.20	17	0.3

3.40	19	0.9
3.60	16	1.3
3.80	28	3.2
4.00	51	4.5
4.20	47	2.0
4.40	28	1.3
4.60	24	3.2
4.80	35	0.8
5.00	28	1.3
5.20	26	0.9
5.40	22	1.5
5.60	20	0.8
5.80	25	0.9
6.00	25	0.3
	Horizontal	
3.50	16	1.1
4.00	48	4.2
4.50	21	3.0

X. 2. c Thistle A31 - 0.5cm spacing data

COLUMN A
10048.06-1077.54 ft

Cor.Dpth(m)	Depth(ft)	Perm(md)
3062.650	10048.06	4751.5
3062.655	10048.08	3111.9
3062.660	10048.10	4452.0
3062.665	10048.11	4248.0
3062.670	10048.13	3173.7
3062.675	10048.15	3968.2
3062.680	10048.16	3459.8
3062.685	10048.18	3563.6
3062.690	10048.20	3173.4
3062.695	10048.21	3305.1
3062.700	10048.23	988.9
3062.720	10048.29	1190.9
3062.725	10048.31	2059.0
3062.730	10048.33	2500.0
3062.735	10048.34	2937.8
3062.740	10048.36	3417.5
3062.745	10048.38	2464.8
3062.750	10048.39	1504.6
3062.755	10048.41	2374.5
3062.760	10048.43	3670.7
3062.765	10048.44	5861.6
3062.770	10048.46	2942.0
3062.775	10048.47	3279.9
3062.780	10048.49	3383.0
3062.785	10048.51	4688.7
3062.790	10048.52	6751.7
3062.795	10048.54	8606.5
3062.800	10048.56	4968.6
3062.805	10048.57	1604.4
3062.835	10048.67	937.0
3062.840	10048.69	1627.0
3062.845	10048.70	1324.8
3062.850	10048.72	368.1
3062.855	10048.74	653.8
3062.860	10048.75	911.2
3062.865	10048.77	1096.4
3062.870	10048.79	1051.8
3062.875	10048.80	1205.4
3062.880	10048.82	214.8
3062.885	10048.84	674.6
3062.890	10048.85	327.1
3062.895	10048.87	843.0
3062.900	10048.88	1315.9
3062.905	10048.90	785.4
3062.910	10048.92	658.6
3062.915	10048.93	928.8
3062.920	10048.95	797.8
3062.940	10049.02	909.7
3062.945	10049.03	1251.2
3062.950	10049.05	845.4
3062.955	10049.07	1324.8
3062.960	10049.08	2276.3
3062.965	10049.10	2118.7
3062.970	10049.11	2188.7
3062.975	10049.13	2480.8
3062.980	10049.15	2287.2
3062.985	10049.16	2696.1
3062.990	10049.18	2286.9
3062.995	10049.20	2112.9
3063.000	10049.21	2750.0
3063.005	10049.23	564.6
3063.010	10049.25	37.6
3063.020	10049.28	837.3
3063.025	10049.29	2108.2
3063.030	10049.31	2541.8
3063.035	10049.33	1651.5
3063.040	10049.34	1205.2
3063.045	10049.36	1283.7
3063.050	10049.38	1358.1
3063.055	10049.39	512.2
3063.060	10049.41	346.2
3063.065	10049.43	267.2
3063.070	10049.44	151.8
3063.075	10049.46	137.1
3063.080	10049.48	189.6
3063.085	10049.49	158.4
3063.090	10049.51	232.6
3063.095	10049.52	115.9
3063.100	10049.54	52.9
3063.105	10049.56	332.0
3063.110	10049.57	165.5
3063.135	10049.66	14.8
3063.140	10049.67	26.8
3063.145	10049.69	100.4
3063.150	10049.71	312.5
3063.155	10049.72	244.2
3063.160	10049.74	12.9
3063.165	10049.75	14.3
3063.170	10049.77	14.6
3063.175	10049.79	32.5
3063.180	10049.80	44.0
3063.185	10049.82	46.7
3063.190	10049.84	14.3
3063.195	10049.85	24.4
3063.230	10049.97	707.7
3063.235	10049.98	531.6
3063.240	10050.00	36.3
3063.245	10050.02	39.5

COLUMN B
10096.06-10123.95ft

Cor.Dpth(m)	Depth(ft)	Perm(md)
3077.280	10096.06	81.6
3077.285	10096.08	17.6
3077.290	10096.10	48.9
3077.295	10096.11	34.4
3077.300	10096.13	73.6
3077.305	10096.15	31.2
3077.310	10096.16	26.7
3077.335	10096.24	31.0
3077.340	10096.26	58.4
3077.345	10096.28	63.1
3077.350	10096.29	31.5
3077.355	10096.31	45.6
3077.360	10096.33	25.5
3077.365	10096.34	41.4
3077.370	10096.36	28.1
3077.375	10096.37	44.0
3077.385	10096.41	16.4
3077.390	10096.42	14.1
3077.395	10096.44	105.4
3077.400	10096.46	98.6
3077.405	10096.47	19.1
3077.410	10096.49	17.9
3077.415	10096.51	17.6
3077.420	10096.52	6.2
3077.425	10096.54	6.3
3077.430	10096.56	11.3
3077.435	10096.57	7.2
3077.440	10096.59	9.8
3077.445	10096.60	4.5
3077.450	10096.62	10.2
3077.455	10096.64	7.3
3077.475	10096.70	12.3
3077.480	10096.72	15.5
3077.485	10096.74	8.3
3077.490	10096.75	29.0
3077.495	10096.77	3.0
3077.500	10096.79	2.9
3077.505	10096.80	4.4
3077.510	10096.82	6.4
3077.515	10096.83	6.0
3077.520	10096.85	7.1
3077.525	10096.87	3.7
3077.530	10096.88	13.2
3077.535	10096.90	3.3
3077.540	10096.92	4.6
3077.545	10096.93	8.4
3077.550	10096.95	16.5
3077.555	10096.97	17.5
3077.560	10096.98	5.2
3077.565	10097.00	15.4
3077.630	10097.21	6.5
3077.640	10097.24	6.2
3077.645	10097.26	27.8
3077.650	10097.28	17.5
3077.655	10097.29	8.3
3077.660	10097.31	30.0
3077.665	10097.33	11.4
3077.670	10097.34	20.6
3077.695	10097.42	24.2
3077.700	10097.44	11.6
3077.705	10097.46	6.7
3077.710	10097.47	12.1
3077.715	10097.49	27.1
3077.720	10097.51	30.4
3077.725	10097.52	19.3
3077.730	10097.54	10.9
3077.735	10097.56	58.4
3077.740	10097.57	29.5
3077.745	10097.59	45.2
3077.750	10097.61	10.3
3077.755	10097.62	10.7
3077.760	10097.64	8.0
3077.765	10097.65	7.7
3077.770	10097.67	12.8
3077.775	10097.69	23.4
3077.780	10097.70	27.1
3077.785	10097.72	38.5
3077.790	10097.74	47.0
3077.795	10097.75	40.6
3077.800	10097.77	33.3
3077.840	10097.90	59.6
3077.845	10097.92	61.1
3077.850	10097.93	99.6
3077.855	10097.95	26.3
3077.880	10098.03	43.7
3077.885	10098.05	37.5
3077.890	10098.06	32.3
3077.895	10098.08	13.7
3077.900	10098.10	29.5
3077.905	10098.11	54.2
3077.910	10098.13	59.5
3077.915	10098.15	26.2
3077.920	10098.16	25.2
3077.925	10098.18	22.6
3077.930	10098.20	72.9
3077.935	10098.21	28.8
3077.940	10098.23	38.1
3077.945	10098.25	44.8

COLUMN C
10124.08-10150.34ft

Cor.Dpth(m)	Depth(ft)	Perm(md)
3085.820	10124.08	92.7
3085.825	10124.10	41.6
3085.830	10124.11	21.1
3085.835	10124.13	38.5
3085.840	10124.15	31.1
3085.845	10124.16	37.5
3085.850	10124.18	69.3
3085.870	10124.25	78.3
3085.875	10124.26	29.3
3085.880	10124.28	39.3
3085.885	10124.29	70.9
3085.890	10124.31	64.8
3085.895	10124.33	43.7
3085.900	10124.34	58.7
3085.905	10124.36	32.3
3085.910	10124.38	66.6
3085.915	10124.39	47.1
3085.920	10124.41	7.1
3085.925	10124.43	12.0
3085.930	10124.44	15.6
3085.935	10124.46	29.4
3085.940	10124.48	13.7
3085.945	10124.49	7.9
3085.950	10124.51	12.4
3085.955	10124.52	16.5
3085.960	10124.54	8.1
3085.965	10124.56	38.2
3085.970	10124.57	45.8
3085.975	10124.59	27.6
3085.980	10124.61	11.0
3085.985	10124.62	5.2
3085.990	10124.64	19.2
3085.995	10124.66	13.6
3086.000	10124.67	11.0
3086.005	10124.69	36.6
3086.010	10124.71	19.0
3086.015	10124.72	28.3
3086.020	10124.74	5.2
3086.025	10124.75	7.5
3086.030	10124.77	4.7
3086.035	10124.79	14.6
3086.040	10124.80	13.2
3086.045	10124.82	19.1
3086.050	10124.84	28.2
3086.055	10124.85	43.9
3086.060	10124.87	11.1
3086.065	10124.89	18.5
3086.070	10124.90	11.5
3086.075	10124.92	7.0
3086.080	10124.93	15.6
3086.085	10124.95	16.1
3086.105	10125.02	27.7
3086.110	10125.03	13.4
3086.115	10125.05	6.3
3086.120	10125.07	8.1
3086.125	10125.08	9.6
3086.130	10125.10	14.3
3086.135	10125.12	10.6
3086.140	10125.13	11.1
3086.145	10125.15	38.9
3086.150	10125.16	14.2
3086.155	10125.18	21.4
3086.160	10125.20	17.3
3086.165	10125.21	20.5
3086.170	10125.23	46.3
3086.175	10125.25	33.8
3086.180	10125.26	14.0
3086.200	10125.33	34.7
3086.205	10125.34	9.4
3086.210	10125.36	12.2
3086.215	10125.38	12.8
3086.220	10125.39	7.7
3086.225	10125.41	6.9
3086.230	10125.43	7.1
3086.235	10125.44	9.1
3086.240	10125.46	13.8
3086.245	10125.48	12.4
3086.250	10125.49	6.5
3086.255	10125.51	12.8
3086.260	10125.53	9.7
3086.265	10125.54	6.7
3086.270	10125.56	18.3
3086.275	10125.57	17.0
3086.280	10125.59	13.8
3086.285	10125.61	8.1
3086.290	10125.62	10.8
3086.295	10125.64	13.2
3086.300	10125.66	13.2
3086.305	10125.67	11.8
3086.310	10125.69	23.2
3086.315	10125.71	14.2
3086.320	10125.72	23.5
3086.325	10125.74	21.4
3086.330	10125.75	14.9
3086.335	10125.77	13.9
3086.340	10125.79	7.5
3086.365	10125.87	21.1
3086.370	10125.89	27.9

COLUMN D
10150.36-10174.1 ft

Cor.Dpth(m)	Depth(ft)	Perm(md)
3093.830	10150.36	55.1
3093.835	10150.38	61.2
3093.840	10150.39	32.7
3093.845	10150.41	30.9
3093.850	10150.43	93.9
3093.855	10150.44	118.6
3093.860	10150.46	127.6
3093.865	10150.48	113.2
3093.870	10150.49	105.3
3093.875	10150.51	106.9
3093.880	10150.53	56.1
3093.885	10150.54	62.8
3093.890	10150.56	6.3
3093.895	10150.57	25.4
3093.900	10150.59	41.4
3093.905	10150.61	91.9
3093.910	10150.62	13.9
3093.915	10150.64	19.3
3093.920	10150.66	25.3
3093.925	10150.67	10.7
3093.930	10150.69	11.4
3093.935	10150.71	4.8
3093.950	10150.75	2.0
3093.960	10150.79	7.3
3093.965	10150.80	12.4
3093.970	10150.82	3.8
3093.975	10150.84	8.5
3093.980	10150.85	5.2
3094.070	10151.15	2.2
3094.125	10151.33	2.4
3094.130	10151.35	5.4
3094.150	10151.41	6.3
3094.155	10151.43	3.0
3094.160	10151.44	3.2
3094.175	10151.49	3.4
3094.200	10151.58	14.0
3094.205	10151.59	3.0
3094.210	10151.61	2.2
3094.215	10151.62	3.4
3094.235	10151.69	2.5
3094.240	10151.71	2.9
3094.250	10151.74	3.2
3094.290	10151.87	2.4
3094.320	10151.97	5.7
3094.325	10151.99	4.1
3094.330	10152.00	5.6
3094.335	10152.02	4.7
3094.340	10152.03	3.2
3094.345	10152.05	5.1
3094.355	10152.08	8.0
3094.360	10152.10	5.8
3094.365	10152.12	5.6
3094.370	10152.13	6.4
3094.385	10152.18	22.4
3094.390	10152.20	9.0
3094.395	10152.21	5.8
3094.400	10152.23	3.5
3094.415	10152.28	3.2
3094.430	10152.33	3.5
3094.435	10152.35	2.0
3094.440	10152.36	2.4
3094.445	10152.38	2.1
3094.460	10152.43	3.8
3094.465	10152.44	5.2
3094.470	10152.46	15.8
3094.475	10152.48	4.7
3094.480	10152.49	41.5
3094.485	10152.51	36.2
3094.490	10152.53	17.1
3094.495	10152.54	11.2
3094.500	10152.56	7.6
3094.505	10152.58	27.4
3094.510	10152.59	10.5
3094.515	10152.61	12.3
3094.520	10152.62	4.8
3094.530	10152.66	23.1
3094.535	10152.67	23.3
3094.540	10152.69	8.3
3094.545	10152.71	6.9
3094.550	10152.72	28.8
3094.555	10152.74	21.2
3094.560	10152.76	11.4
3094.565	10152.77	26.9
3094.570	10152.79	54.7
3094.575	10152.81	21.0
3094.580	10152.82	23.3
3094.585	10152.84	23.9
3094.590	10152.85	52.7
3094.595	10152.87	18.7
3094.600	10152.89	20.0
3094.605	10152.90	22.4
3094.610	10152.92	18.7
3094.615	10152.94	15.3
3094.620	10152.95	26.9
3094.625	10152.97	12.1
3094.630	10152.99	43.1
3094.635	10153.00	18.2
3094.650	10153.05	40.6

3063.250	10050.03	4.6
3063.255	10050.05	6.8
3063.260	10050.07	4.9
3063.265	10050.08	5.4
3063.270	10050.10	2.3
3063.275	10050.12	4.0
3063.290	10050.16	2.4
3063.300	10050.20	2.2
3063.345	10050.34	73.3
3063.350	10050.36	99.2
3063.355	10050.38	478.6
3063.360	10050.39	281.2
3063.365	10050.41	320.4
3063.370	10050.43	362.3
3063.375	10050.44	248.7
3063.380	10050.46	230.8
3063.385	10050.48	82.0
3063.390	10050.49	15.4
3063.395	10050.51	22.5
3063.400	10050.53	71.6
3063.405	10050.54	59.5
3063.410	10050.56	46.5
3063.415	10050.57	6.0
3063.420	10050.59	161.1
3063.425	10050.61	389.3
3063.430	10050.62	26.3
3063.435	10050.64	18.3
3063.440	10050.66	74.4
3063.445	10050.67	2.7
3063.450	10050.69	326.7
3063.455	10050.71	180.5
3063.460	10050.72	192.9
3063.465	10050.74	342.9
3063.470	10050.75	149.0
3063.475	10050.77	227.5
3063.480	10050.79	6.1
3063.485	10050.80	27.0
3063.490	10050.82	90.1
3063.495	10050.84	207.9
3063.500	10050.85	108.3
3063.510	10050.89	2.0
3063.675	10051.43	16.2
3063.680	10051.44	82.0
3063.685	10051.46	150.6
3063.690	10051.48	266.9
3063.695	10051.49	308.3
3063.700	10051.51	114.2
3063.705	10051.53	168.3
3063.710	10051.54	180.5
3063.715	10051.56	209.2
3063.720	10051.58	103.4
3063.725	10051.59	19.6
3063.730	10051.61	158.7
3063.735	10051.62	279.1
3063.740	10051.64	442.9
3063.745	10051.66	494.1
3063.750	10051.67	730.5
3063.755	10051.69	434.0
3063.760	10051.71	1013.8
3063.765	10051.72	289.8
3063.770	10051.74	551.2
3063.775	10051.76	75.2
3063.785	10051.79	15.8
3063.790	10051.80	7.1
3063.795	10051.82	13.1
3063.800	10051.84	66.7
3063.805	10051.85	121.2
3063.810	10051.87	166.1
3063.815	10051.89	41.2
3063.820	10051.90	101.8
3063.825	10051.92	26.2
3063.830	10051.94	151.2
3063.835	10051.95	201.8
3063.840	10051.97	208.1
3063.845	10051.99	232.2
3063.850	10052.00	236.2
3063.855	10052.02	307.1
3063.875	10052.08	63.9
3063.880	10052.10	98.9
3063.885	10052.12	70.3
3063.890	10052.13	72.3
3063.895	10052.15	95.7
3063.900	10052.17	489.6
3063.905	10052.18	526.4
3063.910	10052.20	51.2
3063.915	10052.21	72.3
3063.920	10052.23	53.8
3063.925	10052.25	174.1
3063.930	10052.26	69.5
3063.935	10052.28	104.4
3063.940	10052.30	157.1
3063.945	10052.31	183.5
3063.950	10052.33	368.4
3063.970	10052.40	22.8
3063.975	10052.41	528.1
3063.980	10052.43	604.3
3063.985	10052.44	86.7
3063.990	10052.46	71.1
3063.995	10052.48	93.3
3064.000	10052.49	61.8
3064.005	10052.51	11.4
3064.010	10052.53	155.6
3064.015	10052.54	138.8

3077.950	10098.26	31.8
3077.955	10098.28	60.7
3077.960	10098.29	38.4
3077.965	10098.31	29.0
3077.970	10098.33	42.2
3077.975	10098.34	45.8
3077.980	10098.36	60.4
3077.985	10098.38	55.4
3077.990	10098.39	36.8
3077.995	10098.41	29.2
3078.000	10098.43	26.5
3078.005	10098.44	75.6
3078.010	10098.46	34.4
3078.015	10098.47	56.5
3078.020	10098.49	43.5
3078.025	10098.51	47.5
3078.030	10098.52	28.7
3078.035	10098.54	59.3
3078.040	10098.56	43.8
3078.060	10098.62	41.6
3078.065	10098.64	80.8
3078.070	10098.66	36.5
3078.075	10098.67	41.2
3078.080	10098.69	39.4
3078.085	10098.70	89.7
3078.090	10098.72	72.5
3078.095	10098.74	44.2
3078.100	10098.75	94.6
3078.105	10098.77	42.7
3078.110	10098.79	39.9
3078.115	10098.80	63.4
3078.120	10098.82	86.1
3078.125	10098.84	88.9
3078.130	10098.85	30.1
3078.135	10098.87	22.7
3078.140	10098.88	35.5
3078.145	10098.90	45.9
3078.150	10098.92	80.6
3078.155	10098.93	70.7
3078.160	10098.95	78.3
3078.215	10099.13	48.2
3078.220	10099.15	50.7
3078.225	10099.16	48.0
3078.230	10099.18	121.9
3078.235	10099.20	70.3
3078.240	10099.21	119.9
3078.245	10099.23	105.1
3078.250	10099.25	60.9
3078.255	10099.26	56.7
3078.260	10099.28	80.2
3078.265	10099.29	88.7
3078.270	10099.31	53.8
3078.275	10099.33	39.9
3078.280	10099.34	67.8
3078.305	10099.43	39.0
3078.310	10099.44	55.4
3078.315	10099.46	91.8
3078.320	10099.48	67.8
3078.325	10099.49	72.3
3078.330	10099.51	85.8
3078.335	10099.52	75.8
3078.340	10099.54	108.3
3078.345	10099.56	103.3
3078.350	10099.57	99.2
3078.355	10099.59	81.2
3078.360	10099.61	122.4
3078.365	10099.62	89.6
3078.370	10099.64	71.1
3078.375	10099.66	90.5
3078.380	10099.67	58.4
3078.385	10099.69	89.0
3078.390	10099.71	91.0
3078.395	10099.72	44.7
3078.400	10099.74	118.5
3078.405	10099.75	82.3
3078.575	10100.31	142.2
3078.580	10100.33	78.1
3078.585	10100.34	49.1
3078.590	10100.36	66.6
3078.595	10100.38	91.6
3078.600	10100.39	77.8
3078.605	10100.41	84.3
3078.610	10100.43	160.4
3078.615	10100.44	63.2
3078.620	10100.46	53.9
3078.625	10100.48	62.2
3078.630	10100.49	92.7
3078.635	10100.51	79.3
3078.640	10100.53	70.1
3078.645	10100.54	132.1
3078.650	10100.56	59.9
3078.655	10100.57	61.6
3078.660	10100.59	58.8
3078.665	10100.61	76.0
3078.685	10100.67	60.1
3078.690	10100.69	133.4
3078.695	10100.71	167.5
3078.700	10100.72	176.9
3078.705	10100.74	84.3
3078.710	10100.75	149.3
3078.715	10100.77	58.6
3078.720	10100.79	92.8
3078.725	10100.80	101.3

3086.375	10125.90	18.7
3086.380	10125.92	38.1
3086.385	10125.94	27.3
3086.390	10125.95	14.0
3086.395	10125.97	11.9
3086.400	10125.98	24.1
3086.405	10126.00	13.5
3086.410	10126.02	18.6
3086.415	10126.03	14.8
3086.420	10126.05	17.7
3086.425	10126.07	20.5
3086.430	10126.08	23.0
3086.435	10126.10	20.9
3086.440	10126.12	21.9
3086.445	10126.13	35.3
3086.465	10126.20	45.4
3086.470	10126.21	26.2
3086.475	10126.23	81.7
3086.480	10126.25	11.5
3086.485	10126.26	15.2
3086.490	10126.28	28.2
3086.495	10126.30	59.2
3086.500	10126.31	18.0
3086.505	10126.33	17.1
3086.510	10126.35	13.9
3086.515	10126.36	17.2
3086.520	10126.38	26.5
3086.525	10126.39	14.2
3086.530	10126.41	13.8
3086.535	10126.43	22.6
3086.540	10126.44	13.5
3086.545	10126.46	23.5
3086.550	10126.48	36.8
3086.555	10126.49	25.3
3086.560	10126.51	20.7
3086.565	10126.53	33.8
3086.570	10126.54	25.0
3086.575	10126.56	19.6
3086.580	10126.58	38.2
3086.585	10126.59	23.5
3086.590	10126.61	19.9
3086.595	10126.62	66.5
3086.600	10126.64	15.2
3086.605	10126.66	13.6
3086.610	10126.67	68.2
3086.615	10126.69	18.5
3086.620	10126.71	36.1
3086.625	10126.72	44.3
3086.630	10126.74	28.1
3086.635	10126.76	22.9
3086.640	10126.77	61.0
3086.645	10126.79	26.0
3086.650	10126.80	34.3
3086.655	10126.82	64.5
3086.660	10126.84	66.5
3086.665	10126.85	55.5
3086.670	10126.87	24.4
3086.675	10126.89	30.3
3086.730	10127.07	39.7
3086.735	10127.08	72.6
3086.740	10127.10	39.3
3086.745	10127.12	34.7
3086.750	10127.13	28.8
3086.755	10127.15	87.1
3086.760	10127.17	31.9
3086.765	10127.18	27.2
3086.770	10127.20	24.4
3086.775	10127.21	24.0
3086.780	10127.23	57.5
3086.785	10127.25	16.0
3086.805	10127.31	30.3
3086.810	10127.33	23.0
3086.815	10127.35	23.8
3086.820	10127.36	39.7
3086.825	10127.38	48.4
3086.830	10127.40	29.2
3086.835	10127.41	40.9
3086.840	10127.43	38.3
3086.845	10127.44	42.4
3086.850	10127.46	23.0
3086.855	10127.48	32.0
3086.860	10127.49	83.3
3086.865	10127.51	36.7
3086.870	10127.53	39.6
3086.875	10127.54	64.5
3086.880	10127.56	55.1
3086.885	10127.58	44.2
3086.890	10127.59	35.3
3086.895	10127.61	21.0
3086.900	10127.62	36.2
3086.905	10127.64	31.8
3086.910	10127.66	14.9
3086.915	10127.67	40.1
3086.920	10127.69	21.0
3086.945	10127.77	9.2
3086.950	10127.79	3.6
3086.955	10127.81	3.2
3086.960	10127.82	2.9
3086.965	10127.84	3.1
3086.970	10127.85	3.8
3086.975	10127.87	8.4
3086.980	10127.89	8.6
3086.985	10127.90	5.6

3094.655	10153.07	9.2
3094.660	10153.08	10.7
3094.665	10153.10	4.1
3094.670	10153.12	3.8
3094.675	10153.13	19.1
3094.680	10153.15	5.0
3094.685	10153.17	2.9
3094.695	10153.20	2.1
3094.700	10153.22	2.5
3094.710	10153.25	26.4
3094.715	10153.26	33.6
3094.720	10153.28	24.7
3094.725	10153.30	13.5
3094.730	10153.31	8.0
3094.735	10153.33	4.9
3094.740	10153.35	4.5
3094.750	10153.38	2.2
3094.780	10153.48	56.6
3094.785	10153.49	17.4
3094.790	10153.51	3.4
3094.795	10153.53	3.8
3094.800	10153.54	4.5
3094.825	10153.63	16.4
3094.830	10153.64	10.8
3094.835	10153.66	14.7
3094.840	10153.67	8.6
3094.845	10153.69	4.2
3094.850	10153.71	8.5
3094.855	10153.72	18.1
3094.860	10153.74	13.5
3094.865	10153.76	9.8
3094.870	10153.77	30.5
3094.875	10153.79	12.8
3094.880	10153.81	12.4
3094.885	10153.82	11.4
3094.890	10153.84	25.9
3094.895	10153.86	12.5
3094.900	10153.87	39.2
3094.905	10153.89	41.6
3094.910	10153.90	41.7
3094.915	10153.92	32.7
3094.960	10154.07	18.6
3094.985	10154.15	54.2
3094.990	10154.17	54.9
3094.995	10154.18	30.9
3095.000	10154.20	67.1
3095.005	10154.22	28.2
3095.010	10154.23	78.3
3095.015	10154.25	62.6
3095.020	10154.27	42.1
3095.025	10154.28	34.2
3095.030	10154.30	45.1
3095.035	10154.31	28.8
3095.040	10154.33	68.9
3095.045	10154.35	43.0
3095.050	10154.36	57.1
3095.055	10154.38	45.9
3095.060	10154.40	25.7
3095.065	10154.41	34.8
3095.085	10154.48	42.8
3095.090	10154.50	46.3
3095.095	10154.51	29.4
3095.100	10154.53	45.2
3095.105	10154.54	41.2
3095.110	10154.56	35.9
3095.115	10154.58	18.8
3095.120	10154.59	10.3
3095.125	10154.61	17.1
3095.130	10154.63	6.3
3095.135	10154.64	33.3
3095.140	10154.66	21.8
3095.145	10154.68	4.0
3095.150	10154.69	8.6
3095.155	10154.71	7.4
3095.160	10154.72	6.1
3095.165	10154.74	3.1
3095.185	10154.81	33.6
3095.190	10154.82	9.6
3095.195	10154.84	60.7
3095.200	10154.86	11.6
3095.220	10154.92	65.5
3095.225	10154.94	27.6
3095.230	10154.95	14.4
3095.235	10154.97	5.4
3095.240	10154.99	18.2
3095.245	10155.00	14.8
3095.250	10155.02	43.5
3095.255	10155.04	29.4
3095.260	10155.05	16.9
3095.290	10155.15	6.6
3095.295	10155.17	13.6
3095.300	10155.18	17.5
3095.305	10155.20	10.1
3095.310	10155.22	13.5
3095.315	10155.23	12.0
3095.320	10155.25	30.5
3095.325	10155.27	34.8
3095.330	10155.28	44.1
3095.335	10155.30	29.4
3095.340	10155.32	14.6
3095.365	10155.40	13.0
3095.370	10155.41	24.1
3095.375	10155.43	44.6

3064.020	10052.56	151.7
3064.025	10052.58	281.7
3064.030	10052.59	94.5
3064.035	10052.61	250.3
3064.040	10052.62	430.0
3064.045	10052.64	334.9
3064.055	10052.67	175.0
3064.060	10052.69	227.7
3064.065	10052.71	207.3
3064.070	10052.72	151.1
3064.075	10052.74	150.0
3064.080	10052.76	281.3
3064.085	10052.77	42.4
3064.090	10052.79	179.3
3064.095	10052.81	85.8
3064.100	10052.82	310.2
3064.105	10052.84	125.3
3064.110	10052.85	33.5
3064.115	10052.87	41.4
3064.120	10052.89	72.9
3064.125	10052.90	76.5
3064.130	10052.92	22.6
3064.135	10052.94	197.1
3064.140	10052.95	3.0
3064.145	10052.97	115.5
3064.150	10052.99	264.3
3064.155	10053.00	339.9
3064.160	10053.02	357.3
3064.165	10053.04	187.1
3064.170	10053.05	164.6
3064.175	10053.07	236.0
3064.180	10053.08	163.4
3064.185	10053.10	231.8
3064.190	10053.12	485.9
3064.195	10053.13	248.4
3064.215	10053.20	499.1
3064.220	10053.22	124.5
3064.225	10053.23	4.9
3064.230	10053.25	98.7
3064.235	10053.26	304.9
3064.240	10053.28	158.9
3064.245	10053.30	200.9
3064.250	10053.31	701.7
3064.255	10053.33	223.1
3064.260	10053.35	145.3
3064.265	10053.36	61.8
3064.270	10053.38	18.2
3064.275	10053.40	47.9
3064.300	10053.48	214.8
3064.305	10053.49	457.5
3064.310	10053.51	270.6
3064.315	10053.53	91.7
3064.320	10053.54	334.5
3064.325	10053.56	105.9
3064.330	10053.58	590.6
3064.335	10053.59	654.2
3064.340	10053.61	355.8
3064.345	10053.63	387.8
3064.350	10053.64	431.0
3064.355	10053.66	230.1
3064.360	10053.67	258.5
3064.365	10053.69	429.8
3064.370	10053.71	435.0
3064.375	10053.72	279.6
3064.380	10053.74	652.3
3064.385	10053.76	509.2
3064.390	10053.77	497.7
3064.395	10053.79	300.3
3064.400	10053.81	298.7
3064.405	10053.82	336.1
3064.410	10053.84	572.0
3064.430	10053.90	8.5
3064.435	10053.92	94.9
3064.480	10054.07	246.2
3064.485	10054.08	192.1
3064.490	10054.10	43.1
3064.495	10054.12	71.0
3064.500	10054.13	503.4
3064.505	10054.15	512.9
3064.510	10054.17	448.6
3064.515	10054.18	322.7
3064.520	10054.20	129.1
3064.525	10054.22	128.4
3064.530	10054.23	58.4
3064.535	10054.25	66.2
3064.540	10054.27	47.5
3064.545	10054.28	72.3
3064.550	10054.30	81.7
3064.575	10054.38	17.3
3064.580	10054.40	61.6
3064.585	10054.41	7.8
3064.590	10054.43	23.4
3064.595	10054.45	79.4
3064.600	10054.46	11.2
3064.605	10054.48	31.6
3064.610	10054.50	30.0
3064.615	10054.51	36.1
3064.620	10054.53	91.3
3064.625	10054.54	84.8
3064.630	10054.56	52.2
3064.635	10054.58	111.2
3064.640	10054.59	39.1
3064.645	10054.61	61.7

3078.730	10100.82	45.0
3078.735	10100.84	48.6
3078.740	10100.85	116.2
3078.745	10100.87	124.7
3078.750	10100.89	91.8
3078.755	10100.90	87.3
3078.760	10100.92	70.9
3078.765	10100.94	85.4
3078.770	10100.95	94.9
3078.775	10100.97	92.7
3078.780	10100.98	70.1
3078.800	10101.05	88.5
3078.805	10101.07	138.3
3078.820	10101.12	78.3
3078.825	10101.13	66.7
3078.830	10101.15	38.0
3078.835	10101.17	28.7
3078.840	10101.18	71.3
3078.845	10101.20	61.8
3078.850	10101.21	69.4
3078.855	10101.23	103.8
3078.860	10101.25	97.9
3078.865	10101.26	95.9
3078.870	10101.28	90.2
3078.875	10101.30	133.3
3078.880	10101.31	111.9
3078.885	10101.33	81.8
3078.890	10101.35	69.1
3078.895	10101.36	63.2
3078.900	10101.38	71.8
3078.905	10101.39	40.4
3078.910	10101.41	55.5
3078.915	10101.43	58.5
3078.920	10101.44	133.1
3078.925	10101.46	64.9
3078.930	10101.48	95.8
3078.935	10101.49	47.0
3078.940	10101.51	85.8
3078.945	10101.53	105.1
3078.950	10101.54	112.1
3078.955	10101.56	133.4
3078.960	10101.58	83.0
3078.965	10101.59	127.1
3078.970	10101.61	85.0
3078.975	10101.62	129.0
3078.980	10101.64	105.1
3078.985	10101.66	74.2
3078.990	10101.67	101.9
3078.995	10101.69	63.9
3079.000	10101.71	156.8
3079.005	10101.72	99.0
3079.010	10101.74	127.7
3079.015	10101.76	110.0
3079.020	10101.77	76.4
3079.025	10101.79	59.9
3079.030	10101.80	57.2
3079.055	10101.89	195.4
3079.060	10101.90	163.8
3079.065	10101.92	130.0
3079.110	10102.07	313.7
3079.115	10102.08	452.1
3079.120	10102.10	290.6
3079.125	10102.12	519.3
3079.130	10102.13	325.2
3079.135	10102.15	274.5
3079.140	10102.17	276.4
3079.145	10102.18	269.4
3079.150	10102.20	183.3
3079.155	10102.21	279.0
3079.160	10102.23	177.6
3079.165	10102.25	133.1
3079.170	10102.26	144.9
3079.175	10102.28	254.0
3079.195	10102.35	27.7
3079.200	10102.36	43.1
3079.205	10102.38	36.5
3079.210	10102.40	112.8
3079.215	10102.41	43.5
3079.220	10102.43	52.3
3079.225	10102.44	17.3
3079.230	10102.46	49.7
3079.235	10102.48	30.9
3079.240	10102.49	55.5
3079.245	10102.51	36.9
3079.250	10102.53	52.2
3079.255	10102.54	38.1
3079.260	10102.56	27.7
3079.265	10102.58	37.5
3079.270	10102.59	41.9
3079.275	10102.61	39.2
3079.280	10102.62	48.0
3079.285	10102.64	49.2
3079.290	10102.66	33.3
3079.295	10102.67	84.7
3079.300	10102.69	43.8
3079.305	10102.71	49.6
3079.310	10102.72	33.2
3079.315	10102.74	35.2
3079.320	10102.76	36.7
3079.325	10102.77	45.6
3079.330	10102.79	37.3
3079.335	10102.81	64.2
3079.365	10102.90	35.6

3086.990	10127.92	4.3
3086.995	10127.94	12.7
3087.000	10127.95	6.5
3087.005	10127.97	3.1
3087.010	10127.99	2.6
3087.015	10128.00	2.3
3087.020	10128.02	3.0
3087.030	10128.05	3.3
3087.035	10128.07	3.0
3087.040	10128.08	6.4
3087.045	10128.10	2.0
3087.070	10128.18	3.4
3087.075	10128.20	5.4
3087.080	10128.22	6.5
3087.085	10128.23	13.2
3087.090	10128.25	5.8
3087.095	10128.26	6.1
3087.100	10128.28	6.8
3087.105	10128.30	5.5
3087.110	10128.31	13.7
3087.115	10128.33	57.0
3087.120	10128.35	10.8
3087.125	10128.36	14.0
3087.130	10128.38	11.5
3087.135	10128.40	11.6
3087.140	10128.41	43.4
3087.145	10128.43	7.8
3087.150	10128.45	17.5
3087.155	10128.46	27.0
3087.160	10128.48	16.5
3087.165	10128.49	7.0
3087.170	10128.51	8.9
3087.175	10128.53	7.4
3087.180	10128.54	7.5
3087.185	10128.56	9.5
3087.190	10128.58	9.8
3087.195	10128.59	11.6
3087.200	10128.61	9.7
3087.230	10128.71	19.0
3087.235	10128.72	23.3
3087.240	10128.74	20.8
3087.245	10128.76	22.6
3087.250	10128.77	32.1
3087.255	10128.79	39.0
3087.260	10128.81	13.7
3087.265	10128.82	27.3
3087.270	10128.84	13.7
3087.440	10129.40	33.4
3087.445	10129.41	27.6
3087.450	10129.43	81.8
3087.455	10129.45	21.4
3087.460	10129.46	25.9
3087.465	10129.48	24.0
3087.470	10129.50	26.7
3087.475	10129.51	10.0
3087.480	10129.53	4.9
3087.485	10129.54	4.7
3087.490	10129.56	8.0
3087.495	10129.58	13.3
3087.500	10129.59	13.6
3087.505	10129.61	13.8
3087.510	10129.63	15.1
3087.515	10129.64	3.6
3087.520	10129.66	4.5
3087.525	10129.68	8.3
3087.530	10129.69	12.0
3087.535	10129.71	5.7
3087.540	10129.72	9.6
3087.545	10129.74	7.7
3087.550	10129.76	7.8
3087.555	10129.77	13.1
3087.560	10129.79	14.3
3087.565	10129.81	45.6
3087.570	10129.82	8.8
3087.575	10129.84	9.7
3087.580	10129.86	14.0
3087.585	10129.87	5.6
3087.590	10129.89	18.5
3087.595	10129.91	8.8
3087.600	10129.92	15.3
3087.645	10130.07	27.1
3087.650	10130.09	39.0
3087.655	10130.10	113.9
3087.660	10130.12	136.3
3087.665	10130.13	21.4
3087.670	10130.15	19.6
3087.675	10130.17	26.3
3087.680	10130.18	23.2
3087.695	10130.23	28.7
3087.700	10130.25	30.0
3087.705	10130.27	30.2
3087.710	10130.28	35.9
3087.715	10130.30	30.3
3087.720	10130.32	30.9
3087.725	10130.33	26.6
3087.730	10130.35	25.6
3087.735	10130.36	41.1
3087.740	10130.38	31.9
3087.745	10130.40	27.3
3087.750	10130.41	31.1
3087.755	10130.43	35.2
3087.760	10130.45	35.7
3087.765	10130.46	44.6

3095.380	10155.45	14.9
3095.385	10155.46	8.9
3095.390	10155.48	10.8
3095.395	10155.50	16.4
3095.400	10155.51	31.1
3095.405	10155.53	13.8
3095.410	10155.54	20.8
3095.415	10155.56	31.3
3095.420	10155.58	20.8
3095.425	10155.59	12.7
3095.430	10155.61	14.0
3095.435	10155.63	22.0
3095.440	10155.64	18.7
3095.445	10155.66	16.1
3095.450	10155.68	28.5
3095.455	10155.69	32.0
3095.460	10155.71	41.7
3095.465	10155.73	41.5
3095.470	10155.74	9.5
3095.475	10155.76	33.0
3095.480	10155.77	15.2
3095.485	10155.79	13.2
3095.490	10155.81	33.8
3095.495	10155.82	18.3
3095.500	10155.84	20.3
3095.505	10155.86	14.5
3095.510	10155.87	20.0
3095.515	10155.89	13.8
3095.520	10155.91	13.5
3095.525	10155.92	18.0
3095.555	10156.02	13.7
3095.560	10156.04	18.3
3095.565	10156.05	43.0
3095.570	10156.07	53.3
3095.575	10156.09	67.5
3095.580	10156.10	46.8
3095.585	10156.12	37.2
3095.590	10156.14	45.0
3095.595	10156.15	35.9
3095.600	10156.17	30.1
3095.605	10156.18	44.4
3095.610	10156.20	36.7
3095.615	10156.22	29.7
3095.620	10156.23	39.1
3095.625	10156.25	41.2
3095.630	10156.27	18.4
3095.635	10156.28	19.2
3095.640	10156.30	21.8
3095.645	10156.32	19.7
3095.650	10156.33	16.9
3095.655	10156.35	22.9
3095.660	10156.37	46.1
3095.665	10156.38	42.1
3095.670	10156.40	19.7
3095.685	10156.45	23.9
3095.690	10156.46	26.2
3095.695	10156.48	38.8
3095.700	10156.50	33.9
3095.705	10156.51	38.9
3095.710	10156.53	26.5
3095.715	10156.55	23.9
3095.720	10156.56	26.2
3095.725	10156.58	24.5
3095.730	10156.59	28.4
3095.735	10156.61	20.0
3095.740	10156.63	23.8
3095.745	10156.64	47.8
3095.750	10156.66	40.3
3095.755	10156.68	26.4
3095.760	10156.69	59.8
3095.765	10156.71	67.7
3095.770	10156.73	57.0
3095.775	10156.74	35.9
3095.780	10156.76	18.5
3095.785	10156.78	26.7
3095.790	10156.79	18.7
3095.795	10156.81	16.1
3095.800	10156.82	44.0
3095.825	10156.91	63.0
3095.830	10156.92	38.6
3095.945	10157.30	29.4
3095.950	10157.32	13.3
3095.955	10157.33	24.0
3095.960	10157.35	24.3
3095.965	10157.37	14.0
3095.970	10157.38	15.4
3095.975	10157.40	32.7
3095.980	10157.42	8.9
3095.985	10157.43	9.4
3095.990	10157.45	4.3
3095.995	10157.46	8.5
3096.000	10157.48	2.8
3096.005	10157.50	6.8
3096.010	10157.51	3.1
3096.030	10157.58	24.6
3096.035	10157.60	7.1
3096.040	10157.61	6.9
3096.045	10157.63	7.4
3096.050	10157.64	17.7
3096.055	10157.66	20.3
3096.075	10157.73	7.8
3096.080	10157.74	7.2
3096.085	10157.76	12.0

3064.650	10054.63	100.1
3064.655	10054.64	164.7
3064.660	10054.66	73.2
3064.665	10054.68	68.1
3064.670	10054.69	222.7
3064.675	10054.71	500.9
3064.680	10054.72	128.5
3064.685	10054.74	15.6
3064.690	10054.76	4.2
3064.695	10054.77	13.5
3064.700	10054.79	155.0
3064.705	10054.81	243.9
3064.710	10054.82	162.0
3064.715	10054.84	203.0
3064.720	10054.86	509.6
3064.725	10054.87	286.7
3064.730	10054.89	511.2
3064.735	10054.91	766.3
3064.755	10054.97	63.0
3064.760	10054.99	221.4
3064.765	10055.00	274.9
3064.770	10055.02	191.7
3064.775	10055.04	31.6
3064.780	10055.05	42.2
3064.785	10055.07	120.7
3064.790	10055.09	173.9
3064.795	10055.10	132.7
3064.800	10055.12	202.0
3064.805	10055.13	246.4
3064.810	10055.15	79.0
3064.815	10055.17	176.9
3064.850	10055.28	107.5
3064.855	10055.30	226.9
3064.860	10055.32	149.1
3064.865	10055.33	31.0
3064.870	10055.35	94.5
3064.875	10055.36	113.3
3064.880	10055.38	160.8
3064.885	10055.40	213.0
3064.890	10055.41	98.8
3064.895	10055.43	216.4
3064.900	10055.45	111.4
3064.905	10055.46	122.8
3064.910	10055.48	214.4
3064.915	10055.50	260.3
3064.920	10055.51	607.5
3064.925	10055.53	91.4
3064.930	10055.54	29.2
3064.935	10055.56	43.6
3064.940	10055.58	25.0
3064.945	10055.59	41.3
3064.950	10055.61	19.8
3064.955	10055.63	40.7
3064.960	10055.64	153.6
3064.965	10055.66	84.3
3064.970	10055.68	156.2
3064.975	10055.69	74.5
3064.980	10055.71	106.4
3064.985	10055.73	56.6
3064.990	10055.74	37.4
3064.995	10055.76	54.3
3065.000	10055.77	36.3
3065.025	10055.86	4.1
3065.030	10055.87	56.5
3065.035	10055.89	144.2
3065.040	10055.91	66.5
3065.045	10055.92	61.7
3065.050	10055.94	15.6
3065.055	10055.96	16.3
3065.060	10055.97	48.4
3065.065	10055.99	83.8
3065.070	10056.00	280.0
3065.075	10056.02	122.9
3065.080	10056.04	191.3
3065.085	10056.05	1261.0
3065.090	10056.07	980.9
3065.095	10056.09	430.5
3065.100	10056.10	207.8
3065.105	10056.12	96.1
3065.110	10056.14	159.6
3065.115	10056.15	132.0
3065.120	10056.17	21.6
3065.125	10056.18	62.1
3065.130	10056.20	136.8
3065.135	10056.22	283.2
3065.140	10056.23	176.4
3065.145	10056.25	541.9
3065.165	10056.32	435.1
3065.170	10056.33	337.9
3065.175	10056.35	354.4
3065.180	10056.37	37.1
3065.185	10056.38	135.3
3065.190	10056.40	195.2
3065.195	10056.41	336.9
3065.200	10056.43	244.9
3065.205	10056.45	76.5
3065.210	10056.46	158.6
3065.215	10056.48	391.3
3065.220	10056.50	156.1
3065.225	10056.51	87.4
3065.230	10056.53	229.4
3065.235	10056.55	110.5
3065.240	10056.56	56.9

3079.370	10102.92	24.3
3079.375	10102.94	27.8
3079.380	10102.95	12.3
3079.385	10102.97	42.2
3079.390	10102.99	110.4
3079.395	10103.00	49.2
3079.400	10103.02	71.2
3079.405	10103.04	73.2
3079.410	10103.05	65.5
3079.415	10103.07	210.3
3079.420	10103.08	49.8
3079.425	10103.10	48.1
3079.430	10103.12	52.4
3079.435	10103.13	41.0
3079.440	10103.15	87.3
3079.445	10103.17	43.4
3079.450	10103.18	75.0
3079.455	10103.20	77.7
3079.460	10103.22	44.5
3079.465	10103.23	36.8
3079.470	10103.25	78.8
3079.475	10103.26	47.8
3079.480	10103.28	29.4
3079.485	10103.30	64.0
3079.490	10103.31	36.4
3079.495	10103.33	47.2
3079.500	10103.35	39.5
3079.505	10103.36	39.4
3079.510	10103.38	38.5
3079.515	10103.40	51.6
3079.520	10103.41	76.6
3079.525	10103.43	39.9
3079.530	10103.45	50.8
3079.535	10103.46	48.2
3079.540	10103.48	28.7
3079.545	10103.49	30.4
3079.550	10103.51	31.5
3079.555	10103.53	32.5
3079.560	10103.54	34.0
3079.565	10103.56	26.0
3079.570	10103.58	19.4
3079.575	10103.59	34.0
3079.580	10103.61	24.4
3079.585	10103.63	34.5
3079.590	10103.64	27.9
3079.595	10103.66	28.3
3079.600	10103.67	35.7
3079.605	10103.69	34.3
3079.610	10103.71	38.0
3079.615	10103.72	17.2
3079.620	10103.74	31.7
3079.625	10103.76	23.0
3079.630	10103.77	25.7
3079.635	10103.79	26.5
3079.640	10103.81	26.4
3079.645	10103.82	39.0
3079.650	10103.84	18.9
3079.655	10103.86	20.7
3079.660	10103.87	16.9
3079.665	10103.89	64.8
3079.670	10103.90	19.5
3079.675	10103.92	27.4
3079.680	10103.94	18.3
3079.685	10103.95	20.4
3079.690	10103.97	34.0
3079.695	10103.99	23.3
3079.710	10104.04	52.2
3079.715	10104.05	20.8
3079.720	10104.07	28.3
3079.725	10104.08	21.1
3079.730	10104.10	24.7
3079.735	10104.12	44.0
3079.740	10104.13	20.7
3079.745	10104.15	25.4
3079.750	10104.17	34.7
3079.755	10104.18	23.3
3079.760	10104.20	19.5
3079.765	10104.22	22.7
3079.770	10104.23	19.7
3079.775	10104.25	25.8
3079.780	10104.27	33.0
3079.785	10104.28	30.6
3079.790	10104.30	25.6
3079.795	10104.31	22.6
3079.800	10104.33	43.0
3079.805	10104.35	37.1
3079.810	10104.36	24.5
3079.815	10104.38	72.2
3079.820	10104.40	27.3
3079.825	10104.41	39.7
3079.830	10104.43	23.8
3079.835	10104.45	25.5
3079.840	10104.46	26.0
3079.845	10104.48	29.2
3079.850	10104.50	21.4
3079.855	10104.51	23.1
3079.860	10104.53	25.7
3079.865	10104.54	22.5
3079.870	10104.56	15.8
3079.885	10104.61	15.0
3079.890	10104.63	40.4
3079.895	10104.64	16.5
3079.900	10104.66	31.9

3087.770	10130.48	62.2
3087.775	10130.50	56.1
3087.780	10130.51	40.2
3087.785	10130.53	20.6
3087.790	10130.54	12.9
3087.795	10130.56	13.5
3087.800	10130.58	12.8
3087.805	10130.59	19.2
3087.810	10130.61	21.0
3087.815	10130.63	19.9
3087.820	10130.64	27.7
3087.825	10130.66	24.3
3087.830	10130.68	23.8
3087.835	10130.69	28.8
3087.840	10130.71	25.7
3087.845	10130.73	30.5
3087.850	10130.74	31.7
3087.855	10130.76	33.4
3087.860	10130.77	35.4
3087.865	10130.79	47.2
3087.870	10130.81	23.6
3087.890	10130.87	15.0
3087.895	10130.89	15.1
3087.900	10130.91	10.2
3087.905	10130.92	9.4
3087.910	10130.94	22.7
3087.915	10130.96	19.8
3087.920	10130.97	18.9
3087.925	10130.99	15.1
3087.930	10131.00	17.5
3087.935	10131.02	25.6
3087.940	10131.04	23.2
3087.945	10131.05	14.7
3087.950	10131.07	18.9
3087.955	10131.09	26.6
3087.960	10131.10	27.2
3087.965	10131.12	27.8
3087.970	10131.14	36.3
3087.975	10131.15	47.8
3087.980	10131.17	19.7
3087.985	10131.18	16.1
3088.005	10131.25	38.3
3088.010	10131.27	16.2
3088.015	10131.28	39.1
3088.020	10131.30	27.7
3088.025	10131.32	31.8
3088.030	10131.33	18.6
3088.035	10131.35	24.8
3088.040	10131.37	26.8
3088.045	10131.38	46.5
3088.050	10131.40	38.3
3088.055	10131.41	79.4
3088.060	10131.43	120.1
3088.065	10131.45	84.9
3088.070	10131.46	153.2
3088.075	10131.48	56.6
3088.080	10131.50	65.9
3088.085	10131.51	22.8
3088.090	10131.53	35.6
3088.095	10131.55	84.1
3088.100	10131.56	129.9
3088.105	10131.58	40.6
3088.110	10131.59	42.5
3088.115	10131.61	46.5
3088.120	10131.63	52.9
3088.125	10131.64	69.8
3088.130	10131.66	122.3
3088.135	10131.68	69.6
3088.140	10131.69	79.7
3088.145	10131.71	128.4
3088.150	10131.73	38.7
3088.155	10131.74	38.6
3088.160	10131.76	64.4
3088.165	10131.78	87.7
3088.170	10131.79	75.0
3088.175	10131.81	68.6
3088.180	10131.82	59.3
3088.185	10131.84	38.8
3088.190	10131.86	100.0
3088.195	10131.87	81.6
3088.200	10131.89	81.5
3088.205	10131.91	60.6
3088.210	10131.92	66.5
3088.215	10131.94	160.2
3088.220	10131.96	83.0
3088.225	10131.97	62.2
3088.230	10131.99	120.5
3088.250	10132.05	20.9
3088.255	10132.07	36.8
3088.260	10132.09	22.4
3088.265	10132.10	24.2
3088.270	10132.12	17.1
3088.275	10132.14	23.4
3088.280	10132.15	28.0
3088.285	10132.17	29.2
3088.290	10132.19	19.7
3088.295	10132.20	25.4
3088.300	10132.22	30.9
3088.305	10132.23	12.2
3088.310	10132.25	34.9
3088.315	10132.27	26.2
3088.320	10132.28	42.1
3088.325	10132.30	17.5

3096.090	10157.78	26.9
3096.095	10157.79	35.0
3096.100	10157.81	27.7
3096.105	10157.83	9.5
3096.110	10157.84	4.0
3096.115	10157.86	22.6
3096.120	10157.87	35.9
3096.125	10157.89	39.0
3096.130	10157.91	29.8
3096.135	10157.92	22.3
3096.140	10157.94	21.1
3096.145	10157.96	40.4
3096.150	10157.97	29.1
3096.155	10157.99	33.4
3096.160	10158.01	16.1
3096.165	10158.02	33.6
3096.170	10158.04	3.5
3096.175	10158.05	2.4
3096.180	10158.07	2.8
3096.200	10158.14	3.6
3096.205	10158.15	4.2
3096.210	10158.17	2.2
3096.215	10158.19	2.1
3096.220	10158.20	2.8
3096.225	10158.22	2.5
3096.235	10158.25	2.3
3096.260	10158.33	4.8
3096.265	10158.35	3.8
3096.275	10158.38	3.6
3096.285	10158.42	2.3
3096.290	10158.43	4.0
3096.300	10158.46	9.8
3096.305	10158.48	7.7
3096.310	10158.50	10.2
3096.315	10158.51	2.7
3096.325	10158.55	4.1
3096.335	10158.58	2.8
3096.345	10158.61	3.2
3096.365	10158.68	3.8
3096.370	10158.69	2.5
3096.375	10158.71	2.9
3096.395	10158.78	2.3
3096.415	10158.84	3.4
3096.420	10158.86	6.0
3096.425	10158.87	5.9
3096.430	10158.89	13.1
3096.435	10158.91	8.2
3096.440	10158.92	7.1
3096.445	10158.94	6.0
3096.450	10158.96	2.3
3096.460	10158.99	3.2
3096.465	10159.01	8.6
3096.470	10159.02	6.0
3096.475	10159.04	10.3
3096.480	10159.06	14.4
3096.485	10159.07	8.4
3096.490	10159.09	4.8
3096.495	10159.10	6.6
3096.500	10159.12	8.9
3096.520	10159.19	2.2
3096.530	10159.22	2.7
3096.535	10159.24	3.2
3096.555	10159.30	5.7
3096.560	10159.32	3.6
3096.570	10159.35	4.7
3096.580	10159.38	2.2
3096.585	10159.40	2.3
3096.590	10159.42	4.5
3096.595	10159.43	2.1
3096.615	10159.50	3.3
3096.620	10159.51	4.0
3096.635	10159.56	2.7
3096.640	10159.58	5.1
3096.645	10159.60	4.2
3096.650	10159.61	5.7
3096.655	10159.63	3.7
3096.660	10159.65	2.9
3096.665	10159.66	2.2
3096.670	10159.68	3.2
3096.695	10159.76	2.5
3096.700	10159.78	2.0
3096.735	10159.89	5.8
3096.740	10159.91	4.3
3096.745	10159.92	3.0
3096.820	10160.17	5.1
3096.830	10160.20	2.1
3096.840	10160.24	3.4
3096.865	10160.32	2.3
3096.875	10160.35	2.0
3096.880	10160.37	2.5
3096.885	10160.38	2.4
3096.900	10160.43	2.0
3096.915	10160.48	2.1
3096.925	10160.52	2.2
3096.980	10160.70	3.3
3096.985	10160.71	2.2
3097.010	10160.79	3.8
3097.020	10160.83	2.3
3097.025	10160.84	2.5
3097.040	10160.89	3.7
3097.050	10160.93	3.7
3097.055	10160.94	5.3
3097.060	10160.96	3.9

3065.245	10056.58	157.5
3065.250	10056.59	66.3
3065.255	10056.61	115.2
3065.280	10056.69	18.0
3065.285	10056.71	19.8
3065.290	10056.73	24.4
3065.295	10056.74	65.8
3065.300	10056.76	28.1
3065.305	10056.78	37.3
3065.310	10056.79	25.4
3065.315	10056.81	22.7
3065.320	10056.82	85.1
3065.325	10056.84	16.3
3065.330	10056.86	68.1
3065.335	10056.87	90.6
3065.340	10056.89	56.0
3065.345	10056.91	16.7
3065.425	10057.17	10.5
3065.430	10057.19	164.5
3065.435	10057.20	41.5
3065.440	10057.22	111.2
3065.445	10057.23	79.2
3065.450	10057.25	75.0
3065.455	10057.27	204.5
3065.460	10057.28	102.2
3065.465	10057.30	275.1
3065.470	10057.32	348.5
3065.475	10057.33	328.8
3065.480	10057.35	437.2
3065.485	10057.37	230.2
3065.490	10057.38	217.9
3065.495	10057.40	299.5
3065.500	10057.42	180.0
3065.505	10057.43	190.0
3065.510	10057.45	286.2
3065.515	10057.46	227.3
3065.520	10057.48	90.5
3065.525	10057.50	363.8
3065.530	10057.51	399.8
3065.535	10057.53	133.1
3065.540	10057.55	217.9
3065.545	10057.56	206.3
3065.550	10057.58	174.6
3065.555	10057.60	65.8
3065.560	10057.61	86.0
3065.565	10057.63	63.2
3065.570	10057.64	122.2
3065.575	10057.66	162.1
3065.580	10057.68	237.9
3065.585	10057.69	216.5
3065.590	10057.71	432.0
3065.595	10057.73	430.9
3065.600	10057.74	386.3
3065.605	10057.76	155.2
3065.610	10057.78	36.7
3065.620	10057.81	62.8
3065.625	10057.83	46.0
3065.630	10057.84	191.6
3065.635	10057.86	192.9
3065.640	10057.87	156.7
3065.645	10057.89	64.5
3065.650	10057.91	46.3
3065.655	10057.92	157.3
3065.660	10057.94	170.8
3065.665	10057.96	42.9
3065.670	10057.97	52.4
3065.675	10057.99	63.1
3065.680	10058.01	217.1
3065.685	10058.02	30.9
3065.690	10058.04	11.6
3065.695	10058.05	432.4
3065.700	10058.07	625.2
3065.705	10058.09	434.1
3065.710	10058.10	323.2
3065.715	10058.12	197.3
3065.735	10058.19	57.8
3065.740	10058.20	25.4
3065.745	10058.22	31.3
3065.750	10058.24	58.3
3065.755	10058.25	43.0
3065.760	10058.27	121.5
3065.765	10058.28	111.3
3065.770	10058.30	33.5
3065.775	10058.32	158.8
3065.780	10058.33	70.7
3065.785	10058.35	35.1
3065.790	10058.37	38.4
3065.795	10058.38	85.8
3065.800	10058.40	94.0
3065.805	10058.42	132.0
3065.810	10058.43	87.1
3065.815	10058.45	48.1
3065.820	10058.46	63.5
3065.825	10058.48	75.8
3065.830	10058.50	9.1
3065.840	10058.53	13.9
3065.845	10058.55	3.3
3065.850	10058.56	6.7
3065.870	10058.63	7.9
3065.875	10058.65	10.1
3065.880	10058.66	24.9
3065.885	10058.68	88.6
3065.890	10058.69	184.7

3079.905	10104.68	49.6
3079.910	10104.69	31.7
3079.915	10104.71	41.5
3079.920	10104.72	26.8
3079.925	10104.74	36.8
3079.930	10104.76	46.9
3079.935	10104.77	47.7
3079.940	10104.79	46.4
3079.945	10104.81	42.5
3079.950	10104.82	37.0
3079.955	10104.84	47.3
3079.960	10104.86	50.8
3079.965	10104.87	91.7
3079.970	10104.89	39.8
3079.975	10104.91	45.6
3079.980	10104.92	38.7
3079.985	10104.94	76.2
3080.330	10106.07	63.0
3080.335	10106.09	64.3
3080.340	10106.10	116.5
3080.345	10106.12	102.6
3080.350	10106.14	126.2
3080.355	10106.15	141.6
3080.360	10106.17	126.5
3080.365	10106.18	91.6
3080.370	10106.20	103.9
3080.375	10106.22	101.7
3080.380	10106.23	117.1
3080.385	10106.25	92.5
3080.390	10106.27	70.3
3080.395	10106.28	125.4
3080.415	10106.35	76.6
3080.420	10106.37	104.8
3080.425	10106.38	123.5
3080.430	10106.40	60.6
3080.435	10106.41	103.9
3080.440	10106.43	86.7
3080.445	10106.45	84.9
3080.450	10106.46	161.6
3080.455	10106.48	124.3
3080.460	10106.50	64.0
3080.465	10106.51	55.3
3080.470	10106.53	72.3
3080.475	10106.55	97.2
3080.480	10106.56	26.2
3080.485	10106.58	71.8
3080.490	10106.59	104.0
3080.495	10106.61	113.7
3080.500	10106.63	86.9
3080.505	10106.64	100.5
3080.510	10106.66	60.5
3080.515	10106.68	77.5
3080.520	10106.69	105.1
3080.525	10106.71	45.2
3080.530	10106.73	92.4
3080.535	10106.74	116.0
3080.540	10106.76	83.6
3080.555	10106.81	86.3
3080.560	10106.82	102.0
3080.565	10106.84	77.5
3080.570	10106.86	46.7
3080.575	10106.87	68.9
3080.580	10106.89	67.4
3080.585	10106.91	80.6
3080.590	10106.92	69.3
3080.595	10106.94	78.6
3080.600	10106.96	43.2
3080.605	10106.97	105.5
3080.610	10106.99	84.5
3080.615	10107.00	11.3
3080.620	10107.02	28.5
3080.625	10107.04	15.7
3080.630	10107.05	78.1
3080.635	10107.07	59.4
3080.640	10107.09	72.3
3080.645	10107.10	36.0
3080.650	10107.12	30.3
3080.655	10107.14	21.1
3080.660	10107.15	31.9
3080.665	10107.17	31.4
3080.670	10107.19	23.7
3080.675	10107.20	23.1
3080.680	10107.22	16.8
3080.700	10107.28	31.7
3080.705	10107.30	42.6
3080.710	10107.32	15.7
3080.715	10107.33	24.4
3080.720	10107.35	20.8
3080.725	10107.37	16.4
3080.730	10107.38	16.4
3080.735	10107.40	19.4
3080.740	10107.42	24.4
3080.745	10107.43	33.2
3080.750	10107.45	42.0
3080.755	10107.46	56.5
3080.760	10107.48	41.5
3080.765	10107.50	39.7
3080.775	10107.53	34.3
3080.780	10107.55	14.2
3080.785	10107.56	20.0
3080.790	10107.58	38.8
3080.795	10107.60	14.2
3080.800	10107.61	14.7

3088.330	10132.32	22.1
3088.335	10132.33	32.0
3088.340	10132.35	9.9
3088.345	10132.37	10.7
3088.365	10132.43	22.6
3088.370	10132.45	18.5
3088.375	10132.46	15.0
3088.380	10132.48	16.2
3088.385	10132.50	17.2
3088.390	10132.51	53.2
3088.395	10132.53	43.8
3088.400	10132.55	43.1
3088.405	10132.56	71.5
3088.410	10132.58	80.4
3088.415	10132.60	41.7
3088.420	10132.61	104.1
3088.425	10132.63	21.4
3088.430	10132.64	40.1
3088.435	10132.66	44.6
3088.440	10132.68	42.0
3088.445	10132.69	64.9
3088.450	10132.71	33.5
3088.455	10132.73	13.9
3088.460	10132.74	28.4
3088.465	10132.76	53.6
3088.470	10132.78	72.1
3088.475	10132.79	60.3
3088.480	10132.81	26.9
3088.485	10132.83	77.6
3088.490	10132.84	32.3
3088.495	10132.86	56.0
3088.560	10133.07	8.9
3088.565	10133.09	5.1
3088.570	10133.10	6.3
3088.575	10133.12	17.8
3088.580	10133.14	8.5
3088.585	10133.15	25.7
3088.590	10133.17	9.9
3088.595	10133.19	7.3
3088.600	10133.20	30.3
3088.605	10133.22	3.2
3088.610	10133.24	14.6
3088.615	10133.25	7.8
3088.620	10133.27	18.6
3088.625	10133.28	36.4
3088.630	10133.30	9.8
3088.635	10133.32	18.9
3088.640	10133.33	11.9
3088.645	10133.35	4.2
3088.650	10133.37	8.3
3088.655	10133.38	19.9
3088.660	10133.40	34.9
3088.665	10133.42	12.6
3088.670	10133.43	27.2
3088.675	10133.45	35.5
3088.680	10133.46	42.8
3088.685	10133.48	46.6
3088.690	10133.50	92.7
3088.695	10133.51	67.3
3088.700	10133.53	36.1
3088.705	10133.55	62.2
3088.710	10133.56	18.6
3088.715	10133.58	47.9
3088.720	10133.60	12.8
3088.725	10133.61	23.9
3088.730	10133.63	63.4
3088.735	10133.65	17.5
3088.740	10133.66	67.1
3088.745	10133.68	53.8
3088.750	10133.69	56.3
3088.755	10133.71	18.2
3088.785	10133.81	31.0
3088.790	10133.83	29.5
3088.795	10133.84	19.7
3088.800	10133.86	10.9
3088.805	10133.87	61.7
3088.810	10133.89	37.3
3088.815	10133.91	97.3
3088.820	10133.92	26.4
3088.825	10133.94	31.0
3088.830	10133.96	28.7
3088.835	10133.97	24.1
3088.840	10133.99	57.9
3088.845	10134.01	34.8
3088.850	10134.02	33.7
3088.855	10134.04	55.0
3088.860	10134.06	52.2
3088.865	10134.07	33.5
3088.870	10134.09	68.6
3088.875	10134.10	41.9
3088.880	10134.12	40.8
3088.885	10134.14	37.6
3088.890	10134.15	46.2
3088.895	10134.17	15.7
3088.915	10134.24	85.2
3088.920	10134.25	19.5
3088.925	10134.27	53.5
3088.930	10134.29	27.1
3088.935	10134.30	43.6
3088.940	10134.32	15.0
3088.945	10134.33	45.2
3088.950	10134.35	61.0
3088.960	10134.38	6.2

3097.100	10161.09	3.5
3097.125	10161.17	3.9
3097.150	10161.25	4.2
3097.170	10161.32	2.5
3097.210	10161.45	2.0
3097.245	10161.57	2.7
3097.250	10161.58	7.7
3097.275	10161.66	2.0
3097.360	10161.94	4.1
3097.450	10162.24	4.1
3097.460	10162.27	4.3
3097.480	10162.34	2.3
3097.505	10162.42	4.0
3097.510	10162.43	4.1
3097.515	10162.45	4.2
3097.520	10162.47	3.9
3097.525	10162.48	4.3
3097.530	10162.50	4.2
3097.535	10162.52	4.6
3097.540	10162.53	4.2
3097.545	10162.55	4.2
3097.550	10162.57	4.2
3097.555	10162.58	4.3
3097.565	10162.62	5.3
3097.585	10162.68	4.5
3097.590	10162.70	4.4
3097.595	10162.71	4.3
3097.600	10162.73	4.4
3097.605	10162.75	4.3
3097.610	10162.76	4.3
3097.615	10162.78	4.3
3097.620	10162.80	3.9
3097.625	10162.81	4.3
3097.645	10162.88	4.0
3097.650	10162.89	4.1
3097.655	10162.91	3.9
3097.660	10162.93	4.2
3099.530	10169.06	5.8
3099.535	10169.08	3.2
3099.540	10169.09	2.4
3099.545	10169.11	4.7
3099.555	10169.14	7.9
3099.570	10169.19	2.0
3099.585	10169.24	3.0
3099.610	10169.32	4.1
3099.615	10169.34	2.7
3099.620	10169.36	3.6
3099.625	10169.37	3.5
3099.630	10169.39	2.2
3099.635	10169.41	2.6
3099.640	10169.42	2.9
3099.705	10169.64	2.6
3099.715	10169.67	3.2
3099.720	10169.69	5.1
3099.725	10169.70	4.5
3099.730	10169.72	2.5
3099.735	10169.73	5.6
3099.740	10169.75	4.8
3099.745	10169.77	6.9
3099.750	10169.78	9.2
3099.755	10169.80	10.4
3099.780	10169.88	7.1
3099.815	10170.00	4.1
3099.825	10170.03	4.0
3099.875	10170.19	3.6
3099.880	10170.21	4.3
3099.895	10170.26	7.3
3099.910	10170.31	2.8
3099.920	10170.34	1.9
3099.930	10170.37	2.4
3099.940	10170.41	2.8
3099.980	10170.54	4.7
3099.995	10170.59	3.8
3100.000	10170.60	6.4
3100.005	10170.62	3.8
3100.020	10170.67	2.3
3100.025	10170.69	6.1
3100.050	10170.77	3.3
3100.055	10170.78	5.6
3100.060	10170.80	7.0
3100.065	10170.82	5.4
3100.070	10170.83	8.0
3100.075	10170.85	5.1
3100.080	10170.87	3.8
3100.085	10170.88	3.7
3100.090	10170.90	6.2
3100.095	10170.92	5.4
3100.100	10170.93	2.9
3100.105	10170.95	2.4
3100.120	10171.00	26.2
3100.125	10171.01	6.1
3100.135	10171.05	2.3
3100.140	10171.06	3.2
3100.145	10171.08	9.8
3100.160	10171.13	5.1
3100.235	10171.37	2.0
3100.240	10171.39	3.1
3100.270	10171.49	6.9
3100.280	10171.52	4.1
3100.285	10171.54	8.5
3100.290	10171.56	11.3
3100.295	10171.57	4.0
3100.300	10171.59	4.8

3065.895	10058.71	118.5
3065.900	10058.73	111.4
3065.905	10058.74	88.2
3065.910	10058.76	233.3
3065.915	10058.78	170.6
3065.920	10058.79	182.8
3065.925	10058.81	95.0
3065.930	10058.83	148.6
3065.935	10058.84	39.3
3065.940	10058.86	77.0
3065.945	10058.87	72.1
3065.950	10058.89	25.1
3065.955	10058.91	40.2
3065.960	10058.92	75.4
3065.965	10058.94	33.0
3065.970	10058.96	81.3
3065.975	10058.97	54.8
3065.980	10058.99	28.0
3065.985	10059.01	31.8
3065.990	10059.02	37.6
3065.995	10059.04	10.2
3066.015	10059.10	73.8
3066.020	10059.12	34.9
3066.025	10059.14	71.2
3066.030	10059.15	79.0
3066.035	10059.17	84.2
3066.040	10059.19	91.1
3066.045	10059.20	67.9
3066.050	10059.22	171.0
3066.055	10059.24	33.6
3066.060	10059.25	78.1
3066.065	10059.27	77.0
3066.070	10059.29	99.9
3066.075	10059.30	81.9
3066.080	10059.32	93.5
3066.085	10059.33	60.2
3066.090	10059.35	116.4
3066.095	10059.37	43.1
3066.100	10059.38	42.1
3066.105	10059.40	54.8
3066.110	10059.42	39.4
3066.115	10059.43	43.9
3066.120	10059.45	44.2
3066.125	10059.47	47.1
3066.130	10059.48	73.2
3066.135	10059.50	81.3
3066.140	10059.51	38.8
3066.145	10059.53	68.4
3066.150	10059.55	6.8
3066.155	10059.56	25.5
3066.180	10059.65	98.7
3066.185	10059.66	98.0
3066.190	10059.68	69.4
3066.195	10059.70	68.2
3066.200	10059.71	81.8
3066.205	10059.73	69.8
3066.315	10060.09	2.4
3066.320	10060.11	3.1
3066.325	10060.12	3.5
3066.330	10060.14	4.2
3066.335	10060.15	4.4
3066.340	10060.17	4.6
3066.345	10060.19	4.7
3066.365	10060.25	81.2
3066.370	10060.27	127.3
3066.375	10060.29	108.1
3066.380	10060.30	45.7
3066.385	10060.32	138.9
3066.390	10060.33	140.8
3066.395	10060.35	67.5
3066.400	10060.37	77.9
3066.405	10060.38	142.2
3066.410	10060.40	84.2
3066.415	10060.42	23
3066.420	10060.43	60.8
3066.425	10060.45	62.3
3066.430	10060.47	102.1
3066.435	10060.48	104.5
3066.440	10060.50	121.1
3066.445	10060.52	54.3
3066.450	10060.53	132.5
3066.455	10060.55	184.7
3066.460	10060.56	117.8
3066.465	10060.58	134.8
3066.470	10060.60	110.7
3066.475	10060.61	132.1
3066.480	10060.63	189.1
3066.485	10060.65	137
3066.500	10060.70	37.4
3066.505	10060.71	24.6
3066.510	10060.73	26.4
3066.515	10060.75	30.5
3066.520	10060.76	74.8
3066.525	10060.78	59.8
3066.530	10060.79	103.6
3066.535	10060.81	128.1
3066.540	10060.83	104.1
3066.545	10060.84	155.4
3066.550	10060.86	126.2
3066.555	10060.88	142.1
3066.560	10060.89	212.6
3066.565	10060.91	135.3
3066.570	10060.93	121.7

3080.805	10107.63	9.6
3080.810	10107.64	13.5
3080.815	10107.66	14.6
3080.835	10107.73	72.1
3080.840	10107.74	46.6
3080.845	10107.76	62.3
3080.850	10107.78	31.2
3080.855	10107.79	30.7
3080.860	10107.81	63.1
3080.865	10107.83	33.1
3080.870	10107.84	61.0
3080.875	10107.86	38.7
3080.880	10107.87	56.3
3080.885	10107.89	63.1
3080.890	10107.91	52.6
3080.895	10107.92	75.3
3080.900	10107.94	33.9
3080.905	10107.96	27.7
3080.910	10107.97	23.0
3080.915	10107.99	66.7
3080.920	10108.01	58.5
3080.925	10108.02	46.3
3080.930	10108.04	36.9
3080.935	10108.05	59.3
3080.955	10108.12	67.7
3080.960	10108.14	88.3
3080.965	10108.15	88.1
3080.970	10108.17	41.8
3080.975	10108.19	40.4
3080.980	10108.20	85.6
3080.985	10108.22	75.4
3080.990	10108.24	96.4
3080.995	10108.25	45.9
3081.000	10108.27	34.3
3081.005	10108.28	31.2
3081.010	10108.30	41.6
3081.015	10108.32	56.5
3081.020	10108.33	27.9
3081.025	10108.35	33.4
3081.030	10108.37	25.2
3081.035	10108.38	23.3
3081.040	10108.40	28.7
3081.045	10108.42	56.2
3081.050	10108.43	31.9
3081.055	10108.45	34.1
3081.060	10108.46	29.0
3081.065	10108.48	55.7
3081.070	10108.50	8.1
3081.075	10108.51	21.0
3081.080	10108.53	34.8
3081.085	10108.55	13.7
3081.090	10108.56	13.9
3081.095	10108.58	10.7
3081.100	10108.60	13.5
3081.105	10108.61	39.5
3081.110	10108.63	19.8
3081.115	10108.65	24.8
3081.120	10108.66	13.5
3081.125	10108.68	28.1
3081.130	10108.69	18.0
3081.135	10108.71	17.9
3081.140	10108.73	17.6
3081.145	10108.74	22.5
3081.150	10108.76	14.9
3081.155	10108.78	23.7
3081.160	10108.79	41.1
3081.180	10108.86	46.5
3081.185	10108.87	46.8
3081.190	10108.89	15.7
3081.195	10108.91	22.1
3081.200	10108.92	14.4
3081.245	10109.07	82.7
3081.250	10109.09	32.0
3081.255	10109.10	57.3
3081.260	10109.12	27.6
3081.265	10109.14	101.2
3081.270	10109.15	58.7
3081.275	10109.17	32.4
3081.295	10109.24	18.4
3081.300	10109.25	21.0
3081.305	10109.27	27.2
3081.310	10109.29	34.5
3081.315	10109.30	30.4
3081.320	10109.32	25.7
3081.325	10109.33	35.0
3081.330	10109.35	72.3
3081.335	10109.37	35.1
3081.340	10109.38	43.2
3081.345	10109.40	42.6
3081.350	10109.42	13.6
3081.355	10109.43	23.0
3081.360	10109.45	21.5
3081.365	10109.47	21.4
3081.370	10109.48	35.4
3081.375	10109.50	40.0
3081.380	10109.51	40.6
3081.385	10109.53	34.7
3081.390	10109.55	43.8
3081.395	10109.56	27.8
3081.400	10109.58	6.0
3081.405	10109.60	25.0
3081.410	10109.61	10.4
3081.415	10109.63	20.2

3088.965	10134.40	7.0
3088.970	10134.42	5.3
3088.975	10134.43	12.0
3088.980	10134.45	41.6
3088.985	10134.47	4.1
3088.990	10134.48	31.5
3088.995	10134.50	39.2
3089.010	10134.55	12.7
3089.015	10134.56	10.9
3089.020	10134.58	42.3
3089.025	10134.60	35.0
3089.030	10134.61	71.2
3089.035	10134.63	63.4
3089.040	10134.65	9.3
3089.045	10134.66	39.9
3089.050	10134.68	12.5
3089.055	10134.70	7.7
3089.060	10134.71	46.8
3089.065	10134.73	27.4
3089.070	10134.74	46.9
3089.075	10134.76	31.8
3089.080	10134.78	27.1
3089.085	10134.79	56.3
3089.090	10134.81	10.1
3089.095	10134.83	15.1
3089.100	10134.84	85.9
3089.105	10134.86	36.4
3089.110	10134.88	87.6
3089.115	10134.89	54.2
3089.120	10134.91	27.5
3089.125	10134.92	6.7
3089.130	10134.94	9.6
3089.135	10134.96	21.4
3089.140	10134.97	13.6
3089.145	10134.99	14.1
3089.150	10135.01	43.0
3089.155	10135.02	30.2
3089.160	10135.04	22.0
3089.165	10135.06	20.3
3089.170	10135.07	25.1
3089.190	10135.14	29.0
3089.195	10135.15	36.7
3089.200	10135.17	16.0
3089.205	10135.19	42.5
3089.210	10135.20	57.7
3089.215	10135.22	35.4
3089.220	10135.24	29.9
3089.225	10135.25	11.5
3089.230	10135.27	38.9
3089.235	10135.29	35.8
3089.240	10135.30	33.2
3089.245	10135.32	10.5
3089.250	10135.33	34.6
3089.255	10135.35	24.2
3089.260	10135.37	13.1
3089.265	10135.38	44.4
3089.270	10135.40	56.2
3089.275	10135.42	29.8
3089.280	10135.43	14.6
3089.285	10135.45	25.8
3089.290	10135.47	37.4
3089.295	10135.48	8.8
3089.300	10135.50	22.3
3089.305	10135.52	39.8
3089.310	10135.53	20.9
3089.315	10135.55	12.8
3089.320	10135.56	10.1
3089.325	10135.58	10.3
3089.330	10135.60	16.4
3089.335	10135.61	25.5
3089.340	10135.63	18.9
3089.345	10135.65	29.9
3089.350	10135.66	20.4
3089.355	10135.68	42.2
3089.360	10135.70	30.3
3089.365	10135.71	27.0
3089.370	10135.73	22.7
3089.395	10135.81	33.9
3089.400	10135.83	41.2
3089.405	10135.84	69.5
3089.410	10135.86	47.4
3089.415	10135.88	25.5
3089.420	10135.89	71.8
3089.425	10135.91	21.0
3089.430	10135.93	43.0
3089.435	10135.94	48.6
3089.440	10135.96	28.2
3089.475	10136.07	29.6
3089.480	10136.09	19.6
3089.505	10136.17	60.0
3089.510	10136.19	33.3
3089.515	10136.20	24.3
3089.520	10136.22	60.8
3089.525	10136.24	63.9
3089.530	10136.25	30.1
3089.535	10136.27	64.7
3089.540	10136.29	48.0
3089.545	10136.30	89.7
3089.550	10136.32	33.0
3089.555	10136.34	53.3
3089.560	10136.35	66.6
3089.565	10136.37	49.2
3089.570	10136.38	45.7

3100.305	10171.60	4.4
3100.310	10171.62	6.1
3100.315	10171.64	5.1
3100.320	10171.65	6.2
3100.325	10171.67	6.0
3100.330	10171.69	8.0
3100.335	10171.70	7.9
3100.340	10171.72	11.4
3100.345	10171.74	8.3
3100.350	10171.75	6.5
3100.355	10171.77	4.5
3100.360	10171.79	3.8
3100.365	10171.80	3.7
3100.370	10171.82	3.8
3100.445	10172.06	14.3
3100.450	10172.08	12.3
3100.455	10172.10	6.7
3100.460	10172.11	5.0
3100.465	10172.13	4.0
3100.475	10172.16	2.2
3100.485	10172.20	2.4
3100.490	10172.21	5.9
3100.495	10172.23	2.6
3100.500	10172.24	2.2
3100.515	10172.29	3.0
3100.520	10172.31	5.6
3100.525	10172.33	2.1
3100.535	10172.36	2.9
3100.560	10172.44	4.0
3100.565	10172.46	6.2
3100.570	10172.47	31.6
3100.575	10172.49	3.5
3100.580	10172.51	9.2
3100.585	10172.52	2.8
3100.590	10172.54	6.0
3100.595	10172.56	12.6
3100.600	10172.57	9.5
3100.605	10172.59	6.9
3100.610	10172.61	24.2
3100.615	10172.62	11.3
3100.620	10172.64	27.2
3100.625	10172.65	8.3
3100.630	10172.67	16.1
3100.635	10172.69	38.4
3100.640	10172.70	28.8
3100.645	10172.72	21.9
3100.650	10172.74	32.6
3100.655	10172.75	16.5
3100.680	10172.83	11.8
3100.685	10172.85	17.6
3100.690	10172.87	29.6
3100.695	10172.88	46.9
3100.700	10172.90	19.2
3100.705	10172.92	29.9
3100.710	10172.93	40.2
3100.715	10172.95	45.1
3100.720	10172.97	35.8
3100.725	10172.98	43.7
3100.730	10173.00	33.6
3100.735	10173.02	23.0
3100.740	10173.03	21.2
3100.745	10173.05	9.9
3100.750	10173.06	12.9
3100.755	10173.08	23.0
3100.760	10173.10	8.7
3100.765	10173.11	13.0
3100.985	10173.84	9.7
3100.990	10173.85	3.1
3100.995	10173.87	3.4
3101.000	10173.88	4.0
3101.005	10173.90	4.8
3101.015	10173.93	3.9
3101.020	10173.95	2.9
3101.025	10173.97	4.2
3101.030	10173.98	3.3
3101.035	10174.00	10.7
3101.040	10174.02	10.9
3101.045	10174.03	4.8
3101.050	10174.05	6.5
3101.055	10174.07	22.5
3101.060	10174.08	12.0
3101.065	10174.10	16.7

3066.575	10060.94	132
3066.580	10060.96	110.7
3066.585	10060.97	162.5
3066.590	10060.99	98.8
3066.595	10061.01	126.1
3066.600	10061.02	102.9
3066.605	10061.04	109.3
3066.610	10061.06	21.4
3066.615	10061.07	60.4
3066.620	10061.09	39.1
3066.625	10061.11	41.1
3066.630	10061.12	33.7
3066.635	10061.14	33.7
3066.640	10061.16	61.2
3066.645	10061.17	55
3066.650	10061.19	111.6
3066.655	10061.20	79.8
3066.660	10061.22	76.2
3066.680	10061.29	106.4
3066.685	10061.30	150
3066.690	10061.32	248.6
3066.695	10061.34	213.8
3066.700	10061.35	132.5
3066.705	10061.37	224.3
3066.710	10061.38	236.8
3066.715	10061.40	140.2
3066.720	10061.42	180
3066.725	10061.43	216
3066.730	10061.45	284
3066.735	10061.47	265.7
3066.740	10061.48	300.5
3066.745	10061.50	227.5
3066.750	10061.52	262.9
3066.755	10061.53	302.1
3066.760	10061.55	201.6
3066.765	10061.57	329.9
3066.770	10061.58	314.3
3066.775	10061.60	249
3066.780	10061.61	204.6
3066.785	10061.63	134.7
3066.790	10061.65	165.1
3066.795	10061.66	151.1
3066.800	10061.68	246.3
3066.805	10061.70	316.9
3066.810	10061.71	212.3
3066.815	10061.73	181.4
3066.820	10061.75	282.6
3066.825	10061.76	273.4
3066.830	10061.78	228.1
3066.835	10061.79	340.6
3066.840	10061.81	206.3
3066.845	10061.83	360
3066.850	10061.84	178.2
3066.860	10061.88	116.5
3066.865	10061.89	201.1
3066.870	10061.91	173.4
3066.875	10061.93	60.1
3066.880	10061.94	114.3
3066.885	10061.96	253.9
3066.890	10061.98	231.2
3066.895	10061.99	82.2
3066.900	10062.01	262.3
3066.905	10062.02	159.7
3066.910	10062.04	122.8
3066.915	10062.06	91.9
3066.920	10062.07	98.4
3066.925	10062.09	40.9
3066.930	10062.11	160.3
3066.945	10062.16	159.1
3066.950	10062.17	129.4
3066.955	10062.19	162.1
3066.960	10062.21	197.7
3066.965	10062.22	201
3066.970	10062.24	108.4
3066.975	10062.25	233.9
3066.980	10062.27	125.2
3066.985	10062.29	171.3
3066.990	10062.30	163.1
3066.995	10062.32	122.6
3067.000	10062.34	84.3
3067.005	10062.35	146.4
3067.010	10062.37	95.1
3067.015	10062.39	177.7
3067.020	10062.40	132.4
3067.025	10062.42	41.6
3067.030	10062.43	104.4
3067.035	10062.45	191.7
3067.040	10062.47	186.5
3067.045	10062.48	157.8
3067.050	10062.50	163.3
3067.055	10062.52	291.7
3067.060	10062.53	214.8
3067.065	10062.55	146.6
3067.070	10062.57	242
3067.075	10062.58	130.9
3067.080	10062.60	137
3067.085	10062.62	201
3067.090	10062.63	93.9
3067.095	10062.65	150.1
3067.100	10062.66	157.7
3067.105	10062.68	132.4
3067.110	10062.70	67.7
3067.115	10062.71	126.4

3081.420	10109.65	13.7
3081.425	10109.66	29.6
3081.430	10109.68	33.6
3081.435	10109.70	24.7
3081.440	10109.71	45.1
3081.445	10109.73	12.7
3081.450	10109.74	23.4
3081.455	10109.76	34.1
3081.460	10109.78	39.4
3081.465	10109.79	32.7
3081.485	10109.86	28.9
3081.490	10109.88	37.9
3081.495	10109.89	18.0
3081.500	10109.91	29.2
3081.505	10109.92	46.0
3081.510	10109.94	12.0
3081.515	10109.96	25.6
3081.520	10109.97	31.2
3081.525	10109.99	19.5
3081.530	10110.01	43.0
3081.535	10110.02	36.6
3081.540	10110.04	26.9
3081.545	10110.06	25.6
3081.575	10110.15	20.2
3081.580	10110.17	13.9
3081.585	10110.19	11.3
3081.590	10110.20	13.4
3081.595	10110.22	17.4
3081.600	10110.24	9.9
3081.605	10110.25	9.9
3081.610	10110.27	9.5
3081.615	10110.29	7.0
3081.620	10110.30	7.0
3081.625	10110.32	8.1
3081.630	10110.33	5.6
3081.635	10110.35	4.7
3081.640	10110.37	4.4
3081.645	10110.38	4.1
3081.650	10110.40	3.2
3081.655	10110.42	2.2
3081.670	10110.47	3.8
3081.675	10110.48	4.0
3081.680	10110.50	4.0
3081.690	10110.53	3.7
3081.700	10110.56	2.1
3081.705	10110.58	2.7
3081.710	10110.60	3.6
3081.715	10110.61	5.6
3081.735	10110.68	6.3
3081.740	10110.70	8.2
3081.745	10110.71	11.0
3081.750	10110.73	9.1
3081.765	10110.78	10.2
3081.770	10110.79	8.1
3081.775	10110.81	13.8
3081.780	10110.83	14.5
3081.785	10110.84	22.3
3081.790	10110.86	13.3
3081.795	10110.88	24.2
3081.800	10110.89	37.3
3081.805	10110.91	43.6
3081.810	10110.93	47.8
3081.815	10110.94	43.7
3081.820	10110.96	27.6
3081.825	10110.97	35.3
3081.830	10110.99	29.7
3081.835	10111.01	35.5
3081.840	10111.02	39.3
3081.845	10111.04	40.7
3081.850	10111.06	37.6
3081.855	10111.07	33.2
3081.860	10111.09	26.6
3081.865	10111.11	41.9
3081.870	10111.12	39.8
3081.875	10111.14	16.2
3081.880	10111.16	43.6
3081.885	10111.17	21.9
3081.890	10111.19	25.5
3081.895	10111.20	24.9
3081.900	10111.22	66.7
3081.905	10111.24	38.2
3081.910	10111.25	59.1
3081.915	10111.27	44.7
3081.950	10111.38	24.5
3081.955	10111.40	24.5
3081.960	10111.42	23.7
3081.965	10111.43	27.2
3081.970	10111.45	25.3
3081.975	10111.47	23.3
3081.980	10111.48	22.3
3081.985	10111.50	30.7
3081.990	10111.52	22.1
3081.995	10111.53	27.9
3082.000	10111.55	28.3
3082.005	10111.57	27.5
3082.010	10111.58	19.2
3082.015	10111.60	28.1
3082.020	10111.61	29.6
3082.025	10111.63	18.4
3082.030	10111.65	34.1
3082.035	10111.66	25.0
3082.040	10111.68	29.1
3082.045	10111.70	31.4

3089.575	10136.40	30.7
3089.580	10136.42	40.0
3089.585	10136.43	62.0
3089.590	10136.45	67.9
3089.595	10136.47	39.4
3089.600	10136.48	42.2
3089.605	10136.50	37.0
3089.610	10136.52	42.2
3089.615	10136.53	28.3
3089.620	10136.55	42.3
3089.625	10136.57	32.9
3089.630	10136.58	69.5
3089.635	10136.60	36.8
3089.640	10136.61	64.0
3089.665	10136.70	42.4
3089.670	10136.71	19.3
3089.675	10136.73	6.9
3089.680	10136.75	21.9
3089.685	10136.76	24.8
3089.690	10136.78	13.4
3089.695	10136.79	45.2
3089.700	10136.81	18.1
3089.705	10136.83	30.1
3089.710	10136.84	43.1
3089.715	10136.86	26.0
3089.720	10136.88	16.3
3089.725	10136.89	38.4
3089.730	10136.91	24.7
3089.735	10136.93	29.2
3089.740	10136.94	46.2
3089.745	10136.96	95.0
3089.750	10136.98	21.9
3089.770	10137.04	36.4
3089.775	10137.06	35.8
3089.780	10137.07	25.6
3089.785	10137.09	40.5
3089.790	10137.11	25.5
3089.795	10137.12	34.6
3089.800	10137.14	44.7
3089.805	10137.16	28.7
3089.810	10137.17	42.6
3089.815	10137.19	32.9
3089.820	10137.21	31.6
3089.825	10137.22	32.3
3089.830	10137.24	28.4
3089.835	10137.25	67.8
3089.840	10137.27	96.0
3089.845	10137.29	67.5
3089.850	10137.30	47.1
3089.855	10137.32	67.8
3089.860	10137.34	80.5
3089.865	10137.35	34.5
3089.870	10137.37	50.7
3089.875	10137.39	78.5
3089.880	10137.40	74.3
3089.885	10137.42	107.5
3089.890	10137.43	66.7
3089.895	10137.45	103.0
3089.900	10137.47	32.2
3089.905	10137.48	60.0
3089.910	10137.50	43.0
3089.930	10137.57	100.6
3089.935	10137.58	68.1
3089.940	10137.60	90.5
3089.945	10137.62	89.5
3089.950	10137.63	80.4
3089.955	10137.65	75.0
3089.960	10137.66	59.2
3089.965	10137.68	95.0
3089.970	10137.70	76.1
3089.975	10137.71	85.5
3089.980	10137.73	70.2
3089.985	10137.75	141.3
3089.990	10137.76	75.2
3089.995	10137.78	90.4
3090.000	10137.80	51.9
3090.005	10137.81	52.8
3090.010	10137.83	76.6
3090.015	10137.84	75.5
3090.020	10137.86	92.6
3090.025	10137.88	105.2
3090.030	10137.89	159.8
3090.050	10137.96	143.7
3090.055	10137.98	111.3
3090.060	10137.99	128.4
3090.065	10138.01	72.8
3090.070	10138.03	128.7
3090.075	10138.04	38.6
3090.080	10138.06	22.3
3090.085	10138.07	84.5
3090.090	10138.09	57.9
3090.095	10138.11	53.0
3090.100	10138.12	12.2
3090.105	10138.14	13.3
3090.110	10138.16	38.3
3090.115	10138.17	36.2
3090.120	10138.19	49.2
3090.125	10138.21	2.4
3090.130	10138.22	2.2
3090.135	10138.24	2.2
3090.140	10138.25	3.3
3090.155	10138.30	5.3
3090.165	10138.34	3.4

3067.120	10062.73	197	3082.065	10111.76	23.0	3090.170	10138.35	3.9
3067.125	10062.75	249.3	3082.070	10111.78	41.2	3090.175	10138.37	2.6
3067.130	10062.76	230.6	3082.075	10111.79	30.0	3090.180	10138.39	2.4
3067.135	10062.78	98.1	3082.080	10111.81	28.6	3090.205	10138.47	6.8
3067.140	10062.80	86.7	3082.085	10111.83	24.6	3090.210	10138.48	2.6
3067.145	10062.81	43.3	3082.090	10111.84	25.5	3090.215	10138.50	7.8
3067.150	10062.83	175.3	3082.095	10111.86	21.2	3090.220	10138.52	6.5
3067.155	10062.84	116.8	3082.100	10111.88	26.4	3090.225	10138.53	3.6
3067.160	10062.86	59.5	3082.105	10111.89	32.9	3090.230	10138.55	3.3
3067.165	10062.88	71.4	3082.110	10111.91	28.3	3090.235	10138.57	3.8
3067.170	10062.89	93.7	3082.115	10111.93	20.6	3090.240	10138.58	5.1
3067.175	10062.91	58.7	3082.120	10111.94	25.5	3090.245	10138.60	3.1
3067.180	10062.93	156.3	3082.125	10111.96	24.6	3090.250	10138.62	4.1
3067.220	10063.06	158.2	3082.370	10112.76	28.1	3090.255	10138.63	4.9
3067.225	10063.07	208.9	3082.375	10112.78	55.9	3090.260	10138.65	5.3
3067.230	10063.09	140.1	3082.380	10112.80	48.9	3090.265	10138.67	3.7
3067.235	10063.11	123.2	3082.385	10112.81	34.5	3090.270	10138.68	8.7
3067.240	10063.12	112.8	3082.390	10112.83	68.9	3090.275	10138.70	3.7
3067.245	10063.14	43.6	3082.395	10112.84	104.0	3090.280	10138.71	3.4
3067.250	10063.16	86.2	3082.400	10112.86	66.7	3090.285	10138.73	6.2
3067.255	10063.17	105.9	3082.405	10112.88	67.5	3090.290	10138.75	14.0
3067.260	10063.19	94.9	3082.410	10112.89	74.8	3090.295	10138.76	8.1
3067.265	10063.21	1.9	3082.415	10112.91	67.1	3090.300	10138.78	14.0
3067.270	10063.22	109.5	3082.420	10112.93	52.9	3090.305	10138.80	11.2
3067.275	10063.24	164.7	3082.425	10112.94	62.7	3090.310	10138.81	9.2
3067.280	10063.25	118.6	3082.430	10112.96	47.0	3090.315	10138.83	10.2
3067.285	10063.27	87.9	3082.435	10112.98	55.4	3090.385	10139.06	20.0
3067.290	10063.29	138.3	3082.440	10112.99	58.1	3090.390	10139.08	11.1
3067.295	10063.30	167.1	3082.445	10113.01	34.4	3090.395	10139.09	8.0
3067.300	10063.32	161.2	3082.450	10113.03	48.0	3090.400	10139.11	8.8
3067.305	10063.34	88.1	3082.455	10113.04	36.3	3090.405	10139.12	30.2
3067.310	10063.35	78.9	3082.460	10113.06	55.5	3090.410	10139.14	13.6
3067.315	10063.37	185.1	3082.465	10113.07	93.1	3090.415	10139.16	21.4
3067.320	10063.39	90.4	3082.470	10113.09	84.4	3090.420	10139.17	9.0
3067.325	10063.40	69.9	3082.475	10113.11	64.1	3090.425	10139.19	23.5
3067.330	10063.42	119.4	3082.480	10113.12	78.9	3090.430	10139.21	21.1
3067.335	10063.44	88.6	3082.500	10113.19	42.0	3090.435	10139.22	47.1
3067.340	10063.45	34.4	3082.505	10113.21	38.3	3090.440	10139.24	10.9
3067.345	10063.47	73.1	3082.510	10113.22	44.5	3090.445	10139.26	35.5
3067.350	10063.48	107.8	3082.515	10113.24	30.0	3090.450	10139.27	29.6
3067.355	10063.50	105.4	3082.520	10113.25	35.4	3090.455	10139.29	30.7
3067.360	10063.52	121.3	3082.525	10113.27	39.3	3090.460	10139.30	30.7
3067.365	10063.53	62.3	3082.530	10113.29	32.5	3090.465	10139.32	65.6
3067.370	10063.55	86.3	3082.535	10113.30	45.4	3090.470	10139.34	42.3
3067.375	10063.57	141.4	3082.540	10113.32	29.5	3090.475	10139.35	22.1
3067.380	10063.58	135.7	3082.545	10113.34	34.5	3090.490	10139.40	20.7
3067.385	10063.60	100.4	3082.550	10113.35	39.4	3090.495	10139.42	40.9
3067.390	10063.62	42.3	3082.555	10113.37	30.1	3090.500	10139.44	18.7
3067.395	10063.63	75.1	3082.560	10113.39	40.5	3090.505	10139.45	25.9
3067.400	10063.65	53.3	3082.565	10113.40	37.5	3090.510	10139.47	14.7
3067.405	10063.67	105.7	3082.570	10113.42	45.7	3090.515	10139.49	13.1
3067.410	10063.68	23.6	3082.575	10113.44	39.0	3090.520	10139.50	60.6
3067.415	10063.70	75.1	3082.580	10113.45	34.7	3090.525	10139.52	12.6
3067.420	10063.71	88.3	3082.585	10113.47	37.3	3090.530	10139.53	25.2
3067.425	10063.73	90.0	3082.590	10113.48	38.3	3090.535	10139.55	15.9
3067.430	10063.75	65.5	3082.595	10113.50	54.7	3090.540	10139.57	11.7
3067.435	10063.76	50.4	3082.600	10113.52	42.9	3090.545	10139.58	35.5
3067.440	10063.78	40.7	3082.625	10113.60	80.8	3090.550	10139.60	38.2
3067.445	10063.80	35.1	3082.630	10113.62	41.0	3090.555	10139.62	45.4
3067.450	10063.81	21.4	3082.635	10113.63	45.7	3090.560	10139.63	50.8
3067.455	10063.83	230.5	3082.640	10113.65	79.5	3090.565	10139.65	39.6
3067.460	10063.85	61.1	3082.645	10113.67	68.6	3090.570	10139.67	53.1
3067.465	10063.86	131.4	3082.650	10113.68	72.5	3090.575	10139.68	43.8
3067.470	10063.88	165.0	3082.655	10113.70	76.4	3090.580	10139.70	38.8
3067.475	10063.89	148.1	3082.660	10113.71	55.9	3090.585	10139.71	64.3
3067.480	10063.91	102.8	3082.665	10113.73	87.9	3090.590	10139.73	46.9
3067.485	10063.93	147.4	3082.670	10113.75	39.7	3090.595	10139.75	9.7
3067.490	10063.94	107.4	3082.675	10113.76	43.3	3090.600	10139.76	25.8
3067.495	10063.96	79.7	3082.680	10113.78	74.0	3090.605	10139.78	61.5
3067.500	10063.98	51.4	3082.685	10113.80	43.1	3090.610	10139.80	69.5
3067.505	10063.99	41.8	3082.690	10113.81	58.8	3090.615	10139.81	36.3
3067.510	10064.01	45.3	3082.695	10113.83	97.1	3090.620	10139.83	13.1
3067.515	10064.03	124.4	3082.700	10113.85	68.5	3090.625	10139.85	11.2
3067.520	10064.04	96.0	3082.705	10113.86	29.7	3090.635	10139.88	47.2
3067.525	10064.06	134.2	3082.710	10113.88	69.0	3090.640	10139.90	43.8
3067.530	10064.08	116.4	3082.715	10113.89	52.2	3090.645	10139.91	15.6
3067.535	10064.09	104.3	3082.730	10113.94	88.6	3090.650	10139.93	14.9
3067.540	10064.11	2.9	3082.735	10113.96	70.5	3090.655	10139.94	49.6
3067.545	10064.12	57.8	3082.740	10113.98	77.9	3090.660	10139.96	23.9
3067.550	10064.14	69.4	3082.745	10113.99	61.2	3090.665	10139.98	34.1
3067.555	10064.16	80.7	3082.750	10114.01	79.2	3090.670	10139.99	44.0
3067.560	10064.17	148.0	3082.755	10114.03	46.4	3090.675	10140.01	42.3
3067.565	10064.19	104.2	3082.760	10114.04	68.3	3090.680	10140.03	19.2
3067.570	10064.21	101.5	3082.765	10114.06	72.6	3090.685	10140.04	50.1
3067.575	10064.22	87.8	3082.770	10114.08	60.3	3090.690	10140.06	35.6
3067.580	10064.24	111.2	3082.775	10114.09	101.0	3090.695	10140.08	41.2
3067.585	10064.26	61.9	3082.780	10114.11	84.4	3090.700	10140.09	47.3
3067.590	10064.27	96.7	3082.785	10114.12	77.0	3090.705	10140.11	63.7
3067.595	10064.29	143.1	3082.790	10114.14	100.1	3090.710	10140.12	43.8
3067.600	10064.30	146.4	3082.795	10114.16	54.3	3090.715	10140.14	52.4
3067.605	10064.32	245.7	3082.800	10114.17	97.5	3090.720	10140.16	41.6
3067.610	10064.34	191.1	3082.805	10114.19	115.7	3090.725	10140.17	51.1
3067.615	10064.35	144.6	3082.810	10114.21	98.7	3090.730	10140.19	41.6
3067.620	10064.37	133.0	3082.815	10114.22	127.5	3090.750	10140.26	29.7
3067.625	10064.39	181.9	3082.820	10114.24	138.9	3090.755	10140.27	65.9
3067.630	10064.40	174.4	3082.825	10114.26	168.8	3090.760	10140.29	50.3
3067.635	10064.42	147.5	3082.830	10114.27	118.0	3090.765	10140.31	71.0
3067.640	10064.44	160.1	3082.835	10114.29	198.0	3090.770	10140.32	91.8
3067.645	10064.45	136.3	3082.855	10114.35	60.1	3090.775	10140.34	113.6
3067.650	10064.47	132.6	3082.860	10114.37	139.8	3090.780	10140.35	39.5
3067.655	10064.49	141.4	3082.865	10114.39	117.4	3090.785	10140.37	31.2
3067.660	10064.50	184.8	3082.870	10114.40	106.3	3090.790	10140.39	76.7
3067.665	10064.52	294.2	3082.875	10114.42	156.0	3090.795	10140.40	60.4

3067.670	10064.53	134.8
3067.675	10064.55	64.1
3067.680	10064.57	51.5
3067.685	10064.58	42.0
3067.690	10064.60	87.1
3067.695	10064.62	114.6
3067.700	10064.63	66.7
3067.705	10064.65	47.4
3067.710	10064.67	90.6
3067.715	10064.68	134.8
3067.720	10064.70	50.3
3067.725	10064.71	52.1
3067.730	10064.73	123.9
3067.735	10064.75	203.3
3067.740	10064.76	124.6
3067.745	10064.78	132.7
3067.750	10064.80	127.8
3067.755	10064.81	117.9
3067.760	10064.83	71.9
3067.765	10064.85	3.3
3067.770	10064.86	125.2
3067.775	10064.88	77.3
3067.780	10064.90	126.0
3067.785	10064.91	134.1
3067.790	10064.93	274.9
3067.795	10064.94	251.7
3067.800	10064.96	5.0
3067.815	10065.01	195.6
3067.820	10065.03	252.7
3067.825	10065.04	246.9
3067.830	10065.06	122.8
3067.835	10065.08	133.0
3067.840	10065.09	199.9
3067.845	10065.11	125.2
3067.850	10065.12	191.2
3067.855	10065.14	157.4
3067.860	10065.16	139.4
3067.865	10065.17	131.9
3067.870	10065.19	182.6
3067.875	10065.21	167.3
3067.880	10065.22	263.4
3067.900	10065.29	224.4
3067.905	10065.31	137.3
3067.910	10065.32	170.3
3067.915	10065.34	142.8
3067.920	10065.35	127.0
3067.925	10065.37	107.9
3067.930	10065.39	191.2
3067.935	10065.40	143.3
3067.940	10065.42	147.9
3067.945	10065.44	196.3
3067.950	10065.45	158.4
3067.955	10065.47	47.6
3067.960	10065.49	103.3
3067.965	10065.50	87.6
3067.970	10065.52	240.9
3067.975	10065.54	141.5
3067.980	10065.55	134.8
3067.985	10065.57	129.8
3067.990	10065.58	33.3
3067.995	10065.60	67.9
3068.000	10065.62	74.4
3068.005	10065.63	89.4
3068.010	10065.65	139.9
3068.015	10065.67	78.0
3068.020	10065.68	63.0
3068.025	10065.70	63.9
3068.030	10065.72	86.5
3068.035	10065.73	90.1
3068.040	10065.75	91.9
3068.065	10065.83	173.5
3068.070	10065.85	203.3
3068.075	10065.86	89.3
3068.080	10065.88	87.9
3068.085	10065.90	120.5
3068.090	10065.91	64.7
3068.095	10065.93	134.4
3068.100	10065.95	132.8
3068.135	10066.06	299.7
3068.140	10066.08	433.6
3068.145	10066.09	248.3
3068.150	10066.11	323.9
3068.155	10066.13	145.1
3068.160	10066.14	145.5
3068.165	10066.16	265.4
3068.170	10066.17	343.4
3068.175	10066.19	196.8
3068.195	10066.26	265.3
3068.200	10066.27	268.7
3068.205	10066.29	348.7
3068.210	10066.31	343.9
3068.215	10066.32	210.2
3068.220	10066.34	217.6
3068.225	10066.36	249.3
3068.230	10066.37	265.7
3068.235	10066.39	130.4
3068.240	10066.40	216.0
3068.265	10066.49	128.2
3068.270	10066.50	200.0
3068.275	10066.52	175.8
3068.280	10066.54	101.5
3068.285	10066.55	128.0
3068.290	10066.57	132.5
3082.880	10114.44	101.1
3082.885	10114.45	42.4
3082.890	10114.47	118.9
3082.895	10114.49	97.0
3082.900	10114.50	81.4
3082.905	10114.52	85.0
3082.910	10114.53	105.5
3082.915	10114.55	58.9
3082.920	10114.57	109.7
3082.925	10114.58	77.8
3082.930	10114.60	98.6
3082.935	10114.62	77.3
3082.940	10114.63	87.9
3082.945	10114.65	79.1
3082.965	10114.71	12.4
3082.970	10114.73	42.2
3082.975	10114.75	24.2
3082.980	10114.76	52.2
3082.985	10114.78	45.8
3082.990	10114.80	18.1
3082.995	10114.81	42.9
3083.000	10114.83	18.9
3083.005	10114.85	55.6
3083.010	10114.86	56.9
3083.015	10114.88	75.3
3083.020	10114.90	52.6
3083.070	10115.06	67.6
3083.075	10115.08	67.6
3083.080	10115.09	27.6
3083.085	10115.11	22.3
3083.090	10115.12	47.9
3083.095	10115.14	25.4
3083.110	10115.19	85.2
3083.115	10115.21	61.7
3083.120	10115.22	134.8
3083.125	10115.24	41.7
3083.130	10115.26	23.5
3083.135	10115.27	91.4
3083.140	10115.29	40.4
3083.145	10115.31	55.1
3083.150	10115.32	61.2
3083.155	10115.34	47.1
3083.160	10115.35	24.2
3083.165	10115.37	60.1
3083.170	10115.39	34.5
3083.175	10115.40	16.8
3083.180	10115.42	47.0
3083.185	10115.44	86.1
3083.190	10115.45	33.8
3083.195	10115.47	36.2
3083.200	10115.49	61.2
3083.205	10115.50	58.8
3083.210	10115.52	31.5
3083.215	10115.54	25.2
3083.220	10115.55	29.6
3083.225	10115.57	62.8
3083.230	10115.58	26.0
3083.235	10115.60	72.6
3083.240	10115.62	89.4
3083.245	10115.63	91.3
3083.250	10115.65	47.8
3083.265	10115.70	69.0
3083.270	10115.72	108.0
3083.275	10115.73	68.5
3083.280	10115.75	28.0
3083.285	10115.76	61.6
3083.290	10115.78	34.5
3083.295	10115.80	61.6
3083.300	10115.81	45.3
3083.305	10115.83	35.1
3083.310	10115.85	21.9
3083.315	10115.86	74.7
3083.320	10115.88	27.9
3083.325	10115.90	53.0
3083.330	10115.91	90.6
3083.335	10115.93	82.6
3083.340	10115.95	38.4
3083.345	10115.96	139.5
3083.350	10115.98	73.2
3083.355	10115.99	144.6
3083.360	10116.01	173.8
3083.365	10116.03	91.5
3083.370	10116.04	34.8
3083.375	10116.06	76.7
3083.380	10116.08	109.8
3083.385	10116.09	86.2
3083.405	10116.16	34.3
3083.410	10116.17	54.5
3083.415	10116.19	10.0
3083.420	10116.21	9.2
3083.425	10116.22	15.6
3083.430	10116.24	24.1
3083.435	10116.26	41.0
3083.440	10116.27	73.3
3083.445	10116.29	107.4
3083.450	10116.31	164.5
3083.455	10116.32	183.2
3083.460	10116.34	42.3
3083.465	10116.36	75.1
3083.470	10116.37	109.2
3083.475	10116.39	150.6
3083.480	10116.40	39.3
3083.485	10116.42	37.6
3090.800	10140.42	34.3
3090.830	10140.52	86.7
3090.835	10140.54	76.8
3090.840	10140.55	107.2
3090.845	10140.57	77.0
3090.850	10140.58	105.2
3090.855	10140.60	95.3
3090.860	10140.62	62.5
3090.865	10140.63	37.2
3090.870	10140.65	42.0
3090.875	10140.67	38.6
3090.880	10140.68	58.8
3090.885	10140.70	12.9
3090.890	10140.72	22.9
3090.895	10140.73	30.7
3090.900	10140.75	33.5
3090.905	10140.76	20.1
3090.910	10140.78	37.7
3090.915	10140.80	44.6
3090.920	10140.81	13.3
3090.925	10140.83	15.8
3090.930	10140.85	37.4
3090.935	10140.86	50.2
3090.940	10140.88	40.9
3090.945	10140.90	33.3
3090.950	10140.91	33.7
3090.955	10140.93	46.0
3090.960	10140.95	34.4
3090.965	10140.96	42.4
3090.970	10140.98	26.3
3090.975	10140.99	17.1
3090.980	10141.01	50.8
3090.985	10141.03	66.6
3090.990	10141.04	41.0
3090.995	10141.06	13.9
3091.000	10141.08	12.0
3091.005	10141.09	23.2
3091.010	10141.11	31.4
3091.015	10141.13	28.8
3091.020	10141.14	62.6
3091.025	10141.16	28.8
3091.030	10141.17	45.0
3091.035	10141.19	37.2
3091.040	10141.21	17.2
3091.045	10141.22	39.0
3091.050	10141.24	31.1
3091.055	10141.26	10.2
3091.060	10141.27	19.5
3091.065	10141.29	22.8
3091.070	10141.31	41.0
3091.075	10141.32	52.9
3091.080	10141.34	52.1
3091.085	10141.36	73.1
3091.090	10141.37	44.3
3091.095	10141.39	25.0
3091.100	10141.40	23.3
3091.105	10141.42	38.3
3091.110	10141.44	26.3
3091.115	10141.45	27.1
3091.120	10141.47	40.3
3091.125	10141.49	24.2
3091.130	10141.50	28.5
3091.135	10141.52	23.0
3091.140	10141.54	28.6
3091.145	10141.55	25.8
3091.150	10141.57	11.7
3091.155	10141.58	33.1
3091.160	10141.60	21.6
3091.165	10141.62	34.3
3091.170	10141.63	37.9
3091.175	10141.65	26.1
3091.180	10141.67	41.2
3091.185	10141.68	16.0
3091.190	10141.70	16.7
3091.205	10141.75	43.5
3091.210	10141.77	66.0
3091.215	10141.78	18.6
3091.220	10141.80	24.1
3091.225	10141.81	16.6
3091.230	10141.83	67.6
3091.235	10141.85	39.6
3091.240	10141.86	27.7
3091.245	10141.88	45.4
3091.250	10141.90	108.0
3091.255	10141.91	59.8
3091.260	10141.93	71.6
3091.265	10141.95	116.5
3091.300	10142.06	5.8
3091.305	10142.08	9.4
3091.310	10142.09	4.5
3091.315	10142.11	3.2
3091.330	10142.16	1.9
3091.335	10142.18	2.4
3091.350	10142.22	2.9
3091.365	10142.27	6.1
3091.370	10142.29	7.3
3091.385	10142.34	6.2
3091.395	10142.37	2.5
3091.415	10142.44	2.5
3091.430	10142.49	2.4
3091.435	10142.50	4.5
3091.440	10142.52	7.4
3091.445	10142.54	4.6

3068.295	10066.58	172.6
3068.300	10066.60	149.0
3068.305	10066.62	115.3
3068.310	10066.63	136.0
3068.315	10066.65	153.3
3068.320	10066.67	148.4
3068.325	10066.68	160.7
3068.330	10066.70	138.0
3068.335	10066.72	187.6
3068.340	10066.73	166.3
3068.345	10066.75	120.8
3068.350	10066.77	131.5
3068.355	10066.78	144.5
3068.360	10066.80	159.2
3068.365	10066.81	162.2
3068.370	10066.83	169.8
3068.375	10066.85	137.0
3068.380	10066.86	3.1
3068.385	10066.88	110.7
3068.390	10066.90	131.5
3068.395	10066.91	104.5
3068.400	10066.93	92.7
3068.405	10066.95	165.9
3068.410	10066.96	191.3
3068.415	10066.98	248.7
3068.420	10067.00	147.4
3068.425	10067.01	245.5
3068.430	10067.03	146.6
3068.435	10067.04	130.3
3068.440	10067.06	84.2
3068.445	10067.08	150.8
3068.450	10067.09	237.5
3068.455	10067.11	287.2
3068.460	10067.13	124.6
3068.465	10067.14	198.2
3068.470	10067.16	190.0
3068.475	10067.18	202.5
3068.480	10067.19	235.4
3068.500	10067.26	207.6
3068.505	10067.27	234.5
3068.510	10067.29	286.5
3068.515	10067.31	159.0
3068.520	10067.32	176.4
3068.525	10067.34	200.6
3068.530	10067.36	204.9
3068.535	10067.37	189.2
3068.540	10067.39	99.0
3068.545	10067.41	190.8
3068.550	10067.42	154.7
3068.555	10067.44	72.1
3068.560	10067.45	153.8
3068.565	10067.47	109.7
3068.570	10067.49	182.5
3068.575	10067.50	123.9
3068.580	10067.52	187.0
3068.585	10067.54	153.6
3068.590	10067.55	196.9
3068.595	10067.57	238.1
3068.600	10067.59	155.5
3068.605	10067.60	282.2
3068.610	10067.62	227.9
3068.615	10067.63	161.2
3068.620	10067.65	139.7
3068.625	10067.67	224.5
3068.630	10067.68	135.8
3068.635	10067.70	135.5
3068.640	10067.72	125.6
3068.645	10067.73	233.0
3068.650	10067.75	267.7
3068.655	10067.77	159.9
3068.660	10067.78	137.0
3068.680	10067.85	118.3
3068.685	10067.86	131.1
3068.690	10067.88	170.0
3068.695	10067.90	228.6
3068.700	10067.91	277.9
3068.705	10067.93	284.8
3068.710	10067.95	243.5
3068.715	10067.96	299.7
3068.720	10067.98	160.2
3068.725	10068.00	139.2
3068.730	10068.01	197.7
3068.735	10068.03	219.3
3068.740	10068.04	155.0
3068.745	10068.06	162.0
3068.750	10068.08	247.7
3068.755	10068.09	243.2
3068.760	10068.11	299.2
3068.765	10068.13	198.3
3068.770	10068.14	215.4
3068.775	10068.16	228.8
3068.780	10068.18	149.8
3068.785	10068.19	253.7
3068.790	10068.21	99.4
3068.795	10068.23	228.5
3069.050	10069.06	22.5
3069.055	10069.08	16.2
3069.060	10069.09	39.6
3069.065	10069.11	18.7
3069.070	10069.13	35.9
3069.075	10069.14	20.6
3069.080	10069.16	65.7
3069.085	10069.18	80.9

3083.490	10116.44	45.5
3083.495	10116.45	98.8
3083.500	10116.47	114.8
3083.505	10116.49	37.6
3083.510	10116.50	7.5
3083.515	10116.52	9.2
3083.520	10116.54	31.1
3083.535	10116.58	18.9
3083.540	10116.60	20.3
3083.545	10116.62	27.6
3083.550	10116.63	91.1
3083.555	10116.65	9.7
3083.560	10116.67	40.6
3083.565	10116.68	72.9
3083.570	10116.70	203.0
3083.575	10116.72	147.3
3083.580	10116.73	64.7
3083.585	10116.75	39.4
3083.590	10116.77	69.6
3083.595	10116.78	72.2
3083.600	10116.80	33.8
3083.605	10116.81	57.3
3083.610	10116.83	38.2
3083.615	10116.85	178.8
3083.620	10116.86	114.7
3083.625	10116.88	86.8
3083.630	10116.90	86.3
3083.635	10116.91	27.5
3083.640	10116.93	43.9
3083.645	10116.95	127.9
3083.650	10116.96	77.1
3083.660	10117.00	59.4
3083.665	10117.01	43.3
3083.670	10117.03	73.6
3083.675	10117.04	109.7
3083.680	10117.06	193.0
3083.685	10117.08	142.3
3083.690	10117.09	109.3
3083.695	10117.11	111.4
3083.700	10117.13	192.9
3083.705	10117.14	229.5
3083.710	10117.16	94.2
3083.715	10117.18	119.6
3083.720	10117.19	161.1
3083.725	10117.21	192.1
3083.730	10117.22	79.6
3083.735	10117.24	186.8
3083.740	10117.26	91.4
3083.745	10117.27	78.3
3083.750	10117.29	139.6
3083.755	10117.31	193.4
3083.760	10117.32	109.0
3083.765	10117.34	79.8
3083.770	10117.36	107.3
3083.775	10117.37	116.0
3083.780	10117.39	201.5
3083.785	10117.41	180.5
3083.790	10117.42	125.8
3083.795	10117.44	232.0
3083.800	10117.45	215.5
3083.805	10117.47	100.9
3083.810	10117.49	100.6
3083.815	10117.50	263.6
3083.820	10117.52	215.6
3083.825	10117.54	159.8
3083.830	10117.55	238.3
3083.835	10117.57	142.4
3083.840	10117.59	291.4
3083.845	10117.60	267.3
3083.850	10117.62	144.2
3083.855	10117.63	256.9
3083.860	10117.65	90.2
3083.880	10117.72	189.5
3083.885	10117.73	171.9
3083.890	10117.75	209.6
3083.895	10117.77	201.3
3083.900	10117.78	131.0
3083.905	10117.80	79.6
3083.910	10117.82	166.7
3083.915	10117.83	251.9
3083.920	10117.85	160.4
3083.925	10117.86	181.7
3083.930	10117.88	121.6
3083.935	10117.90	178.9
3083.940	10117.91	119.0
3083.990	10118.08	61.2
3083.995	10118.09	50.4
3084.000	10118.11	37.7
3084.005	10118.13	18.6
3084.020	10118.18	111.6
3084.025	10118.19	115.0
3084.030	10118.21	202.2
3084.035	10118.23	123.8
3084.040	10118.24	132.2
3084.045	10118.26	127.3
3084.050	10118.27	154.5
3084.055	10118.29	191.1
3084.060	10118.31	172.2
3084.065	10118.32	136.0
3084.070	10118.34	69.9
3084.075	10118.36	163.6
3084.080	10118.37	133.4
3084.085	10118.39	193.1

3091.450	10142.55	8.7
3091.455	10142.57	29.7
3091.460	10142.59	9.5
3091.465	10142.60	36.0
3091.470	10142.62	13.6
3091.475	10142.63	8.7
3091.480	10142.65	33.7
3091.485	10142.67	14.0
3091.490	10142.68	2.4
3091.495	10142.70	57.5
3091.500	10142.72	7.7
3091.505	10142.73	11.2
3091.520	10142.78	5.9
3091.525	10142.80	9.0
3091.530	10142.82	5.0
3091.535	10142.83	17.0
3091.540	10142.85	23.1
3091.545	10142.86	71.6
3091.550	10142.88	33.0
3091.565	10142.93	37.1
3091.570	10142.95	31.8
3091.575	10142.96	23.2
3091.580	10142.98	28.4
3091.585	10143.00	34.7
3091.590	10143.01	54.1
3091.595	10143.03	38.6
3091.600	10143.04	33.7
3091.605	10143.06	55.6
3091.610	10143.08	14.4
3091.615	10143.09	29.9
3091.620	10143.11	29.0
3091.625	10143.13	68.6
3091.630	10143.14	36.1
3091.635	10143.16	29.0
3091.655	10143.23	53.0
3091.660	10143.24	74.8
3091.665	10143.26	24.6
3091.670	10143.27	37.3
3091.675	10143.29	31.9
3091.680	10143.31	26.1
3091.685	10143.32	27.4
3091.690	10143.34	32.5
3091.695	10143.36	13.1
3091.700	10143.37	38.5
3091.705	10143.39	74.8
3091.710	10143.41	28.1
3091.715	10143.42	43.7
3091.720	10143.44	33.3
3091.725	10143.46	22.5
3091.730	10143.47	29.5
3091.735	10143.49	71.2
3091.740	10143.50	14.9
3091.745	10143.52	53.2
3091.750	10143.54	15.4
3091.755	10143.55	89.4
3091.760	10143.57	102.8
3091.765	10143.59	41.7
3091.770	10143.60	77.1
3091.775	10143.62	116.9
3091.780	10143.64	112.7
3091.785	10143.65	64.6
3091.805	10143.72	24.3
3091.810	10143.73	68.1
3091.815	10143.75	55.8
3091.820	10143.77	27.8
3091.825	10143.78	43.2
3091.830	10143.80	30.7
3091.835	10143.82	67.8
3091.840	10143.83	44.4
3091.845	10143.85	14.1
3091.850	10143.87	26.1
3091.855	10143.88	41.7
3091.860	10143.90	23.2
3091.865	10143.91	89.3
3091.870	10143.93	41.4
3091.875	10143.95	25.0
3091.880	10143.96	16.6
3091.885	10143.98	20.1
3091.890	10144.00	45.7
3091.895	10144.01	22.4
3091.900	10144.03	78.5
3091.905	10144.05	12.5
3091.910	10144.06	15.9
3091.915	10144.08	22.9
3091.920	10144.09	42.5
3091.925	10144.11	39.8
3091.930	10144.13	71.1
3091.935	10144.14	5.9
3091.940	10144.16	15.9
3091.980	10144.29	58.7
3091.985	10144.31	59.5
3091.990	10144.32	71.4
3091.995	10144.34	137.9
3092.000	10144.36	60.4
3092.005	10144.37	70.4
3092.010	10144.39	109.9
3092.015	10144.41	70.6
3092.020	10144.42	119.1
3092.025	10144.44	109.7
3092.030	10144.46	92.6
3092.035	10144.47	119.2
3092.040	10144.49	146.1
3092.045	10144.50	91.6

3069.115	10069.28	178.8
3069.120	10069.29	145.3
3069.125	10069.31	142.0
3069.130	10069.32	203.7
3069.135	10069.34	167.6
3069.140	10069.36	171.1
3069.145	10069.37	204.4
3069.150	10069.39	131.3
3069.155	10069.41	145.6
3069.160	10069.42	156.4
3069.165	10069.44	160.1
3069.170	10069.46	154.3
3069.175	10069.47	155.9
3069.180	10069.49	182.9
3069.185	10069.50	156.1
3069.190	10069.52	168.8
3069.195	10069.54	163.3
3069.200	10069.55	136.0
3069.205	10069.57	129.4
3069.210	10069.59	127.2
3069.215	10069.60	141.1
3069.220	10069.62	155.7
3069.225	10069.64	113.4
3069.230	10069.65	125.8
3069.235	10069.67	93.3
3069.240	10069.69	118.0
3069.245	10069.70	165.2
3069.250	10069.72	148.9
3069.255	10069.73	158.9
3069.260	10069.75	174.9
3069.265	10069.77	152.8
3069.270	10069.78	160.5
3069.275	10069.80	134.7
3069.280	10069.82	226.5
3069.285	10069.83	310.1
3069.305	10069.90	18.9
3069.310	10069.92	22.9
3069.315	10069.93	13.8
3069.320	10069.95	4.7
3069.325	10069.96	23.1
3069.330	10069.98	15.1
3069.335	10070.00	2.8
3069.340	10070.01	7.6
3069.345	10070.03	11.1
3069.350	10070.05	13.3
3069.355	10070.06	18.9
3069.360	10070.08	13.2
3069.365	10070.10	68.6
3069.370	10070.11	22.6
3069.375	10070.13	22.1
3069.380	10070.14	99.4
3069.385	10070.16	34.7
3069.390	10070.18	70.6
3069.395	10070.19	108.1
3069.400	10070.21	40.0
3069.405	10070.23	84.2
3069.410	10070.24	37.5
3069.415	10070.26	54.0
3069.420	10070.28	72.7
3069.425	10070.29	72.5
3069.430	10070.31	68.3
3069.435	10070.33	28.2
3069.440	10070.34	67.7
3069.445	10070.36	54.1
3069.450	10070.37	21.4
3069.455	10070.39	39.3
3069.460	10070.41	71.3
3069.465	10070.42	58.2
3069.470	10070.44	138.0
3069.475	10070.46	101.4
3069.480	10070.47	104.5
3069.485	10070.49	58.4
3069.490	10070.51	65.5
3069.495	10070.52	44.9
3069.500	10070.54	77.8
3069.505	10070.55	75.4
3069.510	10070.57	72.2
3069.515	10070.59	117.7
3069.520	10070.60	115.8
3069.525	10070.62	85.4
3069.530	10070.64	66.4
3069.535	10070.65	33.9
3069.540	10070.67	44.4
3069.545	10070.69	71.7
3069.550	10070.70	96.0
3069.555	10070.72	15.0
3069.560	10070.74	66.1
3069.565	10070.75	75.3
3069.570	10070.77	91.6
3069.575	10070.78	42.6
3069.580	10070.80	59.9
3069.585	10070.82	47.7
3069.590	10070.83	90.4
3069.595	10070.85	64.7
3069.620	10070.93	42.1
3069.625	10070.95	36.9
3069.630	10070.96	108.2
3069.635	10070.98	92.0
3069.640	10071.00	89.9
3069.645	10071.01	92.3
3069.650	10071.03	96.0
3069.655	10071.05	32.7
3069.660	10071.06	60.1

3084.090	10118.41	138.6
3084.095	10118.42	150.3
3084.100	10118.44	133.0
3084.105	10118.46	37.4
3084.110	10118.47	69.9
3084.115	10118.49	169.7
3084.120	10118.50	156.6
3084.125	10118.52	112.7
3084.130	10118.54	132.8
3084.135	10118.55	85.7
3084.140	10118.57	228.5
3084.145	10118.59	191.6
3084.150	10118.60	156.7
3084.155	10118.62	86.9
3084.160	10118.64	111.9
3084.165	10118.65	156.3
3084.170	10118.67	167.9
3084.175	10118.68	277.8
3084.180	10118.70	145.8
3084.185	10118.72	245.2
3084.190	10118.73	129.0
3084.195	10118.75	233.3
3084.200	10118.77	174.2
3084.205	10118.78	156.4
3084.210	10118.80	170.5
3084.215	10118.82	217.6
3084.235	10118.88	250.1
3084.240	10118.90	266.2
3084.245	10118.91	173.8
3084.250	10118.93	341.7
3084.255	10118.95	356.1
3084.260	10118.96	394.6
3084.265	10118.98	211.6
3084.270	10119.00	145.2
3084.275	10119.01	73.2
3084.280	10119.03	122.5
3084.285	10119.05	87.2
3084.290	10119.06	80.7
3084.295	10119.08	23.2
3084.300	10119.09	102.9
3084.305	10119.11	110.6
3084.310	10119.13	58.9
3084.315	10119.14	58.6
3084.320	10119.16	21.8
3084.325	10119.18	123.0
3084.330	10119.19	72.7
3084.350	10119.26	98.4
3084.355	10119.28	117.9
3084.360	10119.29	56.3
3084.365	10119.31	9.7
3084.370	10119.32	36.1
3084.375	10119.34	69.6
3084.380	10119.36	106.2
3084.385	10119.37	118.5
3084.390	10119.39	134.4
3084.395	10119.41	84.5
3084.400	10119.42	88.1
3084.405	10119.44	165.8
3084.410	10119.46	26.2
3084.415	10119.47	81.6
3084.420	10119.49	77.0
3084.425	10119.50	78.3
3084.430	10119.52	66.2
3084.435	10119.54	122.1
3084.440	10119.55	115.1
3084.445	10119.57	244.1
3084.450	10119.59	162.4
3084.455	10119.60	169.4
3084.485	10119.70	67.9
3084.490	10119.72	120.7
3084.495	10119.73	31.2
3084.500	10119.75	42.5
3084.505	10119.77	113.9
3084.510	10119.78	124.4
3084.515	10119.80	104.2
3084.520	10119.82	131.8
3084.525	10119.83	118.4
3084.530	10119.85	111.3
3084.535	10119.87	152.0
3084.540	10119.88	147.5
3084.545	10119.90	100.6
3084.550	10119.92	107.5
3084.555	10119.93	101.1
3084.560	10119.95	41.6
3084.565	10119.96	140.2
3084.570	10119.98	257.0
3084.575	10120.00	104.9
3084.595	10120.06	41.7
3084.600	10120.08	11.5
3084.605	10120.10	31.2
3084.610	10120.11	42.6
3084.630	10120.18	58.7
3084.635	10120.19	47.5
3084.640	10120.21	46.8
3084.645	10120.23	64.9
3084.650	10120.24	72.4
3084.655	10120.26	82.5
3084.660	10120.28	43.8
3084.665	10120.29	84.0
3084.670	10120.31	62.8
3084.675	10120.33	103.1
3084.680	10120.34	9.9
3084.685	10120.36	19.5

3092.050	10144.52	123.5
3092.055	10144.54	30.1
3092.060	10144.55	26.3
3092.065	10144.57	37.7
3092.070	10144.59	72.9
3092.075	10144.60	99.1
3092.080	10144.62	140.7
3092.085	10144.64	134.9
3092.090	10144.65	107.2
3092.095	10144.67	133.1
3092.100	10144.69	79.8
3092.105	10144.70	111.5
3092.110	10144.72	76.5
3092.115	10144.73	94.3
3092.120	10144.75	123.1
3092.125	10144.77	43.9
3092.130	10144.78	136.1
3092.135	10144.80	72.7
3092.140	10144.82	152.0
3092.145	10144.83	72.7
3092.150	10144.85	120.7
3092.155	10144.87	78.7
3092.160	10144.88	79.1
3092.215	10145.06	77.2
3092.220	10145.08	88.9
3092.225	10145.10	173.7
3092.230	10145.11	84.5
3092.235	10145.13	101.8
3092.240	10145.14	183.0
3092.245	10145.16	100.4
3092.250	10145.18	165.3
3092.255	10145.19	129.4
3092.260	10145.21	143.6
3092.265	10145.23	200.5
3092.270	10145.24	186.2
3092.275	10145.26	119.0
3092.280	10145.28	104.2
3092.285	10145.29	82.9
3092.290	10145.31	170.0
3092.295	10145.33	123.3
3092.300	10145.34	117.7
3092.320	10145.41	141.4
3092.325	10145.42	115.5
3092.330	10145.44	154.4
3092.335	10145.46	118.8
3092.340	10145.47	145.8
3092.345	10145.49	143.4
3092.350	10145.51	135.1
3092.355	10145.52	173.0
3092.360	10145.54	106.6
3092.365	10145.55	153.6
3092.370	10145.57	195.0
3092.375	10145.59	165.3
3092.380	10145.60	99.6
3092.385	10145.62	97.2
3092.390	10145.64	125.1
3092.410	10145.70	208.3
3092.415	10145.72	151.2
3092.420	10145.74	10.0
3092.425	10145.75	59.0
3092.430	10145.77	85.8
3092.435	10145.78	78.6
3092.440	10145.80	19.1
3092.445	10145.82	19.4
3092.450	10145.83	25.8
3092.455	10145.85	20.9
3092.460	10145.87	15.6
3092.465	10145.88	23.4
3092.470	10145.90	56.8
3092.475	10145.92	8.7
3092.480	10145.93	14.5
3092.485	10145.95	5.9
3092.490	10145.96	19.5
3092.495	10145.98	17.6
3092.500	10146.00	28.8
3092.505	10146.01	46.8
3092.510	10146.03	72.0
3092.530	10146.10	26.0
3092.535	10146.11	20.9
3092.540	10146.13	7.4
3092.545	10146.15	28.1
3092.550	10146.16	17.3
3092.555	10146.18	25.6
3092.560	10146.19	8.2
3092.565	10146.21	34.5
3092.570	10146.23	13.5
3092.575	10146.24	59.2
3092.580	10146.26	17.2
3092.585	10146.28	16.2
3092.590	10146.29	23.5
3092.595	10146.31	37.5
3092.600	10146.33	26.1
3092.605	10146.34	170.7
3092.610	10146.36	45.7
3092.615	10146.37	38.2
3092.620	10146.39	27.7
3092.625	10146.41	19.9
3092.630	10146.42	95.7
3092.635	10146.44	95.7
3092.640	10146.46	42.4
3092.645	10146.47	15.0
3092.650	10146.49	38.7
3092.655	10146.51	19.2

3069.665	10071.08	53.3
3069.670	10071.10	70.4
3069.675	10071.11	36.0
3069.680	10071.13	35.1
3069.685	10071.15	53.9
3069.690	10071.16	39.7
3069.695	10071.18	92.8
3069.700	10071.19	14.4
3069.705	10071.21	32.4
3069.710	10071.23	71.1
3069.715	10071.24	83.0
3069.720	10071.26	137.0
3069.725	10071.28	67.8
3069.730	10071.29	74.2
3069.735	10071.31	116.7
3069.740	10071.33	89.8
3069.745	10071.34	83.0
3069.750	10071.36	79.9
3069.755	10071.37	73.3
3069.760	10071.39	85.1
3069.765	10071.41	58.3
3069.785	10071.47	22.5
3069.790	10071.49	34.8
3069.795	10071.51	46.4
3069.800	10071.52	40.0
3069.805	10071.54	20.6
3069.810	10071.56	43.0
3069.815	10071.57	13.9
3069.820	10071.59	27.6
3069.825	10071.60	31.9
3069.830	10071.62	26.5
3069.835	10071.64	44.8
3069.840	10071.65	54.8
3069.845	10071.67	39.2
3069.850	10071.69	58.4
3069.855	10071.70	35.2
3069.860	10071.72	45.7
3069.865	10071.74	57.7
3069.870	10071.75	74.7
3069.875	10071.77	59.3
3069.880	10071.79	52.8
3069.885	10071.80	73.2
3069.890	10071.82	59.1
3069.895	10071.83	60.4
3069.900	10071.85	84.8
3069.905	10071.87	65.4
3069.910	10071.88	42.2
3069.975	10072.10	277.0
3069.980	10072.11	434.4
3069.985	10072.13	305.2
3069.990	10072.15	158.5
3069.995	10072.16	132.5
3070.000	10072.18	169.7
3070.005	10072.20	262.3
3070.010	10072.21	300.2
3070.015	10072.23	195.6
3070.020	10072.24	151.8
3070.025	10072.26	197.7
3070.030	10072.28	243.9
3070.035	10072.29	207.7
3070.040	10072.31	171.0
3070.045	10072.33	196.7
3070.070	10072.41	158.2
3070.075	10072.42	166.1
3070.080	10072.44	181.8
3070.085	10072.46	184.7
3070.090	10072.47	155.7
3070.095	10072.49	121.8
3070.100	10072.51	135.5
3070.105	10072.52	123.8
3070.110	10072.54	114.7
3070.140	10072.64	230.2
3070.145	10072.65	124.2
3070.150	10072.67	107.9
3070.155	10072.69	331.6
3070.160	10072.70	203.9
3070.165	10072.72	222.3
3070.170	10072.74	105.7
3070.175	10072.75	160.5
3070.180	10072.77	220.2
3070.185	10072.79	216.5
3070.190	10072.80	117.2
3070.195	10072.82	204.4
3070.200	10072.83	288.8
3070.205	10072.85	344.3
3070.210	10072.87	108.3
3070.215	10072.88	344.8
3070.220	10072.90	379.7
3070.225	10072.92	218.3
3070.230	10072.93	353.5
3070.235	10072.95	367.8
3070.240	10072.97	155.2
3070.245	10072.98	130.6
3070.250	10073.00	164.8
3070.255	10073.02	202.6
3070.260	10073.03	291.2
3070.265	10073.05	288.6
3070.295	10073.15	184.1
3070.300	10073.16	159.3
3070.305	10073.18	220.7
3070.310	10073.20	179.2
3070.315	10073.21	161.0
3070.320	10073.23	165.2
3084.690	10120.37	54.5
3084.695	10120.39	35.9
3084.700	10120.41	55.9
3084.705	10120.42	60.8
3084.710	10120.44	33.7
3084.715	10120.46	34.7
3084.720	10120.47	59.5
3084.725	10120.49	18.4
3084.730	10120.51	84.1
3084.735	10120.52	21.6
3084.740	10120.54	44.3
3084.745	10120.55	119.5
3084.750	10120.57	40.1
3084.755	10120.59	83.2
3084.760	10120.60	183.1
3084.765	10120.62	86.0
3084.770	10120.64	60.7
3084.775	10120.65	98.4
3084.780	10120.67	48.6
3084.785	10120.69	91.9
3084.790	10120.70	47.4
3084.795	10120.72	43.7
3084.800	10120.74	4.2
3084.805	10120.75	2.2
3084.815	10120.78	3.5
3084.820	10120.80	3.5
3084.900	10121.06	3.9
3084.905	10121.08	3.0
3084.910	10121.10	4.0
3084.915	10121.11	2.2
3084.920	10121.13	5.3
3084.925	10121.15	17.5
3084.930	10121.16	18.2
3084.935	10121.18	9.0
3084.945	10121.21	3.1
3084.950	10121.23	14.1
3084.955	10121.24	32.6
3084.960	10121.26	4.5
3084.965	10121.28	4.3
3084.970	10121.29	10.0
3084.975	10121.31	25.3
3084.985	10121.34	4.4
3084.990	10121.36	21.3
3084.995	10121.37	28.6
3085.000	10121.39	9.1
3085.005	10121.41	25.8
3085.010	10121.42	8.3
3085.015	10121.44	20.0
3085.020	10121.46	26.7
3085.025	10121.47	11.3
3085.030	10121.49	18.6
3085.035	10121.51	11.4
3085.040	10121.52	31.9
3085.045	10121.54	26.9
3085.050	10121.56	73.0
3085.055	10121.57	70.3
3085.060	10121.59	59.1
3085.065	10121.60	69.6
3085.070	10121.62	56.8
3085.075	10121.64	20.8
3085.080	10121.65	35.2
3085.085	10121.67	16.1
3085.090	10121.69	7.7
3085.095	10121.70	6.2
3085.100	10121.72	40.8
3085.105	10121.74	17.3
3085.110	10121.75	42.5
3085.115	10121.77	57.0
3085.120	10121.79	26.3
3085.125	10121.80	30.5
3085.130	10121.82	67.2
3085.135	10121.83	16.7
3085.140	10121.85	24.8
3085.145	10121.87	10.2
3085.150	10121.88	61.3
3085.155	10121.90	3.9
3085.160	10121.92	3.1
3085.165	10121.93	6.7
3085.170	10121.95	3.9
3085.175	10121.97	10.7
3085.180	10121.98	13.2
3085.185	10122.00	6.5
3085.190	10122.01	16.6
3085.195	10122.03	23.0
3085.200	10122.05	40.5
3085.215	10122.10	31.6
3085.220	10122.11	36.8
3085.225	10122.13	8.2
3085.230	10122.15	8.7
3085.235	10122.16	54.9
3085.240	10122.18	24.5
3085.245	10122.20	44.1
3085.250	10122.21	19.2
3085.255	10122.23	46.8
3085.260	10122.24	27.4
3085.265	10122.26	42.7
3085.270	10122.28	30.3
3085.275	10122.29	6.2
3085.280	10122.31	39.3
3085.285	10122.33	23.5
3085.290	10122.34	37.7
3085.295	10122.36	12.9
3085.300	10122.38	89.8
3092.660	10146.52	5.2
3092.665	10146.54	36.8
3092.670	10146.56	28.9
3092.675	10146.57	32.8
3092.680	10146.59	25.3
3092.685	10146.60	27.1
3092.690	10146.62	30.1
3092.695	10146.64	30.3
3092.700	10146.65	24.1
3092.705	10146.67	29.2
3092.710	10146.69	32.5
3092.715	10146.70	37.3
3092.735	10146.77	20.4
3092.740	10146.79	34.0
3092.745	10146.80	21.6
3092.750	10146.82	37.2
3092.755	10146.83	53.4
3092.760	10146.85	54.2
3092.765	10146.87	21.8
3092.770	10146.88	70.1
3092.775	10146.90	85.1
3092.780	10146.92	60.9
3092.785	10146.93	13.8
3092.790	10146.95	22.6
3092.795	10146.97	38.5
3092.800	10146.98	69.8
3092.805	10147.00	43.3
3092.810	10147.01	43.0
3092.815	10147.03	62.5
3092.820	10147.05	40.3
3092.825	10147.06	29.6
3092.830	10147.08	95.1
3092.835	10147.10	91.9
3092.840	10147.11	47.4
3092.845	10147.13	153.1
3092.850	10147.15	140.9
3092.860	10147.18	74.8
3092.865	10147.20	68.2
3092.870	10147.21	36.7
3092.875	10147.23	17.9
3092.880	10147.24	19.5
3092.885	10147.26	33.5
3092.890	10147.28	47.5
3092.895	10147.29	31.9
3092.900	10147.31	20.3
3092.905	10147.33	3.1
3092.910	10147.34	7.3
3092.915	10147.36	20.6
3092.920	10147.38	16.1
3092.925	10147.39	26.8
3092.930	10147.41	10.2
3092.935	10147.42	21.4
3092.940	10147.44	76.0
3092.945	10147.46	39.1
3092.950	10147.47	31.6
3092.955	10147.49	59.3
3092.960	10147.51	71.6
3092.965	10147.52	104.0
3092.970	10147.54	47.5
3092.975	10147.56	82.6
3092.980	10147.57	89.2
3092.985	10147.59	98.5
3093.005	10147.65	94.8
3093.010	10147.67	104.9
3093.015	10147.69	53.4
3093.020	10147.70	77.8
3093.025	10147.72	41.1
3093.030	10147.74	58.1
3093.035	10147.75	81.3
3093.040	10147.77	131.5
3093.045	10147.79	69.6
3093.050	10147.80	109.8
3093.055	10147.82	106.0
3093.060	10147.83	69.5
3093.065	10147.85	109.0
3093.070	10147.87	120.9
3093.075	10147.88	81.5
3093.130	10148.06	221.5
3093.135	10148.08	136.5
3093.140	10148.10	116.1
3093.145	10148.11	176.0
3093.165	10148.18	139.2
3093.170	10148.20	77.1
3093.175	10148.21	83.2
3093.180	10148.23	90.4
3093.185	10148.25	173.4
3093.190	10148.26	117.1
3093.195	10148.28	156.4
3093.200	10148.29	120.9
3093.205	10148.31	141.4
3093.210	10148.33	134.0
3093.215	10148.34	81.6
3093.220	10148.36	132.0
3093.225	10148.38	118.5
3093.230	10148.39	92.4
3093.235	10148.41	99.6
3093.240	10148.43	143.1
3093.245	10148.44	100.0
3093.250	10148.46	112.9
3093.255	10148.47	145.1
3093.260	10148.49	113.5
3093.275	10148.54	2.9
3093.280	10148.56	9.8

3070.325	10073.25	210.8
3070.330	10073.26	310.1
3070.335	10073.28	212.3
3070.340	10073.29	178.0
3070.345	10073.31	431.7
3070.350	10073.33	434.5
3070.355	10073.34	273.5
3070.360	10073.36	365.4
3070.365	10073.38	196.5
3070.370	10073.39	248.4
3070.375	10073.41	266.3
3070.380	10073.43	192.0
3070.385	10073.44	179.7
3070.390	10073.46	246.4
3070.395	10073.47	372.6
3070.400	10073.49	351.7
3070.405	10073.51	491.9
3070.430	10073.59	535.9
3070.435	10073.61	400.1
3070.440	10073.62	253.7
3070.445	10073.64	427.3
3070.450	10073.66	251.4
3070.455	10073.67	204.6
3070.460	10073.69	190.9
3070.465	10073.70	322.4
3070.470	10073.72	366.0
3070.475	10073.74	232.2
3070.480	10073.75	182.5
3070.485	10073.77	218.9
3070.490	10073.79	427.7
3070.495	10073.80	112.5
3070.500	10073.82	76.9
3070.520	10073.88	82.0
3070.525	10073.90	65.0
3070.530	10073.92	121.7
3070.535	10073.93	93.8
3070.540	10073.95	92.7
3070.545	10073.97	90.1
3070.550	10073.98	83.0
3070.555	10074.00	95.0
3070.560	10074.02	79.0
3070.565	10074.03	121.8
3070.570	10074.05	79.1
3070.575	10074.07	107.2
3070.580	10074.08	114.3
3070.585	10074.10	133.9
3070.590	10074.11	132.4
3070.595	10074.13	100.0
3070.600	10074.15	102.7
3070.605	10074.16	106.2
3070.610	10074.18	95.6
3070.615	10074.20	119.7
3070.620	10074.21	115.4
3070.625	10074.23	161.3
3070.630	10074.25	171.6
3070.635	10074.26	92.8
3070.640	10074.28	165.1
3070.645	10074.29	98.7
3070.665	10074.36	160.4
3070.670	10074.38	77.8
3070.675	10074.39	153.5
3070.680	10074.41	124.8
3070.685	10074.43	103.8
3070.690	10074.44	80.6
3070.695	10074.46	104.0
3070.700	10074.48	81.7
3070.705	10074.49	143.7
3070.710	10074.51	116.7
3070.715	10074.52	103.8
3070.720	10074.54	96.7
3070.725	10074.56	125.3
3070.730	10074.57	158.6
3070.735	10074.59	130.4
3070.740	10074.61	78.8
3070.745	10074.62	166.4
3070.750	10074.64	158.2
3070.755	10074.66	152.7
3070.760	10074.67	96.3
3070.765	10074.69	142.8
3070.770	10074.71	73.8
3070.775	10074.72	84.4
3070.780	10074.74	65.5
3070.785	10074.75	70.1
3070.790	10074.77	90.9
3070.795	10074.79	87.8
3070.800	10074.80	40.3
3070.805	10074.82	104.5
3070.810	10074.84	114.2
3070.815	10074.85	206.7
3070.820	10074.87	83.3
3070.825	10074.89	76.5
3070.830	10074.90	105.4
3070.835	10074.92	122.8
3070.840	10074.93	167.6
3070.845	10074.95	157.6
3070.880	10075.07	142.3
3070.885	10075.08	72.9
3070.890	10075.10	98.6
3070.895	10075.12	70.2
3070.900	10075.13	79.1
3070.905	10075.15	67.8
3070.910	10075.16	48.9
3070.915	10075.18	50.4

3085.305	10122.39	32.1
3085.310	10122.41	25.1
3085.315	10122.42	9.4
3085.320	10122.44	34.5
3085.325	10122.46	45.5
3085.330	10122.47	21.9
3085.335	10122.49	59.5
3085.340	10122.51	61.4
3085.345	10122.52	60.5
3085.350	10122.54	16.3
3085.355	10122.56	60.6
3085.360	10122.57	22.1
3085.370	10122.61	8.7
3085.375	10122.62	13.1
3085.380	10122.64	9.7
3085.385	10122.65	6.5
3085.390	10122.67	4.1
3085.395	10122.69	12.7
3085.400	10122.70	6.9
3085.405	10122.72	9.8
3085.410	10122.74	5.6
3085.415	10122.75	3.0
3085.420	10122.77	7.8
3085.425	10122.79	12.8
3085.430	10122.80	5.6
3085.435	10122.82	22.0
3085.440	10122.83	8.1
3085.445	10122.85	9.1
3085.450	10122.87	6.4
3085.455	10122.88	5.7
3085.460	10122.90	5.1
3085.465	10122.92	5.1
3085.470	10122.93	7.8
3085.475	10122.95	7.0
3085.480	10122.97	5.3
3085.485	10122.98	8.2
3085.490	10123.00	4.5
3085.495	10123.02	6.9
3085.500	10123.03	17.1
3085.505	10123.05	14.4
3085.510	10123.06	9.3
3085.515	10123.08	6.6
3085.520	10123.10	9.2
3085.525	10123.11	7.5
3085.530	10123.13	12.0
3085.535	10123.15	7.7
3085.540	10123.16	16.9
3085.545	10123.18	8.3
3085.550	10123.20	6.2
3085.560	10123.23	6.6
3085.565	10123.25	34.2
3085.570	10123.26	16.8
3085.575	10123.28	7.5
3085.580	10123.29	19.2
3085.585	10123.31	17.2
3085.590	10123.33	18.0
3085.595	10123.34	21.5
3085.600	10123.36	21.3
3085.605	10123.38	6.7
3085.610	10123.39	19.1
3085.615	10123.41	27.4
3085.625	10123.44	6.9
3085.630	10123.46	5.6
3085.635	10123.47	5.3
3085.640	10123.49	7.3
3085.645	10123.51	7.4
3085.650	10123.52	7.8
3085.655	10123.54	28.6
3085.660	10123.56	21.6
3085.665	10123.57	14.9
3085.670	10123.59	13.0
3085.675	10123.61	24.4
3085.680	10123.62	27.8
3085.685	10123.64	8.8
3085.690	10123.66	11.8
3085.695	10123.67	39.2
3085.700	10123.69	33.3
3085.705	10123.70	9.3
3085.710	10123.72	8.3
3085.715	10123.74	12.6
3085.720	10123.75	34.1
3085.725	10123.77	28.1
3085.730	10123.79	32.4
3085.740	10123.82	13.4
3085.745	10123.84	6.2
3085.750	10123.85	19.1
3085.755	10123.87	10.4
3085.760	10123.88	11.7
3085.765	10123.90	28.4
3085.770	10123.92	17.3
3085.775	10123.93	33.0
3085.780	10123.95	31.8

3093.285	10148.57	8.1
3093.290	10148.59	11.6
3093.295	10148.61	16.9
3093.300	10148.62	10.6
3093.305	10148.64	8.2
3093.310	10148.66	10.7
3093.315	10148.67	13.2
3093.320	10148.69	22.0
3093.325	10148.70	18.3
3093.330	10148.72	13.2
3093.335	10148.74	3.1
3093.340	10148.75	4.2
3093.345	10148.77	2.9
3093.350	10148.79	3.0
3093.365	10148.84	4.1
3093.380	10148.88	35.3
3093.385	10148.90	134.8
3093.390	10148.92	189.7
3093.395	10148.93	83.3
3093.400	10148.95	62.3
3093.405	10148.97	72.8
3093.410	10148.98	60.6
3093.415	10149.00	23.0
3093.420	10149.02	29.4
3093.425	10149.03	88.9
3093.430	10149.05	110.0
3093.435	10149.07	15.2
3093.440	10149.08	59.8
3093.445	10149.10	27.8
3093.450	10149.11	2.6
3093.455	10149.13	6.5
3093.460	10149.15	8.6
3093.465	10149.16	19.5
3093.485	10149.23	10.3
3093.490	10149.25	32.5
3093.495	10149.26	44.6
3093.500	10149.28	17.4
3093.505	10149.29	22.4
3093.510	10149.31	23.6
3093.515	10149.33	9.7
3093.520	10149.34	5.7
3093.525	10149.36	3.4
3093.530	10149.38	2.7
3093.535	10149.39	21.1
3093.540	10149.41	4.4
3093.545	10149.43	24.6
3093.550	10149.44	17.7
3093.555	10149.46	13.1
3093.560	10149.48	21.8
3093.565	10149.49	14.3
3093.570	10149.51	18.9
3093.590	10149.57	10.3
3093.595	10149.59	4.5
3093.600	10149.61	3.0
3093.605	10149.62	25.9
3093.610	10149.64	44.9
3093.615	10149.66	30.8
3093.620	10149.67	45.2
3093.625	10149.69	36.1
3093.630	10149.71	4.4
3093.635	10149.72	85.3
3093.640	10149.74	27.0
3093.645	10149.75	21.3
3093.650	10149.77	14.1
3093.670	10149.84	28.6
3093.675	10149.85	27.8
3093.680	10149.87	18.0
3093.685	10149.89	21.1
3093.690	10149.90	14.8
3093.695	10149.92	4.4
3093.700	10149.93	5.6
3093.705	10149.95	4.6
3093.715	10149.98	13.8
3093.720	10150.00	37.6
3093.725	10150.02	36.4
3093.730	10150.03	9.6
3093.735	10150.05	62.6
3093.740	10150.07	6.6
3093.745	10150.08	12.3
3093.750	10150.10	23.5
3093.755	10150.12	64.9
3093.760	10150.13	60.3
3093.765	10150.15	122.8
3093.770	10150.16	160.3
3093.775	10150.18	78.4
3093.780	10150.20	76.1
3093.785	10150.21	177.3
3093.790	10150.23	110.3
3093.795	10150.25	43.3
3093.815	10150.31	23.9
3093.820	10150.33	23.6
3093.825	10150.34	38.4

3070.920	10075.20	98.2
3070.925	10075.21	47.2
3070.930	10075.23	53.4
3070.935	10075.25	41.9
3070.940	10075.26	48.6
3070.945	10075.28	52.4
3070.950	10075.30	32.7
3070.955	10075.31	35.8
3070.960	10075.33	46.7
3070.965	10075.34	67.3
3070.970	10075.36	117.8
3070.975	10075.38	80.5
3070.980	10075.39	85.3
3070.985	10075.41	60.3
3070.990	10075.43	73.8
3070.995	10075.44	77.5
3071.000	10075.46	74.6
3071.005	10075.48	101.0
3071.010	10075.49	127.2
3071.015	10075.51	65.4
3071.020	10075.53	74.7
3071.050	10075.62	101.6
3071.055	10075.64	71.8
3071.060	10075.66	48.9
3071.065	10075.67	45.6
3071.070	10075.69	79.3
3071.075	10075.71	121.0
3071.080	10075.72	72.9
3071.085	10075.74	51.5
3071.090	10075.75	33.0
3071.095	10075.77	42.1
3071.100	10075.79	47.6
3071.105	10075.80	39.8
3071.110	10075.82	61.4
3071.115	10075.84	38.2
3071.120	10075.85	72.2
3071.125	10075.87	49.8
3071.130	10075.89	93.2
3071.135	10075.90	71.5
3071.140	10075.92	69.6
3071.145	10075.94	50.5
3071.150	10075.95	81.5
3071.155	10075.97	80.5
3071.160	10075.98	79.7
3071.165	10076.00	65.3
3071.170	10076.02	52.0
3071.175	10076.03	73.3
3071.235	10076.23	27.5
3071.240	10076.25	22.3
3071.245	10076.26	21.7
3071.250	10076.28	46.0
3071.275	10076.36	5.3
3071.280	10076.38	7.3
3071.285	10076.39	9.6
3071.290	10076.41	29.5
3071.295	10076.43	67.5
3071.300	10076.44	65.4
3071.305	10076.46	102.2
3071.310	10076.48	24.4
3071.315	10076.49	109.6
3071.320	10076.51	96.7
3071.325	10076.53	67.8
3071.330	10076.54	24.7
3071.335	10076.56	22.6
3071.340	10076.58	28.2
3071.380	10076.71	124.2
3071.385	10076.72	92.5
3071.390	10076.74	75.7
3071.395	10076.76	58.7
3071.400	10076.77	105.6
3071.405	10076.79	88.4
3071.410	10076.80	102.3
3071.415	10076.82	152.0
3071.625	10077.51	170.1
3071.630	10077.53	90.6
3071.635	10077.54	54.1
3071.640	10077.56	138.7
3071.645	10077.58	151.6
3071.650	10077.59	100.9
3071.655	10077.61	169.0
3071.660	10077.62	278.2
3071.665	10077.64	165.2
3071.735	10077.87	328.9
3071.740	10077.89	436.4
3071.745	10077.90	173.2
3071.750	10077.92	263.8
3071.755	10077.94	154.4
3071.760	10077.95	268.2